

---

Doctoral

Science


---

2001-04-01

## Effect of a Modified Isoindole Backbone on the Electrical Optical and Physical Properties of the Isoindole Organised Semiconductor System

Matthew Boylan  
*Technological University Dublin*

Follow this and additional works at: <https://arrow.tudublin.ie/sciendoc>

 Part of the [Chemistry Commons](#)

---

### Recommended Citation

Boylan, M. (2001). *Effect of a modified isoindole backbone on the electrical optical and physical properties of the isoindole organis semiconductor system*. Doctoral thesis. Technological University Dublin. doi:10.21427/D7FP4N

This Theses, Ph.D is brought to you for free and open access by the Science at ARROW@TU Dublin. It has been accepted for inclusion in Doctoral by an authorized administrator of ARROW@TU Dublin. For more information, please contact [yvonne.desmond@tudublin.ie](mailto:yvonne.desmond@tudublin.ie), [arrow.admin@tudublin.ie](mailto:arrow.admin@tudublin.ie), [brian.widdis@tudublin.ie](mailto:brian.widdis@tudublin.ie).



This work is licensed under a [Creative Commons Attribution-Noncommercial-Share Alike 3.0 License](#)

**EFFECT OF A MODIFIED ISOINDOLE  
BACKBONE ON THE ELECTRICAL,  
OPTICAL AND PHYSICAL PROPERTIES  
OF THE ISOINDOLE ORGANIC  
SEMICONDUCTOR SYSTEM.**

by

Matthew Boylan BSc.

A Thesis presented to  
Dublin Institute of Technology  
for the award of Ph.D.

Prepared under the supervision of Dr. J.F. Cassidy, School of  
Chemistry, Dublin Institute of Technology, Kevin Street and  
Dr. N.M. Hanly, Department of Chemical and Environmental  
Sciences, University of Limerick

School of Chemistry

March 2001

*To Mum & Dad.*

## Declaration

I certify that this thesis which I now submit for examination for the award of Ph.D., is entirely my own work and has not been taken from the work of others save and to the extent that such work has been cited and acknowledged within the text of my work.

This thesis was prepared according to the regulations for postgraduate studies by research of the Dublin Institute of Technology and has not been submitted in whole or in part for an award in any other Institute or University.

Signature Matthew Boylan Date 7/6/01  
Candidate

## Acknowledgements

During these past years I have received much needed help from a number of people. Firstly, I would like to express my sincere thanks to my supervisors Dr. Noreen Hanly and Dr. John Cassidy for their guidance, perseverance and encouragement throughout the course of my studies. I am grateful to John for taking on this role half way through the project, despite his busy work schedule.

I would also like to thank Dr. N. Russell for the use of the facilities and instrumentation within the School of Chemistry, Dublin Institute of Technology, Kevin Street. I would like to thank the D.I.T. for awarding me with the post-graduate scholarship funding, which managed to keep my head above water. Many, many thanks to the technical staff in the department, especially Mr. Sean McGee for showing me how to use the NMR and for solving the many glassware problems I presented to him.

I would like to thank Dr. Anthony Kennedy for his advice and help in both carrying out the research and reporting it. Thank you to Mr. Gordon Chambers of the School of Physics, D.I.T., Kevin Street, for his help in constructing the optics for the spectroelectrochemical experiments and thanks to Mr. Martin Baillie-Johnston for his AutoCAD skills.

To the many post-graduate students that have passed through lab 330, I thank you, as without your very special sense of humour that was always in the air, it may not have been so easy to turn up when things were going bad. Kathy and Steven, in answer to your question, lab 330 will never be the same again, thanks for the laughs.

I am also indebted to my family and my parents to whom this thesis is dedicated, you both have been endlessly supporting and encouraging, which will always be invaluable to me. Finally I would like to thank Gemma Bogle for all her help, support, vibrant encouragement and her very special skill to see everything as a positive, thank you for helping me through it all.

## Abstract

Primarily it was endeavoured to synthesise conducting polymers bearing a modified isoindole backbone with potentially enhanced electrical, optical and physical properties. The addition of electron donating methoxy groups on to the N-methylisoindole system results in alterations to the resultant polymer's optical and physical properties.

The synthesis of the new compounds 5-methoxy-N-methylisoindole and 5,6-dimethoxy-N-methylisoindole was carried out via a devised route. Characterisation of the two new monomers 5-methoxy-N-methylisoindole and 5,6-dimethoxy-N-methylisoindole and the parent N-methylisoindole and their corresponding polymers has also been carried out initially by cyclic voltammetry studies. The oxidation of the monomers and corresponding polymers occurs at decreasing positive potentials with the addition of the methoxy groups. Variation in the dopant anion incorporated into the polymer has also lead to alteration of the polymer properties. The novel poly-5,6-dimethoxy-N-methylisoindole appears to be potentially a soluble organic conductor with rather interesting electrical properties.

Subsequent characterisation of these materials to obtain an insight to their mechanistic properties was carried out. Along with cyclic voltammetry, the nucleation process occurring during polymerisation was studied with current vs time transients. Also cation exchange studies have been carried out.

Finally *in situ* spectroelectrochemical properties of polymers are studied and analysed using the Nernst equation. The band gap of the neutral poly-5-methoxy-N-methylisoindole and poly-5,6-dimethoxy-N-methylisoindole was determined to be ~2.36 eV and ~2.38 eV respectively.

## Table of Contents

	Page No.
Declaration	(i)
Acknowledgements	(ii)
Abstract	(iii)
Table of contents	(iv)

### Chapter 1 – General Introduction

1.1	Organic Semiconductors.	1
1.2	Band Theory and Conduction – Classical Model.	6
1.3	Electronic structure of organic semiconductors – Conduction properties.	10
1.4	Electronic structure of organic semiconductors – Optical properties.	20
1.5	Structure – Property relationship.	21
1.6	Isoindoles as Organic semiconductors.	41
1.7	Applications.	49
1.8	References	53

### Chapter 2 – The Organic Synthesis of Isoindole Monomers

2.1	Introduction	
2.1.1	Synthesis of Isoindoles	58
2.2	Results and Discussion	
2.2.1	Synthesis of N-methylisoindole	82
2.2.2	Strategic route to the formation of 5,6-dimethoxy-N-methylisoindole and its synthesis.	87
2.2.3	Strategic route to the formation of 5-methoxy-N-methylisoindole and its synthesis.	110

2.3	Conclusion	127
2.4	Experimental	
2.4.1	Preparation of $\alpha,\alpha'$ -dibromo-o-xylene	135
2.4.2	Preparation of N-methylisoindole	136
2.4.3	Preparation of 5,6-dimethoxy-N-methylisoindole	137
2.4.4	Preparation of 5-methoxy-N-methylisoindole	140
2.5	References	143

### **Chapter 3 – Preliminary Electrochemical Characterisation of Monomers and Polymers**

3.1	Introduction	
3.1.1	Electrodes	146
3.1.2	Electrochemical Techniques	149
3.1.3	Synthesis of Conducting Polymers	157
3.1.4	Electrochemical Synthesis	157
3.1.5	Preliminary study of electrochemical synthesis	158
3.1.6	Mechanism of Electropolymerisation	160
3.1.7	Factors affecting electrochemical polymerisation and polymer properties.	166
3.2	Results and Discussion	
3.2.1	Cyclic Voltammetric study of the isoindole monomers	170
3.2.2	Chronoamperometric study of Polymer formation	193
3.2.3	Cyclic Voltammetric study of the isoindole polymers	216
3.2.4	Cyclic Voltammetric study of the $\alpha,\alpha'$ -dibromo-o-xylene series.	237
3.3	Conclusion	245



3.4	Experimental	
3.4.1	Cyclic Voltammetric study of the substituted $\alpha, \alpha'$ -dibromo-o-xylenes	250
3.4.2	Cyclic Voltammetric study of N-methylisindole & poly-N-methylisindole	250
3.4.3	Cyclic Voltammetric study of 5-methoxy-N-methylisindole & poly-5-methoxy-N-methylisindole	251
3.4.4	Cyclic Voltammetric study of 5,6-dimethoxy-N-methylisindole & poly-5,6-dimethoxy-N-methylisindole	252
3.4.5	Chronoamperometric study of the growth of polymer films	253
3.5	References	254

## **Chapter 4 – *In situ* Spectroelectrochemical Characterisation of Polymers**

4.1	Introduction	259
4.1.1	Spectroelectrochemical Techniques	261
4.1.2	Analysis of spectroelectrochemical behaviour of conducting polymers using the Nernst Equation	264
4.1.3	Optical studies of Polypyrrole	267
4.1.4	Low band-gap conducting polymers	270
4.1.5	Optical studies of poly-N-methylisindole	271
4.2	Results and Discussion	
4.2.1	Spectroelectrochemistry of poly-N-methylisindole	273
4.2.2	Spectroelectrochemistry of poly-5-methoxy-N-methylisindole	292
4.2.3	Spectroelectrochemistry of poly-5,6-dimethoxy-N-methylisindole	309
4.3	Conclusion	313

4.4	Experimental	315
4.4.1	poly-N-methylisindole	318
4.4.2	poly-5-methoxy-N-methylisindole	318
4.4.3	poly-5,6-dimethoxy-N-methylisindole	319
4.5	References	320

**Chapter 5 – An Electrochemical Study of Ion Exchange behaviour of thin films of Poly-N-methylisindole, Poly-5-methoxy-N-methylisindole and Poly-5,6-dimethoxy-N-methylisindole.**

5.1	Introduction	323
5.2	Results and Discussion	
5.2.1	Ion exchange studies of Poly-N-methylisindole	326
5.2.2	Ion exchange studies of Poly-5-methoxy-N-methylisindole	328
5.2.3	Ion exchange studies of Poly-5,6-dimethoxy-N-methylisindole	330
5.2.4	Ion Concentration Study of Polymers	332
5.3	Conclusion	342
5.4	Experimental	
5.4.1	General experimental	344
5.4.2	Ion exchange studies	344
5.4.3	Cation Concentration Study	345
5.5	References	348
Appendix A-G		349 - 362

# **Chapter 1**

## **General Introduction**

## Chapter 1 – General Introduction

### 1.1 Organic Semiconductors.

A key property of organic polymers, which has propelled their development, is their inability to conduct electricity. In fact the application of polymers in electrical insulation is common place in everyday life. Figure 1.1 illustrates typical electrical conductivities of some common materials and indicates those which are classified as insulators, semi-conductors and metals.

Traditionally polymers were firmly set in the insulator region i.e.  $\sim 10^{-5}$ - $10^{-18}$  siemens per centimetre or  $\text{S cm}^{-1}$ . However, over the past twenty years a new class of organic polymers has been developed with the ability to conduct electricity [1]. These new polymers are part of a larger class of materials called “synthetic metals” because of their metallic like behaviour. Names such as “conducting polymers” and “organic semiconductors” were also assigned to these materials.

The novel concept that organic polymers could conduct electricity and furthermore be fabricated into electrical wires, films and virtually any shape brought scientists of many disciplines together including chemists, physicists, material scientists, engineers and theoreticians, both in academia and industry to work towards a common goal. This common goal was to tailor the properties of these materials so as to enable their wide application [1]. This required a close look at the monomer unit of which these polymers are composed.

In the early 1970's, a key discovery in the evolution of conductive polymers was the high conductivity of polysulfurnitride  $(\text{SN})_x$  [2], an inorganic explosive polymer. Its room temperature conductivity was of the order of  $10^3 \text{ S cm}^{-1}$ , compared with that of  $\sim 6 \times 10^5 \text{ S cm}^{-1}$  for copper and  $\sim 10^{-14} \text{ S cm}^{-1}$  for the known insulator, polyethylene. It was also reported [3] that polysulfurnitride was superconducting at about 0.3 K. By the mid seventies it was observed that the room temperature conductivity of polysulfurnitride could be further

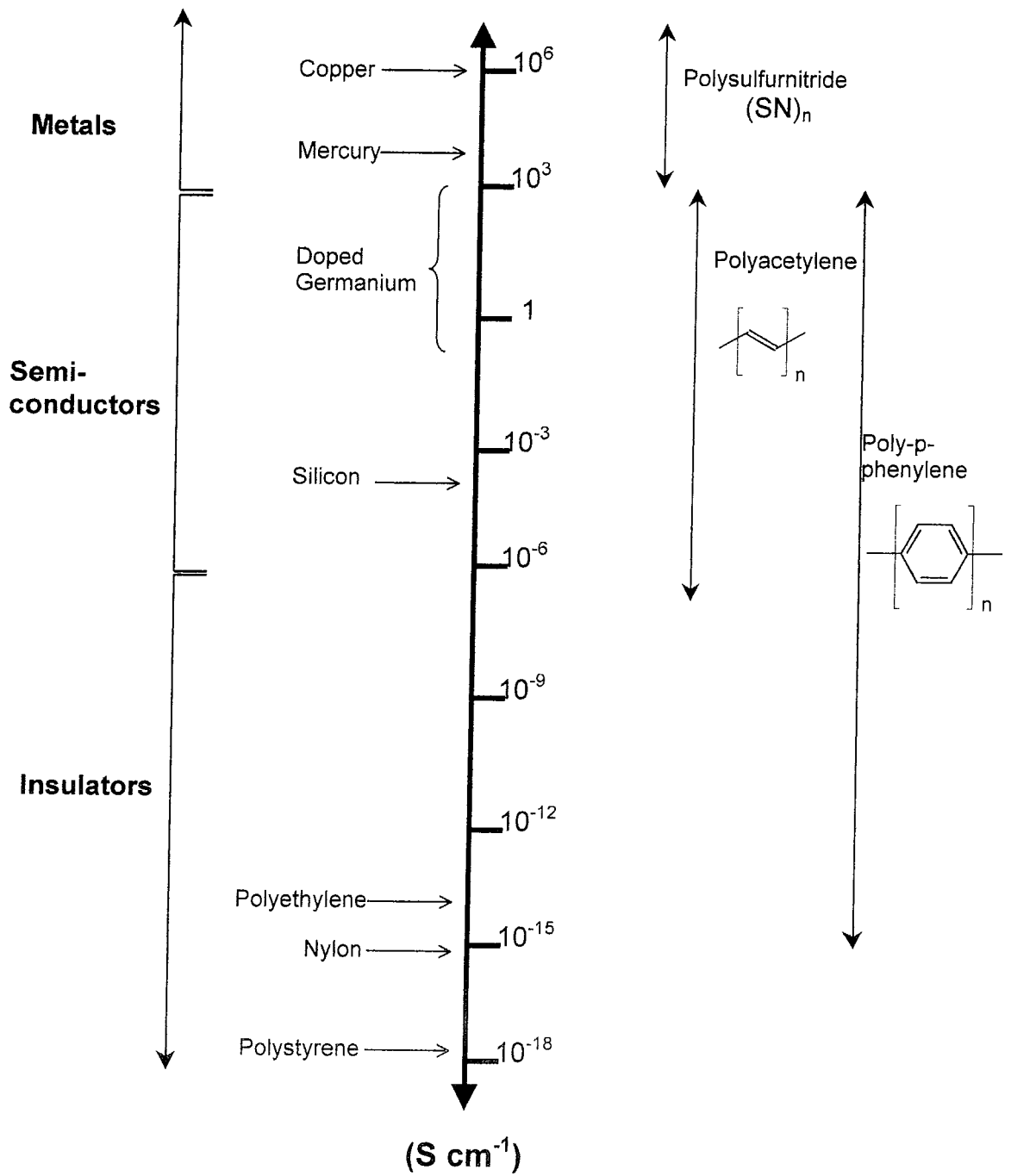


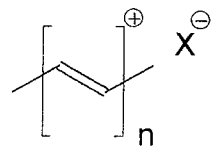
**Figure 1.1:** Ambient temperature conductivities of doped conducting polymers compared to conventional materials.

enhanced by an order of magnitude following exposure to bromine and similar oxidising agents [4]. The resulting conducting material was no longer a neutral polymer, but a polymeric cation, with charge neutrality being preserved by incorporating into the material the reduced form of the oxidising agent.

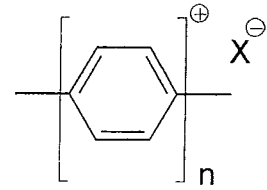
The discovery of conducting polysulfurnitride lead to a huge interest in the possibility that the same redox chemistry could be applied to intrinsically insulating organic materials. A major breakthrough [5] came in 1979 with the discovery that the insulator polyacetylene (**1**); see figure 1.2, consisting of only weakly coupled chains of  $\text{-CH-}$  units with a conductivity in the order of  $10^{-5} \text{ S cm}^{-1}$ , could be made highly conducting ( $\sim 10^3 \text{ S cm}^{-1}$ ) when exposed to an oxidising agent such as iodine, as seen in figure 1.1. Furthermore, the polymer was obtained in the form of shiny coherent films.

The process of oxidation of a polymer in this manner is termed 'doping', whereby the insulating neutral polymer is converted into an ionic complex consisting of a polymeric cation (or anion) and a counter ion which is the reduced form of the oxidising agent (or the oxidised form of the reducing agent). Thus an important criterion in selecting potentially conducting polymers is therefore the ease with which the system can be oxidised or reduced.

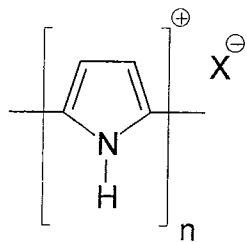
Another key discovery [6] was that of polyparaphenylene (**2**) as shown in figure 1.2. This aromatic polymer upon doping gave a polymer with a high conductivity ( $\sim 10^3 \text{ S cm}^{-1}$ ), demonstrating that polyacetylene was not unique as an organic semiconductor. This lead to the subsequent discovery of a whole series of aromatic based conducting polymers including polypyrrole (**3**) [7], polythiophene (**4**) [8] polyisothianaphthene (**5**) [9] and polyaniline (**6**) [10] as seen in figure 1.2.



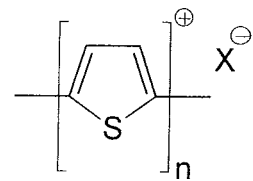
(1)



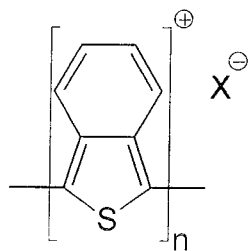
(2)



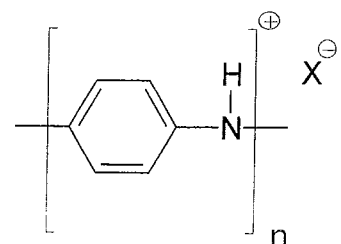
(3)



(4)



(5)



(6)

Figure 1.2: Typical conducting polymers in doped state

All of these conductive polymers had one thing in common, they contained an extended  $\pi$  - conjugated system, i.e. single and double bonds alternating along the polymer chain. The  $\pi$  electrons can also be easily removed or added to form a polymeric ion without much disruption of the  $\sigma$  bonds which are responsible for holding the polymer together.

By the early 1980's optimism was high with a number of predictions being made about the bright future of these new materials, with conducting polymers being used as electrical wires and battery powered devices from watches to cars. Perhaps these predictions would have been realised had the early conductive polymers been processible like conventional organic polymers and their chemical and electronic structures better understood. But far from behaving as plastics, the first conductive polymers were insoluble, infusible and brittle and some were unstable in air [1].

By the mid-1980's, it was realised that if conductive polymers were going to succeed as commercial materials, a few important problems had to be solved. Processibility had to be improved, conductivity enhanced to higher levels, crystallinity increased, and defects reduced. Better characterisation and understanding of polymer structure was also needed [1].

A basic research goal in this field at this time was to understand the relationship between the chemical structure of the repeating unit of polymer and its electrical properties. Such an understanding would enable the electronic, mechanical and other properties of these materials to be tailored at the molecular level.

Building on the exciting discovery of conducting polyacetylene, researchers continued to develop important structure – property relationships, prepared more well-characterised and ordered materials, unfolded novel electrical and optical properties of these materials, and developed a much deeper understanding of the fundamental processes that lead to electron transport in conducting polymers and also photon interactions with conjugated polymers.



Today, research in this field can be sub-divided into the general areas of theory and charge transport, synthesis, processing, properties, and applications of conducting polymers, with the latter enjoying increased amount of interest especially within the last decade [11]. As more and more applications like those envisioned by early researchers are developed this will provide a continuing driving force for further research into this rapidly expanding area. Finally, in October 2000, the Nobel Prize in Chemistry was awarded to Alan J. Heeger, Alan G. MacDiarmid and Hideki Shirakawa “*for the discovery and development of conductive polymers*”, highlighting the tremendous amount of work carried out in this field of research.

### *1.2 Band Theory and Conduction – Classical Model.*

The conduction properties of a conventional material (i.e. metals, semiconductors and insulators) is determined by its electrical structure, and the latter is explained best by simple band theory [12]. Consider a simple diatomic molecule derived from two identical atoms that each has only one electron available for bonding. The energy levels of these two electrons before and after the formation of the bond are shown in figure 1.3. Bond formation involves the generation of two new energy levels – the bonding level, occupied by the two electrons, and the unoccupied antibonding level. This higher level can be populated temporarily if the bonding–level electrons acquire sufficient energy from heat or light to make the transition [12].

According to the same model bond formation in more complex molecules follows the same principle. As each bond is formed an additional bonding and antibonding level is added to the overall electronic structure. Thus, the larger the number of atoms that are linked together in a molecule or ultrastructure, the greater will be the number of bonding and antibonding orbitals. Beyond a certain size of “molecule” or in a high-polymer molecule, or a solid state system, thousands or millions of atoms may be involved and the number of molecular orbitals becomes large. Now the bonding orbitals become crowded together on the energy scale to form a set of closely spaced energy levels known as a bonding band or the valence band (VB).

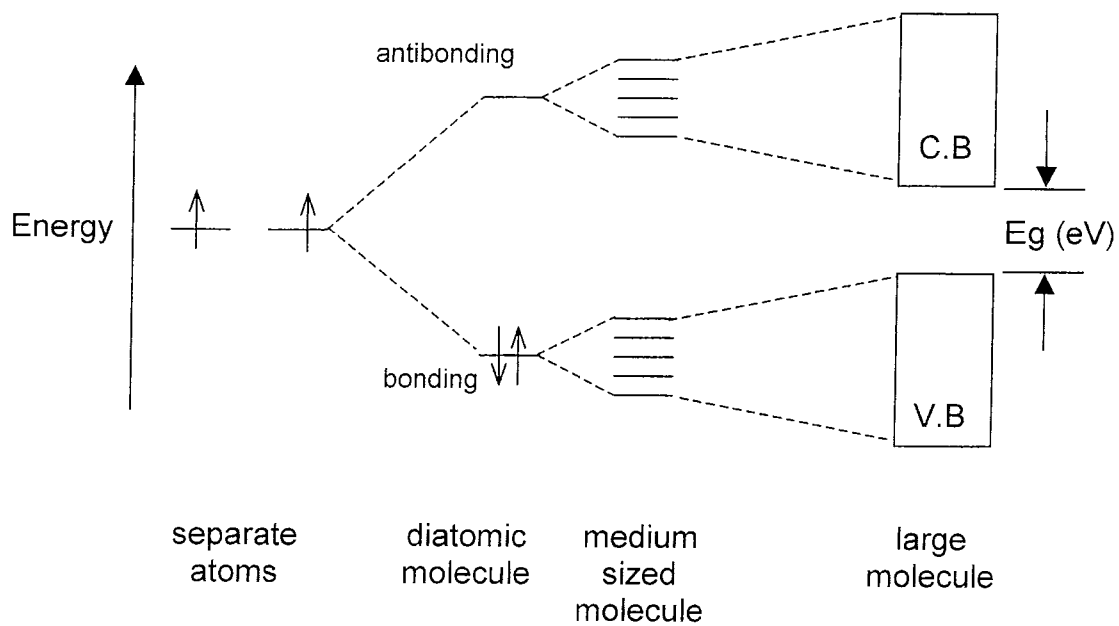


**Figure 1.3:** Progression from atomic orbitals in two isolated atoms, through the formation of a bonding orbital in a simple diatomic molecule and the generation of several bonding orbitals in a medium sized molecule, to the coalescence of orbital energy levels into bands.

The term “band” is used because the energy levels are so closely packed that for all practical purposes they form an energy continuum within which electrons can exchange places and are free to wander throughout the material. A similar crowding and band formation occurs in the case of the antibonding orbitals, which is known as the conduction band (CB). The two bands are usually separated by an energy difference known as the band gap or  $E_g$  and is quantified in terms of electron volts or eV. The magnitude of the band gap and the degree to which the valence band is filled with electrons determine if the material is an insulator, a semiconductor or a metal. These possibilities are shown schematically in figure 1.4.

Insulators have very low conductivity values since although the valence band is full and the conduction band is empty, the band gap is very large, thereby preventing the promotion of electrons, see figure 1.4 (a).

Semiconductors also have a filled valence band and an empty conduction band as shown in figure 1.4 (b). However they possess a band gap small enough to allow the promotion of electrons at room temperature from the valence band to the conduction band, thus giving rise to some conduction.

Metals on the other hand have high conductivities, which are accounted for in one of three ways;

- (i) If the valence band of the material is only partially filled and the conduction band is empty, illustrated in figure 1.4 (c), the electrons in the valence band are free to move within the energy confines of this band, hence giving rise to conduction.
- (ii) If the valence band is full and the conduction band is partially filled, as shown in figure 1.4 (d), the electrons in the conduction band are free to move within the energy confines of this band, again giving rise to conduction.

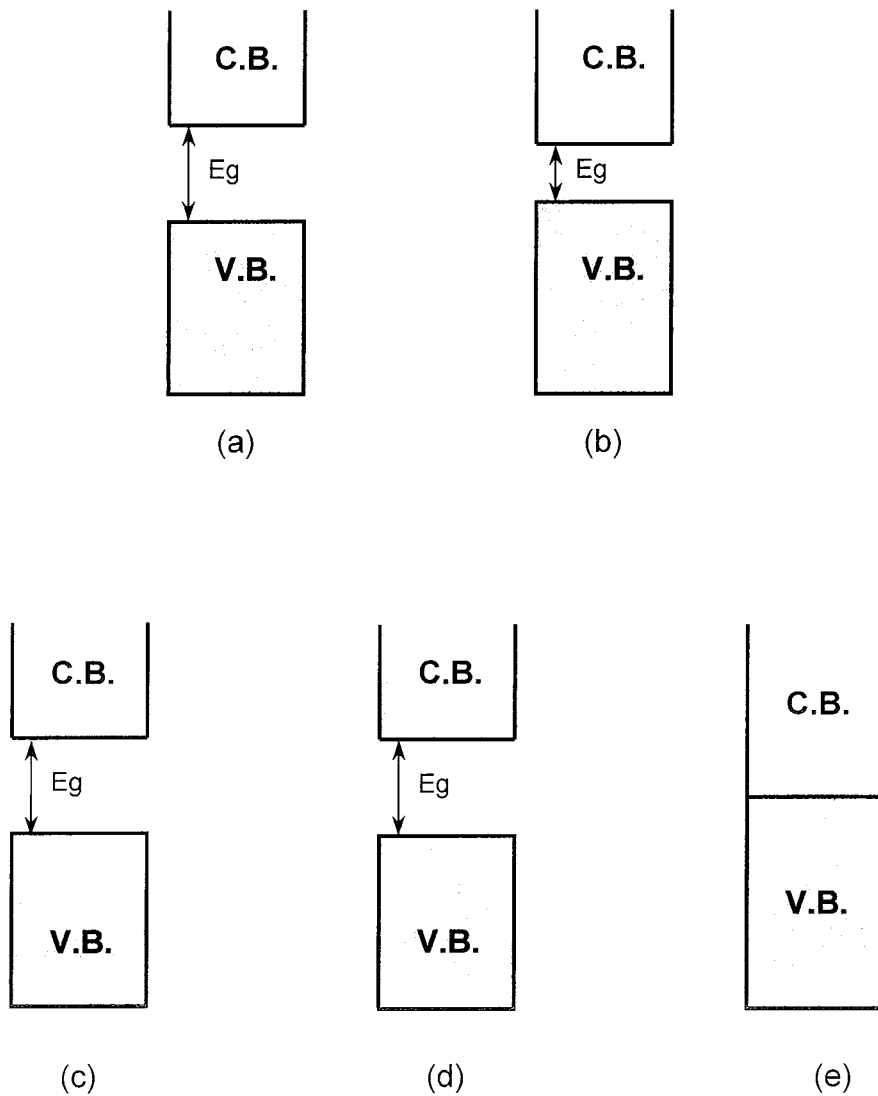


**Figure 1.4:** Band structure, (a) Insulator, (b) Semiconductor, (c) Metal [partially filled valence band], (d) Metal [partially filled conduction band], (e) Metal [no band gap], V.B. = Valence Band, C.B. = Conduction Band

- (iii) If the valence is full and the conduction is empty, as shown in figure 1.4 (e), but there is no band gap, the electrons highest occupied level in the valence band can move freely within the conduction band, thus allowing conduction.

This theory does not however fully explain why some organic polymers can conduct current, as they have neither a partially filled band (conduction or valence) nor do they have a band gap small enough to allow the promotion of enough electrons at room temperature to give rise to a significant conductivity. Hence another model for the electronic structure of organic semiconductors has been proposed and is detailed in the next section.

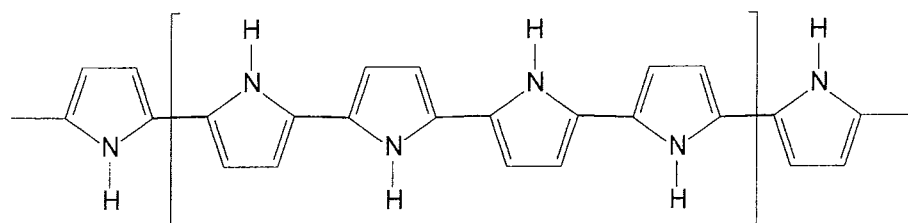
### 1.3 *Electronic structure of organic semiconductors – Conduction properties.*

In order to explain to some degree conduction in organic semiconductors, concepts from physics, including solitons, polarons and bipolarons have been employed since the early 1980's [1, 13].

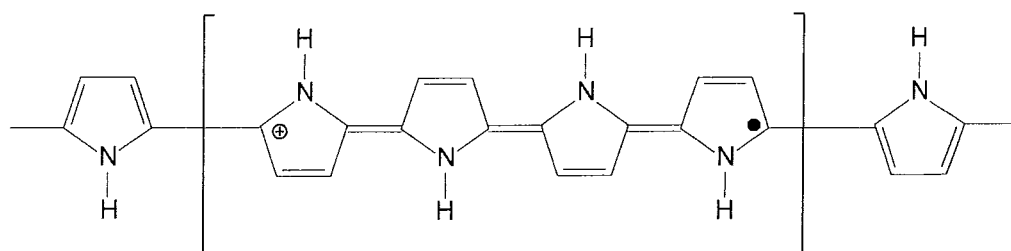
When an electron is removed from the top of the valence band of a neutral conjugated polymer as in figure 1.5 (a), a vacancy (hole or radical cation) is created that does not delocalise completely, as would be expected from the classical theory. Only partial delocalisation occurs, extending over several monomeric units and causing them to deform structurally. A radical cation that is partially delocalised over some polymer segment is called a polaron, as shown for polypyrrole in figure 1.5 (b). It stabilises itself by polarising the medium around it and hence the name polaron.

If another electron is now removed from the already oxidised polymer containing the polaron, two things can happen:

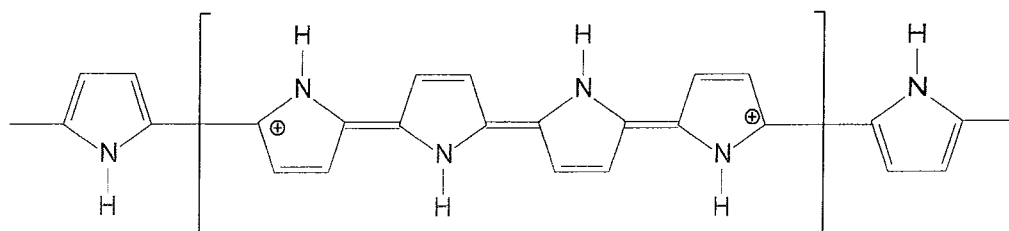
- (i) This electron could come from either a different segment of the polymer chain, thus creating another independent polaron ,
- or,
- (ii) From the first polaron level (remove the unpaired electron) to create a bipolaron as shown for polypyrrole in figure 1.5 (c).



(a)



(b)



(c)

**Figure 1.5:** Formation of polarons and bipolarons in polypyrrole  
 (a) neutral polypyrrole, (b) radical cation or polaron spread over four units,  
 (c) dication or bipolaron spread over four units.

Low doping levels give rise to polarons, whereas higher doping levels produce bipolarons.

The bipolaron also has structural deformation associated with it [1]. The two positive charges of the bipolaron are not independent, but act as a pair. Both polarons and bipolarons are mobile and can move along the polymer chain by the rearrangement of double and single bonds in the conjugated system, as illustrated in figure 1.6.

The energy levels associated with the neutral polymer, the radical cation (or polarons) and dications (or bipolarons) are shown in figure 1.7. The energy level associated with the radical cation represents a destabilised bonding orbital and thus has a higher energy than the energies in the valence band and the antibonding orbital are lower than the conduction band. In other words, its energy levels are located in the band gap [13], figure 1.7 (b). The bipolaron also has distinct energy levels associated with it and these are also in the band gap; figure 1.7 (c). If a great many bipolarons are formed, say as a result of high doping, their energies overlap at the edges, and this creates narrow bipolaron bands in the band gap, as seen in figure 1.7 (d). Polarons have a spin  $\frac{1}{2}$  as is consistent for a radical cation, while bipolarons are spinless [13]. Therefore, in polypyrrole low doping concentrations create paramagnetic polarons, which as the degree of doping increases convert to spinless bipolarons. The nature of charge carriers in conducting polymers, be they polarons, bipolarons or solitons depends on whether the ground state is degenerate or non-degenerate.

Organic conducting polymers can be broadly divided into two types [1], those with degenerate ground state and those with non-degenerate ground states. *Trans*-polyacetylene, the thermodynamically more stable form of polyacetylene, has degenerate ground states [14] i.e. two equivalent resonance forms, where the double bonds can be interchanged with no cost of energy, as shown in figure 1.8.

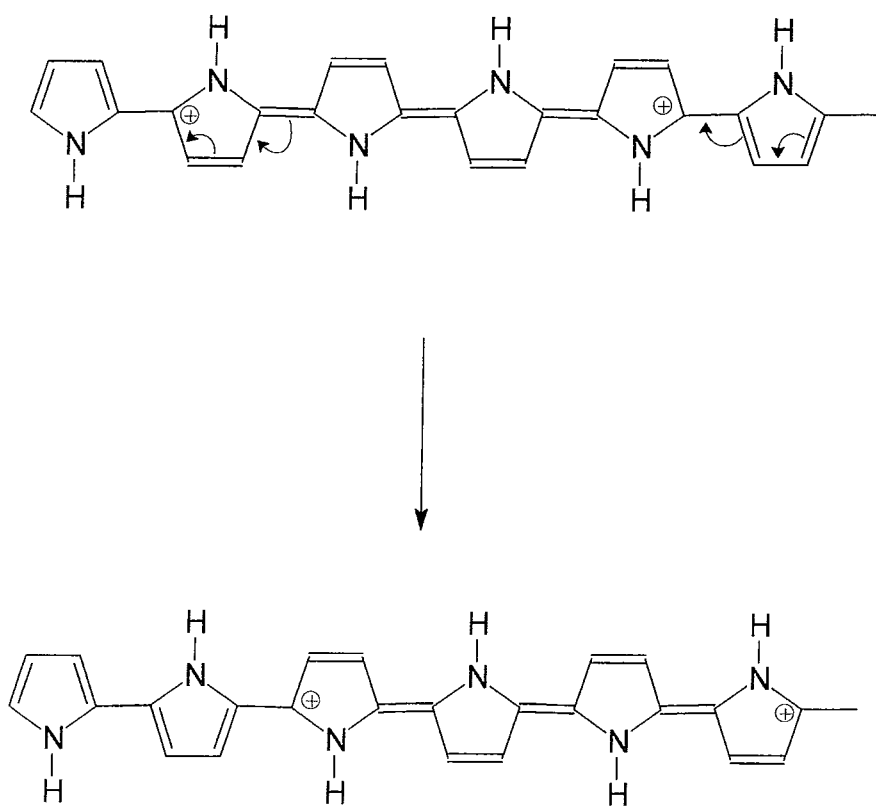


**Figure 1.6:** Bipolaron movement in polypyrrole



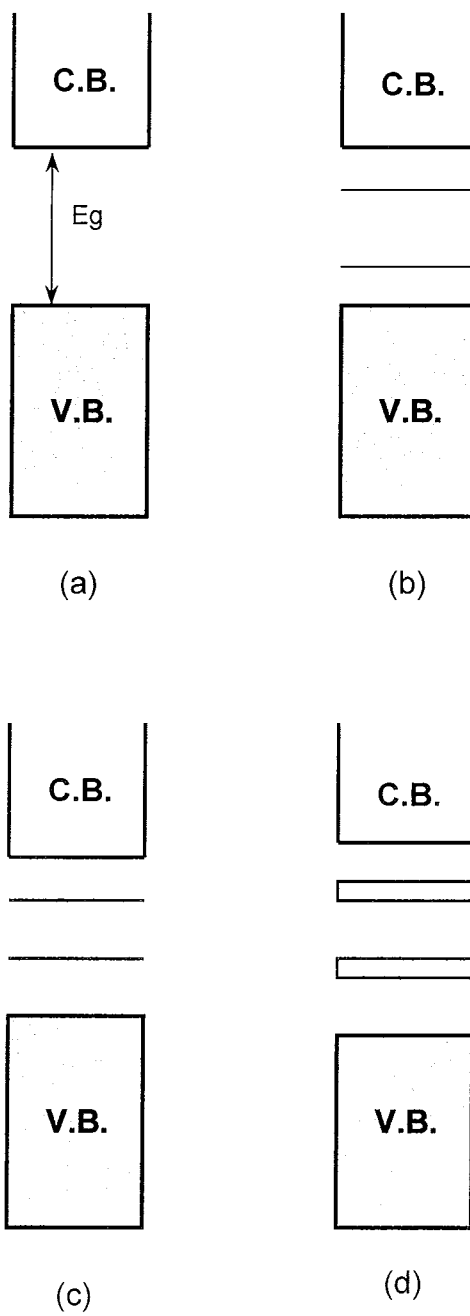


**Figure 1.7:** Band structure and polaron and bipolaron energy levels  
 (a) neutral polymer, (b) polaron mid-gap energy levels, (c) bipolaron mid-gap energy levels, (d) bipolaron mid-gap energy bands

The formation of a dication in *trans*-polyacetylene does not lead to the formation of bipolarons since the dication can separate to form two independent spinless cations known as "solitons" [14], as seen in figure 1.9. The formation of these solitons give rise to mid-gap energy levels and spectroscopic evidence from uv-vis data [13, 15] supports the existence of the mid-gap state. The energy level diagram shown in figure 1.10, shows the mid-gap state associated with a positively charged soliton for *trans*-polyacetylene. The transitions associated with these states also shown where  $h\nu_1$  is the interband transition from the valence to the conduction band and  $h\nu_s$  is the transition from the valence band to the mid-gap level and from the mid-gap level to the conduction band.

Solitons however do not form in polymers with non-degenerate ground states. The aromatic organic conducting polymers are known to have non-degenerate ground states, i.e. two non-equivalent resonance forms, where the quinoid resonance form is of different energy to the corresponding aromatic form [13]. Calculations [16] have shown that the quinoid structure has a lower ionisation potential and a larger electron affinity than the aromatic structure. Figure 1.11 shows the non-degenerate states for polyparaphenylene (2), polypyrrole (3), polythiophene (4) and polyisothianaphthene (5) [1]. Where the degeneracy is lifted, as in these cases, polarons and bipolarons (not solitons) are the dominant mechanism for charge transport. The work undertaken in this study will deal with non-degenerate ground state heterocyclic aromatic organic semiconductors.

In polypyrrole, when polarons are formed, as in the case upon light doping, the energy levels associated with polarons are about 0.5 eV from the band edges [13,15], as shown in figure 1.12 (a). Whereas upon moderate doping levels, associated with bipolaron formation the mid-gap levels are about 0.75 eV from the band edges as in figure 1.12 (b). On heavy doping (~33%) overlap between bipolaron states in the band gap lead to the formation of two bipolaron bands each of which are  $\approx 0.4$  eV wide, as seen in figure 1.12(c).

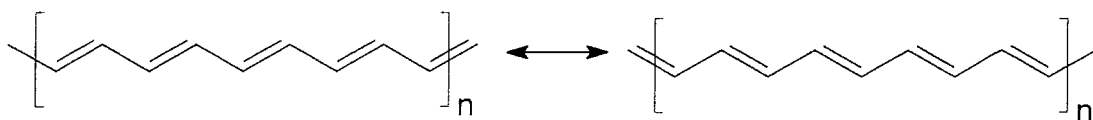


**Figure 1.8:** Degenerate ground states of trans-polyacetylene

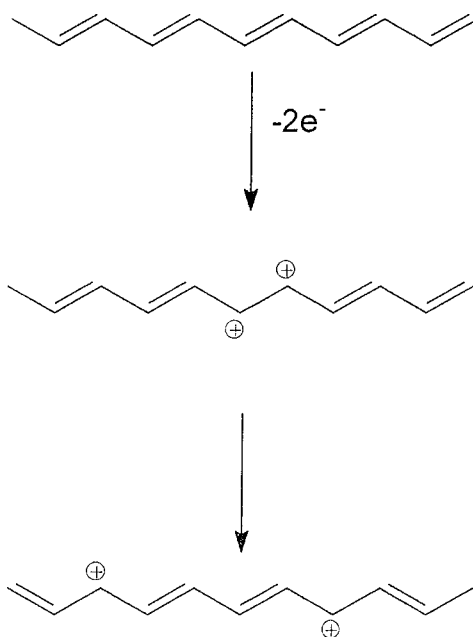


**Figure 1.9:** Soliton formation and dissociation in trans-polyacetylene

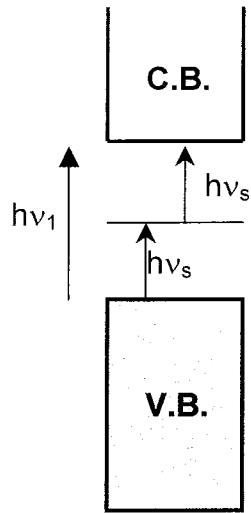
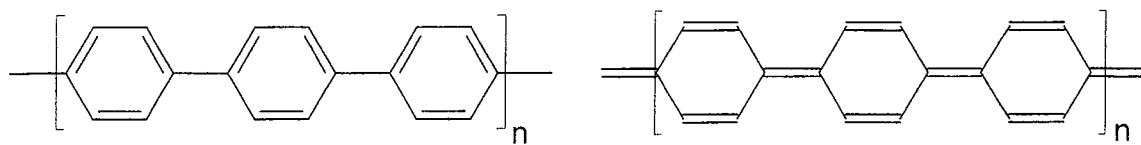
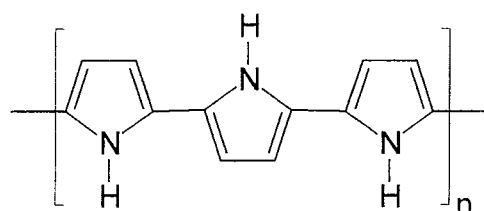


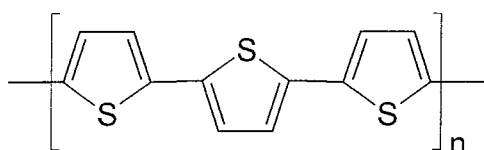
**Figure 1.10:** Mid-gap states due to soliton formation



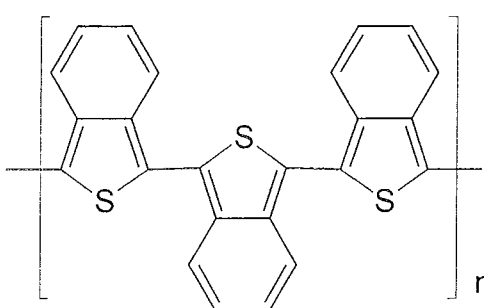
(2)



(3)



(4)



(5)

**Aromatic**

**Quinoid**

**Figure 1.11:** Non-degenerate ground state polymers

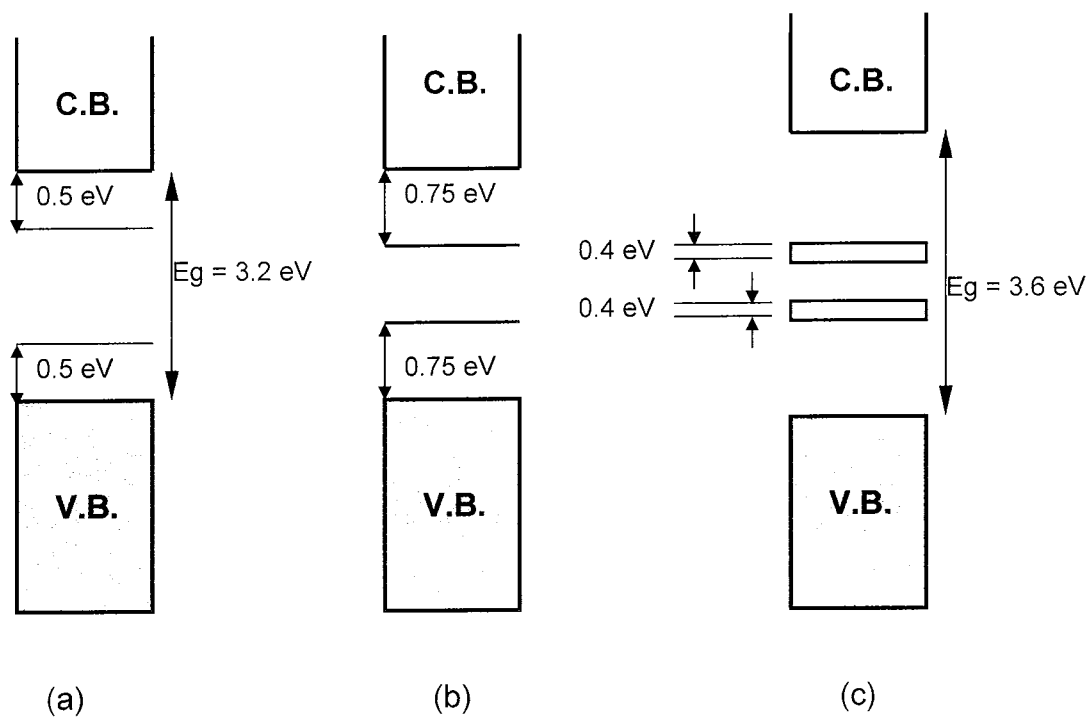


**Figure 1.12:** polaron and bipolaron energy levels in polypyrrole  
 (a) partially oxidised polypyrrole, (b) polaron mid-gap energy levels, (c)  
 bipolaron mid-gap energy bands.

The fact that bipolaron bands originate from states at the edges of the valence and conduction bands also explains why an increase in  $E_g$  is observed from 3.2 eV to 3.6 eV in going from lightly doped polypyrrole to heavy doping levels of  $\approx 33\%$ , which is in agreement with the theoretical predictions [13].

Two aspects of conductivity in conducting polymers must be mentioned. Firstly, these polymers not only conduct along a particular chain, but conduction between chains also occurs, giving rise to interchain mobility [13]. The interchain mobility is the most likely the rate limiting step in determining the observed conductivity. Therefore interchain hopping of solitons and bipolarons is of prime importance and models for interchain hopping have been proposed [17,18]. However contrary to this, investigations into the hopping mechanism in certain cycloalkylpyrroles [19] tentatively precludes bipolarons as being mobile charge carriers. Secondly, as these polymers are rather amorphous in nature, disorder effects need to be properly taken into account to understand conduction in these materials [13].

#### 1.4 *Electronic structure of organic semiconductors – Optical properties.*

The electronic structure for organic semiconductors discussed previously sufficiently explains (although not completely) conduction in these materials. However, it is opportune at this moment to speak briefly about the associated optical properties arising from their electronic structure. The transition of electrons from the valence band to the conduction band gives rise to a polymer, which is highly coloured in the neutral state. On oxidative doping, new low energy transitions have been observed due to the transitions of electrons from the valence band to the new polaron and bipolaron bands within the gap. For example polypyrrole [20] has been found to be yellow in the neutral form ( $\lambda_{\max} \sim 400\text{nm}$ ) and blue/black ( $\lambda_{\max} \sim 540 - 900\text{nm}$ ) in the fully oxidised state. These optical properties can be observed simultaneously by both UV-Vis spectroscopy and electrochemical techniques, termed spectroelectrochemistry.

An increasing drive at the present moment is to synthesise low band gap polymers, (e.g. polyisothianaphthene (**5**)[9]  $E_g \sim 1$  eV), where the polymer is coloured in the undoped state and is transparent or very lightly coloured in the oxidised state. The latter arises since new transitions within the band gap give rise to absorption transitions of lower energy and appear in the near infra-red region of the spectrum. Optical properties are key to the work under study here and will be expanded in greater detail in the appropriate chapters ahead.

### 1.5 Structure – Property relationship.

It is the combination of the electrical and optical properties of these organic semiconductors, coupled with their flexibility, lightness, low cost and low power, (an increasing challenge to the traditional silicon technology) that are enabling the broad application of these materials.

Thus, a fundamental goal in this area of research is to tailor the polymer properties by first specifying the chemical structure of the repeat monomer unit. This dictates the band gap size of the resulting polymer, and subsequently the conduction and optical properties, as well as its physical and mechanical properties. Thus, if the properties are tailored so also will their applications.

One such method of tailoring polymer properties is to functionalise the conjugated backbone with specific substituents, be these present as side chain substituents at key positions or in a fused manner on the monomer repeat unit.

A linear correlation has been found between the oxidation potential and the type of substituent grafted onto the parent monomer system. For example polythiophene (**4**) was first synthesised in 1981 [21,22] with a reported conductivity range of  $10^{-3}$  -  $10^{-1}$  S  $\text{cm}^{-1}$ . Thiophene monomer substituted by a strongly electron-withdrawing group, i.e. 3-nitrothiophene (**8**) in figure 1.13,



had oxidation potentials approximately 0.5 – 0.7V higher than that of thiophene (**4**) and does not electropolymerise [23,24]. Halogen substituted monomers, i.e. 3-bromo-thiophene (**9**) allowed polymerisation but the resulting polymers were poorly conducting [24]. The difficulty in electropolymerisation was attributed to the high reactivity of the corresponding radicals in competitive reactions with the medium [23]. The grafting of electron donating alkoxy groups on the thiophene ring decreases the oxidation potential of the monomer [25], reducing competition with the medium.

Several electron donating 3-alkyl substituted polythiophenes have also been synthesised [26]. Poly(3-hexylthiophene) (**10**), poly(3-octylthiophene) (**11**), poly(3-dodecylthiophene) (**12**) and poly(3-octadecylthiophene) (**13**) as shown in figure 1.14, were all found to be soluble in common organic solvents. However, in these instances no significant change was observed in the  $\pi$ -electronic structure of the polymer. The  $\pi$ -conjugation was seen not to be affected by alkyl substitution, as determined by their electronic spectra.

The conductivity of poly-3-alkylthiophenes however was found to be dependent on the substituent chain length [27, 28]. Conductivity values reported for polythiophene (**4**), poly-3-methylthiophene (**14**) and poly-3-ethylthiophene (**15**) (short alkyl chain substituents) were 190, 450 and 270 S cm<sup>-1</sup> respectively. For longer substituent chains it was observed that the conductivity was dependent upon the substituent chain length. The conductivity decreased with increasing chain length and the values for the hexyl, octyl, dodecyl, and octadecyl - polythiophenes were 95, 78, 67, and 17 S cm<sup>-1</sup> respectively.

Electropolymerisation of 3-methoxythiophene (**16**) [25, 29], figure 1.15, produced polymers with a low degree of polymerisation, i.e. short chain polymers. The conductivity of 0.3 S cm<sup>-1</sup> of a polymer sample increased by a factor of 50 after washing with hexane [30] which extracted the soluble short chain oligomers from the polymer.

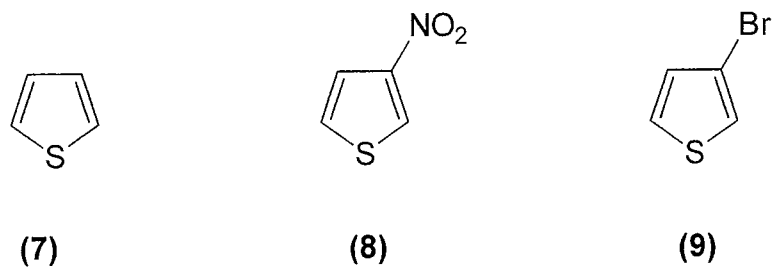
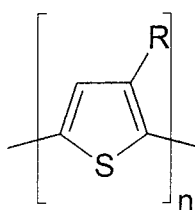


**Figure 1.13:** Substituted thiophenes



- R = n-hexyl **(10)**
- = n-octyl **(11)**
- = n-dodecyl **(12)**
- = n-octadecyl **(13)**
- = methyl **(14)**
- = ethyl **(15)**

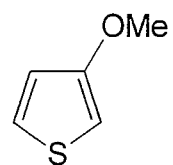
**Figure 1.14:** 3-substituted polythiophenes

More recently long-chain polymers containing methoxy groups have been prepared from 4,4'-dimethoxybithiophene (**17**), figure 1.15, whereas 3,3'-dimethoxybithiophene (**18**) essentially dimerizes [31]. The differences are explained by the higher reactivity of the 4- versus 3-substituted radical cation in these dithiophenes. Attention will be drawn to this at a later stage for comparative purposes within our own work under study.

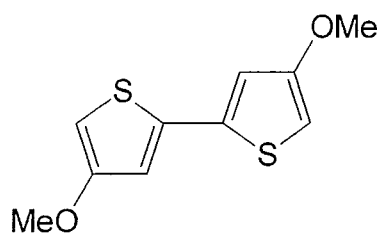
Considering steric effects, the introduction of bulky substituents close to the coupling positions may produce a blocking of the polymerisation process [32]. This is attributable in part to a decrease in reactivity of the growing polymer chain but much more to the fact that the steric constraints produce too few conjugated sequences which are therefore difficult to oxidise and may undergo degradation.

Other substituted thiophenes have led to self-doped conducting polymers [33, 34]. In self-doped polymers, the charge-compensating anion is covalently bound to the polymeric backbone, so that oxidative doping involves the expulsion of cationic species rather than anion insertion. Poly(3-thiophene- $\beta$ -ethanesulphonate) (**19**) and poly(3-thiophene- $\beta$ -butanesulphonate) (**20**) [33] were first prepared with a sulphonate group, which makes the polymer water soluble. Films cast from water solution exhibited a rather short conjugated polymer and conductivities of 1 – 10 S cm<sup>-1</sup> [34].

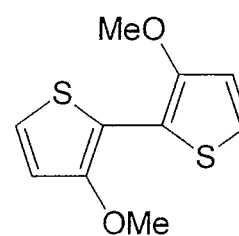
It has been found that the presence of a fused benzene ring at the  $\beta, \beta'$  positions of thiophene resulted in a conducting polymer, namely polyisothianaphthene (**5**) as shown in figure 1.17 which is also conducting ( $\sim 50$  S cm<sup>-1</sup>) [9]. In fact it had the smallest energy gap of any known conjugated organic polymer [35] at the time ( $\sim 1$  eV). It could be prepared electrochemically in the form of highly stable polymer films. The film of polyisothianaphthene also had a low absorption in the visible region making it a highly conductive transparent polymer.



(16)

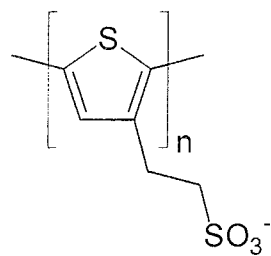


(17)

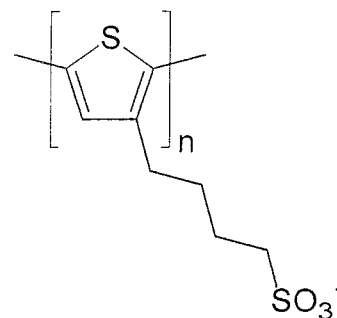


(18)

Figure 1.15: methoxy substituted thiophenes.



(19)



(20)

Figure 1.16: Self doped polythiophenes

The monomer in polyisothianaphthene can be thought of as a thiophene unit with a benzene ring built onto it. The aromatic nature of the six membered benzene ring was thought to affect the electronic structure of the polymer in two ways.

- (i) The many resonance contributors shown in figure 1.18 was expected to lead to higher stability and more nearly equal bond lengths along the pseudopolyene backbone. This should impart a high degree of quinoid character to its backbone, and lead to a decrease in band gap.
- (ii) The presence of the extra benzene ring was not surprisingly thought to increase the  $\pi$ - electron density along the backbone in polyisothianaphthene and thus modify its conduction properties.

Bakhshi and Ladik [35] made an extensive study of the electronic properties of polyisothianaphthene. These properties were compared with that of the parent polymer polythiophene. In this argument the above effects of the fused benzene ring could be supported. The most important electronic properties of polyisothianaphthene and polythiophene are given in table 1.1.

From table 1.1, it can be seen that the ionisation potential of polyisothianaphthene is smaller than that of polythiophene, while its electron affinity is larger. It therefore means that polyisothianaphthene has greater capacity to form conducting materials through both oxidative and reductive doping and can be doped even with weaker electron acceptors (p-doping) or electron donors (n-doping).

Also in the same study it was found that the electron affinity and the ionisation potential of polyisothianaphthene are sensitive to the substitution at the benzene ring. Another point to note was that only the electron affinity value is dependent upon substituting the sulphur atom by another heteroatom. Another study by Kobayashi *et al* [36], also concluded that the reduction of the energy gap compared with that of the parent polythiophene presumably resulted mainly from more possible resonance contributors.

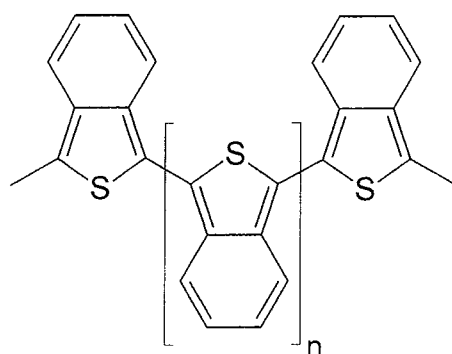


**Figure 1.17:** Polyisothianaphthene

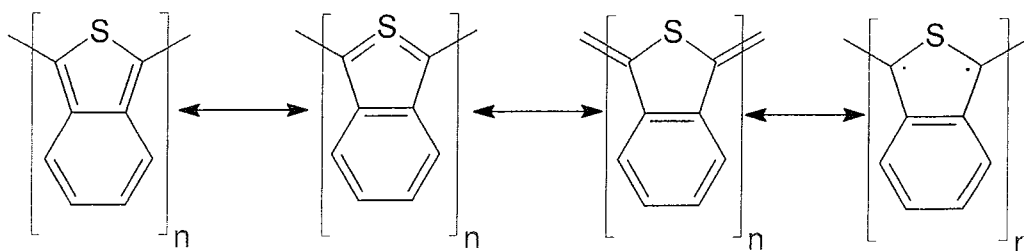


**Figure 1.18:** Various resonance forms of polyisothianaphthene

	<b>PITN</b>	<b>PTP</b>
	<b>/eV</b>	<b>/eV</b>
Valence band width	3.528	2.890
Conduction band width	3.616	5.118
Ionization potential (top of valence band)	7.588	9.499
Electron affinity (negative of the bottom of the conduction band)	3.063	1.362
Band gap	4.524 (~1.0)*	8.137 (2.0)*

**Table 1.1** Calculated electronic properties of polyisothianaphthene (PITN) and polythiophene (PTP) (ref. [35])

\* experimental values.

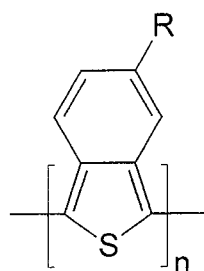
To be potentially useful in electronic applications a material must be environmentally stable, have excellent mechanical and electrical properties and be solution or melt processable. The delocalised electronic structures of  $\pi$ -conjugated polymers, which are responsible for their unusual electronic properties, tend to yield relatively stiff chains with little flexibility and with relatively strong interchain attractive interaction which make them insoluble and non-processable.

Polyisothianaphthene prepared either electrochemically or chemically was insoluble and non-processable, and while it has a low band gap, a new focus to prepare soluble and processable polymers with a low band gap and high conductivity emerged. Since its original preparation [9] the synthesis and study of a number of substituted derivatives have appeared and are discussed below.

Simple alkyl derivatives of polyisothianaphthene have been reported [37- 40]. Introduction of a long chain alkyl substituent ( $C_{10}H_{21}$ ) on carbon-5 of the aromatic ring of the monomer unit, on polymerisation gave poly(5-decylbenzo[c]thiophene) (**22**), figure 1.19, and was found to be soluble and processable [37]. Unfortunately this derivative had an increased band gap between 1.0 – 1.3 eV. In 1990 [38], a patent involving the study of a series of alkyl derivatives emerged. Poly(5-dodecylbenzo[c]thiophene) (**23**) was reported to be soluble in a variety of organic solvents and had a conductivity of  $10^{-2}$  S  $cm^{-1}$ , while the other alkyl substituted polymer Poly(5-octylbenzo[c]thiophene) (**24**) had a reported conductivity [38] of  $10^{-3}$  S  $cm^{-1}$ , however no band gap values were quoted.

In a separate study, the 5-methyl derivative, poly(5-methylbenzo[c]thiophene) (**25**) was reported by Higgins and co-workers [39-41], where the band gap was 1.13 eV and the electrochemical oxidation potential for the monomer was lower than that of isothianaphthene under the same electrochemical conditions. However the polymer oxidation potential was slightly higher than that of polyisothianaphthene, while the potential for n-doping was similar.



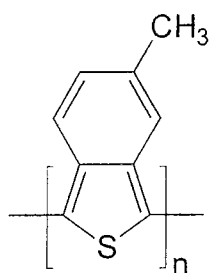


R = C<sub>10</sub>H<sub>21</sub> **(22)**

= C<sub>12</sub>H<sub>25</sub> **(23)**

= C<sub>8</sub>H<sub>17</sub> **(24)**

**Figure 1.19:** 5-alkyl substituted polyisothianaphthenes



**(25)**

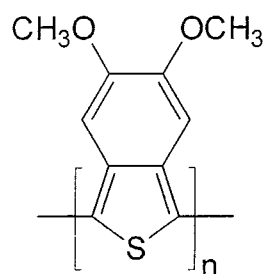
**Figure 1.20:** 5-methyl substituted polyisothianaphthene

One of the earliest claims of the synthesis of electron donating alkoxy derivatives of polyisothianaphthene was in 1988, with a patent claim [42] for the synthesis of poly-5,6-dimethoxy-isothianaphthene (**26**), poly-5-methoxy-isothianaphthene (**27**) and poly(5,6-dioxymethyleneisothianaphthene) (**28**) as shown in figure 1.21. No properties were reported for the two methoxy substituted polymers, however (**28**) [42, 43] was insoluble, but had a band gap of ~1 eV. A thin film of the polymer changed from blue / black in the reduced state to transparent grey in the oxidised state upon electrochemical switching.

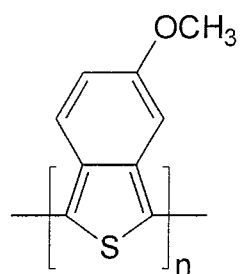
More recently, the synthesis and polymerisation of 5,6-dihexoxyisothianaphthene gave a polymer poly(5,6-dihexoxyisothianaphthene) (**29**) [44] see figure 1.22, with a reported bandgap of 1.0 ~ 1.3 eV. The conductivity for the doped form of the polymer was reported to be  $2 \times 10^{-2} \text{ S cm}^{-1}$ . It concluded that the introduction of the dihexoxy groups at the 5- and 6-positions on the benzene ring of polyisothianaphthene provides light colour (close to colourless) transparent conductive film after doping, and also improved solubility in both the neutral and doped states [44]

The alkyl and alkoxy substituents on the fused benzene ring of polyisothianaphthene are electron donating, however the effects of electron withdrawing groups on the fused ring have also been investigated.

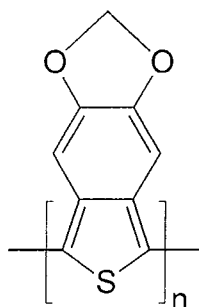
Fluorine-substituted polybenzo[*c*]thiophenes (**30**) and (**31**) were compared with Poly(5,6-dichlorobenzo[*c*]thiophene) (**32**) as shown in figure 1.23. It was shown [41] that there was very little substituent effect on the p-doping potential but there was a significant effect on the n-doping. While the total range in the p-doping values for polyisothianaphthene (**5**), (**25**) and (**30-32**) is only 0.25V, the n-doping values cover a range of 0.9V. In addition these derivatives were reported to be transparent when n-doped [41]. However the properties of (**31**), such as its colour, which was red-purple, was different to those of the others (**5**), (**25**), (**30**) and (**32**), which were blue. Interestingly, the band gap for (**30**) was reported to be 0.95 eV which is slightly lower than that of polyisothianaphthene [41].



(26)

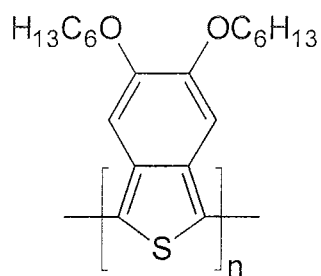


(27)



(28)

Figure 1.21: Alkoxy substituted polyisothianaphthene



(29)

Figure 1.22: poly (5,6-dihexoxyisothianaphthene)

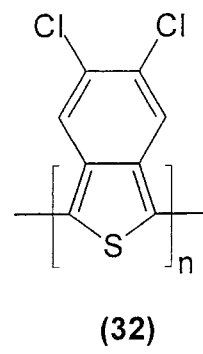
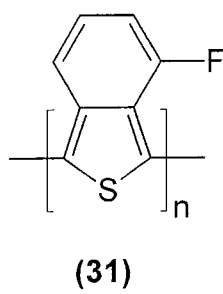
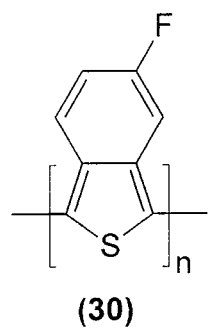


Figure 1.23: Halide substituted polyisothianaphthene

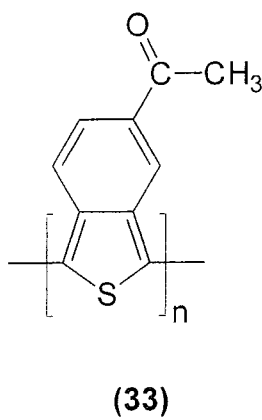


Figure 1.24: poly(5-benzoylbenzo[c]thiophene)

Another electron withdrawing mono substituted polyisothianaphthene was reported in 1989 by Wallnöfer *et al.* [45]. The synthesis and polymerisation of 5-benzoylbenzo[*c*]thiophene gave poly(5-benzoylbenzo[*c*]thiophene) (**33**), figure 1.24, but no data was given on the polymer.

Other derivatives of polyisothianaphthene containing electron-withdrawing groups have been reported in another Japanese patent [46]. Poly(5-cyanobenzo[*c*]thiophene) (**36**) as shown in figure 1.25, electrochemically synthesised in a perchlorate electrolyte gave a conductivity of  $10^{-2}$  S cm<sup>-1</sup>, and a light transmission in the visible region of 65%. This is better than the parent polyisothianaphthene, which showed a doped transmission of only 40% in the same electrolytic media [46]. The doped conductivities and light transmittance of other substituted polyisothianaphthenes (**37 – 40**) are shown in table 1.2.

A system analogous to polythiophene and polyisothianaphthene is that of polypyrrole (**3**) and the relatively unexplored polyisoindole (**41**), as shown in figure 1.26. Polypyrrole is a well known organic semiconductor and extensive research has already been carried out. It was first prepared as a powder in 1916 [47], but it was not until the late seventies [7] when continuous films could be prepared and made conductive, that so much interest was generated. The properties of polypyrrole are found to vary with method of preparation and handling. As a result, there is quite a large amount of literature on structure, properties and mechanism of preparation.

The effect of  $\beta$ -disubstitution on the properties of polypyrrole has also received some attention. The conductivity of poly(3-methylpyrrole) (**42**) is  $10$  S cm<sup>-1</sup>, a factor of four less than polypyrrole (**3**) and similar to that of poly(3,4-dimethylpyrrole) (**43**) [48] see figure 1.27 and table 1.3. By contrast, the conductivity of poly(3,4-diphenylpyrrole) (**44**) [48] is about four orders of magnitude less ( $10^{-3}$  S cm<sup>-1</sup>). In a more recent study, [49] the conductivity of poly(3,4-dimethoxypyrrole) (**45**) [49] was  $6$  S cm<sup>-1</sup>.

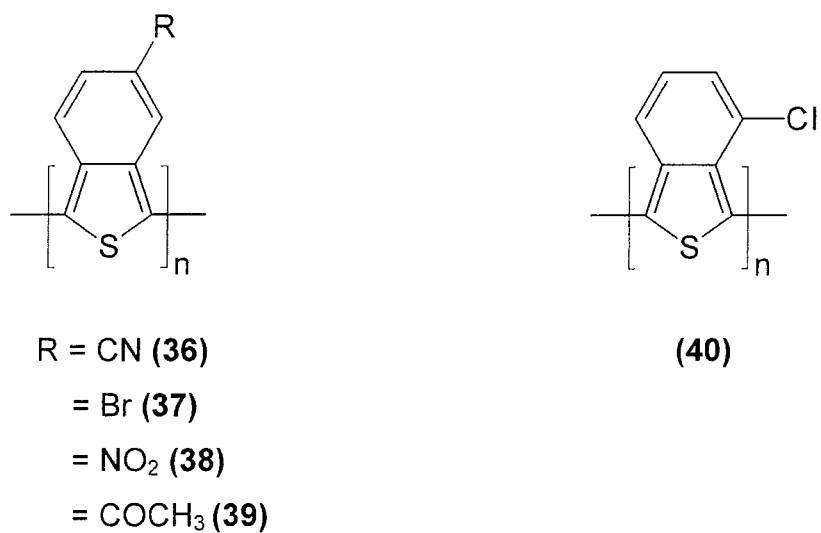
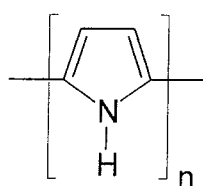


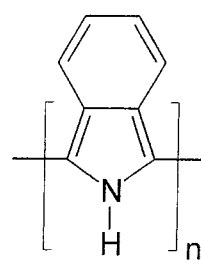
**Figure 1.25:** Polyisothianaphthenes substituted with electron-withdrawing groups

Polymer	Conductivity (S cm <sup>-1</sup> )	% Transmittance
<b>37</b>	10 <sup>-2</sup>	60
<b>38</b>	10 <sup>-2</sup>	55
<b>39</b>	10 <sup>-3</sup>	50
<b>40</b>	10 <sup>-3</sup>	60

**Table 1.2:** The doped conductivities and light transmittance substituted polyisothianaphthenes (**37 – 40**) (ref: [46])

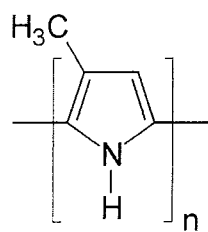


(3)

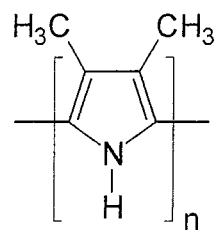


(41)

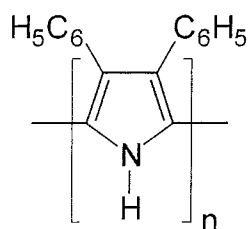
**Figure 1.26:** Polypyrrole and polyisindole



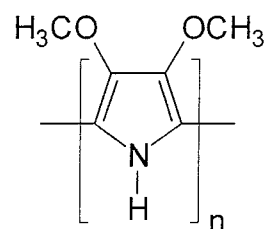
(42)



(43)



(44)



(45)

Figure 1.27:  $\beta$ -substituted polypyrroles

Polymer	Conductivity ( $\text{S cm}^{-1}$ )	$E_{pa} / \text{V}$
3	40	-0.2
42	10	-0.3
43	4	-0.1
44	$10^{-3}$	+0.5

Table 1.3 The conductivities and oxidation potentials of polypyrrole and substituted polypyrroles (42 – 44) (ref. [48])

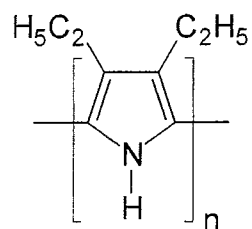


These differences in conductivities were explained on the basis of planarity. The three highly conducting polymers (**3**), (**42**) and (**43**) could be planar, whereas poly(3,4-diphenylpyrrole) (**44**) cannot, thus highlighting the importance of polymer chain planarity to conductivity which is consistent with the basic premise of a delocalised  $\pi$ -system. It is also interesting to note that the redox potential of the highly conducting planar polymers have similar negative potentials with the methoxy substituents (**45**), ( $E_{pa} = -0.5V$  [49]) providing the greatest ease of oxidation, while the poorly conducting non-planar system have a positive redox potential, showing that the latter is more difficult to oxidise.

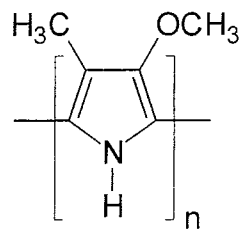
The actual electronic effect of  $\beta$ -substituents on the pyrrole ring on the properties of polypyrrole has been given little importance with the steric effect being predominant.

However, a study [50] on a series of electron donating / withdrawing groups on the  $\beta$ -positions of polypyrrole (**46** – **50**) as shown in figure 1.28, showed that the electronic effect cannot be ignored. Table 1.4 showed that no conducting films could be obtained from the monomers with strong electron withdrawing groups (**48** – **50**), unlike compounds with electron donating substituents (**46**) and (**47**).

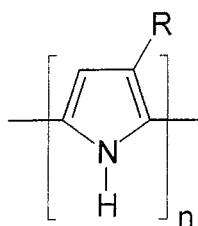
A study of 3,4-dihalopyrroles (**51** – **53**) was also carried out [51], the halogens appearing appropriate because of their relatively low steric hindrance, figure 1.29. The oxidation potentials,  $E_{pa, m}$  and  $E_{pa, p}$ , of both monomers and corresponding polymers respectively shown in table 1.5 were higher than that of polypyrrole, as expected with electron withdrawing substituents. The low conductivity values for the halopyrroles (**51** – **53**) were explained on the basis of both steric (size of substituent) and electronic effects.



(46)



(47)

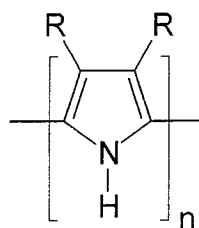
R = COCH<sub>3</sub> (48)= COOCH<sub>3</sub> (49)

= COOH (50)

**Figure 1.28:**  $\beta$ -substituted of polypyrroles with both electron donating and withdrawing groups

Polymer	Conductivity (S cm <sup>-1</sup> )	E <sub>pa</sub> / V
3	3	-0.12
46	2 x 10 <sup>-4</sup>	+0.11
47	2	-0.05
48	-----	-----
49	-----	-----
50	-----	-----

**Table 1.4:** The conductivities and oxidation potentials of polypyrrole and substituted polypyrroles (46 & 47) (ref. [50])



R = Cl (**51**)

= Br (**52**)

= I (**53**)

**Figure 1.29:** Halide substituted polypyrroles

Polymer	Conductivity (S cm <sup>-1</sup> )	E <sub>pa</sub> / V	
		monomer	polymer
<b>3</b>	1-10 <sup>2</sup>	0.94	-0.12
<b>51</b>	2 x 10 <sup>-4</sup>	1.27	+0.97
<b>52</b>	8 x 10 <sup>-3</sup>	1.22	+0.7
<b>53</b>	9 x 10 <sup>-4</sup>	1.07	+0.6

**Table 1.5:** The conductivities and oxidation potentials of polypyrrole and halide substituted polypyrroles (ref. [51])

Substitution of the nitrogen heteroatom in pyrrole has also been investigated. Diaz *et al.* [52] prepared a series of simple N-alkyl substituted polypyrroles (**54** – **59**), figure 1.30, and concluded that the size of substituent showed little variation in electronic factors. This enabled the steric effects of N-substitution on the properties of the polymers to be probed.

With simple N-alkyl substituents (**54** – **58**) the oxidation potential,  $E_{pa, m}$ , of the monomers were very similar, see table 1.6. However, with the larger substituent (**59**) the  $E_{pa, m}$  was higher implying a decrease in the ease of oxidation. This observation was attributed to the steric effect of the substituent, which would disturb the planarity of the rings along the polymer chain. The steric effect of the N-alkyl substituent is again reflected in the conductivity values of the corresponding polymers, where the conductivity decreased with increasing size of alkyl substituent.

#### 1.6 Isoindoles as Organic semiconductors.

The parent isoindole (**41**), figure 1.26, is the nitrogen analogue of isothianaphthene but has the same reactivity as pyrrole. Isoindole itself is unstable and was only first successfully isolated in 1972 [53]. It undergoes a self condensation [54] with the tautomeric form (which will be discussed in detail in chapter 2), and therefore experiments involving N substituted isoindoles predominate as these are more stable, since tautomerisation is no possible.

With polyisothianaphthene the effects of the fused benzene ring that led to higher conductivity and lower band gap were first discovered in the late 1980's, as discussed. Despite some patent reports [55-58] that were ambiguous and unclear, any reported literature on polyisoindole as organic semiconductors did not appear until 1990 [59], when a series of N-substituted isoindoles were examined by Lee *et al.* [59] i.e. poly-N-methylisoindole (**60**), poly-N-octylisoindole (**61**), poly-N-phenylisoindole (**62**), as shown in figure 1.31

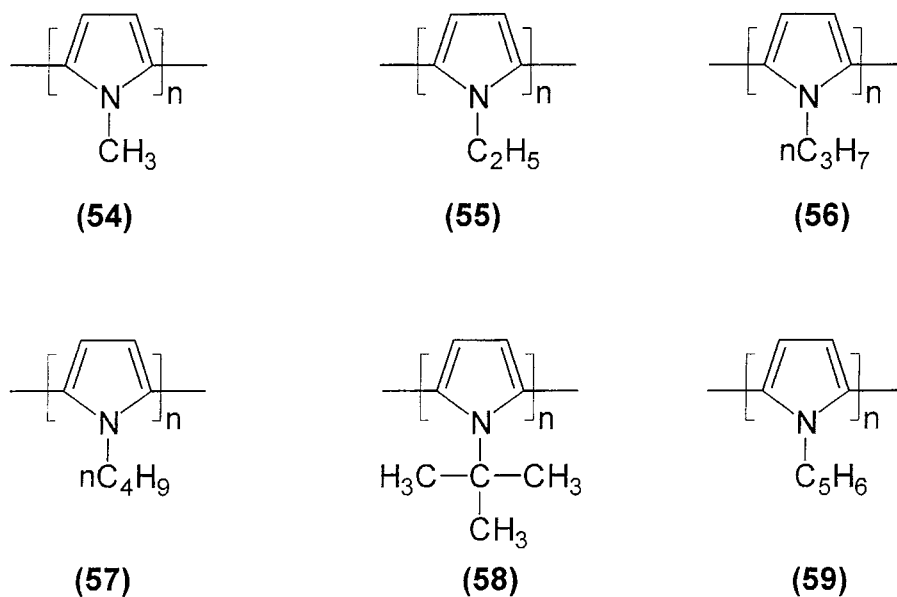


**Figure 1.30:** N-substituted polypyrroles

Polymer	Conductivity (S cm <sup>-1</sup> )	Epa / V monomer	Epa / V polymer
<b>3</b>	29·10 <sup>-2</sup>	+0.12	-0.2
<b>54</b>	10 <sup>-3</sup>	+1.12	+0.45
<b>55</b>	2 x 10 <sup>-3</sup>	+1.22	+0.45
<b>56</b>	10 <sup>-3</sup>	+1.26	+0.5
<b>57</b>	10 <sup>-4</sup>	+1.22	+0.64
<b>58</b>	2 x 10 <sup>-5</sup>	+1.24	+0.6
<b>59</b>	10 <sup>-3</sup>	+1.8	+0.65

**Table 1.6:** The conductivities and oxidation potentials of polypyrrole and N-substituted polypyrroles (ref. [52])

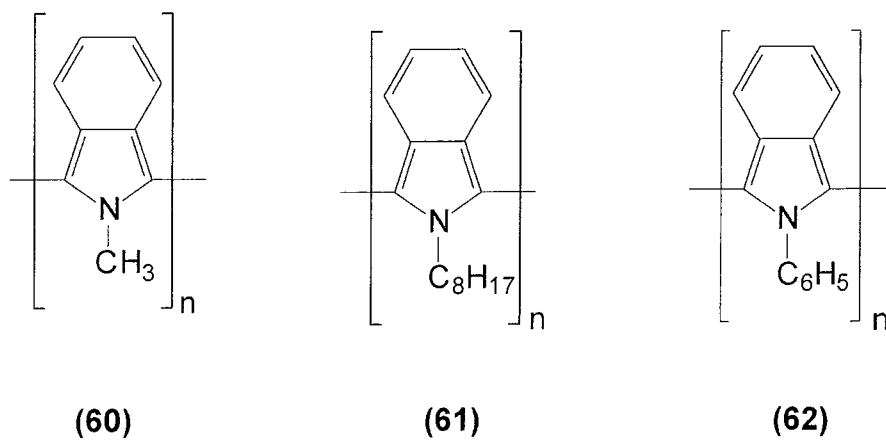


**Figure 1.31:** N-substituted Isoindoles

The report showed that the oxidation potential of these monomers were all lower than that of polypyrrole and therefore polymerised by electrochemical methods quite readily. The conductivities of these polymers were in the range of  $10^{-3}$  to  $10^{-6}$  S cm<sup>-1</sup>. Major emphasis on the steric hindrance of the large N-substituted groups inflicted on the polymer chain were discussed, it concluded,

- (i) The steric strain which disrupts the conjugation of the polymer backbone in poly-N-methylisindole mainly arises from the N-methyl group rather than the benzene ring
- (ii) The steric strain due to N-methyl is much greater in polyisindoles than in polypyrrole.

The order of conductivities of N-substituted polyisindoles seemed to be dependent on the size of the N-substituent. Among the three derivatives, **(60)**, with the smallest substituent has the largest conductivity ( $10^{-3}$  S cm<sup>-1</sup>) while **(62)**, with the largest substituent, has the lowest conductivity ( $10^{-6}$  S cm<sup>-1</sup>). The paper also stated "An apparent non-planarity of poly-N-methylisindole, which results from steric strain due to the methyl, seems to offset the band gap decrease driven by the fused benzene ring". However no band gap values were quoted for any of the polymers other than the inclusion of a visible spectrum of the reduced form of poly-N-methylisindole ( $\lambda_{\text{max}} = 420$  nm)

It was also found [59] that thin films of poly-N-methylisindole **(60)** underwent reversible colour change during redox reactions and were orange in the oxidised form and dark green in the reduced form.

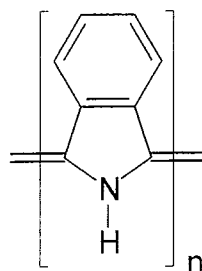
Subsequent to this, two reports [60, 61] on poly-N-methylisindole appeared in 1993. *Rhee et al.* [60] reported preparing poly-N-methylisindole **(60)** chemically and electrochemically as a soluble polymer in DMF and DMSO.

The conductivity of the polymer was found to be in the range of  $10^{-6}$  -  $10^{-4}$  S  $\text{cm}^{-1}$  depending on the extent of doping. Poly-N-methylisoindole also showed good electrochromic properties by changing from golden yellow in the reduced state to dark green in the oxidised state. Another report by Hanly *et al.* [61], where poly-N-methylisoindole (**60**) was again prepared chemically and electrochemically stated the electrochromic switching for poly-N-methylisoindole as metallic gold in the reduced state to transparent colourless in the oxidised form, at the time being only the second reported transparent organic semiconductor. Furthermore the band gap of this polymer was reported [61] to be in the region of 2 eV, which is lower than that for polypyrrole ( $\sim 3.2$  eV). The conductivity of a pressed pellet of electrochemically prepared poly-N-methylisoindole was found to be 0.01 S  $\text{cm}^{-1}$  [61], which is a factor of ten higher than that found by Lee *et al.* [59]. Hanly *et al.* [61] also prepared the polymer chemically and reported a conductivity of 0.007 S  $\text{cm}^{-1}$ .

Nothing appeared in the literature from 1993 until more recently in 1999 when three other papers have appeared [62 – 64] on the isoindole system as organic semiconductors. Huskic *et al.* [62] briefly discussed the formation of polyisoindole (**41**). The report stated that (**41**) was formed as a black precipitate in a 70% yield and had a conductivity of  $3 \times 10^{-4}$  S  $\text{cm}^{-1}$ . However the report had no conclusive evidence of its structure, other than  $^{13}\text{C}$  NMR CP-MAS spectral evidence, which is insufficient. Furthermore, it is difficult to infer if the polymer obtained was in the oxidised or reduced form.

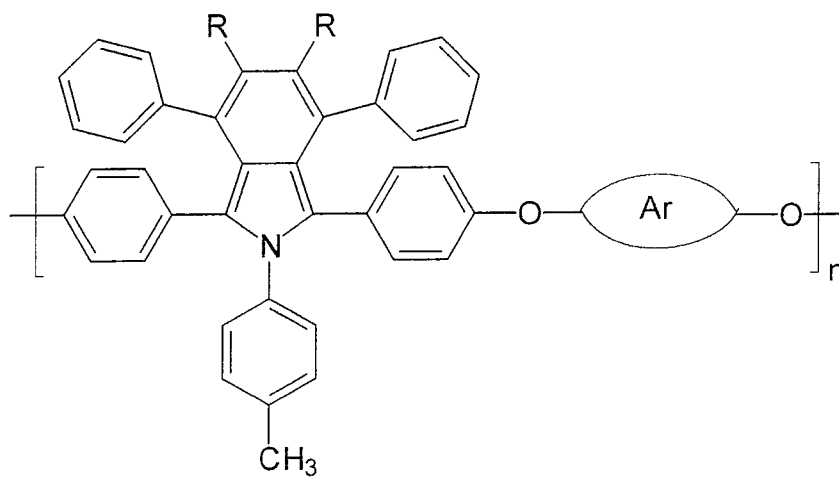
Ding *et al.* [63] reported on the synthesis of highly fluorescent isoindole based polymers. A series of stable highly phenylated isoindoles were formed. The isoindole polymers obtained would more appropriately be called co-polymers of isoindole, were of high molecular weights as reflected in their viscosities and were highly fluorescent. In addition, changes in the fluorescent emission frequencies were observed with different substituents on the isoindole backbone (**63**), see figure 1.33.





(41)

Figure 1.32: Polyisindole



(63) R = H or Ph

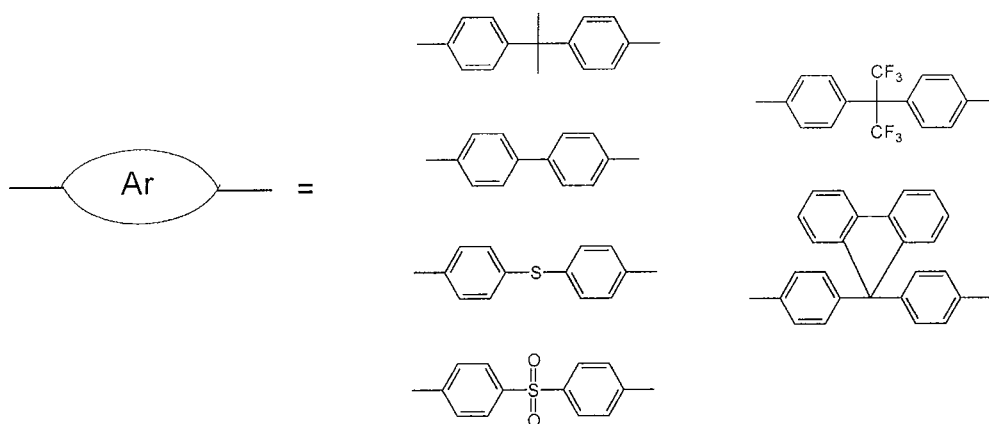
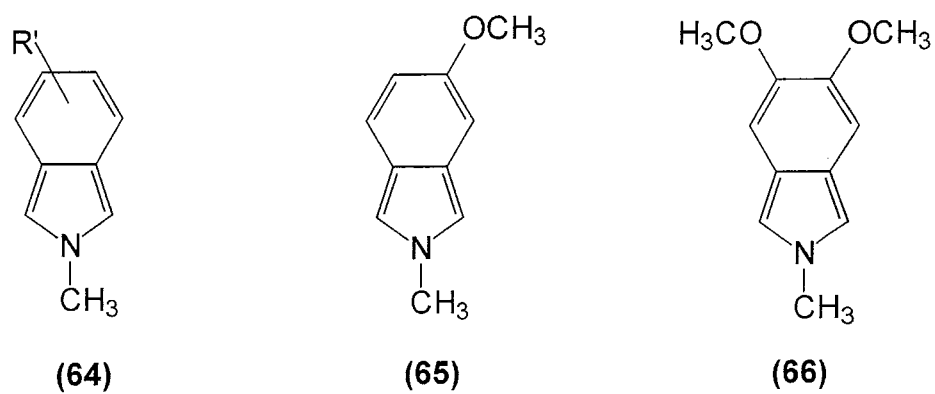


Figure 1.33: Highly fluorescent isoindole based polymers

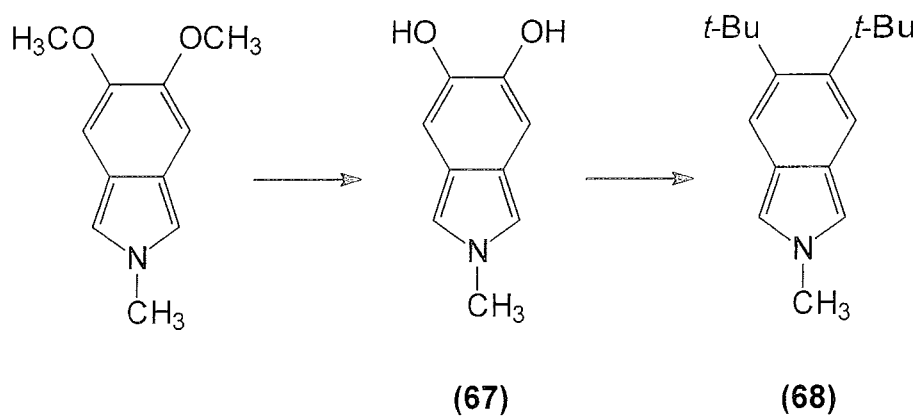
These highly substituted isoindole and polyisoindole reported by Ding *et al.* [63] have been used by Gauvin *et al.* [64] in organic light emitting devices. Highly substituted and fluorescent isoindoles were used in a bilayer type of organic electroeluminescent device, where the role of the polymer is that of a hole transport material. The device performed well against conventional materials and the authors concluded that isoindole be added to the list of possible hole transport materials used in organic light emitting devices

No work has yet been reported on the effect of electron – donating or electron – withdrawing substituents introduced at the six membered ring of the isoindole unit (**64**); see figure 1.34, on the polymer properties, be they electrical, optical, conductive or physical.

At the outset of this work, what was of particular interest was the effect of electron – donating substituents at the 5-position and the 5,6-position of the N-methylisoindole unit and from this, these effects on the polymer properties, be they electronic and/or steric could also be perused. It was initially decided to examine the effects of the methoxy substituent. However, as both 5-methoxy-N-methylisoindole (**65**) and 5,6-dimethoxy-N-methylisoindole (**66**) are unknown compounds, a route to their synthesis would first have to be devised. It was hoped that these methoxy substituents could be readily converted to their hydroxy (**67**) and *t*-butyl (**68**) electron – donating counterparts by appropriate chemical transformations, as shown in scheme 1.1. However, the effect of the methoxy substituent alone on both the monomer and polymer properties opened up a whole field of interest and therefore, neither the hydroxy or *t*-butyl counterparts were perused in this work.



**Figure 1.34:** Methoxy substituted N-methylisindoles



**Scheme 1.1:** Formation of hydroxy and *t*-butyl substituted N-methylisindoles

## 1.7 Applications

The initial interest in conjugated polymers dates from reports of the conducting properties of polyacetylene [65] polypyrrole [66] and polyaniline [67] but for a number of different reasons their future as semiconductors was initially not promising [68]. The development of conjugated polymers with useful semiconducting properties took almost another decade; although there were early reports of diodes made with polyacetylene [69-71], the first reports of devices with potentially useful properties date from the mid-1980s, with field effect transistors (FETs) reported by Koezuka *et al.* [72] based on electrochemically deposited poly (3-methylthiophene).

The projected commercial applications of conducting polymers were based on the promise of a novel combination of light weight, processability, and electronic conductivity. Because of this expectancy most interest focused on the production of light weight rechargeable batteries [73-76]. However, before a commercially realistic model could be achieved the life cycle and the shelf life of the polymer had to be improved.

A number of battery designs using conducting polymers have been described [74]. The active polymeric electrode can be either the anode or the cathode of the cell. Battery cells with conducting polymers as the anode are most common due to difficulties in inserting negative charges into polyheterocycles.

A polypyrrole battery has been developed and tested by BASF and VARTA Batterie AG. The positive electrode consisted of electrochemically synthesised polypyrrole doped with tetrafluoroborate. When polypyrrole was used with a lithium counterelectrode at a cell voltage of 3.5V, a theoretical energy density of 360 W h/kg was estimated for the polypyrrole electrode, although in a practical cell the density was lower [75, 76].

Today the major interest in conducting polymers is in their use as electrochromic displays. The novel behaviour of colour change

accompanying electrochemical change implies that these systems may be used as memory devices, optical switches and electrochromic displays.

Conducting polymers are used as electrochromic devices, which work on a similar principle to the rechargeable battery. Some conducting polymers, such as polyaniline [1], show a whole range of colours as a result of their many protonated and oxidised forms. The electrochromic properties of such polymers can be used to produce a number of electrochromic devices. Electrical potential is applied to cause doping and undoping of the conductive polymer and thus to induce controlled colour changes. In these electrochromic devices if the colour change is to be visible one or both of the electrodes involved must be optically transparent. Indium doped tin oxide glass is commonly used for this purpose. In a 'smart window' [1] which changes colour in response to sunlight or temperature changes both electrodes are transparent. In the transparent (bleached) state of the device, the polymer is in the undoped form. To block sunlight a positive potential is applied, causing oxidative doping of the polymer, which results in intensive colouration of the polymer with good optical contrast. Dopants from the electrolyte enter the polymer structure. To bleach the colour a negative potential is applied to undope the polymer. The response times of an electroactive polymer is determined by the time it takes for the dopant ions to diffuse in and out of the polymer. Typical response time is 100 milliseconds. Smart windows do not require a fast response time. During Summer, smart windows that use a conducting polymer darken to absorb some of the sunlight, thus saving on air-conditioning costs.

#### *Flat-screen televisions*

Organic conducting polymers are currently being developed in the field of flat screen televisions and monitors [78]. A lot of money is being injected into flat panel display technology by companies all over the world. Multi million dollar commercial research programmes have been established by both Eastman, Kodak and Motorola [78], to name a few, as well as a host of companies in Japan, the US and Europe. Small independent firms such as Universal Displays Corporation in the US and Cambridge Display Technologies in the

UK, have been set up specifically to turn the innovation, known as an organic light emitting device (OLED), into a commercial product. Such investment is justified because of the potential of OLEDs to revolutionize the world of television. So far progress has been impressive. These displays were first demonstrated in their present form just over ten years ago. They have active layers only about a thousandth of the thickness of a human hair. Already the best of them are many times brighter per unit area than a conventional television picture tube, and function at less than ten volts, for several tens of thousands of hours. Significantly organic displays are fast enough to handle full motion video, making them suitable for use not only as computer monitors, but also as televisions.

The most impressive features for these displays however, are unusual ones made possible by intrinsic characteristics of their organic constituents [78]. For example, weak intramolecular bonding in these materials permits the active layers to be deposited on thin flexible plastic substrates. The resulting displays could be rolled up or made to conform to surfaces of various contours. Both the active layers and their plastic substrates are so light that the weight of a computer monitor could in principle be reduced to a few grams. The ability of organic semiconductors to form high quality thin films on practically any flat substrate is potentially transformative, because it promises to allow engineers to grow organic electroluminescent devices over large area flat panel displays.

Monochrome organic light emitting devices which emit only green light have been developed for commercial applications by Pioneer Corporation, the Tokyo based electronic giant [78]. They have developed a 2.5 x 10 cm monochrome OLED flatscreen. For eventual use in automobiles to display navigational information the future looks both big and bright for the future production of organic electroluminescent devices in the form of flat panel display screens.

### *Sensors*

Many kinds of sensors using conductive polymers have been described for both chemical and biological uses. The principle of immobilisation of a species adapted to detect a specific gas or ion in solution is important in the application of polypyrroles as sensors. Sensors for the immobilisation of antibodies for viruses and drugs of nucleic sequences can be used in medical diagnostics [79]. Humidity and gas sensors have also been described [80,81].

The applications of organic semiconductors has grown enormously in the last decade and this section only gives a general account of some of the more promising applications. Many reviews of the technical applications have been made [11, 82, 83], where more detailed accounts of these applications are given, and are beyond the scope of this study.

## 1.8 References

- [1] M.G. Kanatzidis, *Chem. Eng. News*, (1990), Dec 3.
- [2] V.V. Walatka, M.M. Labes and J.H. Perlstein, *Phys. Rev. Lett.*, (1973), **31**, 1139.
- [3] R.L. Greene, G.B. Street and L.J. Suter, *Phys. Rev. Lett.*, (1975), **34**, 577.
- [4] W.D. Gill, W. Bludau, R.H. Geiss, P.M. Grant, R.L. Greene, J. Mayerle and G.B. Street, *Phys. Rev. Lett.*, (1977), **38**, 1305.
- [5] H. Shirakawa, E.J. Louis, A.G. MacDiarmid, C.K. Chang & A.J. Heeger, *J. Chem. Soc. Chem. Commun.*, (1979), 662.
- [6] D.M. Ivory, G.G. Miller, J.M. Sowa, L.W. Shacklette, R.R. Chance & R.H. Baughmann, *J. Chem. Phys.*, (1979), **71**, 1506.
- [7] A.F. Diaz, K.K. Kanazawa and G.P. Gardini, *J. Chem. Soc. Chem. Commun.*, (1979), 635.
- [8] G. Tourillon & F. Garnier, *J. Electroanal. Chem.*, (1982), **135**, 173.
- [9] F. Wudl, M. Kobayashi & A.J. Heeger, *J. Org. Chem.*, (1984), **49**, 3382.
- [10] T. Ohaska, Y. Ohnoki, N. Oyama, G. Katagiri & K. Kamisako, *J. Electroanal. Chem.*, (1984), **161**, 399.
- [11] *Handbook of Conducting Polymers*, Vol. 2 (T. J. Skotheim, R.L. Elsenbaumer and J.R. Reynolds ed.), Marcel Dekker, New York, (1998).
- [12] *Molecular structure, Properties and Uses*, **Part V**, 553-572.
- [13] J.L. Bredas and G.B. Street, *Acc. Chem. Res.*, (1985), **18**, 309.
- [14] W.P. Su, J.R. Schrieffer, and A.J. Heeger, *Phys. Rev. Lett.* (1979), **42**, 1698.
- [15] J.J. Ritsko, J. Fink and G. Crecelius, *Solid State Commun.*, (1983), **46**, 477.
- [16] J.L. Bredas, B. Themans, J.G. Fripiat, J.M. Andre, and R.R. Chance, *Phys. Rev. B: Condens. Matter*, (1984), **29**, 6761.
- [17] U.S Patent No: 4,717,762.
- [18] C. Quattrocchi, R. Lazzaroni, and J.L. Bredas, *Macromolecules*, (1993), **26**, 1260.
- [19] G. Wegner and J. R uhe, *Faraday Discuss. Chem. Soc.*, (1989), **88**, 22.
- [20] G. Zotti and G. Schiavon, *Synth. Met*, (1989), **30**, 151.
- [21] A.F. Diaz, *Chem. Scr.*, (1981), **17**, 142.



- [22] A.F. Diaz, J. Crowley, J. Bargon, G.P. Gardini and J. B. Torrance, *J. Electroanal. Chem.*, (1981), **121**, 335.
- [23] R.J. Waltman and J.Bargon, *Can. J. Chem.*, (1986), **64**, 76.
- [24] R.J. Waltman, J.Bargon and A.F. Diaz, *J. Phys. Chem.* (1983), **87**, 1449.
- [25] G. Dian, G. Barbey, and B. Decroix, *Synth. Metals*, (1986), **13**, 281.
- [26] A.O. Patil, A.J. Heeger and F. Wudl, *Chem. Rev.*, (1988), **88**, 183.
- [27] M.A. Sato, S. Tanaka and K. Kaeriyama, *J. Chem. Soc. Chem. Commun.*, (1985), 713.
- [28] M.A. Sato, S. Tanaka and K. Kaeriyama, *Synth. Met.*, (1987), **18**, 229.
- [29] M. Feldhues, G. Kampf, H. Litterer, T. Mecklenburg and P. Wegener, *Synth. Metals*, (1989), **28**, C487.
- [30] S. Tanaka, M. Sato and K. Kaeriyama, *Polym. Commun.*, (1985), **26**, 303.
- [31] M. Dietrich and J. Heinze, *Synth. Met.*, (1991), **41**, 503.
- [32] J. Roncali, R. Garreau, A. Yassar, P. Marque, F. Garnier and M. Lemaire, *J. Phys. Chem.* (1987), **91**, 6706.
- [33] A.O. Patil, Y. Ikenoue, F. Wudl and A.J. Heeger, *J. Am. Chem. Soc.*, (1987), **109**, 1858.
- [34] A.O. Patil, Y. Ikenoue, N. Besescu, N. Colaneri, J. Chen, F. Wudl and A.J. Heeger, *Synth. Met.*, (1987), **20**, 151.
- [35] A.K. Bakhshi and J. Ladik, *Solid State Commun.*, (1987), **61**, 71.
- [36] M. Kobayashi, N. Colaneri, M. Boysel, F. Wudi and A.J. Heger, *J. Chem. Phys.*, (1985), 82(12), 5717.
- [37] M. Pomerantz, B.C. Gill, L.O. Harding, J.J. Tseng & W.J. Pomerantz, *Synth. Met.*, (1993), **55**, 960
- [38] F. Eiji, Jpn. Kokai Tokkyo Koho JP 02 252 726 (1990).
- [39] G. King and S.J. Higgins, *J. Chem. Soc. Chem. Commun.*, (1994), 825.
- [40] G. King, S.J. Higgins, S.E. Garner, and A.R. Hillman, *Synth. Met.* (1994), **67**, 241.
- [41] G. King and S.J. Higgins, *J. Mater. Chem.*, (1995), **5**, 447.
- [42] F. Wudl, A.J. Heeger, Y. Ikenoue, and M. Kobayashi, Eur. Patent Appl. (1988) 0 273 643
- [43] Y. Ikenoue, F. Wudl and A.J. Heeger, *Synth. Met.*, (1991), **40**, 1.
- [44] T-T Hung and S-A Chen, *Polymer*, (1999), **40**, 3881.

- [45] W. Wallnöfer, E. Faulques, H. Kuzmany, and K. Eichinger, *Synth. Met.* (1989), **28**, 533.
- [46] F. Eiji, Jpn. Kokai Tokkyo Koho JP 02 252 727 (1990).
- [47] G.K. Chandler and D. Pletcher, *Chem. Soc.*, (1985), 10 117.
- [48] G.B. Street, T.C. Clarke, R.H. Geiss, V.Y. Lee, A. Nazzal, P. Pfluger & J.C. Scott, *J. Phys. Colloq.*, (1983), **44**, 559
- [49] A. Merz, R. Schwarz and R. Schropp, *Adv. Mater.*, (1992), **4**, No. 6. 409.
- [50] R. Casas, A. Dicko, J.M. Ribo, M.A. Valles, N. Ferrer-Anglada, R. Bonnett, N. Hanly and D. Bloor, *Synth. Met.*, (1990), **39**, 275.
- [51] P. Audebert and G. Bidan, *J. Electroanal. Chem.*, (1985), **161**, 129.
- [52] A.F. Diaz, J. Castillo, K. Kanazawa, J.A. Logan, M. Salmon & O. Fajardo, *J. Electroanal. Chem.*, (1982), **133**, 233.
- [53] R. Bonnet and S.A. North, *Chem. Commun*, (1972), 393.
- [54] R. Bonnet and S.A. North, *Adv. Heterocycl. Chem.*, (1981), **29**, 341.
- [55] Japanese Patent No: JP 02,263,824.
- [56] Japanese Patent No: JP 02,263,825.
- [57] Japanese Patent No: JP 0324,120.
- [58] U.S. Patent No: 4,833,231.
- [59] Y.S. Lee, H. S-W. HU and O.-K Kim, *Mol. Cryst. Lig. Cryst.*, (1990), **190**, 9.
- [60] S.B. Rhee, M-H. Lee, B.S. Moon and Y. Kang, *Korea Polym. J.*, (1993), **1**, No.1, 61-68.
- [61] N.M Hanly, D. Bloor, A.P. Monkman, R. Bonnett and J.M Ribo, *Synth. Met.*, (1993), **60**, 195-198.
- [62] M. Huskic, D. Vanderande and J. Gelan, *Synth. Met.*, (1999), **99**, 143.
- [63] Y. Ding and A.S. Hay, *J. Polymer Science: Part A: Polymer Chemistry*, (1999), **37**,(16), 3293.
- [64] S. Gauvin, F. Santerre, J.P. Dodelet, Y. Ding, A.R. Hill, A.S. Hay, J. Anderson, N.R. Armstrong, T.C. Gorjanc, and M. D'Lorio, *Thin Solid Films*, (1999), **353**, 218.
- [65] C.K. Chiang, C.R. Fincher, Y. W. Park, A. J. Heeger, H. Shirakawa, E. J. Louis, S. C. Gau, and A. G. MacDiarmid, Electrical conductivity in doped polyacetylene, *Phys. Rev. Lett.* (1977), **39**, 1098.

- [66] G. B. Street, Polypyrrole: from powders to plastics, in *Handbook of Conducting Polymers*, Vol. 1 (T. J. Skotheim, ed.), Marcel Dekker, New York, (1986), p. 265
- [67] A. J. Epstein, J. Joo, C.Y. Wu, A. Benatar, C. F. Faisst, J. Zegarski, and A.G. MacDiarmid, Polyanilines: recent advances in processing and applications to welding of plastics, in *Intrinsically Conducting Polymers: An Emerging Technology* (M. Aldissi, ed), NATO ASI Series E, Vol. 246, Kluwer, Dordrecht, (1993), 165.
- [68] R.H. Friend and N. C. Greenham, Electroluminescence in Conjugated Polymers, in *Handbook of Conducting Polymers*, Vol. 2 (T. J. Skotheim, R.L. Elsenbaumer and J.R. Reynolds ed.), Marcel Dekker, New York, (1998), 823.
- [69] P.M. Grant, T. Tani, W. D. Gill, M. Krounbi, and T. C. Clarke, Schottky diodes based on Shirakawa polyacetylene, *J. Appl. Phys.* (1981), **52**, 869.
- [70] E. Ebisawa, T. Kurokawa, and S. Nara, *J. Appl. Phys.* (1983), **54**, 3255.
- [71] J. Kanicki, Polymeric Semiconductor Contacts and Photovoltaic Applications, in *Handbook of Conducting Polymers*, Vol. 1 (T. J. Skotheim, ed.), Marcel Dekker, New York, (1986), p. 544.
- [72] H. Koezuka, A. Tsumara, and T. Ando, Field-effect transistor with polythiophene thin film, *Synth. Met.*, (1987), **18**, 699.
- [73] L.W. Shacklette, R.R. Chance, R.L. Elsenbaumer and R.H. Baughman, *30<sup>th</sup> Power structure Conference, The Electrochemical Society*, (1982), 66.
- [74] J.E. Formmer and R.R. Chance, *Encyclopedia of Polymer Science and Engineering*, Vol. 5, 2<sup>nd</sup> Ed. 462.
- [75] M. Mermillod, J. Tanguy, and F. Petiot, *J. Electroanal. Chem.*, (1986), **133**, 1073.
- [76] J. Gosch, *Electronics*, (1987), **9**, 41.
- [77] D. Naegele and R. Bittihn, *Solid State Ionics*, (1988), **28**, 983.
- [78] P.E. Burrows, S.R. Forrest and M.E. Thompson, "Big, Bright and Organic", *Scientific American*, May (1998).
- [79] T. Shimidzu, T. Iyoda, H. Segewa and M. Fujitsuka, in *Intrinsically Conducting Polymers*: M. Aldissi (ed.), Kluwer Academic, London, 13.
- [80] L.S. Hwang, J.M. Ko, H.W. Rhee, and C.Y. Kim, *Synth. Met.*, (1993), **55-57**, 3671.

[81] J.M. Slater, E.J. Watt, N.J. Freeman, J.P. May and D.J. Weirm, *Analyst*, (1992), **117**, 1265.

[82] A. Kelak and A. Moet, *Functionalised Polymers and their Applications*, Chapman and Hall, 1<sup>st</sup> Ed, (1990).

[83] *Handbook of Organic Conductive Molecules and Polymers*, (H.S. Nalwa Ed.), Chichester: J. Wiley, (1997).

## **Chapter 2**

# **The Organic Synthesis of Isoindole Monomers**

## Chapter 2 – The Organic Synthesis of Isoindole Monomers

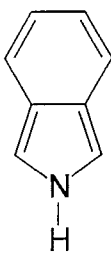
### 2.1 Introduction

The initial work carried out in the field of conducting polymers concentrated on the polymerisation of such monomers as benzene [1], aniline [2], pyrrole [3,4], and thiophene [5,6], and each lead to a polymer containing an extended  $\pi$ -conjugated system. The ready availability of these monomers lead to their easy exploitation, particularly polythiophene and polypyrrole. However, these polyheterocyclics failed to deliver on the expectations envisioned by scientists; namely that of conducting polymers achieving conductivities equal to that of metals. A fundamental goal in this field was to relate the chemical structure of the repeat monomer unit with the electronic, optical and physical properties of the resultant polymer, so as to enable the design of new conjugated polymers with superior properties. Functionalisation of the conjugated backbone, by modification of the monomer species (as discussed in chapter 1), can allow the polymer properties to be tailored at the early stages

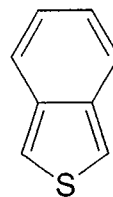
Moreover, the structure of the modified monomer should not inhibit the polymerisation reaction and must preserve and enhance the inherent electronic properties of the  $\pi$ -conjugated parent polymer. Such conditions require a detailed fore knowledge of the electronic and steric effects of substitution on the monomer itself and on the polymerisation reaction and ultimately on the structure and properties of the polymer itself.

#### 2.1.1 Synthesis of Isoindoles

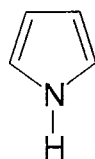
The isoindole system (**1**) is the nitrogen analogue of isothianaphthene (**2**) but has the same reactivity as pyrrole (**3**), see figure 2.1. The isoindoles appeared relatively recently [7], and the parent isoindole (**1**), was not isolated until 1972 [8]. Isoindole is a  $\pi$ -excessive 10- $\pi$ -electron heteroaromatic system and is a resonance hybrid and can be represented in canonical forms



(1)



(2)



(3)

**Figure 2.1:** Isoindole (1), isothianaphthene (2), pyrrole (3)

of the various shown in figure 2.2. Molecular orbital calculations have shown that ground state  $\pi$ -electron density is highest (after Nitrogen) at C-1 (C-3) positions, and that in the benzenoid ring,  $\pi$ -electron density is higher at C-5 (C-6) than at C-4 (C-7). This accords well with the ease of reactivity at C-1 (C-3), the  $\alpha$ ,  $\alpha'$  positions in electrophilic substitution reactions of isoindole [7].

Isoindole is a white solid which becomes discoloured and resinous at room temperature, especially in the presence of air. It may be handled for short periods using vacuum techniques, or in solution under inert atmosphere [8]. The instability has been attributed to a self-condensation reaction with its tautomeric isoindolenine form (**8**), figure 2.3, analogous to that shown by pyrrole under acidic conditions [8].

Various substituted isoindoles can be synthesised by a number of routes, including synthesis from isoindolines, from o-disubstituted benzenes, by retro-cycloaddition, from pyrroles and from phthalimidines, some of which are discussed. Compared with indole, which was prepared in 1866 [9], isoindole as already mentioned was not successfully isolated until 1972 by Bonnett and Brown using a gas-phase pyrolysis technique [8]. 2-Methoxycarbonyloxyisoindoline (**9**) was sublimed at 0.01mm Hg through a silica tube at 500°C, and the desired isoindole was collected at ~77K as shown in scheme 2.1. Shortly after this report, two other routes [10, 11] to isoindole were announced, both involving retro-Diels–Alder reactions. The first, carried out by Bornstein *et al.* [10] employed the gas-phase pyrolysis of (**10**) to give isoindole and ethene, as shown in scheme 2.2. The second route, attributable to Priestley and Warrener [11], involved the retro –Diels – Alder cleavage of the postulated dihydropyridazine (**11**) under very mild conditions as shown in scheme 2.3. Isoindole was separated from (**12**) by sublimation at room temperature.



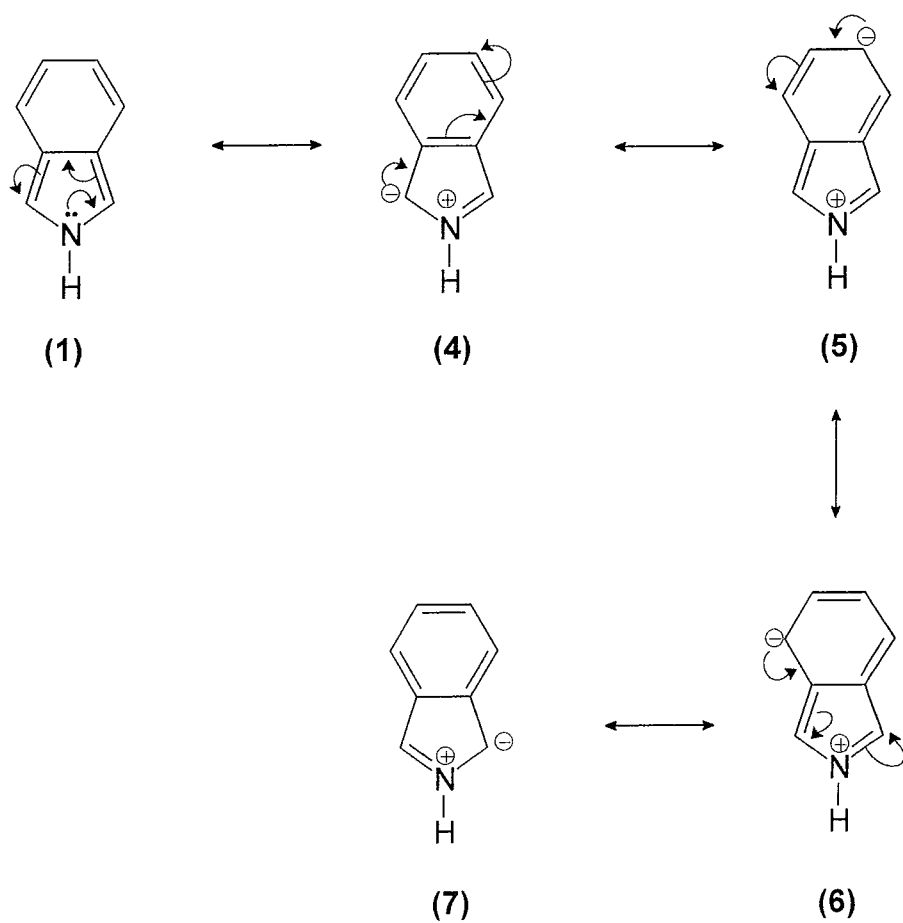


**Figure 2.2:** Canonical forms of Isoindole

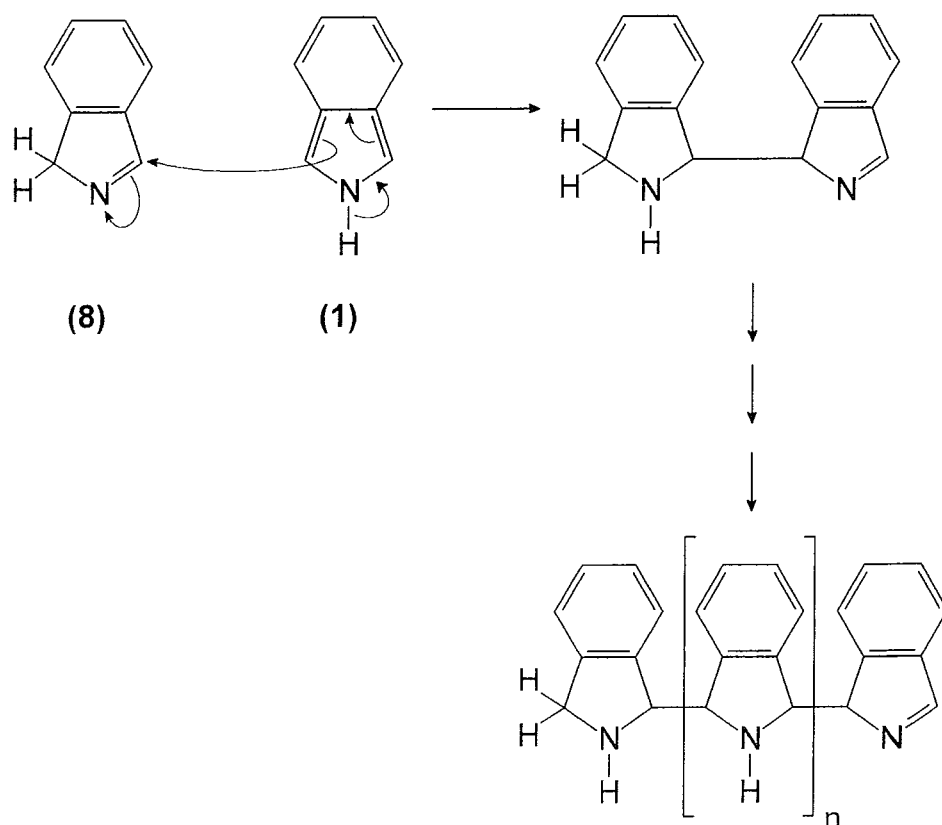
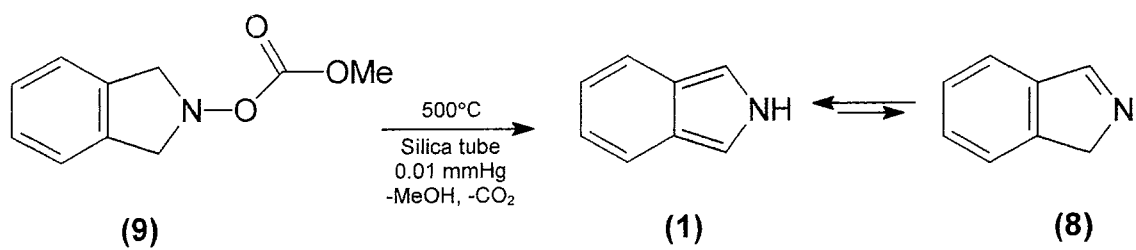
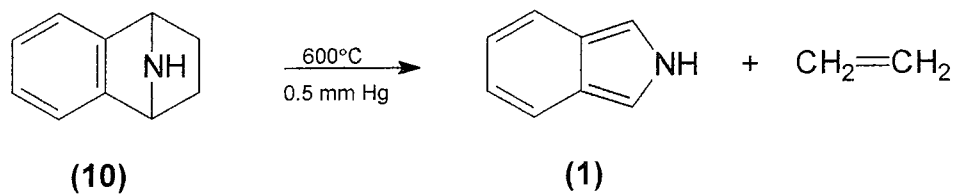


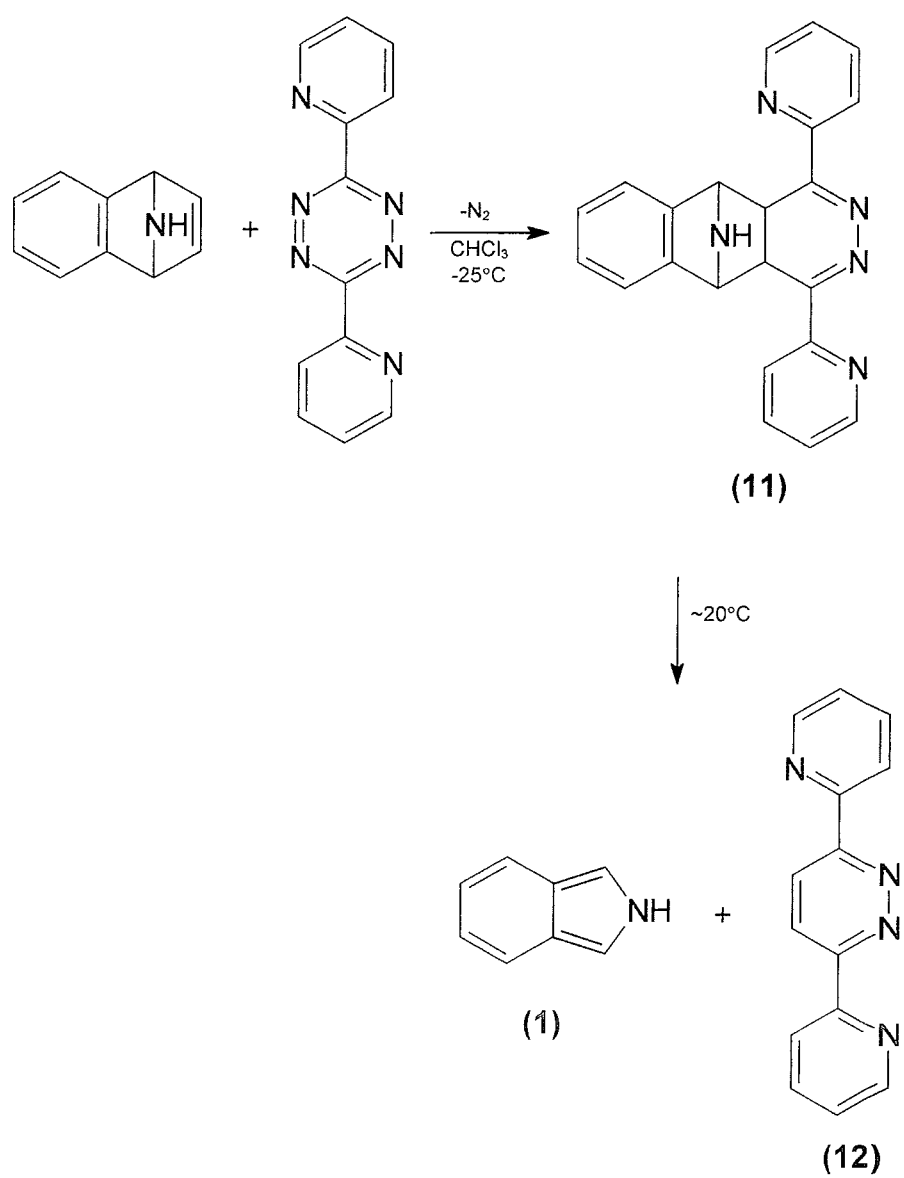
**Figure 2.3:** Self condensation of Isoindole



**Scheme 2.1:** Synthesis of Isoindole; Bonnet & Brown [8]



**Scheme 2.2:** Synthesis of Isoindole; *Bornstein et al.* [10]



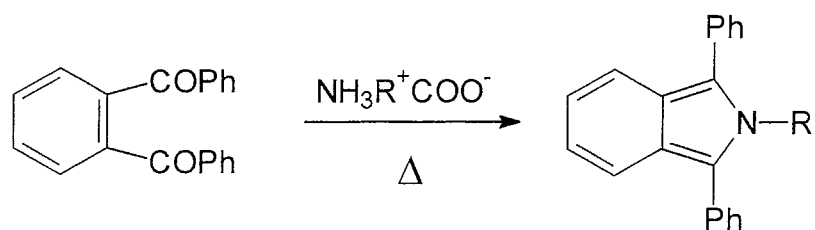
**Scheme 2.3:** Synthesis of Isoindole; Priestley and Warrener [11]

The synthesis of N-substituted isoindoles predominate [7]. These compounds, which cannot tautomerise (unlike the parent isoindole) are more easily prepared and manipulated but they still require the use of an inert atmosphere and refrigeration.

N-substituted isoindoles can be formed from o-disubstituted benzenes whereby the heterocyclic unit is built onto an existing benzenoid ring. Thus 1,3-diphenylisoindole (**13**) can be prepared by a Leuckart reaction [12], on treatment of o-dibenzoylbenzene with ammonium formate [13], as shown in scheme 2.4, but in a low yield (44%). When the reaction is extended to the formation of the N-methyl derivative (**14**) it can only be obtained in a 27% yield. An improved route [14], scheme 2.5, for the formation of 1,3-diphenyl-N-methylisoindole was provided by a similar reaction when 1,2-dibenzoylcyclohexa-1,4-diene (**15a**) was treated with 40% aqueous methylamine in methanol. The desired compound (**16a**) was obtained in a 68% yield, however the starting cyclohexadiene requires very specific preparation. This route can be extended to other substituted isoindoles (**16b**) & (**16c**) by varying the starting cyclohexadiene (**15b**) & (**15c**), scheme 2.5.

The most useful route to a 1-phenylisoindole (**17**), again involving an o-disubstituted benzene as a starting material, namely an  $\alpha$ -phthalimido-o-toluyyl chloride was described by Veber and Lwowski [15] and is shown in scheme 2.6. This reaction gives the desired product in a very good yield (80%) and under mild conditions. In both the 1,3-diphenylisoindole and 1-phenylisoindole compounds, tautomerisation can occur, as with the parent isoindole [13,15].

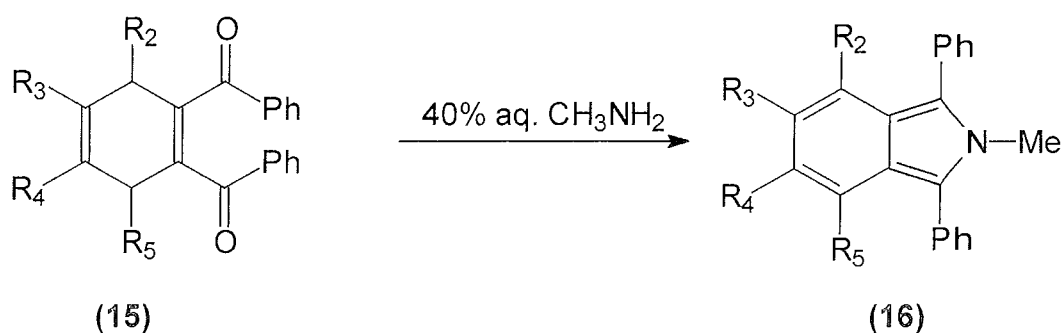
Another route to isoindoles is via the dehydrogenation of isoindolines [16,17], the latter containing a benzenoid ring fused to a saturated 5-membered heterocyclic ring. The alkylation of  $\alpha,\alpha'$ -dibromo-o-xylene (**18**) with p-toluene sulphonamide, scheme 2.7, affords N-tosylisoindoline (**19**) which on subsequent detosylation with HBr gives isoindoline (**20**) in a 63-71% yield [18,19].



**(13)** R = H (44%)

**(14)** R = Me (27%)

**Scheme 2.4:** Synthesis of 1,3-diphenylisoindoles

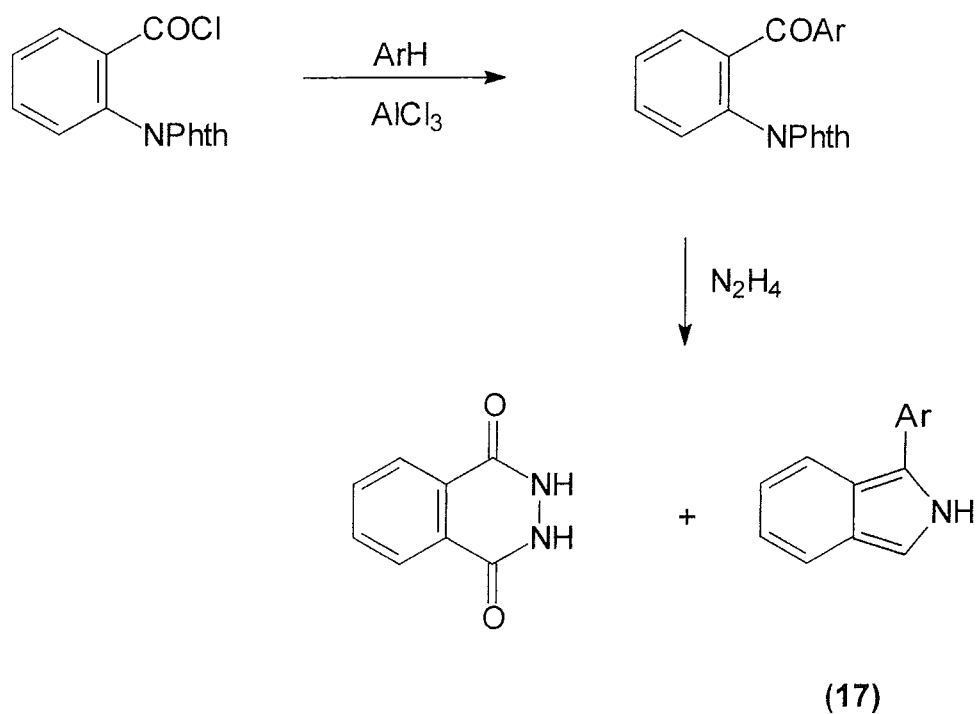


**(15a) & (16a)** R<sub>2</sub>, R<sub>3</sub>, R<sub>4</sub>, R<sub>5</sub> = H (68%)

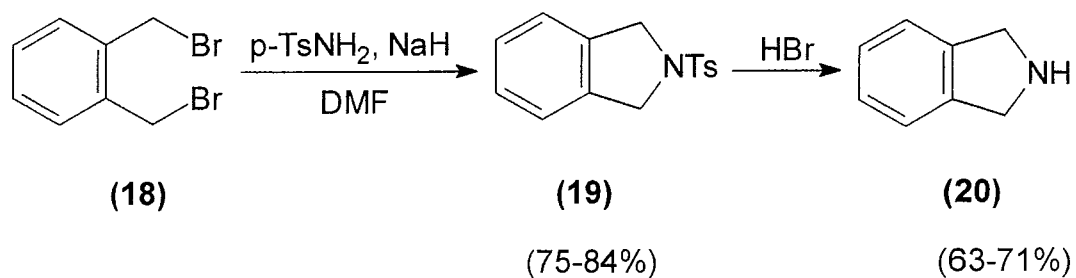
**(15b) & (16b)** R<sub>2</sub> = Me; R<sub>3</sub>, R<sub>4</sub>, R<sub>5</sub> = H (74%)

**(15c) & (16c)** R<sub>3</sub>, R<sub>4</sub> = Me; R<sub>2</sub>, R<sub>5</sub> = H (65%)

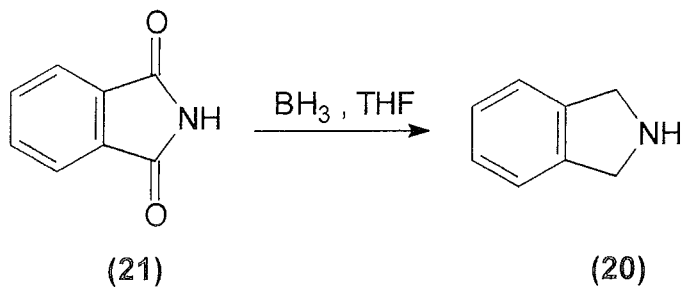
**Scheme 2.5:** Preparation of 1,2,3-trisubstituted Isoindoles



**Scheme 2.6:** Preparation of 1-Arylisindoles



**Scheme 2.7:** Synthesis of Isoindoline (ref. [18, 19])



**Scheme 2.8:** Synthesis of Isoindoline (ref. [20])

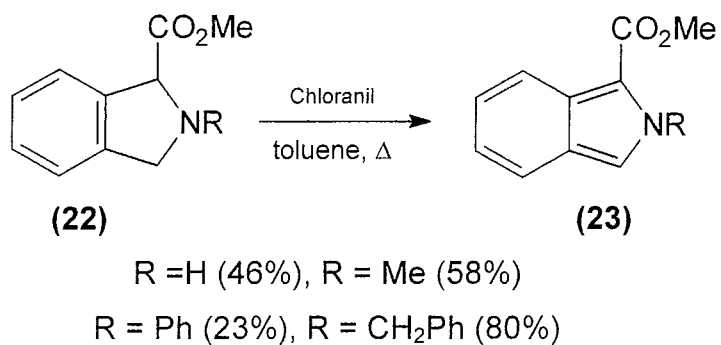


A less cumbersome procedure involving less severe reactants is a one step synthesis [20] by the reaction of phthalimide (**21**) with borane in THF, which affords isoindoline (**20**) in a 50% yield; see scheme 2.8. When a strong electron withdrawing group is present at either C-1 or C-3, such as a methoxycarbonyl group, the isoindoline (**22**) can be conveniently dehydrogenated with a high potential quinone such as chloranil [16] to yield (**23**) as shown in scheme 2.9.

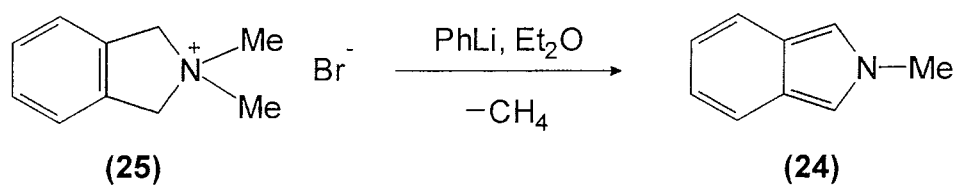
An important method for the preparation of isoindoles is based on their elimination from their corresponding isoindolinium salt, and indeed Wittig's [21] original synthesis of N-methylisoindole (**24**) involved the formation of the isoindolinium salt (**25**); see scheme 2.10. The most useful route, shown in scheme 2.11, is the elimination from a 2-aminoisoindolinium salt under basic conditions [22, 23]; the isoindolinium salt being formed by reaction of a dibromo-o-xylene (**18**) with a hydrazine derivative. The reaction of  $\alpha,\alpha'$ -dibromomethylester-o-xylene (**26**) with phenylhydrazine gives the 1,2,3-trisubstituted iminoisoindoline (**27**) plus the expected 1,2,3-trisubstituted isoindole (**28**) see scheme 2.12.

So far, substitution at the nitrogen atom and the 1, 3 positions of the 5 membered heterocyclic ring have been discussed. However substitution at the fused 6-membered ring on the isoindole unit has also been reported.

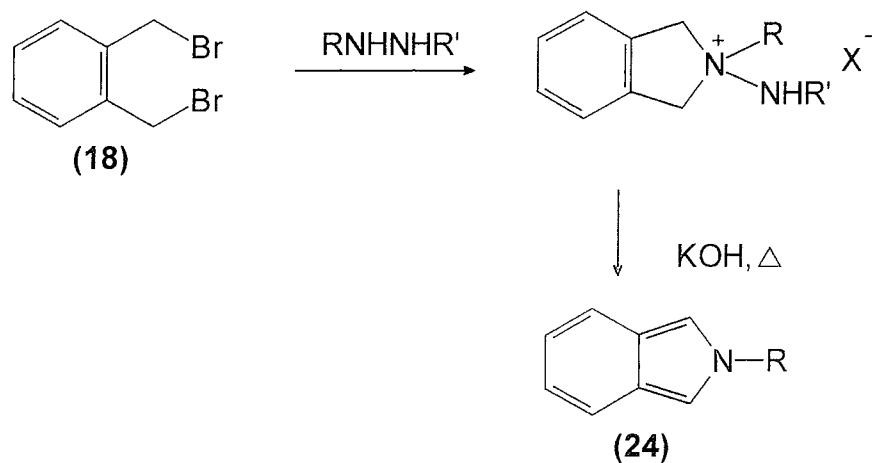
In an approach developed by Kreher and Seubert [24], isoindoline N-oxides undergo an analogous elimination when treated with the acylating agent, such as acetic anhydride in the presence of base. This route has been employed in the preparation of 4,5,6,7-tetrabromoisindole derivatives (**29**); see scheme 2.13. This method has been further developed by Kreher *et al.* [25 – 33] where isoindoles of type (**30**), where N is substituted with R groups such as alkyl [26], allyl [25] and arylalkyl [27] and very frequently *tert*-butyl group [26 - 33], have been synthesised as shown in scheme 2.14.



**Scheme 2.9:** Isoindoles from isoindolines

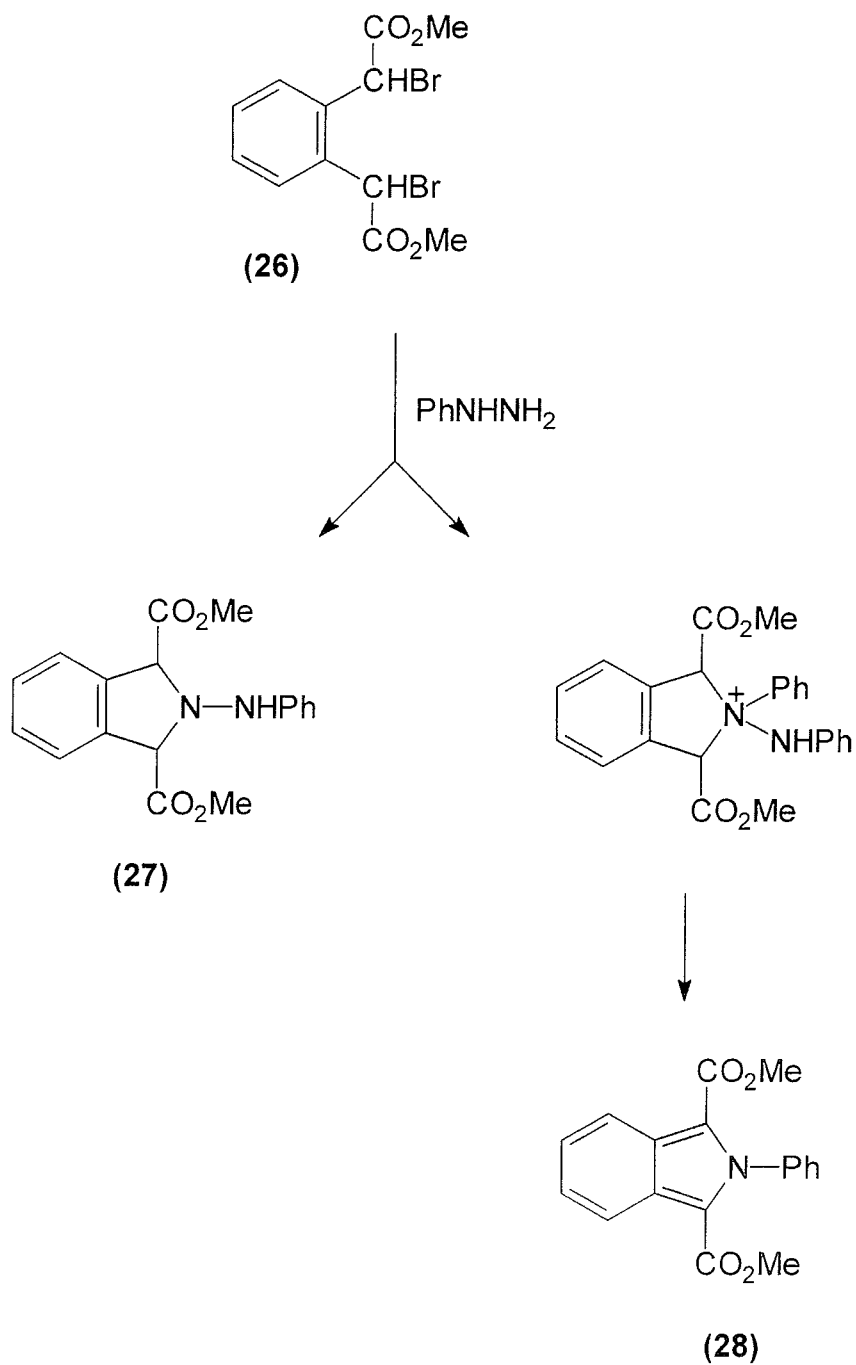


**Scheme 2.10:** Synthesis of N-methylisoindole

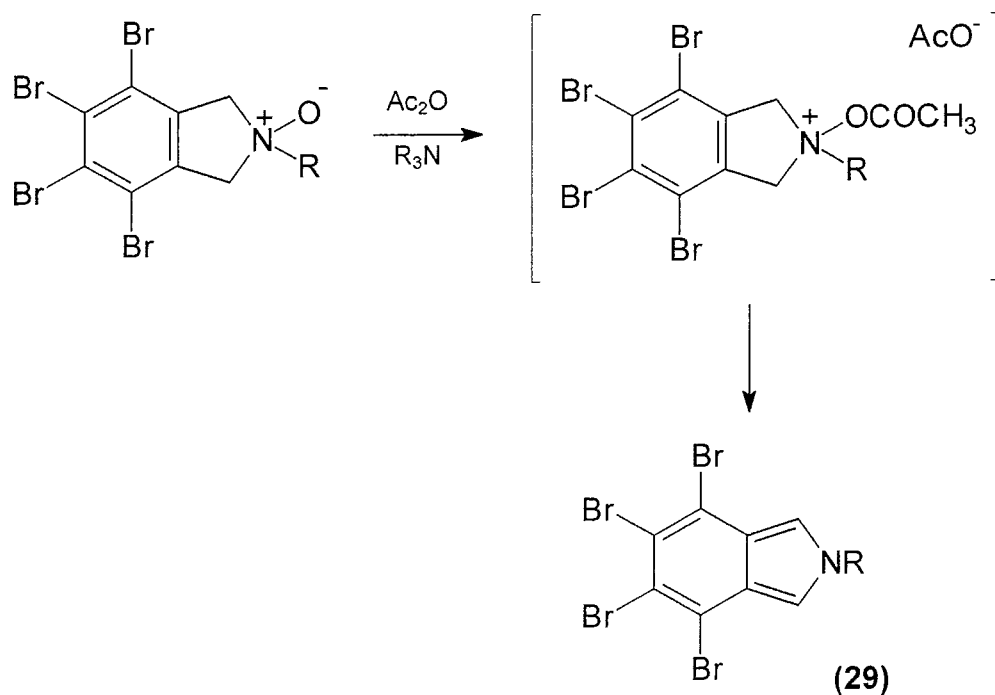


**a:** R = Me, R' = H (70%)  
**b:** R = CH<sub>2</sub>Ph, R' = CO<sub>2</sub> t-Bu (46%)

**Scheme 2.11:** N-substituted Isoindoles from Isoindolinium salts

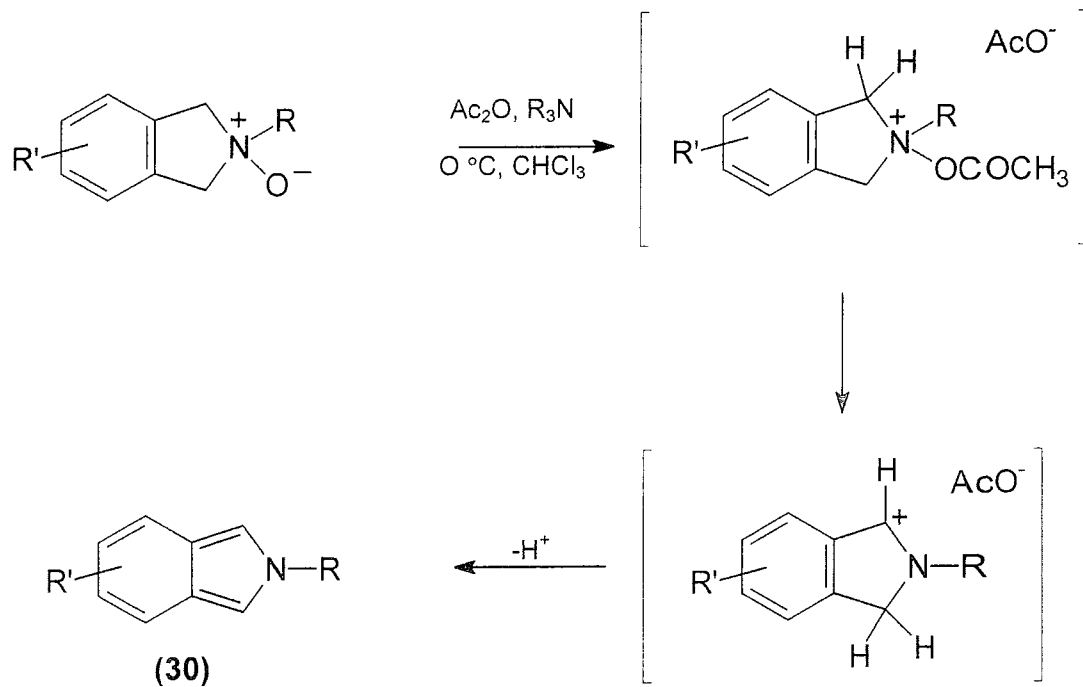


**Scheme 2.12:** Synthesis of 1,2,3-trisubstituted Isoindoles



R = Me (76%), *i*-Pr (78%), *t*-Bu (85%)

**Scheme 2.13:** Synthesis of 4,5,6,7-tetrabromoisoindoles



R = alkyl [26], allyl [25], arylalkyl [27], *tert*-butyl [26 - 33]

R' = methyl [33], nitro [28], chloro [33]

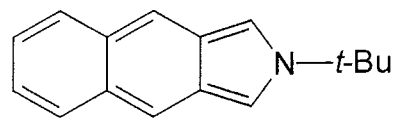
**Scheme 2.14:** Synthesis of isoindoles by Kreher *et al.* (ref. [26-33])

In these instances the 1,3-positions in the system are free but the 6-membered ring can be substituted with R' groups such as, methyl groups [33] nitro groups [28] and chloro groups [33], or it can be condensed with other rings, such as those seen in compounds (31) – (36), in figure 2.4[27, 28-30].

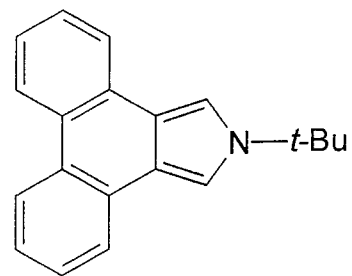
Isoindoles have been obtained [34, 35], via N-methanesulfinylisoindolines on treatment with potassium *tert*-butoxide in dimethylsulfoxide, as shown in scheme 2.15. The 1*H*-isoindoles (37) is formed initially and then isomerises to 2*H*-isoindole (38) as a result of a tautomeric transformation. Another method involving the elimination of propyne from N-propargylisoindolines (39) at a high temperature can serve as a general approach to the synthesis of 2*H*-isoindoles (40) [36,37]; see scheme 2.16. The required isoindoles again can be synthesised from corresponding 1,2-bis(bromomethyl)benzenes (41).

A novel method of synthesis of 1,3-dimethoxyisoindoles (42) have also been proposed [38] as shown in scheme 2.17. It consists of the reduction of phthalimides by magnesium to 3-hydroxyphthalimidine (43), which is converted into 3-methoxyphthalidine (44). The O-alkylation of the latter with CF<sub>3</sub>SO<sub>2</sub>OMe affords 1,3-dimethoxyisoindoliumtrifluoromethane-sulfonate (45), the deprotonation of which with the aid of lithium diisopropylamide leads to the relatively unstable 1,3-dimethoxyisoindoles (42).

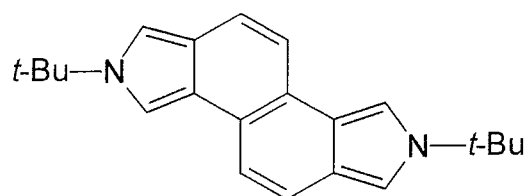
A series of 3-methoxyisoindolenines (46) has been obtained by alkylating 3-oxo-1,2-dihydroisoindolines [39 - 42]; see scheme 2.18. The regioselective O-alkylation in the first stage results in the formation of 3-methoxyisoindolenine triflates (47). Using the same method, a series of 3-alkoxyisoindolenines (48) (13 compounds) [40], containing substituents of different electronic nature R' on the 6-membered ring, has been obtained as shown in scheme 2.19.



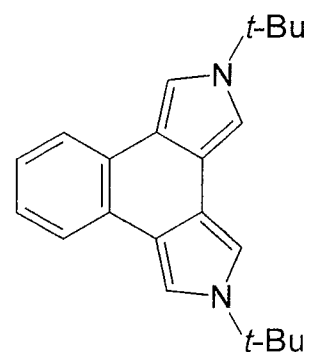
(31)



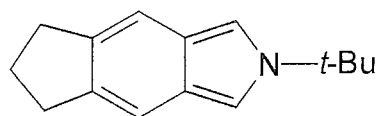
(32)



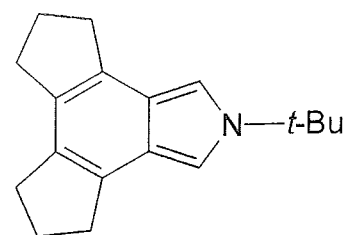
(33)



(34)

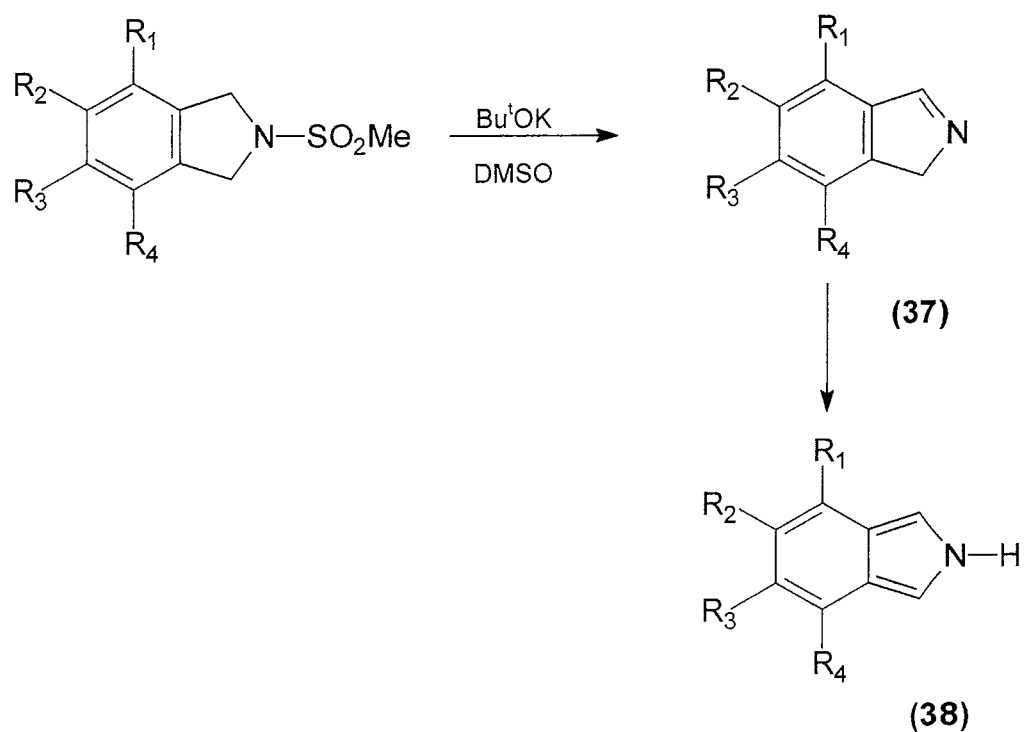


(35)



(36)

**Figure 2.4:** Various cyclic substituted isoindoles

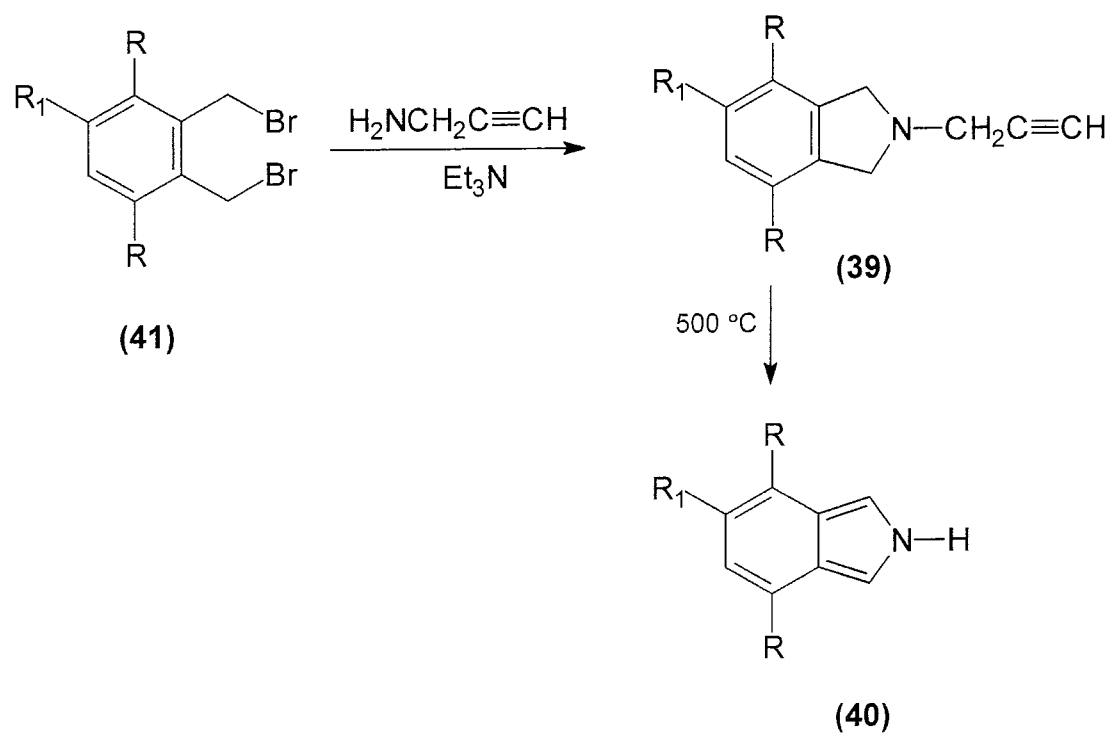


**38a:**  $R_1 = R_2 = R_3 = H$ ;  $R_4 = COBu^t$

**38b:**  $R_1 = R_2 = R_3 = R_4 = Cl$

**38c:**  $R_1 = R_2 = R_3 = R_4 = Br$

**Scheme 2.15:** Synthesis of isoindoles via N-methanesulfonylisoindolines



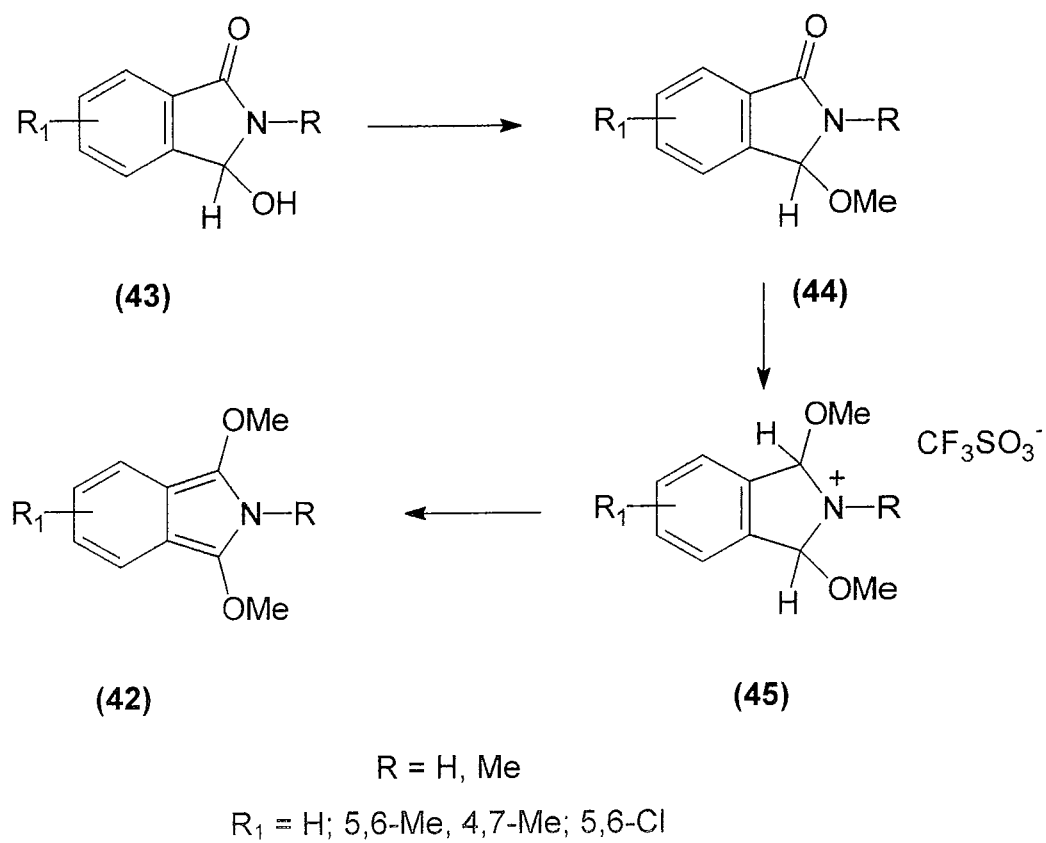
**40a:** R = R<sub>1</sub> = H

**40b:** R = H; R<sub>1</sub> = Bu<sup>t</sup>

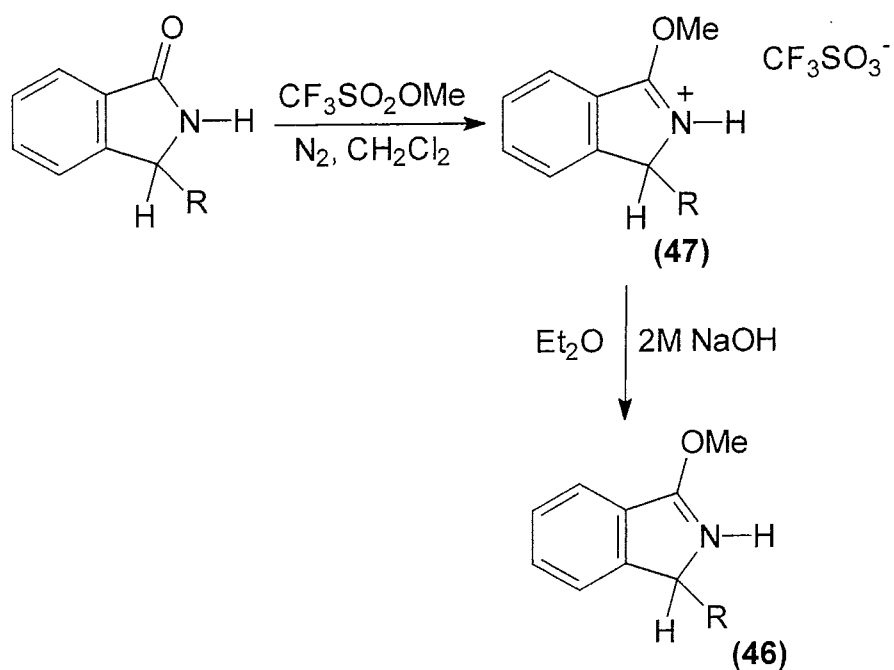
**40c:** R = H; R<sub>1</sub> = COBu<sup>t</sup>

**Scheme 2.16:** Synthesis of isoindoles from corresponding 1,2-bis(bromomethyl)benzenes



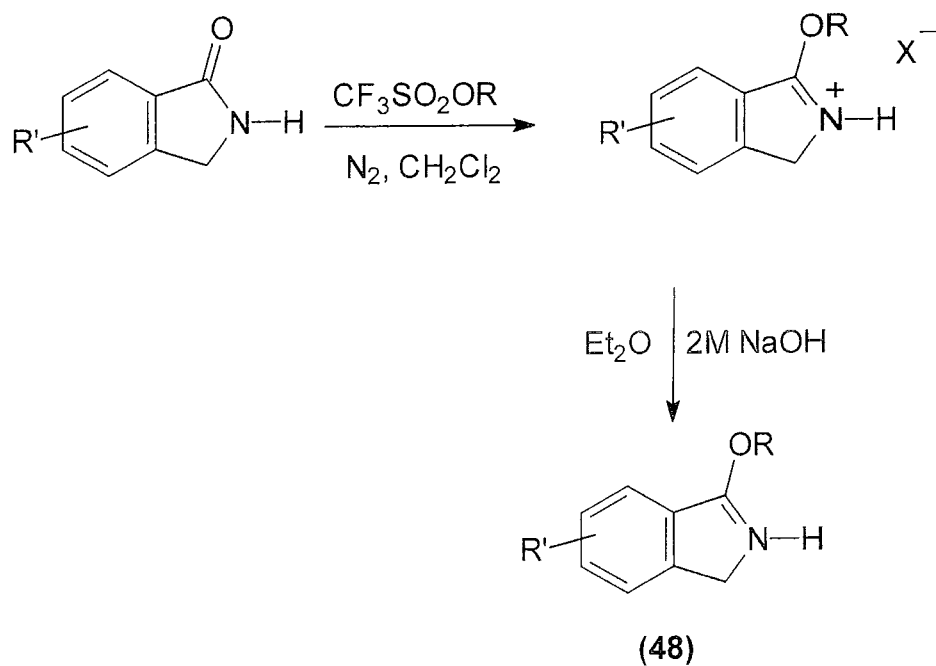


**Scheme 2.17:** Synthesis of 1,3-dimethoxyisoindoles



R = Me (91%); Ph, 4-MePh, 4-ClPh (72-89%); 4-MeOPh (50%)

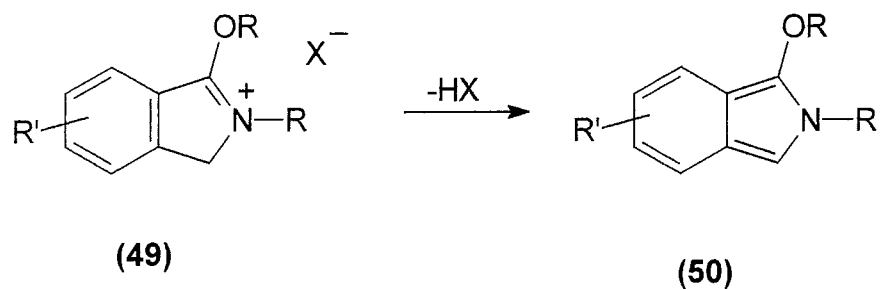
**Scheme 2.18:** Synthesis of 3-methoxyisoindolenines



**Scheme 2.19:** Synthesis of 3-alkoxyisoindolenines

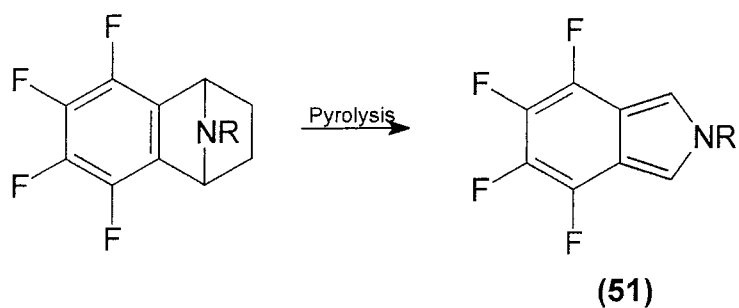
If the isoindolenines (**46**) and (**48**) are alkylated with methyl trifluoromethanesulfonate, then the quaternary salts (**49**) are formed [41, 42]; see scheme 2.20. These are the products of the regioselective N-alkylation which are readily deprotonated after treatment with bases (2M NaOH or lithium diisopropylamide) and are converted into 1-alkoxy-N-methylisoindoles (**50**). Related retro-Diels – Alders reactions as used to form the parent isoindole, see scheme 2.21, have been employed to obtain 4,5,6,7-tetrafluoroisoindole (**51a**) [43], 4,5,6,7-tetrafluoro-N-methylisoindole (**51b**) [44], and 4,5,6,7-tetrachloro-N-*t*-butylisoindole (**52**) [45]. Substituted isoindoles synthesised from pyrroles has also been reported [46]. The condensation of 2,5-disubstituted pyrroles or 1,2,5-trisubstituted pyrroles with 1,4-diones under acidic conditions generates the isoindole system. However the condensation of succinonitrile of 1,2-dibenzoyl ethane (**53**) with the 3,4-diformylpyrrole derivative (**54**) gives the corresponding N-methylisoindole (**55a**) and (**55 b**) in yields of 17 and 50% respectively; see scheme 2.22.

In the study undertaken here the initial objective was to synthesise the novel 5-methoxy-N-methylisoindole (**57**) and 5,6-dimethoxy-N-methylisoindole (**56**), see figure 2.5. As the synthesis of these two compounds have not been previously reported a route to their formation has to be devised. It would only appear reasonable to look at the method of synthesis for the unsubstituted compound, N-methylisoindole (**24**), which has been reported [22], and if appropriate to model the synthesis of these two new compounds along the same route. N-methylisoindole can be successfully formed [22] in a 70% yield, by elimination from its isoindolinium salt, under basic conditions; see scheme 2.11, the latter obtained by the reaction of  $\alpha,\alpha'$ -dibromo-*o*-xylene (**18**) with methylhydrazine. Thus the synthesis of 5-methoxy- and 5,6-dimethoxy-N-methylisoindole will be attempted by elimination reaction from their corresponding isoindolinium salts. Therefore, the starting material for these two isoindoles will have to be a specific substituted  $\alpha,\alpha'$ -dibromo-*o*-xylene type compound, neither of which are readily available. The synthesis of these two new isoindoles will now be discussed.



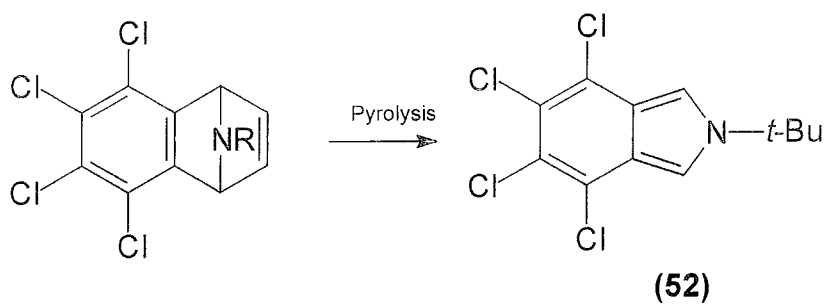
R = alkyl group

**Scheme 2.20:** Synthesis of 3-alkoxyisoindoles



**(a)** R = H [500 °C, 0.5mm]

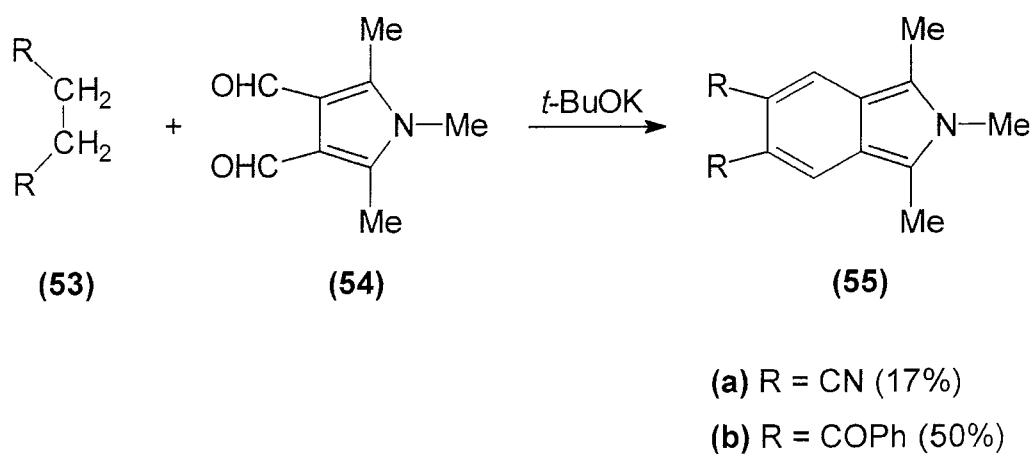
**(b)** R = Me [120 °C, 1 atm]



R = *t*-Bu [200 °C]

( pressure not stated)

**Scheme 2.21:** Synthesis of 4,5,6,7-tetrahaloisoindoles



**Scheme 2.22:** Synthesis of Isoindoles from pyrroles

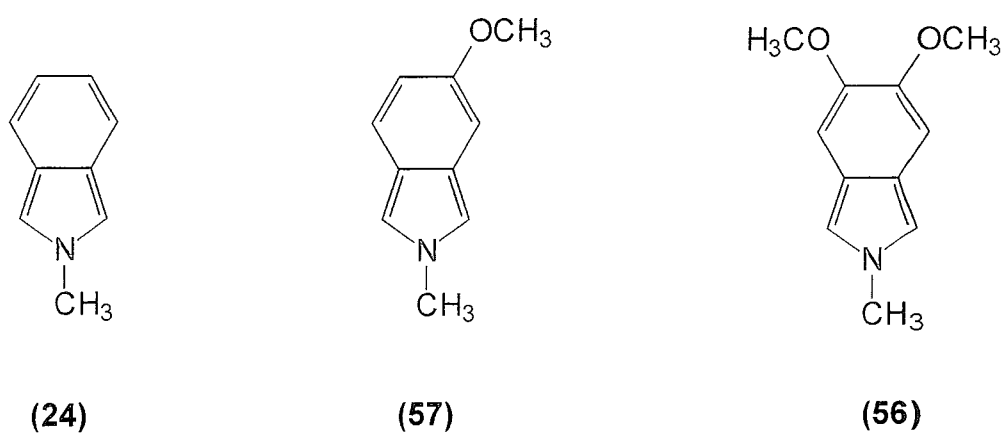


**Figure 2.5:** N-methylisoindole and methoxy substituted N-methylisoindoles

## 2.2 Results and Discussion

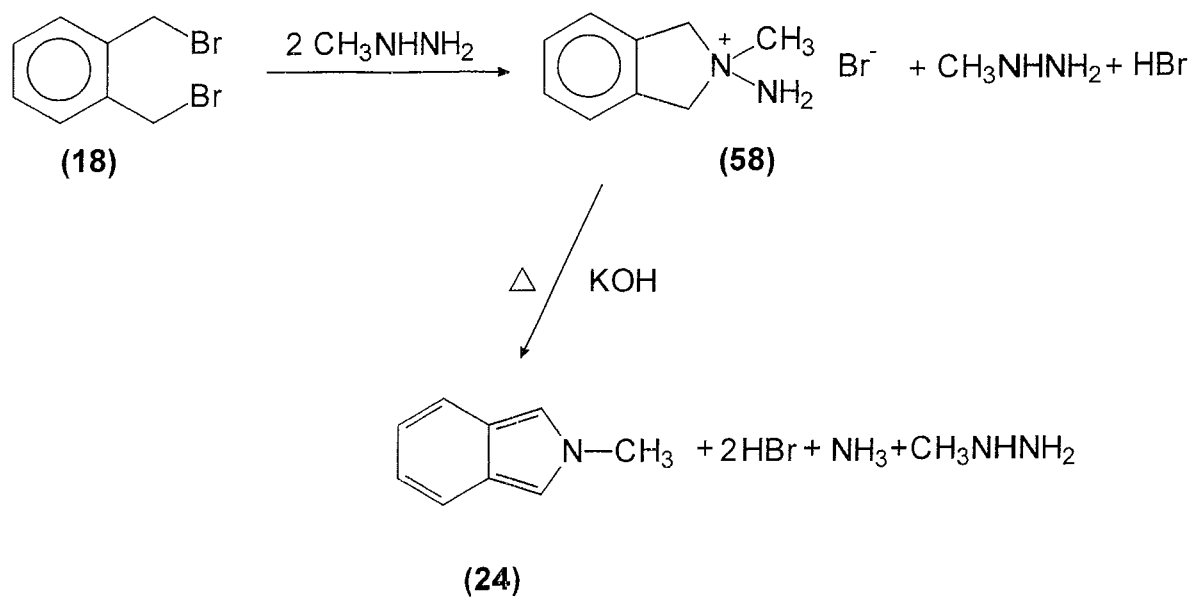
### 2.2.1 Synthesis of N-methylisoindole

N-methylisoindole was synthesised by the method of Zeeh & König [22] as shown in scheme 2.23, involving the reaction of  $\alpha,\alpha'$ -dibromo-o-xylene (**18**) with methylhydrazine, to give the corresponding isoindolinium salt (**58**). Elimination of the N-methylisoindole (**24**) from the salt occurred under basic conditions and heat. A white crystalline product was obtained in a 44% yield, m.p. 88-89°C (lit. [22], 70%, m.p. 90-91°C on sublimation). However, this low yield was due to loss of the product as a result of difficulties encountered with experimental apparatus.

The product was analysed using spectroscopic methods (Appendix A). The UV-Vis spectrum showed a strong absorption at  $\lambda_{\text{max}}$  224nm attributed to the aromatic  $\pi\text{-}\pi^*$  transition, while a broad less intense absorption at 325nm was attributed to vibrational and rotational fine structure.

The infrared spectrum showed ring C=C stretches at  $1618\text{ cm}^{-1}$ , while the band at  $1233\text{ cm}^{-1}$  was attributed to C-N stretches. The peak at  $758\text{ cm}^{-1}$  was indicative of an ortho-disubstituted benzene ring. Finally the band at  $611\text{ cm}^{-1}$  was ascribed to C-H bending at the  $\alpha$  position.  $^1\text{H}$  NMR showed the H<sub>x</sub> and H<sub>x'</sub> protons appearing as a singlet at  $\delta$  7.01 ppm. The multiplets at  $\delta$  7.52 - 7.47 and  $\delta$  6.93 - 6.88 ppm each integrated as two protons. Because of the nature of the aromatic system these signals are each caused by two equivalent protons, and constitute an AA'BB' system. This arises from W coupling due to coupling between H<sub>B</sub>H<sub>B'</sub> and H<sub>A</sub>H<sub>A'</sub> protons. The singlet at  $\delta$  3.94 ppm indicated the N-substituted methyl protons.

$^{13}\text{C}$  NMR spectrum showed only five resonances for the nine carbons present in the molecule, thus implying some equivalence of the carbons. The methyl carbon on the nitrogen atom was clearly seen at  $\delta$ 37.45 ppm. The remaining four resonances were assigned as follows. The resonance



**Scheme 2.23:** Synthesis of N-methylisoindole

$\delta$ 124.61 ppm corresponds to the two equivalent bridging ring carbons C-8 and C-9; the two resonances at  $\delta$ 120.64 and  $\delta$ 119.38 ppm were attributed to the two sets of equivalent carbons of the six membered ring, namely the C-5, C-6 and C-4, C-7 respectively. Finally, the resonance at  $\delta$ 111.73 ppm was assigned to the two equivalent carbons, C-1 and C-3, of the five membered ring.

Like the parent system N-methylisoindole is also a  $\pi$ -excessive 10- $\pi$ -electron heteroaromatic system and is a resonance hybrid and can be represented in canonical forms of the various shown in figure 2.6, based on the canonical forms of isoindole reported by Bonnet *et al.* [7].

The mechanism proposed in this reaction is shown in scheme 2.24. It involves  $S_N2$  attack of the methylhydrazine on any one of the methylene carbon atoms to form a bromide salt. Subsequent loss of hydrogen bromide and intramolecular rearrangement with an  $S_N2$  attack of the other methylene carbon by the nitrogen atom, causes ring closure to give the isoindolinium salt (**58**). When this salt is treated with potassium hydroxide and heat, ammonia is evolved and the resulting isoindolinium salt undergoes loss of hydrogen bromide to give the desired N-methylisoindole (**24**).



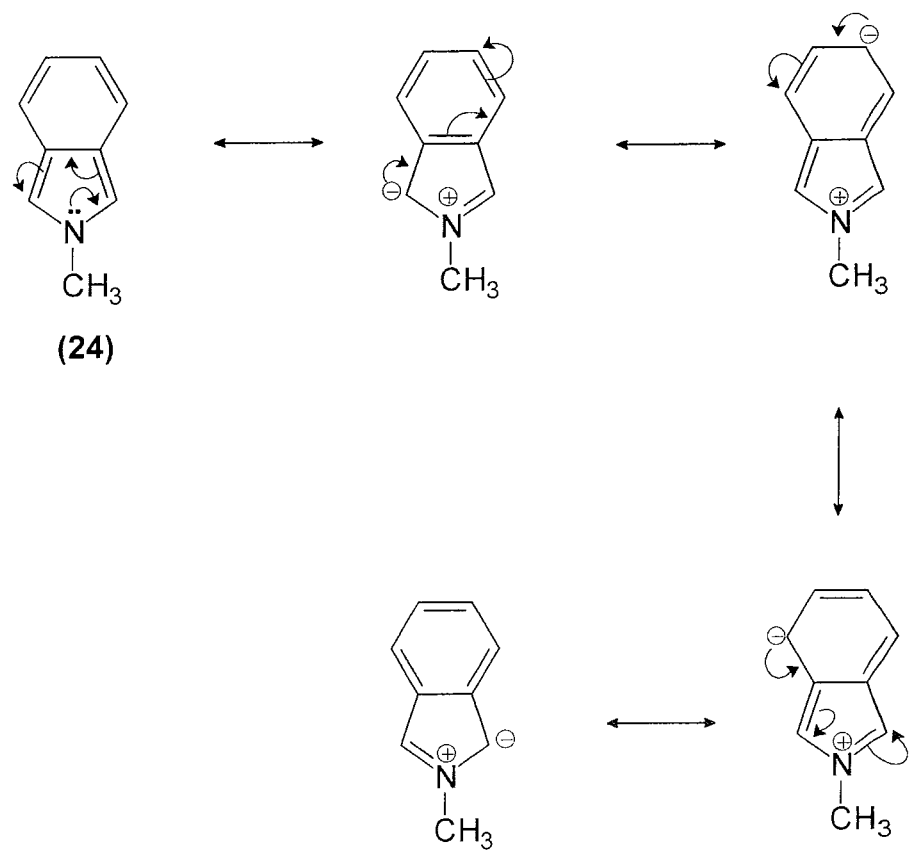
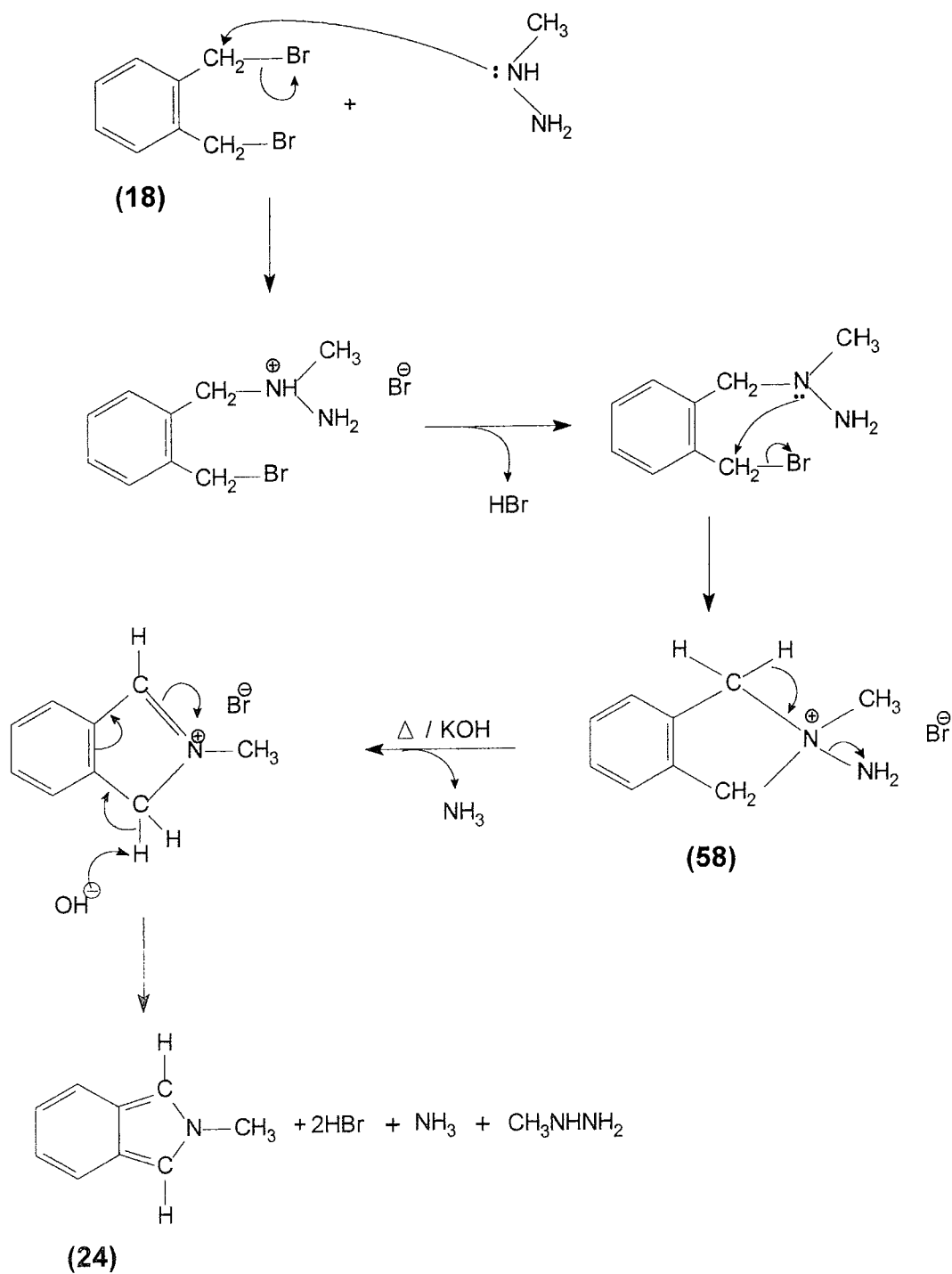


**Figure 2.6:** Canonical forms of N-methylisindole



**Scheme 2.24:** Mechanism for the formation of N-methylisoindole

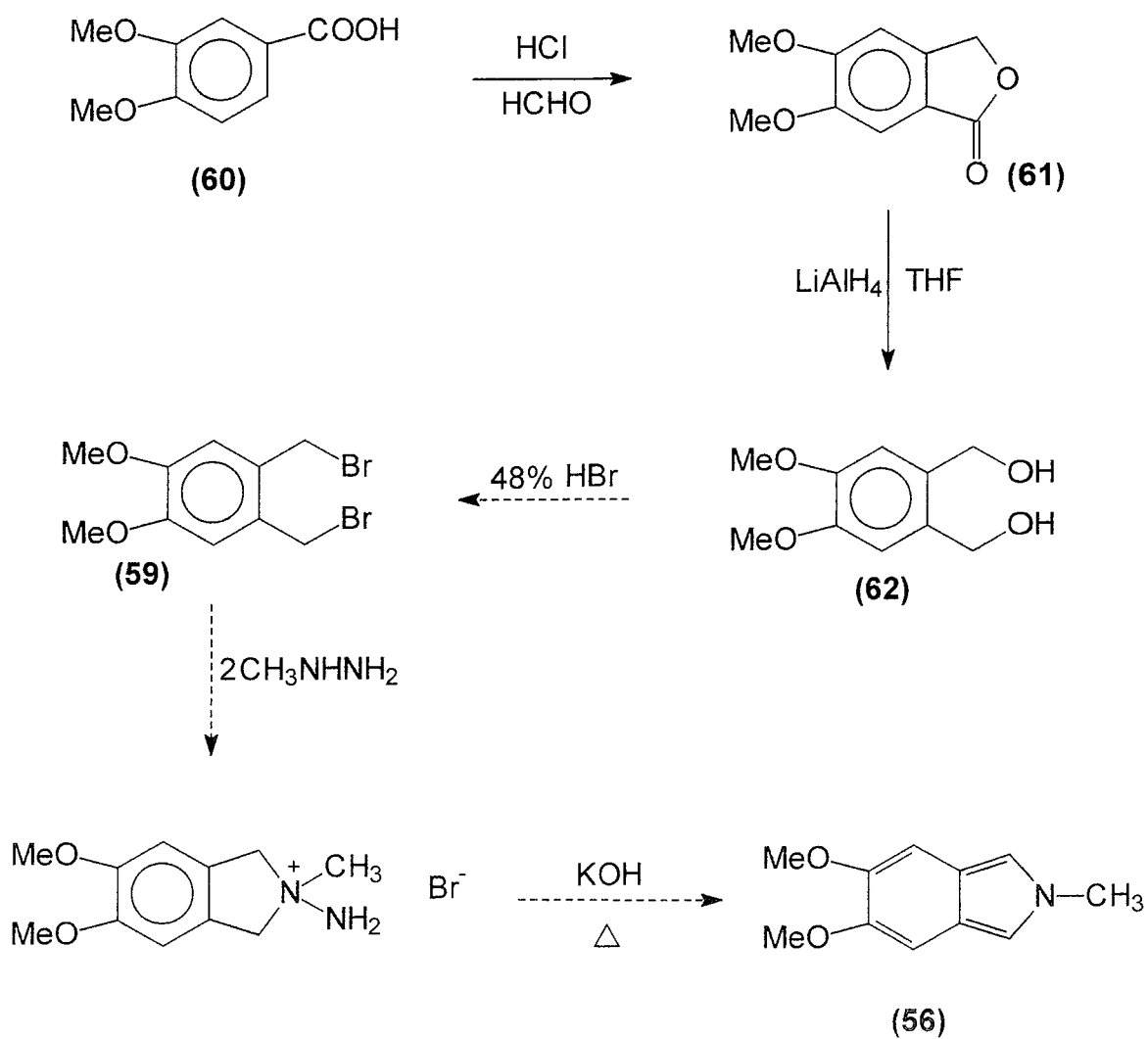
### 2.2.2 Strategic route to the formation of 5,6-dimethoxy-N-methylisoindole (56) and its synthesis.

It was thought that the formation of the target molecule, 5,6-dimethoxy-N-methylisoindole (56), which is an unknown compound, could be obtained following a similar route to that of N-methylisoindole, as shown in scheme 2.23. However, this would require the corresponding starting material 4,5-dimethoxy- $\alpha,\alpha'$ -dibromo-o-xylene (59). This compound is not readily available nor is it a known compound and thus needed to be synthesised. This was unlike the case for the starting material for N-methylisoindole, scheme 2.23, where  $\alpha,\alpha'$ -dibromo-o-xylene (18) was commercially available.

Bhattacharjee & Popp [47] reported that the chloromethylation of commercially available 3,4-dimethoxybenzoic acid (veratric acid) (60), scheme 2.25, gave the lactone 5,6-dimethoxyphthalide (61), which on reduction with lithium aluminium hydride in dry THF afforded 4,5-dimethoxyphthalyl alcohol (62), in an overall yield of 60%.

So far, this pathway still does not lead to the desired starting material (59), but if however the diol (62) were to be reacted with some brominating agent such as 48% hydrobromic acid, the corresponding  $\alpha,\alpha'$ -dibromo-o-xylene (59) should be obtained. For this reaction the bromination conditions need to be established, and this step will be commented in detail later on.

So now having established a route to the starting material (59) the synthesis of 5,6-dimethoxy-N-methylisoindole could be attempted via the multi-step route shown in scheme 2.25; the dashed arrows indicating new synthetic steps leading to new compounds. Each step of the synthetic route to the desired compound is discussed and a mechanism proposed. All the products formed were analysed using spectroscopic methods, including infrared, UV-vis,  $^1\text{H}$  NMR and  $^{13}\text{C}$  NMR spectroscopy.



**Scheme 2.25:** Strategic route to the formation of 5,6-dimethoxy-N-methylisoindole

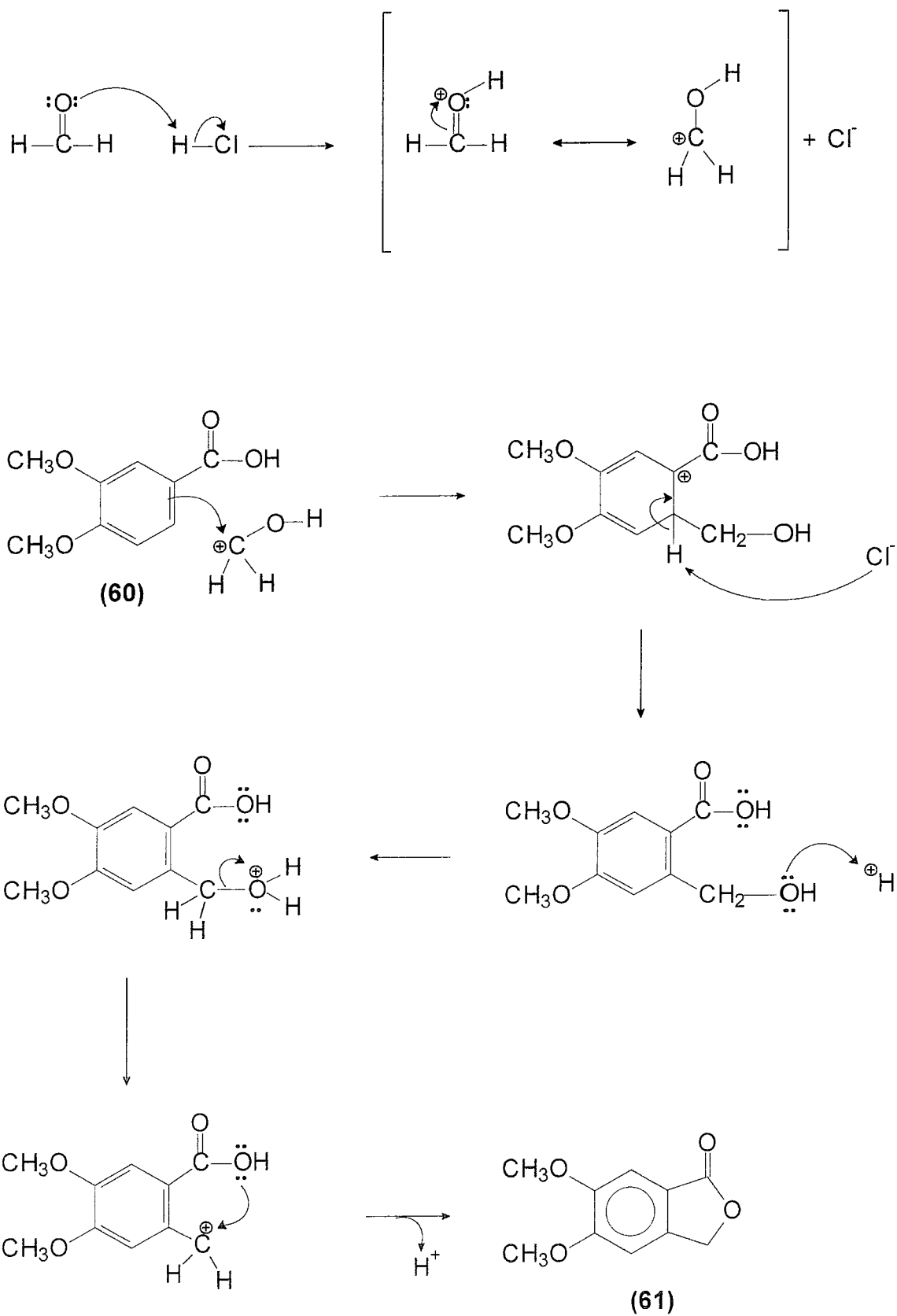
*(a) Formation of 5,6-dimethoxyphthalide (61)*

Following the Bhattacharjee & Popp method [47], chloromethylation of commercially available 3,4-dimethoxybenzoic acid (veratric acid) (**60**) as in scheme 2.25, by reaction of an aqueous solution of 40% formaldehyde with hydrogen chloride gas for seven hours and recrystallisation from methanol, gave the lactone, 5,6-dimethoxyphthalide (**61**), 50% m.p. 146 – 148°C [lit. [47], 66%, m.p. 151 – 154 °C].

The product was characterised by infra-red and nuclear magnetic resonance spectroscopic data (Appendix B). The infra-red spectrum of 5,6-dimethoxyphthalide showed a strong signal at 1753 cm<sup>-1</sup> which was attributed to C=O stretch of the cyclic ester. The band at 1249cm<sup>-1</sup> was due to C-O-C symmetric stretch and 1044 cm<sup>-1</sup> was due to asymmetric stretching of the methoxy carbon-oxygen bond.

No previous literature NMR data has been reported on this compound. <sup>1</sup>H NMR showed two singlets at δ 7.26 and δ6.97 each integrated for one aromatic proton corresponding to (H-7) & (H-4). The resonance at δ5.23 ppm was due to the two methylene protons. The two singlets at δ3.99 and δ3.94 ppm each integrated for three protons and were due to the two methoxy groups. <sup>13</sup>C NMR spectrum of (**61**) showed ten resonances accounting for each of the ten carbons in the compound and was assigned as follows: δ171.33 ppm was due to the carbonyl carbon of the cyclic ester. The resonances at δ154.68 (C-6), δ150.19, (C-5), δ141.02 (C-8), δ117.25 (C-9), δ105.67 (C-7), δ10.338 (C-4) ppm account for the benzoidal ring carbons. Finally the methylene carbon of the cyclic ester resonated at δ68.97 ppm .

The mechanism for the formation of the substituted phthalide (**61**) is proposed as shown in scheme 2.26. Protonation of formaldehyde produces a hydroxymethyl cation, which can exist as two resonance forms. This is then attacked by the electron rich aromatic ring. Removal of proton generates a dimethoxy acid - alcohol. Protonation of the alcohol followed by



**Scheme 2.26:** Mechanism for the formation of 5,6-dimethoxyphthalide

loss of water gives the primary carbocation, as shown. This, on nucleophilic attack by the acid hydroxyl group, followed by loss of a proton gives the lactone (**61**).

*(b) Formation of 4,5-dimethoxyphthalyl alcohol (62)*

Using the Bhattacharjee and Popp [47] method, 5,6-dimethoxyphthalide (**61**) was reduced using lithium aluminium hydride in dry tetrahydrofuran. Recrystallisation of the crude material from toluene gave 4,5-dimethoxyphthalyl alcohol (**62**) in a 66% yield, m.p. 110 – 112 °C, [lit. [47], 91%, m.p. 110 - 111°C], and structure was confirmed by spectroscopic analysis (see Appendix C).

The infra-red showed rather unexpectedly sharp bands at 3463 cm<sup>-1</sup> and 3341 cm<sup>-1</sup> for the O-H stretches of the alcohol group. <sup>1</sup>H NMR showed a singlet at δ6.85 ppm integrated for the two aromatic protons H-3 and H-6. The fine doublet at δ4.58ppm (J = 5.2Hz) was attributed to the two equivalent sets of methylene protons and on a D<sub>2</sub>O shake collapsed to a singlet, suggesting that the methylene protons are weakly coupled to the alcohol proton. The resonance at δ3.61ppm was due to the alcohol proton which disappeared on a D<sub>2</sub>O shake. Finally the singlet at δ3.86ppm, integrated for six protons, was attributed to the six methoxy protons.

<sup>13</sup>C NMR showed five resonances accounting for a ten carbon symmetrical system, and were assigned as follows: δ148.31ppm was due to the two quaternary carbons C-4 and C-5 bonded to the methoxy groups, while δ131.91ppm was due to the two quaternary carbons C-1 and C-2 bonded to the alcohol groups. The other two ring carbons C-3 and C-6 accounted for the resonance at δ113.08ppm. The side chain methylene carbons resonated at δ68.31 and the methoxy at δ55.89ppm.

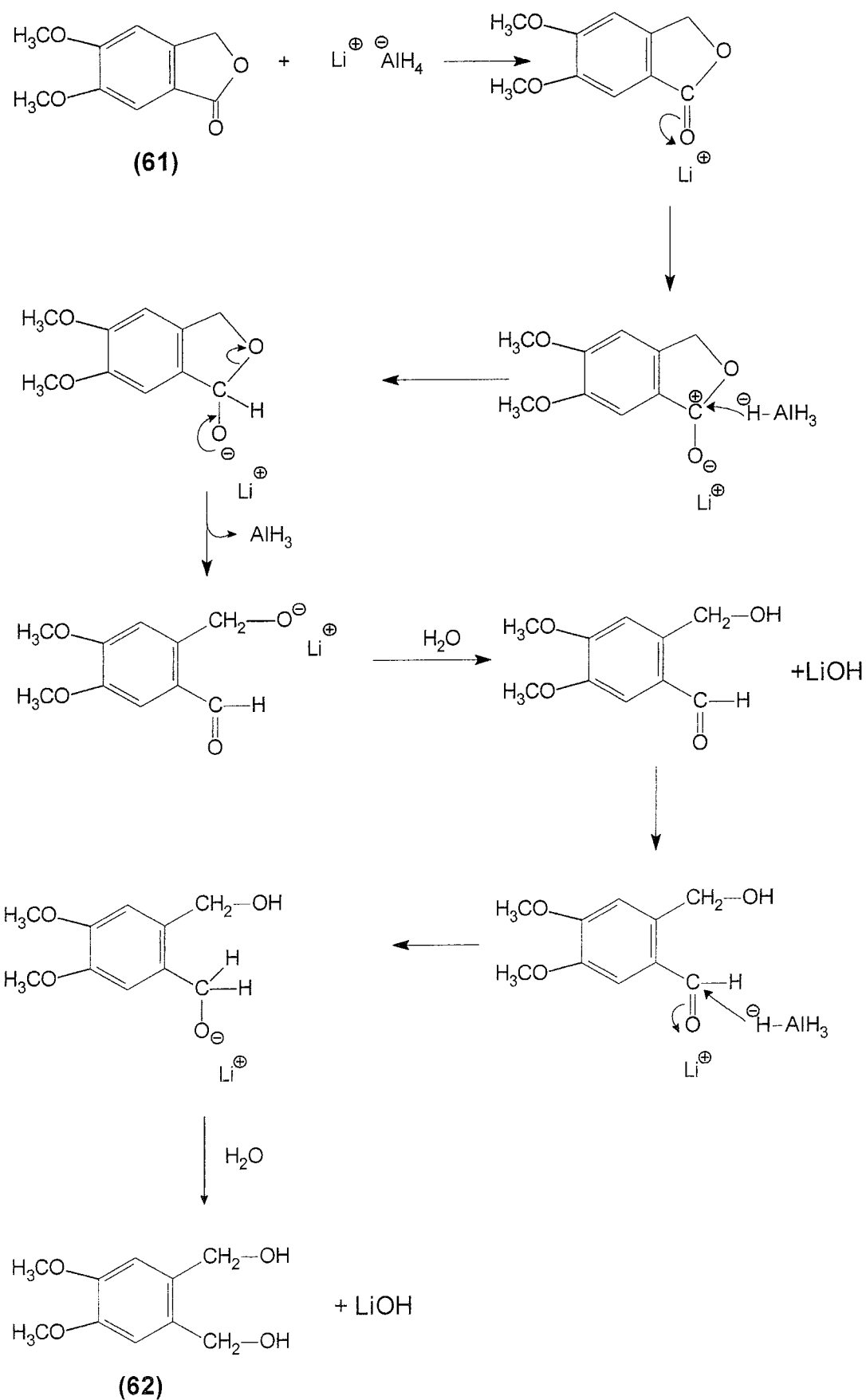
A proposed mechanism for the formation of 4,5-dimethoxyphthalyl alcohol (**62**) is shown in scheme 2.27. The  $\text{Li}^+$  ion coordinates with the carbonyl oxygen and on electron rearrangement forms the carbocation as shown. Attack by the hydride anion from  $\text{AlH}_4^-$  and subsequent ring opening by electron rearrangement results in aldehyde formation and the salt of the alcohol. Protonation (presumably with water) then gives the free alcohol. Finally the aldehyde group is then reduced to a primary alcohol on attack by another hydride ion as shown, which again on protonation with water gives the dimethoxy diol (**62**).

In order to set reaction conditions for the conversion of 4,5-dimethoxyphthalyl alcohol (**62**) to 4,5-dimethoxy- $\alpha,\alpha'$ -dibromo-o-xylene (**59**) it was decided to carry out the bromination of the unsubstituted diol (**63**) which should give the known brominated compound  $\alpha,\alpha'$ -dibromo-o-xylene (**18**) as shown in scheme 2.28. Furthermore literature methods have not synthesised the latter by this route.

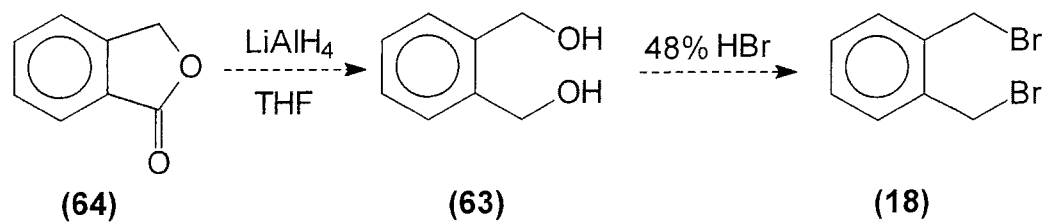
By analogy to the Bhattacharjee & Popp method [47], for the reduction of (**61**) to (**62**) the reduction of the analogous substituted lactone, phthalide (**64**) (commercially available) with lithium aluminium hydride in dry tetrahydrofuran was found to yield o-xylene- $\alpha,\alpha'$ -diol (**63**) in an 83% yield, m.p. 63.4 – 65.2°C [lit. [48], 63 - 65°C]. Subsequent bromination of (**63**) by modifying the Vogel method [49], with 48% hydrobromic acid and concentrated sulphuric acid yielded  $\alpha,\alpha'$ -dibromo-o-xylene (**18**) in an 85% yield, m.p. 92.9 - 95.7°C [lit.[48], 92 - 94°C]. This was identical to an authentic sample of (**18**) (purchased [48]) by comparison of its spectroscopic data.

Thus having set conditions for the conversion of (**64**) to (**18**), scheme 2.28, it was now possible to proceed with the synthesis of the desired 5,6-dimethoxy-N-methylisoindole (**56**), by first synthesising the desired starting material 4,5-dimethoxy- $\alpha,\alpha'$ -dibromo-o-xylene, as shown in scheme 2.25.





**Scheme 2.27:** Mechanism for the formation of 4,5-dimethoxyphthalyl alcohol



**Scheme 2.28:** Synthesis of  $\alpha, \alpha'$ -dibromo-*o*-xylene

(c) *Formation of 4,5-dimethoxy- $\alpha,\alpha'$ -dibromo-o-xylene (59)*

4,5-dimethoxyphthalyl alcohol (**62**) was brominated by modifying the Vogel method [49] used to brominate the unsubstituted diol (**63**). On reaction of (**62**) with 48% hydrobromic acid and concentrated sulphuric acid for 1½ hours yielded the previously unreported 4,5-dimethoxy- $\alpha,\alpha'$ -dibromo-o-xylene (**59**), 90%, m.p. 104.5 – 106.6 °C. Elemental analysis indicates an empirical formula of C<sub>10</sub>H<sub>12</sub>Br<sub>2</sub>O<sub>2</sub>, % calculated C 37.12, H 3.70, Br 49.38, O 9.90, % found C 37.36, H 3.66, Br 49.05, O 9.93.

The infra-red spectrum (Appendix D) of 4,5-dimethoxy- $\alpha,\alpha'$ -dibromo-o-xylene showed a strong CH<sub>2</sub> wagging band observed for -CH<sub>2</sub>Br group at 1203 cm<sup>-1</sup>, and the absence of an O-H absorbance indicative of the starting material. <sup>1</sup>H NMR showed a simple spectrum consisting of only three separate singlets. The singlet at  $\delta$ 6.84 ppm was due to the two aromatic protons H-3 and H-6. The singlet at  $\delta$ 4.63 ppm, integrated for four protons and were attributed to the methylene protons. Finally the singlet at  $\delta$ 3.89 ppm was due to the six methoxy protons as shown in figure 2.7. <sup>13</sup>C NMR showed five resonances accounting for a ten carbon symmetrical system as did the diol, and were assigned as follows:  $\delta$ 149.43 ppm was due to the two equivalent quaternary carbons C-4 and C-5 bonded to the methoxy groups, while  $\delta$ 129.01 ppm was due to the two quaternary carbons C-1 and C-2. The other two ring carbons were accounted for by the resonance at  $\delta$ 113.55 ppm C-3 and C-6. The side chain methylene carbons resonated at  $\delta$ 30.54 and the two methoxy groups at  $\delta$ 55.94 ppm. The assigned <sup>13</sup>C NMR data as shown in figure 2.8, is in agreement with computer [50] predicted values.

A mechanism for the reaction is outlined in scheme 2.29. Protonation of any one of the alcohol groups and subsequent attack by Br<sup>-</sup> in an S<sub>N</sub>2 type manner on the methylene carbon results in the loss of H<sub>2</sub>O (which is a good leaving group) to form a haloalkane side chain. The same process occurs with the second alcohol group. The concentrated sulphuric acid acts as a strong dehydrating agent and removes the water formed in the reaction.

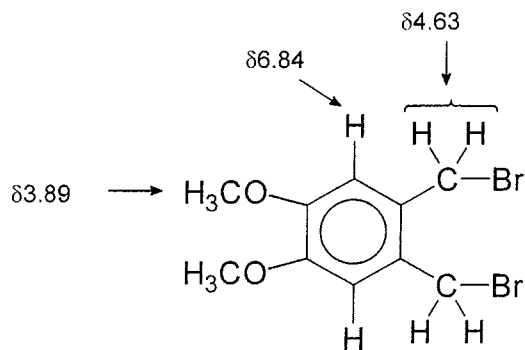


**Figure 2.7:**  $^1\text{H}$  NMR data of 4,5-dimethoxy- $\alpha,\alpha'$ -dibromo-o-xylene  
(values in ppm)

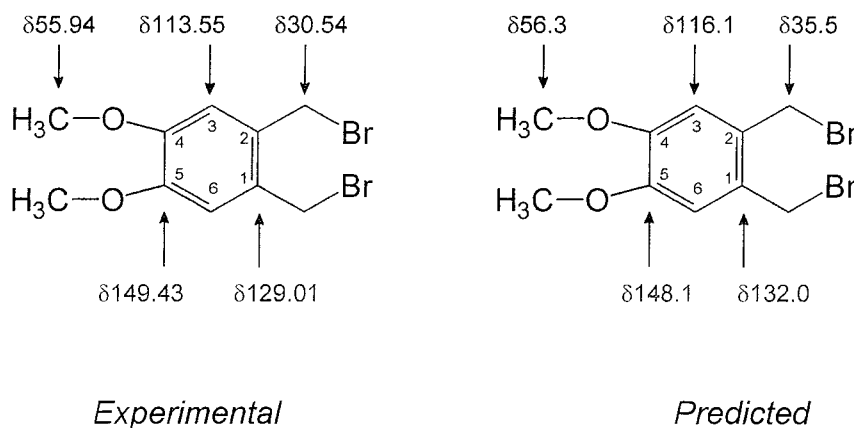
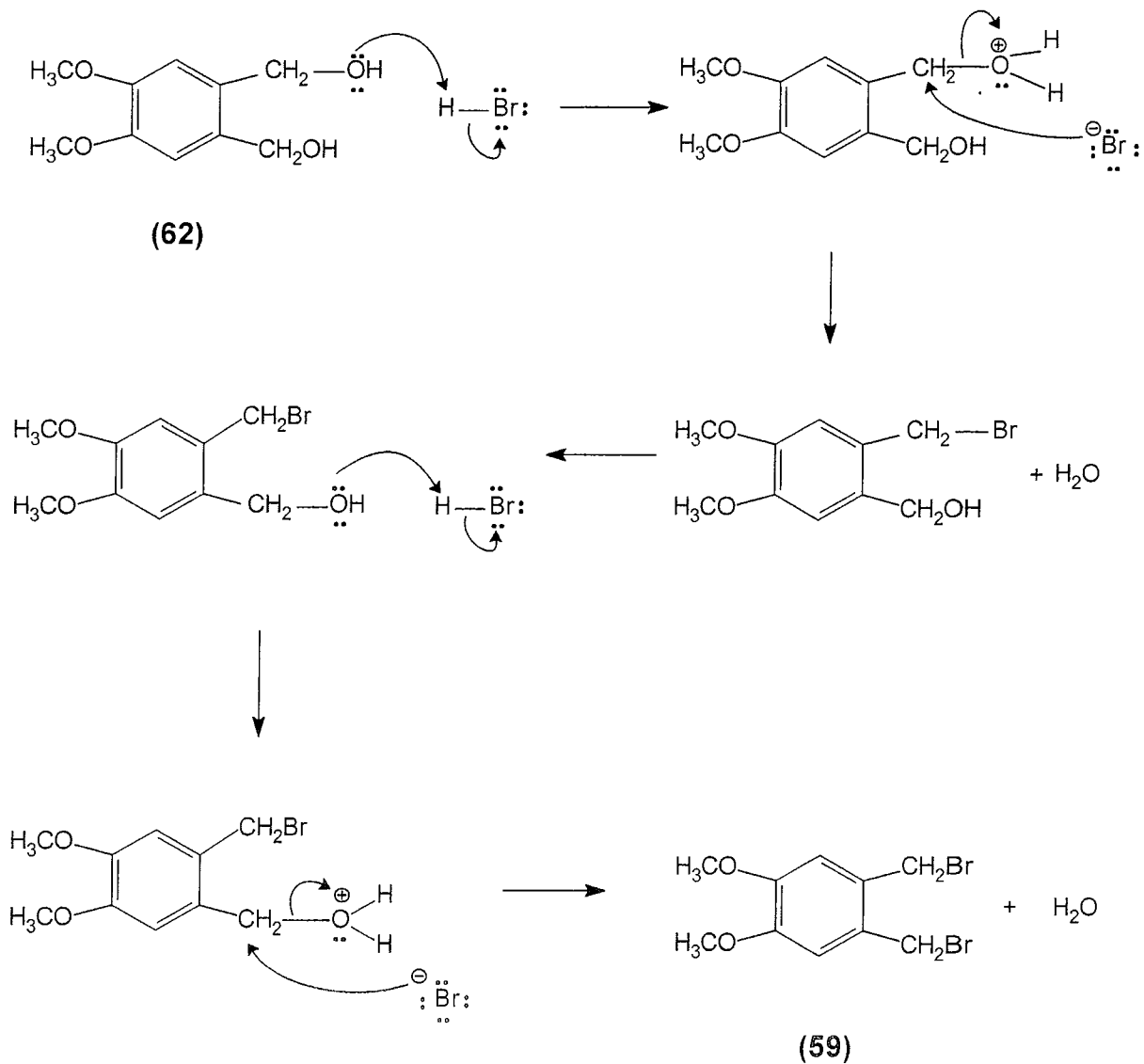


**Figure 2.8:** Experimental and predicted  $^{13}\text{C}$  NMR of 4,5-dimethoxy- $\alpha,\alpha'$ -  
dibromo-o-xylene (values in ppm)

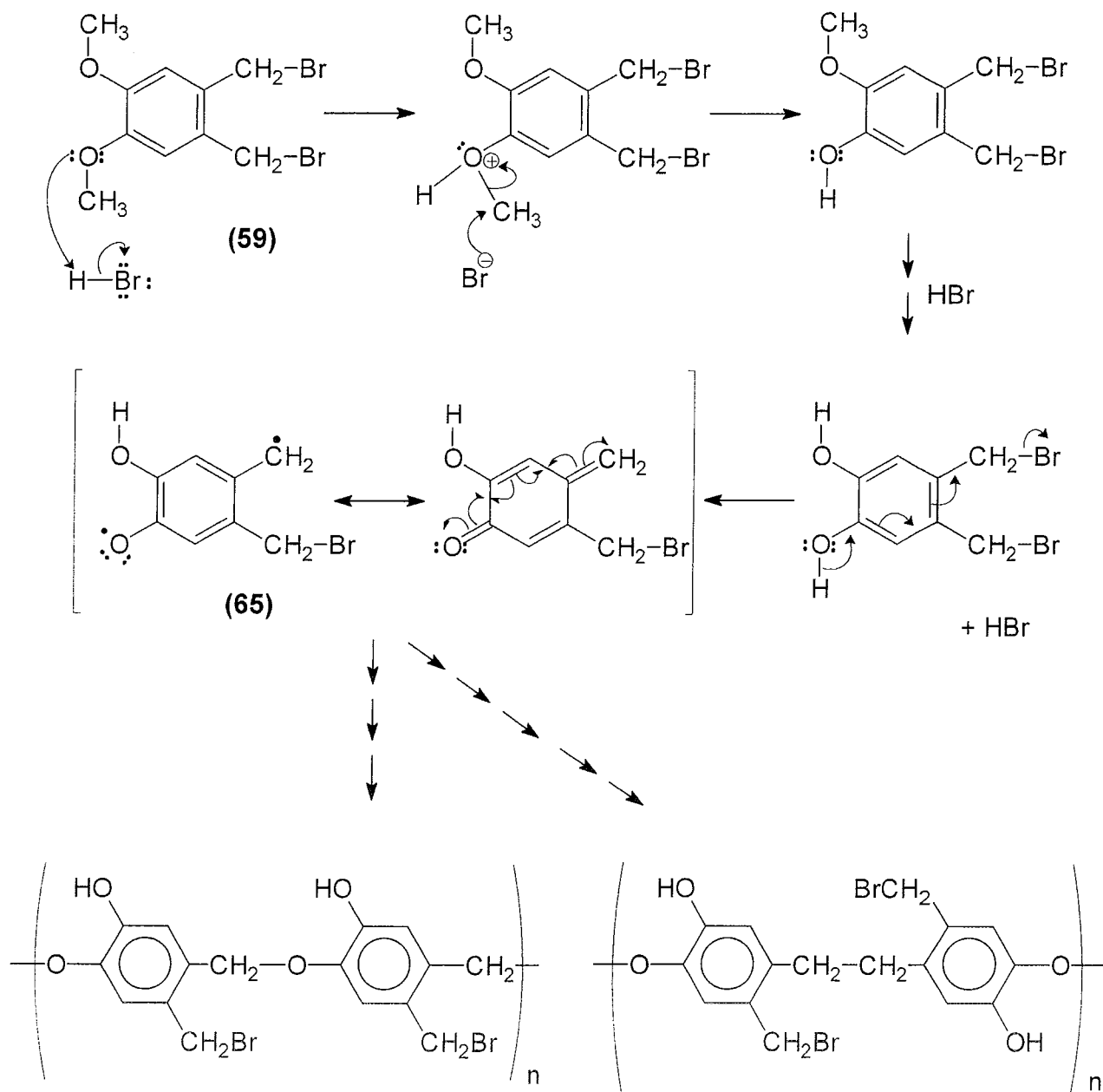


**Scheme 2.29:** Mechanism for the formation of 4,5-dimethoxy- $\alpha,\alpha'$ -dibromo-o-xylene

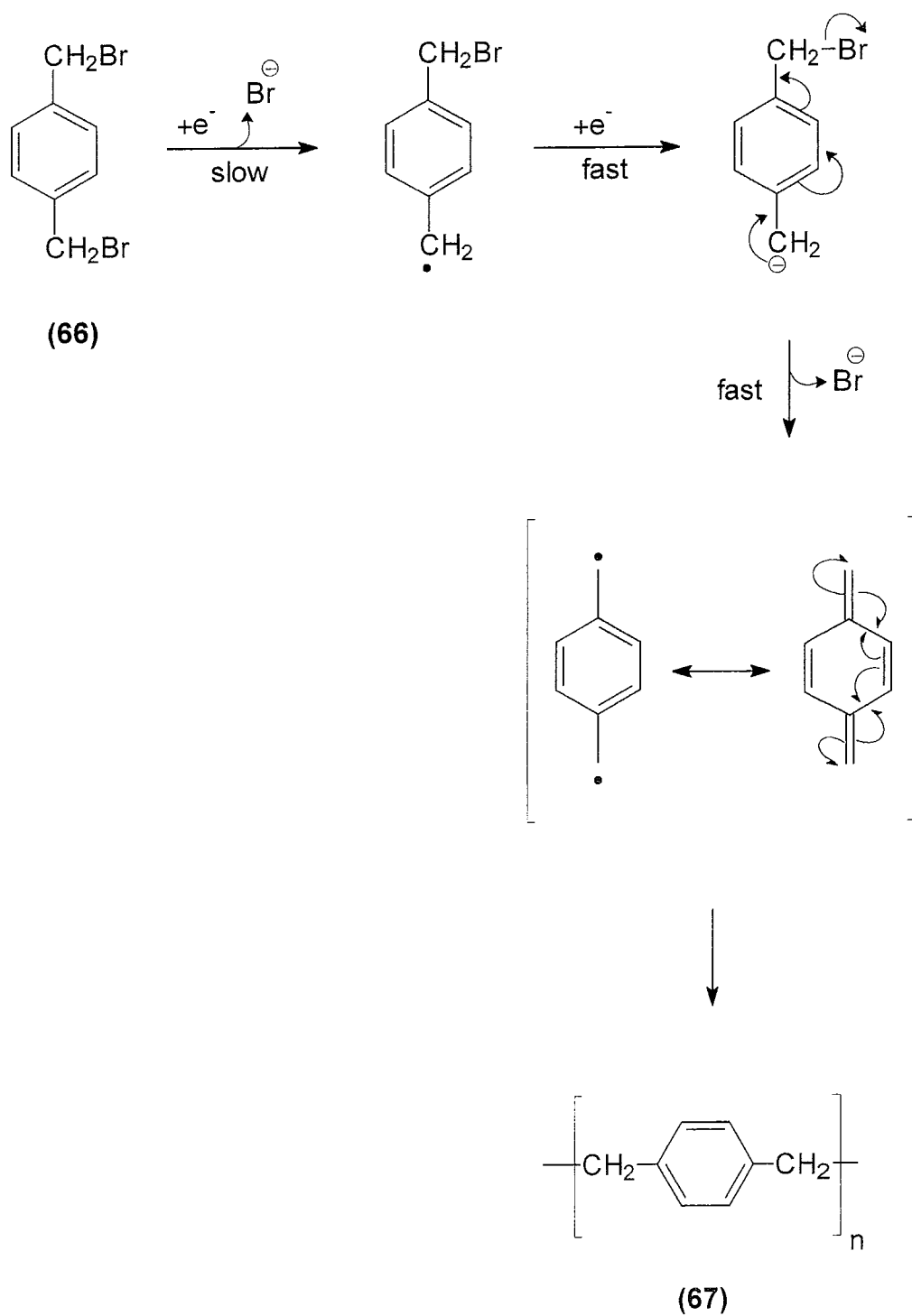
Initially the bromination of 4,5-dimethoxyphthalyl alcohol (**62**) was carried out under the same reaction conditions that were established for the bromination of o-xylene- $\alpha,\alpha'$ -diol (**63**) to form  $\alpha,\alpha'$ -dibromo-o-xylene (**18**). In the latter reaction, 48% hydrobromic acid and concentrated sulphuric acid was added neat to the starting material (**63**) and proved very successful with a 85% yield. However upon repeating under the same reaction conditions for 4,5-dimethoxyphthalyl alcohol (**62**) a black material was produced as soon as the reagents were mixed. This was over come, by further modifying the Vogel method [49] by making the addition with 4,5-dimethoxyphthalyl alcohol to 48% hydrobromic acid and concentrated sulphuric acid in ethanol and the desired product (**59**) was successfully formed, in a 90% yield.

While the unsubstituted dibromo-o-xylene did not produce a black material on reaction with the acids as discussed previously; it is believed that the presence of the electron donating methoxy substituents can lead to a number of possible undesired reactions. Firstly, there is the possibility that the product is forming immediately and subsequent acid cleavage of this alkyl aryl ether occurs, as shown in scheme 2.30. The diradical (**65**) formed could polymerise to form either of the two polymers as illustrated. It has been reported [51, 52], that  $\alpha,\alpha'$ -dibromo-*para*-xylene (**66**) upon electrochemical reduction forms a diradical which can polymerise to give a white polymer poly-o-xylylene (**67**) by the mechanism shown in scheme 2.31. Therefore the electron-donating effect of the methoxy groups has a similar effect as electron donation with an electrochemical reduction.

There is also the possibility that 4,5-dimethoxy- $\alpha,\alpha'$ -dibromo-o-xylene can form the diradical as shown in scheme 2.32 and can react with itself in a manner similar that shown for the electrochemical polymerisation of (**66**). Therefore it is believed that this new compound (**59**), while formed successfully must be treated carefully as it appears to be rather unstable and can lead to a possible number of polymerisation reactions as discussed.

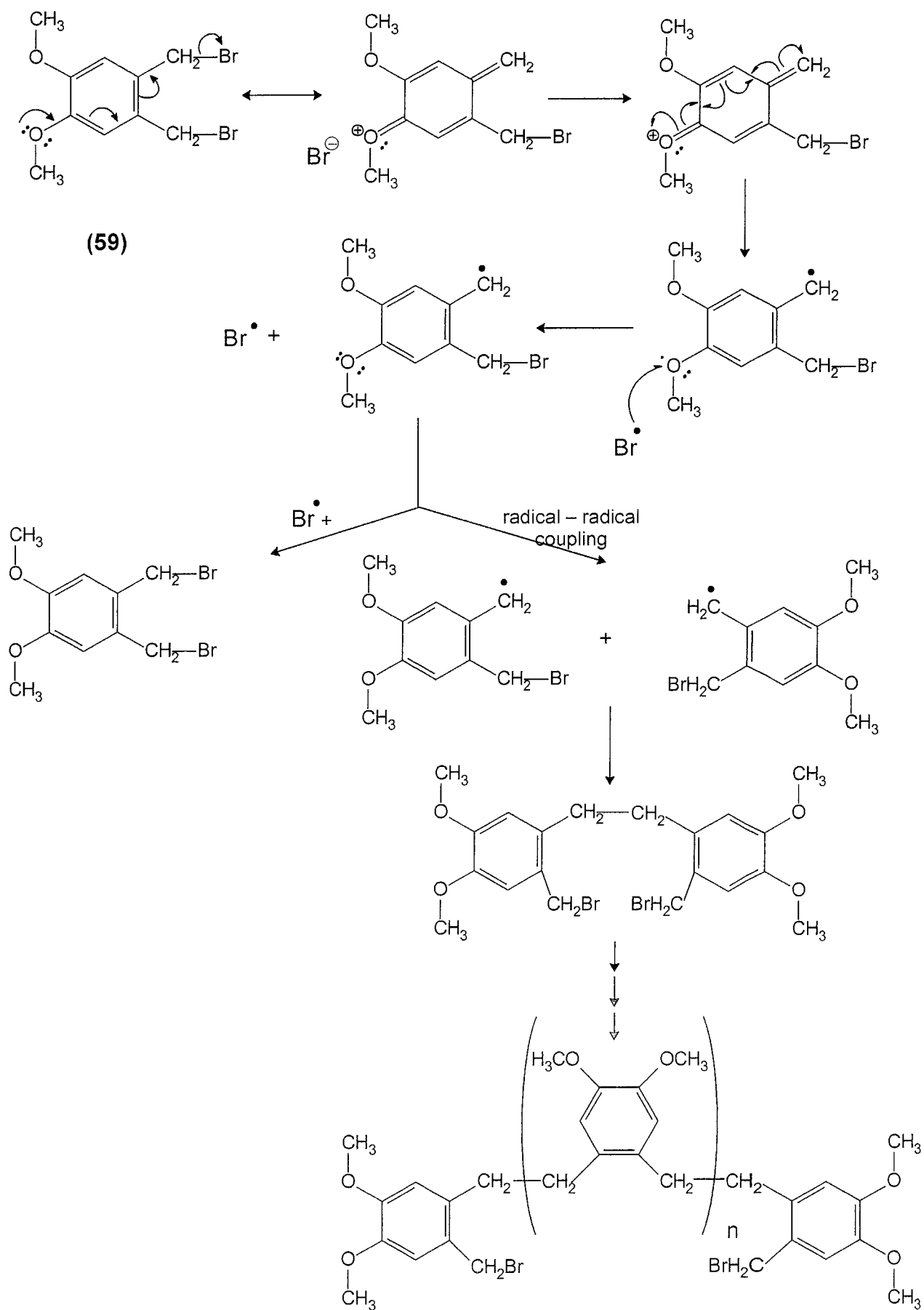


**Scheme 2.30:** Proposed mechanism for the acid cleavage of 4,5-dimethoxy- $\alpha,\alpha'$ -dibromo-o-xylene



**Scheme 2.31:** Mechanism for the electrochemical reduction of  $\alpha, \alpha'$ -dibromo-*para*-xylene





**Scheme 2.32:** Proposed mechanism for the formation 4,5-dimethoxy- $\alpha,\alpha'$ -dibromo-o-xylene diradical and subsequent polymerisation

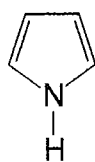
(d) Formation of 5,6-dimethoxy-N-methylisoindole (**56**)

The attempted synthesis of 5,6-dimethoxy-N-methylisoindole was carried out as per the synthesis of N-methylisoindole using the method by Zeeh & König [22], see scheme 2.25. This was done by first reacting 4,5-dimethoxy- $\alpha,\alpha'$ -dibromo-o-xylene (**59**) with methylhydrazine to give the corresponding isoindolinium salt. The product was eliminated by the reaction of the salt with excess base and heat and collected by simultaneous sublimation and was obtained in a 25% yield, m.p. 53-58 °C. The product is somewhat less stable than N-methylisoindole and any elemental analysis attempted gave results outside the acceptable limits. It is believed that the product becomes resinous before an accurate analysis was possible.

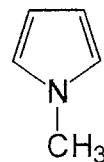
The product structure was confirmed by spectroscopic analysis (Appendix E). The infrared spectrum showed ring C=C stretches at 1504  $\text{cm}^{-1}$ , while the band at 1213  $\text{cm}^{-1}$  was attributed to C-N stretches. The stretch at 1014  $\text{cm}^{-1}$  was due to asymmetric stretching of the methoxy carbon-oxygen bond.

The UV-vis spectrum showed a strong absorption at  $\lambda_{\text{max}}$  222nm attributed to the aromatic  $\pi\text{-}\pi^*$  transition. The  $\lambda_{\text{max}}$  observed for N-methylisoindole was at 224nm showing only a small hypsochromic shift of the  $\lambda_{\text{max}}$  with the addition of the two methoxy groups. UV-vis data reported by Merz *et al.* [53] on pyrrole (**3**) and N-methylpyrrole (**68**) compared with that of 3,4-dimethoxypyrrole (**69**) and 3,4-dimethoxy-N-methylpyrrole (**70**), is shown in table 2.1 and figure 2.9. Their data showed hypsochromic shift in  $\lambda_{\text{max}}$  between (**3**) and (**69**) and on the other hand a relatively large bathochromic shift with the introduction of the methoxy groups onto N-methylpyrrole. The UV-vis spectrum of 5,6-dimethoxy-N-methylisoindole also showed an additional broad transition at 325nm and also weak absorption at 297nm which was absent in the spectrum of N-methylisoindole.

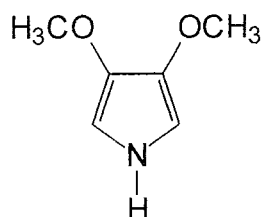
$^1\text{H}$  NMR spectrum of (**56**) displayed a simple spectrum with only three discrete singlets at  $\delta$ 3.88,  $\delta$ 6.77,  $\delta$ 6.86 with respective integration of 9 : 2 : 2.



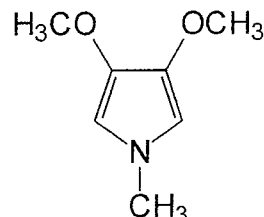
**(3)**



**(68)**



**(69)**



**(70)**

**Figure 2.9:** Methoxy substituted pyrrole and N-methylpyrrole

	<b>3</b>	<b>69</b>	<b>68</b>	<b>70</b>
UV-vis / $\lambda$ (nm) in CH <sub>3</sub> CN	215	212	208	222
$\delta$ - <sup>1</sup> H NMR (ppm) in CDCl <sub>3</sub>				
H-2	6.60	6.23	6.40	6.03
$\delta$ - <sup>13</sup> C NMR (ppm) in CDCl <sub>3</sub>				
C-2	117.3	99.6	122.7	103.4
C-3	107.6	138.1	109.5	137.2
OCH <sub>3</sub>		58.4		58.6
NCH <sub>3</sub>			36.6	36.8

**Table 2.1:** Summary of spectroscopic data of pyrrole and methoxy substituted pyrrole and N-methylpyrrole (**68-70**) (ref [53])

The singlet at  $\delta$ 3.88 was attributed the three N-methyl protons and the six methoxy protons, thus showing that the N-methyl and aromatic methoxy protons are in a similar chemical environment, see figure 2.10. The singlet at  $\delta$ 6.77 was assigned the  $\alpha$ ,  $\alpha'$  protons (H-1 and H-3) on the 5-membered ring and resonated more upfield than the corresponding protons in N-methylisindole at  $\delta$ 7.01. This could suggest a greater electron density at the C-1 and C-3 positions than the same positions in N-methylisindole.

This is in accordance with molecular orbital calculations [54] for N-methylisindole where the  $\pi$ -electron density is highest at the C-1 and C-3 positions, other than the N position, implying that these positions are the main reactive sites on the molecule. The more upfield value for these same protons in 5,6-dimethoxy-N-methylisindole implies an increase in electron density at these two positions on account of the electron donating effect of the methoxy groups. However, the question now arises is this electron donating effect through an inductive effect or through resonance?

Merz et al. [53], when looking at the effect of dimethoxy substitution at the 3,4 positions of pyrrole (**3**) and N-methylpyrrole (**68**), compared the C-2 proton chemical shift of (**3**) with 3,4-dimethoxypyrrole (**69**) and the C-2 proton chemical shift of (**68**) with 3,4-dimethoxy-N-methylpyrrole (**70**), see table 2.1, and saw that in both cases there was an upfield shift due to the methoxy groups. The authors' [53] suggested that this upfield shift at the  $\alpha$ -position points to a greater importance of the inductive effect over the mesomeric effect of the methoxy group. However this would suggest that the methoxy group is more electron donating through inductive effects which is incorrect as the resonance effect of the methoxy group on an aromatic system is far greater than the inductive effect. Therefore, the upfield shift of the H1 and H3 protons is believed to be mainly due to mesomeric effects.

$^{13}\text{C}$  NMR spectrum showed only six resonances for the eleven carbons present in the molecule, thus implying some equivalence of the carbons. The methyl carbon on the nitrogen atom was clearly seen at  $\delta$ 37.24 ppm.

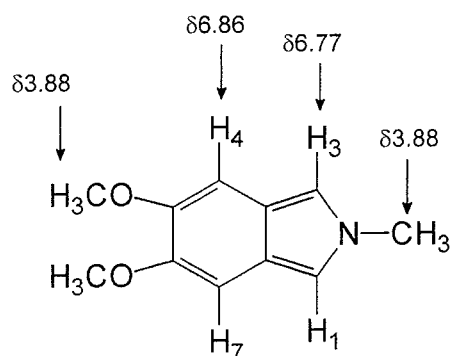


**Figure 2.10:**  $^1\text{H}$  NMR data of 5,6-dimethoxy-N-methylisindole  
(values in ppm)

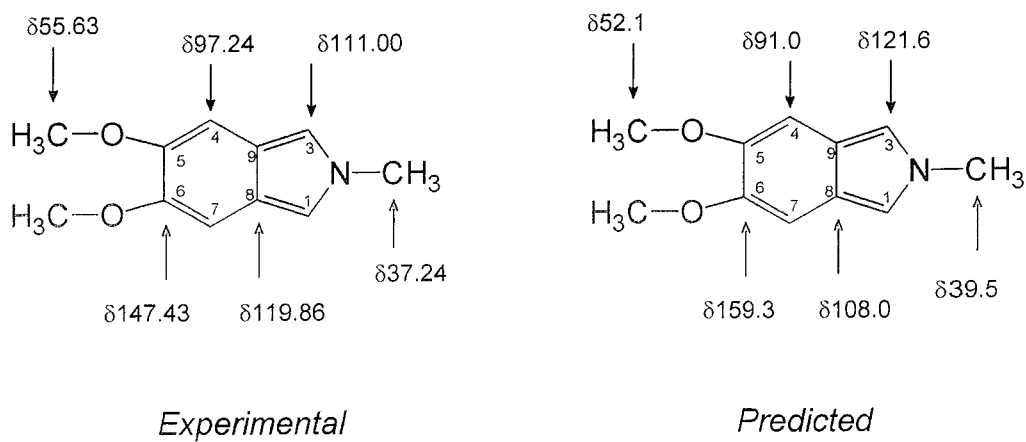


**Figure 2.11:** Experimental and predicted  $^{13}\text{C}$  NMR of 5,6-dimethoxy-N-methylisindole (values in ppm)

The remaining four resonances were assigned as follows. The resonance  $\delta 147.43$  ppm was due to the two quaternary carbons C-5 and C-6, while  $\delta 119.86$  ppm was due to the two equivalent bridging ring carbons C-8 and C-9. The resonance at  $\delta 111.00$  ppm was attributed to C-1 and C-3; the equivalent carbons in N-methylisoindole resonated at a very similar position  $\delta 111.73$  ppm. This is different to the effect observed by Merz *et al.* [54] where the C-2 carbons in both 3,4-dimethoxypyrrole (**69**) and 3,4-dimethoxy-N-methylpyrrole (**70**), resonated considerably upfield from pyrrole (**3**) and N-methylpyrrole (**68**), the same effect as in the proton spectra, see table 2.1. The resonance  $\delta 97.24$  ppm accounted for the other ring carbons C-4 and C-7, while the carbons of the methoxy groups resonated at  $\delta 55.63$  ppm. The assigned  $^{13}\text{C}$  NMR data as shown in figure 2.11, is in agreement with computer [50] predicted values.

Like isoindole and N-methylisoindole, 5,6-dimethoxy-N-methylisoindole is also a  $\pi$ -excessive 10- $\pi$ -electron heteroaromatic system and the various canonical forms are represented in figure 2.12, based on the canonical forms of isoindole reported by Bonnett *et al.* [7]. The mechanism for the reaction proposed is based on the mechanism for the formation for N-methylisoindole, scheme 2.33. Again it involves  $\text{S}_{\text{N}}2$  attack of the methylhydrazine on one of the methylene carbons to form a bromide salt. Subsequent loss of hydrogen bromide and intramolecular rearrangement with an  $\text{S}_{\text{N}}2$  attack of the other methylene carbon by the nitrogen atom, causes ring closure to give the isoindolinium salt. When this salt is treated with potassium hydroxide and heat, ammonia is evolved and the resulting isoindolinium salt undergoes loss of hydrogen bromide to give the desired 5,6-dimethoxy-N-methylisoindole.

The low yield has been attributed to a possible unwanted cleavage of the methoxy groups in the presence of the excess potassium hydroxide leading to the salt (**72**) or (**73**), as shown in scheme 2.34. The base cleavage of the methoxy group was independently examined whereby the starting material 3,4 dimethoxybenzoic acid (**60**) under basic conditions forms the salt (**74**), which is acidified to form 3,4-dihydroxybenzoic acid (**75**); see scheme 2.35.

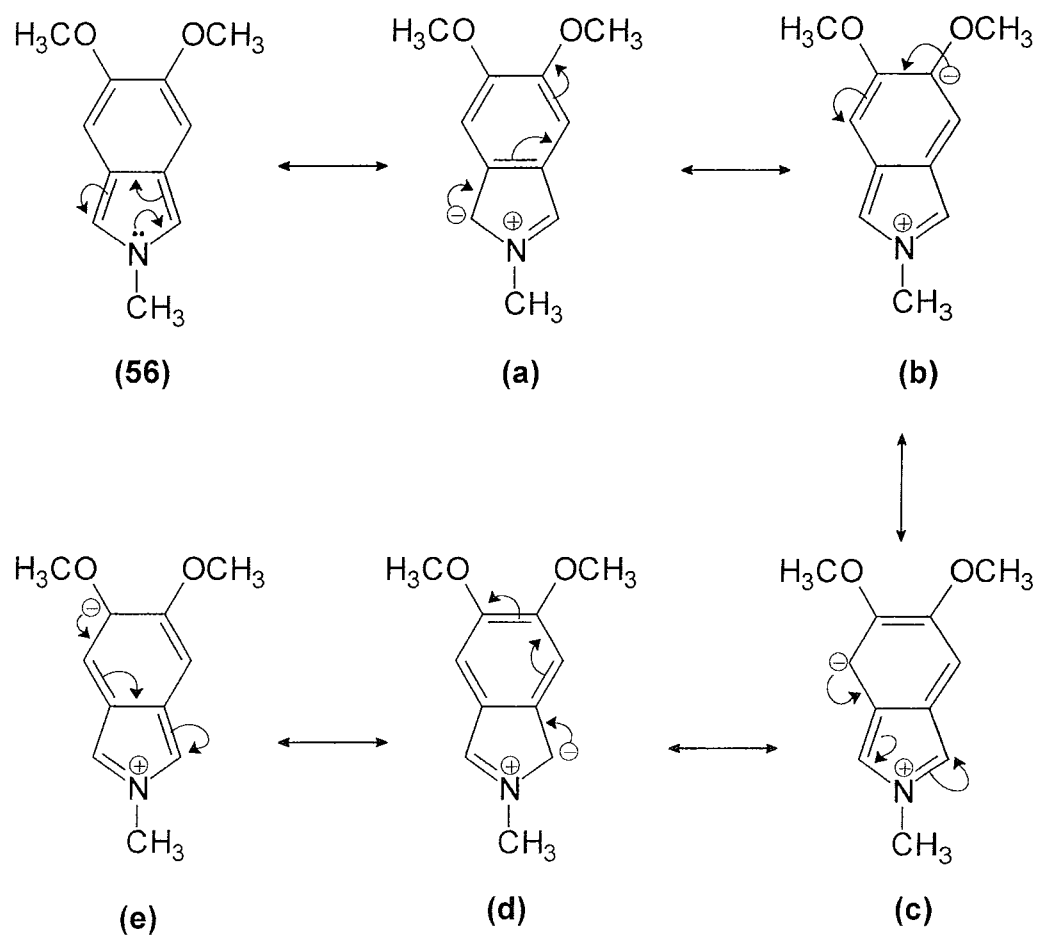
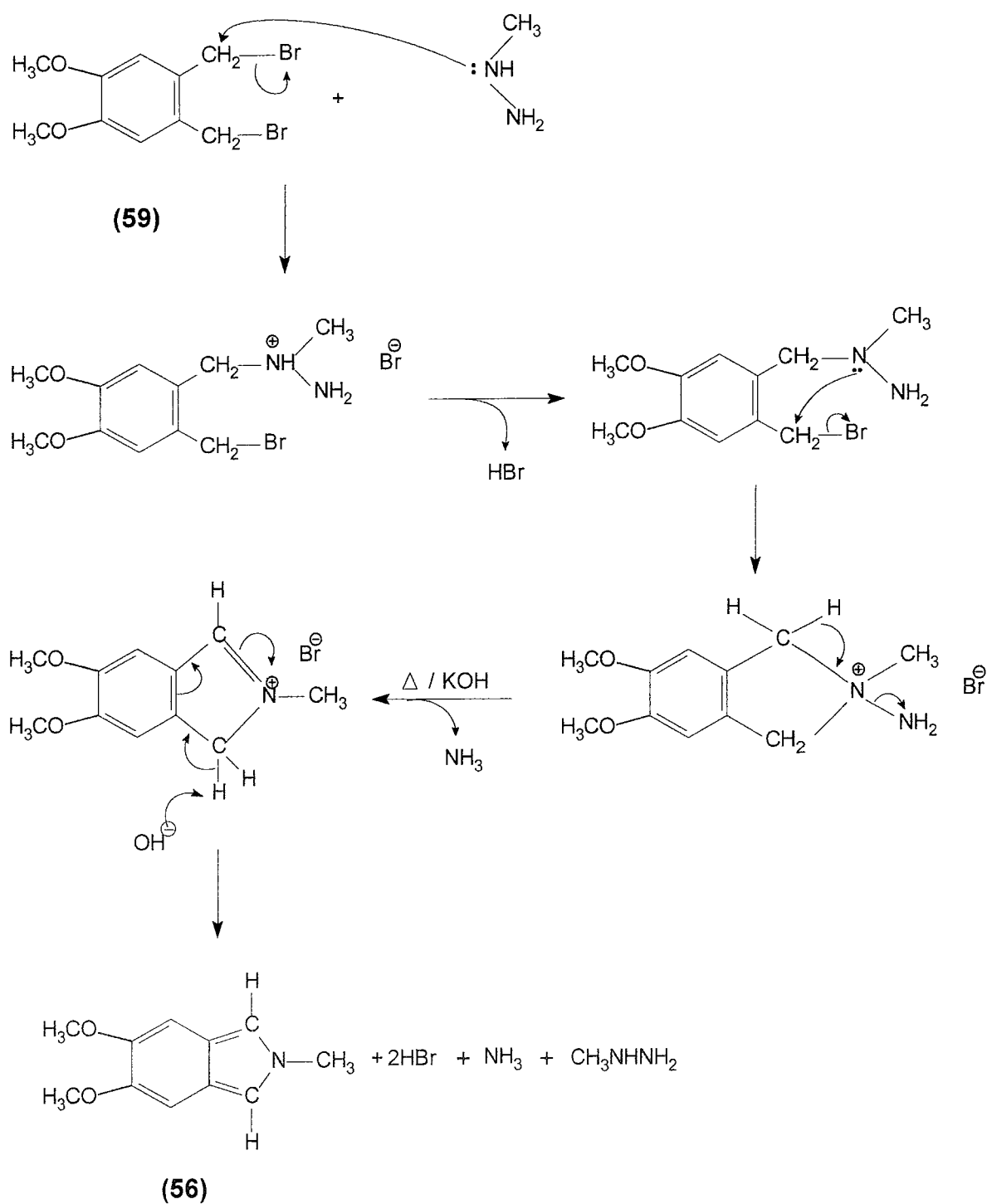
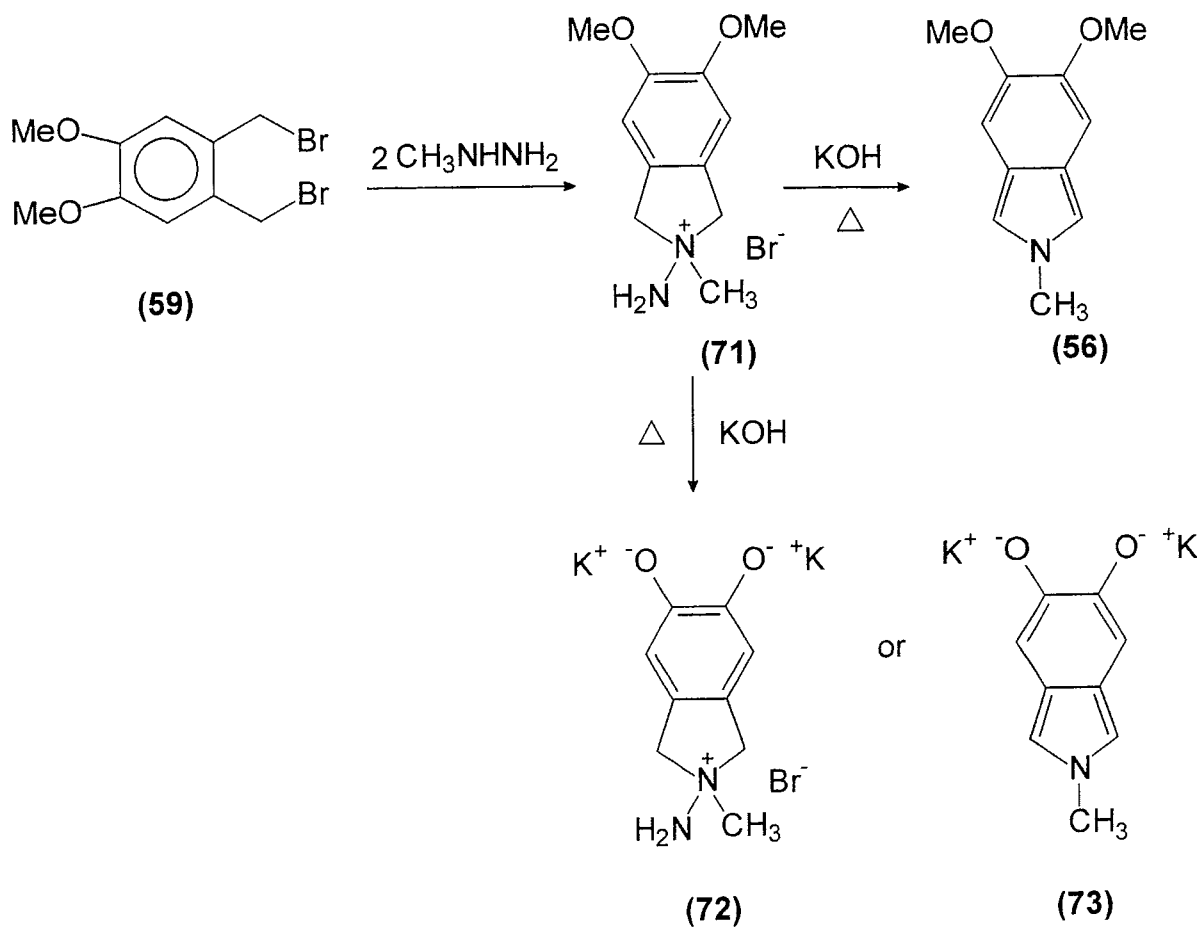


**Figure 2.12:** Canonical forms of 5,6-dimethoxy-N-methylisindole

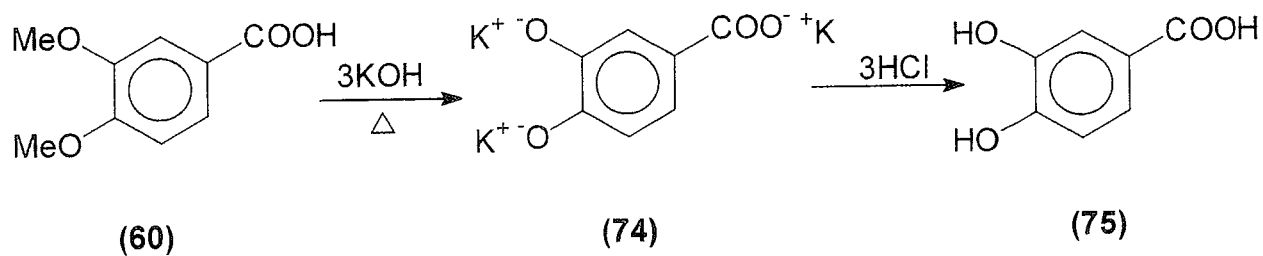


**Scheme 2.33:** Mechanism for the formation of 5,6-dimethoxy-N-methylisoindole





**Scheme 2.34:** Possible unwanted cleavage of the methoxy groups of 5,6-dimethoxy-N-methylisoindole

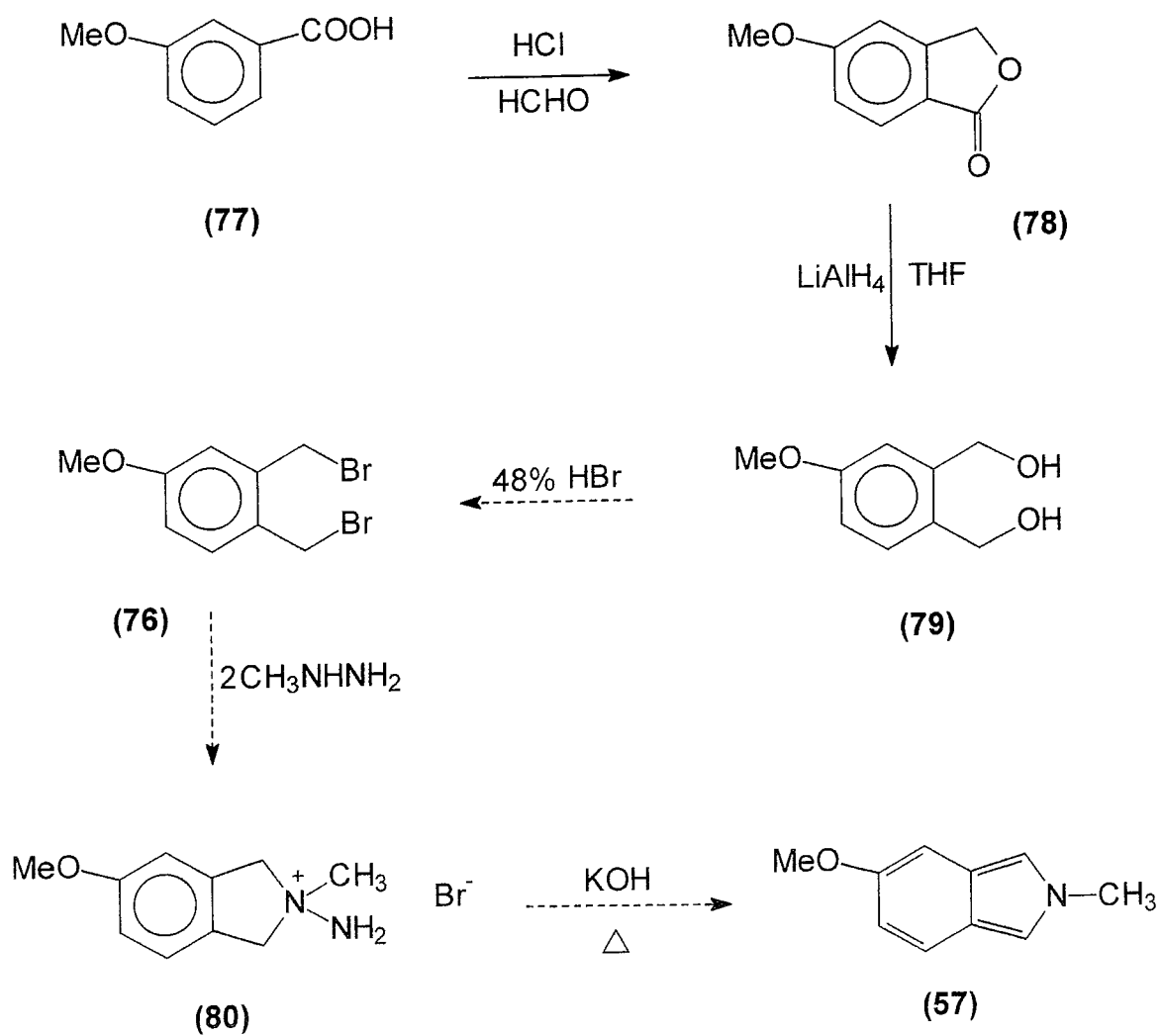


**Scheme 2.35:** Base cleavage of 3,4-dimethoxybenzoic acid.

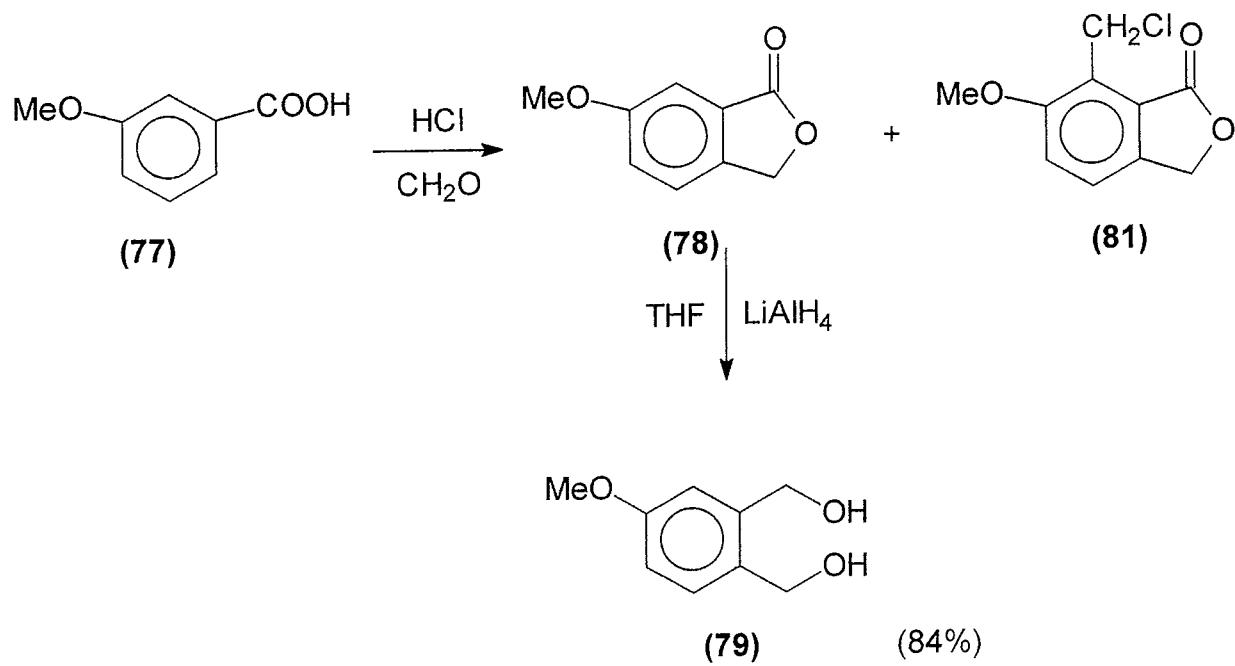
### 2.2.3 Strategic route to the formation of 5-methoxy-N-methylisoindole (**57**) and its synthesis.

Initially it was thought that 5-methoxy-N-methylisoindole (**57**) could be synthesised by a similar route to that used to form 5,6-dimethoxy-N-methylisoindole, as shown in scheme 2.36. This again would involve the synthesis a mono-methoxy substituted  $\alpha,\alpha'$ -dibromo-o-xylene, namely 4-methoxy- $\alpha,\alpha'$ -dibromo-o-xylene (**76**), which like 4,5-dimethoxy- $\alpha,\alpha'$ -dibromo-o-xylene was not commercially available and also needs to be synthesised. Thus again according to the Bhattacharjee & Popp [47] method, chloromethylation of commercially available m-methoxybenzoic acid (**77**), scheme 2.36, should give the lactone 5-methoxyphthalide (**78**), which would then yield the alcohol 4-methoxyphthalyl alcohol (**79**) on reduction with lithium aluminium hydride in dry THF. Then the alcohol could again be brominated to form the desired 4-methoxy- $\alpha,\alpha'$ -dibromo-o-xylene (**76**), leading to the formation of the isoindole (**57**) via the isoindolinium salt (**80**) in the same manner as outlined in scheme 2.36.

Indeed the first reaction in the multistep pathway whereby m-methoxybenzoic acid (**77**) readily condenses with formaldehyde in the presence of HCl to form 5-methoxyphthalide (**78**) had already been reported [55] but the yield obtained was unspecified. Therefore the procedure was repeated as described in the literature [55]. The reaction was carried out many times with varying reaction conditions. The crude yields were repeatedly around 25% and after purification by recrystallisation the yield was reduced to about 17%. The low yields were attributed to the formation of an undesirable second product (**81**) as reported by Bhattacharjee & Popp [47], scheme 2.37. This report also did not specify a yield for this reaction but did however carry out the following reaction whereby the reduction of 5-methoxyphthalide (**78**), with lithium aluminium hydride in dry THF gave 4-methoxyphthalyl alcohol (**79**) in an 84% yield. However, as the first reaction was only the first reaction of a proposed 5-step route to the isoindole, and the yield being so low this route was abandoned, as it would lead the overall yield being unacceptably low.



**Scheme 2.36:** Proposed strategic route to the formation of 5-methoxy-N-methylisindole

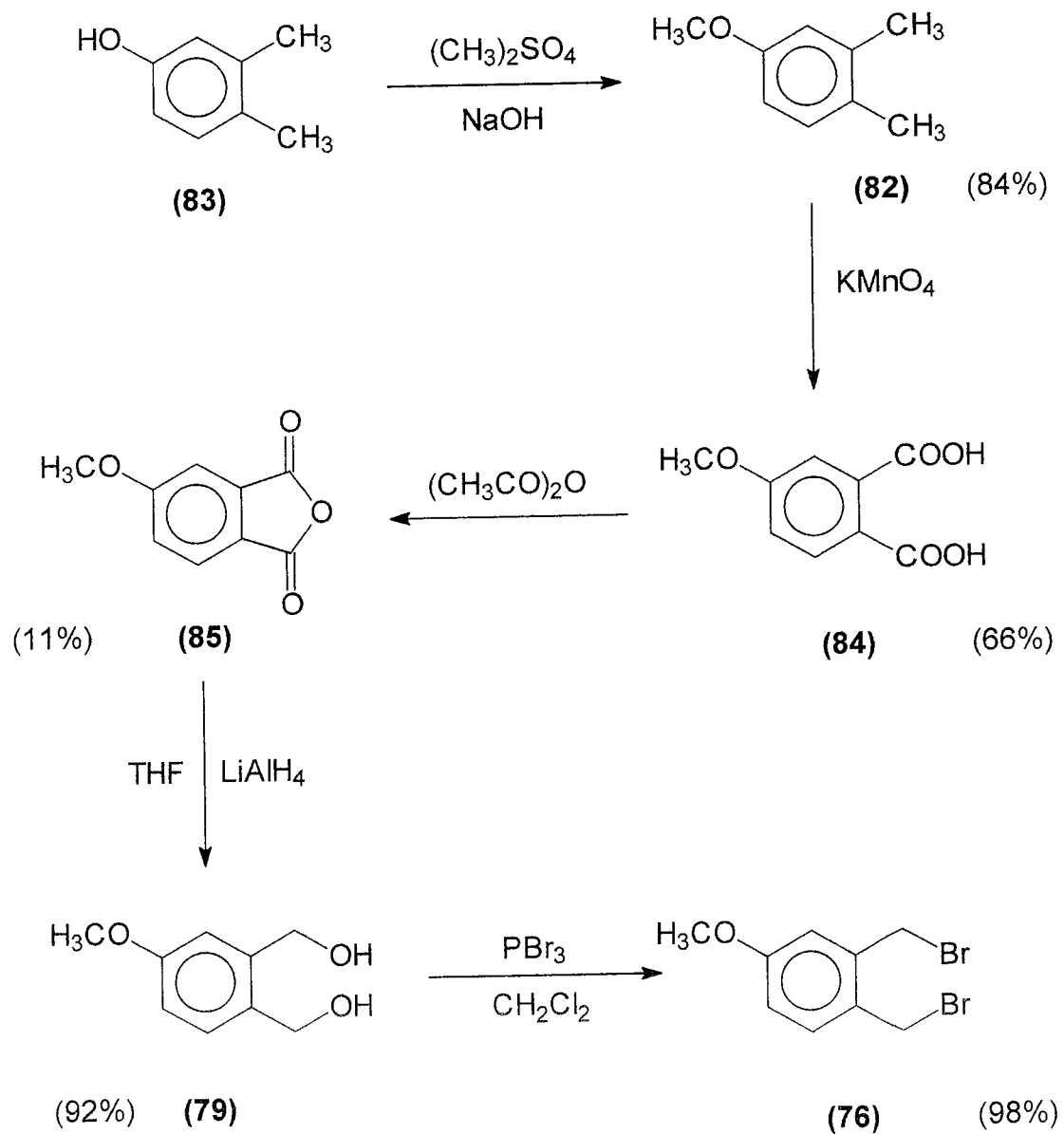


**Scheme 2.37:** Formation of an undesirable second product as reported by Bhattacharjee & Popp [47]

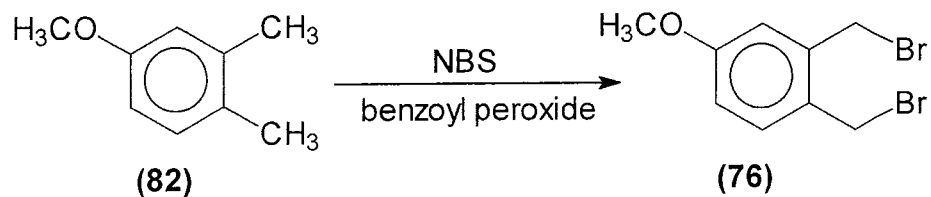
A further literature review revealed that 4-methoxy- $\alpha,\alpha'$ -dibromo-o-xylene (**76**) has been previously synthesised using two different routes [56 – 58]. The target compound was first reported in 1980 by Shetty [56], involving a lengthy five-step route, see scheme 2.38. Later, by two different methods [57,58], the target compound was synthesised by a single-step reaction, by way of a direct bromination of 3,4-dimethyl anisole (**82**) with N-bromosuccinimide and a radical initiator.

Shetty [56] reported the formation of 4-methoxy- $\alpha,\alpha'$ -dibromo-o-xylene via a five step route in a over all yield of 7%, see scheme 2.38. The synthetic route involved 3,4-dimethylphenol (**83**) undergoing a methylation reaction using dimethylsulphate to produce 3,4-dimethyl anisole (**82**), which yielded 4-methoxyphthalic acid (**84**) on oxidation with potassium permanganate. The acid was then reacted with acetic anhydride to give 4-methoxyphthalic anhydride (**85**), which on reduction with lithium aluminium hydride gave 4-methoxyphthalyl alcohol (**79**). Finally the diol was brominated with phosphorous tribromide to give 4-methoxy- $\alpha,\alpha'$ -dibromo-o-xylene (**76**).

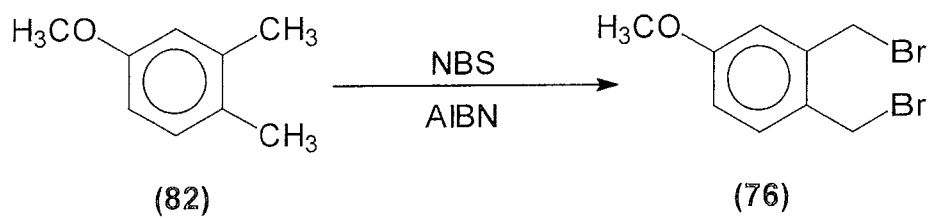
Two subsequent literature reports in early 1997 [57,58] reported the direct bromination of commercially available 3,4-dimethyl anisole (**82**), using N-bromosuccinimide in the presence of a radical initiator. Ohkawa *et al.* [57] carried out the bromination using N-bromosuccinimide and benzoyl peroxide, and obtained (**76**) in a 65% yield, scheme 2.39. The reaction involved refluxing the mixture in carbon tetrachloride for 15 hours followed by a lengthy work-up involving chromatography. In the same year, Wang *et al.* [58] carried out the same reaction, using the same molar ratios of starting material to N-bromosuccinimide. However, they used azo-iso-butyronitrile or AIBN as initiator instead of benzoyl peroxide, as shown in scheme 2.40. This cut the reaction time from 15 hours to just 4 hours. While Wang reported the highest yield of 94%, the purity of the product is in doubt as it was obtained as oil and used it directly for use in another reaction. However, the reported NMR data identifies the product accurately.



**Scheme 2.38:** Formation of 4-methoxy- $\alpha,\alpha'$ -dibromo-o-xylene by Shetty [56]



**Scheme 2.39:** Preparation of (76) by Ohkawa *et al.* [57]



**Scheme 2.40:** Preparation of (76) by Wang *et al.* [58]

(a) Formation of 4-methoxy- $\alpha,\alpha'$ -dibromo-*o*-xylene (**76**)

The bromination of 3,4-dimethyl anisole (**82**) thus was carried out by the latter two methods. Following the Ohkawa *et al.* [57] method 3,4-dimethyl anisole was brominated with N-bromosuccinimide and benzoyl peroxide in carbon tetrachloride to give 4-methoxy- $\alpha,\alpha'$ -dibromo-*o*-xylene (**76**), 38% m.p. 49 – 51 °C [lit. [57], 65% 49 – 50 °C]. The structure of the product was confirmed by infra red and nuclear magnetic resonance data. The reaction using benzoyl peroxide proved to be time consuming with a 15 hour reaction time. Also, it proved difficult to purify, with a TLC analysis of the crude material showing four spots. Even after purification by flash chromatography the product needed to be recrystallised.

The reaction was repeated using the Wang *et al.* [58] method. Bromination of 3,4-dimethyl anisole with N-bromosuccinimide and AIBN as initiator, gave 4-methoxy- $\alpha,\alpha'$ -dibromo-*o*-xylene (**76**). This method proved to be more successful. The reaction time was much shorter only 4 hours and TLC analysis of the crude material showed only three spots. The product was purified by flash chromatography to yield a brown oil as reported by Wang. However, upon standing the oil overnight in a freezer (-20°C) white crystals formed in a 48% yield. The reported [58] yield of 94% was quoted for an oil, with no further purification, m.p. 48.2 - 49.6°C [lit. [56] 49-50°C].

The structure was confirmed by spectroscopic analysis (Appendix F). The infra-red data of 4-methoxy- $\alpha,\alpha'$ -dibromo-*o*-xylene showed a strong CH<sub>2</sub> wagging band observed for the -CH<sub>2</sub>Br group at 1203 cm<sup>-1</sup>, and 1034 cm<sup>-1</sup> is due to asymmetric stretching of the methoxy carbon-oxygen bond.

Assignment of the NMR signals is illustrated in figure 2.13 and 2.14. <sup>1</sup>H NMR showed a doublet at  $\delta$ 7.38 ppm ( $J_{H5,H6}$ =8.6 Hz) and was assigned to the aromatic proton H-6. This signal was the most down field due to the electron withdrawing effect of the halo-methylene group, and was coupled to the adjacent ring proton H-5.



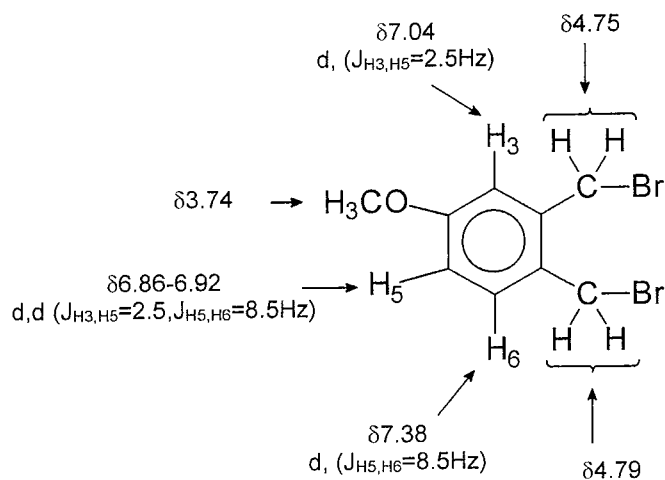


**Figure 2.13:**  $^1\text{H}$  NMR data of 4-methoxy- $\alpha,\alpha'$ -dibromo-o-xylene  
(values in ppm)

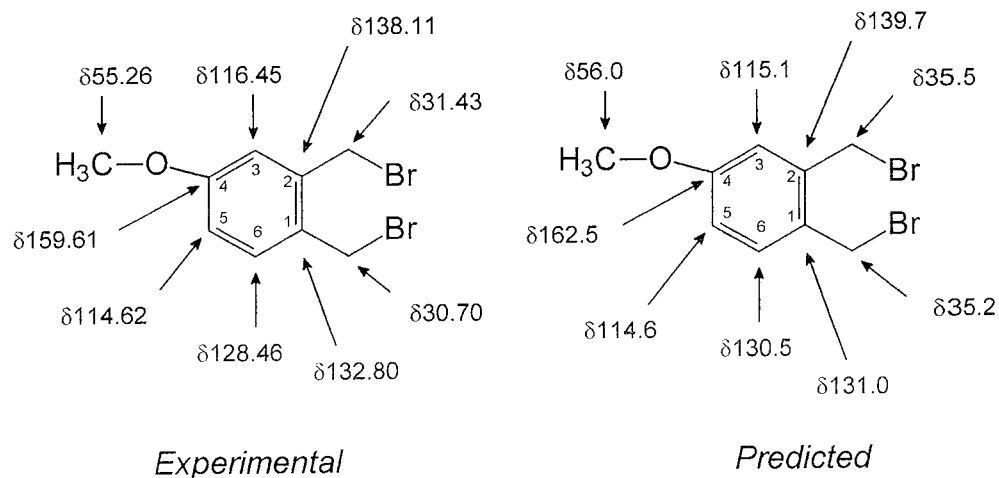
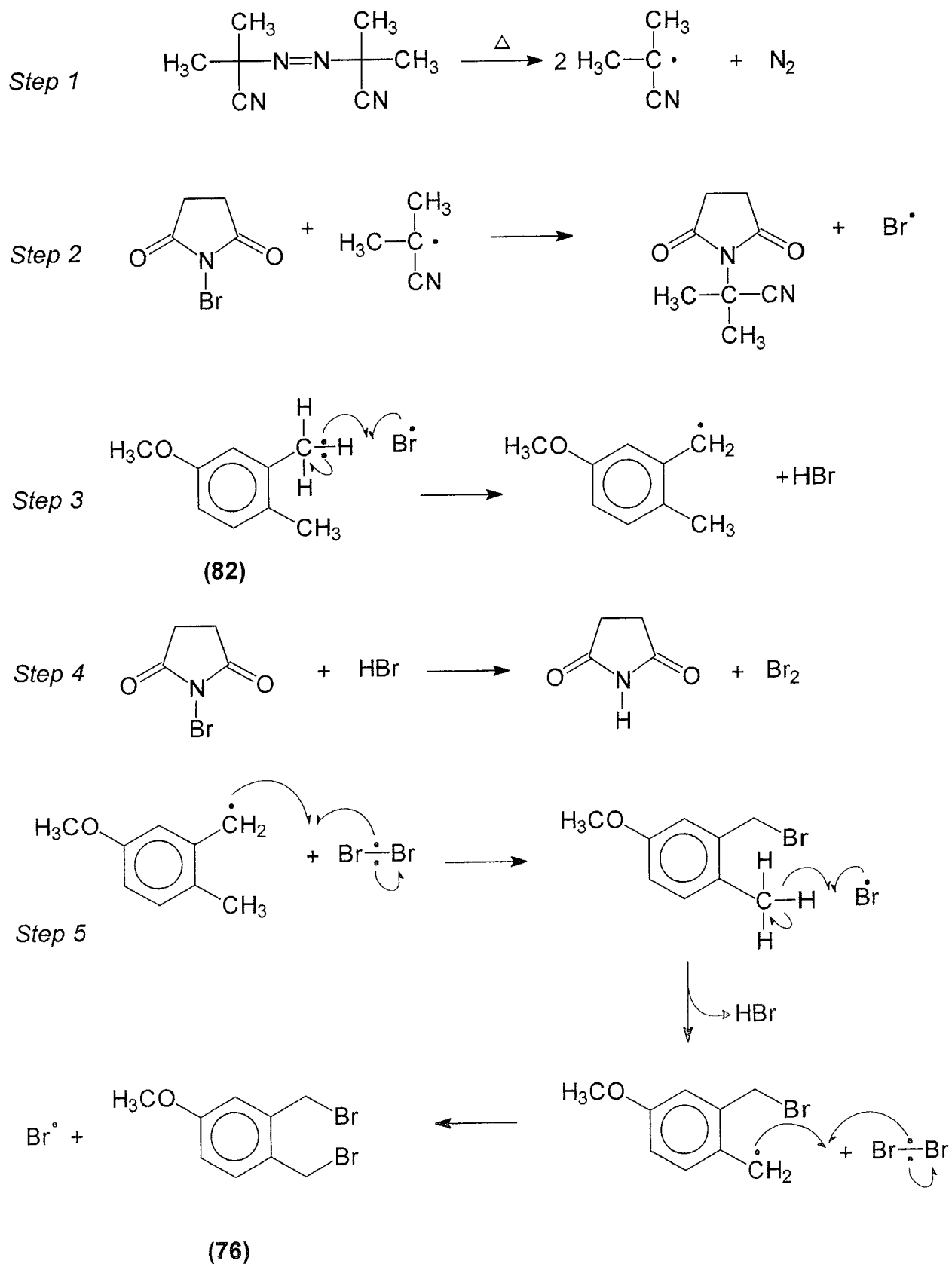


**Figure 2.14:** Experimental and predicted  $^{13}\text{C}$  NMR of 4-methoxy- $\alpha,\alpha'$ -dibromo-o-xylene (values in ppm)

The doublet at  $\delta 7.04$  ppm ( $J_{H3,H5}=2.5$  Hz) was due to H-3, while the doublet at  $\delta 6.86-6.92$  ppm ( $J_{H3,H5}=2.5$ ,  $J_{H5,H6}=8.5$  Hz) was due to H-5 which was coupled to H-6 ( $J=2.5$  Hz) and to H-3 ( $J=8.5$  Hz) arising from W coupling. The doublet at  $\delta 4.77$  ppm integrates for 4 protons and was attributed to the methylene protons. Finally the singlet at  $\delta 3.74$  ppm was due to the methoxy protons.  $^{13}\text{C}$  NMR showed nine resonances accounting for the nine carbons system and were assigned as follows:  $\delta 159.61$  ppm was due to the quaternary carbon bonded to the methoxy group C-4, while  $\delta 138.11$  and  $\delta 132.8$  ppm were due to the quaternary carbons C-1 and C-2 respectively. The resonances at  $\delta 128.46$ ,  $\delta 116.45$  and  $\delta 114.62$  ppm accounted for the remaining benzoidal ring carbons C-6, C-3 and C-5 respectively. The resonance at  $\delta 55.26$  ppm was due to the methoxy carbon, while  $\delta 31.43$  and  $\delta 30.70$  ppm were attributed to the methylene carbons.

The mechanism for the reaction is shown in scheme 2.41. AIBN homolytically cleaves at  $67^\circ\text{C}$  and on reaction with NBS forms the bromine radical as illustrated (step 1 and 2). The latter now reacts with (**82**) (step 3) and results in the formation of hydrogen bromide. Now the HBr reacts with NBS to form  $\text{Br}_2$  (step 4), as the function of the NBS is to provide a source of  $\text{Br}_2$  in a low, steady state concentration. 3,4-dimethyl anisole is then brominated by free radical substitution as shown (step 5).

When the reaction was carried out first, on removal of the solvent, an oily residue remained and upon standing overnight at room temperature it had turned to a black solid and on opening the flask a fuming gas evolved. It was previously found that under strong acidic conditions 4,5-dimethoxy- $\alpha,\alpha'$ -dibromo-o-xylene also produced a black material, as discussed. It was suggested that the dimethoxy product readily polymerises through the  $-\text{CH}_2$  side chain. It is therefore possible that the monomethoxy product also polymerises through the same group and is initiated by the presence of HBr. Upon repeating the reaction again and working it up immediately, the polymerisation reaction is avoided.



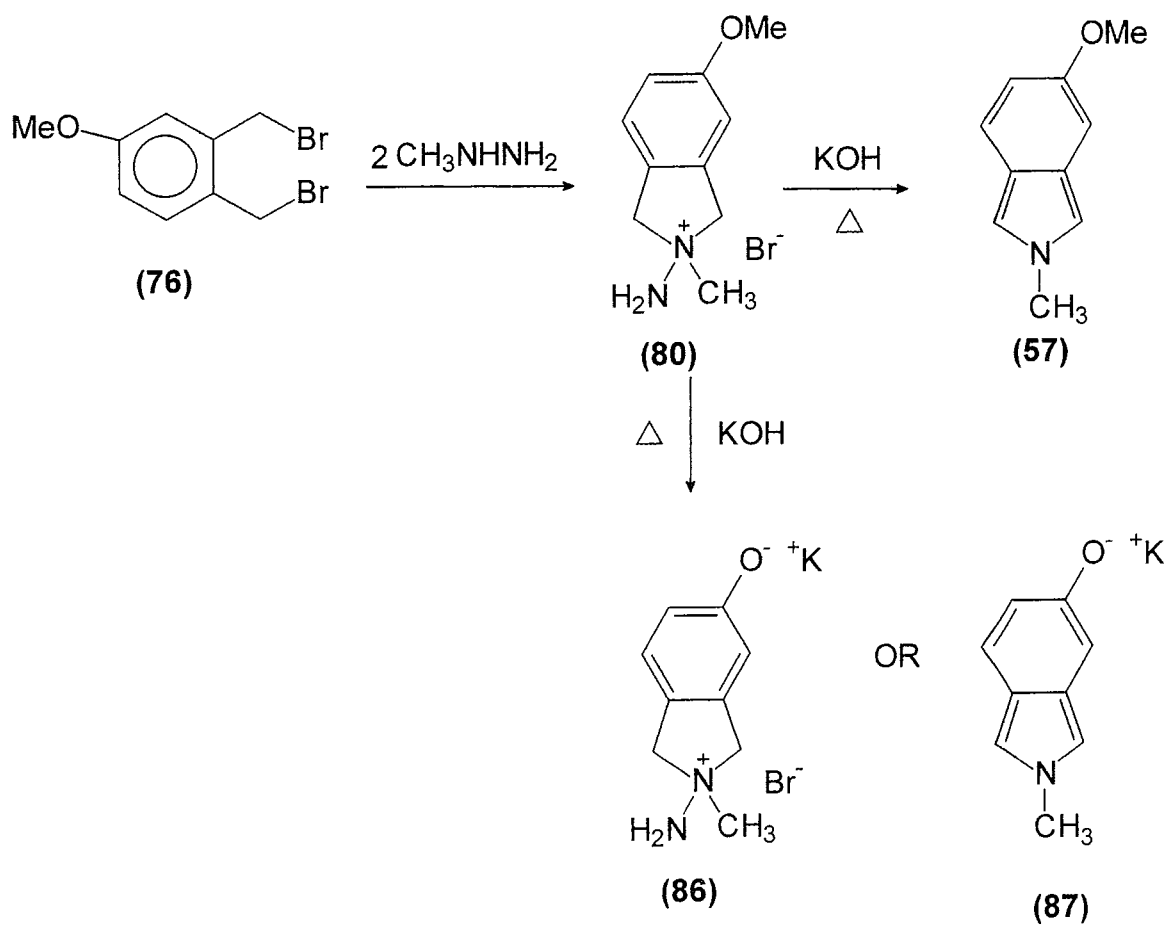
**Scheme 2.41:** Mechanism for the formation of 4-methoxy- $\alpha,\alpha'$ -dibromo-o-xylene

(b) *Formation of 5-methoxy-N-methylisoindole (57)*

The synthesis of 5-methoxy-N-methylisoindole was attempted again using a modified version of the method by Zeeh & König [22]. This was done by first reacting 4-methoxy- $\alpha,\alpha'$ -dibromo-o-xylene (**76**) with methylhydrazine to give the corresponding isoindolinium salt (**80**). The product was eliminated by the reaction of the salt with excess base and heat and collected by a sublimation apparatus. Using the reported reaction conditions [22] the product was formed with a very small yield. The experiment was repeated many times always resulting in the formation of only spectroscopic amounts of product, and the  $^1\text{H}$  NMR consistently showed an impure product.

On carrying out the reaction it was observed that the first step, the reaction of 4-methoxy- $\alpha,\alpha'$ -dibromo-o-xylene with methylhydrazine formed the intermediate isoindolinium salt quite readily. In fact the formation of the salt occurred faster than its dimethoxy-substituted counterpart. The second step, the elimination of 5-methoxy-N-methylisoindole from the salt with solid potassium hydroxide and heat, again occurred faster than with the disubstituted reaction. However it is believed that the reaction conditions for this elimination reaction are too severe, with the presence of base in large excess. It has been proposed that 5-methoxy-N-methylisoindole is forming, but in the presence of such a large amount of base it is further reacting to form the salt (**86**) and/or (**87**) as shown in scheme 2.42.

Therefore it was decided to repeat the reaction again this time using a decreased reaction ratio of starting material to potassium hydroxide. This time the product formed as an oil on the sublimation bulb more readily but still in a small yield 5%. While the sublimation technique worked well for the formation of N-methylisoindole it appeared not so appropriate for (**57**). Thus it was thought that any remaining product could be extracted. This was carried out and again the product was obtained as an oil when the solvent was removed. Both fractions were analysed and the structure of the product was confirmed by spectroscopic analysis (Appendix G).



**Scheme 2.42:** Possible unwanted cleavage of the methoxy group of 5-methoxy-N-methylisoindole

As with 5,6-dimethoxy-N-methylisoindole any elemental analysis of 5-methoxy-N-methylisoindole attempted gave results outside the acceptable limits, and again it is believed that the product becomes resinous before an accurate analysis was possible.

The infrared spectrum showed ring C=C stretches at  $1635\text{ cm}^{-1}$ , while the band at  $1226\text{ cm}^{-1}$  was attributed to a C-N stretch. The stretch at  $1029\text{ cm}^{-1}$  was due to asymmetric stretching of the methoxy carbon-oxygen bond.

The UV-vis spectrum showed a strong absorption at  $\lambda_{\text{max}}\ 225\text{nm}$  attributed to the aromatic  $\pi\text{-}\pi^*$  transition, which was the same as N-methylisoindole (**24**) and 5,6-dimethoxy-N-methylisoindole (**56**). Two other absorptions were observed, one weak absorption at  $279\text{nm}$ , which was absent in the spectrum of N-methylisoindole, but present with 5,6-dimethoxy-N-methylisoindole, and also the broad transition at  $328\text{nm}$  was unchanged from that of N-methylisoindole and 5,6-dimethoxy-N-methylisoindole.

Assignment of the NMR signals is illustrated in figure 2.15 and 2.16.  $^1\text{H}$  NMR showed a doublet at  $\delta 7.40\text{ ppm}$  ( $J_{\text{H4},\text{H6}}=8\text{ Hz}$ ) and was due to the aromatic proton H-4. The singlets at  $\delta 6.96$  and  $\delta 6.91\text{ ppm}$  were attributed to the five membered ring aromatic protons H-1 & H-3 respectively. Taking the position of the H-3 proton on all three isoindoles, there emerges a pattern whereby the resonance appeared more upfield as the number of methoxy substituents increased. This highlights the increased electron density into the reactive  $\alpha,\alpha'$  positions on the isoindole which the methoxy groups provide.

The resonance at  $\delta 6.75\text{ ppm}$  was due to the ring proton H-7. The doublet at  $\delta 6.68 - 6.61\text{ ppm}$  ( $J_{\text{H6},\text{H7}}=2.2, 9\text{ Hz}$ ) was due to H-6 and was coupled to H-7 and coupled to H-4 ( $J_{\text{H4},\text{H6}}=9\text{ Hz}$ ) arising from W coupling. Finally the singlet at  $\delta 3.93\text{ ppm}$  integrated for three protons, and was attributed to the three methoxy protons, while the singlet at  $\delta 3.88$  which also integrated for three proton was due to the N substituted the protons.

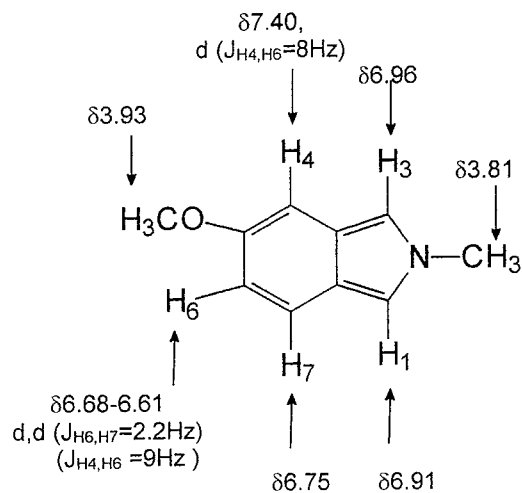


**Figure 2.15:**  $^1\text{H}$  NMR data of 5-methoxy-N-methylisindole (values in ppm)

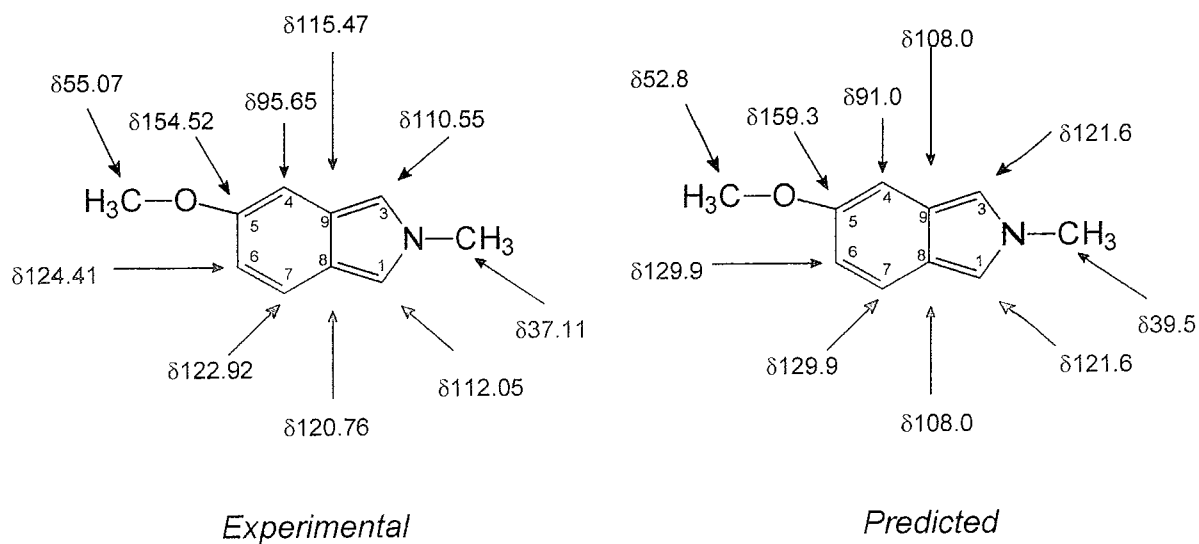


**Figure 2.16:** Experimental and predicted  $^{13}\text{C}$  NMR of 5-methoxy-N-methylisindole (values in ppm)

$^{13}\text{C}$  NMR spectrum showed ten resonances accounting for all ten carbons present in the molecule. The methyl carbon on the nitrogen atom was clearly seen at  $\delta 37.11$  ppm, while the carbons of the methoxy group resonated at  $\delta 55.07$  ppm. The resonance  $\delta 154.52$  ppm was due to the quaternary carbons C-5 and C-6 resonated at  $\delta 124.41$ . The two bridging ring carbons C-8 and C-9 resonated at  $\delta 120.76$  and  $115.47$  ppm respectively. The resonance  $\delta 120.92$  and  $97.24$  ppm accounted for the other ring carbons C-4 and C-7. The resonance at  $\delta 112.05$  and  $110.55$  ppm was attributed to C-1 and C-3, the C-3 in N-methylisoindole and 5,6-dimethoxy-N-methylisoindole resonated at a very similar position  $\delta 111.73$  and  $111.0$  ppm. The assigned  $^{13}\text{C}$  NMR data as shown in figure 2.16, is in some agreement with computer [50] predicted values.

Like isoindole and N-methylisoindole and 5,6-dimethoxy-N-methylisoindole, 5-methoxy-N-methylisoindole is also a  $\pi$ -excessive 10- $\pi$ -electron heteroaromatic system and the various canonical forms are represented in figure 2.17, based on the canonical forms of isoindole reported by Bonnett *et al.* [7].

The mechanism for the reaction proposed is again based on the mechanism for the formation for N-methylisoindole, scheme 2.43. Again it involves  $\text{S}_{\text{N}}2$  attack of the methylhydrazine on one of the methylene carbon to form a bromide salt. Subsequent loss of hydrogen bromide and intramolecular rearrangement with an  $\text{S}_{\text{N}}2$  attack of the other methylene carbon by the nitrogen atom, causes ring closure to give the isoindolinium salt. When this salt is treated with potassium hydroxide and heat, ammonia is evolved and the resulting isoindolinium salt undergoes loss of hydrogen bromide to give the desired 5-methoxy-N-methylisoindole.



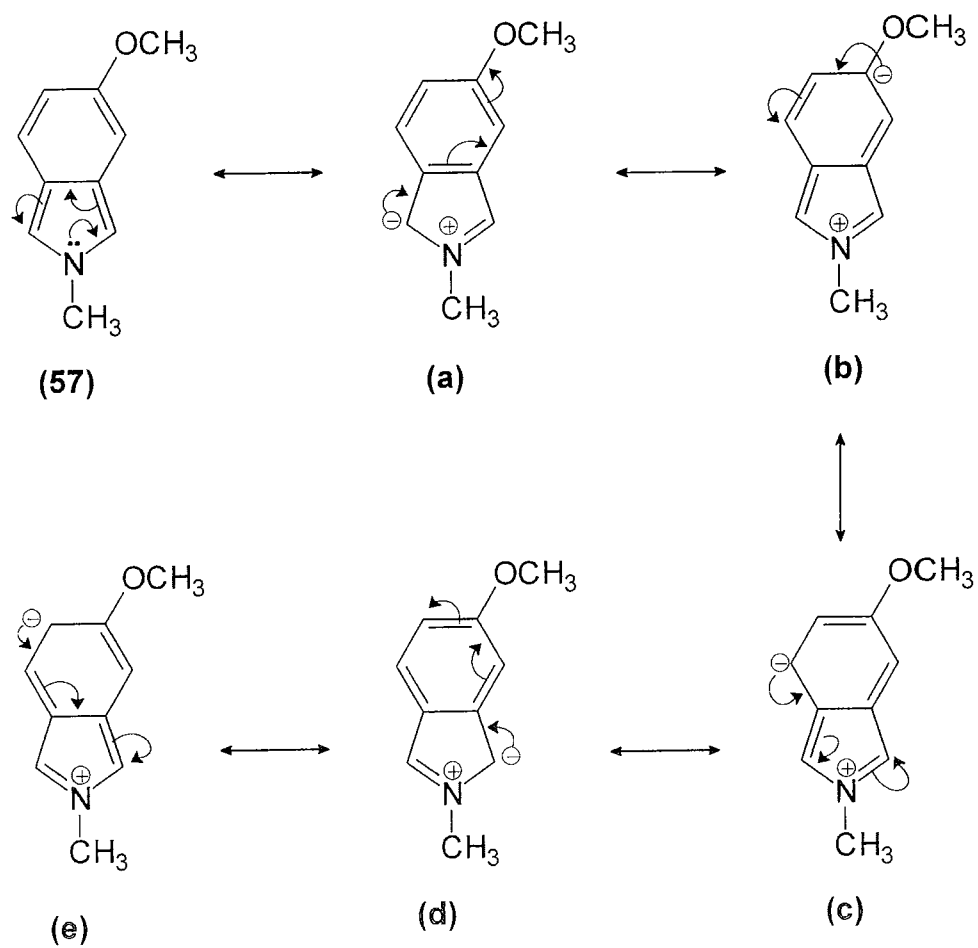
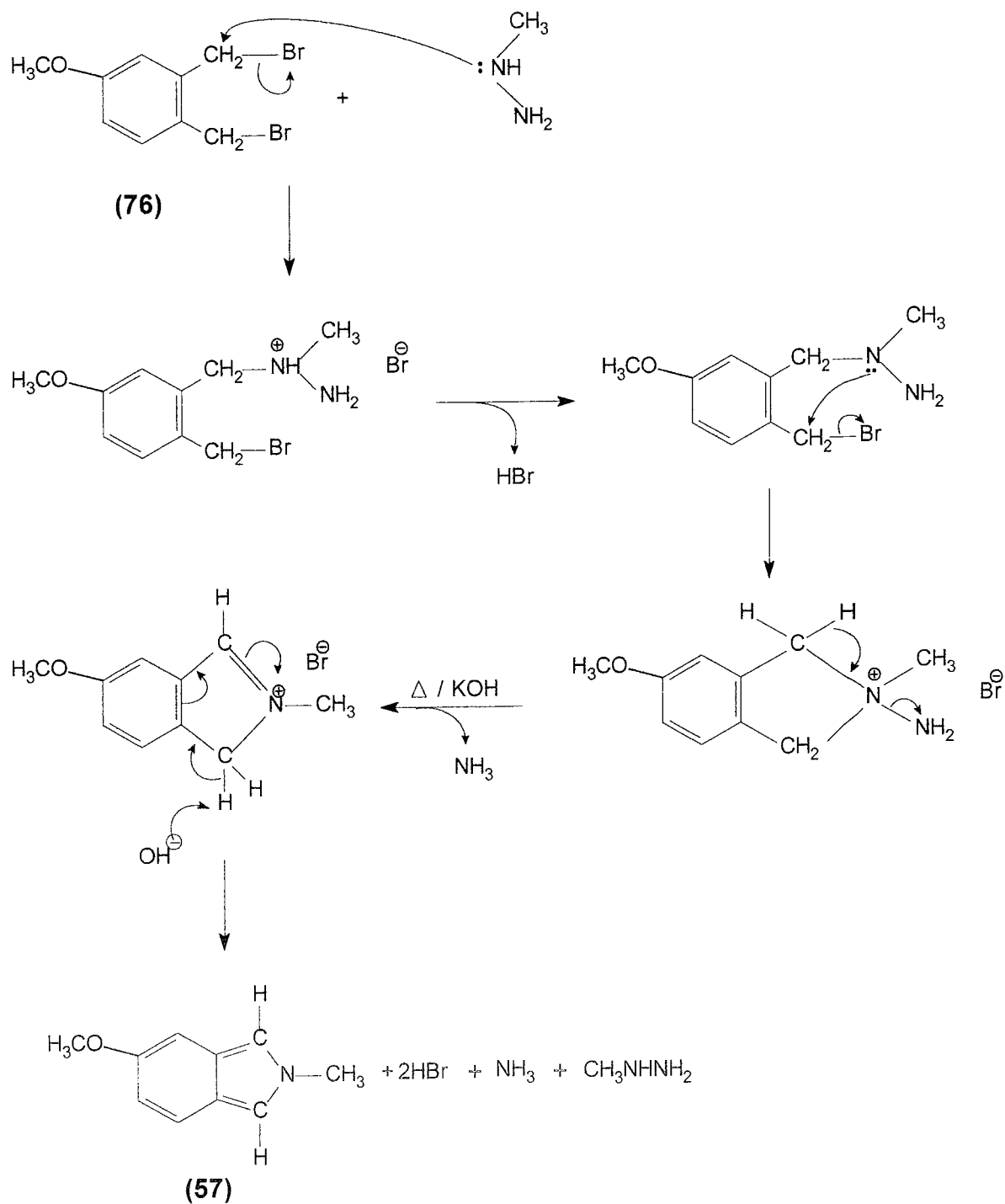


**Figure 2.17:** Canonical forms of 5-methoxy-N-methylisoindole



**Scheme 2.43:** Mechanism for the formation of 5-methoxy-N-methylisoindole

### 2.3 Conclusion

The synthesis of two new compounds, 5-methoxy-N-methylisoindole (**57**) and 5,6-dimethoxy-N-methylisoindole (**56**) has been achieved. The synthetic routes to these compounds are novel and had to be devised.

The synthesis N-methylisoindole (**24**) via the extended route, as shown in scheme 2.23 and 2.28 proved to work very successfully and with relative ease. The phthalide (**64**) was reduced to o-xylene- $\alpha,\alpha'$ -diol (**63**) in an 83% yield, showed a sharp melting point of (63.4 – 65.2 °C) and spectroscopic data showed a pure product and therefore was not recrystallised. o-Xylene- $\alpha,\alpha'$ -diol was brominated with 48% hydrobromic acid to give  $\alpha,\alpha'$ -dibromo-o-xylene (**18**) in a 85% yield and showed sharp melting point and clean spectra. Finally the formation of N-methylisoindole (**24**) in a 44% yield, involved a two step reaction and required some experimental skill as the reaction must be carried out under anhydrous conditions and under an inert atmosphere. This calculates to an over all yield of 31%. While the precursor  $\alpha,\alpha'$ -dibromo-o-xylene is commercially available, its synthesis via this new route offers a further option to the organic chemist for the synthesis of substituted isoindoles.

The synthesis of 5,6-dimethoxy-N-methylisoindole (**56**) via the newly devised route as shown in scheme 2.25, was more difficult. The first step involving the chloromethylation of 3,4-dimethoxybenzoic acid (**60**) gave 5,6-dimethoxyphthalide (**61**) in a yield of 50% which was lower than the reported yield of 65.5% [47]. However while the reported melting point was sharp (154 –155 °C) only infra-red spectroscopic data was reported. In this work nuclear magnetic resonance data ( $^1\text{H}$  and  $^{13}\text{C}$ ) was obtained and showed pure product. 5,6-dimethoxyphthalide was reduced with lithium aluminium hydride and gave 4,5-dimethoxyphthalyl alcohol (**62**), and recrystallised from toluene in a 66% yield with spectroscopic data showing a very pure product. While the literature yield of 91% [47] recrystallised from benzene, is considerably higher, no spectroscopic data was reported.

As already discussed the bromination of 4,5-dimethoxyphthalyl alcohol where 48% hydrobromic acid and concentrated sulphuric acid was added neat, a black material was produced as soon as the reagents were mixed. Indeed when the reaction conditions were finally optimised and 4,5-dimethoxy- $\alpha,\alpha'$ -dibromo-o-xylene was successfully synthesised, it was observed to go black upon standing in air at room temperature. This has been attributed to the compound polymerising as outlined in scheme 2.32. What is also interesting is that the mono substituted, 4-methoxy- $\alpha,\alpha'$ -dibromo-o-xylene also goes black on standing at room temperature. This phenomenon has not been either observed or reported for the unsubstituted  $\alpha,\alpha'$ -dibromo-o-xylene. This would lead to the conclusion that the presence of the electron donating methoxy group on the ring leads to the formation of the radical leading to the formation of the polymer, whether it be mono or di substituted.

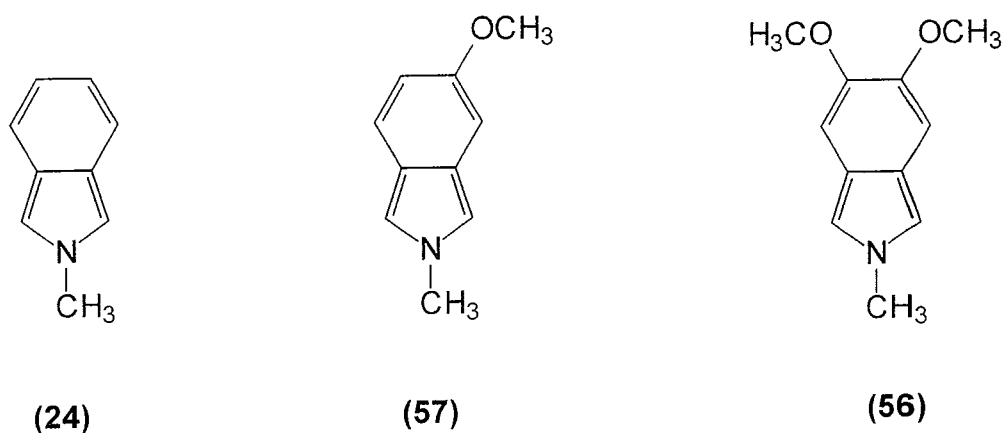
The final step in the formation of 5,6-dimethoxy-N-methylisoindole proved to be very difficult and was repeated many times. As with the synthesis of N-methylisoindole the reaction must be carried out under anhydrous conditions and under an inert atmosphere. The formation of the isoindolinium salt whereby methylhydrazine was simply added to 4,5-dimethoxy- $\alpha,\alpha'$ -dibromo-o-xylene showed that, by making the addition too quickly the salt precipitated out as an oil and stuck to the sides of the reaction vessel. This proved to be very difficult to remove when trying to transfer the salt to the sublimation apparatus and maintaining an inert atmosphere. However, the elimination of the desired isoindole from the salt under basic conditions and heat, carried out in a sublimation apparatus proved the most difficult. Initially, 5,6-dimethoxy-N-methylisoindole was only obtained in spectroscopic amounts. After many repeated attempts the yield was increased to 25% and the product structure was confirmed by nuclear magnetic resonance data. The product, upon handling appeared to less stable than the unsubstituted N-methylisoindole. Also the low yield has been attributed to the cleavage reaction outlined in scheme 2.33.

The devised route to the formation of 5-methoxy-N-methylisoindole was shorter than its disubstituted counterpart. By using commercially available 3,4-dimethoxy anisole (**82**) and brominating directly, the successful synthesis of 4-methoxy- $\alpha,\alpha'$ -dibromo-o-xylene (**76**) with a yield of 38% was achieved much more quickly and efficiently, than using the proposed five step route as shown in scheme 2.38. The formation of 5-methoxy-N-methylisoindole again proved to be difficult with a yield of 5%. However this yield was increased to 25% when more product was obtained by extracting the product from the salt mixture using diethylether.

The effect of the methoxy groups on N-methylisoindole was observed in the analysis of the spectroscopic data summarised in table 2.2. The UV-vis data revealed very little difference in the  $\lambda_{\max}$  of the three isoindoles. However, the  $^1\text{H}$  NMR data highlighted the electronic effects of the methoxy groups much better. The main reactive site on N-methylisoindole the  $\alpha$ -position showed a shift upfield, from  $\delta 7.01$  ppm for N-methylisoindole, to  $\delta 6.91$  and  $6.77$  ppm with the addition of one and two methoxy groups respectively. This, as already discussed, implied that there is a greater electron density at the  $\alpha,\alpha'$ -positions of N-methylisoindole with the addition of the methoxy groups, which should make polymerisation easier.

However, this effect was not observed in the  $^{13}\text{C}$  NMR data where the resonances for the C-3 carbon on the three isoindoles were virtually unchanged around  $\delta 111.0$  ppm. It is interesting to note that the resonances of the protons of the N methyl substituent appeared upfield from the unsubstituted N-methylisoindole implying an increase in electron density into the N methyl bond, while the  $^{13}\text{C}$  NMR data again showed very little change in the resonance for the carbon of the N-methyl substituent.

What can be concluded from this synthesis is that substituted N-methylisoindoles can be formed, by first forming an appropriate substituted  $\alpha,\alpha'$ -dibromo-o-xylene. Indeed other substituted  $\alpha,\alpha'$ -dibromo-o-xylenes have been reported [57,59].



	<b>24</b>	<b>57</b>	<b>56</b>
UV-vis / $\lambda_{\max}$ (nm) in CH <sub>3</sub> CN	224	225	222.5
$\delta$ - <sup>1</sup> H NMR (ppm) in CDCl <sub>3</sub>			
H-3	7.01	6.91	6.77
OCH <sub>3</sub>	/	3.93	3.88
NCH <sub>3</sub>	3.94	3.81	3.88
$\delta$ - <sup>13</sup> C NMR (ppm) in CDCl <sub>3</sub>			
C-3	111.73	110.5	111.0
C-5	120.64	154.52	147.43
OCH <sub>3</sub>	/	55.07	55.63
NCH <sub>3</sub>	37.45	37.11	37.24

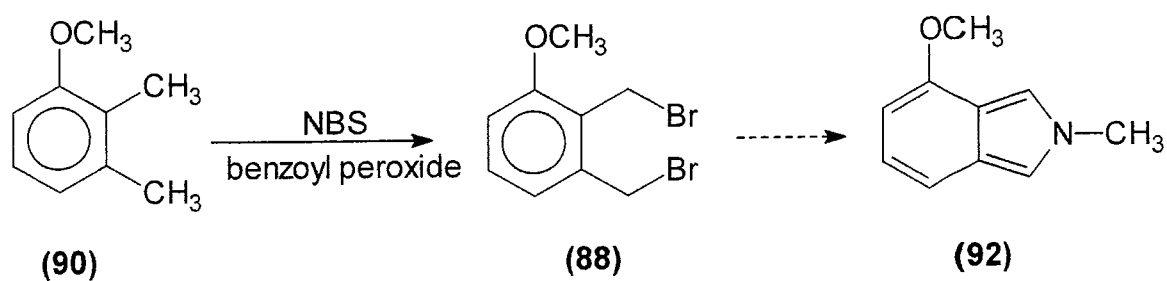
**Table 2.2:** Summary of spectroscopic data for the isoindoles synthesised

Ohkawa *et al.* [57], as well as reporting the the synthesis of 4-methoxy- $\alpha,\alpha'$ -dibromo-o-xylene, also reported the formation of other substituted  $\alpha,\alpha'$ -dibromo-o-xylenes. 2,3-Bis-(bromomethyl)anisole (**88**) and 1,2-bis-(bromomethyl)naphthalene (**89**) were obtained from the corresponding dimethyl derivatives of anisole (**90**) and (**91**) in 68% and 82% respectively. From this we would envisage the formation of the corresponding N-methylisoindoles (**92**) and (**93**) which might be of interest as polymer precursors, as shown in scheme 2.44 and 2.45. However such monomers would lead to polymers with substituents contributing to steric hindrance along the polymer back bone.

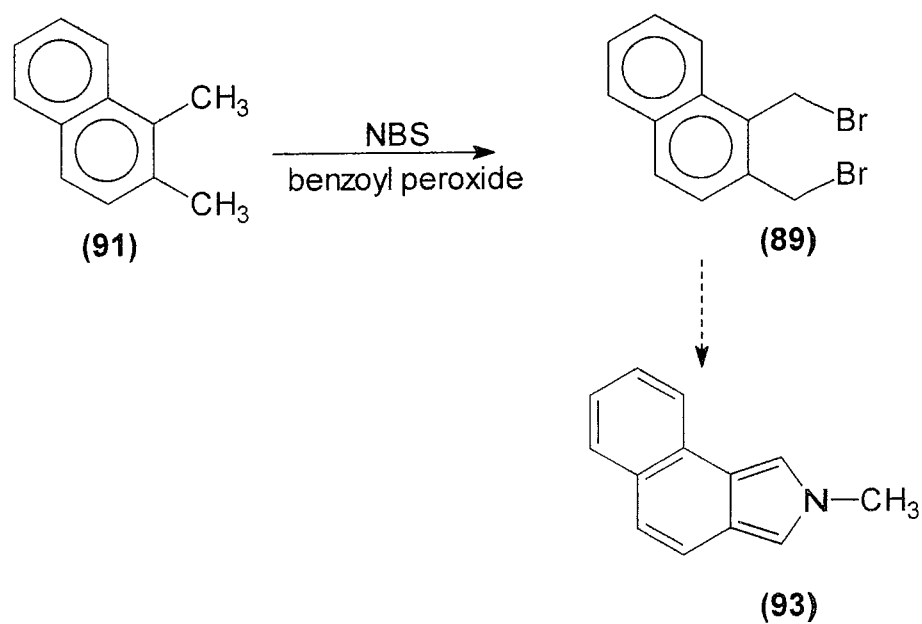
It was further reported [57] that 3,4-bis-(bromomethyl)naphthalene (**94**) was prepared by reduction of the corresponding dicarboxylic acid (**95**) with lithium aluminium hydride in THF followed by the treatment of the diol (**96**) phosphorus tribromide. Again we envisage that the corresponding N-methylisoindole (**97**) could be formed as in scheme 2.46, which would be very useful for purposes of further study on account of the substituent not being in a position to contribute to steric strain along the polymer chain.

Finally, only recently it has been reported [59] in the synthesis of a hexoxy disubstituted isothianaphthene (**98**), the formation of 1,2-bis(bromomethyl)-4,5-hexoxybenzene (**99**) via the route shown in scheme 2.47. From this a 5,6-dihexoy-N-methylisoindole (**100**) could be synthesised.

Following the successful synthesis of the two target monomers, 5-methoxy-N-methylisoindole and 5,6-dimethoxy-N-methylisoindole, they were successfully polymerised and are characterised in the subsequent chapters.

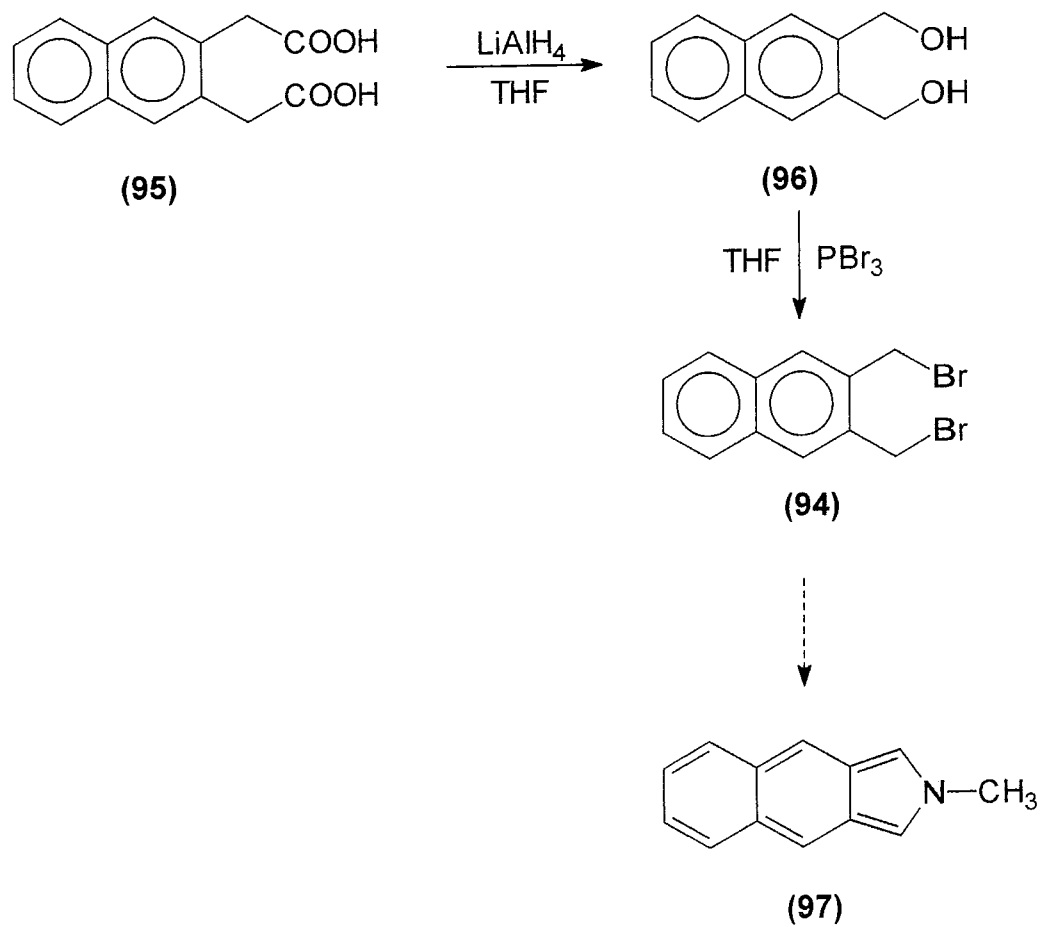


**Scheme 2.44:** Possible formation of methoxy substituted N-methylisindoles from corresponding  $\alpha,\alpha'$ -dibromo-o-xylenes

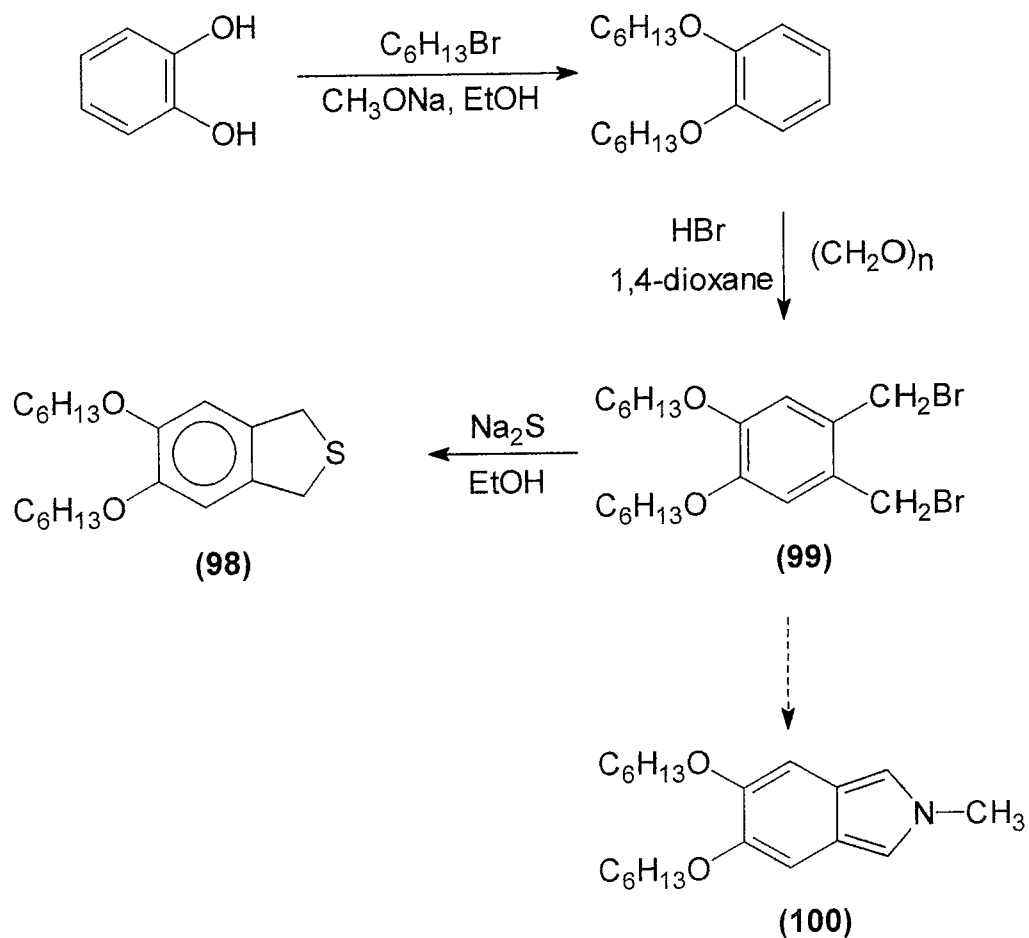


**Scheme 2.45:** Possible formation of N-methylisindoles with a fused benzene ring from corresponding  $\alpha,\alpha'$ -dibromo-o-xylenes





**Scheme 2.46:** Possible formation of N-methylisoindoles with a fused benzene ring from corresponding  $\alpha,\alpha'$ -dibromo-*o*-xylenes



**Scheme 2.47:** Possible formation of hexoxy substituted N-methylisindoles from corresponding  $\alpha, \alpha'$ -dibromo-o-xylenes

## 2.4 Experimental

All infra-red spectra were obtained on a Perkin Elmer FT-IR spectrometer Paragon 1000. Both  $^1\text{H}$  NMR (200 MHz) and  $^{13}\text{C}$  NMR (50 MHz) were obtained on a Varian Gemini 2000, and tetramethylsilane was used as the internal standard. Melting points were recorded using an Electrothermal 9100 melting point apparatus and samples were dried in the Gallenkamp Vacuum Oven. Solvents were either HPLC grade or dried prior to use according to literature methods and all solvents were stored over Na wire.

### 2.4.1 Preparation of $\alpha,\alpha'$ -dibromo-*o*-xylene (**18**)

#### (a) *o*-Xylene $\alpha,\alpha'$ -diol (**63**)

A solution of phthalide (5g, 0.038 moles) in anhydrous tetrahydrofuran (50cm<sup>3</sup>) was added slowly to a suspension of lithium aluminium hydride (3.87g, 0.102 moles) in anhydrous tetrahydrofuran (30 cm<sup>3</sup>) and the mixture was refluxed for 5 hours. The mixture was cooled in an ice bath and the excess lithium aluminium hydride was decomposed by the dropwise addition, with stirring of water (2.5 cm<sup>3</sup>), 15% NaOH (2.5 cm<sup>3</sup>), and another portion of water (7.5 cm<sup>3</sup>) and a white precipitate formed. The precipitate was allowed to settle and the supernatant tetrahydrofuran was decanted off and retained. The precipitate was then washed with hot tetrahydrofuran, and the combined tetrahydrofuran solutions were dried over anhydrous magnesium sulphate, filtered, and the filtrate concentrated *in vacuo* and washed in hot petroleum ether (10mls) to give *o*-xylene  $\alpha,\alpha'$ -diol (4.3g, 83%), m.p. 63.4 - 65.2°C [lit. [48] m.p. 63 - 65°C],  $^1\text{H}$  NMR (200MHz; CDCl<sub>3</sub>)  $\delta$  7.23 (4H, s, Ar H's),  $\delta$  4.49 (4H, s, CH<sub>2</sub> [x2]),  $\delta$  4.41 (2H, br, s, OH [x2], signal disappears on D<sub>2</sub>O shake) ppm.  $^{13}\text{C}$  NMR (50MHz; CDCl<sub>3</sub>)  $\delta$  139.25 (C-1, C-2), 129.51 (C-3, C-6), 128.40 (C-4, C-5), 63.5 (CH<sub>2</sub>OH [x2]) ppm.  $\nu_{\text{max}}$  (KBr), 3243 (br, O-H), 2889, 1607, 1452, 1400, 1212, 1181, 1111, 1037, 1003, 761 (*o*-disubstituted) cm<sup>-1</sup>

(b)  $\alpha$   $\alpha'$  dibromo-*o*-xylene (**18**)

An aqueous solution of 48% hydrobromic acid (1.58 cm<sup>3</sup>, 0.014 moles) was put into a round bottom flask, fitted with a condenser, and placed in an ice bath. To this, concentrated sulphuric acid (1.09 cm<sup>3</sup>, 0.204 moles) was added slowly. To the resulting ice cold mixture *o*-xylene- $\alpha,\alpha'$ -diol (0.7g, 0.005 moles) was added with constant stirring. The reaction mixture was left stirring overnight, then heated for 3 hours 45 minutes on a steam bath. The product was extracted with diethylether and dried overnight over magnesium sulphate, filtered and the filtrate concentrated *in vacuo* to give  $\alpha$   $\alpha'$  dibromo-*o*-xylene (1.1g, 85%), m.p. 92.9 - 95.7 °C [lit. [48] 92 -94 °C]. <sup>1</sup>H NMR (200MHz; CDCl<sub>3</sub>)  $\delta$  7.40 - 7.26,( 4H, m, Ar H's),  $\delta$  4.67 (4H, s, CH<sub>2</sub> [x2]) ppm. <sup>13</sup>C NMR (50MHz; CDCl<sub>3</sub>)  $\delta$  136.56 (C-1, C-2), 131.09 (C-3, C-6), 129.43 (C-4, C-5), 29.92 (CH<sub>2</sub>Br [x2]) ppm.  $\nu_{\max}$  (KBr), 3028, 2356, 1931, 1646, 1492, 1455(m), 1427, 1212, 1186(m), 1072, 947, 835, 765, 737 (s) (*o*-disubstituted) cm<sup>-1</sup>.

2.4.2 Preparation of *N*-methylisoindole [22] (**24**)

A three necked round bottomed flask was fitted with a nitrogen inlet, a dropping funnel and condenser fitted with a calcium chloride drying tube. The flask was charged with a clear pale yellow solution of  $\alpha$ ,  $\alpha'$ -dibromo-*o*-xylene (6.6g, 0.025 moles) in dry diethylether (80 cm<sup>3</sup>). A solution of methylhydrazine (3 cm<sup>3</sup>, 2.6g, 0.055 moles) in dry diethylether (5 cm<sup>3</sup>) was added dropwise from the dropping funnel, with stirring, under a nitrogen atmosphere. A white solid precipitated out, and stirred for a further 2 hours, after which, the solution was allowed to stand overnight under an inert atmosphere. The ether was then decanted off and the reaction vessel was flushed with N<sub>2</sub> to remove any trace ether. Dry powdered potassium hydroxide (17.49g, 0.312 moles) was added to the white solid in small portions with stirring. The reaction mixture was stirred for a further 2 hours. The mixture was then sublimed *in vacuo* (2.0 mbar, 120 °C). The yellow needles formed were dried and weighed to give *N*-methylisoindole (1.4g,

44%), mp 85.5 - 89.0°C [lit. [22] 90 - 91°C]. <sup>1</sup>H NMR (200MHz; CDCl<sub>3</sub>) δ 7.52-7.47 (2H, m, Ar H, H<sub>A</sub>, H<sub>A'</sub>), 7.01 (2H, s, Ar H, H<sub>X</sub>, H<sub>X'</sub>), 6.93-6.88 (2H, m, Ar H, H<sub>B</sub>, H<sub>B'</sub>), 3.94 (3H, s, N-CH<sub>3</sub>) ppm. <sup>13</sup>C NMR (50MHz; CDCl<sub>3</sub>) δ 124.61 (C-8, C-9), 120.64 (C-5, C-6), 119.38 (C-4, C-7), 111.73(C-1, C-3), 37.45 (N-CH<sub>3</sub>) ppm. ν<sub>max</sub> (KBr), 3110, 1618, 1543, 1474, 1408, 1359(C-H), 1329, 1233(C-N), 1135, 1020, 982, 934, 758(o-disubstituted), 611 cm<sup>-1</sup>. UV-vis (CH<sub>3</sub>CN) λ<sub>max</sub> 224, 325nm.

#### 2.4.3 Preparation of 5,6-dimethoxy-N-methylisoindole (56)

##### (a) 5,6-dimethoxyphthalide (61)

The synthesis was carried out following the method of D. Bhattacharjee and F. Popp [47]. A three necked round bottom flask, fitted with a condenser, containing 40% formaldehyde (141 cm<sup>3</sup>, 1.747 moles) was saturated with hydrogen chloride gas generated separately by the dropwise addition of concentrated sulphuric acid to sodium chloride at 20 °C. 3,4-dimethoxybenzoic acid (20g, 0.109 moles) was added with stirring [and remained as a suspension in the solution]. The mixture was heated to 60 - 70 °C, [after 15 minutes the solvent was a deep wine colour, and after 3 hours all the starting material had fully dissolved into solution]. The mixture was heated for a total of 7 hours, during which time hydrogen chloride gas was bubbled slowly through it. It was then allowed to cool and concentrated *in vacuo*, water (70 cm<sup>3</sup>) was added and it was finally neutralised with ammonium hydroxide (5M, 560 cm<sup>3</sup>). The white solid formed was filtered, washed several times with water, air dried and further dried in a dessicator. The product was recrystallised from methanol to give white micro crystals of 5,6-dimethoxyphthalide (10.66g, 50%), m.p. 146 - 148 °C [lit. [47] m.p. 151 - 154°C, 67%]. <sup>1</sup>H NMR (200MHz; CDCl<sub>3</sub>) δ 7.26 (1H, s, Ar H-7), 6.97(1H, s, Ar H.4), 5.23 (2H, s, [CH<sub>2</sub>-O]), 3.99 (3H, s, OCH<sub>3</sub> [C6]) 3.94 (3H, s, OCH<sub>3</sub> [C5]) ppm. <sup>13</sup>C NMR (50MHz; CDCl<sub>3</sub>) δ 171.33 (C=O), 154.68 (C-6), 150.19 (C-5), 141.02(C-8), 117.25(C-9), 105.67(C-7), 103.38(C-4), 68.97(C-3),

56.14(OCH<sub>3</sub>[C6]), 55.96 (OCH<sub>3</sub>[C5])ppm.  $\nu_{\max}$  (KBr), 2937, 2837, 1753(C=O), 1600, 1501, 1451, 1352, 1249, 1225, 1044, 855, 763 cm<sup>-1</sup>.

(b) *4,5-dimethoxyphthalyl alcohol* [47] (**62**)

A warm solution of 5,6-dimethoxyphthalide (8g, 0.041 moles) in anhydrous tetrahydrofuran (150 cm<sup>3</sup>) was added slowly to a suspension of lithium aluminium hydride (4.3g, 0.11 moles) in anhydrous tetrahydrofuran (50 cm<sup>3</sup>), and the mixture was refluxed for 4 hours. The mixture was cooled in an ice bath and excess lithium aluminium hydride was decomposed by the dropwise addition with stirring of water (5 cm<sup>3</sup>), 15% sodium hydroxide (5 cm<sup>3</sup>), and another portion of water (14 cm<sup>3</sup>), and a white precipitate formed. The precipitate was allowed to settle and the supernatant tetrahydrofuran was decanted off and retained. The precipitate was then washed with hot tetrahydrofuran, and the combined tetrahydrofuran solutions were dried over anhydrous magnesium sulphate, filtered, and the filtrate concentrated *in vacuo* to give crude 4,5-dimethoxyphthalyl alcohol (7.12g). Recrystallisation from toluene gave the product as white crystals 5.42g (66%), m.p. 110-112°C [lit. [47] 91%, 110 - 111°C]. <sup>1</sup>H NMR (200MHz; CDCl<sub>3</sub>)  $\delta$  6.85 (2H, s, Ar H's), 4.58 (2H, d, J = 5.2Hz, CH<sub>2</sub>OH [x2] →  $\delta$  4.58, s, on D<sub>2</sub>O exchange), 3.86(6H, s, OCH<sub>3</sub> [x2]), 3.61(2H, br s, OH [x2], exchangeable with D<sub>2</sub>O) ppm. <sup>13</sup>C NMR (50MHz; CDCl<sub>3</sub>)  $\delta$  148.31(C-4, C-5), 131.91(C-1, C-2), 113.08(C-3, C-6), 63.31(CH<sub>2</sub> [x2]), 55.89(OCH<sub>3</sub> [x2]) ppm.  $\nu_{\max}$  (KBr), 3463 (O-H), 3341(O-H), 2924, 1610, 1514, 1452, 1407, 1363, 1286, 1225, 1103, 1011, 979, 877, 852, 753, 703, 549 cm<sup>-1</sup>.

(c) *4,5-dimethoxy- $\alpha$ ,  $\alpha'$ -dibromo-o-xylene* (**59**)

Concentrated sulphuric acid (5.32 cm<sup>3</sup>, 9.8g, 0.1moles) contained in a 250cm<sup>3</sup> round bottom flask, fitted with a condenser, was placed in an ice bath. 48% Hydrobromic acid (11.71 cm<sup>3</sup>, 5.62g, 0.069moles) was then added dropwise with stirring. When the addition was complete, the solution was left

stirring for a further 10 minutes. A solution of 4,5-dimethoxyphthalyl alcohol (5g, 0.025 moles) in ethanol (150 cm<sup>3</sup>) [which formed a clear, colourless solution], was then added dropwise to the solution over a period of 15 minutes. The reaction vessel was removed from the ice bath and stirring continued at room temperature for a further 90 minutes. On completion, the reaction mixture was clear pale yellow in colour, and the solvent was removed *in vacuo*. As the volume of solvent decreased the colour went from pale yellow to increasing darker red to eventually a "blood red" and finally a cream solid fell out of solution. This solid was filtered off and washed several times with water until the washings ran clear. The white solid was air dried, and then finally dried between filter paper and which on leaving in an evacuated desiccator overnight in darkness, gave a creamy white powder of 4,5-dimethoxy- $\alpha$ ,  $\alpha'$ -dibromo-o-xylene (7.3g, 90%), m.p. 104.5 – 106.6°C. <sup>1</sup>H NMR (200MHz; CDCl<sub>3</sub>)  $\delta$ 6.84 (2H, s, Ar H's), 4.63 (4H, s, CH<sub>2</sub>Br [x2]), 3.89 (6H, s, OCH<sub>3</sub> [x2]) ppm. <sup>13</sup>C NMR (50MHz; CDCl<sub>3</sub>)  $\delta$ 149.43(C4, C5), 129.01(C-1, C-2), 113.55(C-3, C-6), 56.94(OCH<sub>3</sub> [x2]), 30.59(CH<sub>2</sub>Br [x2]) ppm.  $\nu_{\max}$  (KBr) 3003, 2954, 1605, 1522, 1460, 1356, 1272, 1238, 1203, 1124, 1090, 1001, 873, 749, 670, 601, 542 cm<sup>-1</sup>, elemental analysis C<sub>10</sub>H<sub>12</sub>Br<sub>2</sub>O<sub>2</sub>, % calculated C 37.1, H 3.7, Br 49.3, O 9.9, % found C 37.36, H 3.66, Br 49.05, O 9.93.

(d) 5,6-dimethoxy-N-methylisoindole (**56**)

A three necked round bottomed flask was fitted with a nitrogen inlet, a dropping funnel and condenser fitted with a calcium chloride drying tube. The flask was charged with a clear pale yellow solution of 4,5-dimethoxy- $\alpha$ ,  $\alpha'$ -dibromo-o-xylene (1g, 3.08mmol) in dry diethylether (35 cm<sup>3</sup>). A solution of methylhydrazine (0.36 cm<sup>3</sup>, 0.311g, 6.07 mmol) in dry diethylether (1.5 cm<sup>3</sup>) was added dropwise from the dropping funnel, with stirring, under a nitrogen atmosphere, over 5 minutes. After the addition of a couple of drops, an immediate white colouration of the solution resulted. On continued addition, the white colour became more intense and an apparent white precipitate had formed. The reaction mixture remained stirring for a further 3

hours, then allowed to stand overnight under an inert atmosphere. On standing overnight the solid turned a slight yellow colour. The ether was decanted and the reaction vessel flushed with N<sub>2</sub> to remove any trace ether, after 10 minutes the sides of the vessel were scrapped to free the solid for stirring. Dry powdered potassium hydroxide (2.156g, 0.0385 moles) was added in portions, with vigorous stirring over 5 minutes. The reaction mixture was stirred for a further 1 hour, all the while under a nitrogen atmosphere. Finally a yellow solid was transferred to a sublimation apparatus and sublimed under high vacuum (3 mmHg), with heating to 80°C in an oil bath, and a clear liquid appeared on the cold finger. After 45 minutes the liquid was removed and the cold finger wiped dry. The high vacuum (0.8 mmHg) was applied to the system, with heating of the oil bath to 80°C, and a white solid began to appear on the finger, as the oil temperature was increased slowly to 115°C, with increasing white solid crystals appearing on the finger. After 1 hour the sublimation was stopped, the salt mixture in the reaction vessel was now deep brown / mustard colour and the white crystals were removed from the finger and stored under nitrogen (0.146g, 25%), m.p. 53 - 58°C. <sup>1</sup>H NMR (200MHz; CDCl<sub>3</sub>) δ6.86 (2H, s, Ar H [H-4, H-7]), 6.77 (2H, s, Ar H [H-1, H-3]), 3.88 (9H, s, OCH<sub>3</sub> [x2], N-CH<sub>3</sub>) ppm. <sup>13</sup>C NMR (50MHz; CDCl<sub>3</sub>) δ147.43 (C-5, C-6), δ119.86 (C-8, C-9), δ111.0 (C-1, C-3), δ97.24 (C-4, C-7), δ55.63 (N-CH<sub>3</sub>), δ37.24 (OCH<sub>3</sub> [x2]). ν<sub>max</sub> (KBr) 3444, 2940, 2836, 1654, 1504, 1450, 1353, 1213, 1139, 1014, 838, 748, 715 cm<sup>-1</sup>. UV-vis (CH<sub>3</sub>CN) λ<sub>max</sub> 222.5, 296, 324.5nm.

#### 2.4.4 Preparation of 5-methoxy-N-methylisoindole (57)

##### (a) 4-methoxy- $\alpha,\alpha'$ -dibromo-o-xylene (76)

N-bromosuccinimide (11.4g, 0.064 moles) was placed in a 250ml round bottom flask with carbon tetrachloride (50cm<sup>3</sup>). The mixture was then stirred and a catalytic amount of AIBN (0.1g) was added. To this mixture 3,4 - dimethyl anisole (4.30g, 0.032 moles) in carbon tetrachloride (50cm<sup>3</sup>) was added slowly with stirring. The mixture was refluxed for four hours and TLC



analysis showed no presence of starting material. The reaction mixture was cooled to 50°C and filtered. The filtrate was then reduced *in vacuo* to leave a dark red residue (8.74g). The product was purified by flash chromatography (ethyl acetate 5:95 hexane) leaving a purified product of 4.51g (48%) m.p. 48.2 - 49.6°C (lit. [56] 49-50°C). <sup>1</sup>H NMR (200MHz; DMSO) δ7.40 (1H, d, Ar H's J<sub>H5,H6</sub>=8.6 Hz), δ7.04 (1H, d, Ar H's J<sub>H3,H5</sub>=2.5 Hz), δ6.81 (1H, dd, Ar H's J<sub>H3,H5</sub>=2.5, J<sub>H5,H6</sub>=8.5 Hz), δ4.77 (4H, d, 2 x CH<sub>2</sub>Br), δ3.74 (3H, s, OCH<sub>3</sub>). <sup>13</sup>C NMR (50MHz; DMSO) δ159.61 (C-4), δ138.11 (C-1), δ132.8 (C-2), δ128.46 (C-6), δ116.45 (C-3), δ114.62 (C-5), δ55.26 (OCH<sub>3</sub>), δ31.4 and δ30.7 ppm (CH<sub>2</sub> [x2]). ν<sub>max</sub> (KBr), 1609.8, 1577.4, 1502.7, 1314.6, 1293.1, 1263.9, 1165.9, 1143.9, 1087.6, 936.0, 893.8, 822.8, 767.6 cm<sup>-1</sup>.

*(b) 5-methoxy-N-methylisoindole (57)*

A three necked round bottomed flask was fitted with a nitrogen inlet, a dropping funnel and condenser fitted with a calcium chloride drying tube. The flask was charged with a clear pale yellow solution of 4-methoxy- $\alpha$ ,  $\alpha'$ -dibromo-*o*-xylene (1.9g, 6.4mmol) in dry diethylether (50 cm<sup>3</sup>). A solution of methylhydrazine (0.75 cm<sup>3</sup>, 0.654g, 0.0142 mol) in dry diethylether (1.5 cm<sup>3</sup>) was added dropwise from the dropping funnel, with stirring, under a nitrogen atmosphere, over 5 minutes. After the addition of a couple of drops, an immediate white colouration of the solution resulted. On continued addition, the white colour became more intense and an apparent white precipitate had formed. The reaction mixture remained stirring for a further 2 hours. The ether was decanted and the reaction vessel flushed with N<sub>2</sub> to remove any trace ether, after 10 minutes the sides of the vessel were scrapped to free the solid for stirring. Dry powdered potassium hydroxide (1.25g, 0.0229moles) was added in portions, with vigorous stirring over 5 minutes, resulting in an exothermic reaction. The reaction mixture was stirred for a further 1 hour. Finally a yellow solid was transferred to a sublimation apparatus and sublimed under high vacuum (0.1 mmHg), with heating to 80°C in an oil bath, and a clear liquid appeared on the cold finger. After 45 minutes the liquid was removed and the cold finger wiped dry, and retained

(0.052g), 5%. The salt mixture in the reaction vessel was now deep brown / mustard colour, and further product was obtained by extracting from this salt with dry ether (0.208g), 20%, total yield 25%.  $^1\text{H}$  NMR (200MHz;  $\text{CDCl}_3$ )  $\delta$ 7.40 (1H, d, Ar H [H-4]  $J_{\text{H4,H6}}=9\text{Hz}$ ), 6.96 (1H, s, Ar H [H-3]), 6.91 (1H, s, Ar H [H-1]), 6.75 (1H, s, Ar H [H-7]), 6.68-6.61 (1H, dd, Ar H [H-6]  $J_{\text{H6,H7}}=2.2, J_{\text{H4,H6}}=9\text{Hz}$ ), 3.93 (3H, s,  $\text{OCH}_3$  [x2]) 3.81 (3H, s  $\text{N-CH}_3$ ) ppm.  $^{13}\text{C}$  NMR (50MHz;  $\text{CDCl}_3$ )  $\delta$ 154.52 (C-5),  $\delta$ 124.41 (C-6),  $\delta$ 122.92 (C-7),  $\delta$ 120.76 (C-8),  $\delta$ 115.47 (C-9),  $\delta$ 112.05 (C-1),  $\delta$ 110.55 (C-3),  $\delta$ 95.65 (C-4),  $\delta$ 55.07 ( $\text{N-CH}_3$ ),  $\delta$ 37.11 ( $\text{OCH}_3$ ).  $\nu_{\text{max}}$  (KBr) 3120, 2940, 2831, 2360, 1635, 1525, 1492, 1479, 1409, 1226, 1164, 1029, 943, 800, 730, 603  $\text{cm}^{-1}$ . UV-vis ( $\text{CH}_3\text{CN}$ )  $\lambda_{\text{max}}$  225, 279, 328.5nm.

## 2.5 References

- [1] P. Kovacic, M.B. Jones, *Chem. Rev.*, (1987), **87**, 357.
- [2] E.M. Genies, *New J. Chem.*, (1989)
- [3] A.F. Diaz, K.K. Kanazawa, and G.P. Gardini, *J. Chem. Soc. Chem. Commun*, (1979), 635.
- [4] A.F. Diaz, J.C. Lacroix, *New J. Chem.*, (1988), **12**, 171.
- [5] A.F. Diaz, *Chem. Scr.*, (1981), **17**, 142.
- [6] J. Roncali, *Chem. Rev.*, (1992), **92**, 711.
- [7] R. Bonnet, and S.A. North, *Adv. Heterocycl. Chem.*, (1981), **29**, 341.
- [8] R. Bonnet and R.F.C. Brown, *Chem. Commun.*, (1972), 393
- [9] A. Baeyer, *Justus Liebigs Ann. Chem.*, (1866), **140**, 295.
- [10] J. Bornstein, D.E. Remy, and J.E. Shields, *Chem. Commun*, (1972), 1149.
- [11] G.M. Priestley and R.N. Warrenner, *Tetrahedron Lett.*, (1972), 4295.
- [12] M.C. Moore in *Organic Reactions*, R. Adams Ed. Wiley, New York, (1949), **vol V**, 304
- [13] J.C. Emmett and W. Lwowski, *Tetrahedron*, (1966), **22**, 1011
- [14] J.D. White, M.E. Mann, H.D. Kirshenbaum and A. Mitre, *J. Org. Chem.*, (1971), **36**, 1048.
- [15] D.F. Veber and W. Lwowski, *J. Am. Chem Soc.*, (1964), **86**, 4152.
- [16] G. Cignarella, R. Cerri, G. Grella and P Sanna, *Gazz. Chim. Ital.*, (1976), **106**, 65.
- [17] G. Cignarella and A. Saba, *Ann Chim.*, (1970), **60**, 765.
- [18] J. Bornstein, J.E. Shields and A.P. Boisselle, *Organic Synthesis*, Wiley, New York, (1973), Coll. Vol., 406.
- [19] J. Bornstein, J.E. Shields and A.P. Boisselle, *Organic Synthesis*, Wiley, New York, (1973), Coll. Vol., 1064.
- [20] R.E. Gawley, S.R. Chamburkhar, A.L. Smith and T.V. Anklekar, *J. Org. Chem.*, (1988), **53**, 5381.
- [21] G. Whittig, H. Tenhaeff, W. Schoch, and G. Koenig, *Justus Liebigs Ann. Chem.*, (1951), **1**, 572
- [22] B. Zeeh and K.H. König, *Synthesis*, (1972), **46**

- [23] P.S. Anderson, M.E. Christy, C.D. Colton, W. Halczenko, G.S. Ponticello and K.L. Shepard, *J. Org. Chem.*, (1979), **44**, 1519.
- [24] R. Kreher, J. Seubert, *Angew. Chem., Int. Ed. Engl.* (1964), **3**, 639; (1966), **5**, 967.
- [25] R. Kreher, U. Feldhoff, J. Seubert, D. Schmitt, *Chem.-Ztg.* (1987), **11**, 155.
- [26] R. Kreher, J. Seubert, D. Schmitt, G. Use, N. Kohl, *Chem.-Ztg.* (1988), **112**, 85.
- [27] R. Kreher, T. Hildebrand, *Chem. Ber.* (1982), **121**, 81.
- [28] G. Use, R. Kreher, *Chem.-Ztg.* (1982), **106**, 143.
- [29] R. Kreher, G. Use, *Heterocycles*, (1982), **19**, 637.
- [30] R. Kreher, N. Kohl, *Chem.-Ztg.* (1986), **110**, 299.
- [31] R. Kreher, T. Hildebrand, *Angew. Chem.*, (1987), **99**, 1325.
- [32] R. Kreher, G. Use, *Angew. Chem.*, (1989), **122**, 337.
- [33] R. Kreher, G. Sewarte-Ross, G. Vogt, *Chem. Ber.*, (1990), **123**, 1719.
- [34] R. Kreher, N. Kohl, G. Use, *Angew. Chem.*, (1982), **94**, 634.
- [35] R. Kreher, K-J Herd, *Chem. Ber.*, (1988), **121**, 1827.
- [36] R. Kreher, J. Seubert, N. Kohl, *Chem.-Ztg.* (1987), **111**, 349.
- [37] R. Kreher, N. Kohl, *Angew. Chem.*, (1984), **96**, 507.
- [38] R. Kreher, M.R. Konrad, *Chem.-Ztg.* (1986), **110**, 363.
- [39] H. Hennige, R. Kreher, J Uhrig, *Synthesis*, (1982), 842.
- [40] H. Hennige, R. Kreher, M.R. Konrad, F. Jelitto, *Chem. Ber.*, (1988), **121**, 243.
- [41] R. Kreher, M.R. Konrad, *Chem.-Ztg.* (1988), **112**, 335.
- [42] R. Kreher, H. Hennige, F. Jelitto, J. Preut, *Z Naturforsch. B. Chem. Sci.*, (1989), **44**, 1132.
- [43] J. Bornstien, D.E. Remy, and J.E. Shields, *Tetrahedron Lett.*, (1974), 4247.
- [44] H. Heaney, S.V. Ley, A.P. Price, and R.P. Sharma, *Tetrahedron Lett.*, (1972) 3067.
- [45] M. Armed and J.M. Vernon, *Chem. Commun.*, (1976), 462.
- [46] R. Kreher, G. Vogt, *Angew. Chem., Int. Ed. Engl.* (1970), **9**, 955.
- [47] D. Bhattacharjee and F. Popp, *J. Pharm Chem.* (1980) **69**. 120.
- [48] Aldrich Chemical Co.

- [49] Vogel, *Textbook of Practical Organic Chemistry*, **5.5**, 563.
- [50] Softshell International, ChemWindows, Version 3.1.4.
- [51] F.H. Covitz, *J. Amer. Chem. Soc.*, (1967), **89**, 5403.
- [52] J.H.P. Utley, Y.Gao and R.Lines, *J. Chem. Soc. Chem. Commun*, (1993), 1540.
- [53] A. Merz, R. Schwarz and R Schropp, *Advanced Materials*, (1992), **4**, (No. 6), 409.
- [54] W. Rettig and J. Wirz, *Helv. Chim. Acta*, (1976), **59**, 1054.
- [55] S.N. Chakravarti and W.E. Perkin, Jr. *J. Chem. Soc.* (1929), 196.
- [56] B.V. Shetty, U.S. Patent 4,210,749, July 1, 1980.
- [57] Ohkawa S., DiGiacomo B., Larson D.L., Takemori A.E., & Portoghese P.S., *J. Med. Chem.* (1997), **40**, 1720 – 1725.
- [58] Wang W., Li T., Attardo G., *J Org. Chem.*, (1997), **62**, 6598 – 6602.
- [59] T.T. Hung and S.A. Chen, *Polymer*, (1999), **40**, 3881-3884.

## **Chapter 3**

# **Preliminary Electrochemical Characterisation of Isoindole Monomers and Corresponding Polymers**

## Chapter 3 – Preliminary Electrochemical Characterisation of Isoindole Monomers and Corresponding Polymers

### 3.1 Introduction

Electrochemistry generally involves having precise control over the application of a potential and the measurement of charge and/or current during an experiment. All of the electrochemical work presented in this thesis was performed in organic media, and the two techniques employed in various experiments, both cyclic voltammetry and potential step are discussed.

#### 3.1.1 Electrodes.

##### (a) Working Electrodes.

The surface of the working electrode defines the interface at which an electrochemical reaction under study is occurring. Therefore, the properties of the working electrode material may be of importance for the study of various different systems. A wide variety of materials have been employed as working electrodes, the most common being platinum and carbon which will be described briefly below.

It has been suggested that the rate of electron transfer across an electrode solution interface may be dependent on the physical and chemical properties of the electrode material [1, 2]. The range of accessible potentials for a particular electrode material is normally limited at negative potentials by the reduction of the supporting electrolyte or the solvent. In the case of indium tin oxide electrodes, reduction of the electrode material sets the cathodic potential limit. At positive potentials, the potential range is normally limited by oxidation of the supporting electrolyte or solvent, or by the oxidation of the electrode material itself to form soluble metal ions or metal oxides. Tables exhibiting the useful potential ranges for different electrode materials are readily available [4, 5]. Therefore, the working electrode material must be judiciously chosen for a particular study.

The design of the working electrode is usually dependent on the experiment to be performed. The working electrode size is variable but for use in cells of small volume an electrode with a small geometric area is commonly employed. It is also necessary that the surface area of the working electrode be smaller than the area of the auxiliary electrode, as the latter acts as a current sink to prevent any current flow into the reference electrode.

In order to obtain consistent results the working electrode must be pretreated to remove surface impurities. Generally this involves polishing the electrode on cloth pads impregnated with a polishing compound such as alumina of a definite particle size. Other methods of pretreatment can involve electrochemically cycling the electrode in supporting electrolyte solutions between the oxygen evolution potential and the hydrogen evolution potential.

Platinum working electrodes are normally used as discs. Mounting of the electrode material normally involves sealing a rod of the solid electrode material in a tube of an inert substance such as teflon or glass. This is done so that a reproducible and easily polished area of the electrode, such as a disc, is exposed.

A platinum working electrode sealed in teflon was employed in this work and the exposed platinum surface was polished using a 0.3  $\mu\text{m}$  alumina slurry on felt to a mirror finish and had a geometric surface area of ca. 0.071  $\text{cm}^2$ .

#### (b) *Reference Electrodes*

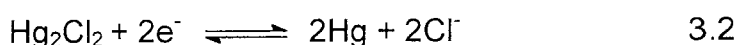
An ideal reference electrode should exhibit the following properties [6] (a) it should be reversible and contain both the oxidized and the reduced form of a redox couple, both of which should be stable, (b) its potential should be stable with time, (c) its potential should not change when a small amount of current has passed through the electrode, (d) it should show little dependence on temperature.



The reference electrode is employed as a source of a fixed potential. Since the potential at the reference electrode is fixed, any change in the voltage applied by the potentiostat is felt at the working electrode – solution interface. The most common reference electrodes employed in fundamental studies are the saturated calomel electrode or the silver – silver chloride electrode. The saturated calomel electrode consists of a half – cell containing mercury and mercurous chloride in contact with a solution of saturated potassium chloride, represented as follows [7]



and has the following half – cell reaction



The saturated solution of KCl employed in this electrode has a high density and must be retained in the electrode by the use of a ceramic, glass or vycor frit so that it does not leak out into the test solution.

### (c) Counter Electrodes.

The current generated at the working electrode is forced to flow through the counter electrode by the potentiostat, thereby preventing any current flowing into the reference electrode. This prevents any internal polarisation of the reference electrode. To allow the current to pass without difficulty through the counter electrode its area is greater than that of the working electrode. The counter electrode should also be insoluble and inert to the supporting electrolyte solution thereby preventing contamination of the test solution. Platinum or carbon is commonly used as the counter electrode material. The counter electrode employed throughout this work was glassy carbon rod.

### 3.1.2 Electrochemical Techniques.

#### (a) *Cyclic Voltammetry Experiments*

Cyclic voltammetry is an extension of linear sweep voltammetry. Linear sweep voltammetry involves applying a potential ramp as a function of time to the working electrode. In cyclic voltammetry the potential is cycled between two potentials. The potential time profile is triangular in shape. A substantial amount of the mathematics derived for linear sweep voltammetry can be applied to cyclic voltammetry. The use of this theory in conjunction with experimental results enables the determination of kinetic parameters [8].

The triangular waveform is normally generated as follows; The initial potential  $E_1$  is normally chosen such that no current flows at that potential. The potential is then swept at a rate  $v$ , termed the scan rate, to a potential  $E_2$ , known as the switching potential. At the switching potential  $E_2$  the sweep is reversed, normally at the same scan rate usually quoted in volts per second; see figure 3.1. This process can be continued once the potential reaches  $E_1$  or it can be halted. It is usually inconvenient to deal with the standard redox potential of a system since its measurement involves the determination of activity coefficients. To avoid this a formal potential,  $E_f$  is defined. A general cell is considered with the following general reaction occurring at the right hand electrode



and the left hand electrode consisting of the standard hydrogen electrode. The formal potential  $E_f$  is defined as the measured potential of the cell when (i) the species O and R are present at concentrations such that  $[O] / [R]$  is equal to one and (ii) other species in the system are at known and designated concentrations [9]. If the formal potential of the redox couple lies in the region between  $E_1$  and  $E_2$  then as the potential approaches  $E_f$  electron transfer begins.

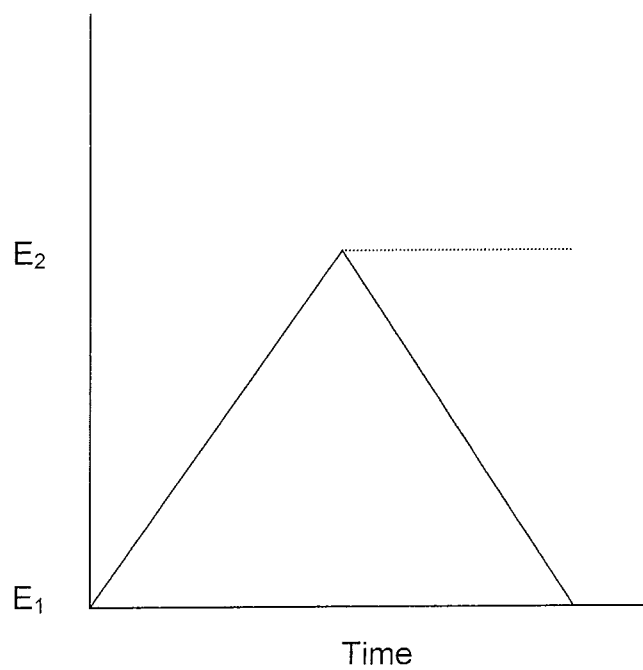


**Figure 3.1:** The applied potential waveform for cyclic voltammetry.

Let the sweep from  $E_1$  to  $E_2$  be the anodic scan where oxidation of the redox couple occurs and the reverse sweep be the cathodic scan where reduction of the product of the anodic scan occurs, as shown in figure 3.2. Once oxidation occurs a diffusion layer begins to extend out into the solution resulting in a greater distance across which the reactant must travel. This increasing diffusion layer thickness results in a peak arising in the cyclic voltammogram. After the switching potential as the potential approaches  $E_r$  reduction of the product occurs and the diffusion layer containing the product is depleted.

Theory describing the signal obtained by applying a triangular potential waveform to a solution of a species exhibiting reversible electrochemistry has been presented [10-12]. From this work a number of useful diagnostic parameters have been developed. The peak separation  $\Delta E_p$  (mV) is a useful diagnostic parameter of Nernstian systems. Although it has a slight dependence on the switching potential it is always close to  $58/n$  mV at  $25^\circ\text{C}$  for a reversible system. A problem which may be encountered in employing this diagnostic test is the presence of uncompensated resistance in the cell. This may induce a larger peak to peak separation than that predicted. The potential at half – height for a linear sweep voltammogram has been shown to be removed from the peak potential for a reversible species by  $26.5/n$  mV at  $25^\circ\text{C}$ . Varying the scan rate has been shown to have no effect on the peak potential for a reversible system but does cause a change in the peak current. Randles and Sevcik [10, 11] have presented the equation relating the peak current to the scan rate as follows,

$$i_p = 0.4463nAF\left(\frac{nF}{RT}\right)^{1/2} C^*D^{1/2} \nu^{1/2} \quad 3.4$$

where  $i_p$  is the peak current in amps,  $\nu$  is the scan rate in  $\text{V s}^{-1}$ , and the other terms have their usual meaning.

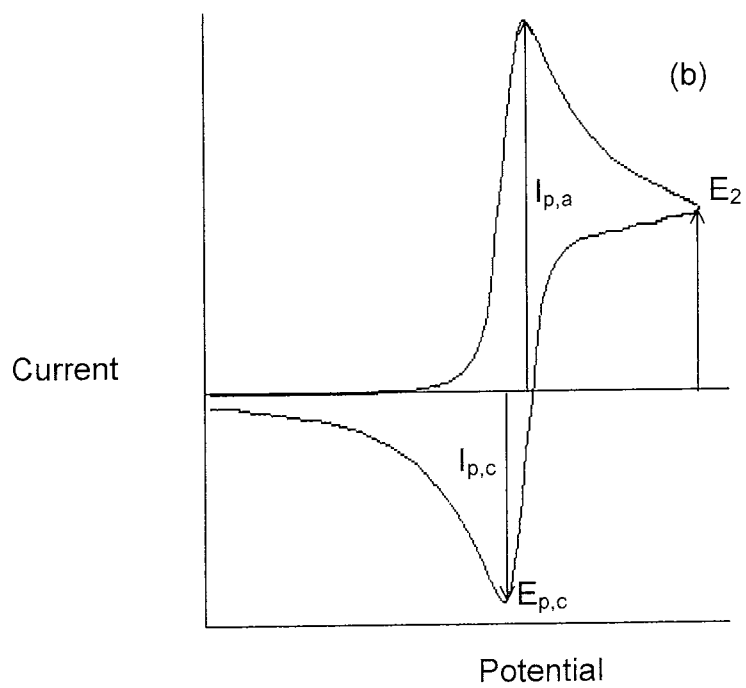


**Figure 3.2:** The resulting cyclic voltammogram obtained as a function of applied potential.

Possibly the most common application for cyclic voltammetry is the preliminary electrochemical characterisation of a system. The cyclic voltammogram obtained provides information on the reversibility of a system and on the potential regions in which the species is electrochemically active.

Cyclic voltammetry has also been found to be of value when studying surface bound species. Here we can consider the irreversible adsorption or the confinement to the electrode surface of a species which exhibits reversible electrochemistry. In this case, if Langmuir adsorption is assumed the peak potentials for both the reduction and the oxidation processes are found to be coincident [13-17] as can be seen in figure 3.3. The peak currents are found to be related to the scan rate according to the following relationship which applies to a thin layer situation or a surface confined species

$$|i_p^c| = \left( \frac{n^2 F^2 A \Gamma}{4RT} \right) v \quad 3.5$$

Where  $|i_p^c|$  represents the magnitude of the cathodic current and  $\Gamma$  is the surface excess of the reactant in mol cm<sup>-2</sup>.

#### *(b) Theory of Potential Step Experiments*

Potential step techniques in electrochemistry involve changing the potential of the working electrode rapidly from one potential value,  $E_1$ , to another  $E_2$ .  $E_1$  is usually chosen to be a potential where no current flows. A current time response (chronoamperometry) or a charge-time response (chronocoulometry) can be recorded. Most potential step techniques are carried out where diffusion is the only form of mass transport present.

The potential time profile applied to the working electrode is illustrated in figure 3.4. The potential of the working electrode can be stepped into 2 separate regions. These regions are where the current is purely diffusion controlled or diffusion and kinetically controlled. The current-time transient

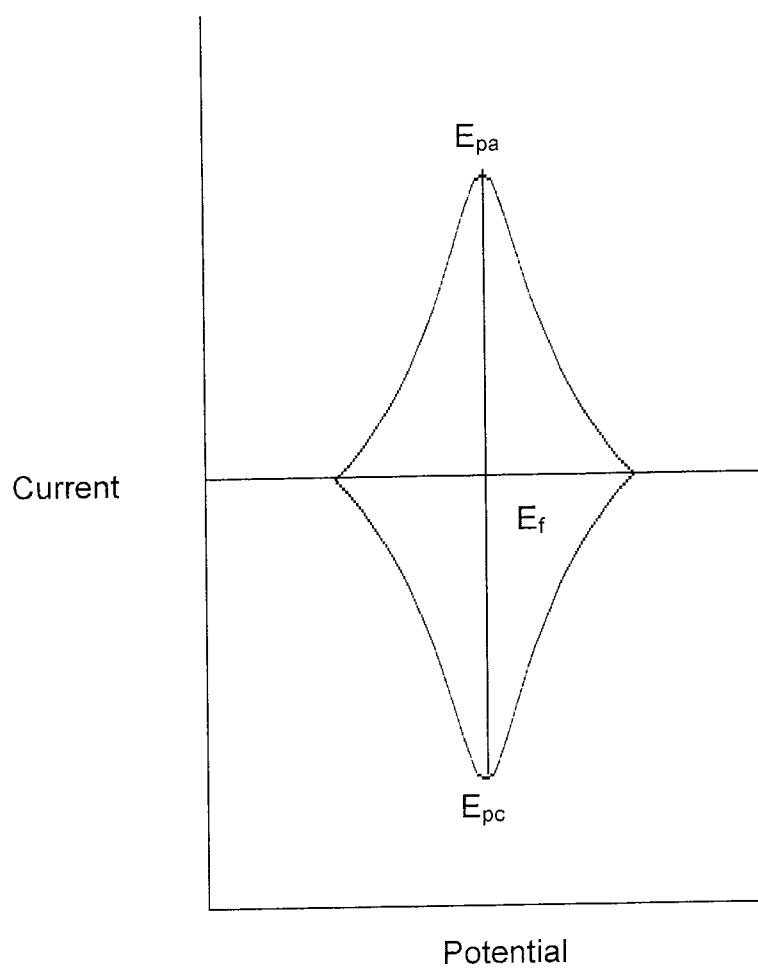


**Figure 3.3:** A cyclic voltammogram obtained for a species confined to an electrode surface.  $E_{pa}$  and  $E_{pc}$  are the anodic and cathodic peak potentials respectively which are both equal to  $E_f$ .

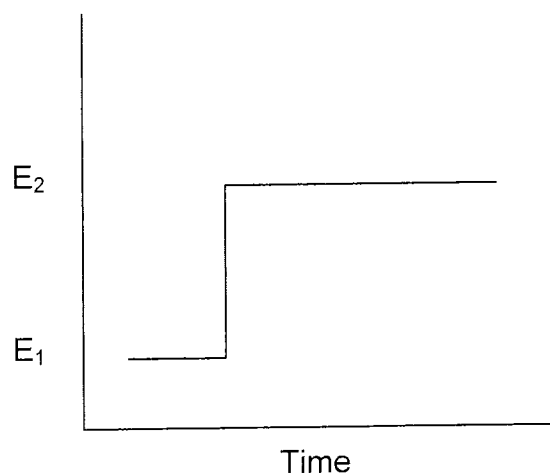


**Figure 3.4:** The potential – time profile for a single potential step chronoamperometric experiment

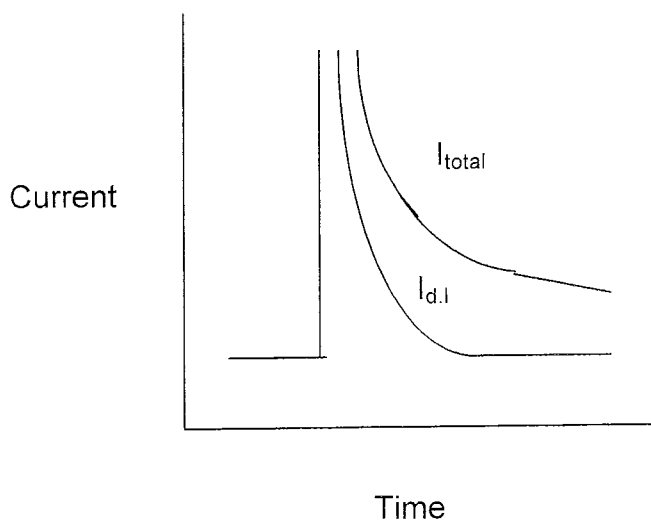


**Figure 3.5:** Current time transient for a potential step experiment. The total current and the double layer charging current components are shown.



produced for the reaction 3.3, when the current is diffusion controlled is illustrated in figure 3.5. It can be seen from that there are two components to the current, one being the associated faradaic current and also the double layer charging current. This is one problem associated with potential step techniques, the presence of the double layer current. This current usually takes in the order of a few hundred microseconds to decay and depends on electrolyte concentration.

The response to a potential step for reaction 3.3, into a diffusion controlled region can be explained by considering the growth of the diffusion layer out into solution. If the potential of the working electrode is stepped to a large positive overpotential, rapid oxidation of species R at the electrode surface will occur. Effectively, the surface concentration of R decreases from bulk solution value to zero. At short times the concentration of R will only have changed from its initial bulk solution value, at points close to the electrode surface, and hence the concentration profile will be steep. As time increases, diffusion occurs, causing the concentration profiles to relax further out into solution.

The response will be a transient where the current density falls with time, as seen in figure 3.5.

The resulting Faradaic current is governed for linear one dimensional diffusion by the equation [11]

$$i = \left( \frac{nFAD^{1/2}C^*}{(\pi t)^{1/2}} \right) \quad 3.6$$

where n is the number of electrons transferred, D is the diffusion coefficient and C\* is the bulk concentration of the reactant. This equation has been used to determine if an electrode reaction is diffusion controlled within the applied potential range and values of the diffusion coefficient for species may be determined once the electrochemical area A is known. If the potential is

stepped into a region of mixed control, kinetic parameters, such as rate constants, can also be determined [18].

### 3.1.3 *Synthesis of Conducting Polymers*

Traditionally conducting polymers have been directly synthesised by electrochemical methods [19-28]. The major advantage with this method is that polymerisation may be controlled instrumentally and the polymer is obtained as a film suitable for further electrochemical analysis. Thus, electrochemistry plays the dual role of a synthetic and an analytical tool.

However, electrochemical synthesis is not the only method of synthesising organic semiconducting materials. Chemical [29-41] and more recently photochemical polymerisation [42-47] have been reported. The principal advantage of chemical methods is related to the possibility of mass production at low cost [48]. On the other hand, electrochemical methods offer materials with better conducting properties [48] and for some applications, such as the construction of electronic devices, electrochemical polymerisation offers the possibility of in-situ formation. In general conducting polymers can also be obtained as free standing films [49-52], powders [42,53,54] or composites [55-62] and all are generally insoluble, thus making their characterisation difficult.

### 3.1.4 *Electrochemical Synthesis*

Of the three methods of synthesis, the electrochemical route has been the most explored, where the polymers can be grown either potentiostatically or galvanostatically [21,26,48,63-66]. The flow of an anodic current in a simple electrochemical cell, through a solution containing a solvent, an electrolyte and the monomer can promote, in some specific electrical conditions, the generation of a polymeric film on the anode (platinum, gold, aluminium, ITO, etc). With the correct conditions a polymeric layer can be formed within a few seconds. As the electrochemical potential needed for monomeric oxidation is significantly higher than charging (or doping) the formed polymer,

the polymer is directly obtained in its conducting state. The film thickness can easily be controlled by the electrical charge employed during polymerisation.

The experimental requirements are not difficult, as it is possible to work at ambient pressure and temperature, and in some cases, with an aqueous solvent. The most restrictive condition is the requirement of an inert atmosphere when using oxygen sensitive monomers or dark conditions for light sensitive monomers. As well as easy experimental conditions, the electrochemical route can yield a wealth of information. It can allow the reaction pathway to be probed and give an insight into the mechanism for the polymerisation, which may be extended to the chemical and photochemical routes, with obvious variation.

#### 3.1.5. *Preliminary study of electrochemical synthesis*

The study of the electrosynthesis of any conjugated polymer is subject to similar restrictions, imposed by the necessity for a suitable solvent / electrolyte system in which the synthesis can be performed. As the polymerisation reaction proceeds via radical cation intermediates, the process will be very sensitive to the nucleophilicity of the environment in the region near the electrode surface. In this sense there are some limitations on the choice of the solvent and the electrolyte.

In general, the flow of an anodic current through an electrochemical system of the monomer, a solvent and an electrolyte can initiate the following reactions:

- (a) Formation of an oxide layer on the metal (from water or residual water)
- (b) Oxidation of monomer on the metal or metal oxide layer
- (c) Oxidation of the solvent
- (d) Oxidation of the electrolyte

Under the correct conditions, whereby polymerisation occurs leading to an electrode coating, the chemical nature of the electrode surface changes. Reactions (a-d) will occur at different potentials on a new electrode and a new metal-polymer interface appears producing new reactions [48]:

(e) Polymer oxidation

(f) Polymer degradation

The approach to the study of the electrochemical generation of conducting polymer films must be initiated by the study of the potential range where these different processes occur. For this purpose it is convenient to know the potential window of the working electrode in the supporting electrolyte. Cyclic voltammetry of the working electrode in the background solution (in the absence of the monomer) allows confirmation of the potential window of work, as well as confirmation of a clean system.

When, for instance in the case of pyrrole present in solution, a voltammetric study allows the identification of the potential ranges where oxidation or polymerisation of the monomer takes place. It is also convenient to know the potential ranges where monomer and electrolyte oxidation and polymer oxidation and reduction take place on the working electrode coated with a thin film of polymer. In general the shapes of these cyclic voltammograms depend on the nature of the solvent and the electrolyte. As a preliminary conclusion, the choice of the supporting electrolyte used for an electropolymerisation process is based on the potential window of the electrode / supporting electrolyte system.

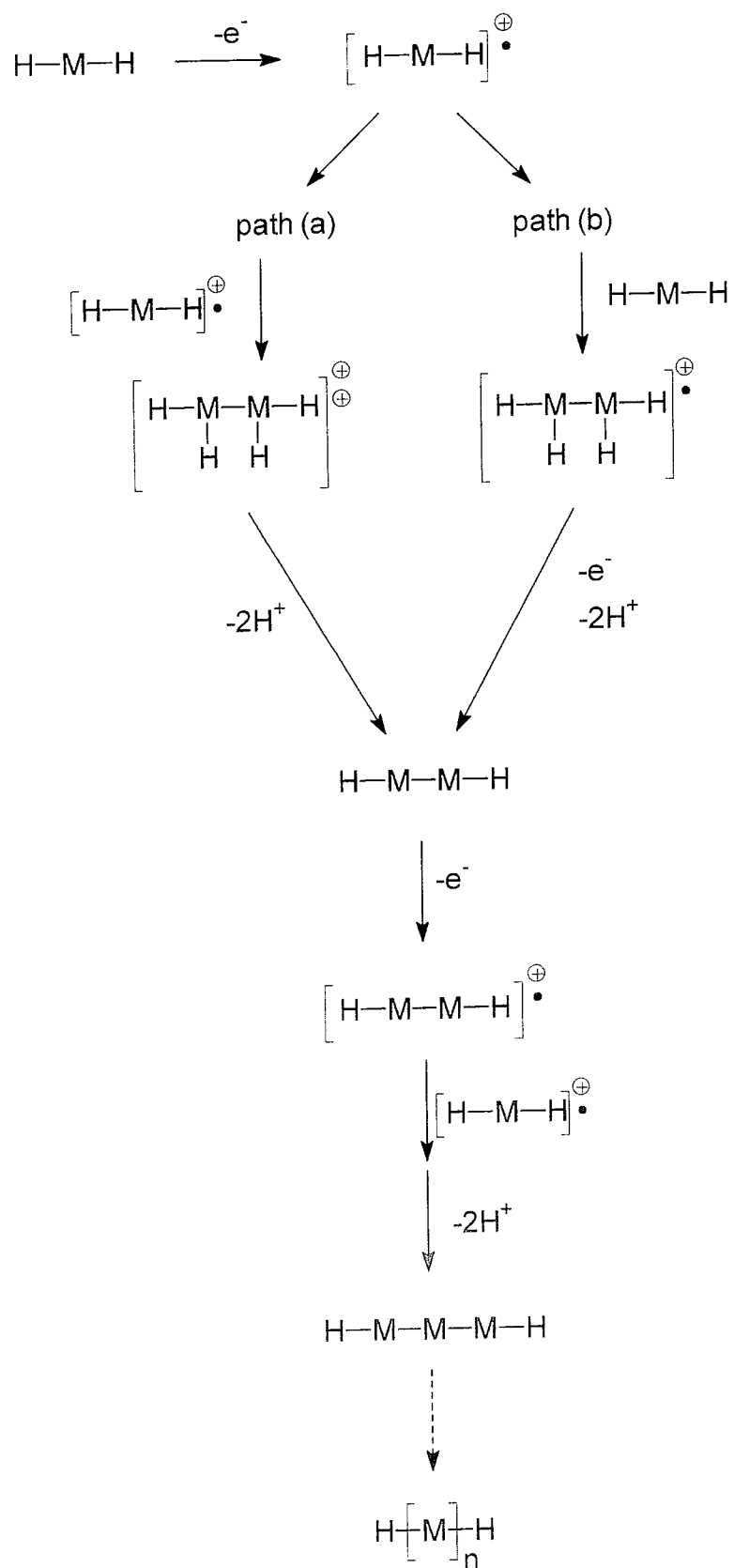
Because isoindoles have the same reactivity to pyrroles, it is useful to review electrochemical work carried out on pyrrole. Cyclic voltammetric studies of pyrrole solutions by Otero *et al.* [67] reveal that the oxidisation is irreversible. This suggests that the intermediate radical cations are unstable and rather reactive. Cyclic voltammograms were recorded with polypyrrole layer in water with background electrolyte 0.1M LiClO<sub>4</sub> on a platinum disk electrode, gives the oxidation peak of polypyrrole occurring at an anodic potential of 600

mV [67]. After reversing the direction of sweep from the first oxidation wave, a corresponding cathodic wave resulting from the reduction of the oxidised polymer is observed. Subsequent anodic sweeps reveal the growth of the polymer film from a monomer solution by an increase in charge involved in polymer oxidation and reduction.

### 3.1.6 Mechanism of Electropolymerisation

Scheme 3.1 shows the polymerisation of an aromatic monomer, where H-M-H represents an aromatic ring with hydrogens on the two active carbon centres. Initially loss of an electron (oxidation) results in the formation of a radical cation  $\text{H-M-H}^{\cdot+}$  which can lead to polymer formation by either of two routes. It can take path (a) in which it couples with another radical cation (radical-radical coupling) to give a dication which on loss of two protons affords the dimeric species H-M-M-H. Alternatively the radical cation can take route (b) in which it undergoes coupling with a monomer molecule, by electrophilic attack on the monomer. Both pathways have been investigated and results seem to point towards path (a) as the most favourable route.

Firstly, it has been argued [22] that radical-radical coupling does not take place as the coulombic repulsion forces between the positively charged species is too great to overcome. Kinetic studies however reveal evidence to support radical-radical coupling [21, 26, 68-70]. Genies et al. [68] have proved that polypyrrole films grow at a rate directly proportional to time, implying that the rate determining step is the radical ion coupling and not diffusion of the monomer to the electrode surface. Furthermore, the polymerisation reaction only proceeds when the potential is sufficiently high to oxidise the monomer. At these potentials the concentration of the neutral monomer at the electrode is virtually zero, thereby decreasing the possibility of radical-monomer coupling. The initial combination product of this coupling reaction is the dication dihydromer  $(\text{HMH})^{2+}_2$ , which, as said before, subsequently deprotonates to produce the neutral dimer H-M-M-H. The dimer is then oxidised, coupled with another radical cation and again deprotonated to give the next highest homologue.

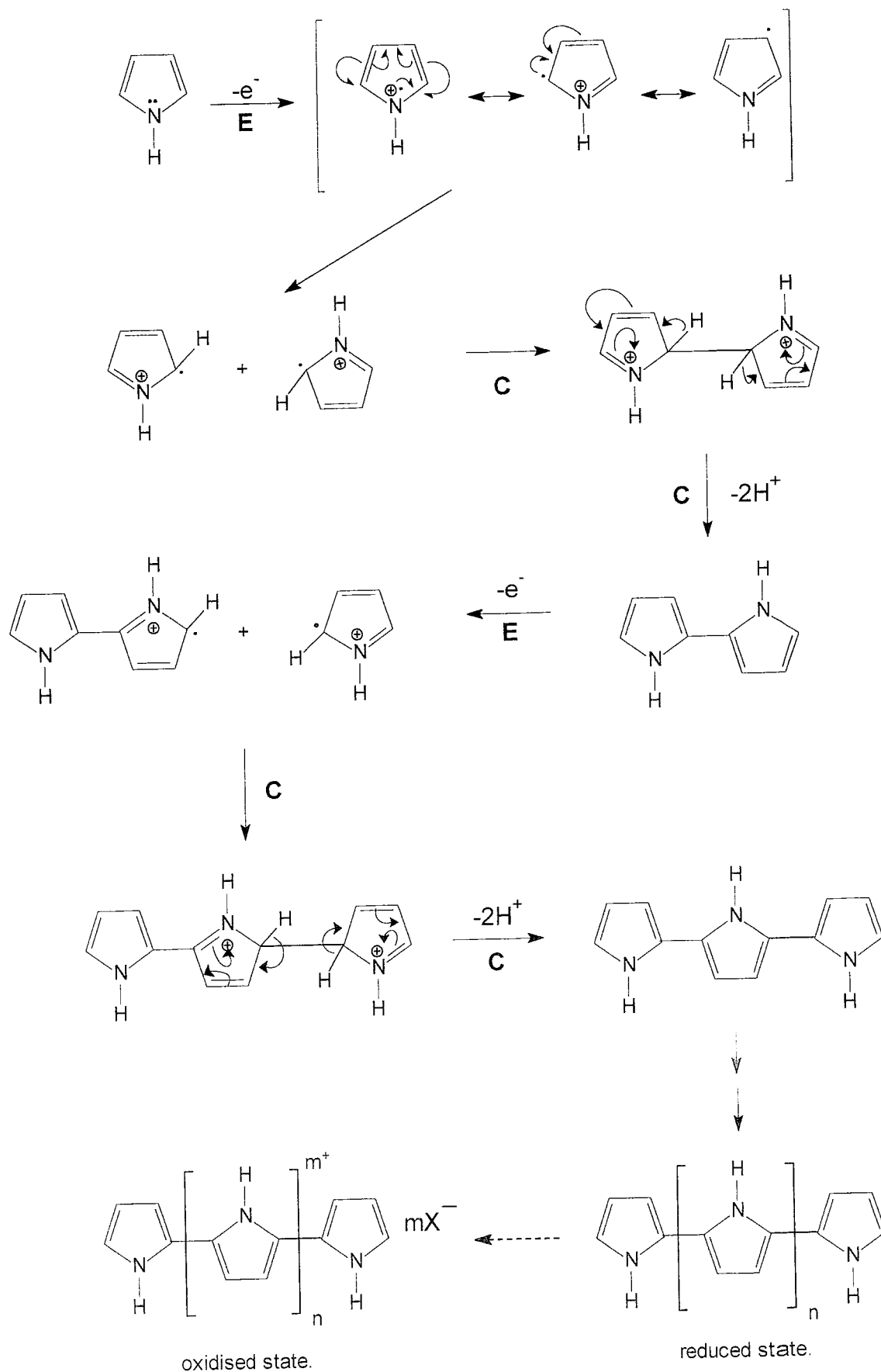


**Scheme 3.1:** Mechanism of the polymerisation of conducting polymers

The polymerisation proceeds in this manner until long chain polymers are formed. Under steady state conditions [69] the coupling reaction is reported to occur between the radical cations of the oligomers and the radical cation of the monomer as the dimer, trimer and polymer are more easily oxidised than the monomer. At this potential, oxidation of the polymer backbone is possible and movement of the anion X into the film results in the formation of oxidised polymer.

Scheme 3.2 shows the proposed polymerisation pathway of polypyrrole via radical – radical coupling. Cyclic voltammograms of polypyrrole films in background electrolyte [21,26,68] show that 2.2 – 2.4 F mol<sup>-1</sup> are required during film formation. 2 F mol<sup>-1</sup> are attributed to the polymerisation of pyrrole and the excess charge 0.2 – 0.4 F mol<sup>-1</sup> correspond to the irreversible oxidation or doping of the polymer, which occurs simultaneously with polymer generation. The polymerisation process can be considered as a condensation reaction, where the protons in the  $\alpha$ -position are eliminated, as can be deduced by the decrease in the pH of the electrolyte solution during film growth. On the other hand, characterisation of the polymer by different techniques confirms that the basic structure of the monomeric subunit survives in the polymer. These facts, together with the absence of polymerisation in  $\alpha$ -substituted pyrroles suggest that polymerisation of pyrroles leads to linear polymers whose monomeric units are  $\alpha,\alpha'$ - bonded, although  $\beta$ -linkages have also been detected [48].

Genies *et al.* [68] proposed the general mechanism for the electropolymerisation of pyrrole via radical-radical coupling, as shown in scheme 3.2. The first step consists of the oxidation of the monomer to form a radical cation. The second step involves formation of a dimer by radical-radical coupling, with two protons being eliminated from the doubly charged dihydrodimer to form a neutral species. As the dimer is more easily oxidised than the monomer, due to the increased stability of the radical cation formed, it is readily oxidised to the cation and undergoes a further coupling with the monomer radical cation.



**Scheme 3.2:** Mechanism for the polymerisation of Polypyrrole



From this scheme, electropolymerisation proceeds through successive electrochemical (E) and chemical (C) steps. Therefore this chain-propagation corresponds to a cascade of ECC steps. The chain growth is terminated either when the radical cation of the growing chain becomes too unreactive or, more likely, when the reactive end of the chain becomes sterically blocked from further reaction [71].

As already mentioned the oxidative polymerisation goes through very reactive radical cation intermediates that couple irregularly. The 2,5 coupling mode is ideal because it produces straight chains, which line up better than branched chains and also conduct better because conjugation between double and single bonds is maximized [72]. However, instead of coupling at the carbons in the 2 and 5 positions of pyrrole, non-2, 5 coupling between the five membered heterocyclic pyrrole units leads to polymers that are branched or crosslinked, as shown in figure 3.6. Some experiments, using X-ray photoelectron spectroscopy on polypyrrole, found that about 30% of carbon-carbon linkages between pyrrole rings are not the ideal 2,5 type [72]. The pyrrole units couple non-selectively because the initial oxidation of the monomer produces this very reactive radical cation species. Although 2,5 coupling is favoured theoretically, the less desirable 2,3 coupling does not take much more energy. In addition, accidental hydrogenation of the polymer backbone can occur, which destroys the conjugation between double and single bonds and therefore lowers the conductivity [73].

In polymer formation, the pyrrole units have positive charges, which are balanced by a variety of dopant ions. Anions are expelled from the polymer film (undoping) when a negative potential is applied to the film, thus reducing it to the neutral state. Conversely, when a positive potential is applied to oxidize the neutral film (doping), anions are taken up. During the doping - undoping process, the volume of the film changes by as much as 50%, depending on the specific volume of dopant anion [72]. Also dramatic colour changes may occur because the visible spectra of the doped and undoped film are very different.

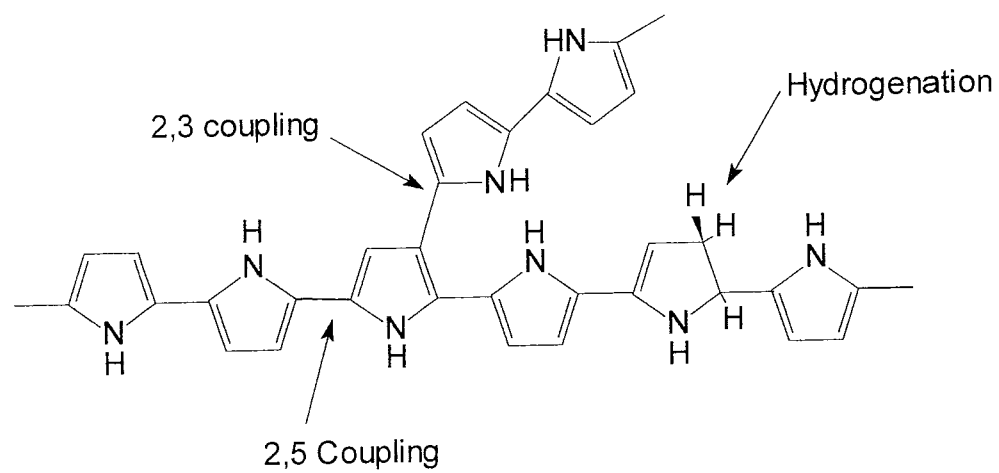
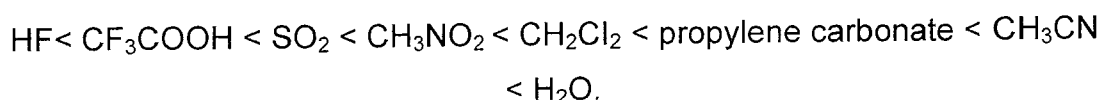


**Figure 3.6:** 2,5 and 2,3 coupling of Polypyrrole

### 3.1.7 Factors affecting electrochemical polymerisation and polymer properties.

#### (a) Solvent

Assuming that the polymerisation pathway of organic monomers to yield conjugated polymers proceeds via radical cation intermediates, it becomes apparent that the reaction will be sensitive to the nucleophilicity of the environment. Because of this most reported [63] electrochemical polymerisation studies have been performed in aprotic solvents which are poor nucleophiles and the order of nucleophilicity for certain solvents is shown;



Studies [65] carried out on pyrrole, thiophene and benzene concluded that film formation was influenced by the strength of the interaction between the solvent and the radical cation intermediates. A solvent capable of stabilising a charged intermediate will enhance the lifetime of the radical cation and therefore increase its chances of reacting before it can diffuse away from the electrode surface.

#### (b) Dopant anion

Good polymer films are generally not produced when the anion is a halide since halides are relatively nucleophilic and are easily oxidised [50]. In a study on the relative competitiveness of counter anions it was observed that films doped with the *p*-toluene sulphonate anion had a conductivity 5-10 times greater than those doped with the nitrate anion [74,75]. This effect of the counter ion was also attributed to the basicity of the ion and it was found by Kuwabata *et al.* [76] that the conductivity of the polymer decreases with increasing dopant basicity. However, if the dopant anion in the polymer is exchanged for a different anion the conductivity remains almost unchanged,

thus implying that the anions effect on the polymer occurs during the polymerisation [77]. Li & Fan [78] studied the competing effects of dopants to try to explain this phenomenon. They prepared films of polypyrrole in both an equimolar mixture of p-toluene sulphonate and nitrate and also in an equimolar mixture of p-toluene sulphonate and perchlorate. The combustion analysis of these films showed that in both cases, a much higher percentage of the sulphonate ion was present. The results indicated that doping of the polymer film during polymerisation was selective and p-toluene sulphonate was favourable both for doping and for forming a good polymer film.

The conductivity and the morphology of the polymer can be controlled to a certain extent by varying the dopant. The supporting electrolyte should therefore have the correct nucleophilicity, as well as a high degree of dissociation. For this reason tetraalkylammonium salts are therefore the most commonly used salts as they have a high degree of dissociation and good solubility in the appropriate solvents.

Variation of anion also produces changes in the mechanical strength of the polymer as well as dramatic changes in the morphology of the growing surfaces. Polypyrrole films containing p-toluenesulphonate as the anion were found to give better mechanical strength [79]. Moreover, the films containing tetrafluoroborate and perchlorate anions were found to be less stable, in terms of storage under ambient conditions, than films containing the p-toluenesulphonate anion [51]. It can therefore be seen that the properties of the polymer film can be conveniently altered by changing the incorporated anion.

The stability of the radical cation is probably the most important consideration for the formation of polymer films [79]. Radical cations with intermediate stability seem to possess the chemical selectivity to favour radical-radical coupling. The more stable cations diffuse away from the electrode and produce soluble products, whereas less stable radical cations are more reactive and will react indiscriminately with solvent and other nucleophiles in

the region near the electrode. The yield of polymer is therefore reduced and the polymer molecular weight is lowered.

In chapter 2, the successful synthesis of the monomers was discussed, namely N-methylisindole (**1**), 5-methoxy-N-methylisindole (**2**) and 5,6-dimethoxy-N-methylisindole (**3**); see figure 3.7. In carrying out a preliminary electrochemical characterisation, namely a cyclic voltammetric study of the new monomers, it is hoped that the effect of the methoxy groups can be seen. It would also be of interest to determine if these substituents have any electrochemical effect on the resulting polymers. Therefore, cyclic voltammetric studies were also carried out on the polymers. Chronoamperometric studies also carried out under identical experimental conditions may show the effect, if any, of the methoxy groups on the nucleation and growth of these polymeric films.

From these preliminary studies the effects of the substitution of a methoxy group along the polymer backbone, on the electronic and physical properties of the N-methylisindole system can be examined.

What is also of interest is to see the effects of the methoxy substituent present in the precursor molecule, namely  $\alpha,\alpha'$ -dibromo-o-xylene (**4**), 4-methoxy- $\alpha,\alpha'$ -dibromo-o-xylene (**5**) and 4,5-dimethoxy- $\alpha,\alpha'$ -dibromo-o-xylene (**6**), as shown in figure 3.8. By using cyclic voltammetry the differences in the precursor's electrochemistry is discussed.

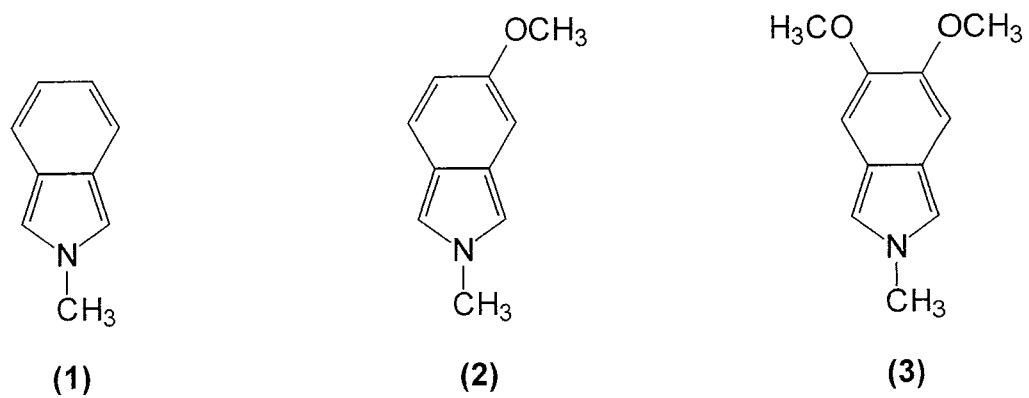


**Figure 3.7:** Methoxy substituted isoindoles

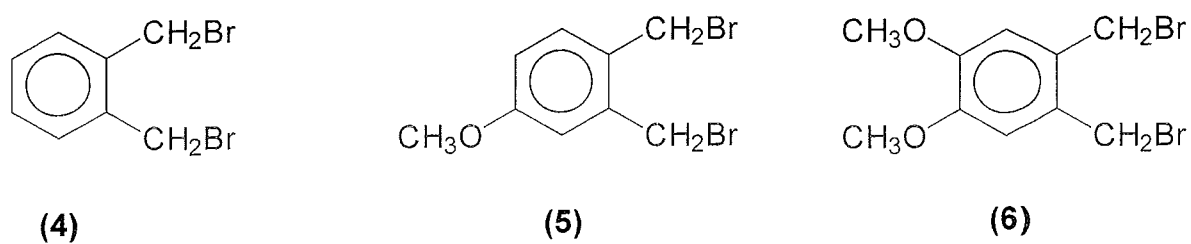


**Figure 3.8:** Methoxy substituted  $\alpha, \alpha'$ -dibromo-o-xylenes

### 3.2. Results and Discussion

The substituted isoindole monomers and precursor compounds which were synthesised (see chapter 2: The Organic Synthesis of Isoindole Monomers) were characterised for electrochemical behaviour. All electrochemical experiments were carried out in a single compartment cell using a three electrode configuration, with a platinum disc as a working electrode and a glassy carbon rod used as auxiliary electrode and all potentials were quoted with respect to a saturated calomel electrode (SCE). A cyclic voltammetric study was carried out on the three monomers, N-methylisoindole (**1**), 5-methoxy-N-methylisoindole (**2**) and 5,6-dimethoxy-N-methylisoindole (**3**). It was necessary to characterise the monomers in this way to determine if polymerisation was possible and if so, to optimise polymerisation conditions.

Initially a cyclic voltammetric study was carried out on all three monomers, under the same experimental conditions, i.e. electrode / electrolyte / solvent system, to see if the effects of the methoxy substituents would be seen. The cyclic voltammetry of N-methylisoindole has already been reported [80,81], and in both cases platinum was used as working electrode and acetonitrile as solvent. However, Rhee *et al.* [80] reported the electrochemical synthesis of poly-N-methylisoindole in lithium bromide, while Hanly *et al.* [81] used tetrabutylammonium perchlorate as electrolyte. In this study the cyclic voltammetric study of the monomers was first carried out in lithium perchlorate in acetonitrile, however lithium bromide was not suitable to study the electrochemistry of the monomer species as the electrolyte itself oxidised at a potential lower than that of the monomers. Therefore it was decided to repeat the study using p-toluene sulphonate, which as discussed earlier generally yield polymers with better mechanical strength.

#### 3.2.1 Cyclic Voltammetric study of the isoindole monomers.

##### *Lithium perchlorate*

Cyclic voltammetric studies of N-methylisoindole (**1**) ( $7.6 \times 10^{-3}$  mol dm<sup>-3</sup>) in 0.1M LiClO<sub>4</sub> in degassed acetonitrile (25cm<sup>3</sup>) showed irreversible oxidation of

the monomer; see figure 3.9 (a), and its anodic peak potential  $E_{pa}$  is +0.54V (SCE), corresponding to a one electron oxidation. This is in good agreement with previous findings [47], which state that cyclic voltammetric studies of the more stable (arylated) isoindoles have shown peak potentials at  $\sim 0.7V$  (SCE) for a one electron oxidation. Also on the first cycle the backward sweep intersects the forward sweep between +0.05V and +0.45V. Between these potentials the backward sweep current is higher than that of the forward sweep indicating the formation of the film by a nucleation and growth mechanism [81]. Cyclic voltammetry studies of 5-methoxy-N-methylisoindole (**2**) ( $8.6 \times 10^{-3} \text{ mol dm}^{-3}$ ) and 5,6-dimethoxy-N-methylisoindole (**3**) ( $7.8 \times 10^{-3} \text{ mol dm}^{-3}$ ) in 0.1M LiClO<sub>4</sub> in degassed acetonitrile, also showed irreversible oxidation of the monomer species; see figure 3.9 (b) & (c). The anodic peak potential  $E_{pa}$  is +0.49V and +0.44V (SCE) respectively, again corresponding to a one electron oxidation.

On comparing the cyclic voltammograms, the monomer oxidation potential is lower when a methoxy substituent is introduced onto the six membered ring and is even lower when a second methoxy substituent is introduced. It can be concluded that the monosubstituted and disubstituted N-methylisoindoles are increasingly easier to oxidise respectively, due to the increased electron density that the electron donating methoxy groups provide. This difference in oxidation potentials has also been observed with 3,4 dimethoxy substituted pyrroles. Merz *et al.* [82] showed that the electrochemical oxidation of 3,4-dimethoxypyrrole (**9**) and 3,4-dimethoxy-N-methylpyrrole (**10**) see figure 3.10, occurs at considerably more negative potentials than those of pyrrole (**7**) and N-methylpyrrole (**8**) respectively.

Also with 5-methoxy-N-methylisoindole and 5,6-dimethoxy-N-methylisoindole on the first cycle the backward sweep intersects the forward sweep between +0.02V and +0.36V, +0.1V and +0.31V respectively; see figure 3.10 (b) and (c), again evident of film formation by a nucleation and growth mechanism.



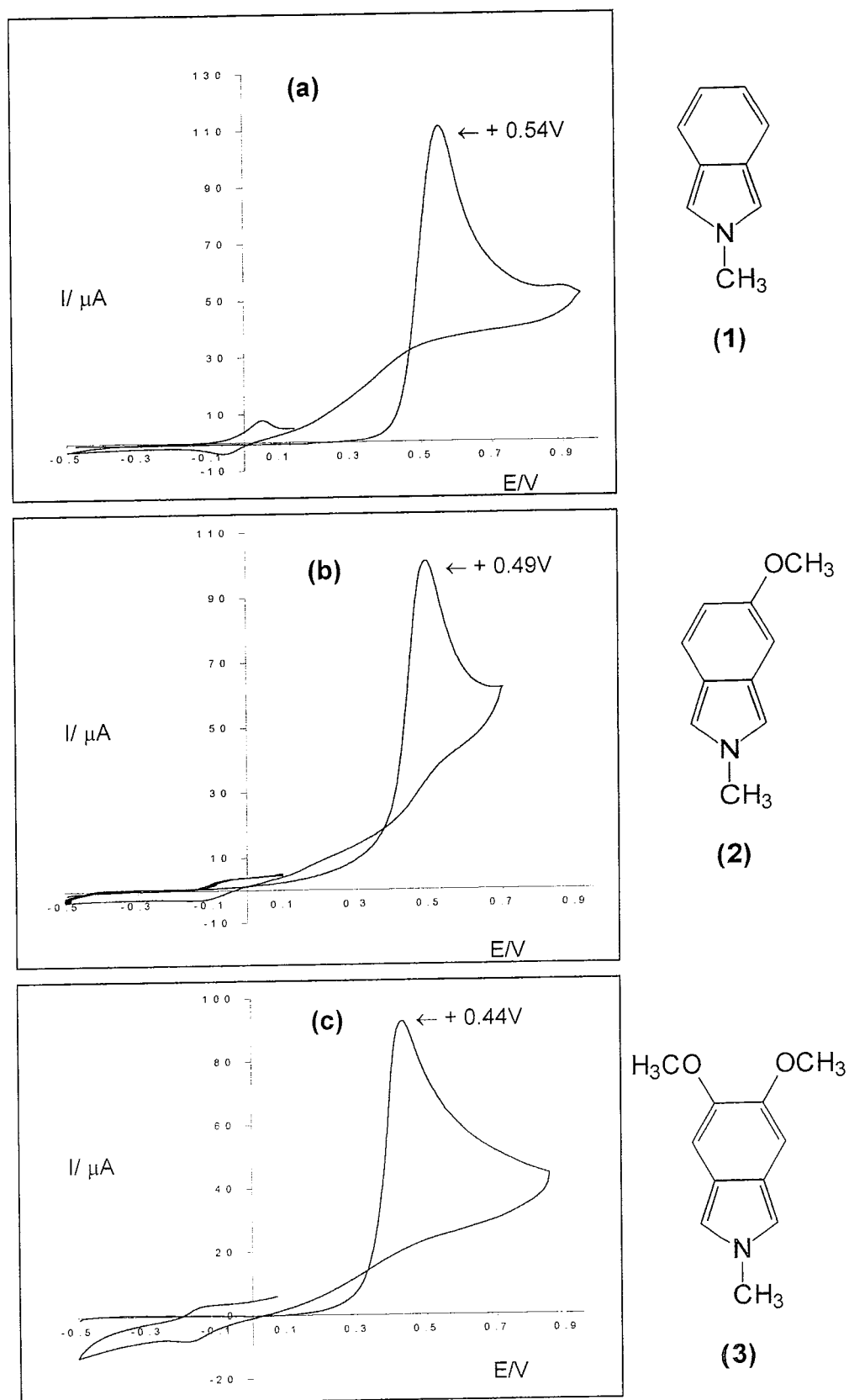
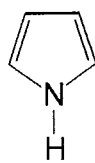
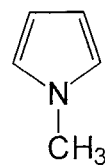


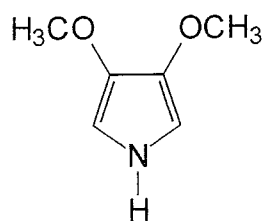
**Figure 3.9:** Cyclic voltammogram of (a) N-methylisindole (1), (b) 5-methoxy-N-methylisindole (2) and (c) 5,6-dimethoxy-N-methylisindole (3) on Pt in 0.1M LiClO<sub>4</sub> in CH<sub>3</sub>CN vs SCE at scan speed 50 mV/sec.



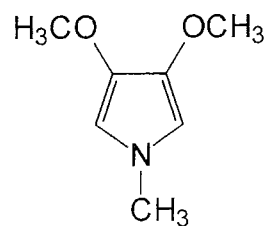
(7)



(8)



(9)



(10)

Figure 3.10.

It can be further noted for N-methylisindole that an oxidation and reduction peak due to polymer formation appears at +0.05V and -0.06V respectively. This is also observed for 5-methoxy-N-methylisindole at -0.07V and -0.11V and for 5,6-dimethoxy-N-methylisindole at -0.16V and -0.17V.

It can be noted in the case of N-methylisindole that  $E_{pa}$  of the monomer on the second sweep (+0.46V) is lower than the first (+0.54V); see figure 3.11 (a). This implies that the oxidation of the monomer is now taking place on a "new" electrode surface, namely the forming polymer film, and that oxidation is easier on this polymer electrode surface than on the bare electrode. This observation was also reported [83] in the electrochemical studies of polypyrrole. The increase in roughness of the new film, compared with the bare electrode provided more nucleation sites and encouraged monomer oxidation, allowing the monomer oxidation to take place at lower potentials on the polymer than on the underlying metal of the electrode.

This drop in  $E_{pa, m}$  on the second sweep was also observed with the new substituted monomers (2) and (3). However in the case of 5-methoxy-N-methylisindole, figure 3.11 (b), the difference between the first sweep (+0.49V) and the second sweep (+0.47V) is 20mV, which is not as large as that for N-methylisindole (80 mV). The same can be said for 5,6-dimethoxy-N-methylisindole, where the  $E_{pa}$  on the second sweep (+0.42V) is only slightly lower than the first (+0.44V), again corresponding to a difference of 20mV; see figure 3.11 (c).

On consecutive sweeping on each of the three monomers, shown in figure 3.12, only N-methylisindole and 5-methoxy-N-methylisindole showed increasing polymer layer formation. In both cases the monomer  $E_{pa}$  decreases on every consecutive cycle, implying easier oxidation of the monomer each time. However, on consecutive cycles the polymer oxidation and reduction peaks of poly-N-methylisindole increase significantly, whereas with the same number of consecutive sweeps the oxidation and reduction peaks of poly-5-methoxy-N-methylisindole are not as pronounced and the polymer layer does not deposit as readily.

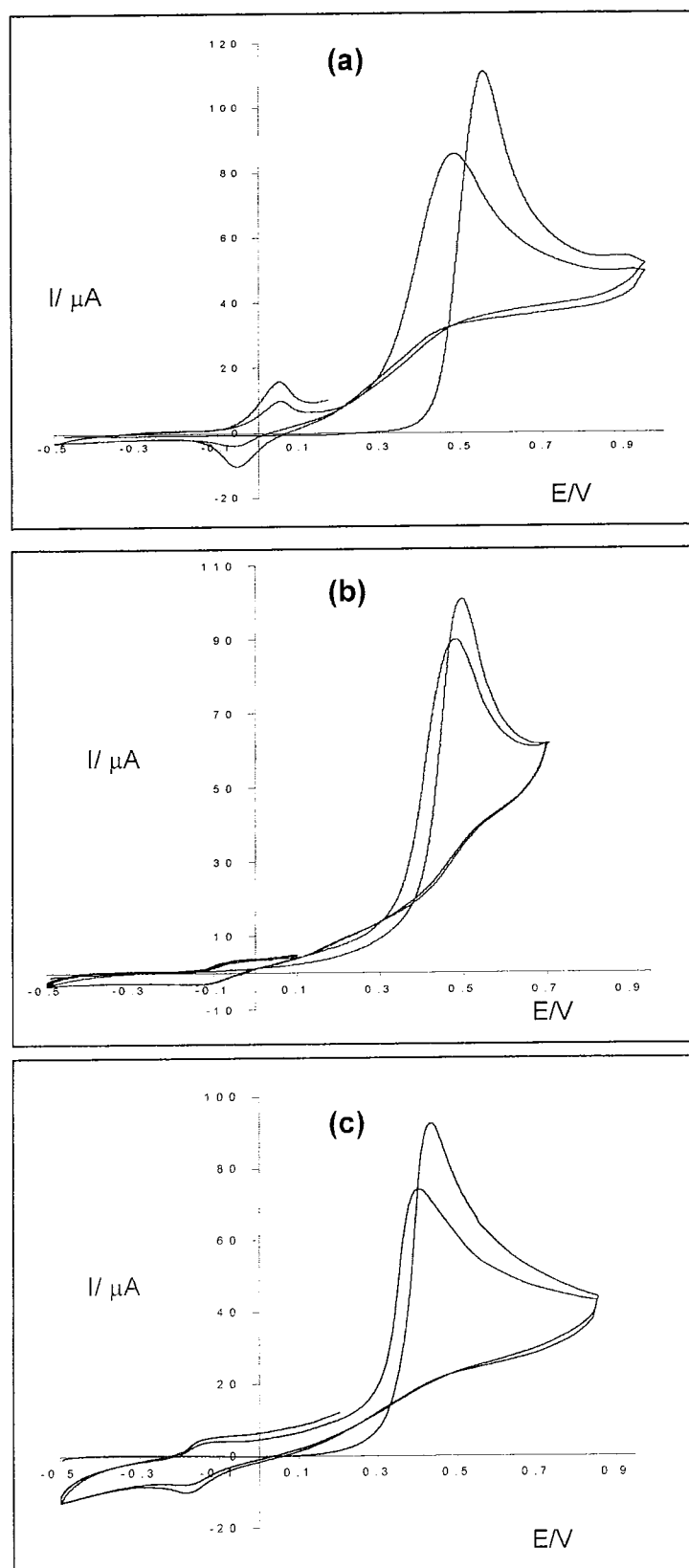


**Figure 3.11:** Consecutive sweeps of (a) N-methylisindole (b) 5-methoxy-N-methylisindole and (c) 5,6-dimethoxy-N-methylisindole on Pt in 0.1M  $\text{LiClO}_4$  in  $\text{CH}_3\text{CN}$  vs SCE at scan speed 50 mV/sec.

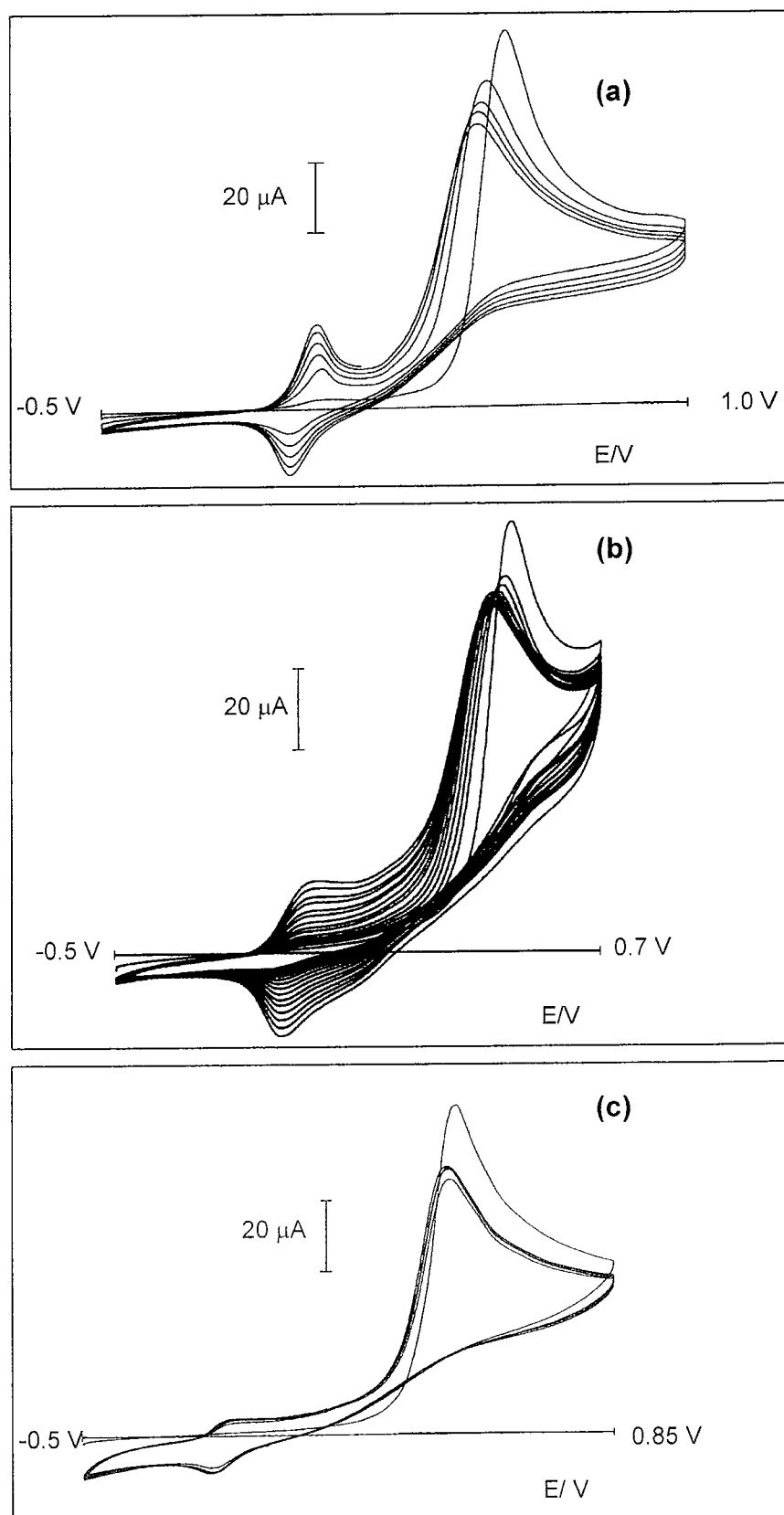


**Figure 3.12:** Consecutive sweeping of (a) N-methylisindole (b) 5-methoxy-N-methylisindole and (c) 5,6-dimethoxy-N-methylisindole on Pt in 0.1M LiClO<sub>4</sub> in CH<sub>3</sub>CN vs SCE at scan speed 50 mV/sec.

On consecutive cycles of 5,6-dimethoxy-N-methylisindole no change in the monomer  $E_{pa}$  was observed; see figure 3.12 (c). This is significantly different from the cases of N-methylisindole and 5-methoxy-N-methylisindole. However, on continuous oxidation of 5,6-dimethoxy-N-methylisindole, a dark green material was seen 'streaming' from the electrode surface, which had not been observed at any time for N-methylisindole or 5-methoxy-N-methylisindole. It appears that the bulk of the newly formed polymer is not forming a significant film and is streaming from the electrode, and oxidation is thus repeatedly occurring on the bare electrode. This is consistent with the observation that on consecutive cycles the polymer oxidation and reduction peaks do not increase to any significant degree, unlike the corresponding polymers of poly-N-methylisindole and poly-5-methoxy-N-methylisindole. This implies that short chain oligomers are being formed and are soluble or the polymer itself is soluble. Short chain oligomer formation was observed in the polymerisation poly-3,4-dimethoxy-N-methylpyrrole (**10**) [82] in  $(n\text{-Bu})_4\text{NClO}_4 / \text{CH}_3\text{CH}$ , where an initial formation of dark green soluble oligomers were observed, before the electrode became partly covered with a dark brown film.

These initial cyclic voltammetric experiments show quite clearly the successful formation of layers of poly-N-methylisindole and poly-5-methoxy-N-methylisindole. However, in order to try and discover why 5,6-dimethoxy-N-methylisindole is not forming a significant layer of polymer on the electrode, the mechanism for the polymerisation of all three monomers must be probed.

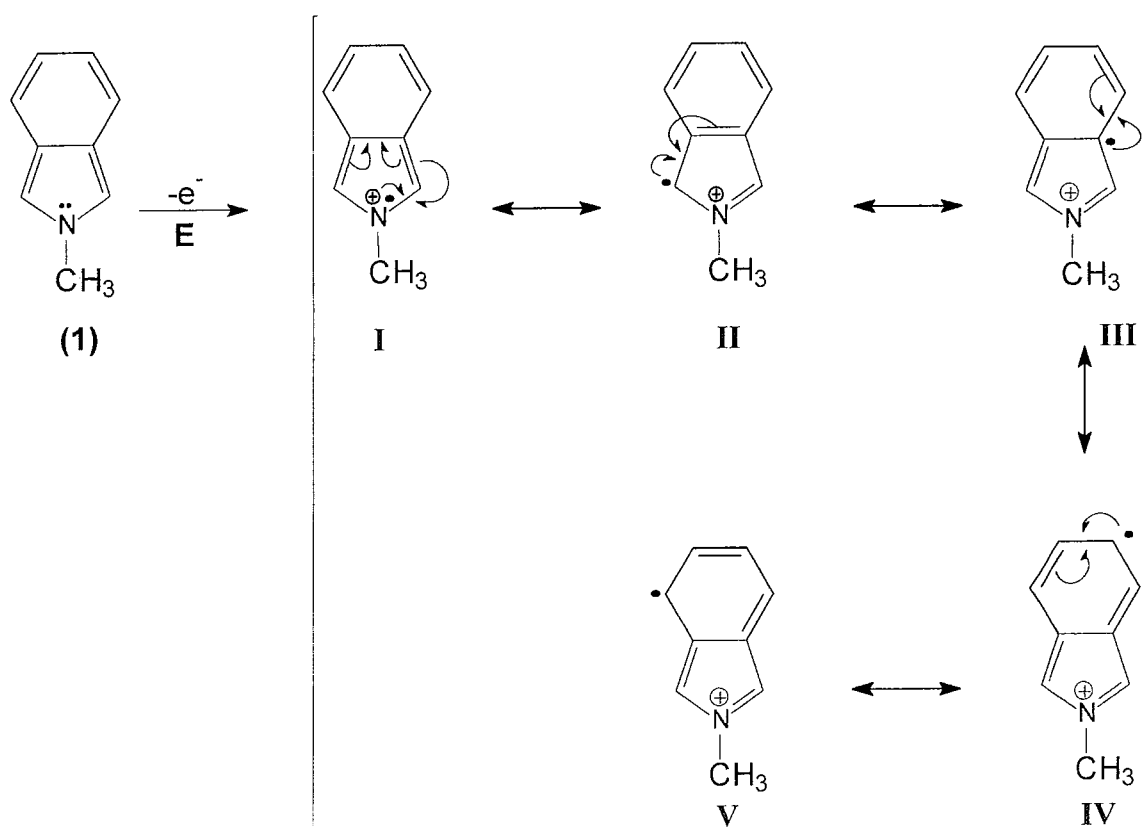
The simple fact that all three monomers show irreversible oxidation and oxidation and reduction of the forming polymer layer, shows that the two new isindoles, 5-methoxy-N-methylisindole and 5,6-dimethoxy-N-methylisindole do polymerise. A proposed mechanism for the polymerisation of the three isindoles are shown in schemes 3.3 to 3.6, and is based on the mechanism of polypyrrole as proposed by Genies *et al.* [68].

The first step consists of the oxidation of the monomer to form a radical cation and is illustrated for N-methylisindole in scheme 3.3. Diaz and Lacroix [79] reported that the stability of the radical cation is probably the most important consideration for the formation of polymer films. The more stable cations diffuse away from the electrode and produce soluble products, whereas less stable radical cation are more reactive and will react indiscriminately with the solvent and other nucleophiles in the region near the electrode.

Scheme 3.4 and 3.5 show the formation of the radical cation and the various resonance structures for 5-methoxy-N-methylisindole (**2**) and 5,6-dimethoxy-N-methylisindole (**3**) respectively. The presence of the methoxy substituents lead to an extra resonance structure which N-methylisindole cannot form. This resonance form (**VI**) is quinoidal in and is particularly stable, with every atom on the ring (other than the H) having the octet number of electrons.

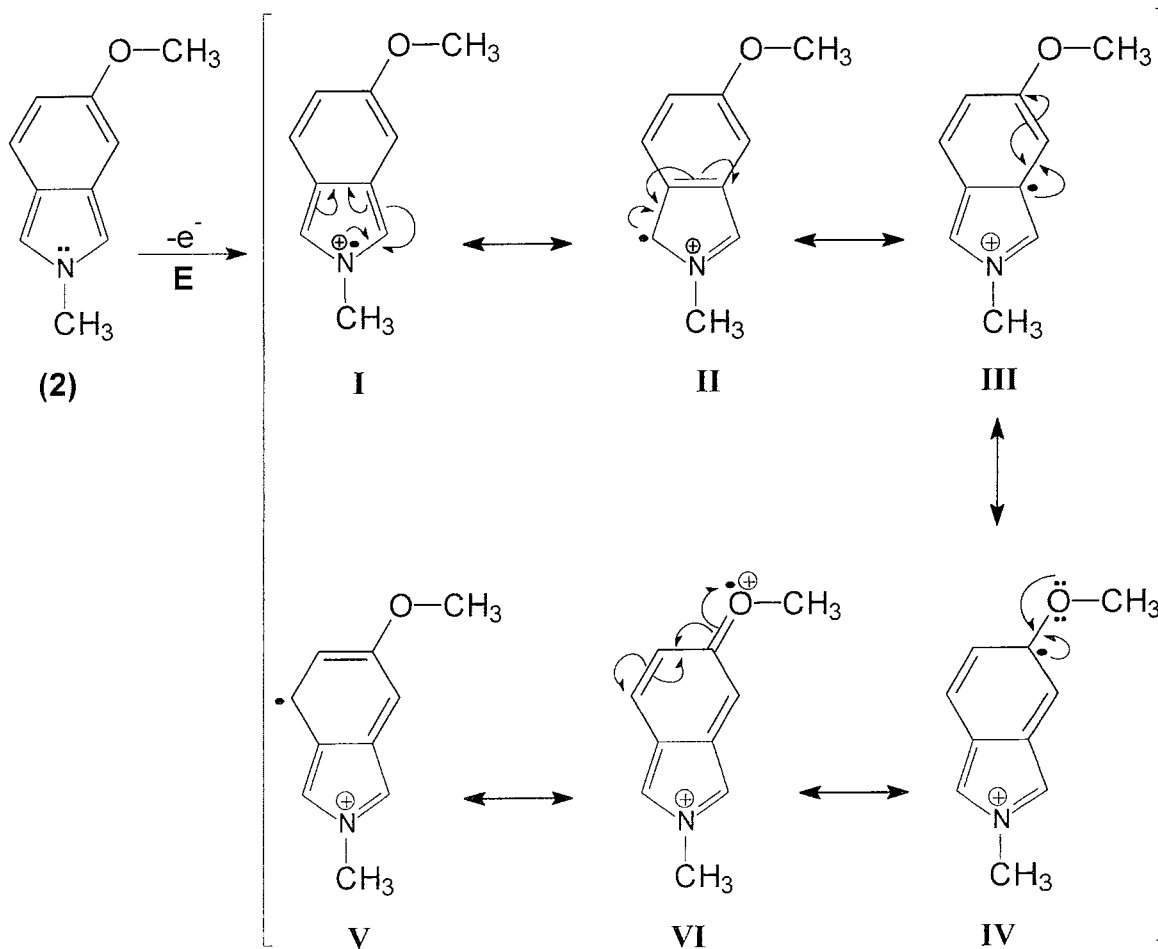
The formation of the monomer radical cation of 5-methoxy-N-methylisindole and 5,6-dimethoxy-N-methylisindole shows that both can form the very stable quinoidal structure but this still does not explain why the latter still does not form a significant polymeric layer, while the former does.

Dietrich and Heinze [84] reported that the electropolymerisation of 3-methoxythiophene (**11**) lead to a polymer with very short chain length and was soluble in aprotic solvents. By contrast, the electropolymerisation of 4,4'-dimethoxybithiophene (**12**) lead to a stable coating of polymeric material which was insoluble in aprotic solvents. The authors [84] stressed the importance of the stability of the radical cation in forming polymeric layers, and it was the low reactivity of the radical-cation of the dimer and/or oligomer which stop the polymerisation process. Scheme 3.6 shows the formation of the radical cation dimer (determined in this study) of 3-methoxy thiophene (**11**). The quinoidal structure (**III**) is stabilised through resonance. By contrast, the formation of the 4,4'-dimethoxybithiophene (**12**) radical cation, illustrated in scheme 3.7, shows the corresponding quinoidal structure (**III**)

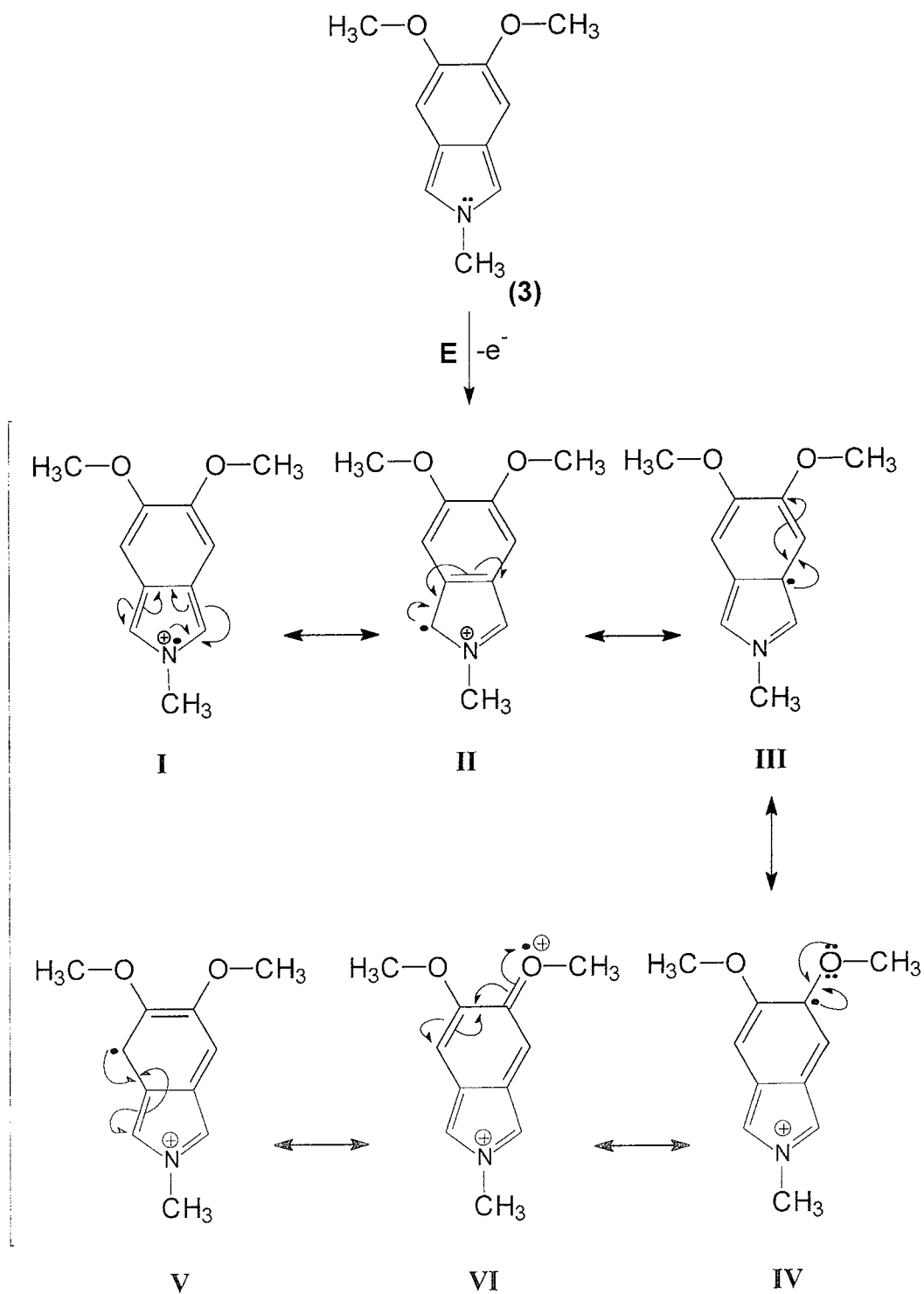


**Scheme 3.3:** Oxidation of N-methylisindole monomer

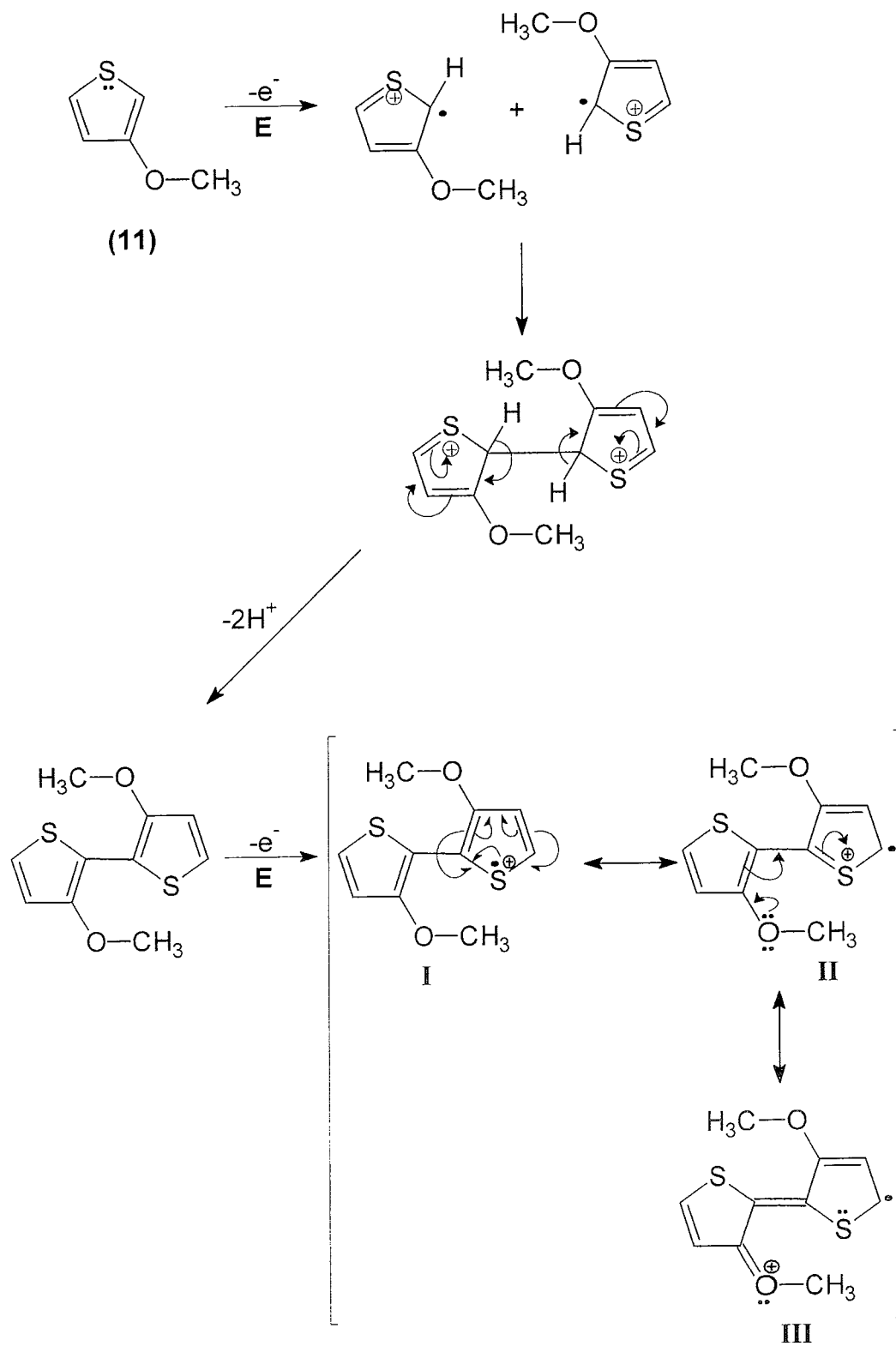




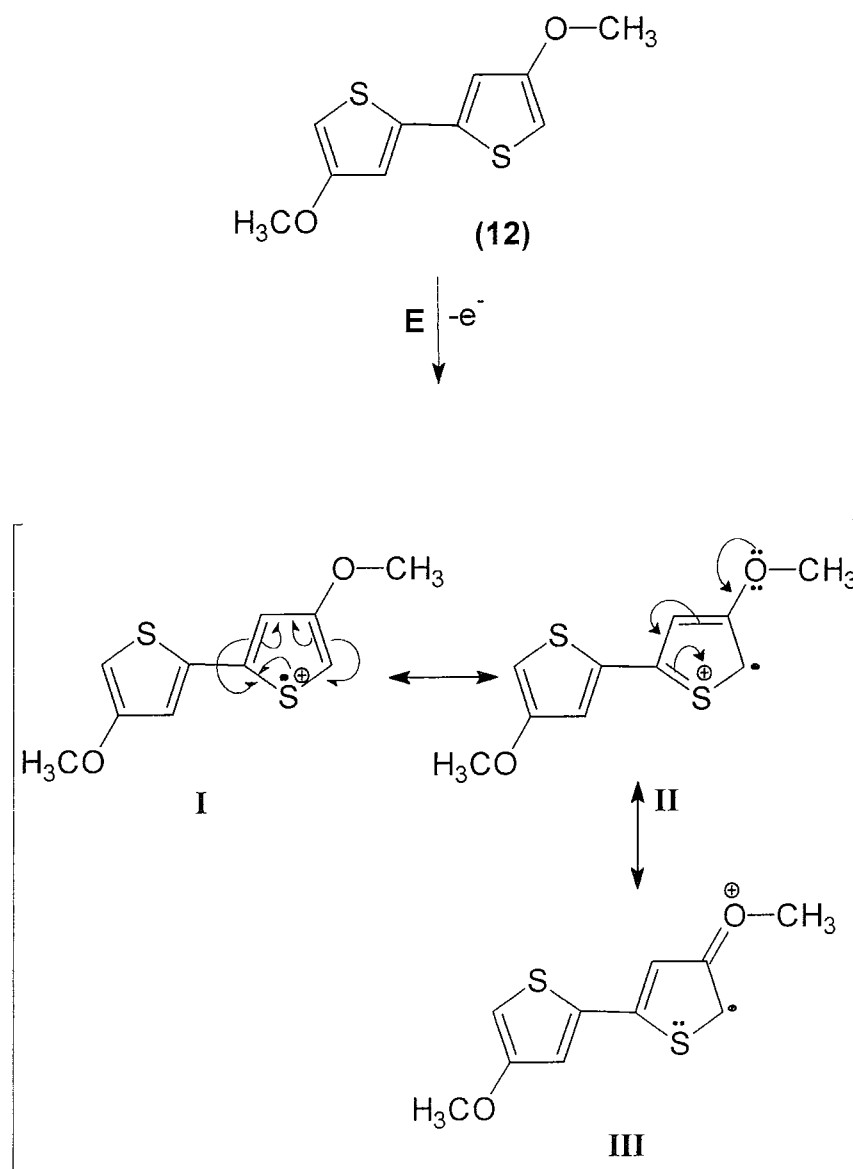
**Scheme 3.4:** Oxidation of 5-methoxy-N-methylisindole monomer



**Scheme 3.5:** Oxidation of 5,6-dimethoxy-N-methylisindole monomer



**Scheme 3.6:** Formation of 3-methoxythiophene (11) radical cation dimer



**Scheme 3.7:** Formation of 4,4'-dimethoxybithiophene (12) radical cation dimer

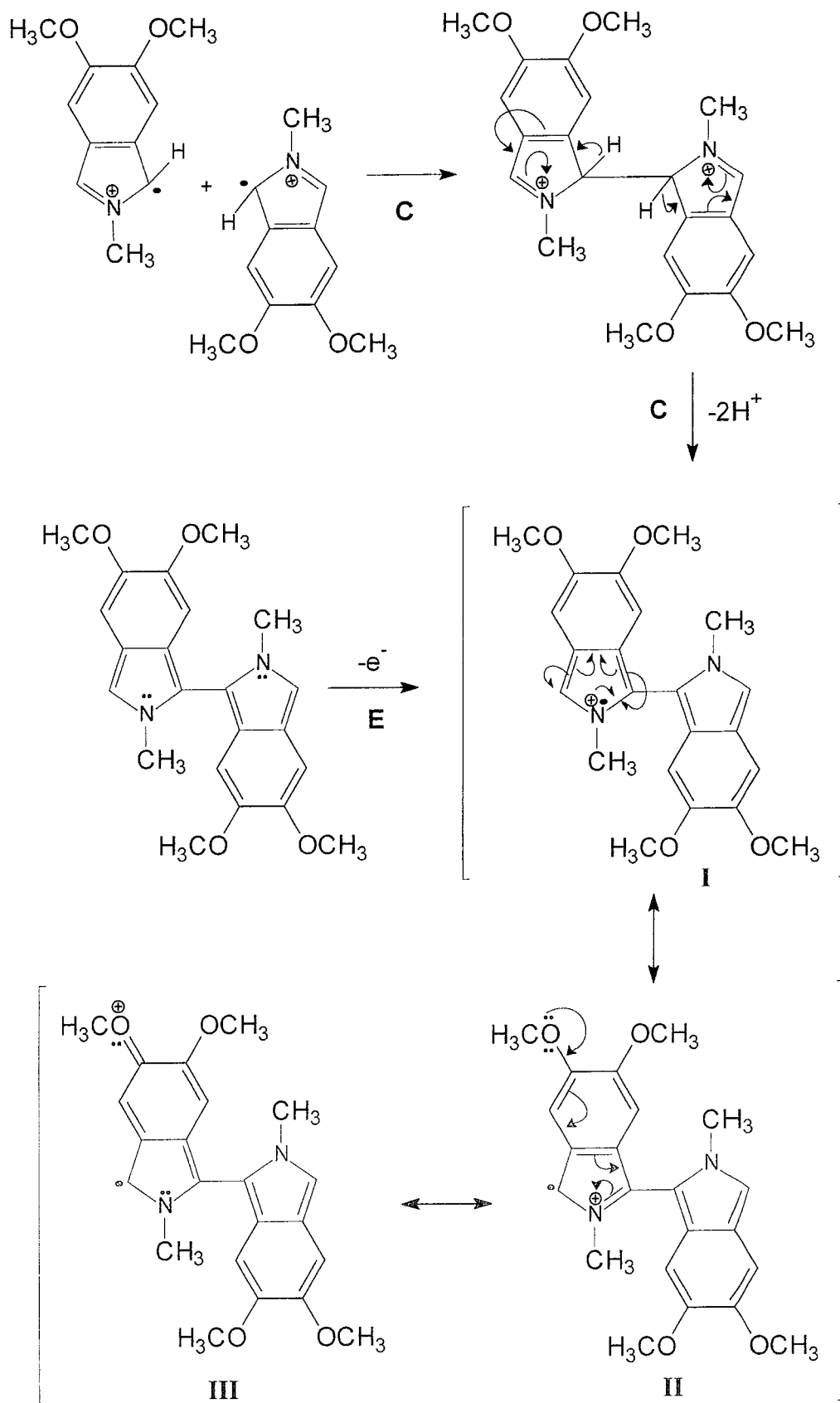
is less stable and therefore continues to polymerise to form polymer of long chain length.

Scheme 3.8 shows the formation of the 5,6-dimethoxy-N-methylisoindole radical cation dimer and the various possible resonance structures. The quinoidal structure (**III**) is very stable for a number of reasons; (a) every carbon atom (except the carbon with the radical electron) has an octet number of electrons, (b) the ring nitrogen no longer has a positive charge which also increases the stability, and (c) the adjacent ring provides extra electron density making it more stable than the corresponding monomer radical cation. Therefore these very stable radical cations diffuse away from the electrode and will tend not to form long chain polymers.

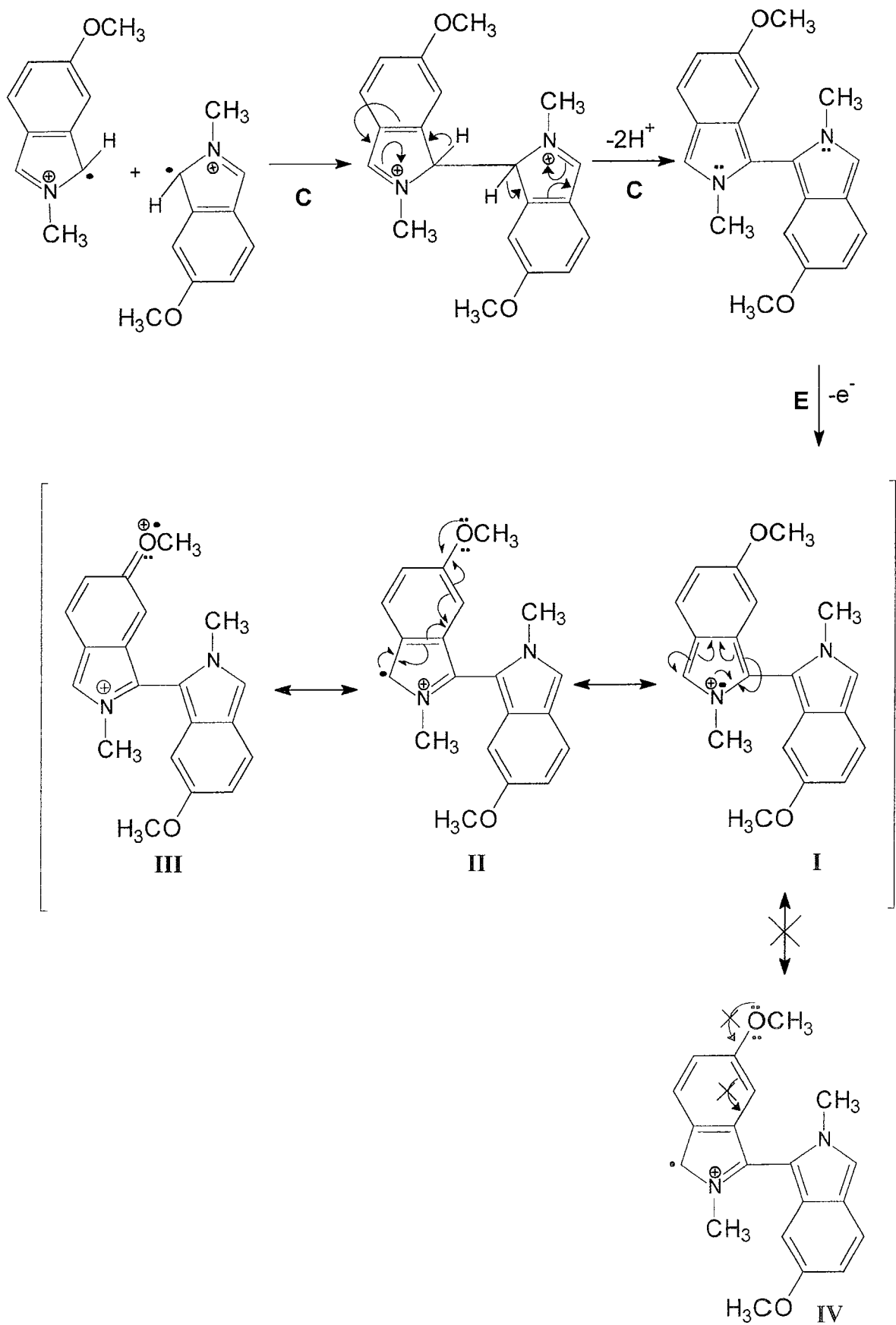
The formation of the 5-methoxy-N-methylisoindole radical cation dimer is illustrated in scheme 3.9, where the very stable quinoidol structure cannot be formed (i.e structure (**IV**)), and therefore 5-methoxy-N-methylisoindole is expected to continue to polymerise to form longer chain polymers.

The full polymerisation mechanism for all three monomers is shown in scheme 3.10. After the formation of the radical cation monomer, the second step involves radical cation – radical cation coupling to form the doubly charged dihydrodimer. Subsequent loss of two protons yields the dimer. As the dimer is more easily oxidised than the monomer, due to the increased stability of the formed radical cation, it is reoxidised to the corresponding cation and undergoes a further coupling with the monomer radical cation.

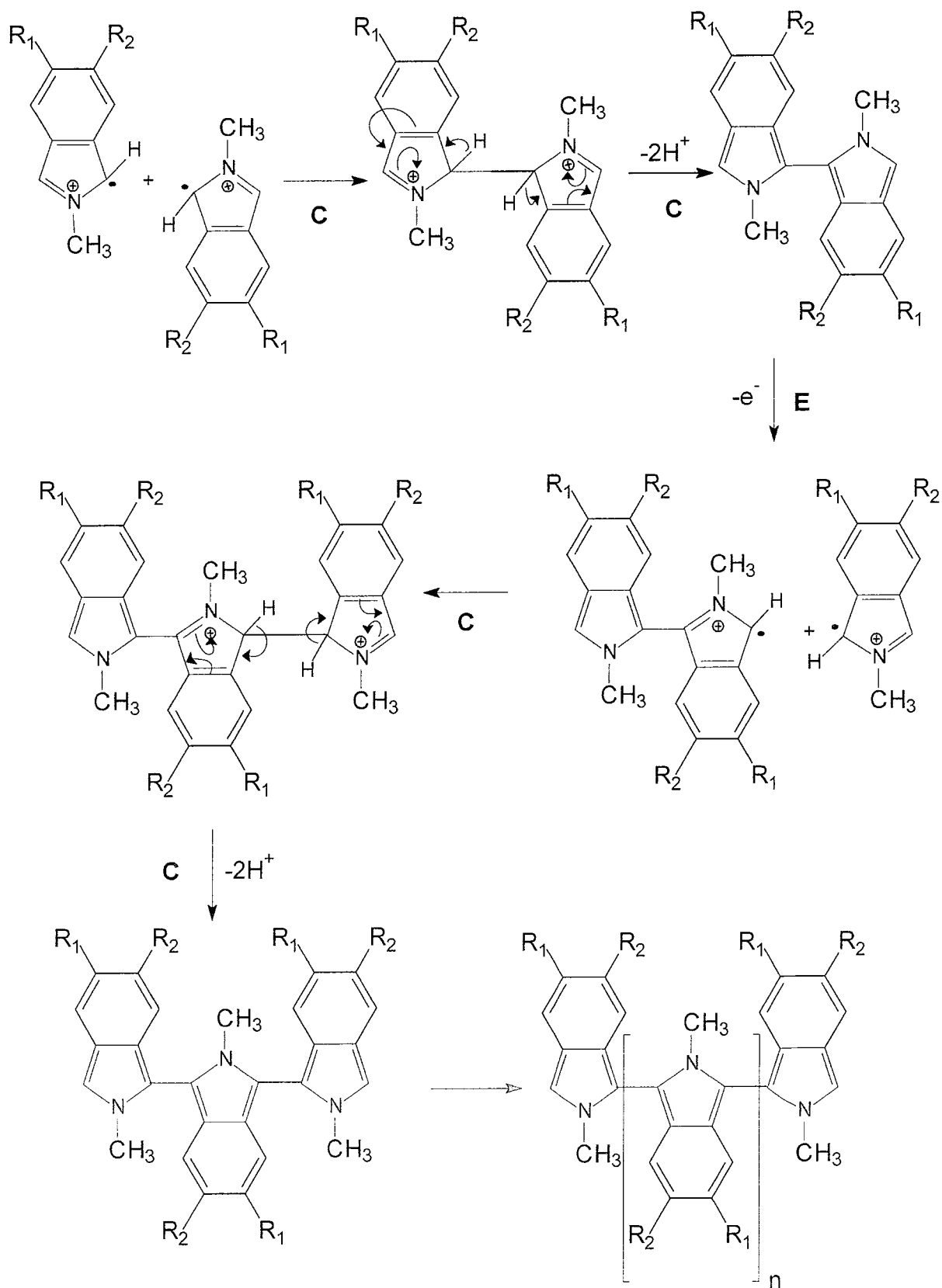
From this scheme, electropolymerisation proceeds through successive electrochemical (E) and chemical (C) steps. Therefore this chain-propagation corresponds to a cascade of ECC steps. The chain growth is terminated either when the radical cation of the growing chain becomes too unreactive, which in the case of 5,6-dimethoxy-N-methylisoindole is when only short chain are formed or when the reactive end of the chain becomes sterically blocked from further reaction [71].



**Scheme 3.8:** Formation of 5,6-dimethoxy-N-methylisoindole radical cation dimer



**Scheme 3.9:** Formation of 5-methoxy-N-methylisoindole radical cation dimer



**Scheme 3.10:** Mechanism for the polymerisation of the Isoindole monomers

N-methylisoindole (**1**) =  $R_1 = R_2 = H$

5-methoxy-N-methylisoindole (**2**) =  $R_1 = H, R_2 = OCH_3$

5,6-dimethoxy-N-methylisoindole (**3**) =  $R_1 = R_2 = OCH_3$



*Tetraethylammonium p-toluene sulphonate:*

As stated in the introduction (see section 3.1.7) variation in the dopant anion can have both chemical and physical effect on the resulting polymers. Diaz and Lacoix [79] found polypyrrole films containing p-toluene sulphonate as the anion were found to give better mechanical strength. Since there was difficulties in forming a significant polymeric layer of 5,6-dimethoxy-N-methylisindole, the cyclic voltammetry studies of the three isindole monomers were repeated with tetraethylammonium p-toluene sulphonate in acetonitrile as the supporting electrolyte.

Cyclic voltammetry studies of N-methylisindole (**1**) ( $7.6 \times 10^{-3}$  mol dm<sup>-3</sup>) in 0.1M (Et)<sub>4</sub>N(O<sub>3</sub>SC<sub>6</sub>H<sub>4</sub>CH<sub>3</sub>) in degassed acetonitrile (25cm<sup>3</sup>) again showed irreversible oxidation of the monomer; see figure 3.13 (a), and its anodic peak potential  $E_{pa}$  was +0.73V (SCE). Repeating the experiment with 5-methoxy-N-methylisindole (**2**) ( $2.6 \times 10^{-2}$  mol dm<sup>-3</sup>) and 5,6-dimethoxy-N-methylisindole (**3**) ( $7.8 \times 10^{-3}$  mol dm<sup>-3</sup>), under the same conditions, also showed irreversible oxidation of the monomer, as shown in figure 3.13 (b) & (c). The corresponding anodic peak potentials  $E_{pa}$  were +0.58V and +0.48V (SCE) respectively.

On comparing cyclic voltammograms, a similar pattern like that observed with lithium perchlorate as dopant emerges, where by, the monomer oxidation potential decreases when the methoxy substituent is introduced onto the six membered ring and is even lower when a second methoxy substituent is introduced in 5-methoxy-N-methylisindole. It can be concluded again that electronic effect of the methoxy groups makes the monomer easier to oxidise.

It can be noted that after two sweeps; see figure 3.14, the  $E_{pa}$  of all the monomers is lower on the second sweep than the first. As was the case in using lithium perchlorate as electrolyte, this implies that the oxidation of the monomer is easier on this polymer electrode surface than on the bare electrode. What is also evident from figure 3.14 is that for N-methylisindole

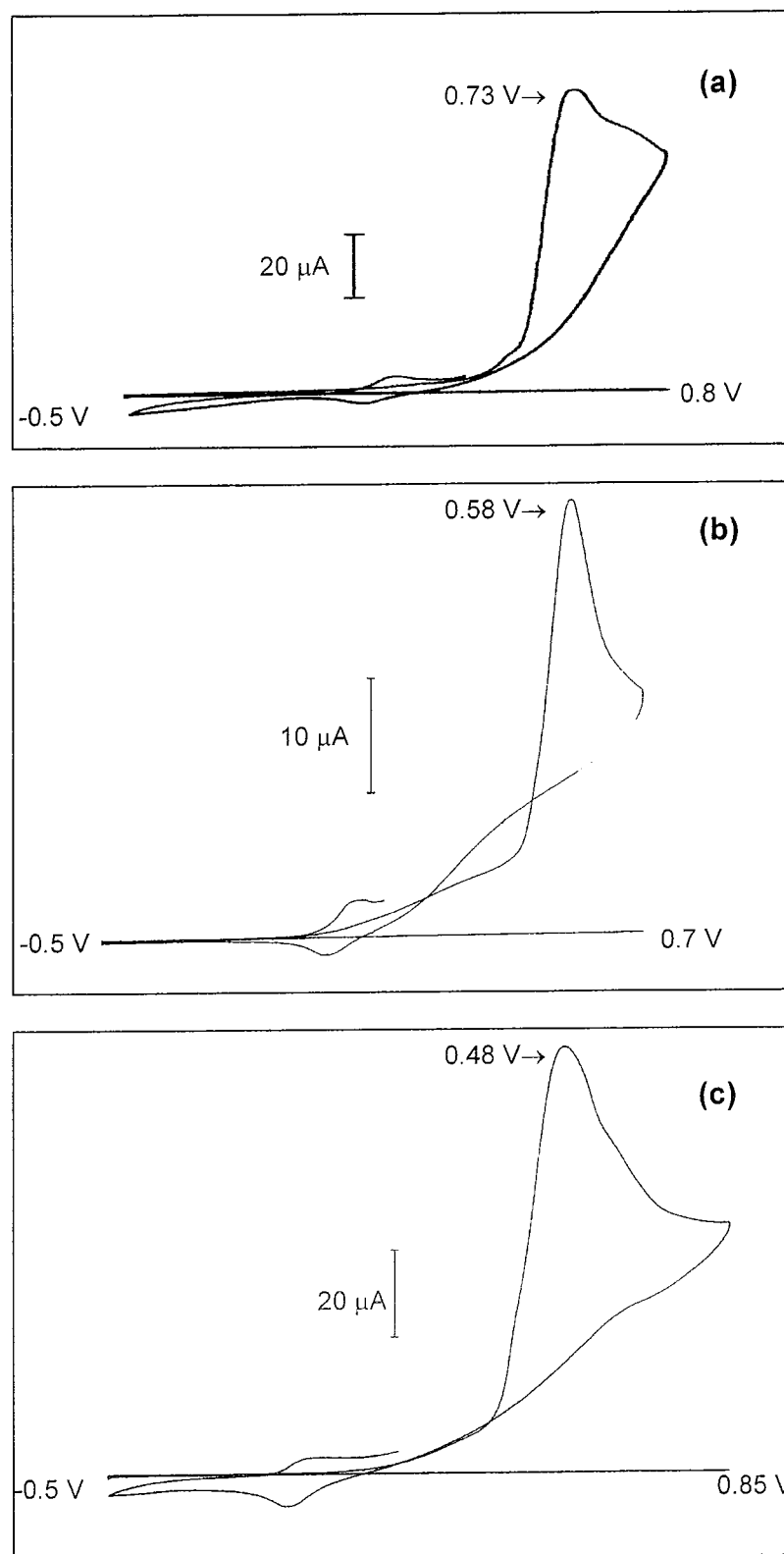


**Figure 3.13:** Cyclic voltammogram of (a) N-methylisindole (b) 5-methoxy-N-methylisindole and (c) 5,6-dimethoxy-N-methylisindole on Pt in 0.1M  $(Et)_4N(O_3SC_6H_4CH_3)$  in  $CH_3CN$  vs SCE at scan speed 50 mV/sec.

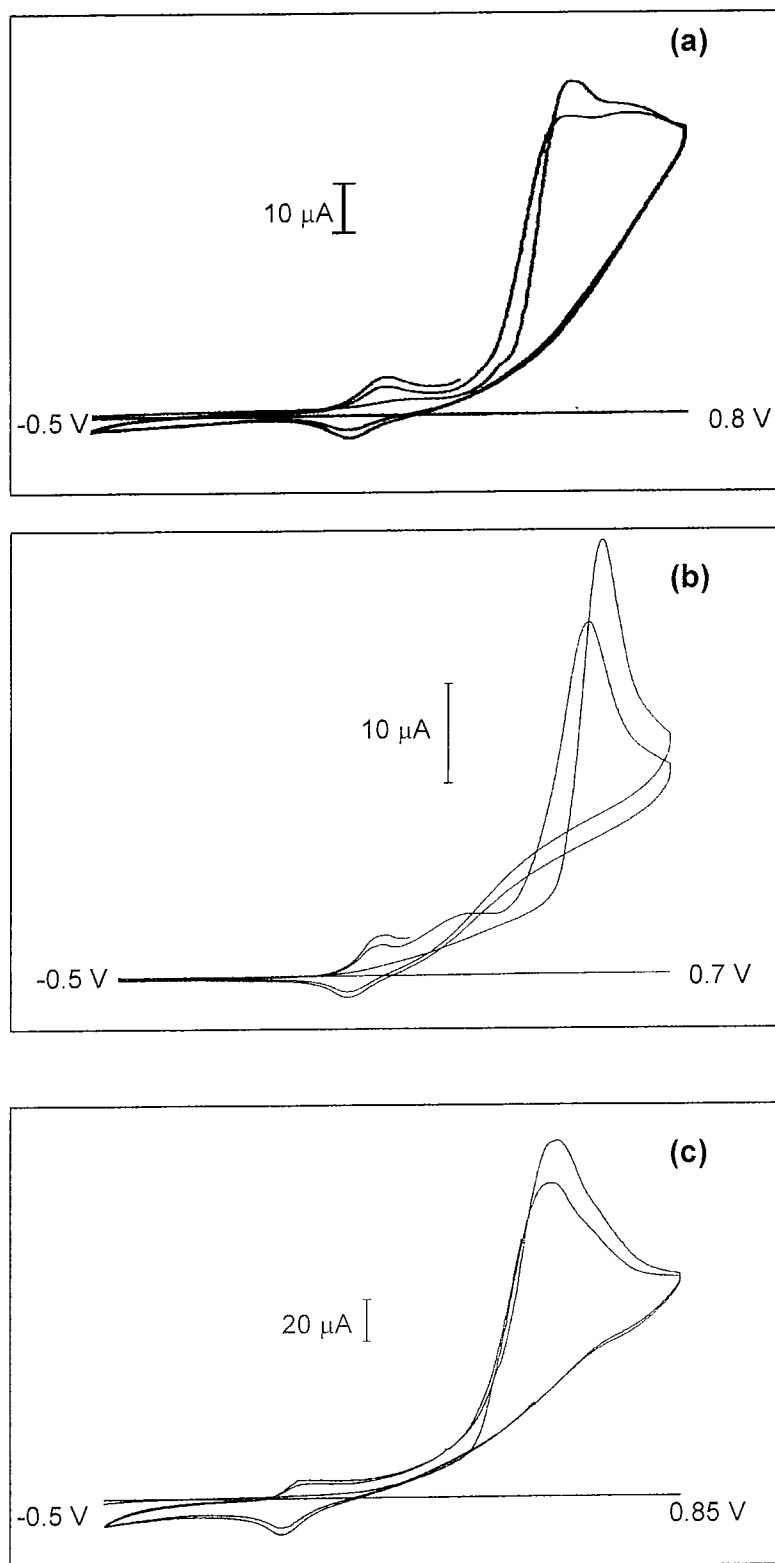


**Figure 3.14:** Consecutive sweeps of (a) N-methylisindole (b) 5-methoxy-N-methylisindole and (c) 5,6-dimethoxy-N-methylisindole on Pt in 0.1M  $(\text{Et})_4\text{N}(\text{O}_3\text{SC}_6\text{H}_4\text{CH}_3)$  in  $\text{CH}_3\text{CN}$  vs SCE at scan speed 50 mV/sec.

and 5,6-dimethoxy-N-methylisindole, there is a second peak on the shoulder of the monomer oxidation peak, and for 5-methoxy-N-methylisindole there appears to be a second peak just after the polymer oxidation peak. These anomalous peaks were not observed for any of the three monomers when using lithium perchlorate as electrolyte.

Consecutive sweeps of N-methylisindole and 5-methoxy-N-methylisindole in p-toluene sulphonate does show the monomer oxidation occurring at lower potentials, similar to that observed for both monomers in lithium perchlorate as electrolyte; see figure 3.15 (a) and (b). However, 5,6-dimethoxy-N-methylisindole is consistent in both electrolytes where on consecutive sweeping the monomer oxidation remains largely unchanged with no continuous polymer growth, as seen in figure 3.15 (c). Again continuous oxidation of 5,6-dimethoxy-N-methylisindole in p-toluene sulphonate, a dark green material was observed 'streaming' from the electrode surface, as reported for the same polymer with perchlorate as electrolyte.

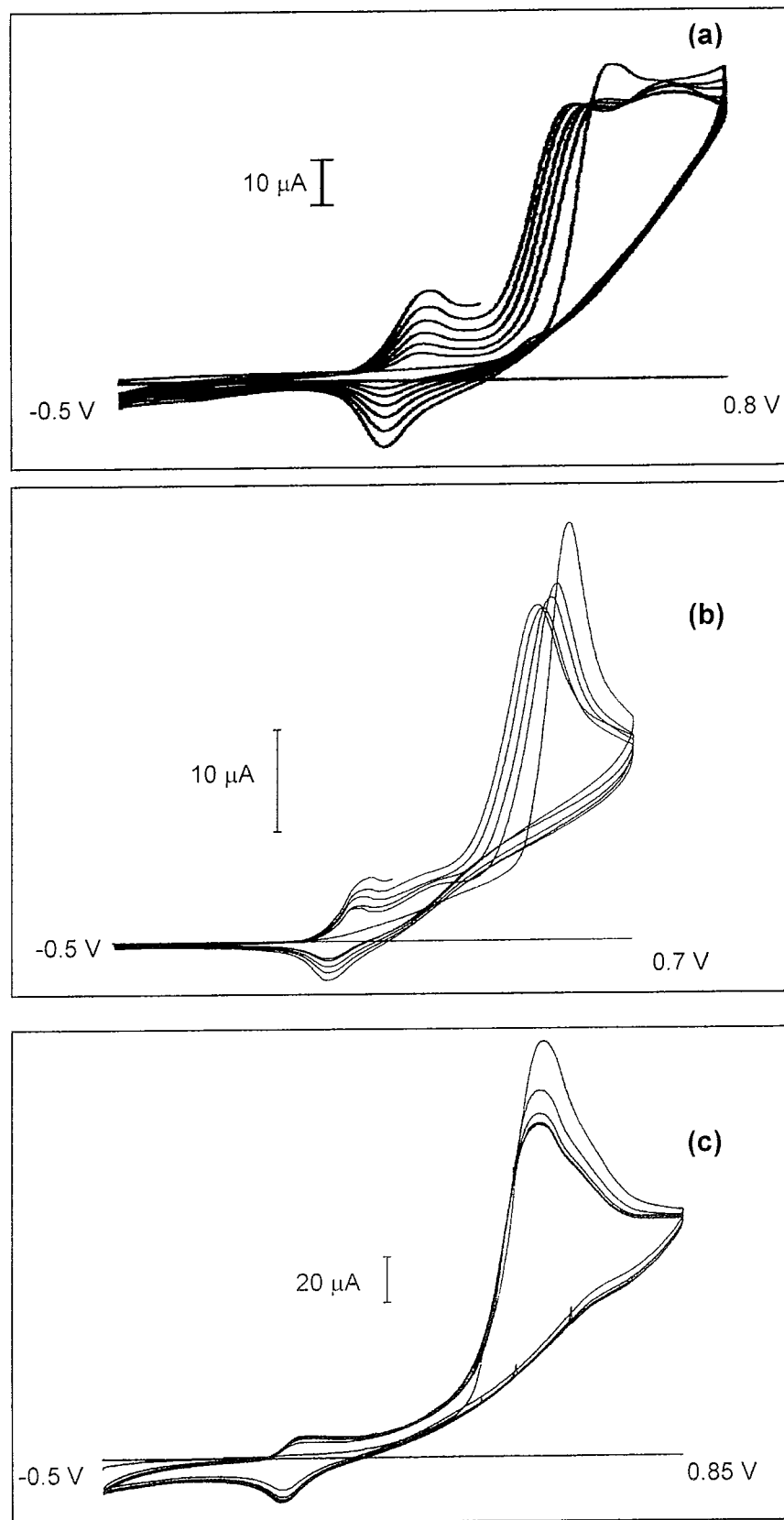


**Figure 3.15:** Consecutive sweeping of (a) N-methylisindole (b) 5-methoxy-N-methylisindole and (c) 5,6-dimethoxy-N-methylisindole on Pt in 0.1M  $(\text{Et})_4\text{N}(\text{O}_3\text{SC}_6\text{H}_4\text{CH}_3)$  in  $\text{CH}_3\text{CN}$  vs SCE at scan speed 50 mV/sec.

### 3.2.2 Chronoamperometric study of Polymer formation

It is evident from the initial cyclic voltammetric study of the three monomers that film formation was occurring differently and indeed with the increase in the number of methoxy groups on N-methylisoindole, film formation was occurring less readily under the electrochemical conditions. Cyclic voltammetry only permits intermittent monitoring of the coating process, the variation of potential with time makes the layer formation mechanism difficult to follow. Nucleation and growth processes are more effectively investigated using chronoamperometry. In this technique, the potential is stepped from a value where nucleation does not occur to a value where nucleation and subsequent growth occurs. The shape of the resultant current-time transient is examined to determine the nature of the nucleation/growth process. Besides being a very simple experimental technique, the form of the chronoamperometric current response is also quite readily quantified in terms of simple mathematical models. A study was performed on the growth of the polymers to see if the nucleation process involved in each case was the reason for the distinct differences witnessed in the study of their cyclic voltammetry. Chronoamperometric experiments for N-methylisoindole, 5-methoxy-N-methylisoindole and 5,6-dimethoxy-N-methylisoindole were all carried out with lithium perchlorate as background electrolyte

#### *N-methylisoindole*

Figure 3.16 (a) & (b) shows a series of potential step experiments from a base voltage of 0.0V to values ranging from 0.2V to 0.4V (SCE) (from the foot of the voltammetric wave almost to the top of its peak). Different current-time responses were observed as the applied potential was increased. The shape of the current-time transients is similar to those reported for the growth of polythiophene and polypyrrole [85,86]. The electrodeposition of polythiophene was examined quantitatively by Hillman *et al* [85] and a similar approach for the analysis of such curves is employed here.

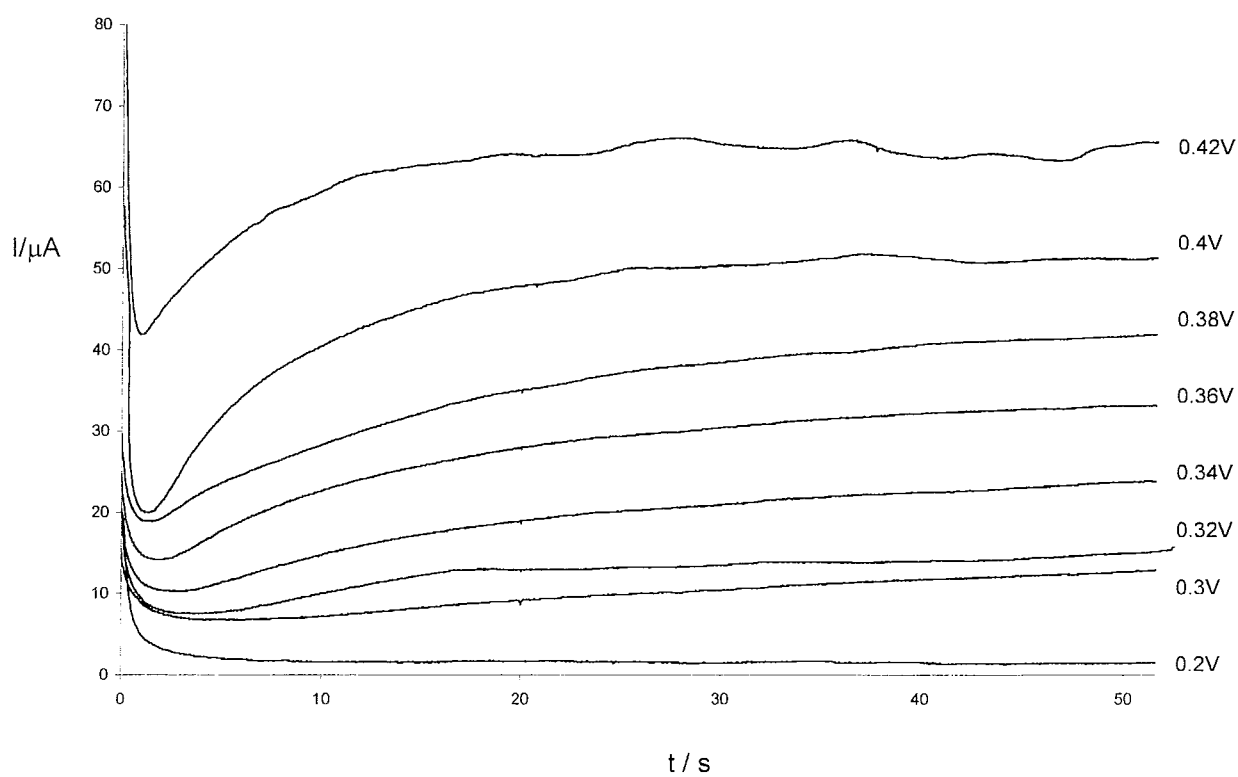


**Figure 3.16 (a):** Current-time transients for the growth of poly-N-methylisindole perchlorate at platinum from a solution containing 7.63mM N-methylisindole in 0.1M LiClO<sub>4</sub> in CH<sub>3</sub>CN as a function of potential (SCE).

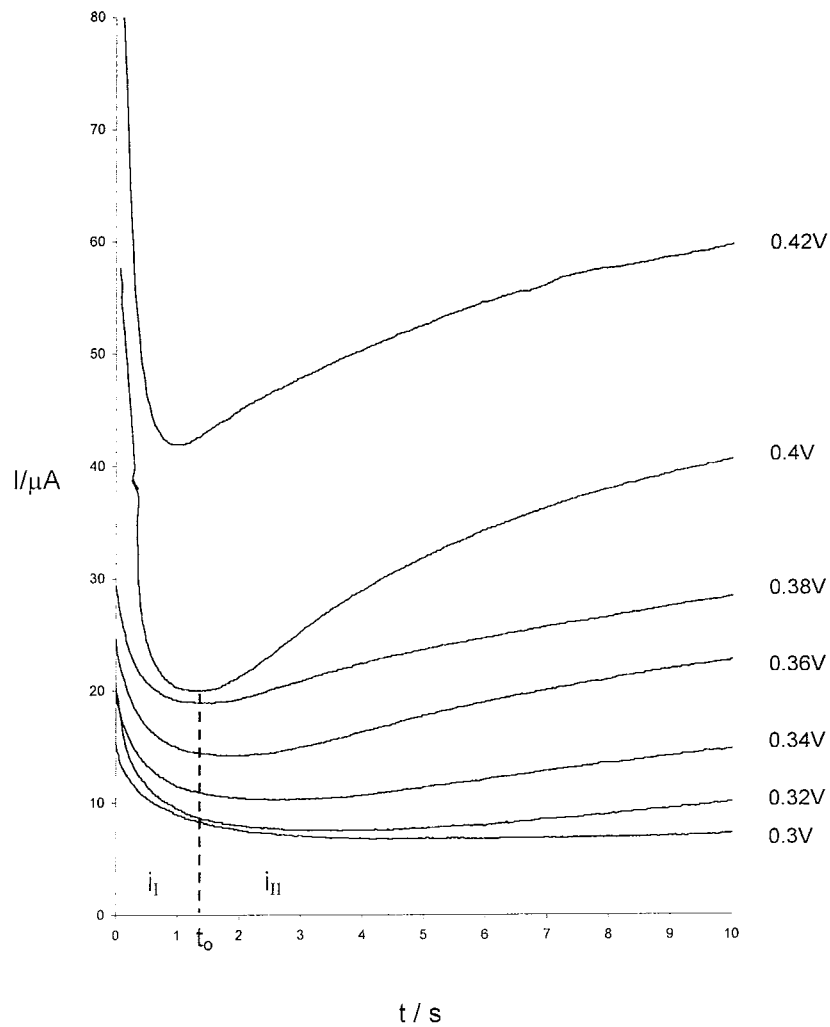


**Figure 3.16 (b):** Current-time transients obtained for poly-N-methylisoindole perchlorate deposition at short times. Regions I and II are presented and  $t_0$  for the transient obtained at 0.4V. The deposition conditions are the same as those employed for figure 3.16(a)



Three regions of the transients are of note.

- (a) The current-time profile resulting from a potential step begins with a rapid increase in current or a current spike (observed over short time) followed by a decay in current to a local minimum, as shown in figure 3.16 (a).
- (b) This local minimum is then followed by an increase in current to a plateau; see figure 3.16(b).
- (c) Following the plateau a slow or rapid decrease in current is observed depending on the applied potential.

This final region was not observed for the current-time profile of N-methylisoindole. This analysis therefore involves dividing up the transient into two regions. The sharp rise and fall of the transient current at short times is designated as region I. This initial current spike is not totally associated with double layer charging, but may also be ascribed to a number of possibilities such as monomer oxidation and polymer deposition [86]. The minimum following this spike in the transient for N-methylisoindole was found to occur at progressively shorter times as the applied potential is increased, as shown in figure 3.16 (b). This finding is in agreement with that reported by Hillman [85]. It had been proposed that in this region an initial monolayer of polymer forms and the current minimum observed just prior to the onset of the rising current response corresponds to the transient between initial monolayer and subsequent multilayer coverage [85]. They have also defined a time  $t_0$ , the time corresponding to the current minimum, to be an estimate of the time required to produce a monolayer coverage of polymer on the electrode. Therefore,  $t_0^{-1}$  was also defined as a crude measure of an electrochemical rate constant for the growth of the monolayer [85].

A plot of  $\ln(t_0^{-1})$  or  $-\ln(t_0)$  versus applied potential is presented in figure 3.17. The plot exhibits reasonable linearity between 0.3V and 0.42V (SCE) indicating Tafel type behaviour.

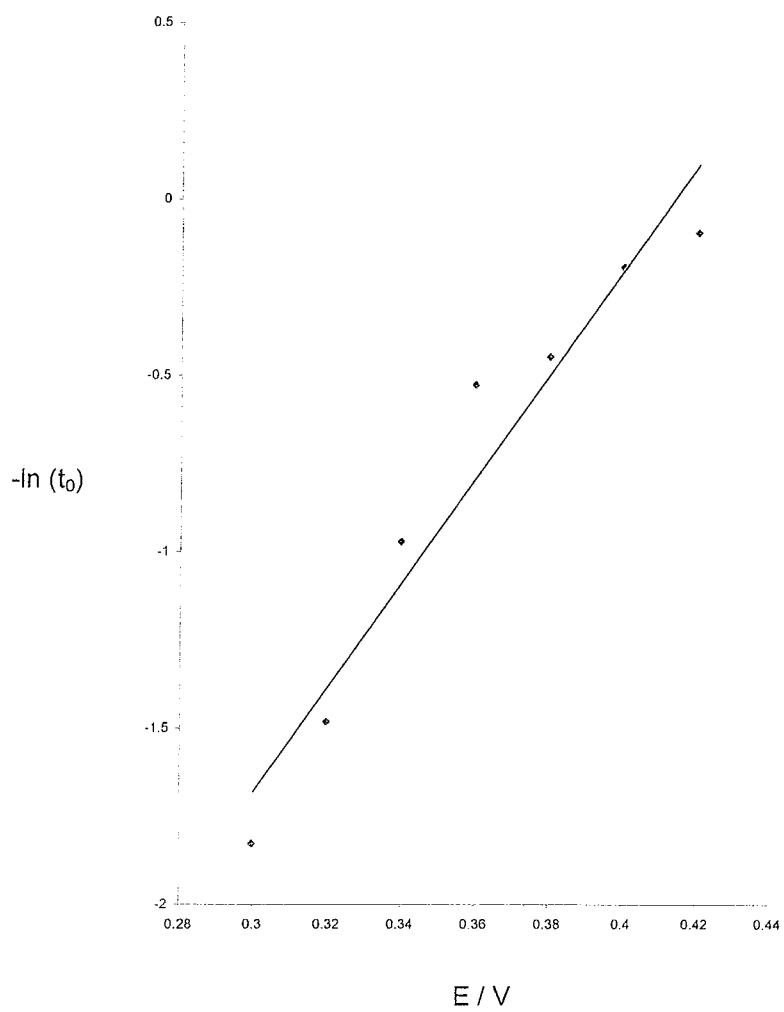


**Figure 3.17:** A plot of  $-\ln (t_0)$  versus applied potential for the transients presented in figure 3.16 (b) for N-methylisindole.

The rising current following the minimum is designated as region II; see figure 3.16 (b). The rise in current becomes more evident as the applied potential is increased. This region represents the current due to a second nucleation and growth process on the monolayer of polymer formed in region I, therefore there is now nucleation/growth on an organic substrate.

At short times prior to the overlap of centres growing on the organic substrate, the current can be given by

$$i \propto k^m t^{m-1} \quad (3.7.)$$

for instantaneous nucleation and n-dimensional growth or,

$$i \propto k^m t^m \quad (3.8)$$

for progressive nucleation followed by n-dimensional growth, where  $m=1, 2, 3$ .  $k$  denotes the growth rate parameter, and will depend on the magnitude of the applied potential via the Butler-Volmer equation (eqn 3.9)

$$k = k^0 \exp\left(\frac{(1-\alpha)nF(E-E^0)}{RT}\right) \quad (3.9)$$

where  $k^0$  = preexponential factor,  $\alpha$  = symmetry factor,  $n$  = no. of electrons transferred,  $F$  = Faradays constant,  $(E-E^0)$  = over potential,  $R$  = gas constant, and  $T$  = temperature.

Simplified analytical expressions for the current observed for nucleation/growth at short times are presented in table 3.1. Hillman *et al* [85], point out that the growth of the film in region I of the transient may not be complete before the region II nucleation begins. Therefore it is necessary to correct for the time taken for the complete growth of the monolayer in region I. The current in region II,  $i_{II}$  hence can be expressed as

$$i_{II} = (\text{constant}) (t-t_0)^m \quad (3.10)$$

Plots of  $i_{II}$  against  $(t-t_0)^2$  where  $m=2$  are shown in figure 3.18 as a function of potential.

Nucleation type	Growth Type		
	1-Dimensional	2-Dimensional	3-Dimensional
Instantaneous	$i = [nFN_oSk]$	$i = [2\pi nF(M/\rho)hN_0k^2t]$	$i = [2\pi nF(M/\rho)^2k^3t^2]$
Progressive	$i = [nFk_gN_oSkf]$	$i = [\pi nF(M/\rho)hk_gN_0k^2t^2]$	$i = [2\pi nFM^2k_gN_0k^3t^3/3\rho^2]$

Symbols:  $F$  = Faraday constant,  $M$  = molar mass ( $\text{g mol}^{-1}$ ),  $\rho$  = density ( $\text{gcm}^{-3}$ )  
 $k_g$  = nucleation rate constant ( $\text{s}^{-1}$ ),  $N_o$  = number density of nucleation sites ( $\text{cm}^{-2}$ ),  $k$  = growth rate parameter ( $\text{mol cm}^{-2} \text{s}^{-1}$ ),  $h$  = height of growth centre,  $S$  = area of growth centre.

**Table 3.1:** Simplified expressions for transient current describing nucleation and growth at short times before overlap occurs between growing centres.

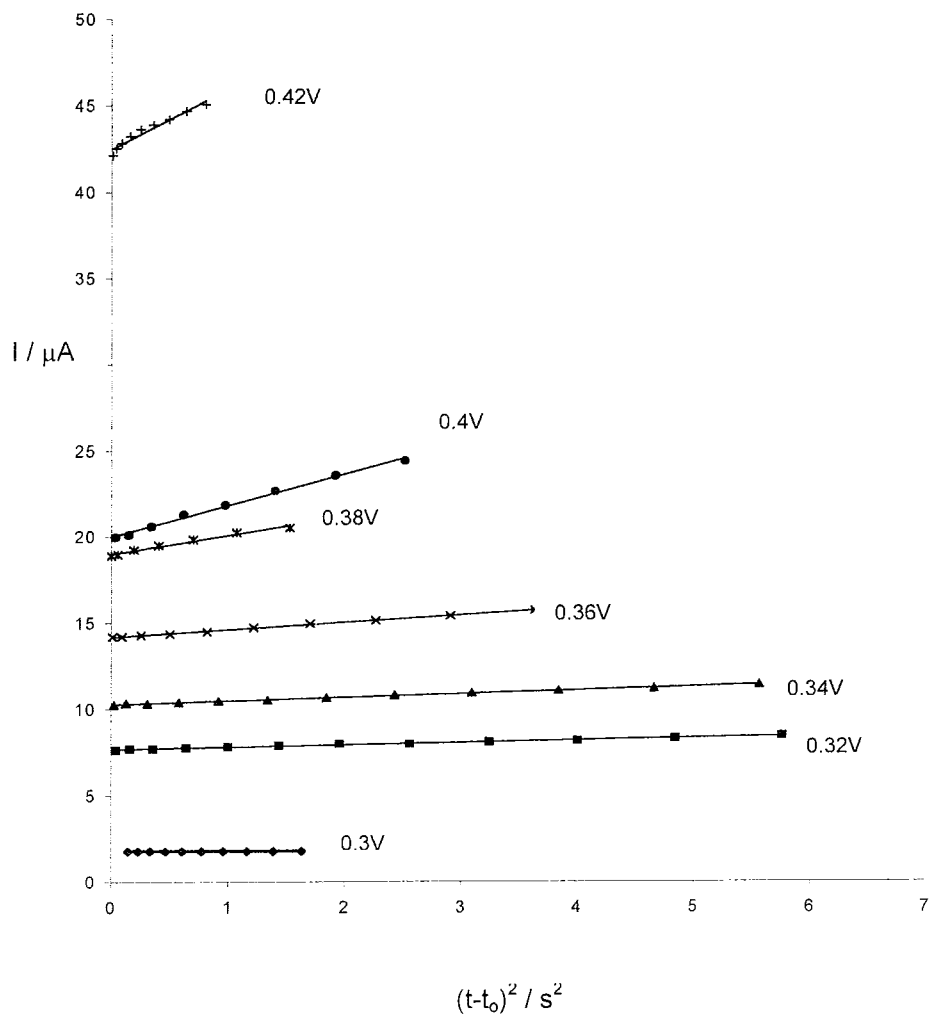


**Figure 3.18:** A plot of  $i_{II}$  versus  $(t-t_0)^2$  as a function of applied potential for the transients presented in figure 3.16 (b) for N-methylisindole.

Reasonable linearity was obtained at short times indicating that the governing equation is

$$i_{II} = (\text{constant}) (t-t_0)^2 \quad (3.11)$$

This value of  $m=2$  is in agreement with the reported analysis of polythiophene [85] and polypyrrole [86]. At longer times as the nucleation and growth of the film progresses, the plot will depart from linearity due to overlap of growth centres. The time dependence of nucleation and growth can therefore be assumed to be a squared dependence. This means that the nucleation process is either two dimensional with progressive nucleation or three dimensional following instantaneous nucleation (see table 3.1).

From table 3.1, note that the slope of  $i$  versus  $t^2$  plot, should be proportional to  $k^2$  for two-dimensional progressive mechanism and to  $k^3$  for the three-dimensional instantaneous mechanism. Since the growth parameter  $k$  is dependent on the applied potential via the Butler-Volmer equation  $k^2$  can be expressed by squaring equation 3.9,

$$k^2 = k^{o2} \exp\left(\frac{2(1-\alpha)nF(E-E^0)}{RT}\right) \quad (3.12)$$

becomes

$$\ln k^2 = \ln k^{o2} + \left(\frac{2(1-\alpha)nF}{RT}\right) (E-E^0) \quad (3.13)$$

Therefore since  $i_{II} \propto k^2$ , the log of the slope of  $i_{II}$  verses  $(t-t_0)^2$  is plotted against potential and the resulting slope  $S$  will be

$$S = \left(\frac{d \log[di/d(t-t_0)^2]}{dE}\right) \quad (3.14)$$

For progressive nucleation followed by two-dimensional growth

$$S = \left(\frac{2(1-\alpha)F}{2.303 RT}\right) = 16.9 \text{ V}^{-1} \quad (3.15)$$

for  $T=298\text{K}$ ,  $n=1$  and  $\alpha= 0.5$ .

On the other hand, by cubing equation 3.9,  $k^3$  can be expressed as

$$S = \left( \frac{3(1-\alpha)F}{2.303 RT} \right) = 25.3 \text{ V}^{-1} \quad (3.16)$$

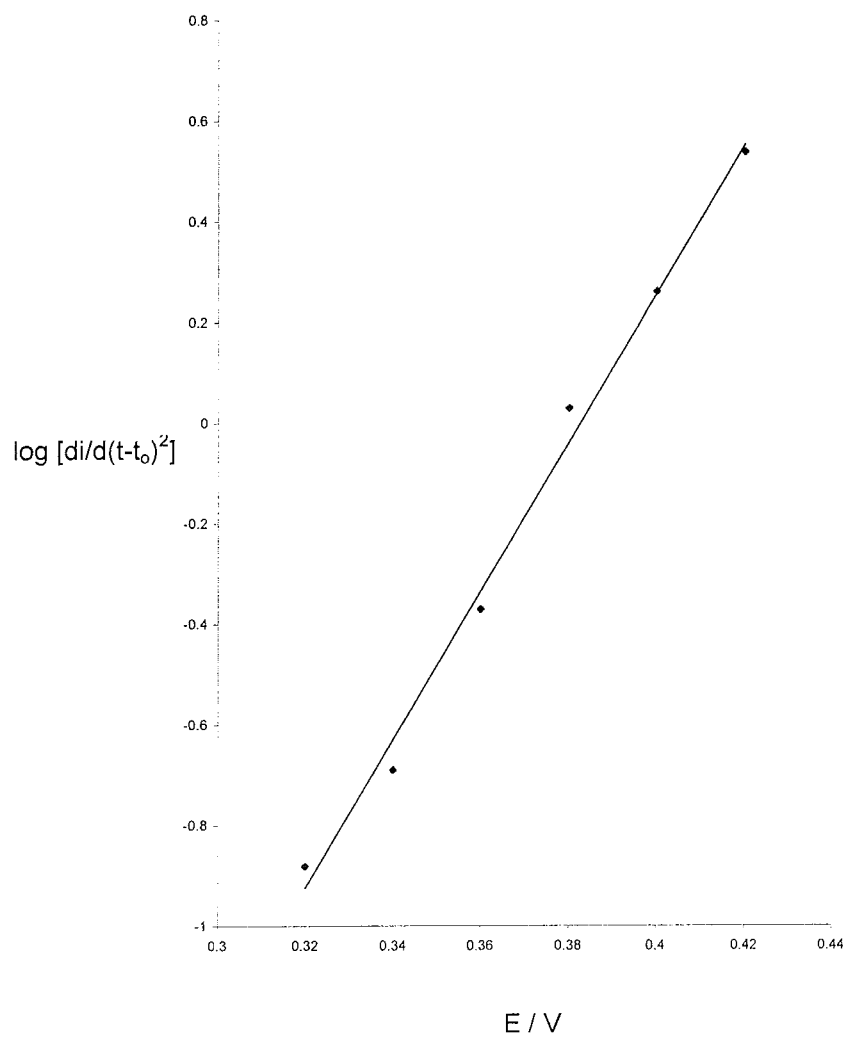
for instantaneous nucleation and three-dimensional growth.

Figure 3.19 shows a plot of the log of the slope of  $i_{II}$  verses  $(t-t_0)^2$  against potential. The plot exhibits reasonable linearity with a slope of  $14.76\text{V}^{-1}$ . Based on this result the data would suggest that the growth of poly-N-methylisindole is two-dimensional with progressive nucleation. This is different to that reported [86] for the formation of polypyrrole, where three-dimensional growth following instantaneous nucleation was observed.

At long times in the current-time profile a steady-state response is observed; see figure 3.16 (a). Since the growth parameter  $k$  obeys the Butler-Volmer equation, the steady-state current response should exhibit Tafel-type behaviour when plotted as a function of potential, i.e.,  $\log i$  verses  $E$  will be linear. A Tafel plot of N-methylisindole at 50 seconds shows good linearity, as seen in figure 3.20. The theoretical Tafel slope  $S_T$  is

$$S_T = \left( \frac{(1-\alpha)F}{2.303 RT} \right) = 8.4 \text{ V}^{-1} \quad (3.17)$$

for  $T=298\text{K}$ ,  $n=1$  and  $\alpha= 0.5$ . The slope of the experimental plot is  $7.48\text{V}^{-1}$  indicating Tafel-type behaviour at long times as expected.



**Figure 3.19:** A plot of the slopes for  $i_{II}$  versus  $(t-t_0)^2$  against applied potential



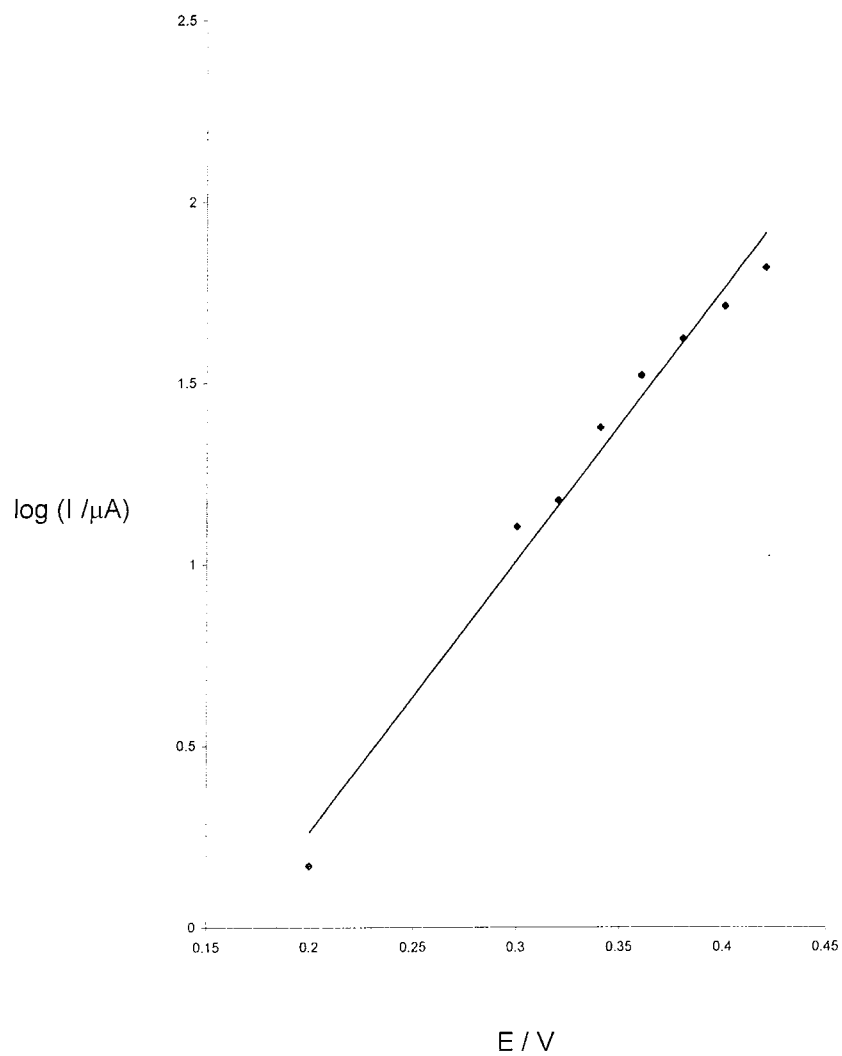


**Figure 3.20:** A Tafel plot of the steady-state section of chronoamperometric current-time response at 50 seconds for N-methylisindole for the transients presented in figure 3.16 (b).

### *5-methoxy-N-methylisindole*

Transients obtained for the nucleation and growth of poly-5-methoxy-N-methylisindole at several different potentials are shown in figure 3.21 (a & b). As with N-methylisindole the current-time profiles are divided into two regions. Region I, the time before the local current minimum ( $t_0$ ) and region II, where the current increases after  $t_0$ . As with N-methylisindole a third region as described for other conducting polymers [85] was not observed.

In region I the initial monolayer of poly-5-methoxy-N-methylisindole is deposited when the curves reach a minimum  $t_0$ . A plot of  $-\ln(t_0)$  versus potential exhibit reasonable linearity between 0.3V and 0.4V (SCE), indicating Tafel-type behaviour; see figure 3.22.

In region II a rise in current after  $t_0$  was observed as with N-methylisindole. The current  $i_{II}$  in region II is given by equation 3.10. A plot of  $i_{II}$  versus  $(t-t_0)$  where  $m=1$  is shown in figure 3.23. Reasonable linearity was obtained at short times indicating that the governing equation is

$$i_{II} = (\text{constant}) (t-t_0) \quad (3.18)$$

This relationship is quite different from that of N-methylisindole where  $m=2$  leading to progressive nucleation and two-dimensional growth. From table 3.1 the slope of a plot of  $i$  versus  $t$  should be proportional to  $k$  for progressive nucleation and one-dimensional growth (needles), and  $k^2$  for instantaneous nucleation and two-dimensional growth. The growth parameter  $k$  is dependent on the applied potential via the Butler-Volmer equation (eqn 3.9). A slope of  $i_{II}$  versus  $(t-t_0)$  is plotted against potential and the resulting slope is given by

$$S = \left( \frac{d \log[di/d(t-t_0)]}{dE} \right) \quad (3.19)$$

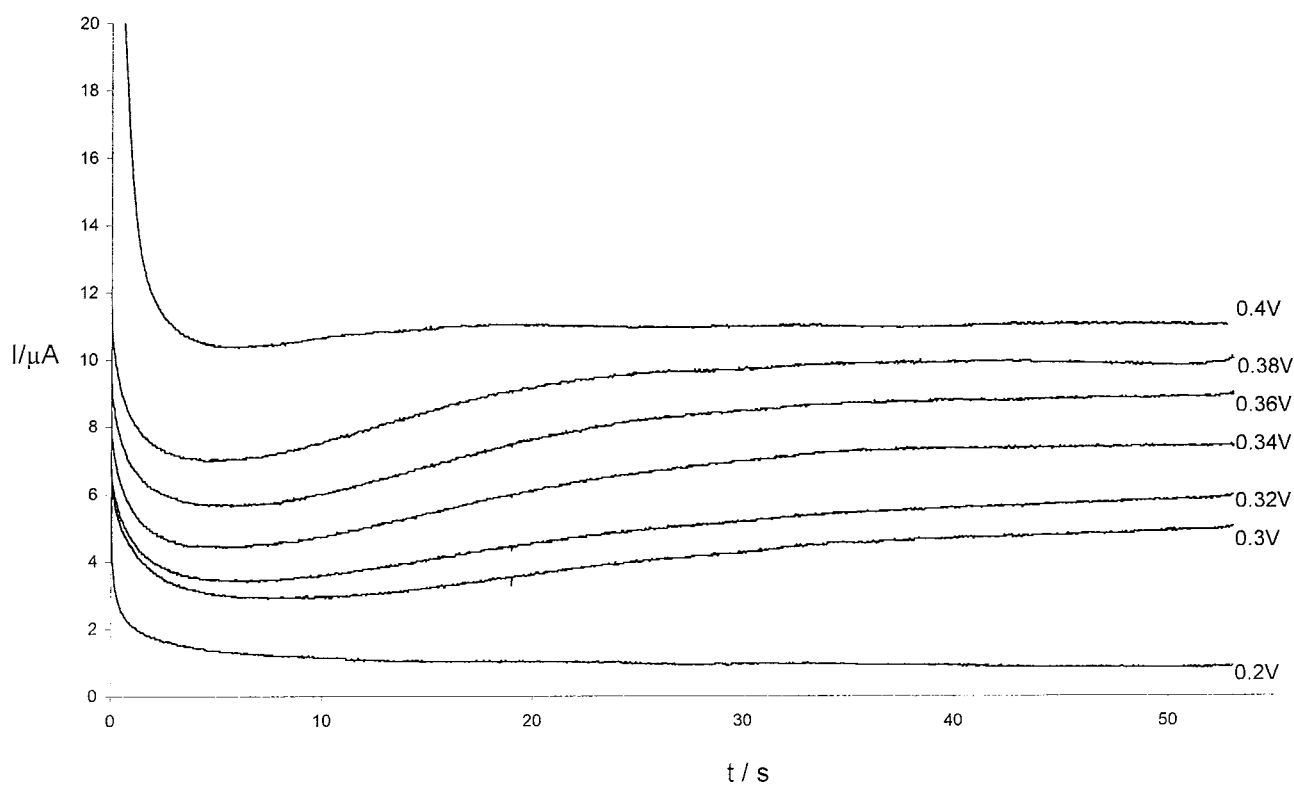


**Figure 3.21 (a):** Current-time transients for the growth of poly-5-methoxy-N-methylisindole perchlorate at platinum from a solution containing 9.3mM 5-methoxy N-methylisindole in 0.1M LiClO<sub>4</sub> in CH<sub>3</sub>CN as a function of potential (SCE).

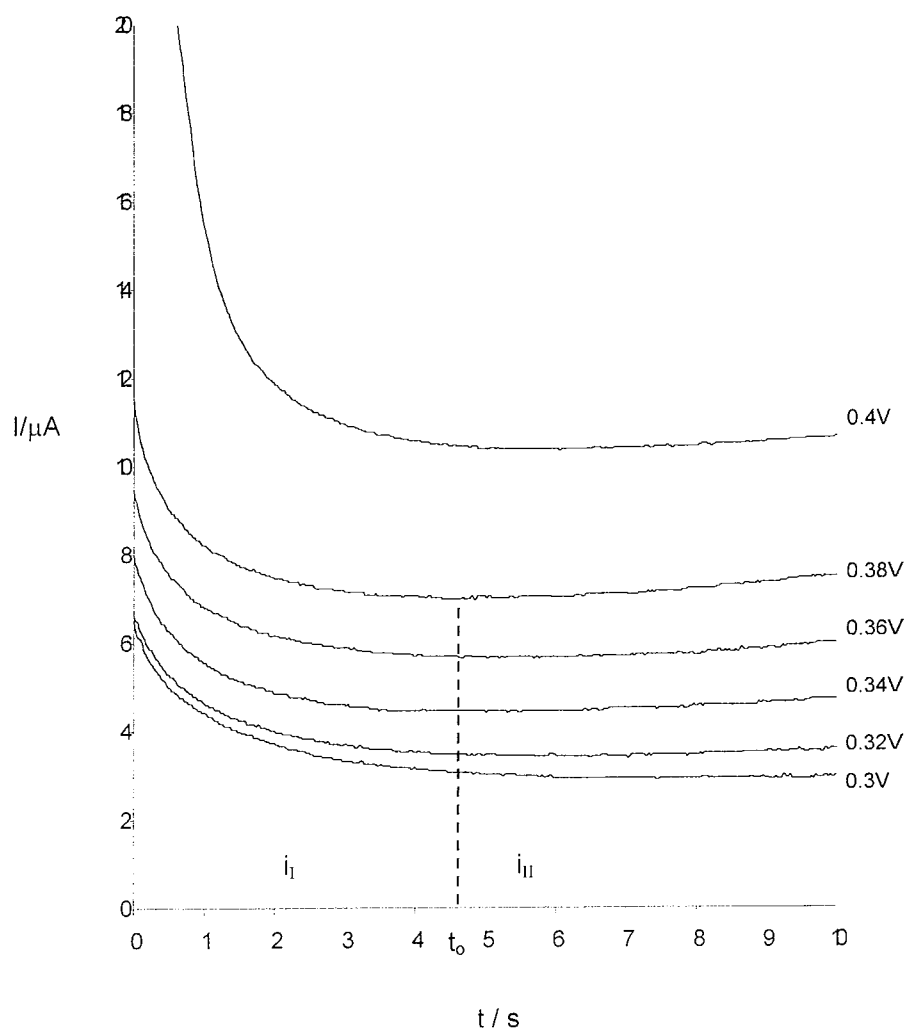


**Figure 3.21 (b):** Current-time transients obtained for poly-5-methoxy-N-methylisoindole perchlorate deposition at short times. Regions I and II are presented and  $t_0$  for the transient obtained at 0.38V. The deposition conditions are the same as those employed for figure 3.21(a)

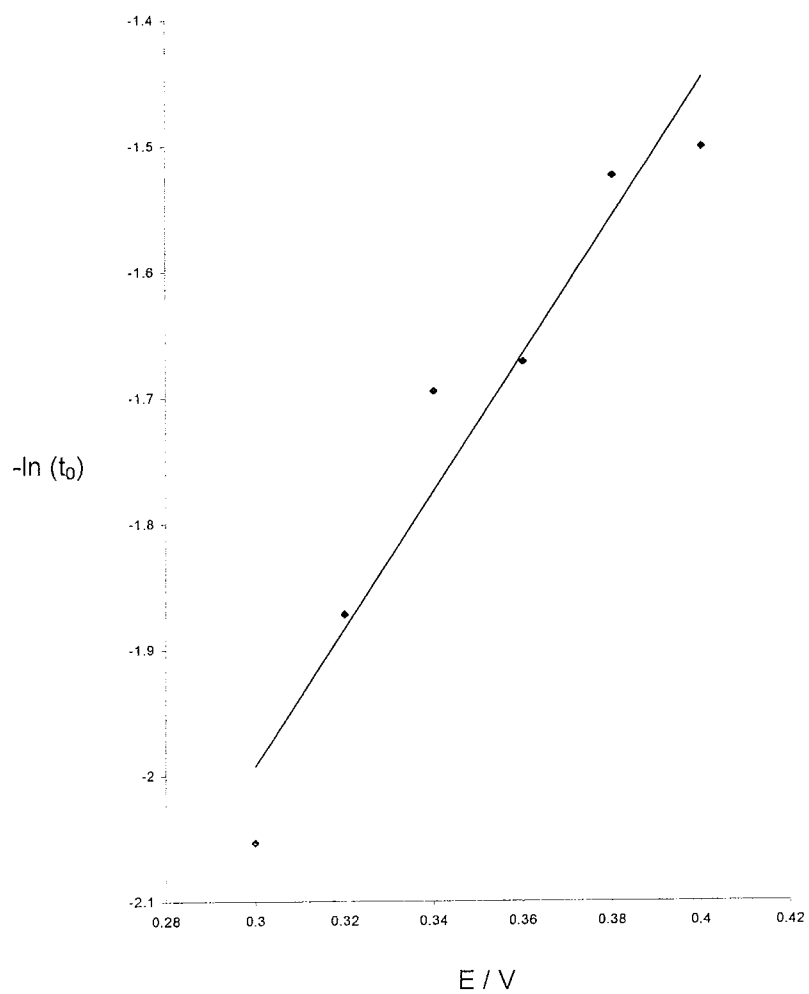


**Figure 3.22:** A plot of  $-\ln (t_0)$  versus applied potential for the transients presented in figure 3.21 (b) for 5-methoxy-N-methylisindole.

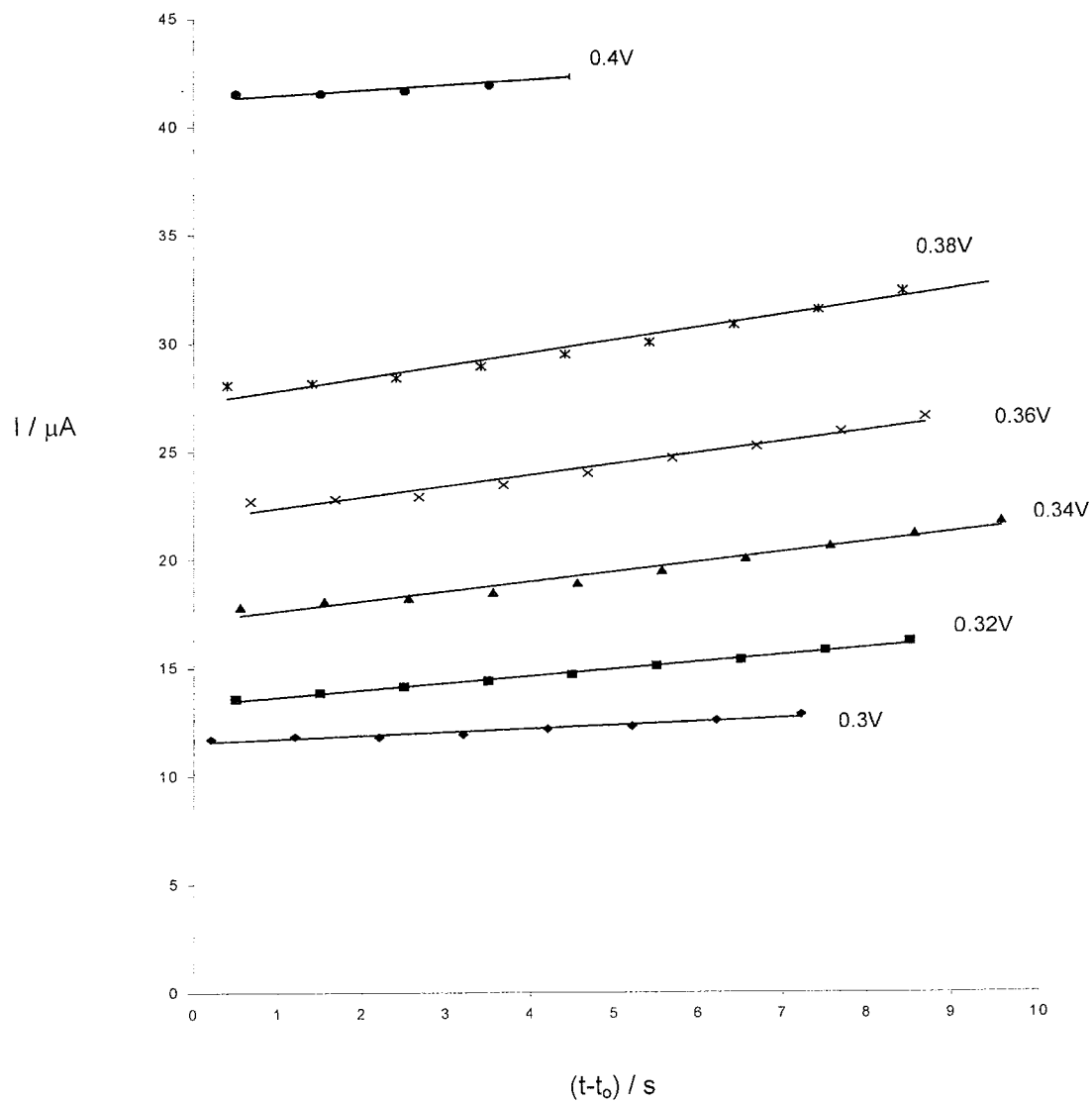


**Figure 3.23:** A plot of  $i_{II}$  versus  $(t-t_0)$  as a function of applied potential for the transients presented in figure 3.21 (b) for 5-methoxy-N-methylisoindole .

From this progressive nucleation and one-dimensional growth can be given by

$$S = \left( \frac{(1-\alpha)F}{2.303 RT} \right) = 8.4 \text{ V}^{-1} \quad (3.20)$$

where  $T=298\text{K}$ ,  $n=1$  and  $\alpha=0.5$ . On the other hand, by squaring equation 3.9,  $k^2$  can be expressed as

$$S = \left( \frac{2(1-\alpha)F}{2.303 RT} \right) = 16.9 \text{ V}^{-1} \quad (3.21)$$

for instantaneous nucleation and two-dimensional growth.

Figure 3.24 shows a plot of the slope of  $i_{II}$  verses  $(t-t_0)$  against potential. The plot exhibits good linearity with a slope of  $8.42\text{V}^{-1}$ . This result agrees well with an instantaneous nucleation and one-dimensional growth.

At long times in the current-time profile; see figure 3.21 (a), a steady-state response is observed as with N-methylisindole. Again, a Tafel-type behaviour would be expected to permit at these longer times. A Tafel plot of 5-methoxy-N-methylisindole at 50 seconds shows good linearity, as seen in figure 3.25. The slope of the plot is  $6.87\text{V}^{-1}$ , somewhat adrift of the theoretical Tafel slope of  $8.4\text{V}^{-1}$  as expressed in equation 3.17.

It is interesting that the mechanism of nucleation for the polymer formation differ between N-methylisindole and 5-methoxy-N-methylisindole, which suggests perhaps the steric effects of the methoxy group effect the nature of layer deposition. However is must be stressed that these chronoamperometric experiments were only carried out once. Therefore it would be valuable to repeat the work to obtain a statistical verification of the models, as polymer nucleation and growth can be affected by electrode morphology, which can change, whether the electrode is polished.

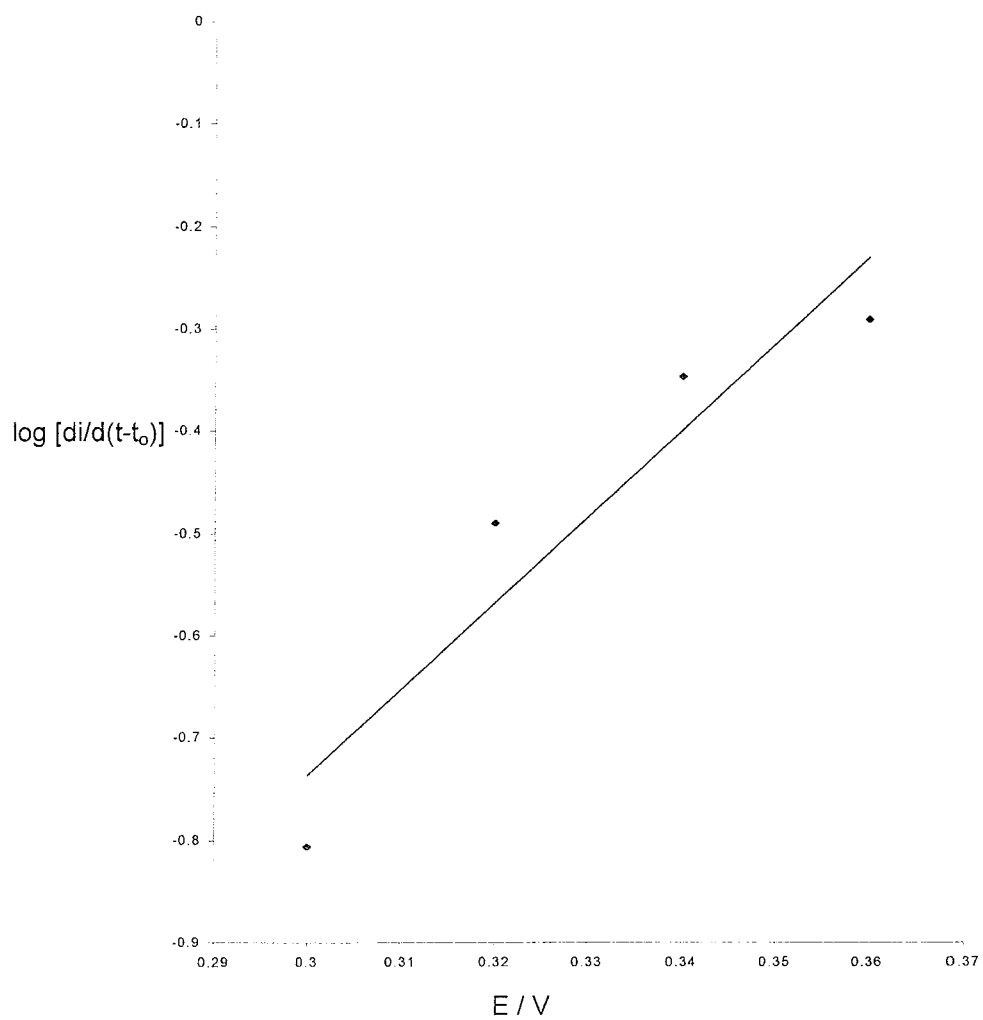


**Figure 3.24:** A plot of the slopes for  $i_{II}$  versus  $(t-t_0)$  against applied potential



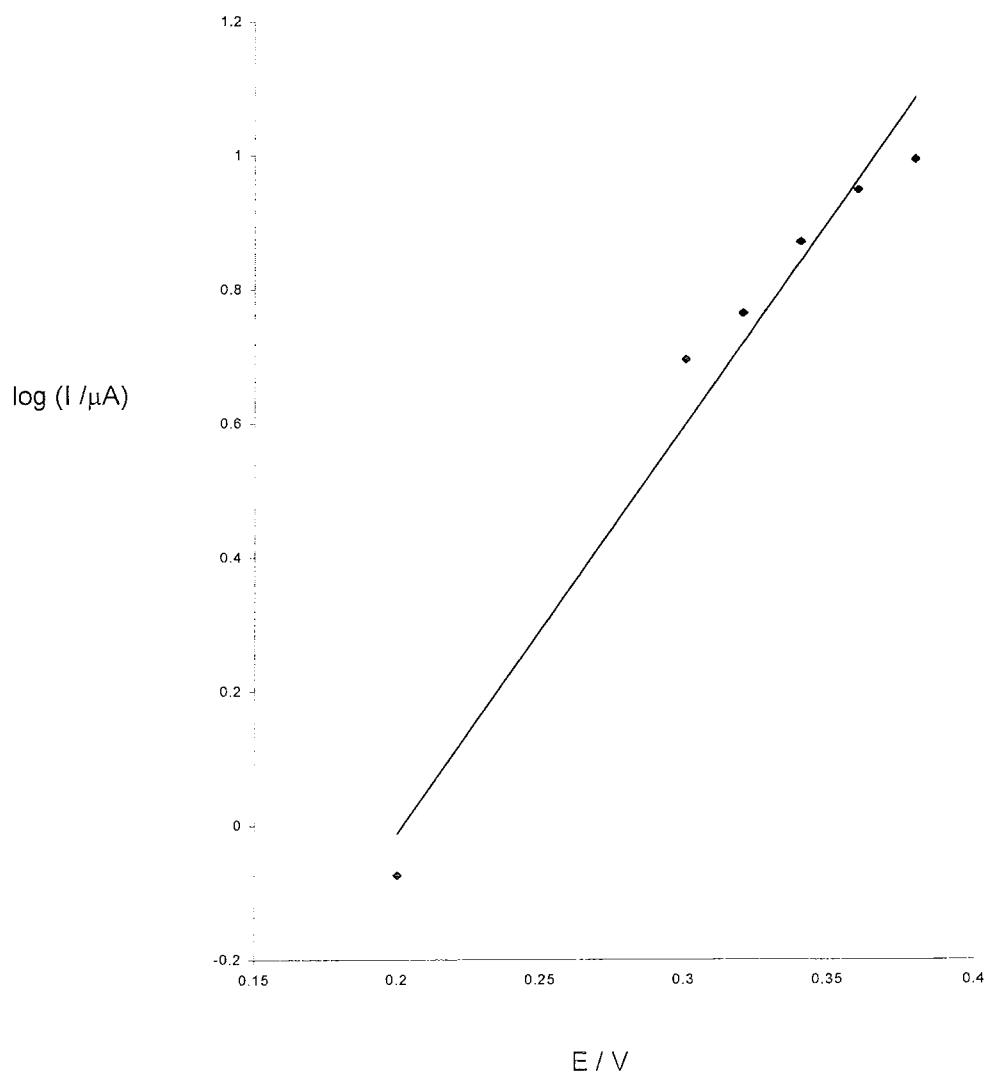


**Figure 3.25:** A Tafel plot of the steady-state section of chronoamperometric current-time response at 50 seconds for 5-methoxy-N-methylisoindole for the transients presented in figure 3.21 (b).

### *5,6-dimethoxy-N-methylisoindole*

Figure 3.26 shows a current-time profile as a function of potential for 5,6-dimethoxy-N-methylisoindole. Unlike N-methylisoindole and 5-methoxy-N-methylisoindole the current decay over time is with no local minimum indicative of monolayer coverage at all voltages. There is some indication of layer formation though it is masked by current due to oligomer formation and therefore, there is little evidence of nucleation activity. This is complimentary to the conclusions from the cyclic voltammetry where the oxidation potential of several consecutive sweeps remained unchanged and no crossover of the forward and backward sweeps suggesting that little nucleation and growth was occurring at the electrode surface; see figure 3.12. At longer times the current obtained a steady-state response and a Tafel plot of  $\log i$  versus potential is shown in figure 3.27. A slope of  $6.8V^{-1}$  is somewhat away from the expected theoretical Tafel slope of  $8.4V^{-1}$ .

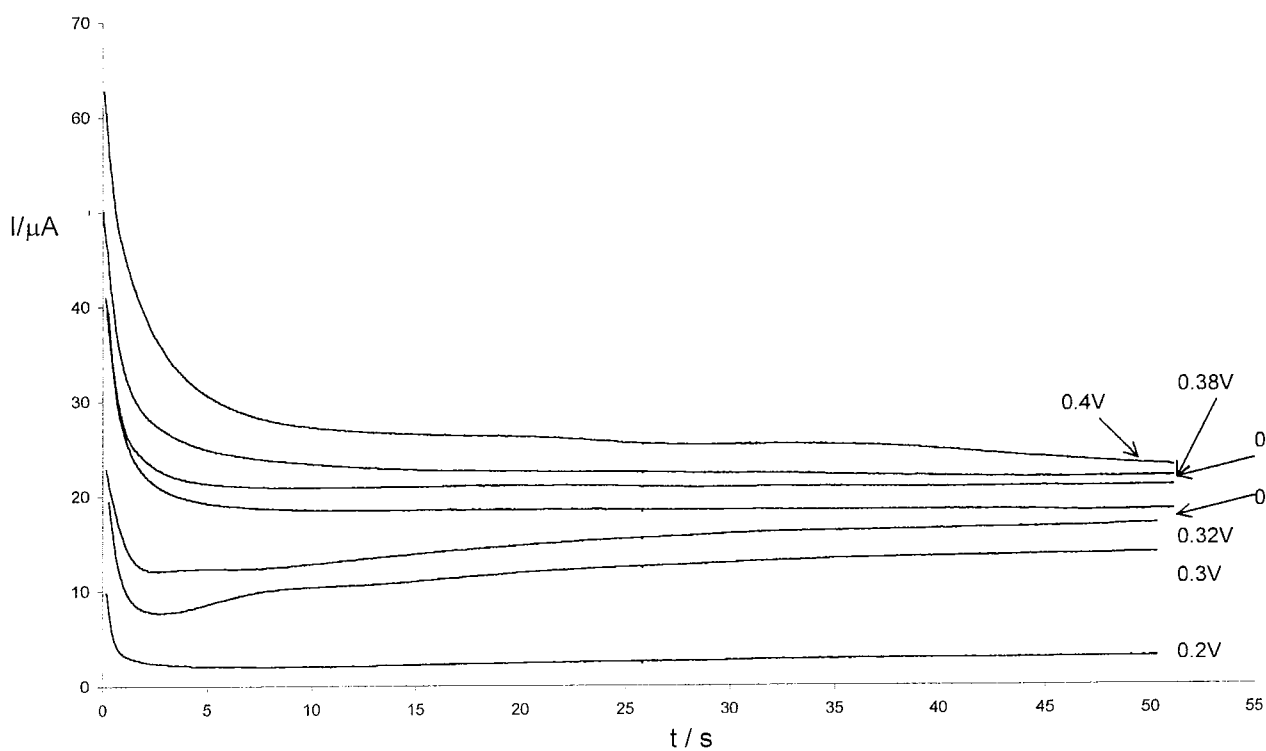


**Figure 3.26** : Current-time transients for the growth of poly-5,6-dimethoxy-N-methylisindole perchlorate at platinum from a solution containing 8.37mM 5,6-dimethoxy-N-methylisindole in 0.1M LiClO<sub>4</sub> in CH<sub>3</sub>CN as a function of potential (SCE).

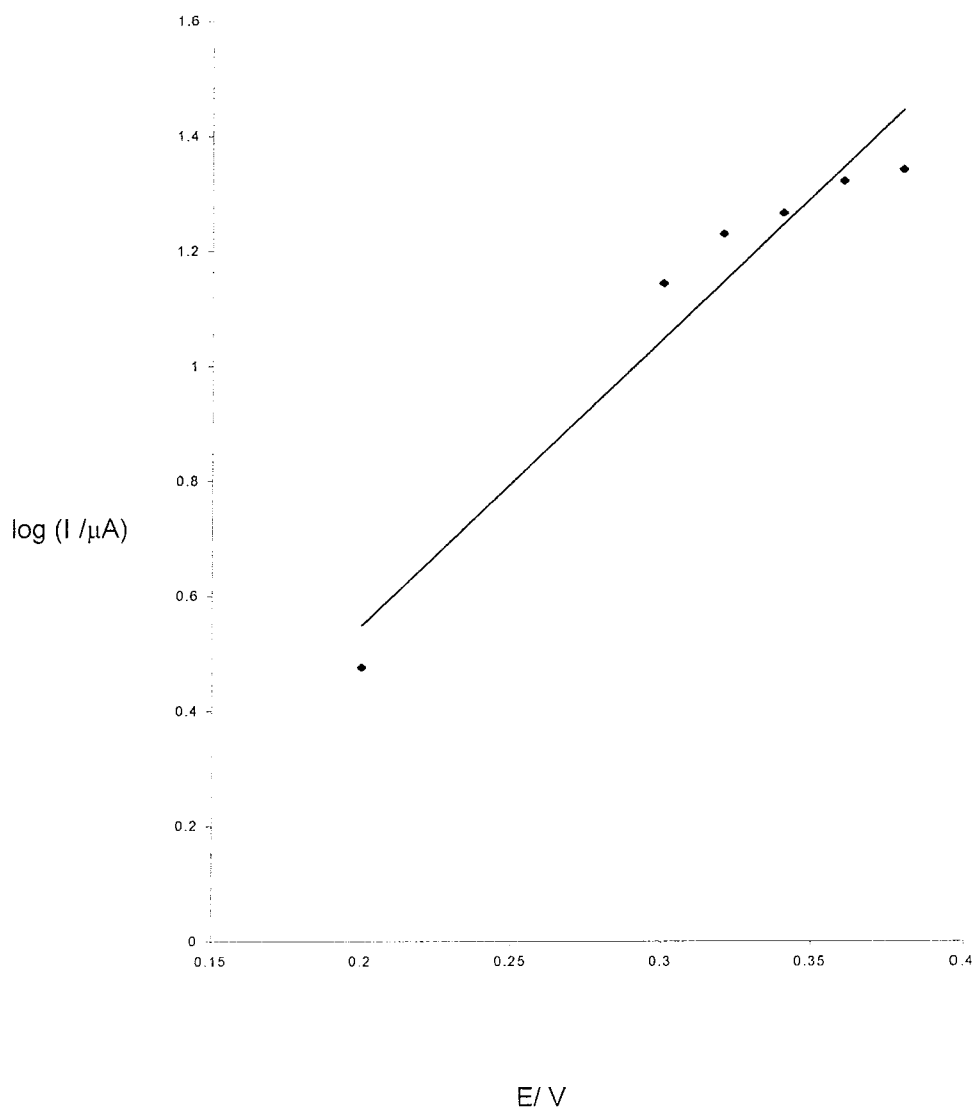


**Figure 3.27:** A Tafel plot of the steady-state section of chronoamperometric current-time response at 50 seconds for 5,6-dimethoxy-N-methylisoindole for the transients presented in figure 3.26.

### 3.2.3 Cyclic Voltammetric study of the Isoindole polymers.

The thin films of poly-N-methylisoindole, poly-5-methoxy-N-methylisoindole and poly-5,6-dimethoxy-N-methylisoindole were formed on a platinum electrode by continuous sweeping in monomer solution as shown in figures 3.12 and 3.15, in lithium perchlorate and tetraethylammonium p-toluene sulphonate respectively. The three polymers were also formed in lithium bromide by continuous sweeping in monomer solution, however the potential limits were  $-0.5\text{V}$  to  $+0.4\text{V}$  as after this upper limit the oxidation of the electrolyte salt occurs. After the polymer films were formed the electrode was washed with supporting electrolyte and then placed in fresh electrolyte solution following which cyclic voltammograms were recorded.

#### *Lithium perchlorate:*

Cyclic voltammetric studies of [Pt] poly-N-methylisoindole perchlorate are shown in figure 3.28(a). The potential was swept from  $-0.5\text{V}$  to  $+0.25\text{V}$  at six different scan speeds, i.e. 10, 20, 40, 50, 80, 100 mV/sec.  $E_{pa}$  and  $E_{pc}$  values for the polymer at 50 mV/sec are  $+0.04\text{V}$  and  $-0.02\text{V}$  respectively, corresponding to a  $\Delta E$  ( $E_{pa} - E_{pc}$ ) of 60 mV, while not equal to zero is indicative of thin film behaviour. The  $i_{pa}/i_{pc} = 1.03$  for the measured values  $i_{pa}=17\mu\text{A}$  &  $i_{pc}=16.5\mu\text{A}$  at 50 mV/sec, implies good reversibility of the redox reaction, i.e the oxidation and reduction of the polymer film. On plotting scan speed  $\nu$  verses  $i_{pa}$  and  $i_{pc}$ ; see figure 3.28 (b), the resulting linear plot is characteristic of a redox process of a surface localised material. The surface coverage  $\Gamma = 2.8 \times 10^{-8}$  moles/cm<sup>2</sup>, assuming oxidation of the polymer occurs over four repeat monomer units, based on that calculated for polypyrrole [26].

An interesting feature of the cyclic voltammogram is the high capacitive current, attributed to the charging of a pseudo-capacitance [87] in the doped state. This was also reported on cyclic voltammograms carried out on poly-N-methylisoindole in other electrolytic media, namely tetrabutylammonium perchlorate in  $\text{CH}_3\text{CN}$  [81] and lithium bromide in  $\text{CH}_3\text{CN}$  [80].

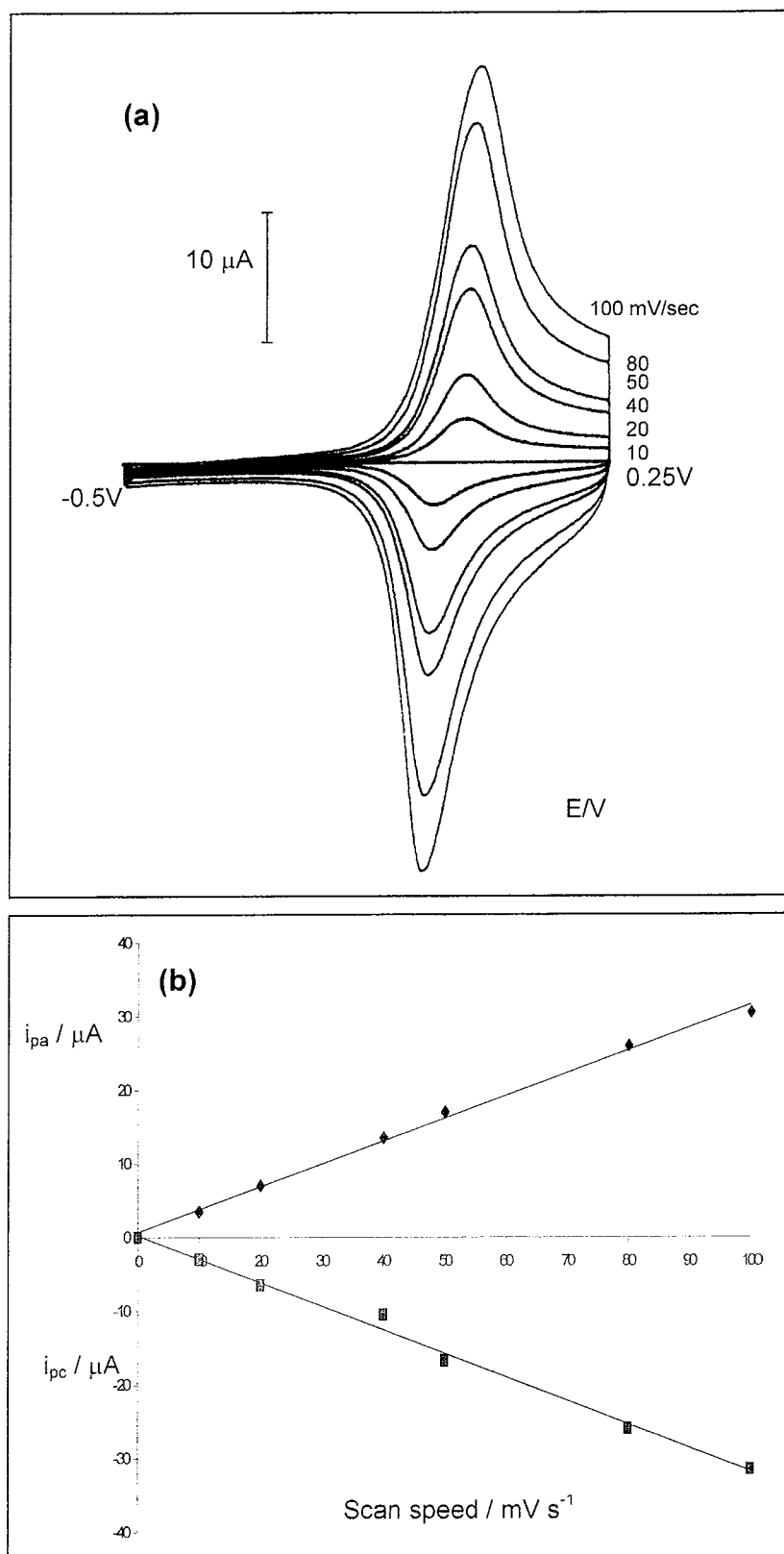


**Figure 3.28:** (a) Cyclic voltammogram of [Pt] poly-N-methylisindole perchlorate in  $0.1 \text{ M LiClO}_4$  in  $\text{CH}_3\text{CN}$  vs SCE at various scan speeds (b) plot of  $i_{pa}$  &  $i_{pc}$  versus scan speed for poly-N-methylisindole perchlorate

A high contrast electrochromic change was also observed on cycling the system from an oxidised state to a reduced state: in the oxidised state the polymer was a transparent or 'colour neutral', whereas in the reduced state it has a metallic gold appearance, also observed in tetrabutylammonium perchlorate [81]. This is in contrast to findings, in lithium bromide [80], where the polymer was dark green in the oxidised state and golden yellow in the reduced state.

Figure 3.29 (a) shows the cyclic voltammogram of poly-5-methoxy-N-methylisindole perchlorate cycling between  $-0.5\text{V}$  and  $0.3\text{V}$  at different scan speeds.  $E_{pa}$  and  $E_{pc}$  values for the polymer at  $50\text{ mV/sec}$  are  $-0.03\text{V}$  and  $-0.07\text{V}$  respectively, corresponding to  $\Delta E$  ( $E_{pa} - E_{pc}$ ) of  $40\text{ mV}$ , showing thin film behaviour, as with N-methylisindole perchlorate. The  $i_{pa}/i_{pc} = 1.3$  for the measured values  $i_{pa}=15\mu\text{A}$  &  $i_{pc}=-19.5\mu\text{A}$  at  $50\text{ mV/sec}$ , again implying good reversibility of the redox reaction. A plot of scan speed versus  $i_{pa}$  and  $i_{pc}$ ; see figure 3.29 (b), is also linear, again indicating a redox process of a surface localised material. The surface coverage  $\Gamma = 5.3 \times 10^{-8}\text{ moles/cm}^2$ , is very close to that for poly-N-methylisindole, indicating a similar amount of polymer layer covering the electrode surface. What is of more significance, is that the  $E_{pa}$  at  $50\text{ mV/sec}$  of poly-5-methoxy-N-methylisindole perchlorate is less positive than poly-N-methylisindole perchlorate and hence oxidises more easily than poly-N-methylisindole. This shows that the electron donating effects of the methoxy substituent, which lowered the  $E_{pa}$  of the monomer, is now affecting the polymer oxidation properties also.

Again the cyclic voltammogram shows a high capacitive current and a high contrast electrochromic change on cycling the system from an oxidised state to a reduced state. In the oxidised state the polymer is transparent or 'colour neutral', whereas in the reduced state it has a metallic gold appearance as with poly-N-methylisindole. Therefore, not only is poly-5-methoxy-N-methylisindole a new conducting polymer with a significantly lower  $E_{pa}$  and  $E_{pc}$ , but it also has electrochromic properties leading to possible applications.

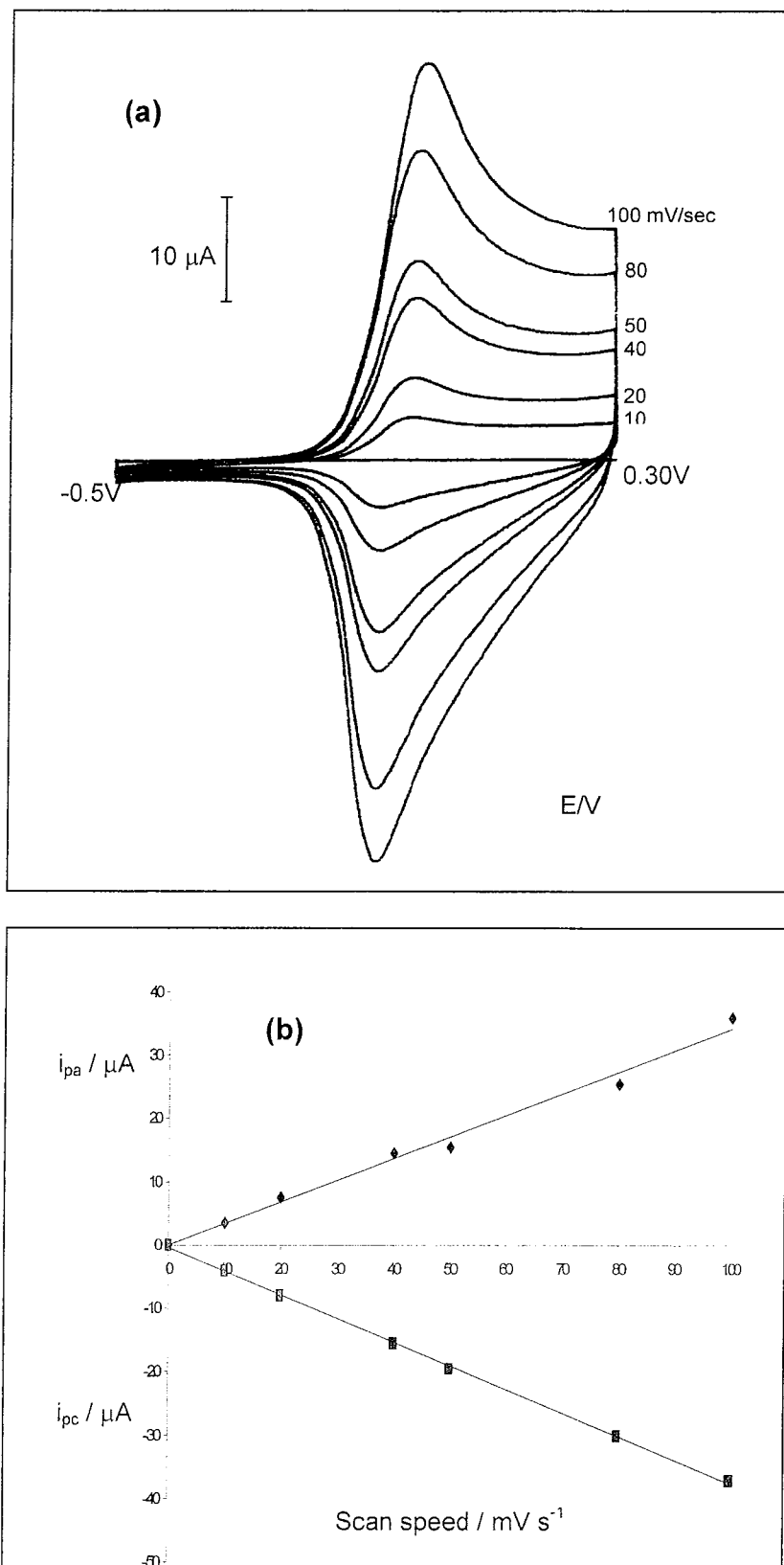


**Figure 3.29:** (a) Cyclic voltammogram of [Pt] poly-5-methoxy-N-methylisindole perchlorate in 0.1 M  $\text{LiClO}_4$  in  $\text{CH}_3\text{CN}$  vs SCE at various scan speeds (b) plot of  $i_{pa}$  &  $i_{pc}$  versus scan speed.



Obtaining a thin film of poly-5,6-dimethoxy-N-methylisindole perchlorate grafted onto the electrode surface was more difficult than poly-N-methylisindole and poly-5-methoxy-N-methylisindole. On attempting to grow the polymer film by continuous scanning of the monomer at 50 mV/sec, polymeric material was observed streaming away from the electrode as previously discussed (see section 3.2.1), however a very thin film of poly-5,6-dimethoxy-N-methylisindole remained. This film on the platinum electrode was washed with supporting electrolyte and then placed in fresh electrolyte solution as before. Cyclic voltammetric studies of [Pt] poly-5,6-dimethoxy-N-methylisindole perchlorate are shown in figure 3.30 (a). The potential was swept from  $-0.5\text{V}$  to  $0.03\text{V}$  at four different scan speeds, i.e. 20, 50, 80, 100 mV/sec.  $E_{pa}$  and  $E_{pc}$  values for the polymer at 50 mV/sec are  $-0.16\text{V}$  and  $-0.17\text{V}$  respectively corresponding to  $\Delta E$  value of  $10\text{mV}$ .

Compared with poly-N-methylisindole and poly-5-methoxy-N-methylisindole with that of poly-5,6-dimethoxy-N-methylisindole, the  $E_{pa}$  values at 50 mV/sec, the polymer oxidation potential is lower when a methoxy substituent is introduced onto the six membered ring and is even lower when a second methoxy substituent is introduced. This is the same as the trend found in the  $E_{pa}$  values for the monomer species, and therefore, it can be concluded that the mono- and di- substituted poly-N-methylisindoles are increasingly easier to oxidise respectively, possibly due to the increased electron density that the electron donating methoxy groups provide.

These results are contrary to cyclic voltammetry recorded for polyisothianaphthene (**13**) and its derivatives poly-5-methylisothianaphthene (**14**) [88] and poly-5,6-dioxymethyleneisothianaphthene (**15**) [89]; see figure 3.31. The methyl substituent (**14**), which is electron donating, showed little change in the oxidation potential from that from the parent system (**13**) [88]. Cyclic voltammetry recorded for (**15**) showed the  $E_{pa}$  at  $+0.68\text{V}$  (Ag/AgCl) and under the same conditions the  $E_{pa}$  for (**13**) was  $+0.36\text{V}$ , this is contrary to expectations, where no redox potential lower effect of the dioxymethylene group was observed.

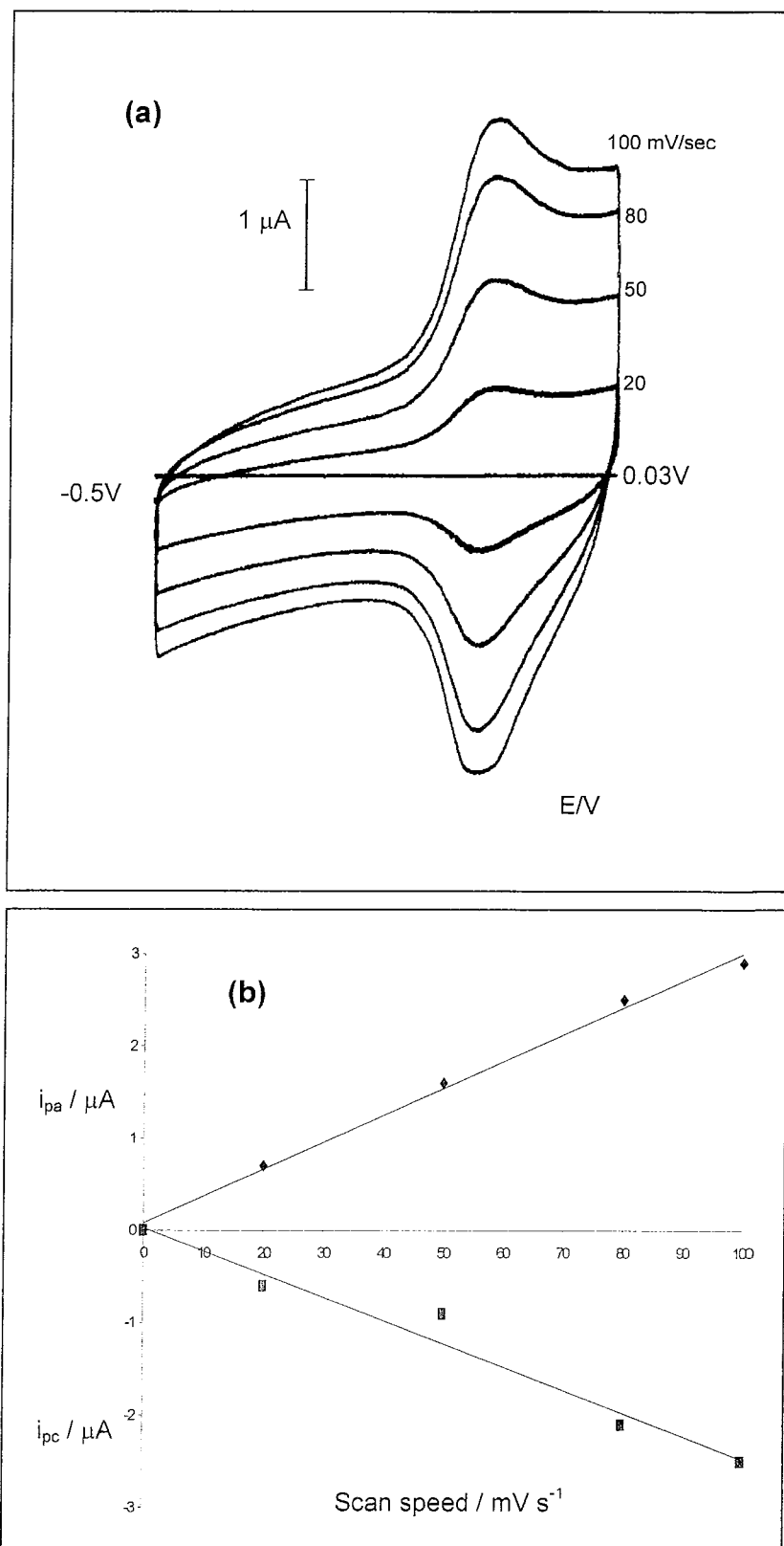


**Figure 3.30:** (a) Cyclic voltammogram of [Pt] poly-5,6-dimethoxy-N-methylisoindeole perchlorate in 0.1 M LiClO<sub>4</sub> in CH<sub>3</sub>CN vs SCE at various scan speeds (b) plot of  $i_{pa}$  &  $i_{pc}$  versus scan speed

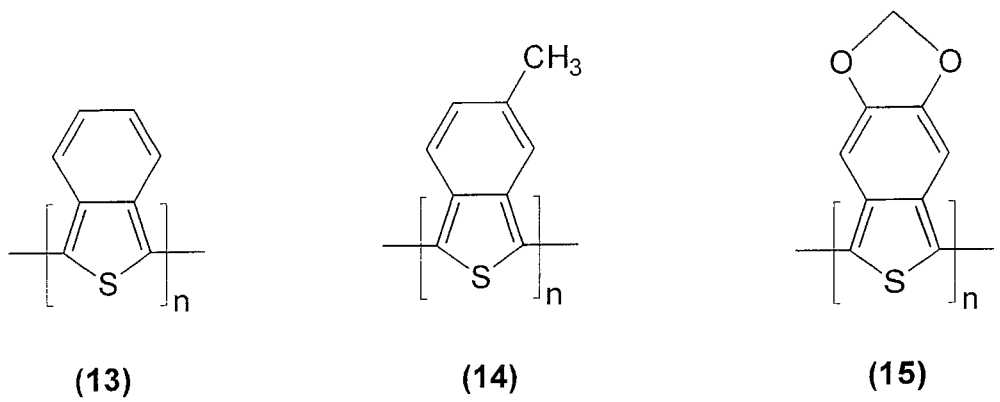


**Figure 3.31:** Substituted Polyisothianaphthene

The value for  $i_{pa}/i_{pc}$  was 1.19 for  $i_{pa}=2.5\mu\text{A}$  &  $i_{pc} = -2.1 \mu\text{A}$  at 80 mV/sec, which again implies good reversibility of the redox reaction. On plotting scan speed  $v$  versus  $i_{pa}$  and  $i_{pc}$ ; see figure 3.30 (b), the resulting linear plot is again characteristic of a redox process of a surface localised material as observed with poly-N-methylisindole. The surface coverage  $\Gamma = 2 \times 10^{-9}$  moles/cm<sup>2</sup> is a order of magnitude lower than the surface coverage of poly-N-methylisindole and poly-5-methoxy-N-methylisindole, which is expected considering the poor polymer formation of the dimethoxy polymer.

Finally unlike poly-N-methylisindole and poly-5-methoxy-N-methylisindole, no electrochromic properties were observed for poly-5,6-dimethoxy-N-methylisindole. However it cannot be concluded that it does not have electrochromic properties, as the films formed were very thin and not visible on the electrode.

#### *Tetraethylammonium-p-toluene sulphonate:*

Cyclic voltammetric studies of the polymers were repeated with tetraethylammonium p-toluene sulphonate in acetonitrile as the supporting electrolyte. The thin film formed from the continuous scanning of N-methylisindole, still on the platinum electrode was washed with supporting electrolyte and then placed in fresh electrolyte solution 0.1M (Et)<sub>4</sub>N(O<sub>3</sub>SC<sub>6</sub>H<sub>4</sub>CH<sub>3</sub>) / CH<sub>3</sub>CN. Cyclic voltammetry studies of [Pt] poly(N-methylisindole) p-toluene sulphonate are shown in figure 3.32 (a). The potential was swept from -0.5V to + 0.4V at six different scan speeds, i.e. 10, 20, 40, 50, 80, 100 mV/sec.  $E_{pa}$  and  $E_{pc}$  values for the polymer at 50 mV/sec are +0.23V and +0.12 V respectively giving  $\Delta E$  of 110 mV is large, compared with  $\Delta E$  of poly-N-methylisindole perchlorate (60mV). The  $i_{pa}=34\mu\text{A}$  &  $i_{pc} = -33 \mu\text{A}$  at 50 mV/sec and the value for  $i_{pa}/i_{pc} = 1.03$ , again confirms good reversibility of the redox reaction. The surface coverage  $\Gamma = 10.3 \times 10^{-8}$  moles/cm<sup>2</sup>, which would indicate a thicker film than that deposited with the perchlorate, as expected.

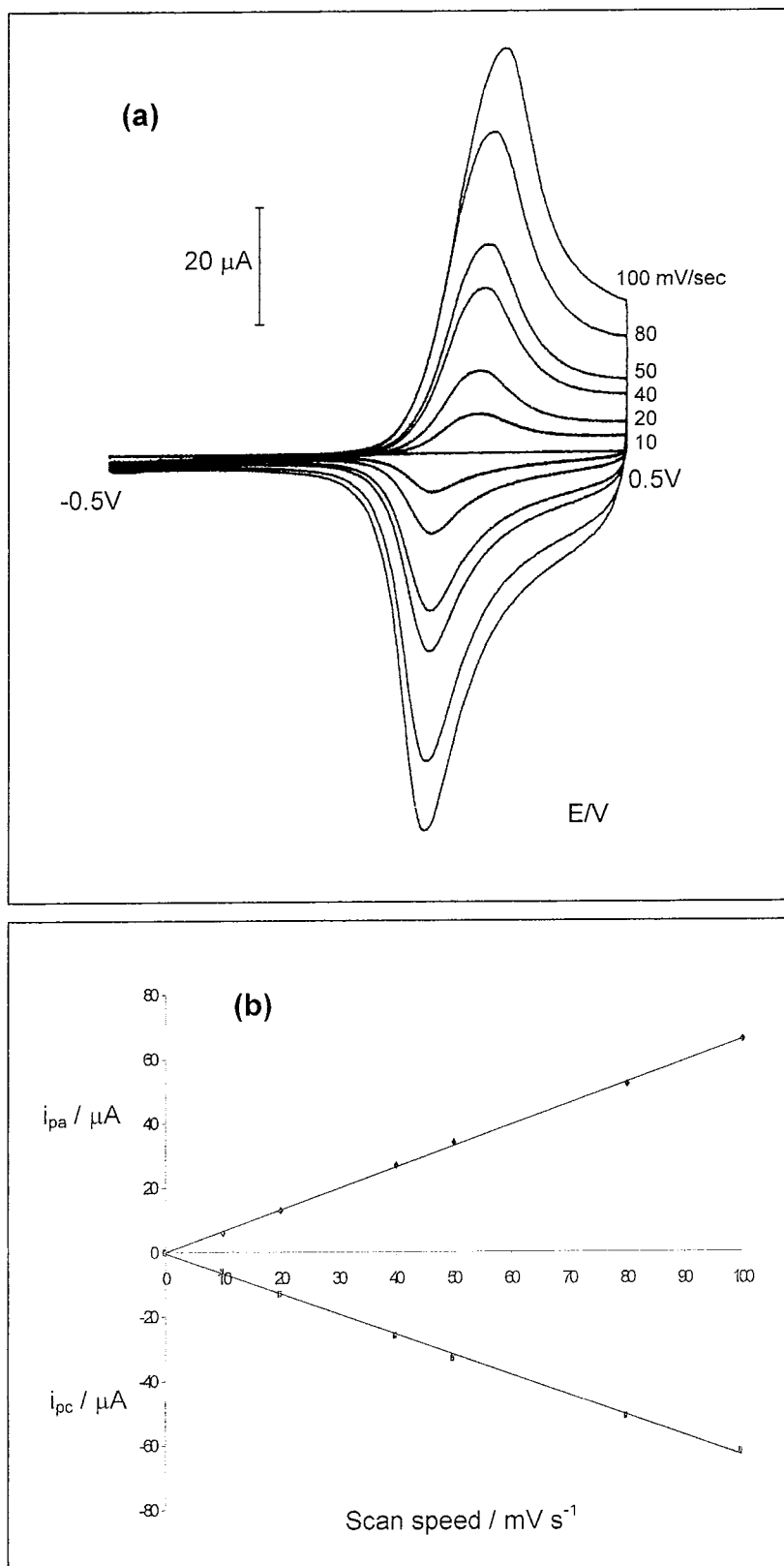


**Figure 3.32:** (a) Cyclic voltammogram of [Pt] poly-N-methylisindole p-toluene sulphonate in 0.1 M  $(\text{Et})_4\text{N}(\text{O}_3\text{SC}_6\text{H}_4\text{CH}_3)$  in  $\text{CH}_3\text{CN}$  vs SCE at various scan speeds (b) plot of  $i_{pa}$  &  $i_{pc}$  versus scan speed

On plotting scan speed  $v$  versus  $i_{pa}$  and  $i_{pc}$ ; see figure 3.32(b), the resulting linear plot is characteristic of a redox process of a surface localised material, the same as poly-N-methylisindole perchlorate. Furthermore the voltammogram does not change on bubbling nitrogen in front of the working electrode. On comparing the  $E_{pa}$  and  $E_{pc}$  values for poly-N-methylisindole perchlorate, +0.04V and -0.02V respectively at 50mV/sec, which are lower, shows that the polymer doped with perchlorate is more easily oxidised than the polymer doped with p-toluene sulphonate. This is possibly due to the greater ease of movement of the less bulky perchlorate anion.

As before a high capacitive current is evident and is attributed to the charging of a pseudo-capacitance [87] in the doped state, see figure 3.32 (a). Again a high contrast electrochromic change was also observed, as with poly-N-methylisindole perchlorate, where in the oxidised state the polymer is transparent colourless or 'colour neutral', whereas in the reduced state it has a metallic gold appearance.

Figure 3.33 (a) shows the cyclic voltammetry of poly-5-methoxy-N-methylisindole p-toluene sulphonate cycling between -0.5V and 0.3V at different scan speeds.  $E_{pa}$  and  $E_{pc}$  values for the polymer at 50 mV/sec are +0.12V and +0.04V respectively, corresponding to  $\Delta E$  ( $E_{pa} - E_{pc}$ ) of 80 mV, again the  $\Delta E$  is larger with p-toluene sulphonate than perchlorate. The  $i_{pa}/i_{pc} = 1.24$  at 50 mV/sec, are a little high though the cyclic voltammogram can be seen to be not ideal since a second oxidation peak is observed. This second peak was also observed when forming the layer in monomer solution; see figure 3.14 (b), however it was not observed in the cyclic voltammograms of poly-5-methoxy-N-methylisindole on lithium perchlorate.

A plot of scan speed versus  $i_{pa}$  and  $i_{pc}$ ; see figure 3.33 (b) is also linear, again indicating a redox process of a surface localised material. The surface coverage  $\Gamma = 6.2 \times 10^{-8}$ , which is slightly higher than that of poly-5-methoxy-N-methylisindole perchlorate, and correlates well with  $\Delta E$  values indicating a thicker film formation in p-toluene sulphonate.

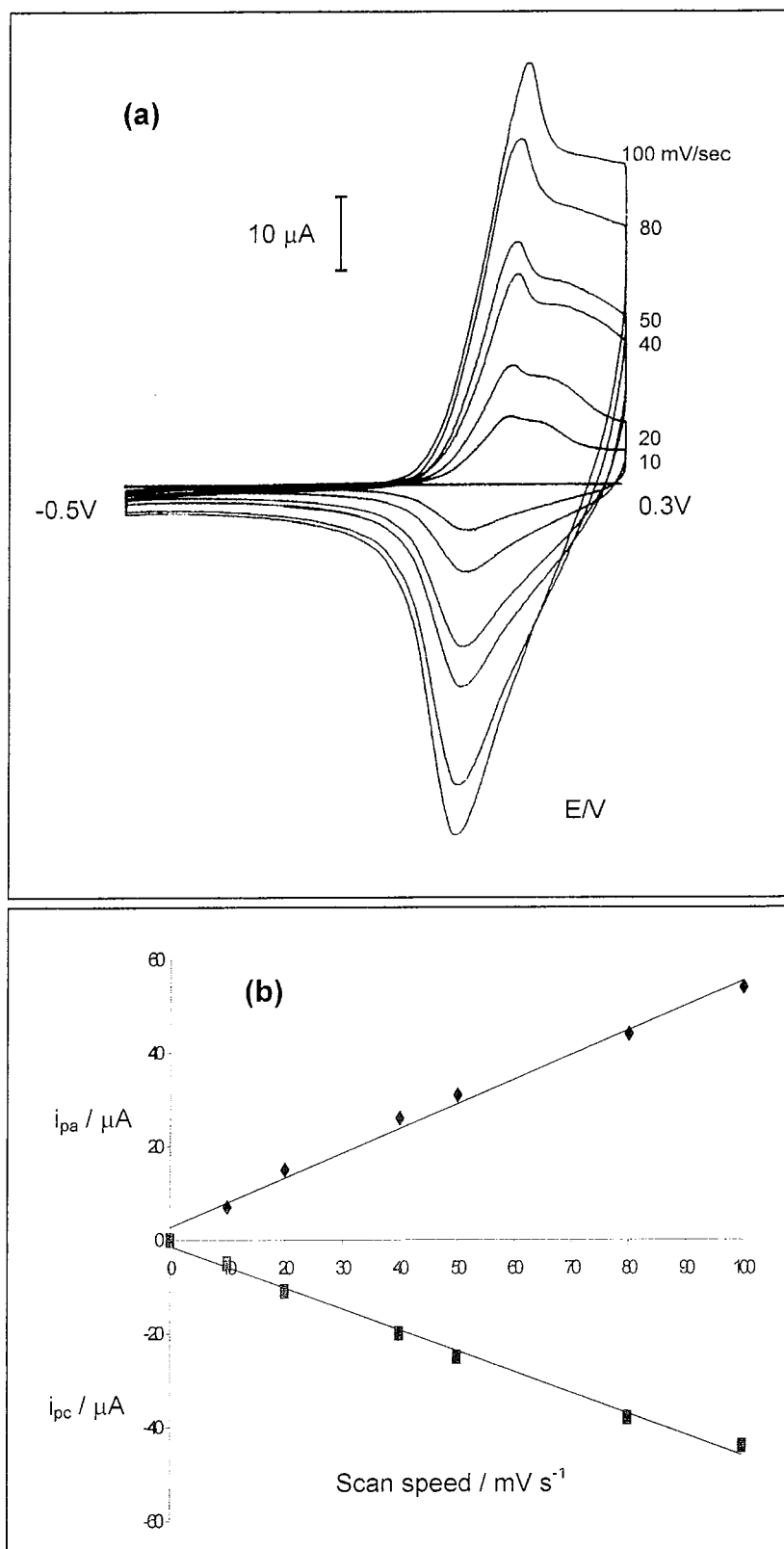


**Figure 3.33:** (a) Cyclic voltammogram of [Pt] poly-5-methoxy-N-methylisindole p-toluene sulphonate in 0.1 M  $(\text{Et})_4\text{N}(\text{O}_3\text{SC}_6\text{H}_4\text{CH}_3)$  in  $\text{CH}_3\text{CN}$  vs SCE at various scan speeds (b) plot of  $i_{pa}$  &  $i_{pc}$  versus scan speed

The  $E_{pa}$  and  $E_{pc}$  at 50 mV/sec of poly-5-methoxy-N-methylisindole p-toluene sulphonate are less positive than N-methylisindole p-toluene sulphonate and hence can be oxidised more easily than N-methylisindole. The mono methoxy substituent is now easier to oxidise regardless of dopant. Again the cyclic voltammogram shows a high capacitive current and a high contrast electrochromic change on cycling the system from an oxidised state to a reduced state. In the oxidised state the polymer is transparent or 'colour neutral', whereas in the reduced state it has a metallic gold appearance as with N-methylisindole.

As with using lithium perchlorate as electrolyte obtaining a thin film of poly-5,6-dimethoxy-N-methylisindole on the electrode surface was more difficult than N-methylisindole. The thin film formed on the platinum electrode was washed with supporting electrolyte and then placed in fresh electrolyte solution as before. Cyclic voltammetry studies of [Pt] poly-5,6-dimethoxy-N-methylisindole p-toluene sulphonate are shown in figure 3.34 (a). The potential was swept from  $-0.5V$  to  $0.0V$  at four different scan speeds, i.e. 20, 50, 80, 100 mV/sec.  $\Delta E$  at 50 mV/sec is 10 mV, which is the same as  $\Delta E$  of poly-5,6-dimethoxy-N-methylisindole perchlorate.  $i_{pa}=2.4\mu A$  &  $i_{pc}=2.2\mu A$  at 50 mV/sec and the value for  $i_{pa}/i_{pc} = 1.09$ , which implies good reversibility of the redox reaction. On plotting scan speed  $v$  versus  $i_{pa}$  and  $i_{pc}$ ,; see figure 3.34 (b), the resulting linear plot is characteristic of a redox process of a surface localised material now observed with both polymers in both electrolyte's. The surface coverage of  $\Gamma = 2 \times 10^{-9}$  moles/  $cm^2$  is equal to that for poly-5,6-dimethoxy-N-methylisindole perchlorate and further highlights the difficulties in forming a significant layer of this disubstituted polymer.

On comparing the  $E_{pa}$  and  $E_{pc}$  values for poly-5,6-dimethoxy-N-methylisindole perchlorate,  $-0.16V$  and  $-0.17V$  respectively at 50 mV/sec which are lower, shows that the polymer doped with perchlorate is more easily oxidised than the polymer doped with p-toluene sulphonate. This trend also occurs with poly-N-methylisindole and poly-5-methoxy-N-methylisindole.



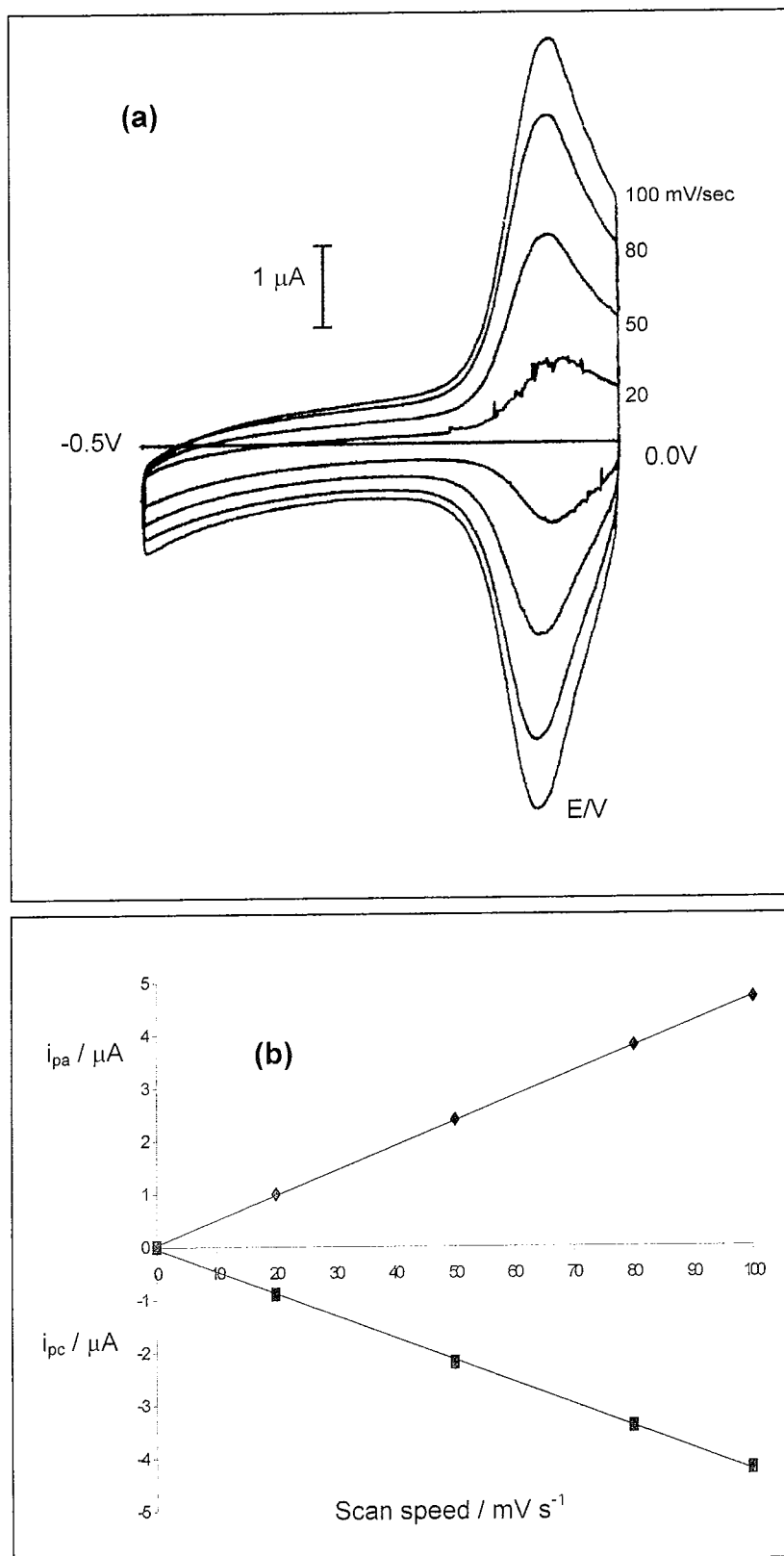


**Figure 3.34:** (a) Cyclic voltammogram of [Pt] poly-5,6-dimethoxy-N-methylisoindole p-toluene sulphonate in 0.1 M (Et)<sub>4</sub>N(O<sub>3</sub>SC<sub>6</sub>H<sub>4</sub>CH<sub>3</sub>) in CH<sub>3</sub>CN vs SCE at various scan speeds (b) plot of  $i_{pa}$  &  $i_{pc}$  versus scan speed

### *Lithium bromide:*

Cyclic voltammetry studies of the polymers were repeated with lithium bromide in acetonitrile as the supporting electrolyte. The thin film formed from the continuous scanning of monomer, still on the platinum electrode was washed with supporting electrolyte and then placed in fresh electrolyte solution 0.1M LiBr / CH<sub>3</sub>CN. The cyclic voltammogram and resulting plots of  $i_{pa}$  &  $i_{pc}$  versus scan speed are shown in figures 3.35 to 3.37. As with the other two electrolytes the  $E_{pa}$  and  $E_{pc}$  for the polymers is lower with an increasing number of methoxy substituents on the N-methylisindole sub-unit. The main results for lithium bromide as supporting electrolyte and the other electrolytes are tabulated in table 3.3.

Finally in analysing the cyclic voltammetric and chronoamperometric data, the different results for the three polymers have been mainly attributed to the electronic effect of the methoxy substituent, while little has been commented any possible steric effects.

It has been found [90] that not only is the position of coupling important, but also the sequence in which the monomer units couple. N-methylisindole and 5,6-dimethoxy-N-methylisindole are symmetrical molecules. These molecules lead to structurally regular polymers and couple through the 1- and 3- positions, where the 3- position is the "Head" and the 1- position is the "Tail", and are denoted as *regioregular* or *HT* polymers, as shown in figure 3.38 and 3.39

However, 5-methoxy-N-methylisindole is asymmetrical and leads to polymers with four possible regiochemical couples, as shown in figure 3.40. The first of these orientations is *regioregular* 3-1 ; 3-1 or head-to-tail coupling (HT-HT), the other three orientations are structurally irregular and are denoted as *regioirregular* or *non-HT* [90] as shown in figure 3.40.

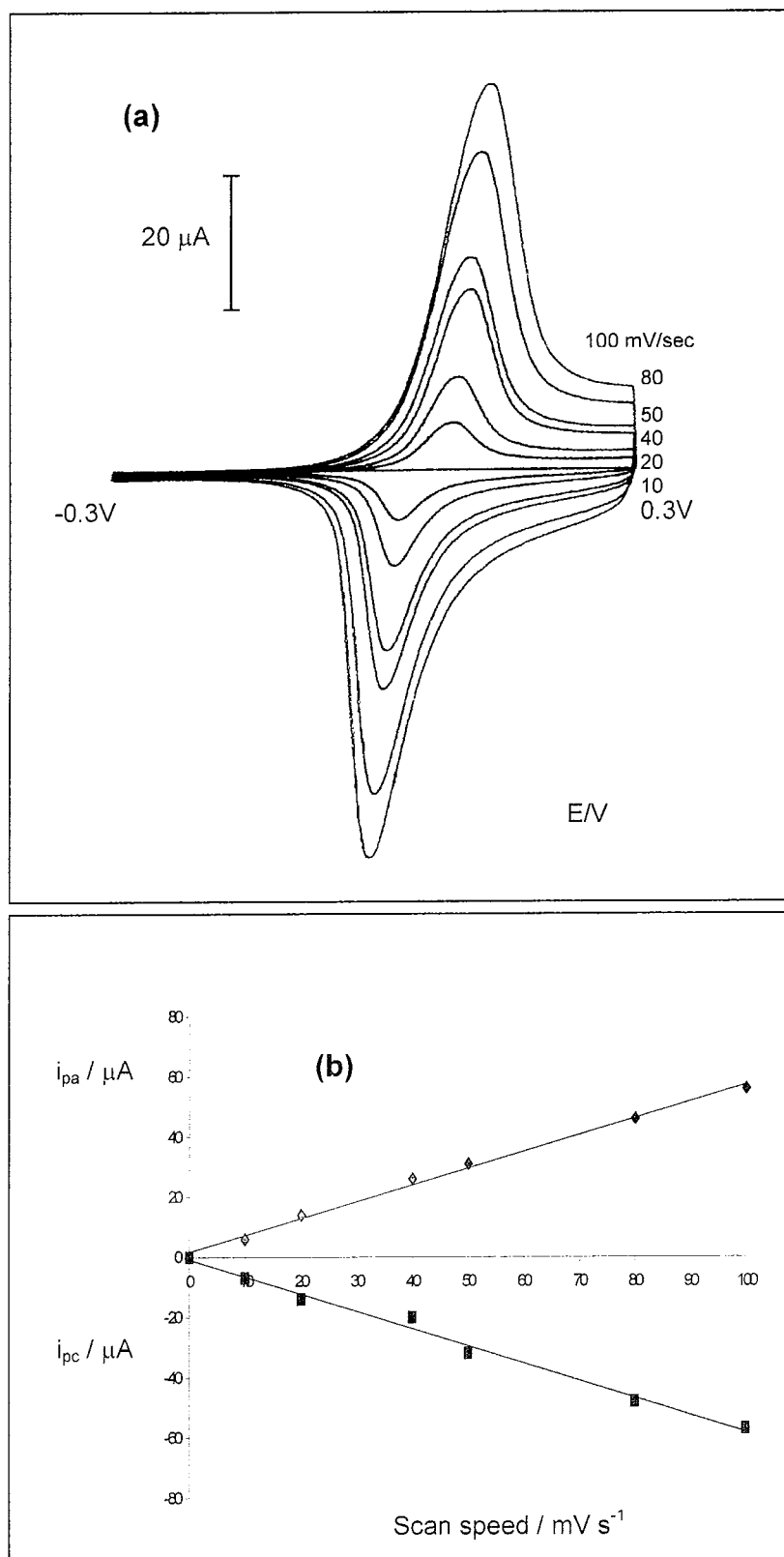


**Figure 3.35:** (a) Cyclic voltammogram of [Pt] poly-N-methylisoindole bromide in 0.1 M LiBr in  $\text{CH}_3\text{CN}$  vs SCE at various scan speeds (b) plot of  $i_{pa}$  &  $i_{pc}$  versus scan speed

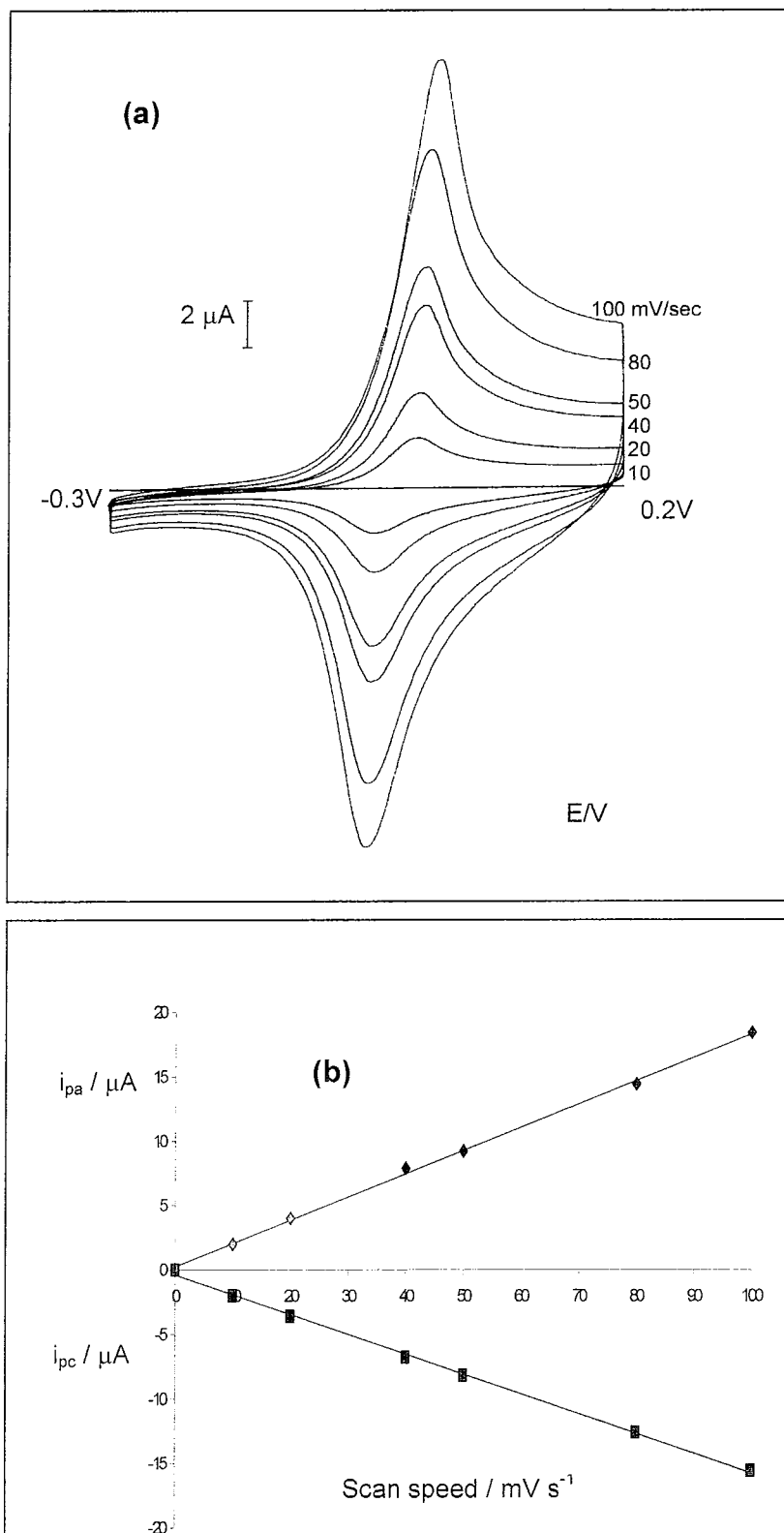


**Figure 3.36:** (a) Cyclic voltammogram of [Pt] poly-5-methoxy-N-methylisoindole bromide in 0.1 M LiBr in  $\text{CH}_3\text{CN}$  vs SCE at various scan speeds (b) plot of  $i_{pa}$  &  $i_{pc}$  versus scan speed

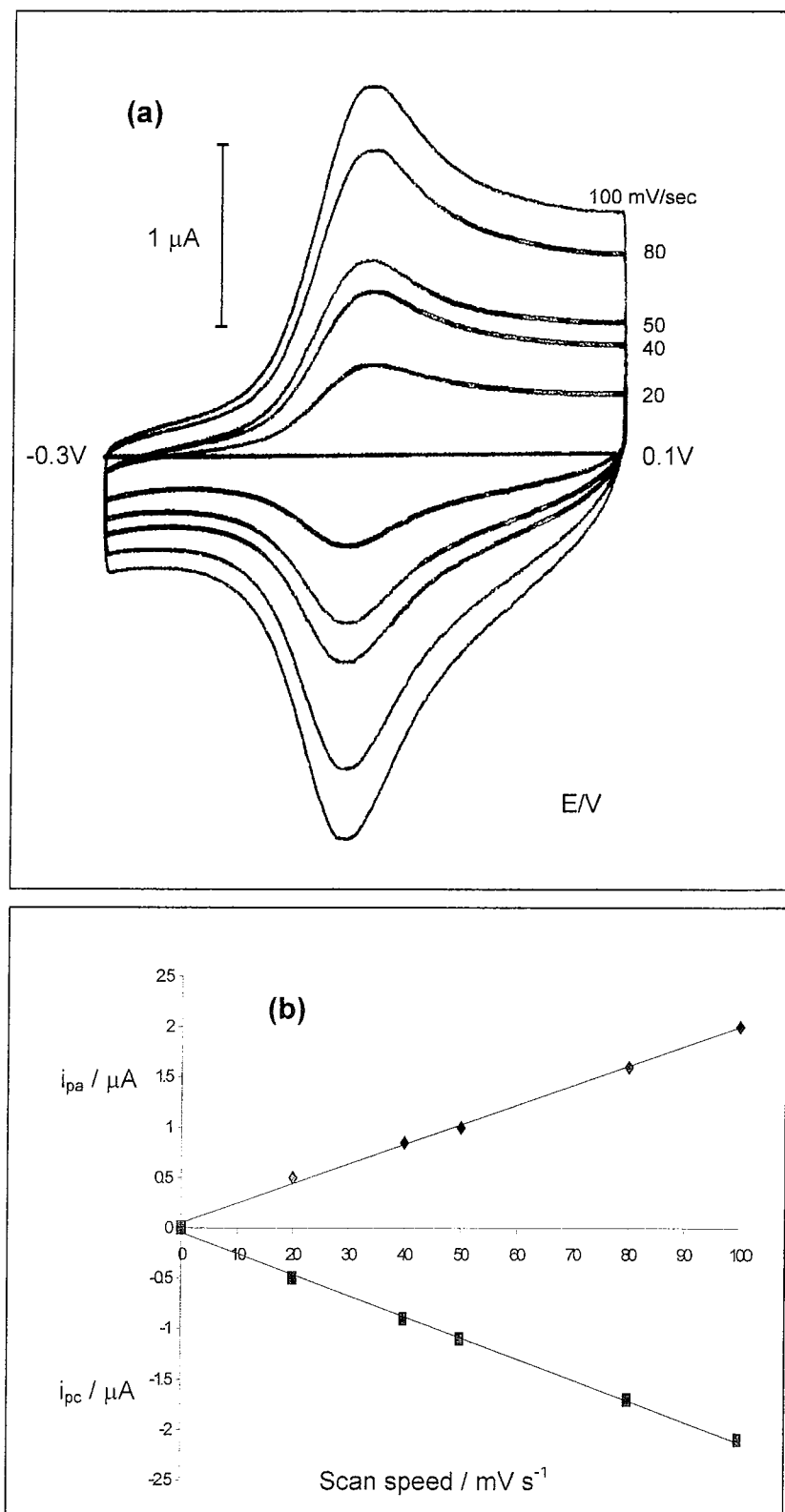


**Figure 3.37:** (a) Cyclic voltammogram of [Pt] poly-5,6-dimethoxy-N-methylisindole bromide in 0.1 M LiBr in  $\text{CH}_3\text{CN}$  vs SCE at various scan speeds (b) plot of  $i_{pa}$  &  $i_{pc}$  versus scan speed

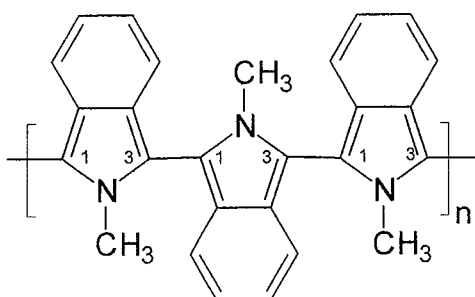


**Figure 3.38:** Regioregular poly-N-methylisoidole

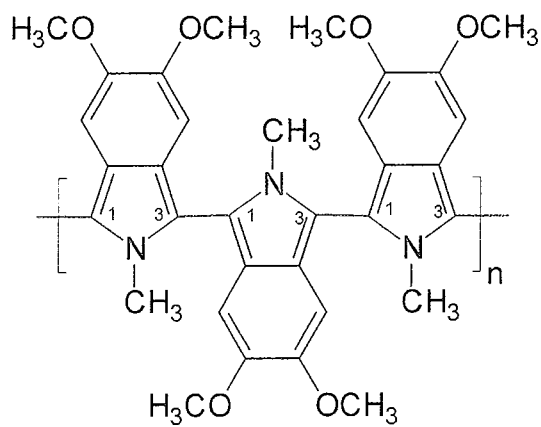
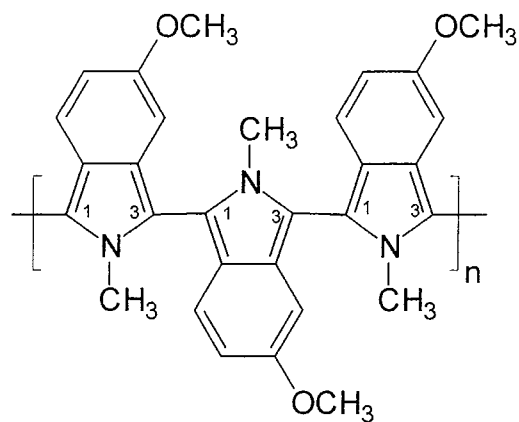
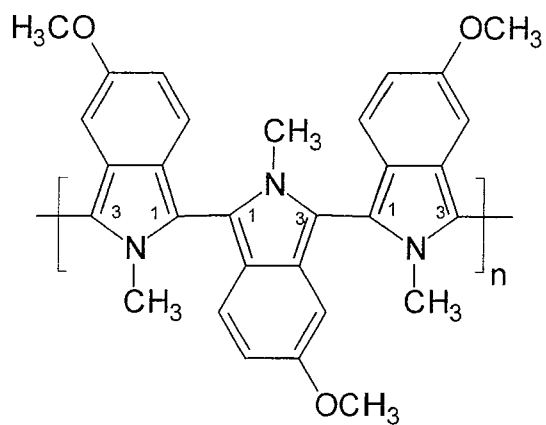


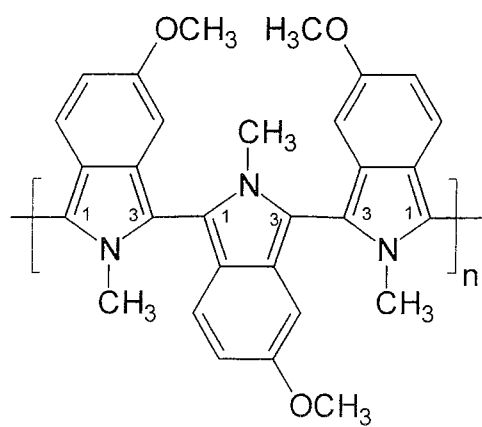
**Figure 3.39:** Regioregular poly-5,6-dimethoxy-N-methylisoidole



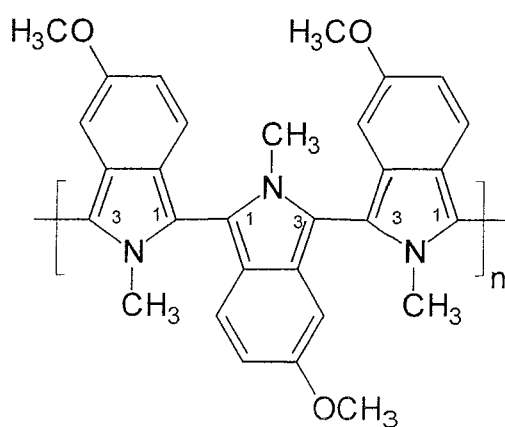
HT-HT coupling  
(3-1 ; 3-1)



TT-HT coupling  
(1-1 ; 3-1)



HT-HH coupling  
(3-1 ; 3-3)



TT-HH coupling  
(1-1 ; 3-3)

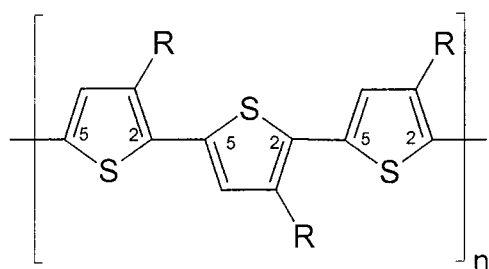
**Figure 3.40:** Regioisomers of poly-5-methoxy-N-methylisoindole

It has been found [90] that chemically prepared 3-alkylthiophene, (an asymmetrical molecule) has three orientations available when two thiophene rings are coupled between the 2- and 5- positions, where the 2- position is the "Head" and the 5- position is the "Tail". The first of these orientations is 2,5' or head-to-tail coupling (HT), the second is 2,2' or head-to-head coupling (HH), and the third is 5,5' or tail-to-tail coupling (TT), as shown in figure 3.41. All of the above methods afford products with three possible regiochemical couples: HH. TT and HT. This leads to a mixture four chemically distinct regioisomers when 3-substituted (asymmetric) thiophene monomers are employed [91,92]; see figure 3.41.

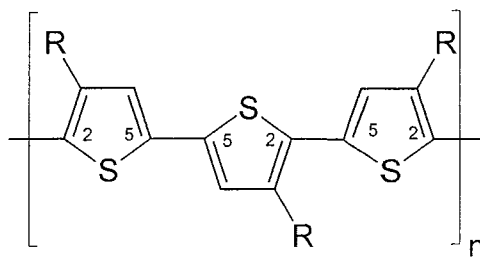
These orientations of poly-3-alkylthiophenes have been found to have resultant effects on the polymer conductivity and band-gap [90]. The electrochemistry of these polymers has also been reported [93, 94], whereby cyclic voltammetry of the regioregular poly-3-alkylthiophene showed two reversible oxidations, while the regioirregular poly-3-alkylthiophene showed only one [94].

It must be noted that reports on poly-3-alkylthiophenes are for the chemically prepared form and that direct experimental evidence for the formation of such regiochemical isomers in electrochemically prepared poly-5-methoxy-N-methylisoindole was not observed.

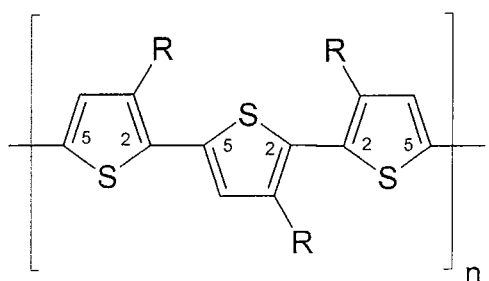




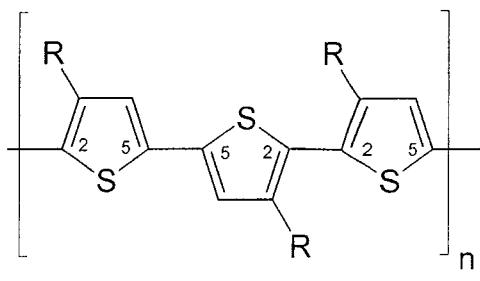
HT-HT coupling  
(2-5 ; 2-5)



TT-HT coupling  
(5-5 ; 2-5)



HT-HH coupling  
(2-5 ; 2-2)



TT-HH coupling  
(5-5 ; 2-2)

**Figure 3.41:** Regiochemical isomers of poly-3-alkylthiophenes

### 3.2.4 Cyclic Voltammetric study of the $\alpha,\alpha'$ -dibromo-*o*-xylene series.

$\alpha,\alpha'$ -dibromo-*o*-xylene (**4**) 4-methoxy- $\alpha,\alpha'$ -dibromo-*o*-xylene (**5**) and 4,5-dimethoxy- $\alpha,\alpha'$ -dibromo-*o*-xylene (**6**); see figure 3.8, were also characterised to see the effect if any, of the methoxy substituent. The electrochemical reduction of compound (**4**) has only been reported [95, 96], whereby the polarographic reduction [95] of all three isomers, *ortho* (**4**), *meta* (**16**) and *para* (**17**)  $\alpha,\alpha'$ -dibromoxylens was discussed. Repeating the experiments under the same reported [95] polarographic conditions, with electrolyte consisting of tetraethylammonium bromide (TEAB) in N, N-dimethylformamide (DMF), lead to poor polarograms. It was decided to modify the conditions whereby a solid carbon electrode was used as working electrode and the compounds analysed using cyclic voltammetry.

Figure 3.42 shows the cyclic voltammogram of the electrochemical reduction of  $\alpha,\alpha'$ -dibromo-*o*-xylene (**4**) ( $5 \times 10^{-3}$  mol dm<sup>-3</sup>), 4-methoxy- $\alpha,\alpha'$ -dibromo-*o*-xylene (**5**) ( $5 \times 10^{-3}$  mol dm<sup>-3</sup>), and 4,5-dimethoxy- $\alpha,\alpha'$ -dibromo-*o*-xylene (**6**) ( $5 \times 10^{-3}$  mol dm<sup>-3</sup>) in 0.1M TEAB in degassed DMF. The cyclic voltammogram of (**4**) shows two cathodic peaks  $E_{pc}$  at  $-1.46V$  and  $-1.64V$  (SCE). Compounds (**5**) and (**6**) also shows two cathodic peaks  $E_{pc}$  at  $-1.52V$  /  $-1.75V$  and  $-1.53V$  /  $-1.88$  (SCE) respectively. What is notable is that the first  $E_{pc}$  remains largely unchanged. However the second cathodic peak shifts more negative as the number of methoxy substituents on the ring increases.

This negative shift in potential has also been observed for the reduction of other organic halides. Streitweiser and Perrin [97] using polarography showed the half wave potentials of *p*-methoxybenzylchloride to differ by  $-0.025V$  from that of benzylchloride. However, for the methoxy substituted  $\alpha,\alpha'$ -dibromo-*o*-xylene series the shift is of the order of  $-0.1V$ .

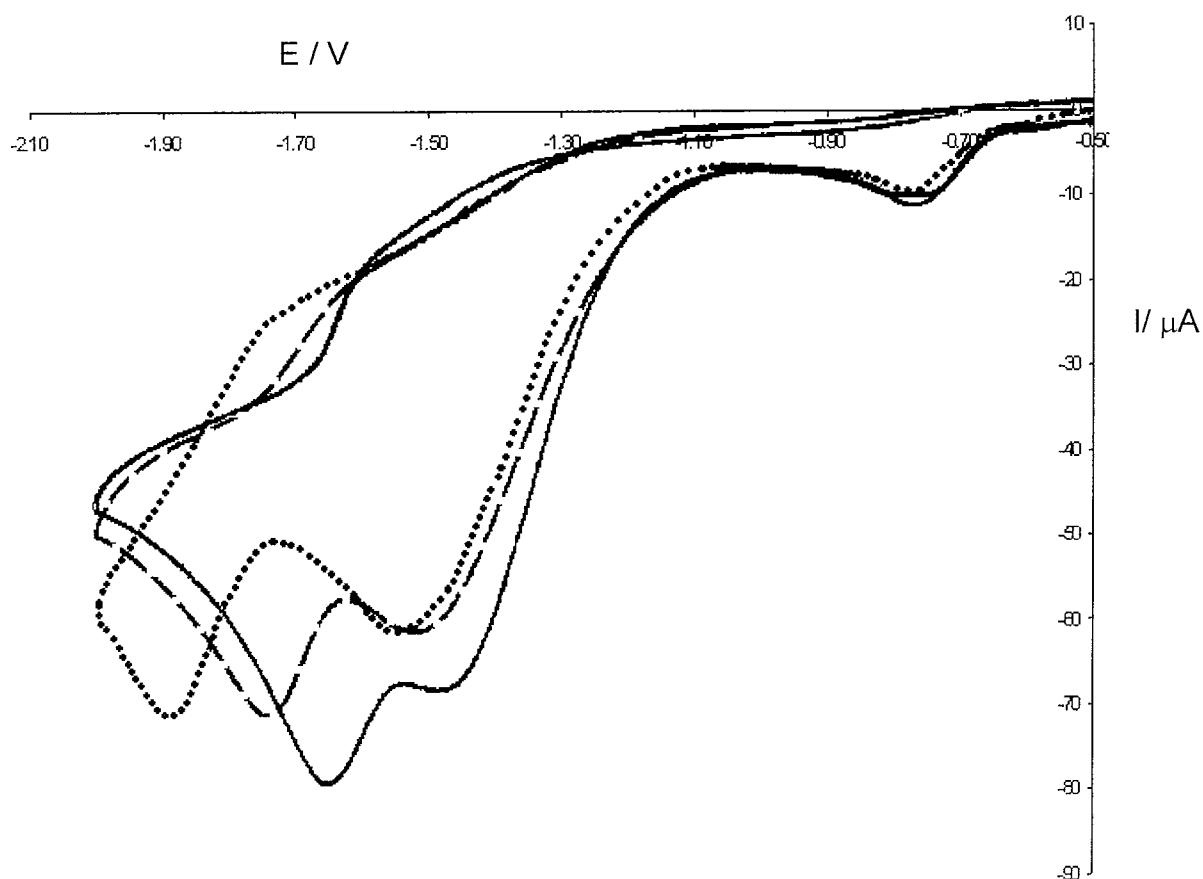


**Figure 3.42:** Cyclic Voltammogram of  
 [—]  $\alpha,\alpha'$ -dibromo-*o*-xylene (**4**) ( $5 \times 10^{-3}\text{M}$ ),  
 [— — —] 4-methoxy- $\alpha,\alpha'$ -dibromo-*o*-xylene (**5**) ( $5 \times 10^{-3}\text{M}$ ), and  
 [••••••••] 4,5-dimethoxy- $\alpha,\alpha'$ -dibromo-*o*-xylene (**6**) ( $5 \times 10^{-3}\text{M}$ ),  
 on carbon in 0.1M TEAB in DMF vs SCE at 50 mV/sec

The main results for the polarographic reduction reported by Covitz [95] are shown in table 3.2. The para isomer  $\alpha,\alpha'$ -dibromo-p-xylene (**17**) showed two reduction potentials at  $-0.8$  and  $-1.72$  V (SCE) and upon macroscale electrolysis afforded poly-p-xylylene (**18**) as a white solid and a small amount of a cyclic dimer, p-cyclophane (**19**). The ortho isomer  $\alpha,\alpha'$ -dibromo-o-xylene (**4**) exhibited two polarographic waves at  $-0.61$  and  $-1.58$  V (SCE). Its macroscale electrolysis also afforded a white polymeric product, which was identified as poly-o-xylylene (**20**). On the other hand  $\alpha,\alpha'$ -dibromo-m-xylene (**16**) exhibited only one polarographic wave at  $-1.32$  V (SCE) and upon macroscale reduction afforded m-xylene (**21**) only.

The nature of the products on electrolysis of  $\alpha,\alpha'$ -dibromo-p-xylene (**17**) strongly suggested that p-xylylene (**22**) was the intermediate [95], see scheme 3.11. The appearance of the second polarographic wave was also indicative of the xylylene intermediate, since only the para and ortho isomers displayed two waves, leading to poly-p-xylylene (**18**) and poly-o-xylylene (**20**). The meta isomer, for which no stabilised xylylene structure is possible yielded m-xylene only.

Scheme 3.12 shows the most probable mechanism for the reduction of  $\alpha,\alpha'$ -dibromo-p-xylene, as reported by Covitz [95]. The first wave leads to the formation of the xylylene intermediate. After the xylylene is formed it can undergo two alternative routes. The xylylene intermediate can either react chemically, to yield poly-p-xylylene (**18**), or undergo a further electrochemical reduction to form a dianion, which is then protonated by the solvent to yield p-xylene. Covitz [60] also stated that the *ortho* isomer would be expected to react in the same fashion and therefore suggested a similar mechanism for the reduction of  $\alpha,\alpha'$ -dibromo-o-xylene. Therefore a proposed mechanism for the electrochemical reduction of the (**4**) and the mono- and di-substituted  $\alpha,\alpha'$ -dibromo-o-xylenes (**5**) and (**6**), is shown in scheme 3.13, and is based on the mechanism put forward by Covitz [95].

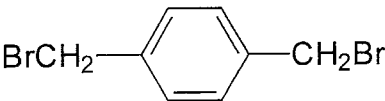
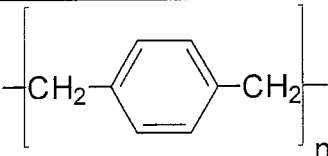
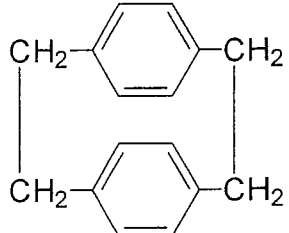
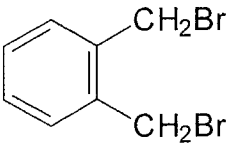
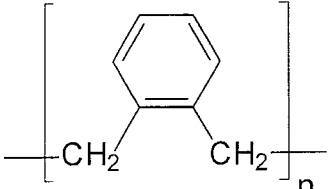
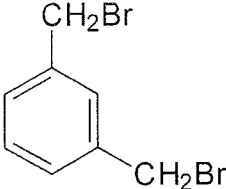
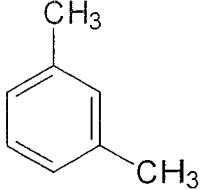
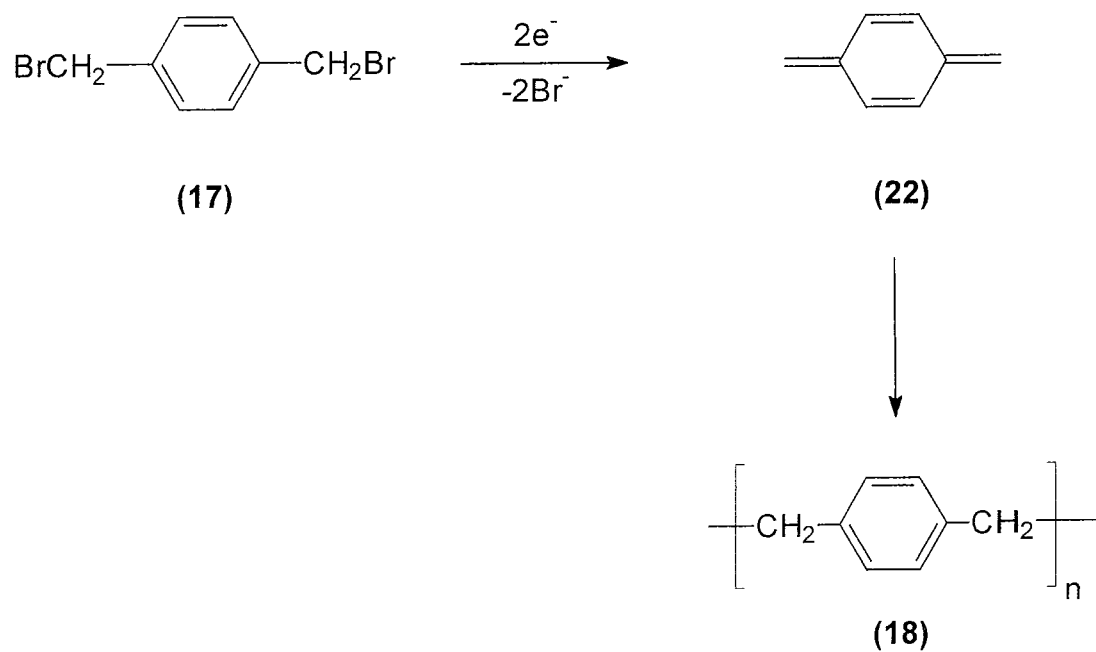
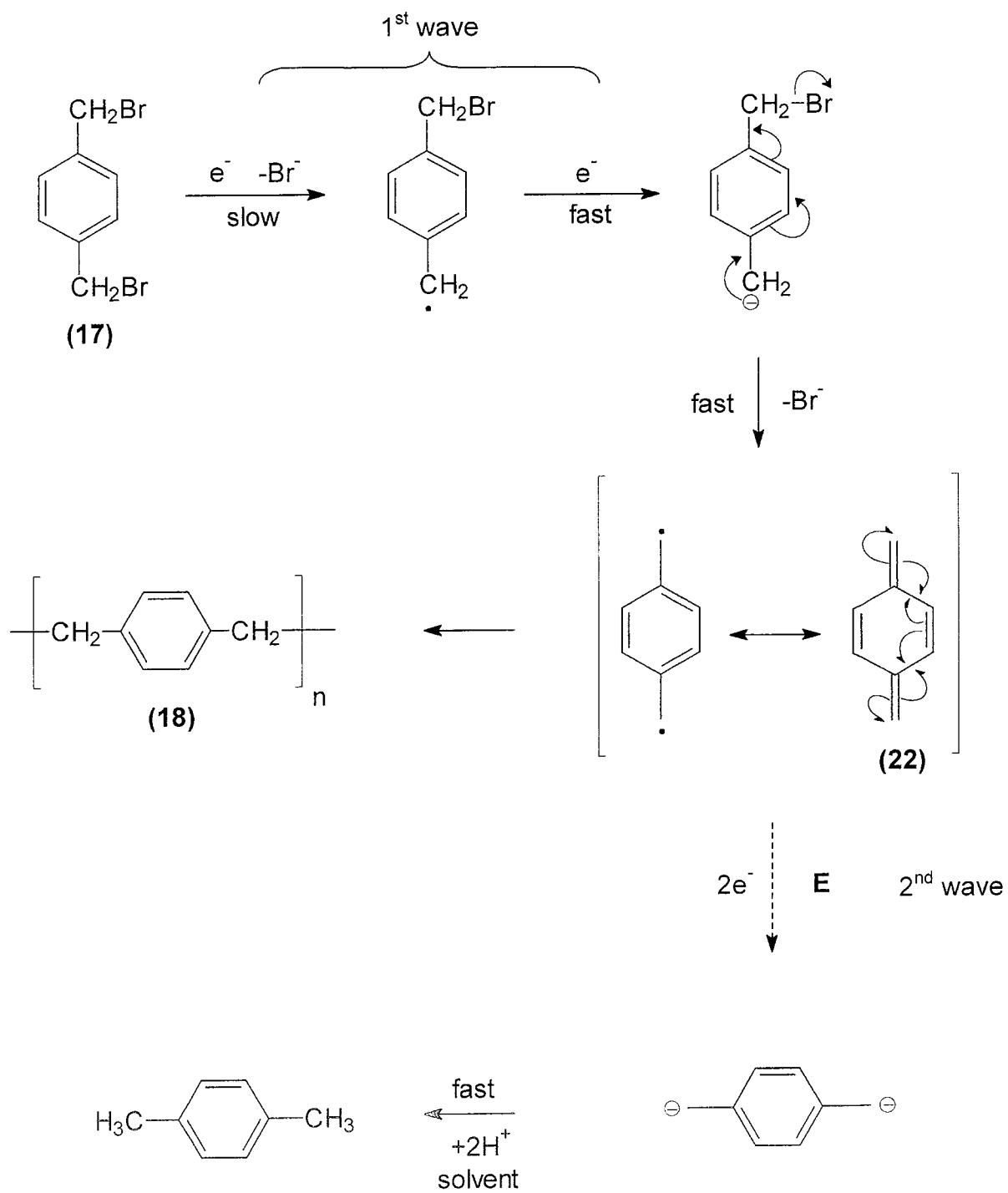
Compound	$E_{1/2}$ V (SCE)	Products
 <p>(17)</p>	<p>-0.80</p> <p>-1.72</p>	 <p>(18) 90%</p>  <p>(19) 5-10%</p>
 <p>(4)</p>	<p>-0.61</p> <p>-1.58</p>	 <p>(20)</p>
 <p>(16)</p>	<p>-1.32</p>	 <p>(21)</p>

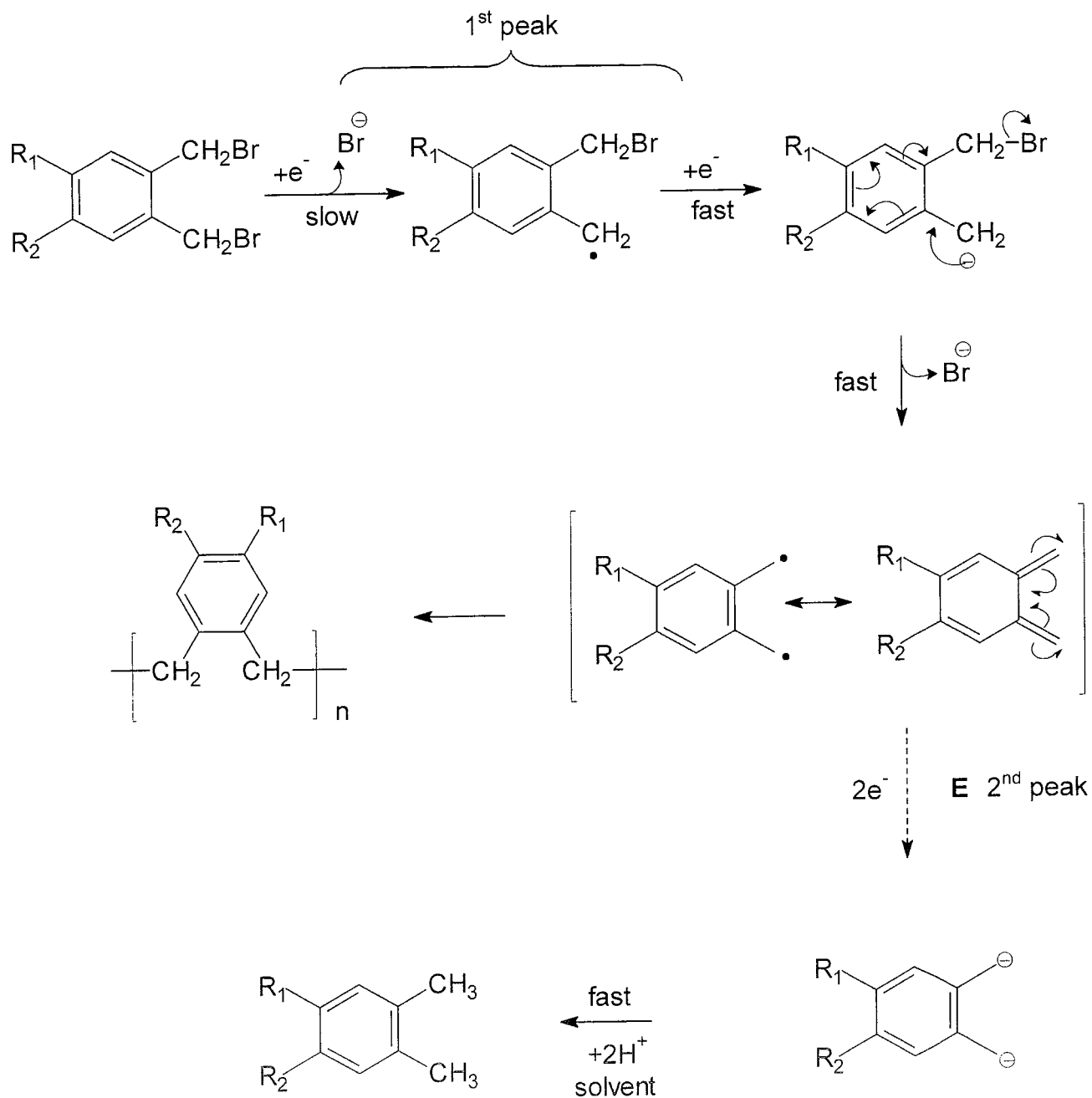
Table 3.2



**Scheme 3.11:** Electrochemical reduction of  $\alpha, \alpha'$ -dibromo-*para*-xylene



**Scheme 3.12:** Mechanism for the electrochemical reduction of  $\alpha, \alpha'$ -dibromo-*para*-xylylene



**Scheme 3.13:** Mechanism for the electrochemical reduction of methoxy substituted  $\alpha, \alpha'$ -dibromo-*ortho*-xylenes

$\alpha, \alpha'$ -dibromo-*o*-xylene (**4**) =  $\text{R}_1 = \text{R}_2 = \text{H}$

4-methoxy- $\alpha, \alpha'$ -dibromo-*o*-xylene (**5**) =  $\text{R}_1 = \text{H}, \text{R}_2 = \text{OCH}_3$

4,5-dimethoxy- $\alpha, \alpha'$ -dibromo-*o*-xylene (**6**) =  $\text{R}_1 = \text{R}_2 = \text{OCH}_3$



Thus in the present study, the reduction of  $\alpha,\alpha'$ -dibromo-o-xylene, 4-methoxy- $\alpha,\alpha'$ -dibromo-o-xylene and 4,5-dimethoxy- $\alpha,\alpha'$ -dibromo-o-xylene, the first reduction potential observed suggests the formation of the corresponding xylylene intermediates, with only negligible variation in the reduction potential going from the unsubstituted, to the mono- and di-substituted  $\alpha,\alpha'$ -dibromo-o-xylenes. However, the presence of the methoxy groups is clearly seen in the second reduction peak.

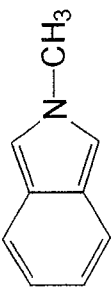
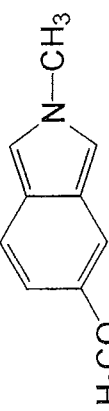
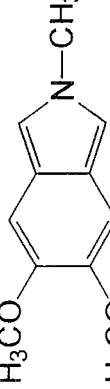
The difference in this second peak shows the methoxy effects on the chemistry of the intermediate. Under cyclic voltammetric conditions the formation of o-xylene is more probable when explaining the second peak, together with the fact that no white precipitate indicative of poly-o-xylylene was observed at any time during the experiment. The methoxy groups are electron donating in an aromatic system; the addition of electrons into the xylylene intermediate to form the dianion becomes more difficult leading to a negative shift in the second reduction peak. Therefore, as the number of methoxy substituents on the ring increases, the more electron rich the ring becomes, hence making it increasingly difficult to electrochemically reduce the system.

### 3.3 Conclusion

In carrying out preliminary cyclic voltammetric studies of the isoindole monomers, the effect of the methoxy group has been observed. The simple fact that all three monomers show irreversible oxidation and subsequent oxidation and reduction of the forming polymer layer shows that the two new isoindoles, 5-methoxy-N-methylisoindole and 5,6-dimethoxy-N-methylisoindole do polymerise.

The main results of the cyclic voltammetry are shown in table 3.3. On comparing results, the monomer oxidation potential is lower as the number of methoxy substituents on the isoindole unit increase. It can be concluded that the monosubstituted and disubstituted N-methylisoindoles are increasingly easier to oxidise, due to the increased electron density that the electron donating methoxy groups provide. This trend follows regardless of what supporting electrolyte is used. From the cyclic voltammograms of the monomers it is evident that polymer layer formation was forming quite differently for the different monomers. N-methylisoindole forms a film quite readily, as does 5-methoxy-N-methylisoindole, however, 5,6-dimethoxy-N-methylisoindole does not form a thin film as readily, as polymeric (or oligomeric) material was observed streaming away from the electrode surface. This was not observed at any time with N-methylisoindole or 5-methoxy-N-methylisoindole. This has been attributed to the presence of the two methoxy groups leading to more stable radical cations than the unsubstituted and mono-substituted N-methylisoindole, which results in poly-5,6-dimethoxy-N-methylisoindole diffusing away from the electrode to form a soluble polymer.

These initial results were supported by chronoamperometric study of the monomers. From a detailed analysis of the current-time profile obtained for all three monomers, the following conclusions can be made. The growth of poly-N-methylisoindole is two-dimensional with progressive nucleation, while poly-5-methoxy-N-methylisoindole film formation is via instantaneous nucleation and one dimensional growth.

Monomer	Electrolyte in CH <sub>3</sub> CN	Dopant X <sup>-</sup>	Monomer E <sub>pa</sub> V (SCE)	[Pt] polymer X <sup>-</sup> at 50 mV/sec			Γ/ moles/cm <sup>2</sup>	
				E <sub>pa</sub> /V	E <sub>pc</sub> /V	E <sub>pa</sub> -E <sub>pc</sub>		i <sub>pa</sub> /i <sub>pc</sub>
 N-methylisoindole	LiClO <sub>4</sub>	ClO <sub>4</sub> <sup>-</sup>	0.54 (1 <sup>st</sup> scan) 0.46 (2 <sup>nd</sup> scan)	+0.04	-0.02	60mV	1.03	2.8 x 10 <sup>-8</sup>
	Et <sub>4</sub> N-p-TsO	p-TsO <sup>-</sup>	0.73 (1 <sup>st</sup> scan) 0.60 (2 <sup>nd</sup> scan)	+0.23	+0.12	110mV	1	10.3 x 10 <sup>-8</sup>
	LiBr	Br <sup>-</sup>	-----*	+0.1	+0.02	80mV	0.96	6.4 x 10 <sup>-8</sup>
 5-methoxy-N-methylisoindole	LiClO <sub>4</sub>	ClO <sub>4</sub> <sup>-</sup>	0.49(1 <sup>st</sup> scan) 0.47 (2 <sup>nd</sup> scan)	-0.02	-0.07	50mV	1.3	5.3 x 10 <sup>-8</sup>
	Et <sub>4</sub> N-p-TsO	p-TsO <sup>-</sup>	0.58(1 <sup>st</sup> scan) 0.53(2 <sup>nd</sup> scan)	+0.12	0.04	80mV	1.24	6.2 x 10 <sup>-8</sup>
	LiBr	Br <sup>-</sup>	-----*	0.0	-0.04	40mV	1.12	1.8 x 10 <sup>-8</sup>
 5,6-dimethoxy-N-methylisoindole	LiClO <sub>4</sub>	ClO <sub>4</sub> <sup>-</sup>	0.44 (1 <sup>st</sup> scan) 0.42 (2 <sup>nd</sup> scan)	-0.16	-0.17	10mV	1.05	2 x 10 <sup>-9</sup>
	Et <sub>4</sub> N-p-TsO	p-TsO <sup>-</sup>	0.48 (1 <sup>st</sup> scan) 0.42 (2 <sup>nd</sup> scan)	-0.06	-0.07	10mV	1.09	2 x 10 <sup>-9</sup>
	LiBr	Br <sup>-</sup>	-----*	-0.1	-0.11	10mV	0.9	1.3 x 10 <sup>-9</sup>

\* E<sub>pa</sub> was not recorded as the LiBr oxidised at lower potentials than the monomers examined.

**Table 3.3:** Summary of cyclic voltammetric data for the monomers and polymers formed

This result is quite surprising, as the cyclic voltammetry for the two monomers were very similar, and seemed to show a similar nucleation mechanism. 5,6-dimethoxy-N-methylisindole current-time profile shows no evidence of nucleation and growth which would be in agreement with the cyclic voltammetry. All three monomers show Tafel-type behaviour for monomer oxidation at long times.

Table 3.3 shows the  $E_{pa}$  and  $E_{pc}$  for all polymers with three different electrolytes and the following conclusions can be made. The methoxy effect on the N-methylisindole sub unit can be seen on the resulting polymer. The  $E_{pa}$  and  $E_{pc}$  becomes increasingly negative for the polymers with increasing number of methoxy substituents. Therefore, the polymers are easier to oxidise due to the increase in electron density that the electron donating methoxy groups provide. This trend occurs regardless of supporting electrolyte. It can also be noted that for all polymers doped with perchlorate, oxidation and reduction potentials are lower than the polymers doped with p-toluene sulphonate, possibly due to the greater ease of movement of the less bulky perchlorate anion. Also by examining the  $\Delta E$  values and the surface coverage  $\Gamma$  for the polymeric films formed with p-toluene sulphonate, they seem to be thicker as the  $\Delta E$  and  $\Gamma$  values increased. The electrochromic properties of poly-5-methoxy-N-methylisindole showed a high contrast electrochromic change, metallic gold in the reduced form and transparent in the oxidised form, the same electrochromic change was observed for poly-N-methylisindole (discussed in more detail in Chapter 4). From a preliminary electrochemical investigation, the effects of the methoxy substituents in N-methylisindole, 5-methoxy-N-methylisindole and 5,6-dimethoxy-N-methylisindole can be readily seen.

Cyclic voltammetric study of the precursors, namely  $\alpha,\alpha'$ -dibromo-o-xylene, 4-methoxy- $\alpha,\alpha'$ -dibromo-o-xylene and 4,5-dimethoxy- $\alpha,\alpha'$ -dibromo-o-xylene shows some interesting results. Firstly the first  $E_{pc}$  remains largely unchanged. However the second cathodic peak shifts more negative as the number of methoxy substituents on the ring increases. These findings have

shown that the first cathodic peak is due to the formation of a xylylene intermediate and that substituent effects in the formation of this intermediate are minimal. However, these methoxy substituents have an observable effect on the formed xylylene intermediate, and as the number of methoxy substituents on the ring increases, the more electron rich the ring becomes, hence making it increasingly difficult to electrochemically reduce. This manifests in a shift in potential of the second cathodic peak.

### 3.4 Experimental

All electrochemical experiments were carried out in a 20 cm<sup>3</sup> & 50 cm<sup>3</sup> single compartment cell using a three electrode configuration. A platinum disc, with an exposed surface area of 7.1 mm<sup>2</sup>, sealed in Teflon was employed as a working electrode. In some experiments (where stated) a carbon tip, with an exposed surface area of 7.1 mm<sup>2</sup>, sealed in Teflon was used as a working electrode. A glassy carbon rod was used as auxiliary electrode and all potentials are quoted with respect to a saturated calomel electrode (SCE). The working electrode was pretreated prior to each experiment by polishing with 0.3 μm alumina powder. The auxiliary and reference electrodes were washed thoroughly with deionised water and background electrolyte.

Potential control and current measurement was performed with a H.B. Thompson DGR16 waveform generator and an EG&G model 362 scanning potentiostat and voltammograms were recorded on a Bryans 60100 model X-Y recorder.

Experiments involving anhydrous acetonitrile was of HPLC grade (Aldrich) and dimethylformamide was reagent grade with further purification by distillation. Electrolyte salts (Aldrich, 99+%) were dried in the vacuum oven where necessary. Water was distilled and deionised. Before all experiments, the electrolyte solution was degassed gently with oxygen free nitrogen for approximately ten minutes and a background cyclic voltammogram was recorded to ensure purity. The species under examination was introduced to the cell by dissolving it in a small amount of degassed electrolyte and was added to the solution using a pasteur pipette. The solution was then further degassed for five minutes. A blanket of nitrogen was maintained over the solution throughout the experiment. The temperature for all experiments was ambient.

### 3.4.1 Cyclic voltammetric studies of the substituted $\alpha, \alpha'$ -dibromo-*o*-xylene

#### *$\alpha, \alpha'$ -dibromo-*o*-xylene*

A cell containing a freshly made solution 0.1M TEAB in anhydrous dimethylformamide (10cm<sup>3</sup>) was flushed with nitrogen and  $\alpha, \alpha'$ -dibromo-*o*-xylene (13.2mgs,  $5 \times 10^{-5}$  moles, 5 mM) was added as already outlined. A carbon tip electrode was used as a working electrode, with glassy carbon auxiliary electrode and saturated calomel electrode as the reference. A ramp potential was then applied to the solution via a potentiostat and ramp generator, between the limits -0.5V and -2.0V at scan speed of 50mV/sec.

#### *4-methoxy- $\alpha, \alpha'$ -dibromo-*o*-xylene*

As above with 4-methoxy- $\alpha, \alpha'$ -dibromo-*o*-xylene (14.7mgs,  $5 \times 10^{-5}$  moles, 5 mM) in 0.1M TEAB in anhydrous dimethylformamide (10cm<sup>3</sup>).

#### *4,5-dimethoxy- $\alpha, \alpha'$ -dibromo-*o*-xylene*

As above with 4,5-dimethoxy- $\alpha, \alpha'$ -dibromo-*o*-xylene (16mgs,  $5 \times 10^{-5}$  moles, 5 mM) in 0.1M TEAB in anhydrous dimethylformamide (10cm<sup>3</sup>).

### 3.4.2 Cyclic Voltammetric studies of *N*-methylisindole & poly-*N*-methylisindole

#### *Lithium perchlorate:*

A cell containing a freshly made solution 0.1M LiClO<sub>4</sub> in anhydrous acetonitrile (25cm<sup>3</sup>) was flushed with nitrogen and *N*-Methylisindole (25mgs,  $1.9 \times 10^{-4}$  moles, 7.6 mM) was added as already outlined. A ramp potential was then applied to the solution via a potentiostat and ramp generator, between the limits -0.5V and +1.0V at scan speed of 50mV/sec. The platinum electrode containing a thin film of Poly-*N*-Methylisindole perchlorate was then removed from the solution rinsed in electrolyte and placed in fresh electrolyte solution. Cyclic voltammogram were then obtained by cycling the potential between -0.5V and +0.25V at six different scan speeds, 10, 20, 40, 50, 80, 100, mV/sec.

*Tetraethylammonium-p-toluene sulphonate:*

As above with N-Methylisindole (25mgs,  $1.9 \times 10^{-4}$  moles, 7.6 mM) 0.1M  $(\text{Et})_4\text{N}(\text{O}_3\text{SC}_6\text{H}_4\text{CH}_3)$  in anhydrous acetonitrile ( $25 \text{ cm}^3$ ). The polymer grown between the limits -0.5V to +0.8V, and the polymeric thin film between the limits -0.5V to +0.4V.

*Lithium bromide:*

As above with N-methylisindole (10mgs,  $7.63 \times 10^{-5}$  mole, 7.6 mM) in 0.1M LiBr in anhydrous acetonitrile ( $10 \text{ cm}^3$ ). The polymer grown between the limits -0.5V to +0.5V, and the polymeric thin film between the limits -0.3V to +0.3V.

*3.4.3 Cyclic Voltammetric studies of 5-methoxy-N-methylisindole & poly-5-methoxy-N-methylisindole*

*Lithium perchlorate:*

A cell containing a freshly made solution 0.1M  $\text{LiClO}_4$  in anhydrous acetonitrile ( $10\text{cm}^3$ ) was flushed with nitrogen and 5,-methoxy-N-Methylisindole (14mgs,  $8.6 \times 10^{-5}$  moles, 8.6 mM) was added as already outlined. A ramp potential was then applied to the solution via a potentiostat and ramp generator, between the limits -0.5V and +0.7V at scan speed of 50mV/sec. The platinum electrode containing a thin film of Poly-5-methoxy-N-Methylisindole perchlorate was then removed from the solution, rinsed in electrolyte and placed in fresh electrolyte solution. Cyclic voltammogram were then obtained by cycling the potential between -0.5V and +0.3V at six different scan speeds, 10, 20, 40, 50, 80, 100, mV/sec.

*Tetraethylammonium-p-toluene sulphonate:*

As above with 5-methoxy-N-Methylisindole (42mgs,  $2.6 \times 10^{-4}$  moles, 0.026 M) in 0.1M  $(\text{Et})_4\text{N}(\text{O}_3\text{SC}_6\text{H}_4\text{CH}_3)$  in anhydrous acetonitrile ( $10 \text{ cm}^3$ ). The polymer grown between the limits -0.5V to +0.75V, and the polymeric thin film between the limits -0.5V to +0.3V.



*Lithium bromide:*

As above with 5-dimethoxy-N-methylisoindole (12mgs,  $7.45 \times 10^{-5}$  mole, 7.4 mM) in 0.1M LiBr in anhydrous acetonitrile ( $10 \text{ cm}^3$ ). The polymer grown between the limits -0.5V to +0.5V, and the polymeric thin film between the limits -0.3V to +0.2V.

#### 3.4.4 Cyclic Voltammetric studies of 5,6-dimethoxy-N-methylisoindole & poly-5,6-dimethoxy-N-methylisoindole

*Lithium perchlorate:*

A cell containing a freshly made solution 0.1M LiClO<sub>4</sub> in anhydrous acetonitrile ( $20\text{cm}^3$ ) was flushed with nitrogen and 5,6-dimethoxy-N-methylisoindole (25mgs,  $1.3 \times 10^{-5}$  moles, 6.5mM) was added as already outlined. A ramp potential was then applied to the solution via a potentiostat, between the limits -0.5V and +0.85V at scan speed of 50mV/sec. The platinum electrode containing a thin film of Poly-5,6-dimethoxy-N-methylisoindole perchlorate was then removed from the solution, rinsed in electrolyte and placed in fresh electrolyte solution. Cyclic voltammograms were then obtained by cycling the potential between -0.5V and 0.0V at four different scan speeds, 20, 50, 80, 100, mV/sec.

*Tetraethylammonium-p-toluene sulphonate:*

As above with 5,6-dimethoxy-N-methylisoindole (25mgs,  $1.3 \times 10^{-5}$  moles, 6.5mM) in 0.1M (Et)<sub>4</sub>N(O<sub>3</sub>SC<sub>6</sub>H<sub>4</sub>CH<sub>3</sub>) in anhydrous acetonitrile ( $20 \text{ cm}^3$ ). The polymer grown between the limits -0.5V to +0.85V, and the polymeric thin film between the limits -0.5V to 0.0V.

*Lithium bromide:*

As above with 5,6-dimethoxy-N-methylisoindole (12mgs,  $6.2 \times 10^{-5}$  mole, 6.2 mM) in 0.1M LiBr in anhydrous acetonitrile ( $10 \text{ cm}^3$ ). The polymer grown between the limits -0.5V to +0.5V, and the polymeric thin film between the limits -0.3V to +0.1V.

### 3.4.5 Chronoamperometric study of the growth of polymeric films

#### *N-methylisoindole*

A cell containing a freshly made solution of 0.1M LiClO<sub>4</sub> in anhydrous acetonitrile (10 cm<sup>3</sup>) was flushed with nitrogen and N-methylisoindole (10mgs,  $7.63 \times 10^{-5}$  mole, 7.63 mM) was added as already outlined. The working electrode was polished using 0.3 $\mu$ m alumina between each recording.

#### *5-methoxy-N-methylisoindole*

As above with 5-methoxy-N-methylisoindole (15mgs,  $9.31 \times 10^{-5}$  mole, 9.3mM)

#### *5,6-dimethoxy-N-methylisoindole*

As above with 5,6-dimethoxy-N-methylisoindole (16mgs,  $8.37 \times 10^{-5}$  mole, 8.37mM)

### 3.5 References

- [1] J. O'M. Bockris, A. K. N. Reddy, *Modern Electrochemistry*, Vol. 2, Plenum Press, New York, (1970), pp. 1156 – 1170.
- [2] S. Trassati, *J. Electroanal. Chem.*, (1972), **39**, 163.
- [3] A.T. Kuhn, C. J. Mortimer, G. C. Bond, J. Lindley, *J. Electroanal. Chem.*, (1972), **34**, 1.
- [4] D. T. Sawyer, J. L. Roberts, Jr., *Experimental Electrochemistry for Chemists*, Wiley, New York, (1974), pp. 60 – 74, 170 – 171.
- [5] C. K. Mann, *J. Electroanal. Chem.*, (1969), **3**, 57.
- [6] D. T. Sawyer, J. L. Roberts, Jr., *Experimental Electrochemistry for Chemists*, Wiley, New York, (1974), p. 34.
- [7] C. D. Schmulbach, T. V. Oomen, *Anal. Chem.*, (1973), **45**, 820.
- [8] Southampton Electrochemistry Group, *Instrumental Methods in Electrochemistry*, Ellis Horwood, Chicester, (1985), p. 178 – 228.
- [9] A. J. Bard, L. R. Faulkner, *Electrochemical Methods, Fundamentals and Applications*, Wiley, New York, (1980), p. 51.
- [10] J. E. B. Randles, *Trans. Faraday Soc.*, (1948), **44**, 327
- [11] A. Sevcik, *Collect. Czech. Chem. Commun.*, (1948), **13**, 349.
- [12] R. S. Nicholson, I. Shain, *Anal. Chem.*, (1964), **36**, 706.
- [13] E. Laviron, *Bull. Soc. Chim. France*, (1967), 3717.
- [14] S. Srinivasan, E. Gileadi, *Electrochim. Acta*, (1966), **11**, 321.
- [15] E. Laviron, *J. Electroanal. Chem.*, (1974), **52**, 355.
- [16] E. Laviron, *J. Electroanal. Chem.*, (1974), **52**, 395.
- [17] A. P. Brown, F. C. Anson, *Anal. Chem.*, (1977), **49**, 1589.
- [18] A. J. Bard, L. R. Faulkner, *Electrochemical Methods, Fundamentals and Applications*, Wiley, New York, (1980)
- [19] A.F. Diaz, K.K. Kanazawa and G.P. Gardini, *J. Chem. Soc. Chem. Commun.*, (1979), 635.
- [20] T.F. Otero & E. de Azelain, *Polymer Commun.*, (1988), **29**, 21.
- [21] J Pprejza, I. Lundstrom & T. Skotheim, *J. Electrochem. Soc.*, (1982), **129**, 1685
- [22] S. Asavapiriyant, G.K. Chandler, G.A. Gunwardena & D. Pletcher, *J. Electroanal. Chem.*, (1984), **177**, 229

- [23] A.F. Diaz, J.I. Castillo, J.A. Logan & W.Y. Lee. *J. Electroanal. Chem.*, (1981), **129**, 115
- [24] M. Delamar, P-C. Lacaze, J.Y. Dumousseau & J.E. Dubois, *Electrochim. Acta.*, (1982), **27**, 61
- [25] G.K. Chandler & D. Pletcher, *Chem. Soc. Periodical Reports: Electrochemistry*, (1985), **10**, 117
- [26] A. Diaz, *Chim. Scripta*, (1981), **17**, 145
- [27] K.K. Kanazawa, A.F. Diaz, W.D. Gill, P.M. Grant, G.B. Street, G.P. Gardini & J.F. Kwak, *Synth. Met.*, (1979), **1**, 329
- [28] M. Deitrich. J. Mortensen & J. Heinze, *J. Chem. Soc. Chem. Commun.*, (1986), 1131.
- [29] A. Tsumura, H. Koezuka, S. Tsunoda & T. Ando, *Chem. Lett.*, (1986), 863
- [30] S. Callavaro, A. Colligiani & G. Cum, *J. Therman Anal.*, (1992), **38**, 2649
- [31] R.E. Myers, *J. Electron. Mater.*, (1986), **15**, 61
- [32] V. Bocchi & G.P. Gardini, *J. Chem. Soc. Chem. Commun.*, (1986), 148
- [33] S. Rapi, V. Bocchi & G.P. Gardini, *Synth. Met.*, (1988), **24**, 217
- [34] N.G. Neoh, T.C. Tan & E.T. Kang, *Polymer*, (1988), **29**, 553
- [35] T.H. Chao & J. Maroh, *J. Polym. Sci. Part A*, (1988), **26**, 743
- [36] Y. Kudoh, *Synth. Met.*, (1996), **79**, 17.
- [37] M. Salmon, *J. Polym. Sci. Polymer Lett.*, (1982), **20**, 187.
- [38] A. Mohammadi, M-A. Hasan, B. Liedberg, I. Lundstrom & W.R. Salaneck, *Synth. Met.*, (1986), **14**, 189
- [39] E.T. Kang, K.G. Neoh & H.C. Ti, *Solid State Commun.*, (1986), **60**, 457
- [40] S.P. Armes & B. Vincent, *J. Chem. Soc. Chem. Commun.*, (1987), 288.
- [41] N. Toshima & O. Ihata, *Synth. Met.*, (1996), **79**, 165.
- [42] T. Iyoda, M. Kitano & T. Shimidzu, *J. Chem. Soc. Chem. Commun.*, (1991), 1618
- [43] M. Catellani, T. Caronna & S.V. Meille, *J. Chem. Soc. Chem. Commun.*, (1994), 1911
- [44] J-M. Kern & J.P. Sauvage, *J. Chem. Soc. Chem. Commun.*, (1989), 657
- [45] H. Segawa, T. Shimidzu & K. Honda, *J. Chem. Soc. Chem. Commun.*, (1989), 132.

- [46] I. Rodriguez & J.G. Velasco, *J. Chem. Soc. Chem. Commun.*, (1990), 387.
- [47] F. Wudl, M. Kobayashi & A.J. Heeger, *J. Org. Chem.*, (1984), **49**, 3383.
- [48] J. Rodriguez, H.-J. Grande & T.F. Otero, *Handbook of Conducting Conductive Molecules and Polymers*, (H.S. Nalwa Ed.) Chichester: J. Wiley, (1997), **Vol. 2**, 415 - 466.
- [49] P. Chandrasekhar, A.M. Masulaitis & R.W. Gumbs, *Synth. Met.*, (1990), **36**, 303.
- [50] A. F. Diaz & J. Bargon, *Handbook of Conducting Polymers*, Ed. T.A. Skotheim, (1986), **Vol. 1**, 82.
- [51] A. F. Diaz & B. Hall, *IBM J. Res. Develop*, (1983), **37**, 342.
- [52] A.F. Diaz, J. Castillo, K.K. Kanazawa, J.A. Logan, M. Salmon & O. Fajardo, *J. Electroanal. Chem.*, (1982), **133**, 233.
- [53] P. Audebert & G. Bidan, *Synth. Met.* (1986), **14**, 71.
- [54] M. Kobayashi, J. Chen, T.C. Chung, F. Moraes, A.J. Heeger & F. Wudl, *Synth. Met.*, (1984), **9**, 77.
- [55] Z. Cai, J. Lei, W. Liang, V. Menon & C.R. Martin, *Chem. Mater.*, (1991), **3**, 960.
- [56] R.M. Penner & C.R. Martin, *J. Electrochem. Soc.*, (1986), **133**, 310.
- [57] R.M. Penner & C.R. Martin, *J. Electrochem. Soc.*, (1986), **133**, 2206.
- [58] A. Mohammadi, I. Lundstrom, O. Inganas & W.R. Salaneck, *Polymer*, (1990), **31**, 395.
- [59] J.C. Wittmann & P. Smith, *Nature*, (1991), **352**, 414.
- [60] C.R. Martin, L.S. VanDyke & Z. Cai, *Electrochim. Acta.*, (1992), **37**, 1611.
- [61] C.R. Martin, R. Parthasarathy & V. Menon, *Synth. Met.*, (1993), **55**, 1165.
- [62] J. Lei, V.P. Menon & C.R. Martin, *Polym. Adv. Tech.*, (1993), **4**, 124.
- [63] J. Heinze, A. Mertz & H.J. Schafer, *Topics in Current Chemistry*, (1990), Ed. E. Steckham.
- [64] K.K. Kanazawa, A.F. Diaz, R.H. Geiss, W.D. Gill, J.F. Kwak, J.A. Logan, J.F. Rabolt & G.B. Street, *J. Chem. Soc. Chem. Commun.*, (1979), 854.
- [65] K. Imanishi, M. Satoh, Y. Yasuda, R. Tsushima & S. Aoki, *J. Electroanal. Chem.*, (1988), **242**, 203.

- [66] J. Ruhe, C. Krohnke, T.A. Ezquerra, F. Kremer & G. Wegner, *Ber. Bunsenges. Phys. Chem.*, (1987), **91**, 885.
- [67] T.F. Otero, R. Tejada and A.S. Elola, *Polymer*, (1987), **29**, 651.
- [68] E.M Genies, G. Bidan & A.F. Diaz, *J. Electroanal. Chem. Interfacial Electrochem.*, (1983), **149**, 101.
- [69] J.F. Ambrose and R.F. Nelson, *J. Electrochem. Soc.*, (1968), **115**, 1159.
- [70] J.F. Ambrose, L.L. Carpenter and R.F. Nelson, *J. Electrochem. Soc.*, (1975), **122**, 876.
- [71] G.B. Street, T.C. Clarke, R.H. Geiss, V.Y. Lee, A. Nazzal, P. Pfluger & J.C. Scott, *J. Phys. Colloq.*, (1983), **44**, 559.
- [72] M.G. Kanatzidis, *Chem. Eng. News*, (1990), Dec 3.
- [73] M. Kobayashi, N. Colaneri, M. Boysel, F Wudi and A.J. Heeger, *J. Chem. Phys.*, (1985), **82**(12), 5717.
- [74] A.F. Diaz and K.K. Kanazawa, *Extended Linear Chain Compounds*, (J.S. Millar Ed.) Plenum, New York, (1983), **vol. 3**, 417.
- [75] R. Qian and J. Qiu, *Polymer*, (1987), **19**, 157.
- [76] S. Kuwabata, J. Nakamura and H. Yonemara, *J. Chem. Soc. Chem. Commun.*, (1988), 779.
- [77] Q. Pei and R. Qian, *Polymer and Biomaterials*, (H. Fang, Y. Han and L. Huang Eds.), (1991), 159.
- [78] Y. Li and Y. Fan, *Synth Met.*, (1996), **79**, 225.
- [79] A.F. Diaz and J.C. Lacroix, *New J. Chem.*, (1988), **12**, 171
- [80] S.B. Rhee, M-H. Lee, B.S. Moon and Y. Kang, *Korea Polym. J.*, (1993), **1**, No.1, 61-68.
- [81] N.M Hanly, D. Bloor, A.P. Monkman, R. Bonnett and J.M Ribo, *Synth. Met.*, (1993), **60**, 195-198.
- [82] A.Merz, R. Schwarz and R. Schropp, *Adv. Mater.*, (1992), **4**, No. 6. 409.
- [83] T.F. Ottero, R. Tejada and A.S. Elola, *Polymer*, (1987), **28**, 651.
- [84] M. Dietrich and J. Heinze, *Synth Met.*, (1991), **41-43**, 503.
- [85] A.R. Hillman, E.F. Mallen, *J. Electroanal. Chem.*, (1987), **220**, 351.
- [86] M.E.G Lyons, *Advances in Chemical Physics*, (1996), Vol. XCIV.
- [87] N. Mermilliod, J. Tanguy and F. Petiot, *J. Electrochem. Soc.*, (1986), **133**,
- [88] G. King and S.J. Higgins, *J. Chem. Soc., Chem Commun.*, (1994), 825.

- [89] Y. Ikenoue, F. Wudl and A.J. Heeger, *Synth. Met.*, (1991), **40**, 1
- [90] R.D. McCullough and P.C. Ewbank, *Handbook of Conducting Polymers*, Vol. 2 (T. J. Skotheim, R.L. Elsenbaumer and J.R. Reynolds ed.), Marcel Dekker, New York, (1998), 225.
- [91] M. Sato and H. Morrii, *Polym. Commun.*, (1991), **32**, 42.
- [92] M. Sato and H. Morrii, *Macromolecules*, (1991), **24**, 1196.
- [93] J. Roncali, *Chem. Rev.*, (1992), **92**, 711.
- [94] R.D. McCullough, S. Tristram-Nagle, S.P. Williams, R.D. Lowe, and M. Jayaraman, *J. Am. Chem. Soc.*, (1993) **115**, 4910.
- [95] F.H. Covitz, *J. Amer. Chem. Soc.*, (1967), **89**, 5403.
- [96] J. H. P. Utley, Y. Gao and R. Lines, *J. Chem. Soc.:Chem Commun*, (1993) 1540.
- [97] A. Streitwieser, Jr., & C. Perrin, *J. Am. Chem. Soc.*, (1964), **86**, 4938.

## **Chapter 4**

### ***In situ* Spectroelectrochemical Characterisation of Isoindole Polymers**



## Chapter 4 – The *In-situ* Spectroelectrochemical Characterisation of Isoindole Polymers.

### 4.1 Introduction

Since the discovery of the redox nature of conjugated polymers, various electrochemical techniques have been used, both to carry out the doping reaction and to characterise the doped polymer. By applying the appropriate potential to an electrode coated with a conducting polymer layer, it is possible to reduce the layer to the neutral form or oxidise the layer to the conducting form. Much work has been carried out in studying the electrode processes by experiments that involve more than the usual electrochemical variables of current, charge and potential. Some of the reasons for this work have been to provide ways for collating information about electrochemical systems that could not be gathered by purely electrochemical means [1]. The *in-situ* measurement of absorption spectra of layers coated on to electrode surfaces as a function of potential is known as spectroelectrochemistry. By using this technique it is possible to obtain an insight into the electronic properties of conducting polymers. Indeed the most interesting and useful phenomenon that can be observed with spectroelectrochemistry is the electrochromic properties of a layer of polymer with changes in doping.

Electrochromism is the ability of a chemical species to be electrochemically switched between different colours [2]. It results from the generation of different visible region electronic absorption bands on switching between redox states. The typical changes in the absorption spectrum for oxidised and neutral layer of polypyrrole [3] are shown in figure 4.1. The polymer was yellow in the neutral form and showed a maximum at about 400nm, while the maximum oxidised form was blue/black in colour corresponding to a broad absorption maximum at 540nm and extending to 900nm [3].

The optical properties of a conducting polymer are important to the understanding of the basic electronic structure of the polymer. Since the charge on the polymer moves along the conjugation of the  $\pi$  - backbone, the

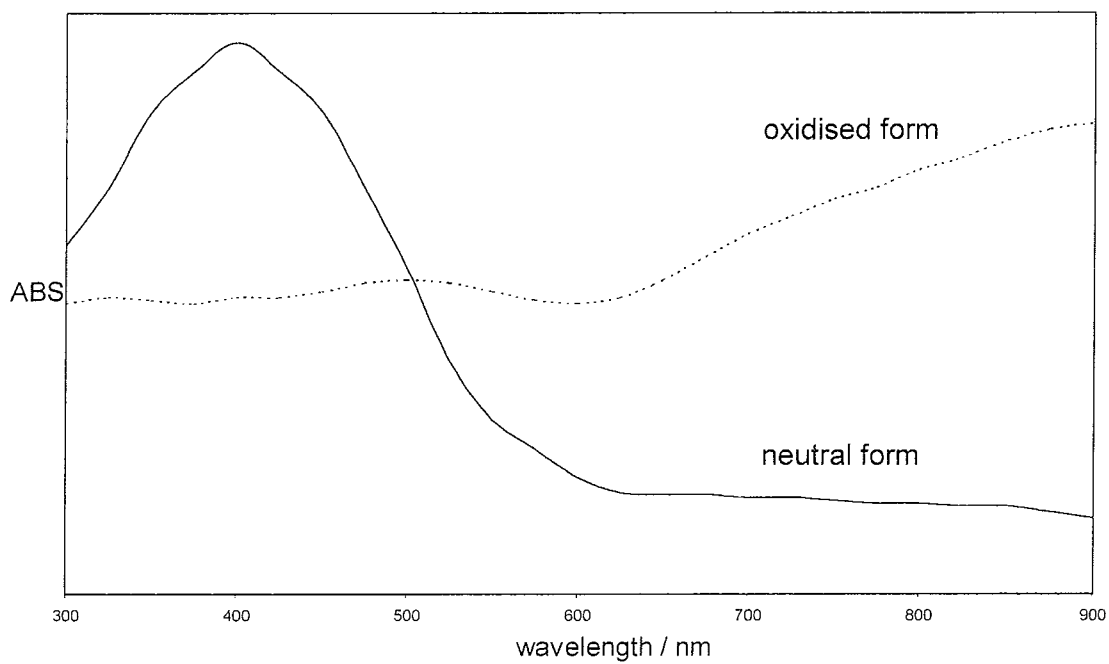


**Figure 4.1:** Typical changes in the absorption spectrum for a conducting polymer for the oxidised and neutral forms. (ref. [3])

amount of  $\pi$  - conjugation in the polymer is one of the major factors that determines the electronic spectra and hence the colour of the polymer. Thus UV-vis spectroscopy is a powerful probe for characterising the electronic processes and hence optical properties that occur in the polymer in the undoped, doped and during doping states.

#### 4.1.1 Spectroelectrochemical Techniques

The simplest spectroelectrochemical experiment [1] is to direct a light beam through a transparent electrode and to measure absorbance changes resulting from the species produced or consumed in the electrode process. A typical experimental arrangement for transmission spectroscopy is illustrated in figure 4.2. The main prerequisite of such a system is an optically transparent electrode (OTE). These OTE's may be thin films of a semiconductor e.g. doped  $\text{SnO}_2$  or  $\text{In}_2\text{O}_3$  or a thin layer metal, e.g. Au or Pt, deposited on a glass, quartz or plastic substrate. Alternatively such cells may be constructed with electrodes of fine wire mesh mini grids with several hundred wires per centimetre [1]. A disadvantage with this set-up is that it can generally only accommodate a two-electrode system as the cell must be small enough to fit inside conventional spectrometers, and therefore no reference electrode is usually used. Cell configurations are sometimes awkward with the auxiliary electrode on one side of the  $\text{SnO}_2$  leading to non-uniform current distribution. Also  $\text{SnO}_2$  can have quite a large I.R. drop across the electrode surface leading to incorrectly quoted potential values.

A way of accommodating a three electrode system is to use reflectance mode spectroelectrochemistry, as illustrated in figure 4.3. Using this system the source and detector are encased into a probe assembly and is placed in front of the working electrode. Since the data recorded is in reflectance mode there is no need for an OTE and a standard platinum tip electrode can act as the working electrode. Consequently the cyclic voltammetry recorded is much better than using an OTE as working electrode.

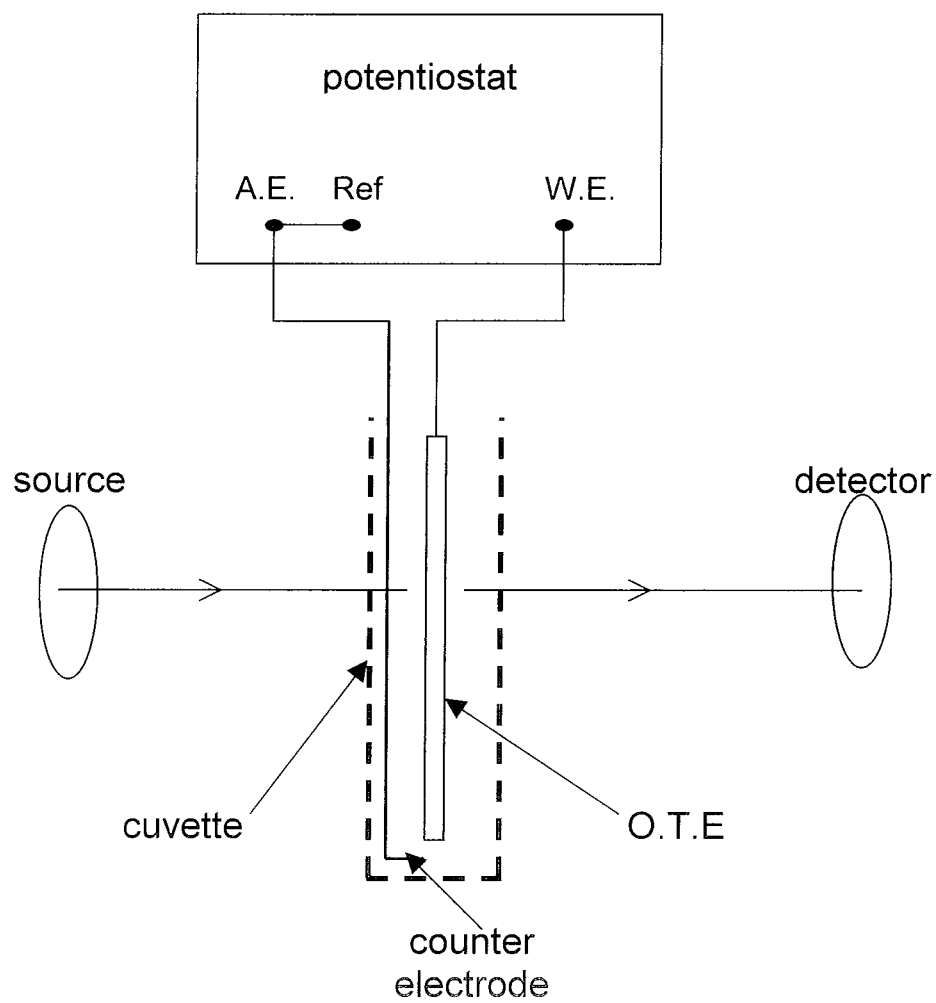


**Figure 4.2:** Schematic diagram for transmission mode spectroelectrochemistry

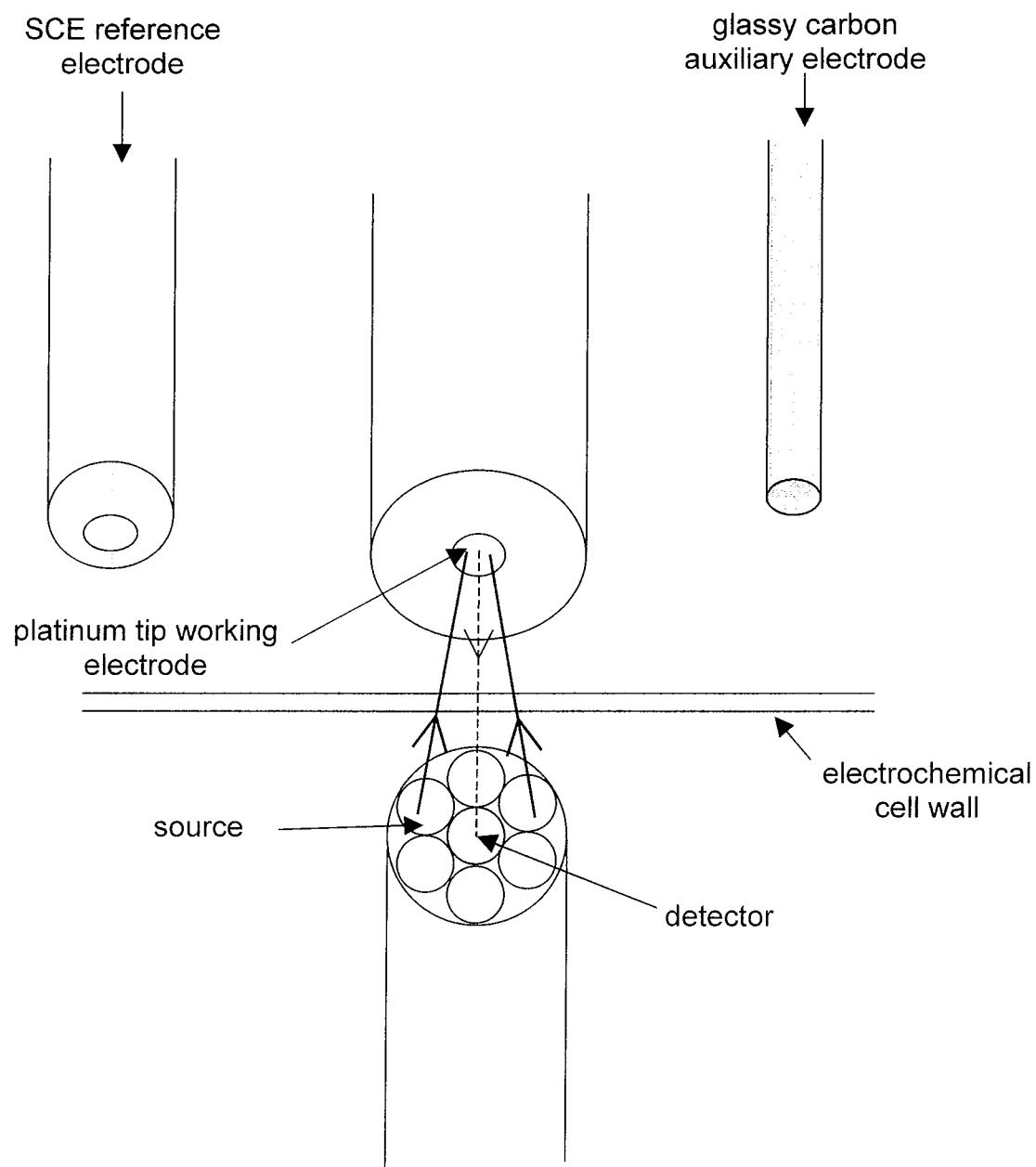


**Figure 4.3:** Schematic diagram of reflectance mode spectroelectrochemistry

The source and detector optical fibres lead into a probe assembly where the source fibre is split into six fibres encircling the detector fibre. A spectrum is recorded at the bare electrode as a reference. The spectrum recorded can be plotted in both transmission and absorption mode as with normal UV-VIS spectroscopy. The spectrometer used in this study consisted of an Ocean Optics Inc, S2000 fibre optic spectrometer with an Ocean optics Inc, LS-1 tungsten halogen lamp as a source and only has a detectable range between 400nm and 850nm,

#### 4.1.2 *Analysis of spectroelectrochemical behaviour of conducting polymers using the Nernst Equation.*

The absorption spectra of a number of conducting polymers including polypyrrole [4, 5, 6] polythiophenes [5, 7], and polyaniline [8] have been quantitatively analysed using the Nernst equation, and the formal electrode potentials and “n-values”, i.e. the number of electrons transferred during the redox reaction, were obtained. Marque and Roncali [7] carried out comparative spectroelectrochemical studies of three substituted polythiophenes and analysed the deviations of the Nernst plots (i.e.  $E$  vs.  $\log[\text{ox}]/[\text{red}]$ ) from linearity in terms of (i) the coulombic interaction between charged sites, and (ii) the mechanical work required to expand the polymer lattice by the insertion of counterions and solvent molecules. The important points in this study [7] were that the redox reaction of conducting polymers can be described by one “monomer unit”, not by several monomers units of the polymers. Therefore the treatment of the redox reactions of conducting polymers in terms of monomer units is known as the “monomer unit model”.

In addition, redox reactions of the conducting polymers have been analysed [4] using the Nernst equation in terms of polaron/bipolaron model. This model treats the polymers as several monomer units having +1 or +2 charges, and describes the redox reaction of these polymers by these units. Therefore, the number of electrons transferred during the redox reactions, i.e. “n-value” is +1 or +2 by this model. According to such analysis [6], excess chemical potentials must be introduced to correct the large deviations

between the Nernst equation and the Nernst plot obtained from the absorption plots. They were attributed to the coulombic interactions among polarons and bipolarons.

Recording the UV-VIS spectra as a function of applied potential, the faradaic and capacitive contributions of the redox behaviour can in principle be separated. There has been much discussion [9-13] concerning the cyclic voltammetry of conducting polymers, and the question as to what fraction of the observed total current is faradic and what fraction is capacitive? Experimental data suggests that the redox chemistry of polypyrrole can be divided into three regions [9],

- (1) At a low potential regime where the polymer is an electronic insulator. The oxidation of this reduced form of polypyrrole appears to depend on the diffusion of anions into the layer [10, 11].
- (2) At a high potential regime where polypyrrole is conducting. Both oxidation and reduction appear to be capacitive in this region.
- (3) At intermediate potentials where the polymer is conducting and where a peak current occurs due to layer oxidation.

Faradaic current involves charge transfer across interface while capacitive current involves charge storage at an interface. Such interfaces are analogous to electrode/electroactive solution interfaces. Conventional faradaic electron transfer occurs across such an interface [12]. Charge is also stored at such an interface. Oxidation of the insulating form of polypyrrole is analogous to the oxidation of a redox polymer [12]. The completely oxidised, conductive form of polypyrrole is highly porous [9], as can be seen in figure 4.4. The "pore space" is filled with electrolyte phase similar to the external electrolyte. The important interface in this case is the interface between the molecular wire and the electrolyte incorporated into the polymer pore space.

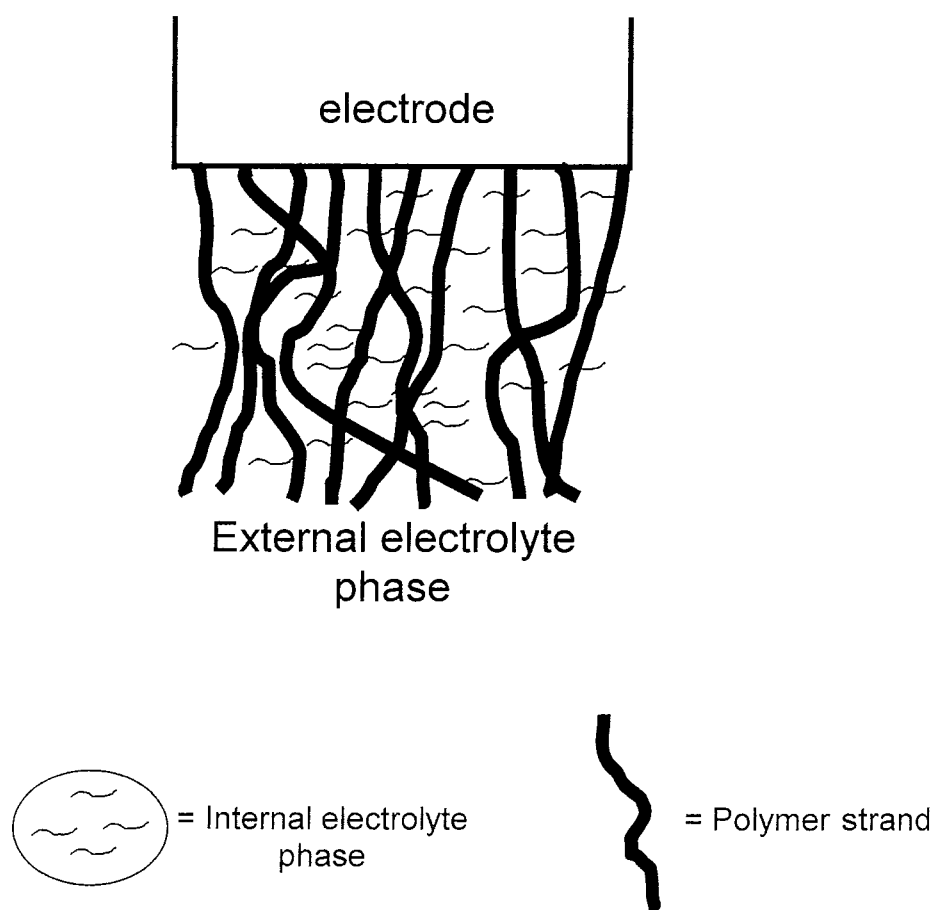


**Figure 4.4:** Simple heuristic model for the morphology of completely oxidised polypyrrole on an electrode surface [9]



Capacitive charge is not transported across the molecular wire/internal electrolyte interface, but is, accumulated at the surface. Therefore, in this high potential region, the process resembles a purely capacitive process. Martin and Cai [9] felt that in the intermediate potential regime both insulating and conductive regions exist within the film. They felt that both faradaic and capacitive mechanisms were at work here. The advantage of this model is that it shows no clear dividing line between anions moving toward molecular wire for faradaic or capacitive reasons. Kalaji and Peter [13] analysed the small-amplitude periodic transmittance of polyaniline films and concluded that the a.c response of the film is dominated by faradaic processes. They were unable to solve the discrepancy between a.c. and cyclic voltammetry capacitance values. They believed that the capacitive current observed is not truly capacitive but a "pseudo-capacitance".

In the work under study here, spectroelectrochemical analysis of the polymer films formed coupled with cyclic voltammetry was expected to shed some further insights into the structure and redox behaviour of these polymers.

#### 4.1.3 Optical studies of Polypyrrole.

Optical studies carried out on neutral polypyrrole by Street *et al.* [14] showed two peaks, one around 1239 nm (1 eV) and another at 387 nm (3.2 eV). The latter was assigned to a  $\pi - \pi^*$  interband transition. Optical studies were also carried out on polypyrrole as a function of doping levels [3, 14-22,]. Yakushi *et al.* [15] reported, aside from the interband transition again appearing around 380 nm three other bands. At moderate levels of doping three features evolve at 1770 nm (0.7 eV), 885 nm (1.4 eV) and 590 nm (2.1 eV). At very high doping levels, the 1.4 eV feature disappears with two mid-gap transitions now appearing at 1239 nm (1 eV) and 459 nm (2.7 eV). These trends along with the blue shift in of the interband transition wavelength were interpreted by Bredas *et al.* [16] to be in good agreement with a polaron/bipolaron model. Subsequent studies by Genies and Pernaut. [17], have utilised UV-VIS spectroelectrochemistry on polypyrrole thin films in

aprotic media, i.e.  $\text{CH}_3\text{CN} - \text{LiClO}_4$ , with a more restricted optical range. As well as the interband transition at 370 nm (3.4 eV), these authors reported two mid-gap transitions at 440 nm (2.8 eV) and 540 nm (2.3 eV). Two further studies [3, 18], again both using  $\text{CH}_3\text{CN}$  and tosylate [3] and perchlorate [18] as counterions showed that the spectral signatures of the two studies were broadly similar, having features appearing at 400 nm (3.1 eV), 540 nm (2.3 eV) and 900 nm (1.4 eV). Moreover, Zotti and Schiavon [3] reported the colour of the film as yellow in the neutral form, while the maximum oxidised form was blue/black, as previously discussed.

Later reports [4, 19, 20] are largely in agreement with initial reported UV-VIS spectroscopy. Amemiya and co-workers [4] reported three significant absorption peaks at 410 nm (3 eV), 530 nm (2.3 eV) and 910 nm (1.4 eV), and consequently analysed the spectroelectrochemical behaviour of polypyrrole using the Nernst equation, as previously discussed. Son and Rajeshwar [19], when studying the effect of  $\text{O}_2$  on the stability of polarons and bipolarons, reported peaks at 400 nm (3.1 eV), 540 nm (2.28 eV) and owing to instrumental limitations, observed only the onset of a peak at 820 nm, which they attributed to the 1.4 eV reported by previous authors [3, 14 – 18].

More recent reports [20-22] have incorporated UV-VIS spectroelectrochemistry with other techniques such as electron – spin resonance or EPR and Raman scattering and have reported similar spectra to those previously discussed. Some differences in the optical data reported by the various authors may be rationalised within the framework of polymer and instrumentation variability (e.g. bandwidth and resolution), although the influence of solvent and electrolyte cannot be discounted [19].

The optical spectrum of neutral polypyrrole shows only one absorption band at 390nm (3.2eV) [19] which was assigned  $\omega_1$  showing only the band gap transition as can be seen in figure 4.5 (a). At moderate doping levels there

were three absorption bands at 1770nm (0.7 eV), 885nm (1.4 eV) and 590nm (2.1 eV) and were attributed to  $\omega_2$ ,  $\omega_3$  and  $\omega_4$  respectively, which were due to

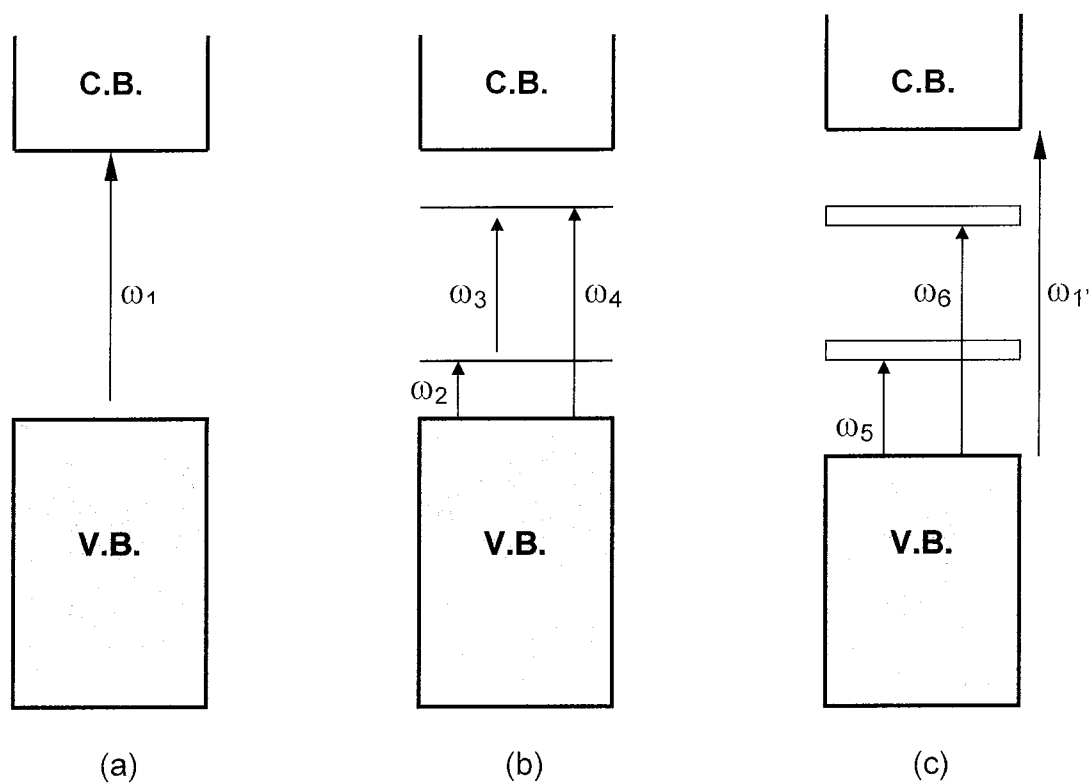


**Figure 4.5:** Polaron and bipolaron mid-gap states in polypyrrole

(a) neutral polypyrrole (b) light doping (c) heavy doping

C.B. = Conduction Band ; V.B. = Valence Band

polarons energy level as shown in figure 4.5 (b). At high doping levels the transition  $\omega_3$  (1.4eV) disappeared with two mid-gap transitions appearing at 1240nm (1.0 eV)  $\omega_5$  and 459nm (2.7 eV)  $\omega_6$ , as seen in figure 4.5 (c). Also the band gap transition  $\omega_1$  had shifted from  $\approx 390\text{nm}$  (3.2eV) to  $\approx 330\text{nm}$  (3.6 eV)  $\omega_1'$ , in going from the neutral polymer to the heavily oxidised polymer, again confirming that bipolaron bands originate from states at the edges of the valence and conduction bands.

#### 4.1.4 *Low band-gap conducting polymers*

Many well-studied conducting polymers with the band gaps of 2eV have been reported, including for example, poly-p-phenylene (2.7 eV) [23, 24], poly-p-phenylene vinylene (2.4 eV) [25, 26], polythiophene (2.0-2.1 eV) [27, 28] and polypyrrole (3.2 eV) as previously discussed. Low band gap conducting polymer have been defined as polymers with a band gap lower than 1.5 eV [29]. With this definition in mind the first of the low band gap conducting polymer was polyisothianaphthene [30], with a band gap of 1 eV, as discussed in Chapter 1 isothianaphthene may be considered as a thiophene unit with a fused benzene ring. The effect of the ring lowered the band gap in the resulting polymer by 1eV. The polyisothianaphthene also could be reversibly doped and undoped with the process accompanied by a high contrast electrochromic change [31], yellow in the reduced form and 'colour neutral' in the oxidised form. It was also found that the optical density of the doped film was found to be very small in the visible part of the spectrum, thereby making it the first example of a 'transparent' highly conducting polymer [32].

Electron donating methoxy substituted polythiophene have been reported [33] with lower band gap than the parent system. Poly-4,4'-dimethoxybithiophene [33] (see scheme 3.7, P183) reported a band gap for the neutral polymer of 1.6 eV and was deep blue in the neutral state and light grey in the doped state. Interestingly further substitution to the polyisothianaphthene has not resulted in lowering the band gap to any great

degree. Poly-5,6-dioxymethyleneisothianaphthene [34, 35] (see figure 3.31, P 222) was found to have a band gap similar to that of polyisothianaphthene of  $\sim 1$  eV. The neutral form was deep blue while the doped form was grey and transparent [34]. More recently, poly-5,6-dihexoxyisothianaphthene (see scheme 2.47, P134) was reported [36] to have a band gap of 0.95 eV, which is lower than polyisothianaphthene, and also exhibited a high contrast and reversible colour change from bluish black in the neutral state to transparent light yellow (close to colourless) in the doped state.

#### 4.1.4 Optical studies of poly-N-methylisindole

In the case of polythiophene the effect of a fused benzene ring dramatically lowered the band gap. The band gap for polypyrrole was 3.2 eV, as discussed, but on benz-fusion has the potential to be lower with the predicted band gap of polyisindole at 1.06 eV [37], the latter being unstable with no experimental value thus far been reported. However, UV-VIS spectroelectrochemical data and electrochromic properties of poly-N-methylisindole have also been reported [38 – 42].

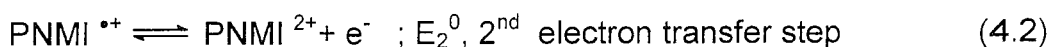
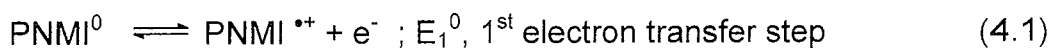
Lee *et al.* [38] reported that N-methylisindole underwent reversible colour changes during redox reactions and was orange in the oxidised form and dark green in the reduced form. Also the absorption spectrum was reported for the reduced form of poly-N-methylisindole only with a peak around 420 nm. Hanly *et al.* [39] however reported this electrochromic change as metallic gold in the reduced form and transparent in the oxidised form. Furthermore the same author reported the spectroelectrochemistry of poly-N-methylisindole with absorption at 431 nm (2.87 eV) in the reduced form and two peaks at 595 nm (2.09 eV) and 1400 nm (0.89 eV) for the oxidised form. Finally Rhee *et al.* [40] using reflectance spectroscopy, as opposed to the normal transmission spectroscopy, recorded similar UV-VIS spectroelectrochemical data. More recently, highly substituted polyisindoles have been reported [41, 42] to be high fluorescent, but the band gap was reported to be only 3.2eV [42].

To obtain a further insight into the electrochromic behaviour observed for poly-N-methylisindole, poly-5-methoxy-N-methylisindole and poly-5,6-dimethoxy-N-methylisindole in Chapter 3, in-situ spectroelectrochemical experiments were carried out. A thin layer of polymer was grown electrochemically and as the potential was increased in a stepwise fashion the spectra were recorded. Spectral data can therefore be gathered when the film is at equilibrium. Previous studies on poly-N-methylisindole have only reported the band gap value from the spectroelectrochemistry presented, as discussed. In addition to this, in this study the optical absorbance data was used to obtain absorbance versus wavelength measurements with varying potentials. This data was subsequently used to obtain Nernst plots and to estimate the bandgap of the three polymers. Cyclic voltammograms recorded simultaneously with the spectroscopic measurements were analysed to shed some further insights into both the faradaic and capacitive contributions to the redox behaviour of these polymers.

## 4.2. Results and Discussion

### 4.2.1 Spectroelectrochemistry of poly-N-methylisindole

The UV-vis absorption spectrum of a preformed layer of poly-N-methylisindole perchlorate on platinum in 0.1M LiClO<sub>4</sub> in CH<sub>3</sub>CN as a function of applied potential is shown in figure 4.6. The potential of the working electrode was set at -0.5 V and spectra were recorded between 400 and 850 nm when a steady state current was obtained after each potential was applied. The potential was first increased to -0.1V in intervals of 100mV and then increased to +0.5V in intervals of 25mV. For ease of discussion, figure 4.7 shows the absorption spectrum of the polymer at three different applied potentials, indicating neutral [PNMI<sup>0</sup>], partially oxidised [PNMI<sup>•+</sup>] and fully oxidised [PNMI<sup>2+</sup>] forms of the polymer layer, or more correctly no doping, low levels of doping and higher levels of doping. The redox mechanism of poly-N-methylisindole oxidation, based on that of polypyrrole [43] can be expressed as follows:



At -0.5V (vs SCE) the polymer was in the neutral form and the spectrum showed a  $\lambda_{\text{max}}$  at 430 nm (2.88 eV). This peak corresponds to an interband transition from the valence band to the conduction band or  $\pi - \pi^*$  transition, indicated as  $\omega_1$  in figure 4.8 (a). This is in good agreement with the literature value [39] where the reported  $\lambda_{\text{max}}$  of neutral poly-N-methylisindole was 430nm (2.87 eV). At +0.15V (vs SCE) the polymer was partially oxidised. The spectrum showed a significant  $\lambda_{\text{max}}$  at 600 nm (2.07eV) and this can be attributed to the electronic transitions  $\omega_2$ , arising from the formation of polarons, as seen in figure 4.8 (b).

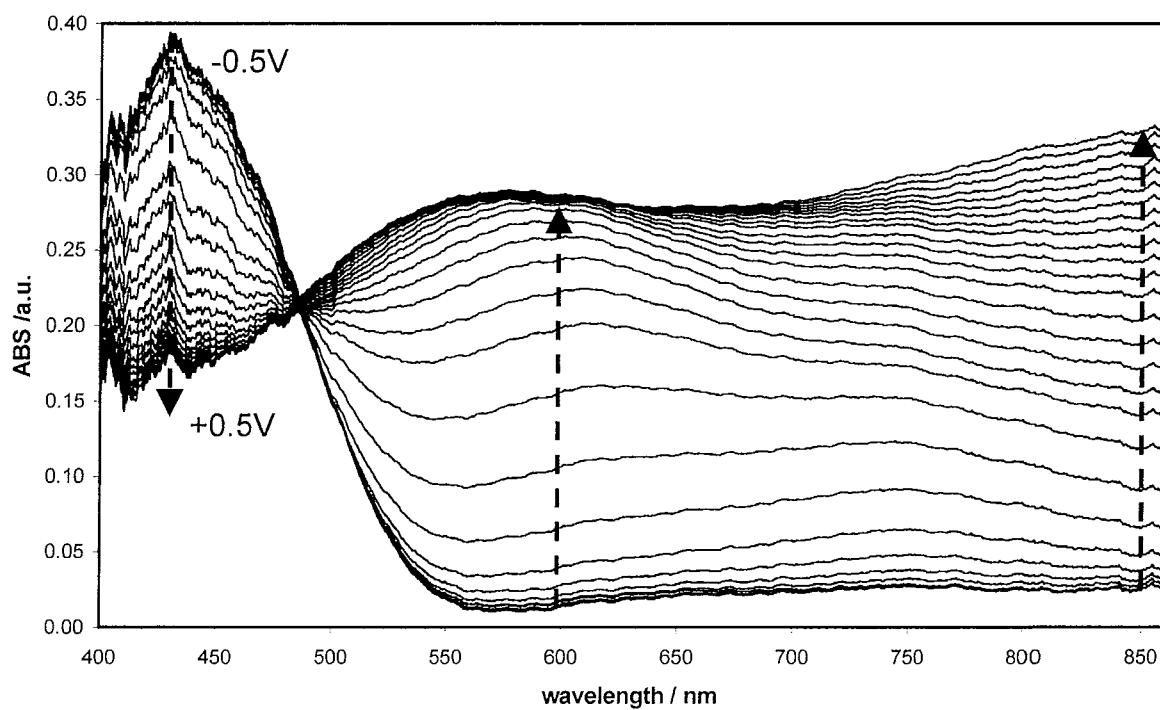


**Figure 4.6:** A series of absorption spectra of [Pt] poly-N-methylisoindole perchlorate in 0.1M LiClO<sub>4</sub> in CH<sub>3</sub>CN vs SCE at a applied potential of  $-0.5\text{V}$  to  $+0.5\text{V}$ .



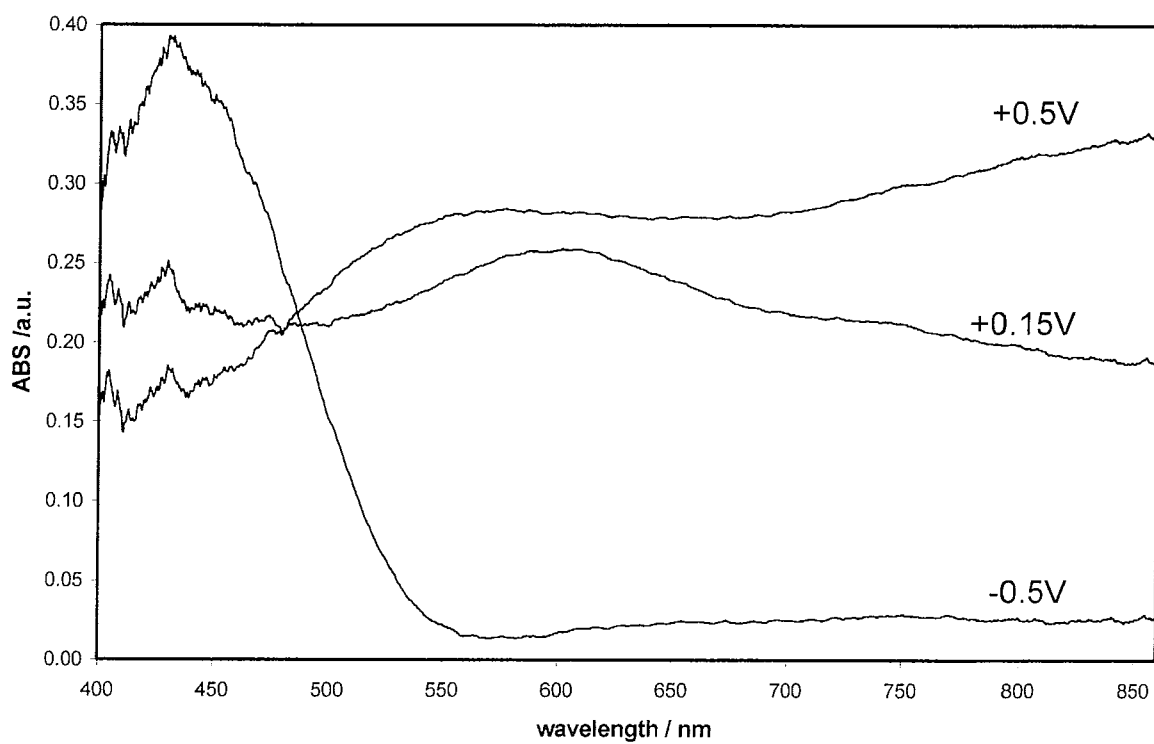


**Figure 4.7:** The absorption spectra of [Pt] poly-N-methylisoindole perchlorate in 0.1M LiClO<sub>4</sub> in CH<sub>3</sub>CN vs SCE at the applied potentials of -0.5V, +0.15 and +0.5V.

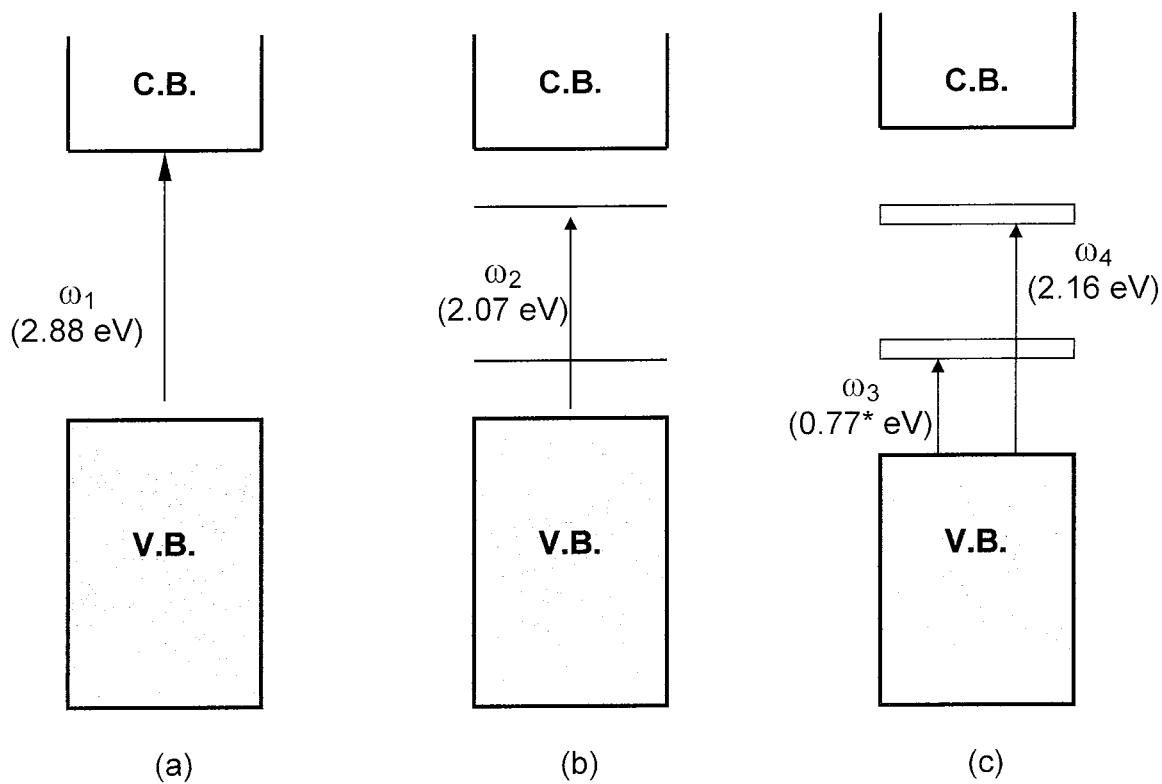


**Figure 4.8:** Electronic transitions of poly-N-methylisindole  
 (a) neutral form (b) partially oxidised form (c) fully oxidised form.

**C.B.** = Conduction Band ; **V.B.** = Valence Band

\* projected on the basis of literature values [39]

What this signifies is that polarons are now the main charge carrier at this doping level. With the peak at 430 nm decreasing, the concentration of neutral poly-N-methylisindole has decreased while the concentration of partially oxidised [PNMI<sup>•+</sup>] and fully oxidised [PNMI<sup>2+</sup>] forms of poly-N-methylisindole within the layer have increased.

At +0.5V (vs SCE) the polymer was fully oxidised or had high doping levels. The spectrum now showed a shift in  $\lambda_{\text{max}}$  600 nm (2.07 eV) to 575 nm (2.16 eV) and a new absorption at 850 nm (1.46 eV). The peak at 575 nm was attributed to the transition of electrons from the valence band to the 2<sup>nd</sup> bipolaron band  $\omega_4$ . The increasing peak at 850 nm has been attributed to the promotion of an electron from the valence band to the 1<sup>st</sup> bipolaron band  $\omega_3$ , figure 4.8 (c), although this absorption band was found by Hanly *et al.* [39] to continue to approximately 1600nm (0.77 eV)  $\omega_3$ , in the near-I.R. region.

The energy of the  $\pi - \pi^*$  transition or  $\omega_1$  transition ( $\lambda_{\text{max}} = 430\text{nm}$ , 2.88 eV) in figure 4.8, for the neutral polymer does not give the true band gap value, but only an estimation. However, the latter can be obtained using a simple graphical method, as proposed by Josowicz and Blackwood [44].

If the energy bands are assumed to be parabolic, the absorption coefficient,  $\alpha$ , is related to the photon energy [45] by

$$(\alpha h\nu)^{2/n} = B (h\nu - E_g) \quad (4.4)$$

where  $h$  is Plancks constant,  $\nu$  is the frequency of the incident radiation,  $E_g$  is the bandgap energy and  $B$  a some constant,  $n$  is a parameter which takes the value of 1 for direct transitions and 4 for indirect transitions. Note that the wavelength,  $\lambda$ , is related to  $\nu$  by the eqn 4.5, where  $c$  is the velocity of light.

$$\nu = c/\lambda \quad (4.5)$$

So using the section of the spectra immediately to the right of the 430nm peak and plotting the relative absorption intensity times  $h\nu$ , all raised to the power of 2 (direct) or  $\frac{1}{2}$  (indirect) versus  $h\nu$ , an estimation of the bandgap energy of neutral poly-N-methylisindole can be obtained. The straight line graph corresponding to  $n=1$ , is shown in figure 4.9, and is the same as that found for polypyrrole [4]. This showed that indeed  $\omega_1$  was a direct transition. From the intercept on the abscissa a value for the bandgap energy of 2.42 eV was obtained, which is lower than the estimated band gap from the  $\lambda_{\max} = 430\text{nm}$  (2.88 eV). However, this is higher than the reported bandgap for poly-N-methylisindole [39] of  $\sim 2$  eV. This difference may partly be due to the band tailing caused by the amorphous structure of poly-N-methylisindole.

The variations in absorption at 430 nm, 600 nm and 850 nm with changing potential are given in figure 4.10. At these wavelengths the concentration of the neutral, partially oxidised and fully oxidised species can be monitored, hence a concentration profile for the three species was obtained. The absorption at 430 nm from  $-0.5\text{V}$  and  $-0.1\text{V}$  remained unchanged. This was complementary to the cyclic voltammetric studies carried out on poly-N-methylisindole perchlorate in Chapter 3, which showed no electrochemical activity in this potential window. Between  $-0.1\text{V}$  and  $+0.35\text{V}$  the absorption decreases before levelling off to a constant value from  $+0.35\text{V}$  to  $+0.5\text{V}$ . At 600 nm the absorption profile mirrored that of the 430 nm profile, where the absorption remains constant between  $-0.5\text{V}$  and  $-0.1\text{V}$ , again complementary to the cyclic voltammetry. Between  $-0.1\text{V}$  and  $+0.3\text{V}$  the profile increases and then levelled off at  $+0.3\text{V}$  to  $0.5\text{V}$ . Finally the absorption at 850 nm again was constant between  $-0.5\text{V}$  and  $-0.1\text{V}$  and then increased constantly up to  $+0.5\text{V}$ .

The variation in absorption with potential at 430 nm was less pronounced than the corresponding absorbance change at 600 nm and 850 nm. This can be attributed to the fact that the transitions at 600 and 850 nm are not well defined and there may be some overlap of more than one transition.

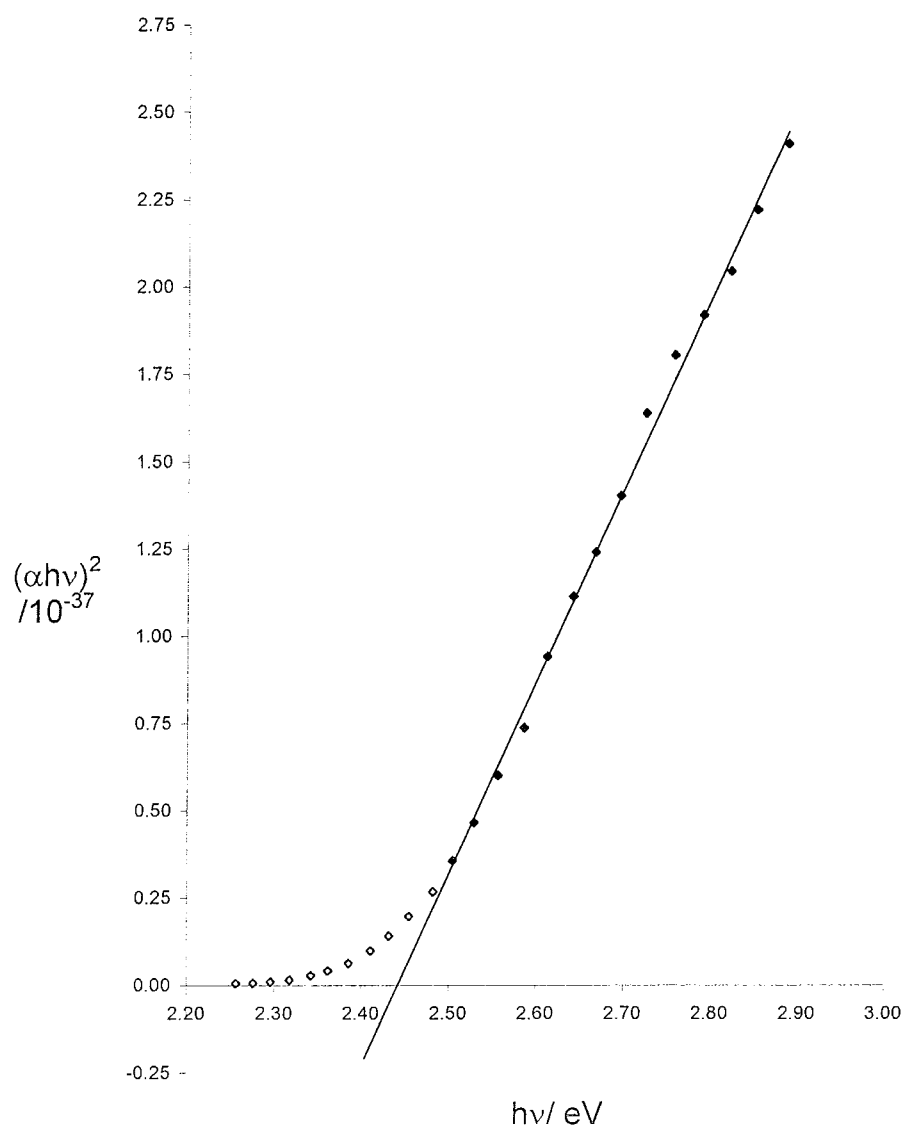


**Figure 4.9:** Plot of  $(\alpha h\nu)^2$  versus  $h\nu$  for a layer of neutral [Pt] poly-N-methylisindole in 0.1M LiClO<sub>4</sub> in CH<sub>3</sub>CN (vs SCE) with an applied potential of -0.5 V in order to determine the bandgap energy.

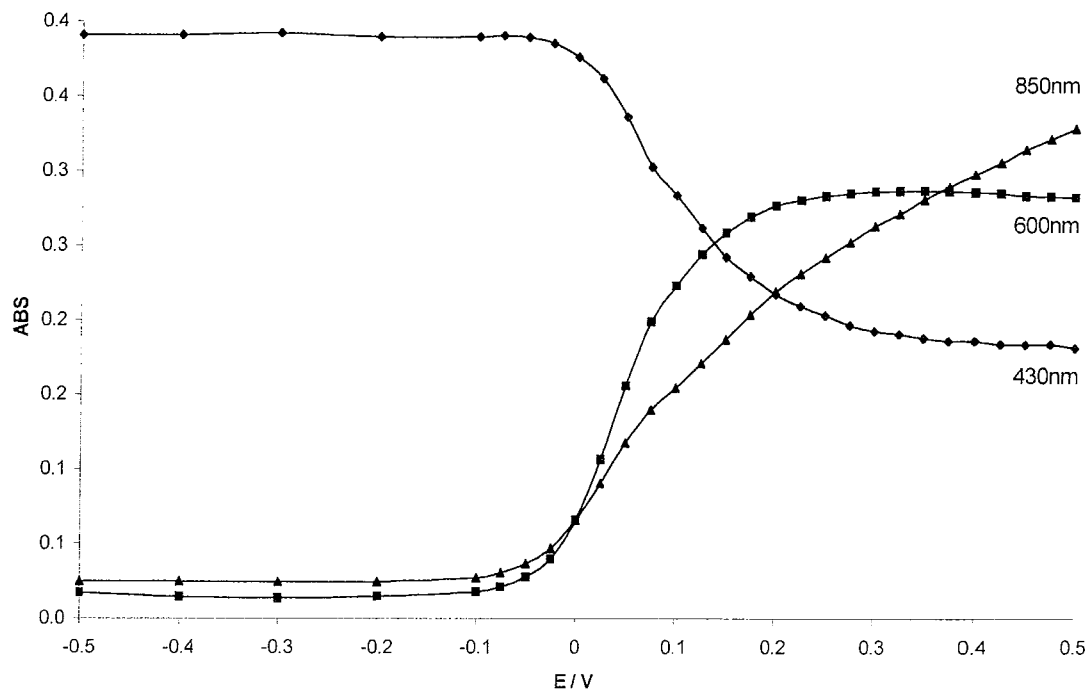


**Figure 4.10:** Plot of variation in absorbance with applied potential for a layer of poly-N-methylisindole perchlorate at 430 nm, 600 nm and 850 nm.

### *Nernst model of poly-N-methylisoindole system*

Previous workers have utilised the Nernst equation to analyse spectroelectrochemical behaviour of polypyrrole films [4 – 6] as previously discussed, to give formal potentials and “n-values”, (the apparent number of electrons transferred during the redox reaction). This same method of analysis was also applied in this study of the spectra of poly-N-methylisoindole. The following assumptions were necessary to apply the Nernst equation [4] to the data, which are,

- (i) the overlapping of absorption spectra are neglected,
- (ii) only three species, neutral monomers, partially oxidised monomers (polarons) and fully oxidised monomers (bipolarons), exist in the film at a given potential and
- (iii) only two reactions occur (a) between neutral monomers and slightly oxidised monomers (polarons) and (b) between slightly oxidised monomers (polarons) and fully oxidised ones (bipolarons).

The “monomer unit” model was used here. This treats the redox reaction of the poly-N-methylisoindole films in terms of the N-methylisoindole monomer unit. This work assumed that the absorption at approximately 430nm was due to  $\pi$ - $\pi^*$  transition of the neutral N-methylisoindole monomer [4, 44]. While 850nm was taken as the wavelength at which the broad band due to the fully oxidised monomers existed.

The absorption data is treated according to the Nernst equation, assuming Beers Law,

at 430nm the equation for T= 298K is

$$E = E_1^0 + (0.059/n_1) \log ([NMI^{+n_1}]/[NMI^0])$$

$$E = E_1^0 + (0.059/n_1) \log \{[(\Delta Abs)_{\max} - \Delta Abs] / \Delta Abs\} \quad (4.6)$$

At 850nm the equation is

$$E = E_2^0 + (0.059/n_3) \log ([NMI^{+n_2}]/[NMI^{+n_1}])$$

$$E = E_2^0 + (0.059/n_3) \log \{ \Delta Abs / [(\Delta Abs)_{max} - \Delta Abs] \} \quad (4.7)$$

where E is the potential applied to the electrode,  $E_1^0$ ,  $E_2^0$  are the formal electrode potentials,  $n_1$  and  $n_3$  are the number of electrons transferred and  $NMI^0$ ,  $NMI^{+n_1}$ ,  $NMI^{+n_2}$ , correspond to the neutral monomer, partially oxidised monomer and the fully oxidised monomer respectively. The  $\Delta Abs$ ' are the absorbance changes relative to the fully oxidised spectrum at 430nm and relative to the fully reduced spectrum at 850nm. The  $(\Delta Abs)_{max}$  is the maximum absorbance change between fully oxidised and fully reduced states. The contributions of counterions are omitted for convenience.

As observed by Amemiya and co-workers, the plots obtained are not linear [4], but linear regions are obtained in certain potential windows. The Nernst plots of poly-N-methylisindole at 430 nm and 850 nm, as determined by equation 4.6 and 4.7 respectively, are shown in figure 4.11 and 4.12. From the slope and the intercept the n-values and the formal electrode potentials were obtained as  $n_1 = 0.45$ ,  $n_3 = 0.32$ ,  $E_1^0 = +0.15V$ , and  $E_2^0 = +0.17V$ . The fact that the  $n_1$  and  $n_3$  values are less than one implies that oxidation of poly-N-methylisindole to form a radical cation or polaron occurs over many units of polymer, while further oxidation to form the dication or bipolaron again occurs over many units of polymer. One would expect  $n_1$  and  $n_3$  to be equal as reported by Amemiya *et al.* [4].  $E_1^0$  occurs at a lower potential than that of  $E_2^0$  implying a greater ease in oxidation of neutral poly-N-methylisindole to the radical cation (eqn. 4.1) than the oxidation of radical cation to the dication (eqn 4.2). The small difference in  $E_1^0$  and  $E_2^0$  confirms that K in eqn 4.3 is also small.



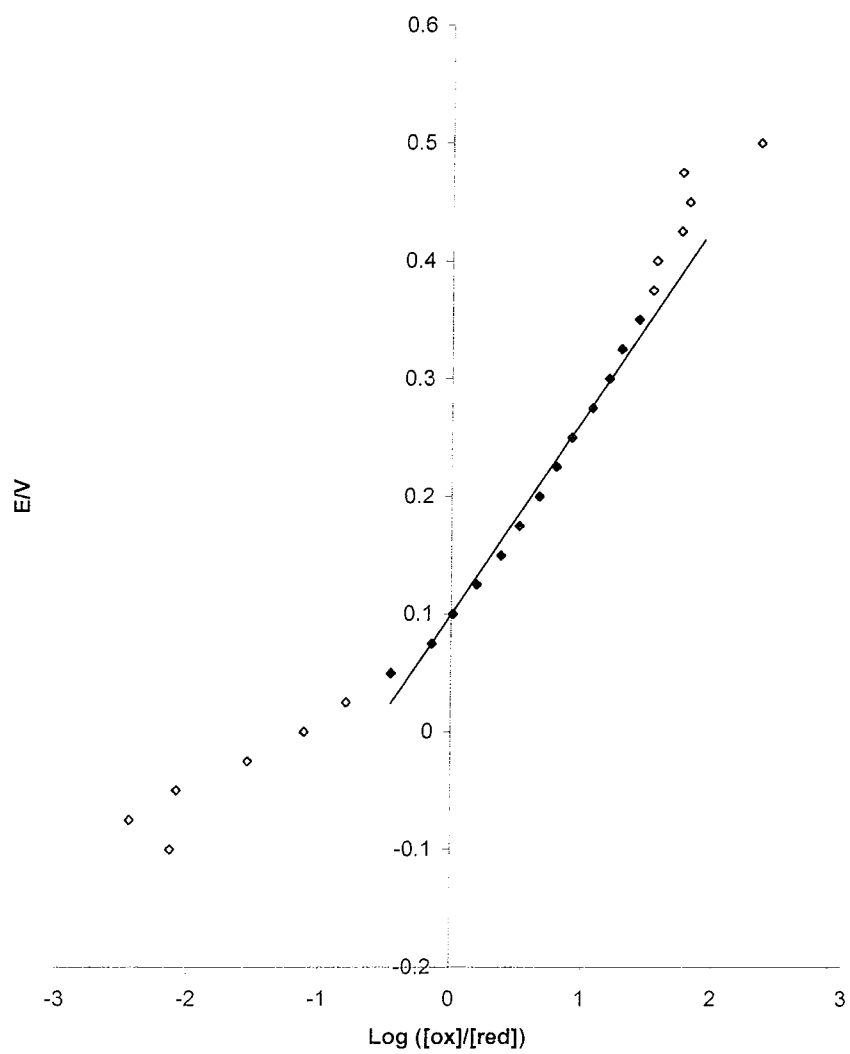


**Figure 4.11:** Nernst plot calculated from the absorbance at 430 nm for poly-N-methylisindole perchlorate in 0.1M LiClO<sub>4</sub> in CH<sub>3</sub>CN (vs SCE).

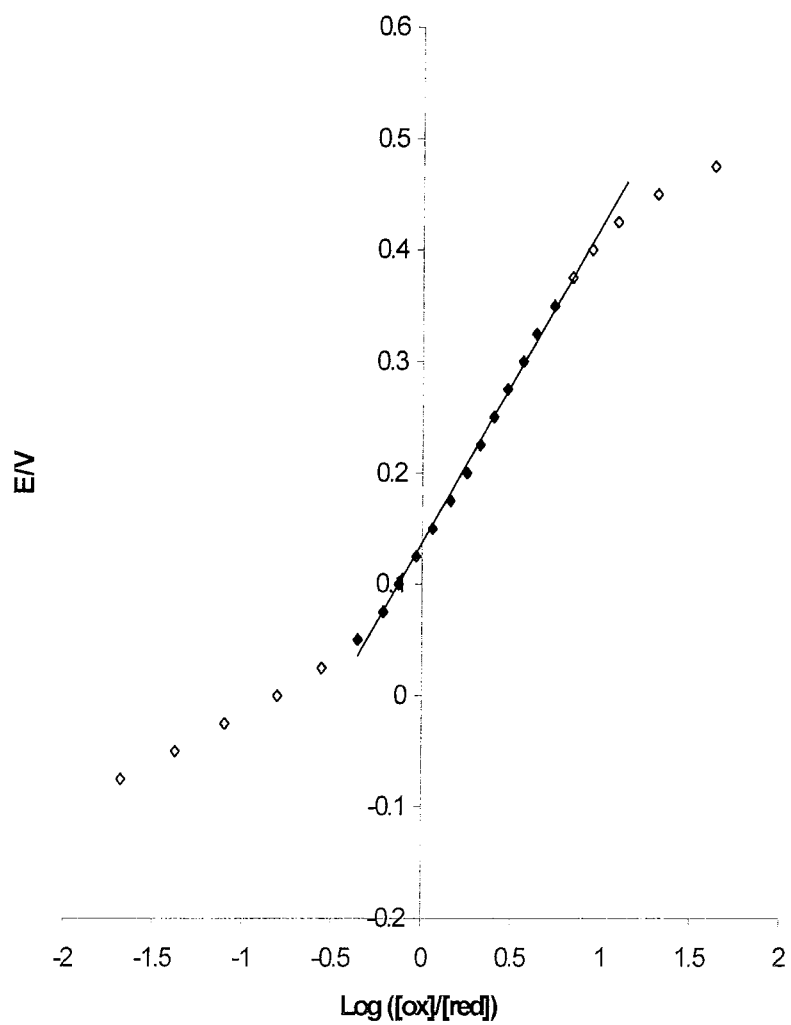


**Figure 4.12:** Nernst plot calculated from the absorbance at 850 nm for poly-N-methylisindole perchlorate in 0.1M LiClO<sub>4</sub> in CH<sub>3</sub>CN (vs SCE).

The theoretical concentration profile of the three species contained within the layer can also be predicted by eqn. 4.1 to 4.3 and 4.8, where C is the total amount of polymer and is constant.

$$[\text{NMI}^0] + [\text{NMI}^{+n_1}] + [\text{NMI}^{+n_2}] = C \quad (4.8)$$

Let,

$$\left(\frac{[\text{NMI}^{+n_1}]}{[\text{NMI}^0]}\right) = x \quad \left(\frac{[\text{NMI}^{+n_2}]}{[\text{NMI}^{+n_1}]}\right) = y \quad (4.9)$$

therefore:

$$[\text{NMI}^{+n_1}] = x[\text{NMI}^0] \quad [\text{NMI}^{+n_2}] = y [\text{NMI}^{+n_1}] \quad (4.10)$$

Now expressions for  $[\text{NMI}^{+n_1}]$  and  $[\text{NMI}^{+n_2}]$  can be substituted into equation 4.8.

$$[\text{NMI}] + x[\text{NMI}] + y[\text{NMI}^{+n_1}] \quad (4.11)$$

$$[\text{NMI}] + x[\text{NMI}] + xy[\text{NMI}] \quad (4.12)$$

$$[\text{NMI}] (1+x+xy) = C \quad (4.13)$$

Now expressions for each species can be expressed in term of x and y.

$$\left(\frac{[\text{NMI}]}{C}\right) = \left(\frac{1}{1+x+xy}\right) \quad (4.14)$$

$$\left(\frac{[\text{NMI}^{+n_1}]}{C}\right) = \left(\frac{x[\text{NMI}]}{C}\right) = \left(\frac{x}{1+x+xy}\right) \quad (4.15)$$

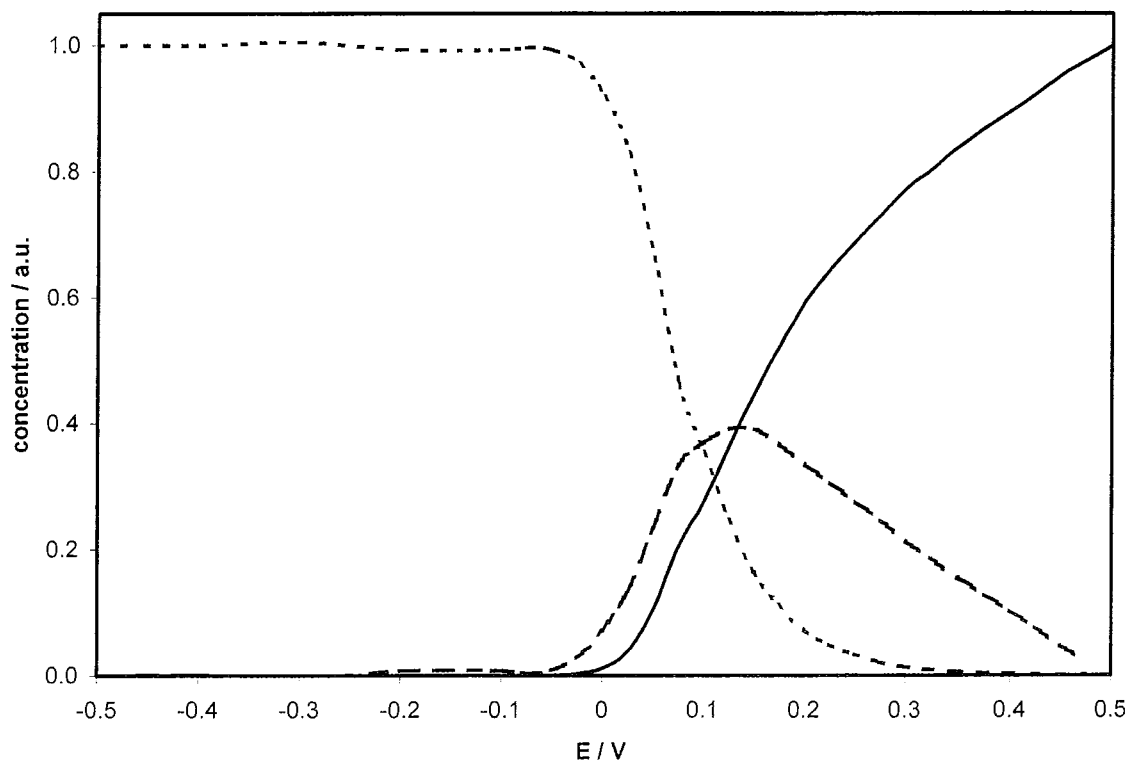
$$\left(\frac{[\text{NMI}^{+n_2}]}{C}\right) = \left(\frac{xy[\text{NMI}]}{C}\right) = \left(\frac{xy}{1+x+xy}\right) \quad (4.16)$$

In practical terms what  $x$  and  $y$  mean has already been defined by the Nernst equation 4.6 and 4.7. Therefore  $x = \{[(\Delta\text{Abs})_{\text{max}} - \Delta\text{Abs}]/ \Delta\text{Abs}\}$  at 430nm and  $y = \{\Delta\text{Abs}/[(\Delta\text{Abs})_{\text{max}} - \Delta\text{Abs}]\}$  at 850nm.

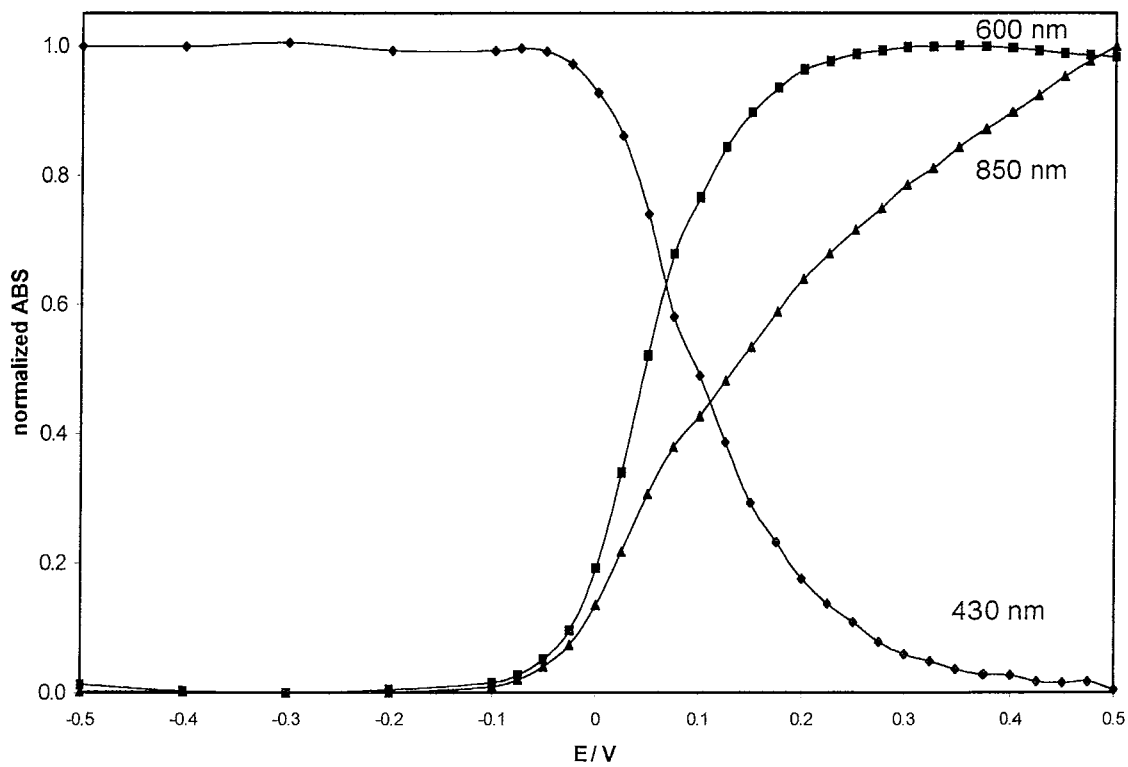
The predicted normalised concentration profile for the three species was plotted using eqn 4.8 to 4.16, and is shown in figure 4.13. At low potentials the concentration of the neutral species is equal to  $C$ . As the applied potential is increased the concentration profile of the neutral species decreases as it becomes oxidised, hence at the same time the concentration profile of the partially oxidised species increases to a maximum, which is approximately half the total concentration  $C$  and then falls back to zero as the partially oxidised polymer becomes fully oxidised. The concentration of the fully oxidised species goes from a zero level to a maximum equal to  $C$ , with a profile similar to that of the neutral species. Such plots have also been determined for polypyrrole [4] and have a similar profile.

Figure 4.14 shows the plot of figure 4.10 in normalised form, and figure 4.15 shows the overlay of figures 4.13 and 4.14. What is interesting to note is that both the neutral species observed at 430 nm and the fully oxidised species at 850 nm have concentration profiles similar to the predicted profiles derived by equation 4.8. However the concentration profile of the partially oxidised species observed at 600 nm does not follow the predicted profile. Instead of the partially oxidised species further oxidises to become fully oxidised as shown with equation 4.17, the concentration profile remains steady. This leads to the possibility that there is some kinetic factor, i.e.  $k_1$  is fast and  $k_2$  is slow. Indeed the sluggish response to the concentration profile of the fully oxidised species could also be attributed to another redox mechanism occurring with the polymer layer involving a two-state transition, again with slow kinetics  $k_3$ , as depicted in equation 4.18.





**Figure 4.13:** predicted concentration profile of neutral form [·····], partially oxidised [ - - -] and fully oxidised [—] forms of poly-N-methylisoindole as derived by eqn. 4.6.



**Figure 4.14:** Plot of normalised absorption versus applied potential for a layer of poly-N-methylisoindole at 430 nm, 600 nm and 850 nm.

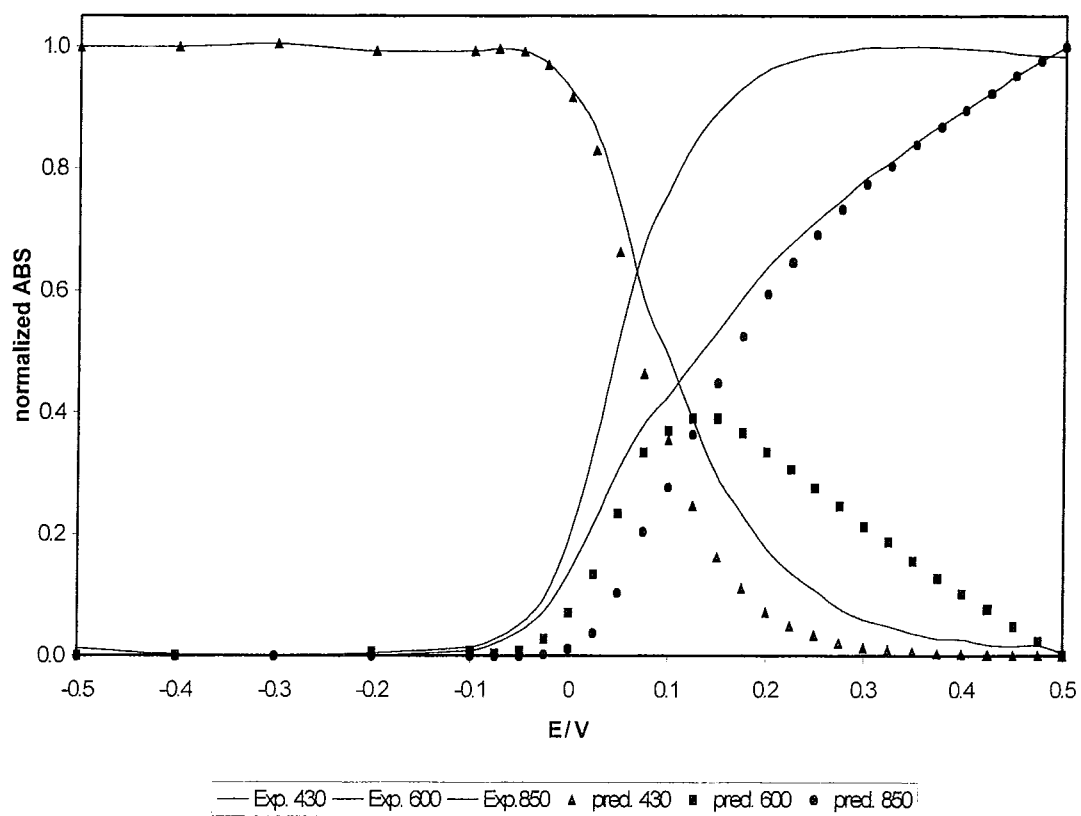


**Figure 4.15:** Overlay of predicted concentration profile (figure 4.13) and experimental concentration profile (figure 4.14).

This mechanism (eqn. 4.18) was suggested by Son and Rajeshwar [19] where spectroelectrochemistry of polypyrrole under an O<sub>2</sub> saturated environment was carried out and they concluded that the radical cation or polaron state of polypyrrole is unstable and leads directly to this two- state transition. Also figure 4.6 shows only one isosbestic point for poly-N-methylisoindeole at around 490 nm similar to that reported in literature [39], suggested that both the partially oxidised form and fully oxidised form of poly-N-methylisoindeole exist within the layer and that both redox mechanism equation 4.17 and 4.18 occur in the layer. It must also be noted that the concentration profile of the partially oxidised species was plotted from absorption data at 430nm and 850nm and not directly from the spectrum in figure 4.6.

Finally, if a plot of the change in absorbance at 850nm with change in potential,  $dA/dE$ , was plotted against applied potential, a curve which was related to a cyclic voltammogram of the thin layer species is obtained. Here the absorption is monitored at sampled potentials at equilibrium. This curve is depicted in figure 4.16(a) and is the spectroscopic analogue of a cyclic voltammogram, figure 4.16 (b). The C.V, if plotted on the same axis, can help to yield information as to what fraction of the total current is faradaic and what is due to double-layer charging. The graph of current versus potential is representative of the total current, while the  $dA/dE$  versus  $E$  curve shows only the faradaic component of current. As can be seen from the superimposition of the two curves, there must be a large double-layer charging component as the current fails to decay back to zero after the current peak. However as can be seen from figure 4.16 (a), the  $dA/dE$  vs  $E$  profile of the poly-N-methylisoindeole drops off to zero after the peak showing thin layer faradaic behaviour.



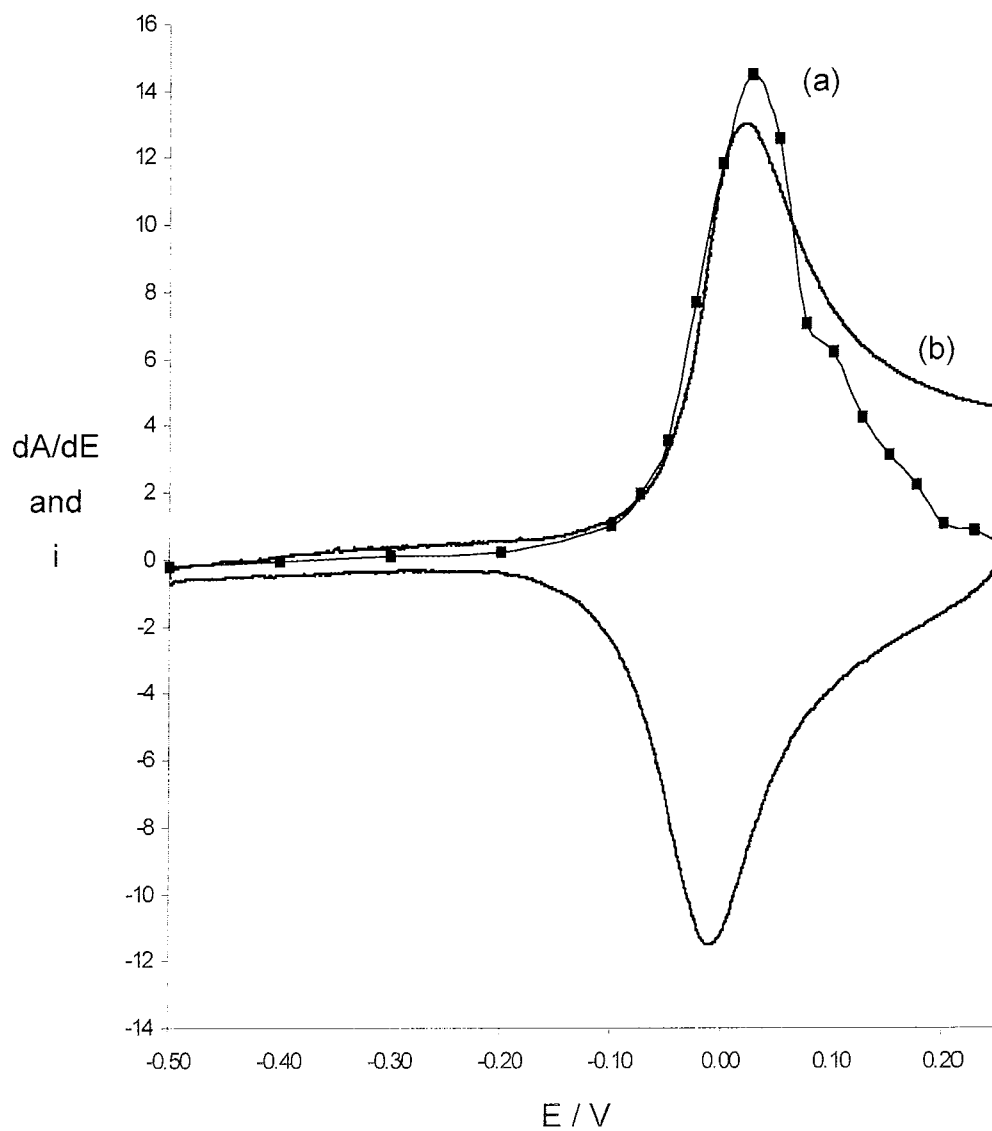
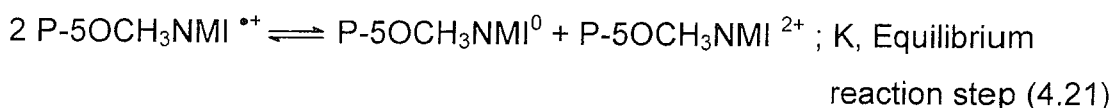
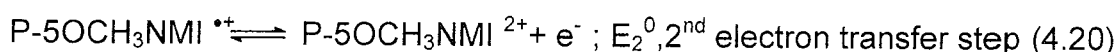
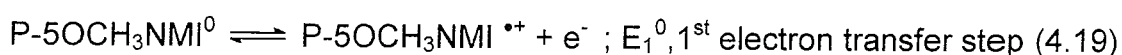


**Figure 4.16:** Plot of (a)  $dA/dE$  versus potential at 850 nm and (b) cyclic voltammogram of [Pt] poly-N-methylisindole in 0.1M  $LiClO_4$  in  $CH_3CN$  vs SCE.

#### 4.2.2. Spectroelectrochemistry of poly-5-methoxy-N-methylisindole

The optical absorption of a poly-5-methoxy-N-methylisindole perchlorate layer formed in 0.1M LiClO<sub>4</sub> in CH<sub>3</sub>CN on platinum as a function of applied potential is shown in figure 4.17. The potential of the working electrode was set at -0.5 V and spectra were recorded between 400 and 850 nm when a steady state current was obtained after each potential was applied. The potential was first increased to -0.1V in intervals of 100mV and then increased to +0.3V in intervals of 25mV and finally increased to +0.75V in intervals of 50mV. For ease of discussion, figure 4.18 shows the absorption spectrum of the polymer at three different applied potentials, indicating neutral [P-5OCH<sub>3</sub>NMI<sup>0</sup>], partially oxidised [P-5OCH<sub>3</sub>NMI<sup>\*+</sup>] and fully oxidised [P-5OCH<sub>3</sub>NMI<sup>2+</sup>] forms of the polymer layer, or no doping, low and high levels of doping. The redox mechanism of poly-5-methoxy-N-methylisindole oxidation based on that of poly-N-methylisindole (eqn. 4.1 – 4.3) can be expressed as follows:



At - 0.5V (vs SCE) the polymer was in the neutral form and the spectrum showed a  $\lambda_{\text{max}}$  at 430 nm (2.88 eV); the same as poly-N-methylisindole. This peak corresponded to an interband transition from the valence band to the conduction band or  $\pi - \pi^*$  transition illustrated as  $\omega_1$  in figure 4.19 (a). At +0.15V (vs SCE) the polymer was partially oxidised. The spectrum showed a significant  $\lambda_{\text{max}}$  at 580 nm (2.14eV) and has been attributed to the electronic transitions arising from the formation of polarons,  $\omega_2$  as seen in figure 4.19 (b). The equivalent transition in poly-N-methylisindole occurred at a longer wavelength 600 nm (2.07 eV) for the same applied potential and suggests

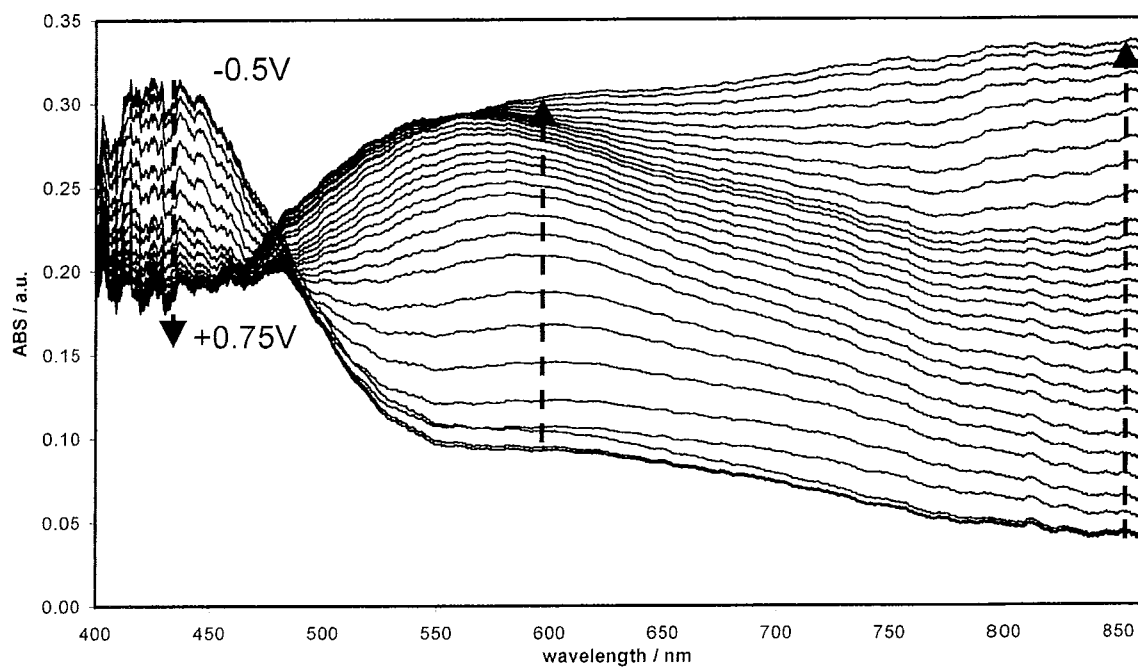


**Figure 4.17:** A series of absorption spectra of [Pt] poly-5-methoxy-N-methylisindole perchlorate in 0.1M LiClO<sub>4</sub> in CH<sub>3</sub>CN vs SCE at applied potentials of -0.5V to +0.75V.

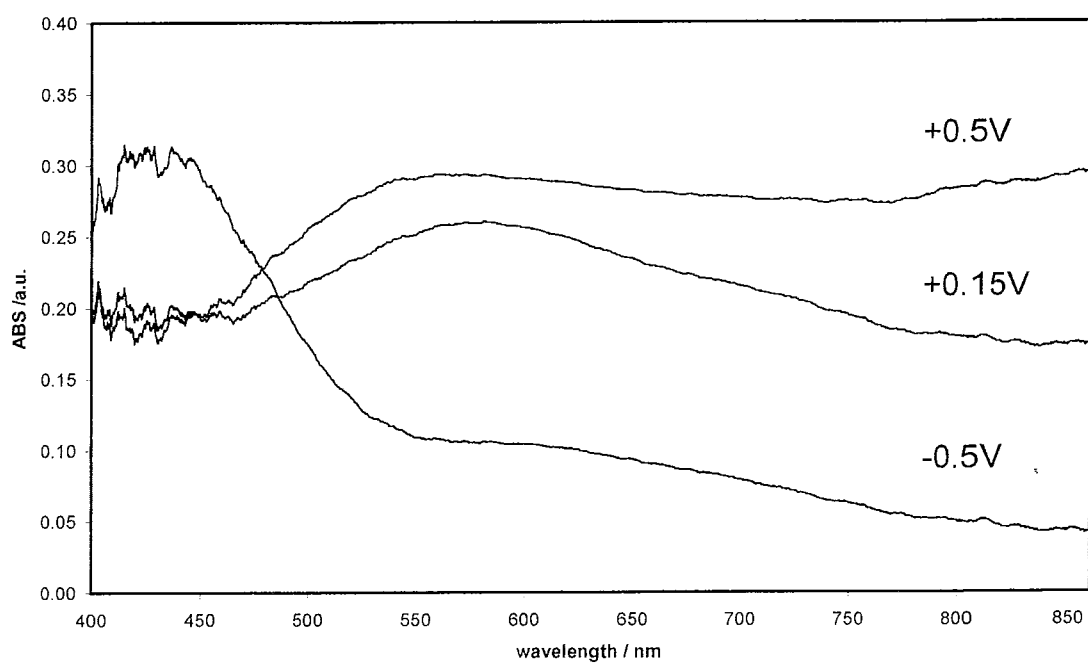


**Figure 4.18:** The absorption spectra of [Pt] poly-5-methoxy-N-methylisindole perchlorate in 0.1M LiClO<sub>4</sub> in CH<sub>3</sub>CN vs SCE at the applied potentials of -0.5V, +0.15V and +0.5V.

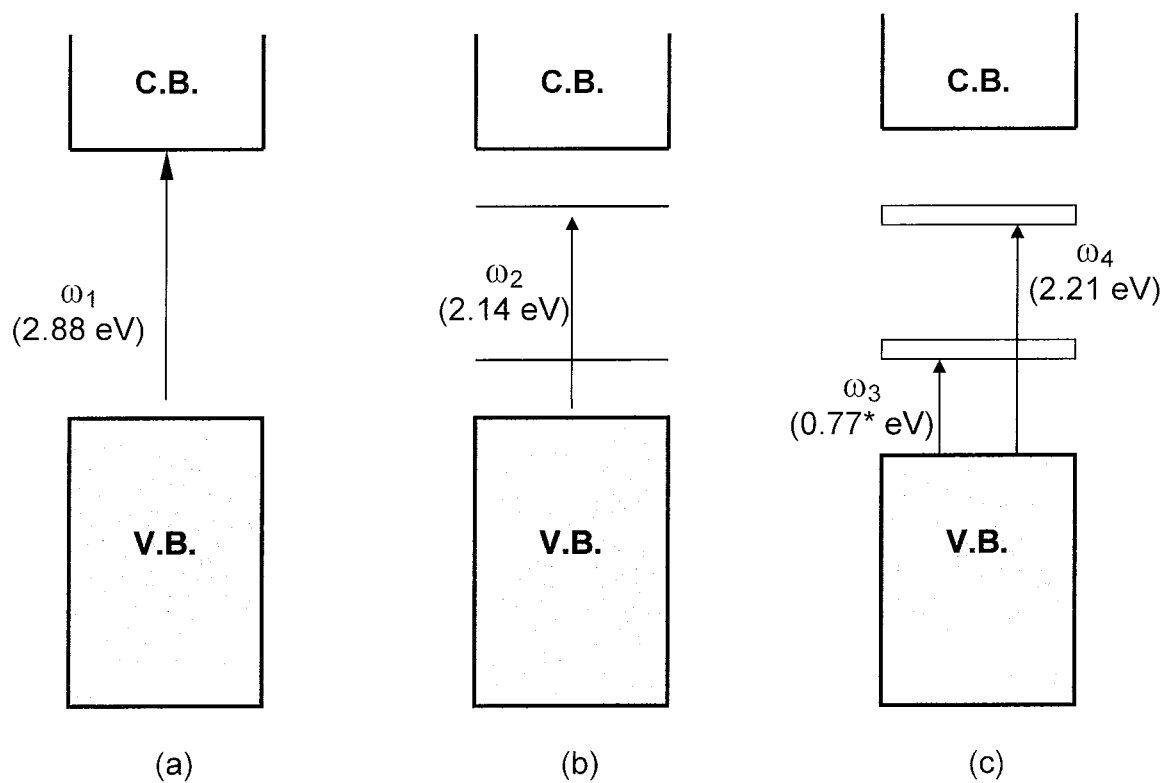


**Figure 4.19:** Electronic transitions of poly-5-methoxy-N-methylisindole  
 (a) neutral form (b) partially oxidised form (c) fully oxidised form.

**C.B.** = Conduction Band ; **V.B.** = Valence Band

\* projected on the basis of literature values [39]

that polaron energy levels for the methoxy substituted polymer exist at higher energy. As with poly-N-methylisindole polarons are the main charge carrier at this doping level, with the peak at 430 nm decreasing, the concentration of neutral poly-5-methoxy-N-methylisindole has decreased while the concentration of slightly oxidised [P-5OCH<sub>3</sub>NMI<sup>•+</sup>] and fully oxidised [P-5OCH<sub>3</sub>NMI<sup>2+</sup>] forms of poly-5-methoxy-N-methylisindole within the layer have increased.

At +0.5V (vs SCE) the polymer was fully oxidised, and the spectrum now shows a shift in  $\lambda_{\text{max}}$  at 580 nm (2.14 eV) to 560 nm (2.21 eV) and an increasing absorption at 850 nm (1.46 eV). The band at 560 nm was attributed to the transition of electrons from the valence band to the 2<sup>nd</sup> bipolaron band  $\omega_4$ . The increasing peak at 850 nm has been attributed to the promotion of an electron from the valence band to the 1<sup>st</sup> bipolaron band  $\omega_4$ , figure 4.19 (c), and it is believed that this absorption band continues to approximately 1600nm (0.77 eV)  $\omega_3$ , as found by Hanly *et al.* [39].

An estimation of the bandgap energy of neutral poly-5-methoxy-N-methylisindole, i.e. transition  $\omega_1$  in figure 4.19 can again be obtained as in the case with poly-N-methylisindole. Figure 4.17 showed a  $\lambda_{\text{max}}$  at 430 nm for an applied potential of -0.5V for the neutral polymer. Using equation 4.4 and 4.5 the nature of the transition and the bandgap can be determined.

So again using the section of the spectra immediately to the right of the 430 nm band and plotting the relative absorption intensity times  $h\nu$ , all raised to the power of 2 (direct) or  $\frac{1}{2}$  (indirect) versus  $h\nu$  can yield an estimation of the bandgap energy of neutral poly-5-methoxy-N-methylisindole. The straight line graph of the linear region between 430 nm and 520 nm corresponds to  $n=1$ , as shown in figure 4.20. This showed that indeed  $\omega_1$  is a direct transition, as found with poly-N-methylisindole. From the intercept on the abscissa a value for the bandgap energy of 2.36 eV was obtained, 0.06 eV lower than that of poly-N-methylisindole. It can be concluded that neutral poly-5-methoxy-N-methylisindole has a lower bandgap than neutral

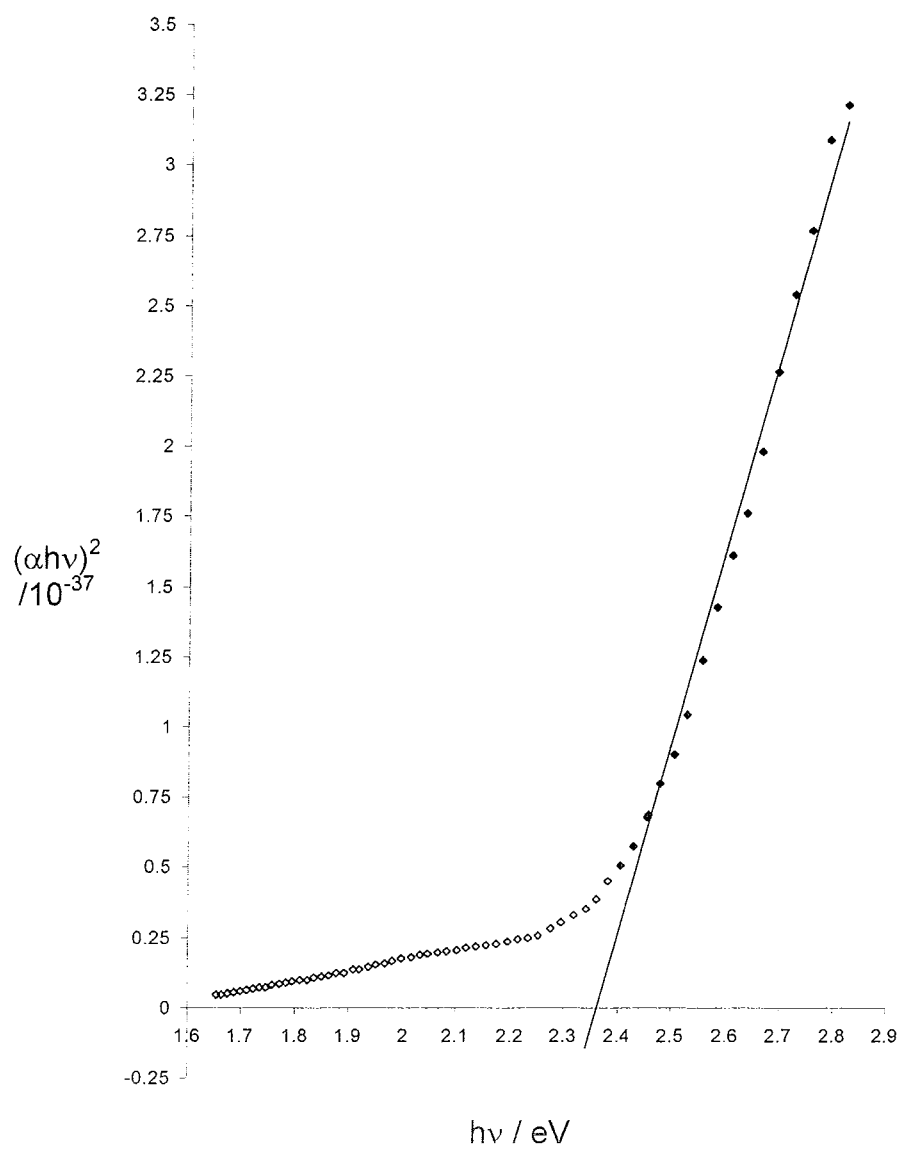


**Figure 4.20:** Plot of  $(\alpha h\nu)^2$  versus  $h\nu$  for a layer of neutral [Pt] poly-5-methoxy-N-methylisoindole in 0.1M LiClO<sub>4</sub> in CH<sub>3</sub>CN (vs SCE) with an applied potential of -0.5 V in order to determine the bandgap energy.

poly-N-methylisindole using the same experimental set-up and method to determine the bandgap. This lowering of the bandgap may arise from the electron donating effect of the methoxy group on the polymer backbone. This small lowering of the band gap with the addition of a methoxy group on the 6-membered ring is similar to that observed for polyisothianaphthene whereby, dioxymethylene [34, 35] and dihexoxy [36] introduced on to the 5- and 6-positions of the ring had little effect on the polymer band gap. This result also shows that determining the band gap of the polymers by just using the  $\lambda_{\max}$  directly from the spectra is not sufficient, as the  $\lambda_{\max}$  for both poly-N-methylisindole and poly-5-methoxy-N-methylisindole were at 430nm (2.88 eV).

The variations in absorption at 430 nm, 565 nm and 850 nm with changing potential are given in figure 4.21. At these wavelengths the concentration of the neutral, slightly oxidised and fully oxidised species can be monitored, hence a concentration profile for the three species was obtained, as before. The absorption at 430 nm from  $-0.5V$  and  $-0.1V$  remained unchanged. This was complementary to the cyclic voltammetric studies carried out on poly-5-methoxy-N-methylisindole perchlorate in Chapter 3, which showed no electrochemical activity in this potential window. Between  $-0.1V$  and  $+0.2V$  the absorption decreased before levelling off to a constant value from  $+0.2V$  to  $+0.75V$ . At 565 nm the absorption profile mirrored that of the 430 nm profile, where the absorption remains constant between  $-0.5V$  and  $-0.1V$ , again complementary to the cyclic voltammetry. Between  $-0.1V$  and  $+0.375V$  the profile increases and then levelled off at  $+0.35V$  to  $0.75V$ . Finally the absorption at 850 nm again was constant between  $-0.5V$  and  $-0.1V$  and then increased constantly up to  $+0.75V$ .

The variation in absorption with potential at 430 nm was less pronounced than the corresponding absorbance change at 565 nm and 850 nm. This can be attributed to the fact that the transitions at 600 and 850 nm are not well defined and there may be some overlap of more than one transition, as in the case with poly-N-methylisindole.



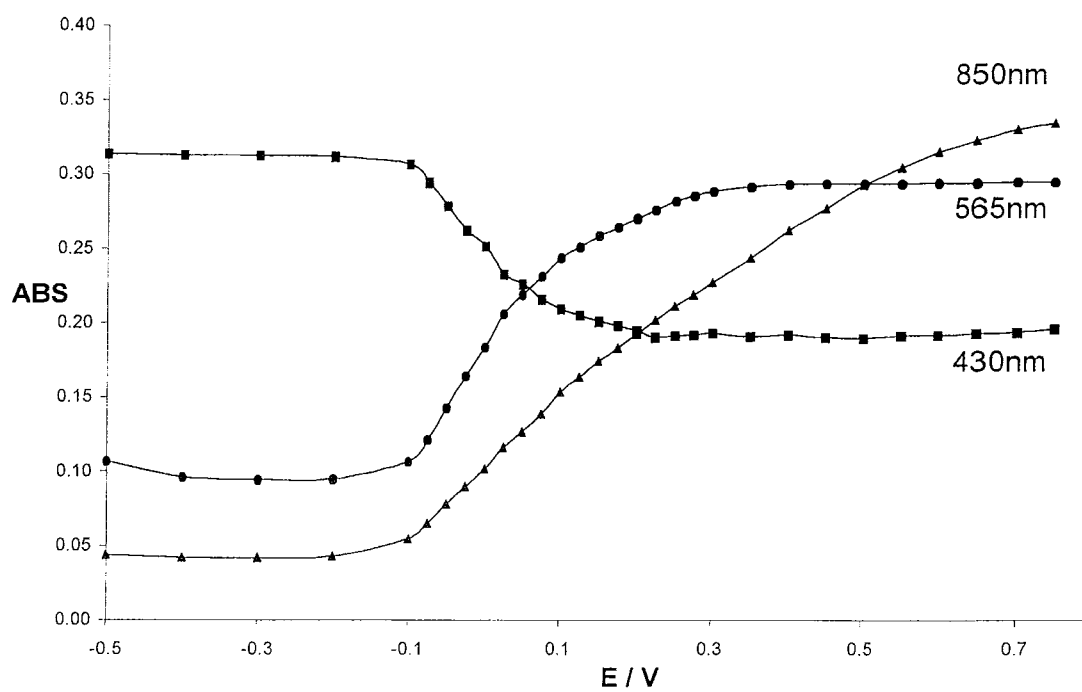


**Figure 4.21:** Plot of variation in absorbance with applied potential for a layer of poly-5-methoxy-N-methylisindole perchlorate at 430nm, 600nm and 850nm.

### *Nernst model of poly-5-methoxy-N-methylisindole*

As with poly-N-methylisindole, poly-5-methoxy-N-methylisindole was analysed using the Nernst equation. The absorption data is treated according to the Nernst equation, assuming Beers Law,

at 430nm the equation for T= 298K is

$$E = E_1^0 + (0.059/n_1) \log ([5OCH_3NMI^{+n_1}]/[5OCH_3NMI^0])$$
$$E = E_1^0 + (0.059/n_1) \log \{[(\Delta Abs)_{max} - \Delta Abs] / \Delta Abs\} \quad (4.22)$$

At 850nm the equation is

$$E = E_2^0 + (0.059/n_3) \log ([5OCH_3NMI^{+n_2}]/[5OCH_3NMI^{+n_1}])$$
$$E = E_2^0 + (0.059/n_3) \log \{\Delta Abs / [(\Delta Abs)_{max} - \Delta Abs]\} \quad (4.23)$$

where E is the potential applied to the electrode,  $E_1^0$ ,  $E_2^0$  are the formal electrode potentials,  $n_1$  and  $n_3$  are the number of electrons transferred and  $5OCH_3NMI^0$ ,  $5OCH_3NMI^{+n_1}$ ,  $5OCH_3NMI^{+n_2}$ , correspond to the neutral monomer, partially oxidised monomer and the fully oxidised monomer respectively.  $\Delta Abs$  and  $(\Delta Abs)_{max}$  are defined as previously stated. Once again the contribution of counterions were omitted for convenience.

The Nernst plots of poly-5-methoxy-N-methylisindole at 430 nm and 850 nm, as determined by equation 4.22 and 4.23 respectively are shown in figure 4.22 and 4.23. As observed poly-N-methylisindole, the plots obtained are not linear, but linear regions are obtained in certain potential windows. From the slope and the intercept the n-values and the formal electrode potentials were obtained as  $n_1 = 0.42$ ,  $n_3 = 0.15$ ,  $E_1^0 = +0.003V$ , and  $E_2^0 = +0.19V$ . The fact that the  $n_1$  and  $n_3$  values are less than one implies that oxidation of poly-5-methoxy-N-methylisindole to form a radical cation or polaron occurs over

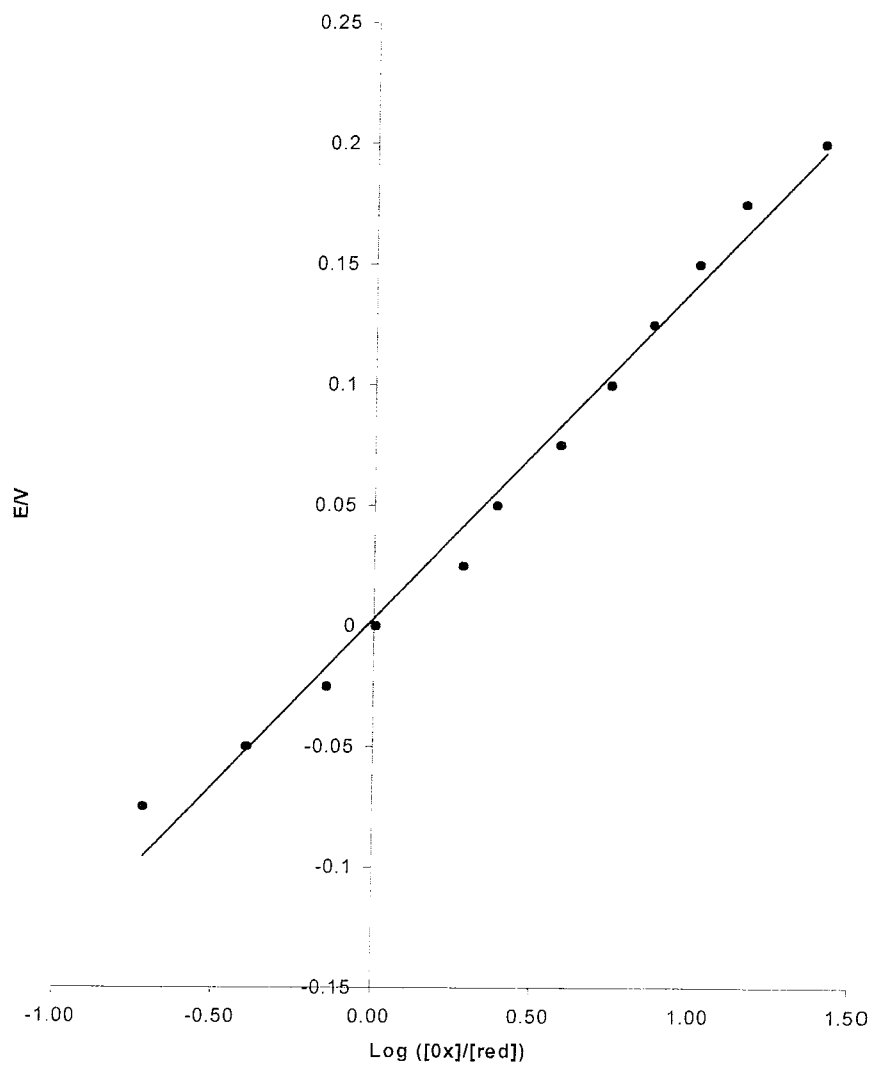


**Figure 4.22:** Nernst plot calculated from the absorbance at 430 nm for poly-5-methoxy-N-methylisoindole perchlorate in 0.1M LiClO<sub>4</sub> in CH<sub>3</sub>CN (vs SCE).

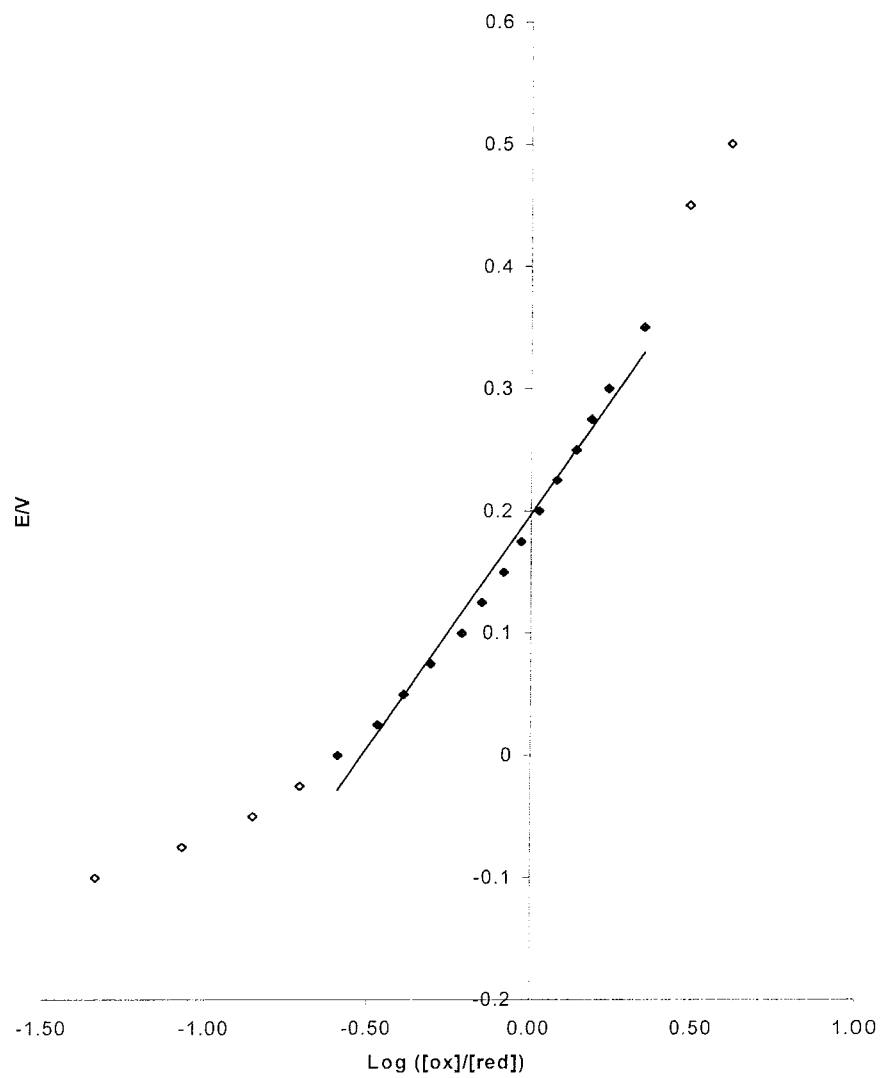


**Figure 4.23:** Nernst plot calculated from the absorbance at 850 nm for poly-5-methoxy-N-methylisindole perchlorate in 0.1M LiClO<sub>4</sub> in CH<sub>3</sub>CN (vs SCE).

many units of polymer, while further oxidation to form the dication or bipolaron again occurs over many units of polymer.  $E_1^0$  occurs at a lower a potential than that of  $E_2^0$  implying a greater ease oxidation of the neutral species (eqn. 4.19.) than oxidation of the radical cation (eqn. 4.20) species. What is also interesting is that  $|E_1^0 - E_2^0|$  is much greater than in the case of poly-N-methylisindole and therefore implies that K in eqn. 4.21 will also be greater.

The theoretical concentration profile of the three species contained within the layer of poly-5-methoxy-N-methylisindole were predicted using eqn 4.24, in the same way as with poly-N-methylisindole and using the same equations 4.8 to 4.16.

$$[5\text{OCH}_3\text{NMI}^0] + [5\text{OCH}_3\text{NMI}^{+n_1}] + [5\text{OCH}_3\text{NMI}^{+n_2}] = C \quad (4.24)$$

The predicted concentration profile for the three species was plotted as shown in figure 4.24. At low potentials the concentration of the neutral species is equal to C. As the applied potential is increased the concentration profile of the neutral species decreases as it becomes more oxidised, hence at the same time the concentration profile of the partially oxidised species increases to a maximum, which is approximately half the total concentration C and then falls back to zero as slightly oxidised polymer becomes fully oxidised. The concentration of the fully oxidised species goes from a zero level to a maximum equal to C, with a profile similar to that of the neutral species.

Figure 4.25 shows the plot of figure 4.21 in normalised form, and figure 4.26 shows the overlay of figures 4.24 and 4.25. What is interesting to note is that as with poly-N-methylisindole both the neutral species observed at 430 nm and the fully oxidised species at 850 nm have concentration profiles similar to the predicted profiles derived by equation 4.26. However the concentration profile of the partially oxidised species observed at 565 nm does not follow the predicted profile, again this is evident with the unsubstituted isindole.

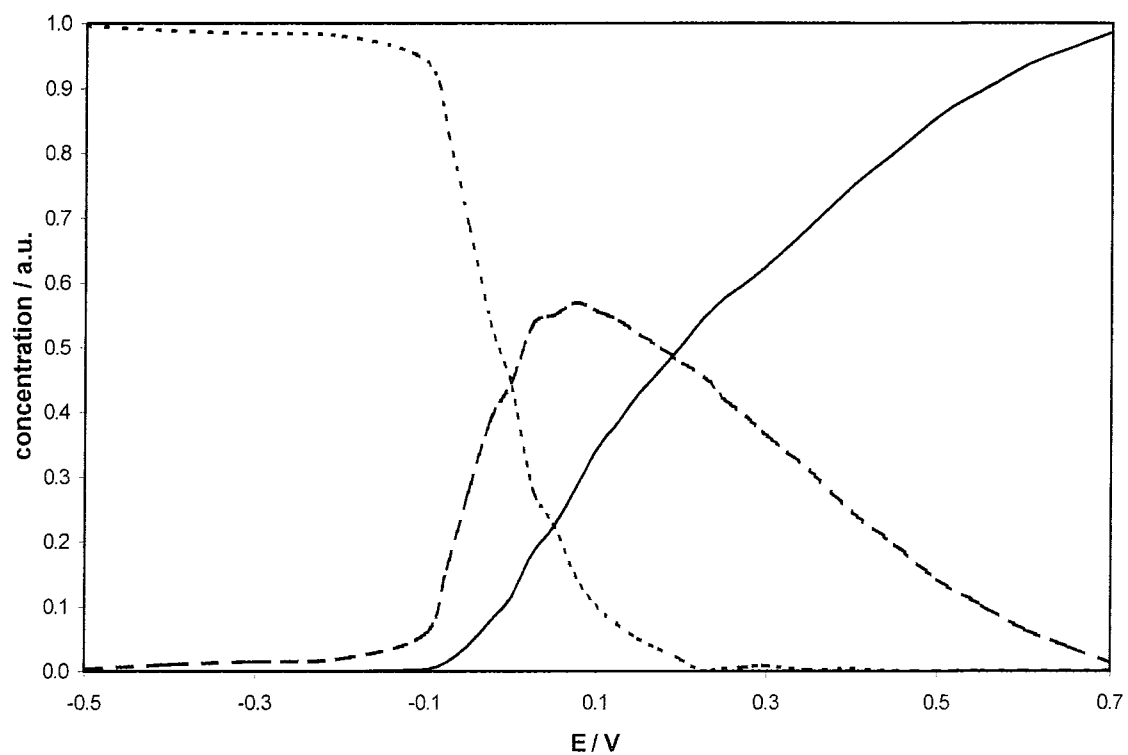


**Figure 4.24:** Predicted concentration profile of neutral form [·····], partially oxidised [ - - -] and fully oxidised [—] forms of poly-5-methoxy-N-methylisoindole as derived by eqn. 4.24.

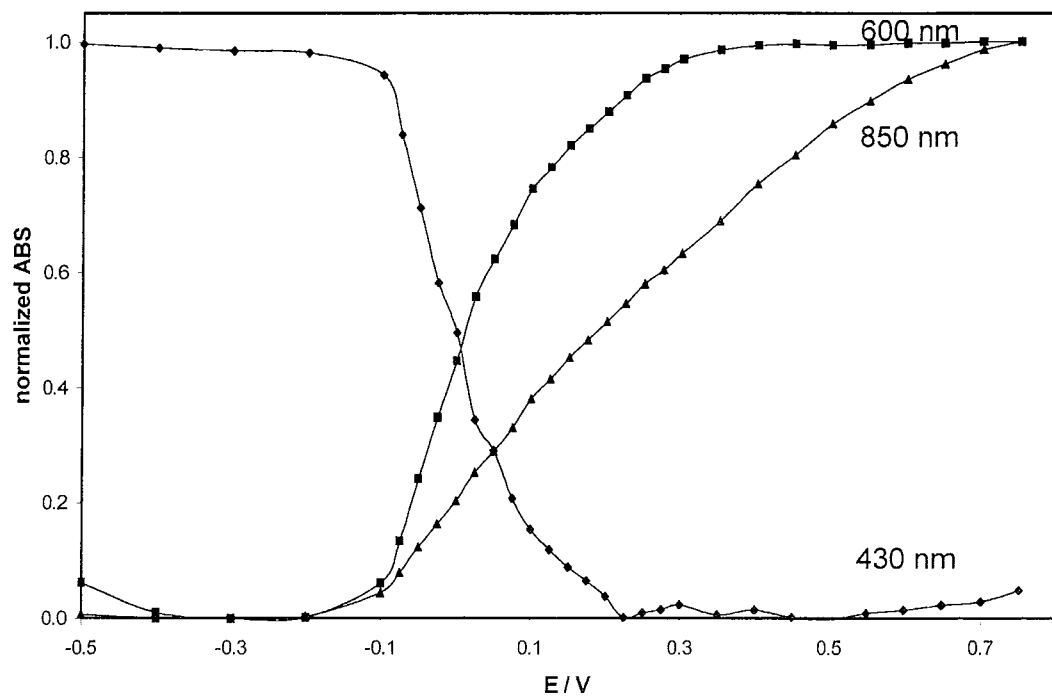


**Figure 4.25:** Plot of normalised absorption versus applied potential for a layer of poly-5-methoxy-N-methylisoindole at 430 nm, 565 nm and 850 nm.

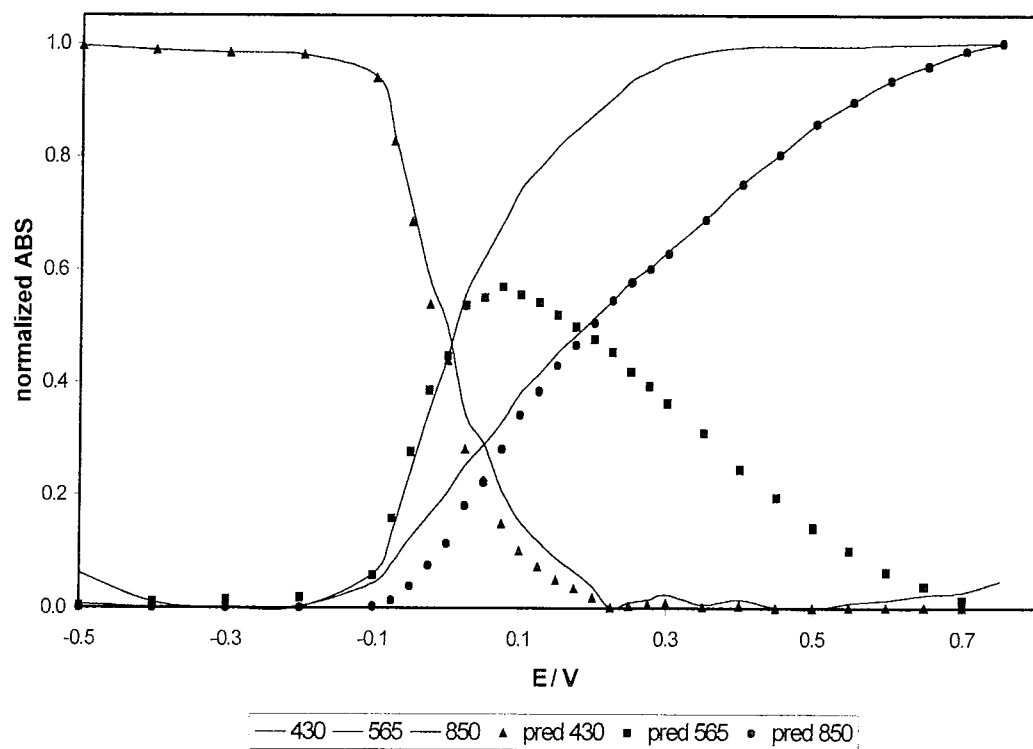


**Figure 4.26:** Overlay of predicted concentration profile (figure 4.24) and experimental concentration profile (figure 4.25).



Instead of partially oxidised species further oxidising to become fully oxidised as predicted by equation 4.25, the concentration profile remains steady. The data is very similar as the poly-N-methylisindole data, which leads to the same conclusion of the possibility that there is some kinetic factor, i.e.  $k_1$  is fast and  $k_2$  is slow. Again a the sluggish response to the concentration profile of the fully oxidised species could also be attributed to the of another redox mechanism occurring with the polymer layer involving a two-state transition, again with slow kinetics  $k_3$ , as depicted in equation 4.26.

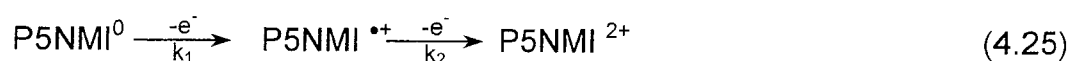
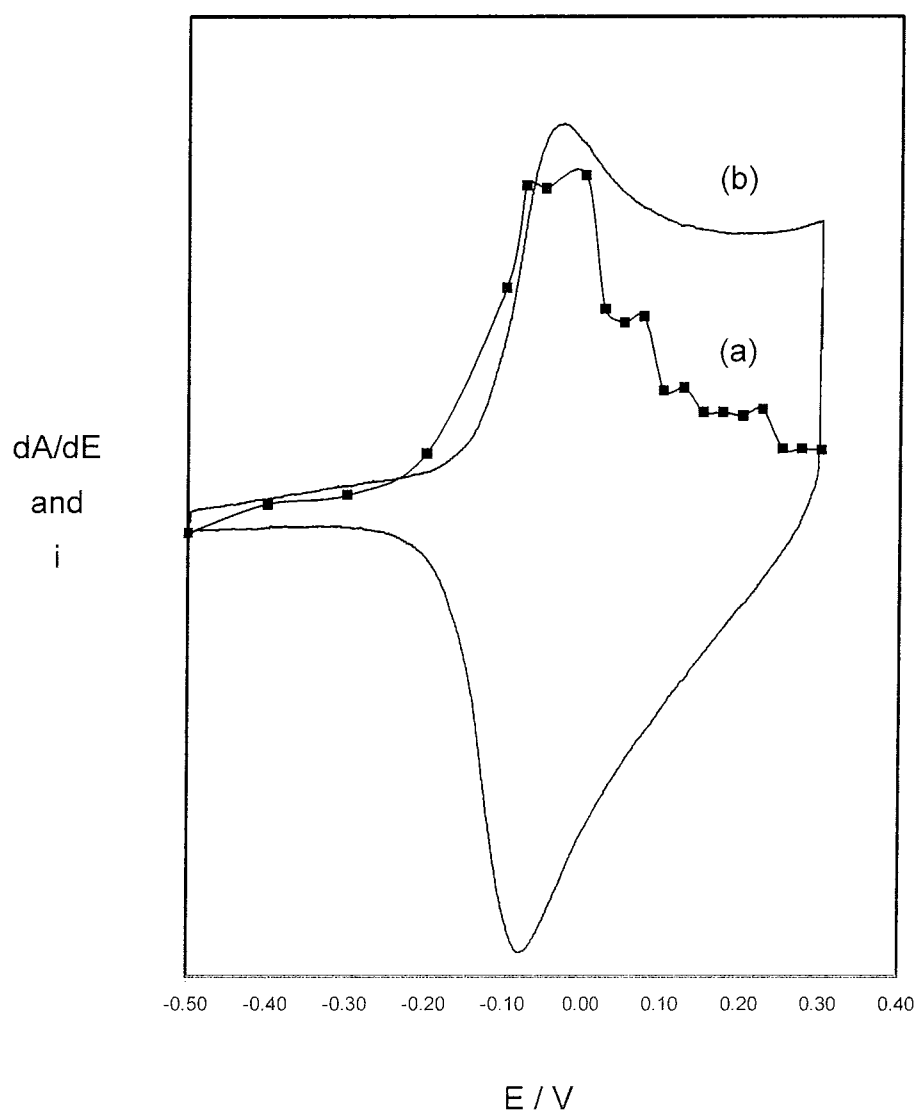


Figure 4.27 (a) shows a plot of the change in absorbance at 850nm with change in potential,  $dA/dE$ , against applied potential, and is the spectroscopic analogue of a cyclic voltammogram, figure 4.27 (b). The graph of current versus potential is representative of the total current, while the  $dA/dE$  versus E curve shows only the faradaic component of current. As can be seen from the superimposition of the two curves, there must be a large double-layer charging component as the current fails to decay back to zero after the peak. However as can be seen from figure 4.27 (b), the  $dA/dE$  vs E profile of the poly-5-methoxy-N-methylisindole drops off to zero, once again showing thin layer faradaic behaviour.



**Figure 4.27:** Plot of (a)  $dA/dE$  at 850nm versus potential and (b) cyclic voltammogram of [Pt] poly-5-methoxy-N-methylisindole in 0.1M  $\text{LiClO}_4$  in  $\text{CH}_3\text{CN}$  vs SCE.

#### 4.2.3 Spectroelectrochemistry of poly-5,6-dimethoxy-N-methylisindole

It was not possible to obtain a U.V.-vis absorption spectrum of a poly-5,6-dimethoxy-N-methylisindole perchlorate layer, as any layer formed was too thin, not visible to the naked eye and not detectable by the spectrometer. The experiment was repeated in p-toluene sulphonate, which from the electrochemical analysis carried out in Chapter 3, was known to give films with better mechanical strength. However, no spectroelectrochemical data of poly-5,6-dimethoxy-N-methylisindole p-toluene sulphonate was obtained either. In chapter 3, cyclic voltammetric studies of 5,6-dimethoxy-N-methylisindole in 0.1M p-toluene sulphonate produced a very thin polymeric film, not visible to the naked eye, along with green material oligomeric material observed streaming from the electrode surface. It was decided to record the spectral change, if any, poly-5,6-dimethoxy-N-methylisindole in the presence of monomer. By cycling between  $-0.5\text{V}$  and  $+0.75\text{V}$  at  $50\text{ mV/sec}$  a spectrum was recorded at  $-0.5\text{V}$ ,  $-0.05\text{V}$  (small peak due to oxidation of polymer),  $+0.3\text{V}$ ,  $+0.5\text{V}$  and  $0+75\text{V}$  (before, on and after monomer oxidation) on the forward sweep, and at  $-0.05\text{V}$  (peak due to polymer reduction) and  $-0.5\text{V}$  again. The spectra are seen in figure 4.28, and an absorption at  $450\text{ nm}$  ( $2.75\text{ eV}$ ) was observed for all spectra. This is not surprising considering the soluble nature of poly-5,6-dimethoxy-N-methylisindole. In the case of poly-N-methylisindole and poly-5-methoxy-N-methylisindole, spectra were recorded as the potential was increased in a stepwise fashion. The total concentration of polymeric material whether it was in a neutral or oxidised state remain constant, i.e. contained within the film. Therefore as the potential was increased the concentration of neutral polymer decreased resulting in a decrease in absorbance at  $430\text{ nm}$ . In this situation, the monomer is oxidised all the time and the polymeric material formed, the majority of it is diffusing away from the electrode surface before it can be oxidised further, as discussed in detail in Chapter 3.

As the potential was swept forward there was an increase in absorption at  $600\text{ nm}$  ( $2.07\text{ eV}$ ) and  $850\text{ nm}$  ( $1.46\text{ eV}$ ). This has been attributed to either oligomeric and/or polymeric material at the electrode surface long enough to

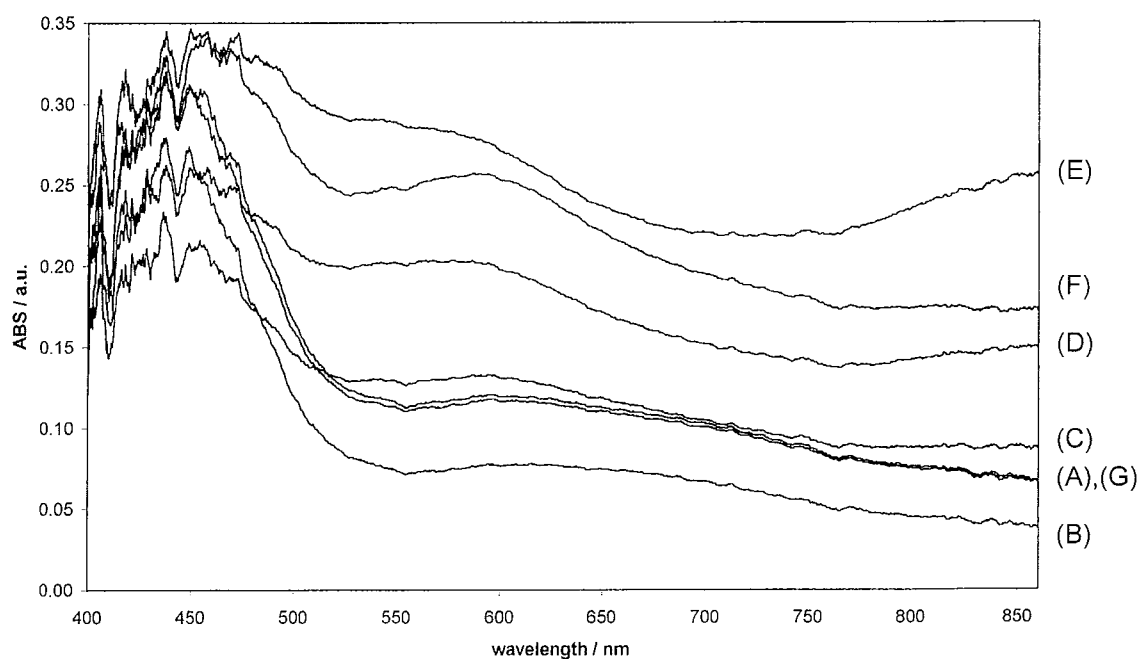


**Figure 4.28:** A series of absorption spectra of [Pt] poly-5,6-dimethoxy-N-methylisindole p-toluene sulphonate in 0.1M p-TsO<sup>-</sup> in CH<sub>3</sub>CN vs SCE, recorded while sweeping at 50 mV/sec forward at (A) -0.5V, (B) -0.05V, (C) +0.3V, (D) +0.5V, (E) +0.75V, and backward at (F) -0.05V and (G) -0.5V.

be oxidised leading to the formation of radical cations and dications. What is interesting to note is that the peak at 450 nm corresponding to valence band to conduction band transition of neutral poly-5,6-dimethoxy-N-methylisindole is of lower energy than that of poly-N-methylisindole and poly-5-methoxy-N-methylisindole. It was decided to determine the bandgap of neutral poly-5,6-dimethoxy-N-methylisindole using the graphical method [44]. The spectrum recorded at  $-0.5\text{V}$  corresponded to the neutral as the peaks at 600nm and 850 nm are at a minimum.

So again using the section of the spectra immediately to the right of the 450 nm peak to 550 nm and plotting the relative absorption intensity times  $h\nu$ , all raised to the power of 2 (direct) or  $\frac{1}{2}$  (indirect) versus  $h\nu$  can yield an estimation of the bandgap energy of neutral poly-5,6-dimethoxy-N-methylisindole. The straight line graph of the linear region between 430 nm and 510 nm corresponds to  $n=1$ , as shown in figure 4.29. This shows a direct interband transition. From the intercept on the abscissa a value for the bandgap energy of 2.38 eV was obtained. This is lower than the determined bandgap for poly-N-methylisindole but higher than poly-5-methoxy-N-methylisindole. However this result is somewhat in doubt as different experimental conditions, including a different electrolyte was used to calculate the bandgap of poly-5,6-dimethoxy-N-methylisindole.

A Nernstian analysis of the spectroelectrochemical data was not carried as with the other two polymers the assumption discussed in section 4.2.1, whereby only three species, neutral, partially oxidised (polarons) and fully oxidised (bipolarons) monomer, can exist in the film at a given potential, does not apply here.

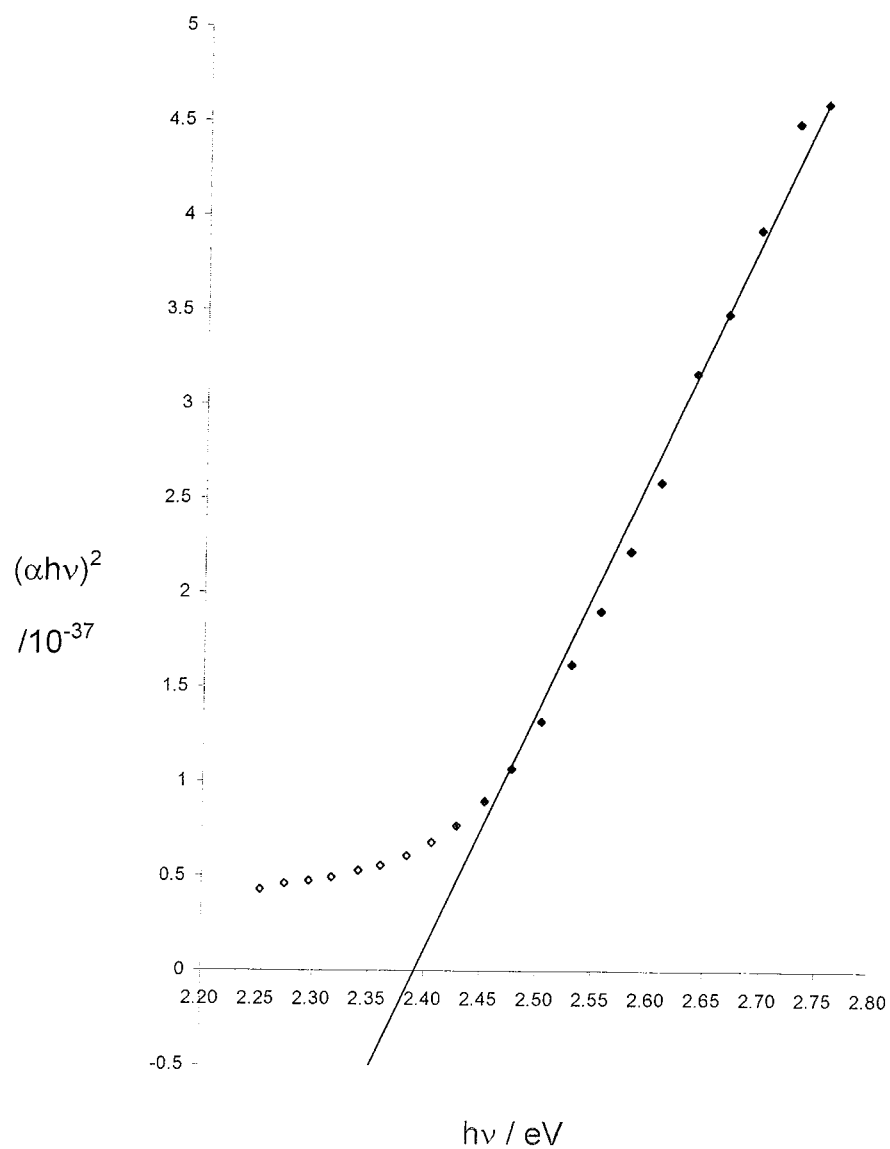


**Figure 4.29:** Plot of  $(\alpha h\nu)^2$  versus  $h\nu$  for [Pt] poly-5,6-dimethoxy-N-methylisindole in 0.1M p-TsO<sup>-</sup> in CH<sub>3</sub>CN (vs SCE) at a potential of -0.5 V. In order to determine bandgap

### 4.3 Conclusion

Using reflectance mode spectrometry, (the experimental arrangement which was designed and constructed in the lab), a detailed analysis of the spectroelectrochemistry of the three polymers, i.e. poly-N-methylisindole, poly-5-methoxy-N-methylisindole and poly-5,6-dimethoxy-N-methylisindole was carried out. The determination of the bandgap of the neutral polymers using the graphical method [44] showed that poly-5-methoxy-N-methylisindole had the lower at 2.36 eV, than poly-N-methylisindole at 2.42 eV. This has been attributed possibly to the to the electron donating effects of the methoxy group which leads to an increase in electron density along the polymer backbone. Unfortunately a bandgap of poly-5,6-dimethoxy-N-methylisindole was determined under different conditions, and while the bandgap value of 2.38 eV is between that of poly-N-methylisindole and poly-5-methoxy-N-methylisindole, it would be expected to be lower than the mono substituted polymer, as the presence of two methoxy groups would give an even greater electron density along the polymer backbone. An analysis of the spectroelectrochemical data using the Nernst equation, showed that for poly-N-methylisindole and poly-5-methoxy-N-methylisindole the  $n_1$  and  $n_3$  values are less than one. It was expected that both values would be equal, however in both cases  $n_1$  was greater than  $n_3$ . Again in both cases,  $E_1^0$  was lower than  $E_2^0$  indicating that oxidation of the neutral polymer was easier than the oxidation of the radical cation species.

An analysis of the concentration profile of neutral, partially oxidised and fully oxidised species of polymer has lead to the possibility of two redox mechanism occurring within the polymer layer. The first involves the oxidation of neutral polymer to radical cation and the further oxidation to dication. The second involves a direct 2-electron oxidation of neutral polymer to the dication. It is possible that both reaction mechanisms are occurring with in the polymer layer.

The inherent advantage of the experimental arrangement is that it allows for the simultaneous monitoring of absorption and current while changing the applied potential. From the curve of  $dA/dE$  versus applied potential, superimposed on the cyclic voltammetry of the polymer at platinum, one can clearly see double layer charging component of the cyclic voltammetric current, for both poly-N-methylisindole and poly-5-methoxy-N-methylisindole.

Finally, poly-5-methoxy-N-methylisindole which is a new conducting polymer, can be reversibly doped and undoped with the process accompanied by a high contrast electrochromic change, metallic gold in the reduced form and transparent in the oxidised form. This is the same electrochromic change observed with poly-N-methylisindole. It is this property of both polymers which leads to the greater potential for applications for these polymers.



#### 4.4 Experimental

Electrochemical experiments were carried out in a 50 cm<sup>3</sup> single compartment quartz cell using a three electrode configuration. A platinum disc, with an exposed surface area of 7.1 mm<sup>2</sup>, sealed in Teflon was employed as a working electrode. A glassy carbon rod was used as auxiliary electrode and all potentials are quoted with respect to a saturated calomel electrode (SCE). The working electrode was pretreated prior to each experiment by polishing with 0.3 µm alumina powder. The auxiliary and reference electrodes were washed thoroughly with deionised water and background electrolyte.

Potential control and current measurement was performed with a H.B. Thompson DGR16 waveform generator and an EG&G model 362 scanning potentiostat and voltammograms were recorded on a Bryans 60100 model X-Y recorder. The cyclic voltammograms were digitised using WinDIG 2.5.

The reflectance spectra of polymer films were examined *in-situ* in a single compartment cell using a three electrode configuration as shown in figure 4.30 and 4.31. The UV absorbance spectra were obtained with an Ocean Optics Inc, S2000 fibre optic spectrometer. The source is an Ocean Optics Inc, LS-1 tungsten halogen lamp. The distance between the working electrode and the probe assembly was approximately 1 cm.

Anhydrous acetonitrile was of HPLC grade (Aldrich) and dimethylformamide was reagent grade with further purification by distillation. Electrolyte salts (Aldrich, 99+%) were dried in the vacuum oven where necessary. Water was distilled and deionised. Before all experiments, the electrolyte solution was degassed gently with oxygen free nitrogen for approximately ten minutes and a background cyclic voltammogram was recorded to ensure purity. The species under examination was introduced to the cell by dissolving it in a small amount of degassed electrolyte and was added to the solution using a pasteur pipette. The solution was then further degassed for five minutes.

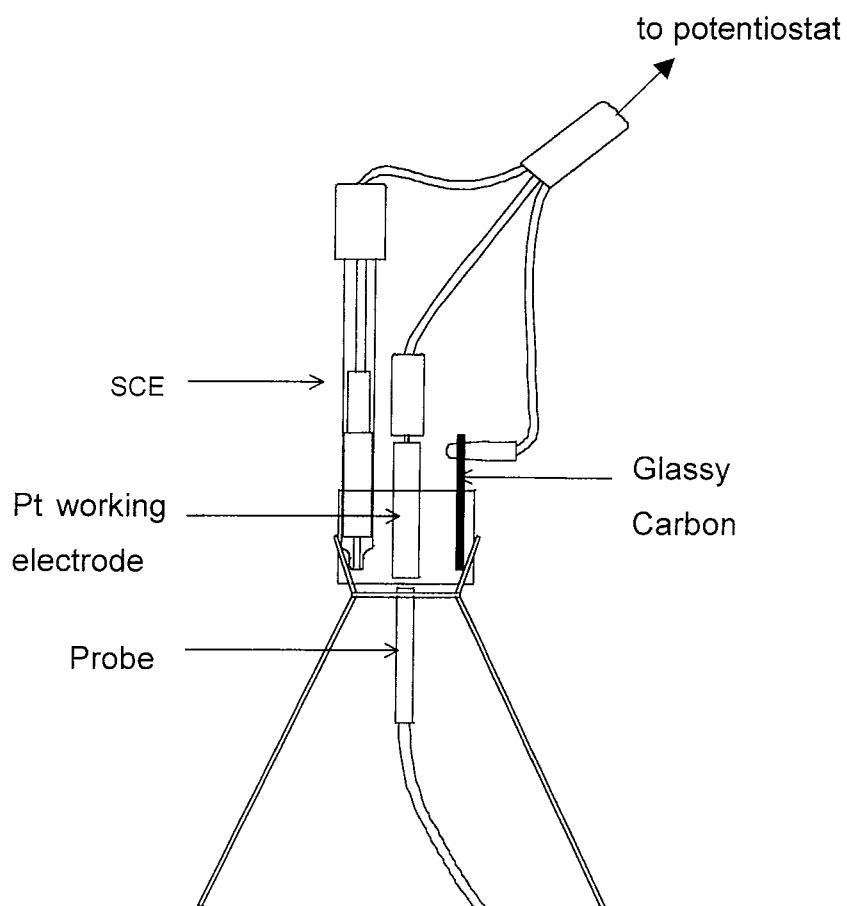


**Figure 4.30:** Schematic diagram of the experimental set-up used in reflectance mode spectroelectrochemistry.

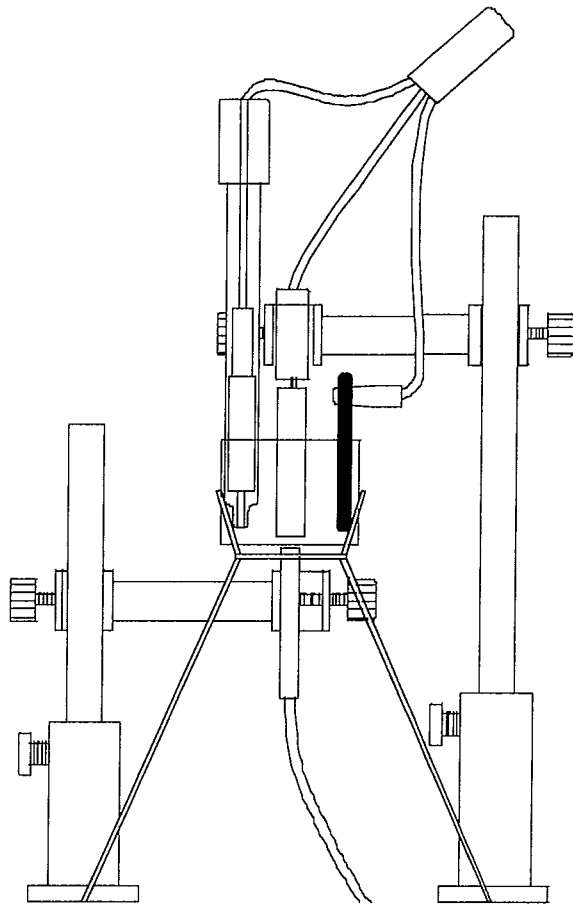


**Figure 4.31:** Full experiment assembly

A blanket of nitrogen was maintained over the solution throughout the experiment. The temperature for all experiments was ambient.

#### 4.4.1 Poly-*N*-methylisindole

A cell containing a freshly made solution of 0.1M LiClO<sub>4</sub> in anhydrous acetonitrile (10 cm<sup>3</sup>) was flushed with nitrogen and *N*-methylisindole (25mgs,  $1.9 \times 10^{-4}$  mole, 19 mM) was added as already outlined. A thin film was grown by electrochemically cycling the solution between the limits of –0.5V and +0.85V at a scan speed of 50 mV/sec for 8 cycles. The working electrode containing the layer was then removed and rinsed thoroughly with electrolyte and then placed in the spectroelectrochemical cell in fresh electrolyte solution; see figure 4.30, and aligned directly on top of the probe. A cyclic voltammogram was obtained between the limits of –0.5V and +0.5V at 50mV/sec. The potential of the working electrode was set at –0.5 V and a spectrum was recorded between 400 and 850 nm. The applied potential was first increased to –0.1V in intervals of 100mV and then increased to +0.5V in intervals of 25mV. During the application of each potential value the current was monitored and spectra were only recorded when current decreased to a steady state which took about 2 minutes. The cell was left undisturbed during the experiment.

#### 4.4.2 Poly-5-methoxy-*N*-methylisindole

As above, with 5-methoxy-*N*-methylisindole (15mgs,  $9.31 \times 10^{-5}$  mole, 9.3mM) film grown between –0.5V and +0.7V at 50 mV/sec for 12 cycles. After transferring to the spectroelectrochemical cell a cyclic voltammogram was obtained between the limits of –0.5V and +0.3V at 50mV/sec. The potential of the working electrode was set at –0.5 V and a spectrum was recorded between 400 and 850 nm. The applied potential was first increased to –0.1V in intervals of 100mV and then increased to +0.3V in intervals of 25mV. Finally the applied potential was increased to +0.75V in intervals of 50mV. During the application of each potential value the current was monitored and spectra were only recorded when current decreased to a

steady state which took about 2 minutes. The cell was left undisturbed during the experiment.

#### 4.4.3 *Poly-5,6-dimethoxy-N-methylisindole*

The spectroelectrochemical cell containing a freshly made solution of 0.1M  $(\text{Et})_4\text{N}(\text{O}_3\text{SC}_6\text{H}_4\text{CH}_3)$  in anhydrous acetonitrile ( $10 \text{ cm}^3$ ) was flushed with nitrogen and 5,6-dimethoxy-N-methylisindole (20mgs,  $1.04 \times 10^{-4}$  mole, 10mM) was added as already outlined. A cyclic voltammogram was obtained between the limits of  $-0.5\text{V}$  and  $+0.75\text{V}$  at 50mV/sec and spectra were recorded instantaneously at seven points along the cycle.

#### 4.5 References

- [1] A.J. Bard, L.R. Faulkner, *Electrochemical Methods, Fundamentals and Applications*, Wiley, New York, (1980), 577- 578.
- [2] R.J. Mortimer, *Chemical Society Reviews*, (1997), **26**, 147.
- [3] G. Zotti and G. Schiavon, *Synthetic Metals*, (1989), **30**, 151.
- [4] T. Amemeiya, K. Hashimoto, A. Fujishima and K. Itoh, *J. Electrochem. Soc.* (1991), **138**, 2854.
- [5] E. M. Peters and J.D. Van Dyke, *Journal of Polymer Science: Part A, Polymer Chemistry*, (1992), **30**, 1891.
- [6] M. Nechtschein, F. Devreux, F Genoud, E. Vieil, J.M. Pernaut and E. Genies, *Synth. Met.*, (1986), **15**, 59.
- [7] P. Marque and J. Roncali, *J. Phys. Chem.*, (1990), **94**, 8614.
- [8] H.A. El-Rahman, *Polymer International*, (1997), **44**, 481.
- [9] C.R. Martin and Zhiahua Cai, *J. Electroanal. Chem.*, (1991), **300**, 35.
- [10] P.M. Penner, L.S. Van Dyke, C.R. Martin, *J. Phys. Chem.*, (1988), **92**, 5274.
- [11] P.M. Penner and C.R. Martin, *J. Phys. Chem.*, (1989), **93**, 984.
- [12] C.E.D. Chidsey, R.W. Murray, *Science (Washington D.C.)*, (1986), **231**, 25.
- [13] M. Kalaji and L.M. Peter, *J. Chem. Soc., Faraday Trans.*, (1991), **87** (6), 853.
- [14] G.B. Street, T.C. Clarke, M. Kroumbi, K. Kanazawa, V. Lee, P. Pfluger, J.C. Scott and G.B. Weisser, *Mol. Cryst. Liq. Cryst*, (1982), **83**, 253.
- [15] K. Yakushi, L.J. Lauchlan, T.C. Clarke and G.B. Street, *J. Chem. Phys.*, (1983), **79**, 4774.
- [16] J.L. Bredas, J.C. Scott, K. Yakushi and G.B. Street, *Phys. Rev. B*, (1984), **30**, 1023.
- [17] E.M. Genies and J-M. Pernaut, *J. Electroanal. Chem.*, (1985), **191**, 111.
- [18] Y. Tezuke, K. Aoki and K. Shinozaki, *Synth. Met.*, (1989), **30**, 369.
- [19] Y. Son and K. Rajeshwar, *J. Chem. Soc. Faraday Trans.*, (1992), **88**(4), 605.
- [20] P. Rapta, A. Neudeck, A. Petr and L. Dunsch, *J. Chem. Soc. Faraday Trans.*, (1998), **94**, 3625.

- [21] T.F. Otero and M. Bengoechea, *Langmuir*, (1999), **15**, 1323.
- [22] A. Neudeck, A. Petr and L. Dunsch, *J. Phys. Chem.*, (1999), **103**, 912.
- [23] G. Grem, G. Leditzky, B. Ullrich, and G. Leising, *Synth. Met.*, (1992), **51**, 383.
- [24] G. Grem, G. Leditzky, B. Ullrich, and G. Leising, *Adv. Mater.*, (1992), **36**, 4.
- [25] K. Yoshino, T. Takiguchi, S. Hayashi, D. H. Park, and R. Sugimoto, *Jpn. J. Appl. Phys.* (1986) **25**, 881.
- [26] J. Obrzut and F. E. Karasz, *J. Chem. Phys.* (1987) **87**, 2349.
- [27] M. Sato, S. Tanaka, and K. Kaeriyama, *Synth. Met.* (1986) **14**, 279.
- [28] T. C. Chung, J. H. Kaufman, A. J. Heeger, and F. Wudl, *Phys. Rev. B* (1984) **30**, 702.
- [29] M. Pomerantz, *Handbook of Conducting Polymers 2<sup>nd</sup> Ed*, (T.A. Skotheim, R.L. Elsenbaumer, and J.R. Reynolds Eds.), Marcel Dekker, New York, (1998), 278.
- [30] F. Wudl, M. Kobayashi, and A.J. Heeger, *J. Org. Chem.*, (198), **49**, 3382.
- [31] A.K. Bakhshi and J. Ladik, *Solid State Commun.*, (1987), **61**, 71.
- [32] J.D. Stenger Smith, *Chem. Eng. News*, (1991), **69**, 3.
- [33] M. Dietrich and J. Heinze, *Synth. Met.* (1991), **41-43**,
- [34] F. Wudl, A.J. Heeger, Y. Ikenoue, and M. Kobayashi, *Eur. Patent Appl.* (1988) 0 273 643.
- [35] Y. Ikenoue, F. Wudl and A.J. Heeger, *Synth. Met.*, (1991), **40**, 1.
- [36] T-T Hung and S-A Chen, *Polymer*, (1999), **40**, 3881.
- [37] J. Pranata, R.H. Grubbs and D.A. Dougherty, *J. Am. Chem. Soc.*, (1988), **110**, 3430.
- [38] Y.S. Lee, H. S-W. Hu and O.-K Kim, *Mol. Cryst. Liq. Cryst.*, (1990), **190**, 9.
- [39] N.M Hanly, D. Bloor, A.P. Monkman, R. Bonnett and J.M Ribo, *Synth. Met.*, (1993), **60**, 195-198.
- [40] S.B. Rhee, M-H. Lee, B.S. Moon and Y. Kang, *Korea Polym. J.*, (1993), **1**, No.1, 61-68.
- [41] Y. Ding and A.S. Hay, *J. Polymer Science: Part A: Polymer Chemistry*, (1999), **37**,(16), 3293.

- [42] S. Gauvin, F. Santerre, J.P. Dodelet, Y. Ding, A.R. Hill, A.S. Hay, J. Anderson, N.R. Armstrong, T.C. Gorjanc, and M. D'Lorio, *Thin Solid Films*, (1999), **353**, 218.
- [43] F. Li and W.J. Albery, *J. Chem. Soc. Faraday Trans.*, (1991), **87**, 151.
- [44] D. Blackwood and M. Josowicz, *J. Phys. Chem.*, (1991), **95**, 493.
- [45] Yu. V. Pleskov, Yu. Ya. Gurevick, *Semiconductor Photoelectrochemistry*; Bartlett, P.N.; (translated from Russian), Plenum: New York, (1986).



## **Chapter 5**

### **An Electrochemical Study of Ion Exchange behaviour of Conducting Polymer films.**

## Chapter 5 – An Electrochemical Study of Ion Exchange Behaviour of Conducting Polymer films.

### 5.1 *Introduction*

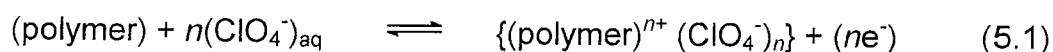
The earliest reported application of intrinsically conducting polymers has been the use of free-standing polymers as sensor devices [1]. These sensors, namely polyacetylene [2] were designed to detect and measure levels of “doping” within the same material upon exposure to vapour-phase dopants. These early experiments concentrated on investigating the doping mechanism of polyacetylene, but served to inspire the early pursuit of research into sensor applications of conducting polymers [1]. The versatility of conducting polymers resides in the inherent ability of these materials to undergo a wide range of molecular interactions that have the potential to be “engineered” into the material during synthesis [1]. The extent of the interaction may be controlled after synthesis, in-situ, using simple electrical stimuli. This capacity coupled with the fact that such interactions are intimately involved in determining electrical properties of conducting polymers provides the basis for a powerful sensor technology.

Chemical and biological sensors using conducting polymers are generally formed from films of the polymers fabricated on a pattern of metal or semiconductor electrodes, and are classified as electrochemical sensors [1]. Such sensors have the advantage of relatively low cost and simplicity with such sensors being miniaturised. The output signal from electrochemical sensors is readily converted to an easily interpretable form using microelectronics and computer technology. Thus specialised personnel are not necessarily required for their use. Conducting polymers have been used as modified electrode sensors, using electrochemical techniques such as potentiometry, amperometry, conductimetry and voltammetry [1].

Using potentiometry, for example, the conducting polymer serves as a sensing membrane and the signal results from changes in the open-circuit potential of the polymer modified electrode [1]. These changes result from

the (i) shifts in the dopant anion equilibrium within the polymer film, modulated by the concentration of dopant anion in the test solution, (ii) ion-exchange processes with other anion within the test solution, (iii) redox equilibria at the underlying metal electrode, and (iv) further redox reactions of the polymer membrane leading to a change in its redox composition. Hence in studying conducting polymers, as well as the redox activity, it can be beneficial to include a study of the ion exchange behaviour. From this it is possible to obtain an insight into the redox mechanistic properties of the polymer, leading to possible application in sensor technology.

The redox nature of conducting polymers can be summarised as the following oxidation/reduction equilibrium:



The application of positive potential to a neutral polymer film promotes the departure of electrons from the polymer chains. Counter ions have to penetrate from the solution through the solid polymer to compensate the generated positive charges, retaining electroneutrality [3]. Although it is clear that this counter ion insertion is not comparable to the classical doping of typical semiconductors, in electrochemical terminology the redox reaction is also called doping. Otherwise, electrochemical oxidation is accompanied by an important change in free volume related to the swelling of the polymeric entanglement, facilitated by electro-static repulsions between positive charges appearing in neighbouring chain, which can be transformed into a macroscopic movement by construction of a electrochemomechanical device [4]. In this way, channels are opened allowing counter ions to penetrate into the solid polymer [5]. Opposite processes occur during reduction, whereby electrons are injected into the polymer, counter ions are expelled in to the solution and the polymer network close again. Therefore electrochemical switching leads to ion movement and the mechanism of ionic charge depends on whether the polymer is in its electronically insulating or conductive states [6,7].

When the polymer is electronically conductive, charge transport may occur uniformly throughout the bulk of the polymer phase via a capacitive-like mechanism [8]. In contrast, when insulating charge is injected at the film surface and is then transported into the bulk solution via a diffusion process. There is still some confusion as to whether the polymer redox reaction begins at the polymer/electrode interface or at the polymer/solution interface [9,10]. Probably, this will depend in the degree of compacting of the polymeric entanglement attained during reduction or on the counterion size. One can appreciate difficulty since when the layer is neutral, charge is injected at the layer / electrode side. However, the electrolyte is at the layer / solution side.

Some applications of polypyrrole, such as drug delivery devices, require specific ion transport. Control of the ion transport process requires determination of the identity of the mobile ion, which is complicated by the fact that there are several ions present in the system. Moreover, Shimidzu *et al.* [11,12] demonstrated that ion transport in polypyrrole can be modified by the use of polymeric anions as dopants. Miller *et al.* [13] proved that the electrochemical switching of polypyrrole could achieve controlled release of a small anion such as  $\text{ClO}_4^-$ , while the incorporation of an immobile polyanion such as polystyrene sulfonate resulted in cation specific transport. The latter polyanion becomes trapped within the polypyrrole matrix due to its large size, and perhaps more importantly its entanglement with the polypyrrole chains. This incorporation, in this manner, increases the stability and the mechanical strength of polypyrrole and improves electrical conductivity and electroactivity [14,15]. In this work, the electrochemical behaviour of poly-N-methylisindole, poly-5-methoxy-N-methylisindole and poly-5,6-dimethoxy-N-methylisindole formed in lithium perchlorate was observed in fresh background electrolyte of tetraethylammonium-p-toluene sulphonate. Also, the effect of background electrolyte concentration was studied in an effort to afford data on the ion exchange behaviour of the polymer films. To date, no such studies have been reported for poly-N-methylisindole, and since poly-5-methoxy-N-methylisindole and poly-5,6-dimethoxy-N-methylisindole are new polymers, the work carried out here is novel.

## 5.2 Results and Discussion

### 5.2.1 Ion Exchange studies of poly-N-methylisindole

Figure 5.1 shows the cyclic voltammetry of a thin film of poly-N-methylisindole perchlorate, with the first sweep (a), recorded in 0.1M LiClO<sub>4</sub> in CH<sub>3</sub>CN. Subsequent sweeps (b), (c), and (d) were recorded in 0.1M (Et)<sub>4</sub>N(O<sub>3</sub>SC<sub>6</sub>H<sub>4</sub>CH<sub>3</sub>) in CH<sub>3</sub>CN. The cyclic voltammogram (a) showed an anodic peak potential  $E_{pa}$  of +0.06V and cathodic peak potential  $E_{pc}$  of -0.01V (vs SCE). The  $|E_{pa} - E_{pc}|$  or  $\Delta E$  of 70mV does not by itself indicate thin layer behaviour. However, the similar peak height and symmetry does indicate that the layer behaves with resistance or slow kinetics. The second cyclic voltammogram (b) corresponds to the first sweep of poly-N-methylisindole perchlorate in 0.1M (Et)<sub>4</sub>N(O<sub>3</sub>SC<sub>6</sub>H<sub>4</sub>CH<sub>3</sub>). A positive shift in both the  $E_{pa}$  and  $E_{pc}$  was observed, to +0.18 V and +0.08 V (vs SCE) respectively. This shift in the  $E_{pa}$  of 120mV for the same polymer layer would suggest that the movement of the larger p-toluene sulphonate anion in and out of the polymer matrix was slightly more difficult. A similar result was observed with polypyrrole [16]. The  $E_{pa}$  of polypyrrole on a perchlorate aqueous solution was higher than in Cl<sup>-</sup> indicating that polypyrrole in a ClO<sub>4</sub><sup>-</sup> solution is slightly more difficult to oxidise. This was attributed to the larger ionic size of the perchlorate ion, which reduces the anion mobility in the polymer. Also the peak current is smaller in the p-toluene sulphonate indicating that the polymer oxidises and reduces to a lesser degree.

The  $\Delta E$  for sweep (b) also increased from 70 mV to 100mV again indicating the difficulty of the p-toluene sulphonate ion movement. Subsequent sweeps (c) and (d) showed that the  $E_{pa}$  had shifted slightly less positive than sweep (b) and remained constant at +0.15V (vs SCE). With the layer already introduced to the new electrolyte, movement of p-toluene sulphonate anion is slightly easier than in the initial sweep. Also the  $\Delta E$  for sweeps (c) and (d) are lower than that of (b) at 80 mV again indicating greater ease of movement of the anion. However, even with poly-N-methylisindole

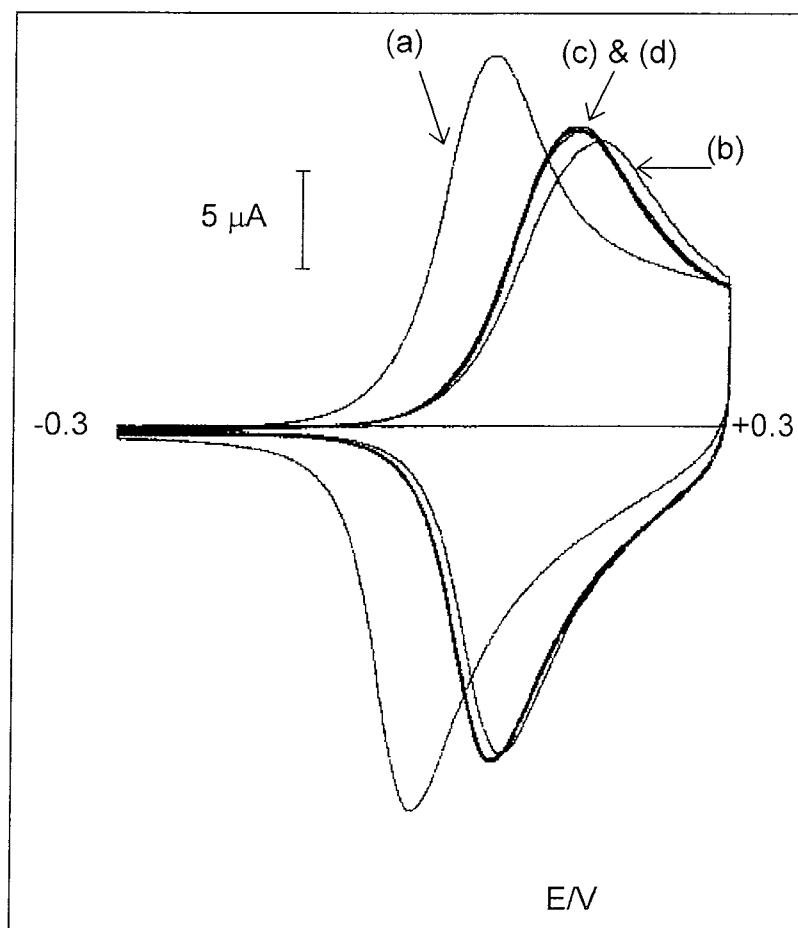


**Figure 5.1:** Cyclic voltammograms of [Pt] poly -N-methylisindole perchlorate in (a) 0.1M LiClO<sub>4</sub>, (b) 1<sup>st</sup> sweep in 0.1M (Et)<sub>4</sub>N(O<sub>3</sub>SC<sub>6</sub>H<sub>4</sub>CH<sub>3</sub>), (c) 2<sup>nd</sup> in 0.1M (Et)<sub>4</sub>N(O<sub>3</sub>SC<sub>6</sub>H<sub>4</sub>CH<sub>3</sub>) and (d) 3<sup>rd</sup> in 0.1M (Et)<sub>4</sub>N(O<sub>3</sub>SC<sub>6</sub>H<sub>4</sub>CH<sub>3</sub>) in CH<sub>3</sub>CN at scan speed of 50 mV/sec.

accommodating the new electrolyte environment, the smaller perchlorate anion has greater ease of movement with a considerable lower anodic peak potential, than the larger p-toluene sulphonate anion. One inherent assumption is that the cation does not play a role. However, the differences in the cyclic voltammograms could be due to contributions from different levels of ion pairing depending on the cation.

### 5.2.2 Ion Exchange studies of poly-5-methoxy-N-methylisindole

The ion exchange behaviour of poly-5-methoxy-N-methylisindole was very similar to that of poly-N-methylisindole. Figure 5.2 shows the cyclic voltammogram of poly-5-methoxy-N-methylisindole perchlorate recorded in 0.1M LiClO<sub>4</sub> in CH<sub>3</sub>CN, sweep (a), and sweeps (b), (c) and (d) were recorded in 0.1M (Et)<sub>4</sub>N(O<sub>3</sub>SC<sub>6</sub>H<sub>4</sub>CH<sub>3</sub>) in CH<sub>3</sub>CN. Sweep (a) showed E<sub>pa</sub> and E<sub>pc</sub> of -0.03V and -0.08V (vs SCE) respectively, which corresponds to a ΔE of 50mV, which again indicated thin layer behaviour. Sweep (b) corresponds to the first sweep of poly-5-methoxy-N-methylisindole perchlorate in 0.1M (Et)<sub>4</sub>N(O<sub>3</sub>SC<sub>6</sub>H<sub>4</sub>CH<sub>3</sub>). As with poly-N-methylisindole a positive shift was observed in both the E<sub>pa</sub> and E<sub>pc</sub>, to +0.08 V and +0.01 V (vs SCE) respectively. This corresponded to a shift in E<sub>pa</sub> of 110 mV, which was remarkably similar to the initial shift in E<sub>pa</sub> of poly-N-methylisindole and again would suggest the movement of the larger p-toluene sulphonate anion is more difficult than that of the perchlorate anion. Also the ΔE for sweep (b) is 70 mV again considerably higher than that of poly-5-methoxy-N-methylisindole in 0.1M LiClO<sub>4</sub>. The behaviour of subsequent sweeps (c) and (d) was again similar to that of poly-N-methylisindole, where the E<sub>pa</sub> had shifted slightly less positive than sweep (b) and remained constant at +0.06V (vs SCE). The movement of anions behaved in the same way in both the unsubstituted and mono methoxy substituted systems, whereby the larger p-toluene sulphonate anion was less mobile the smaller perchlorate anion.

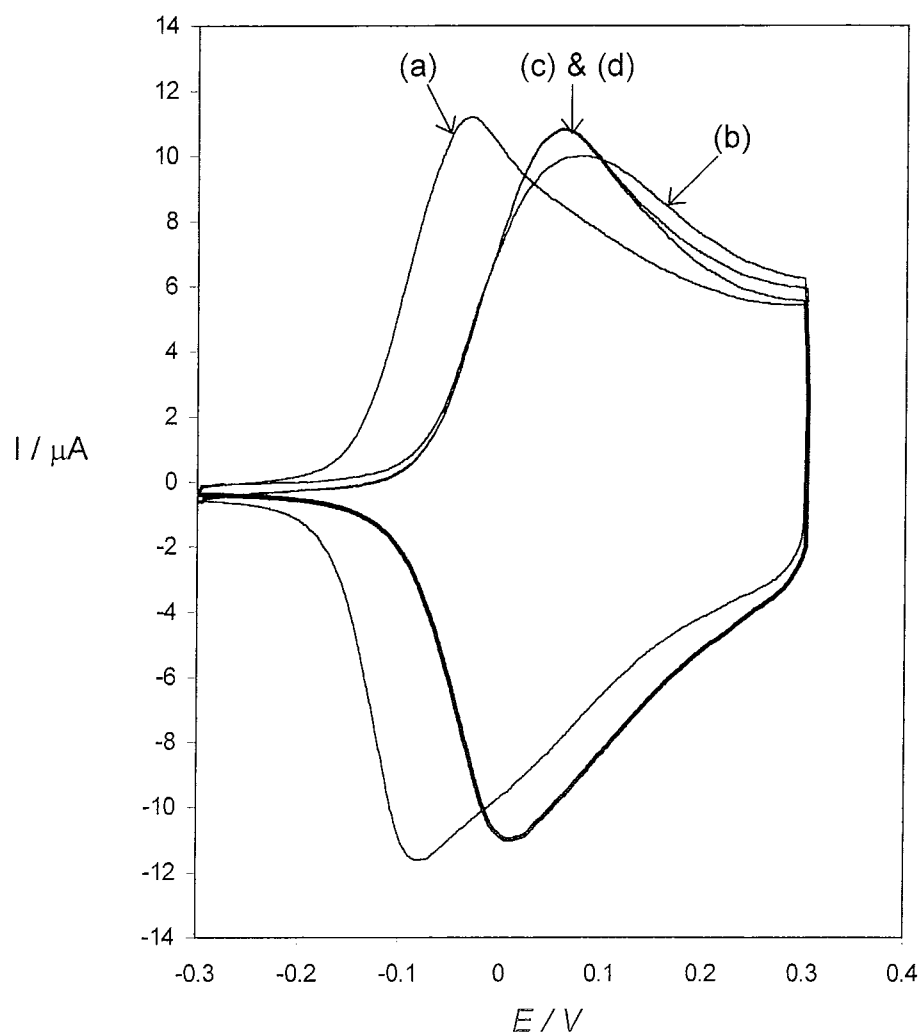


**Figure 5.2:** Cyclic voltammograms of [Pt] poly-5-methoxy-N-methylisoidole perchlorate in (a) 0.1M  $\text{LiClO}_4$ , (b) 1<sup>st</sup> sweep in 0.1M  $(\text{Et})_4\text{N}(\text{O}_3\text{SC}_6\text{H}_4\text{CH}_3)$ , (c) 2<sup>nd</sup> in 0.1M  $(\text{Et})_4\text{N}(\text{O}_3\text{SC}_6\text{H}_4\text{CH}_3)$  and (d) 3<sup>rd</sup> in 0.1M  $(\text{Et})_4\text{N}(\text{O}_3\text{SC}_6\text{H}_4\text{CH}_3)$  in  $\text{CH}_3\text{CN}$  at scan speed of 50 mV/sec.



### 5.2.3 Ion Exchange studies of poly-5,6-dimethoxy-N-methylisindole

Obtaining ion exchange data for a thin film of poly-5,6-dimethoxy-N-methylisindole proved quite difficult. As with the preliminary electrochemical experiments discussed in chapter 4, any film of poly-5,6-dimethoxy-N-methylisindole was very thin and not visible to the electrode surface. However figure 5.3 shows a somewhat different behaviour to that of poly-N-methylisindole and poly-5-methoxy-N-methylisindole.

Sweep (a) corresponds to poly-5,6-dimethoxy-N-methylisindole perchlorate in 0.1M LiClO<sub>4</sub> in CH<sub>3</sub>CN and shows a broad E<sub>pa</sub> peak at - 0.1V and an E<sub>pc</sub> at -0.13 V (vs SCE). The ΔE of 30mV confirmed a very thin layer of polymer on the electrode. However this is not accurate value since the anodic peak is not clear. On introducing poly-5,6-dimethoxy-N-methylisindole perchlorate to 0.1M (Et)<sub>4</sub>N(O<sub>3</sub>SC<sub>6</sub>H<sub>4</sub>CH<sub>3</sub>) in CH<sub>3</sub>CN the E<sub>pa</sub> peak shifts 98 mV positive to just below the potential limit to -0.02 V (vs SCE), which is consistent with the other two polymers. However, subsequent sweeps in 0.1M (Et)<sub>4</sub>N(O<sub>3</sub>SC<sub>6</sub>H<sub>4</sub>CH<sub>3</sub>) showed the anodic and cathodic current responses decreased slightly and while not observable for the E<sub>pa</sub>, the E<sub>pc</sub> increased until it reached a constant value after approximately eleven sweeps. This behaviour is quite different from that of poly-N-methylisindole and poly-5-methoxy-N-methylisindole where the E<sub>pa</sub> and E<sub>pc</sub> remained unchanged and then current response remained constant after three sweeps. The value of these results are that there is evidence of poly-5,6-dimethoxy-N-methylisindole layer formed on the electrode and that the peaks are not due to the presence of impurities.

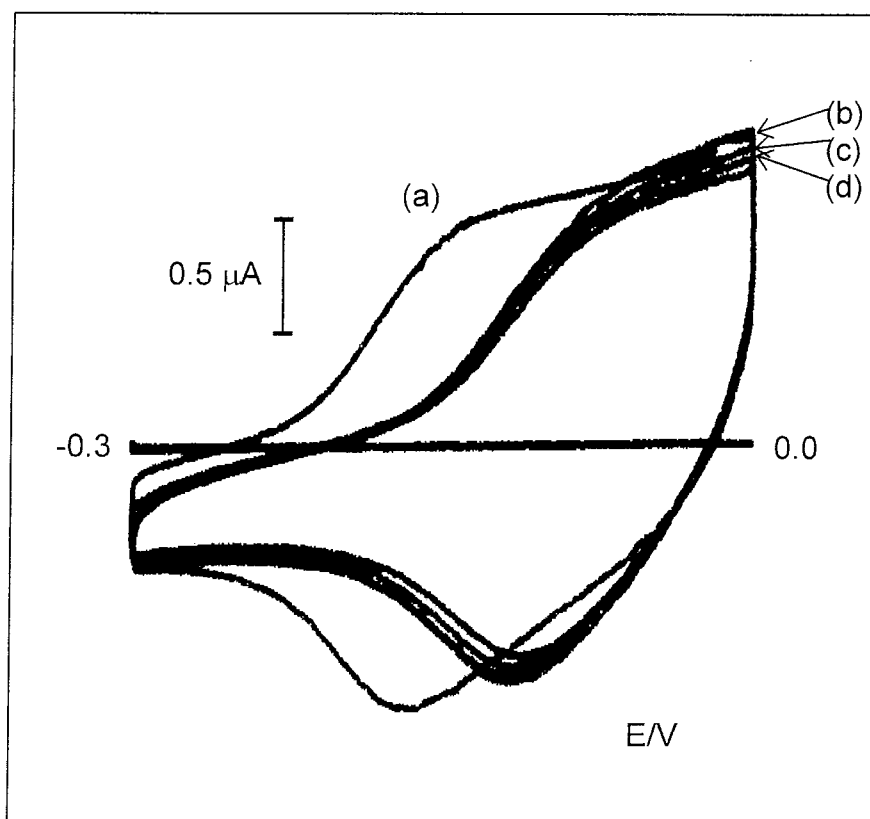


**Figure 5.3:** Cyclic voltammograms of [Pt] poly-5,6-dimethoxy-N-methylisindole perchlorate in (a) 0.1M LiClO<sub>4</sub>, (b) 1<sup>st</sup> sweep in 0.1M (Et)<sub>4</sub>N(O<sub>3</sub>SC<sub>6</sub>H<sub>4</sub>CH<sub>3</sub>), (c) 2<sup>nd</sup> in 0.1M (Et)<sub>4</sub>N(O<sub>3</sub>SC<sub>6</sub>H<sub>4</sub>CH<sub>3</sub>) and (d) 3<sup>rd</sup> in 0.1M (Et)<sub>4</sub>N(O<sub>3</sub>SC<sub>6</sub>H<sub>4</sub>CH<sub>3</sub>) in CH<sub>3</sub>CN at scan speed of 50 mV/sec.

#### 5.2.4 Ion Concentration Study of Polymers

The effects of changing the concentration of background electrolyte on the voltammetry of the polymers is shown in figures 5.4 – 5.6. A thin film of polymer was formed in a 0.1M LiClO<sub>4</sub> in CH<sub>3</sub>CN, and then removed and rinsed thoroughly with electrolyte. Following this, a “breaking in” process was carried out by placing the layer in 0.05M LiClO<sub>4</sub> solution and cycled until a steady state was obtained, then one cyclic voltammogram was recorded. This process was repeated with the same layer in 0.125M, 0.25M, 0.5M, and 0.75M LiClO<sub>4</sub> electrolyte solution.

Figure 5.4 shows the cyclic voltammogram of poly-N-methylisindole perchlorate in (a) 0.05M and (b) 0.75M LiClO<sub>4</sub> in CH<sub>3</sub>CN. The difference in the voltammetry was clear with a 98mV shift in the anodic peak potential  $E_{pa}$  from 0.1V to 0.02V upon increasing the background electrolyte concentration. The change in the cathodic peak  $E_{pc}$  was 100mV from +0.03V to -0.07V. A similar behaviour was observed with poly-5-methoxy-N-methylisindole perchlorate as shown in figure 5.5. The change in  $E_{pa}$  was again 100mV from 0.0V to -0.1V and the shift in  $E_{pc}$  was 90mV from -0.07V to -0.16V.

The experiment was repeated for poly-5,6-dimethoxy-N-methylisindole, as shown in figure 5.6, and as with other cyclic voltammetry observed with this polymer the anodic peak was considerably broader than the cathodic peak. However, a shift of 60mV in the  $E_{pa}$  was observed from -0.11V to -0.17V, and a shift of 60mV in the  $E_{pc}$  from -0.15V to -0.21V.

A similar method was used by Breen et al [17], to study the effect of cation concentration on a layer of polypyrrole incorporating [Fe(CN)<sub>6</sub>]<sup>4-</sup> as an anion. In this work cyclic voltammetry was used to oxidise and reduce the incorporated molecule causing the injection ejection of cations, and hence the electrochemistry of the [Fe(CN)<sub>6</sub>]<sup>4-</sup> was under study. In the work carried out here it is the layer of polymer that is undergoing oxidation and reduction, rather than a probe molecule.

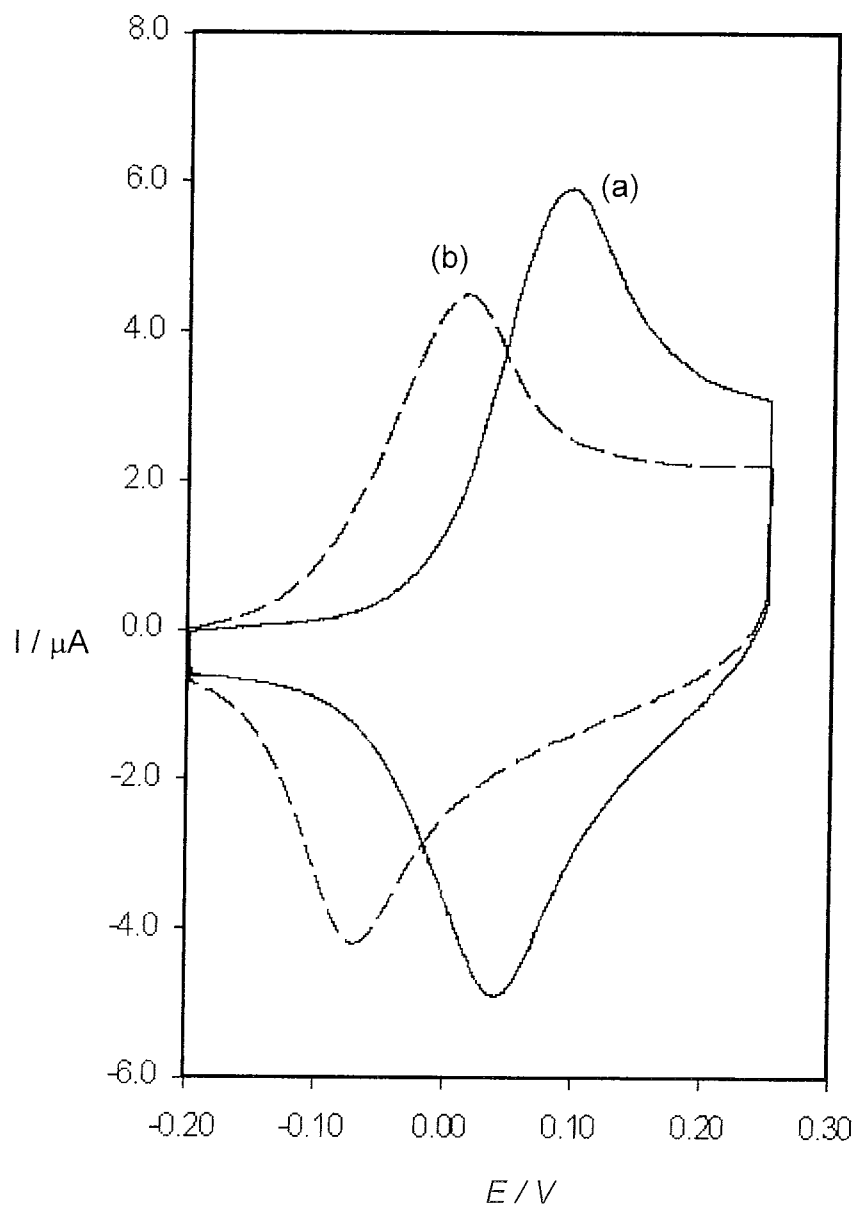


**Figure 5.4:** Cyclic Voltammograms of [Pt] poly-N-methylisoindole perchlorate, formed in 0.1M LiClO<sub>4</sub> in CH<sub>3</sub>CN vs SCE sweep (a) in 0.05M LiClO<sub>4</sub> and sweep (b) in 0.75M LiClO<sub>4</sub>, at scan speed 50 mV/sec

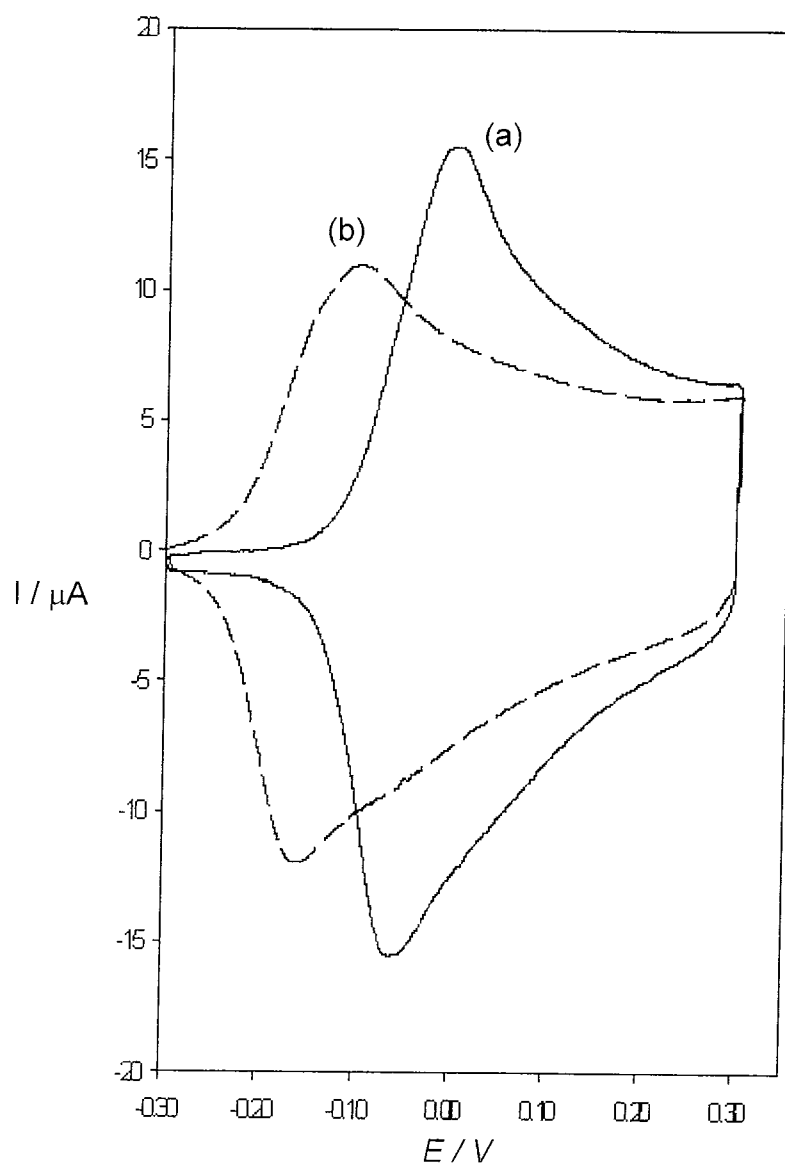


**Figure 5.5:** Cyclic Voltammograms of [Pt] poly-5-methoxy-N-methylisindole perchlorate, formed in 0.1M  $\text{LiClO}_4$  in  $\text{CH}_3\text{CN}$  vs SCE sweep (a) in 0.05M  $\text{LiClO}_4$  and sweep (b) in 0.75M  $\text{LiClO}_4$ , at scan speed 50 mV/sec

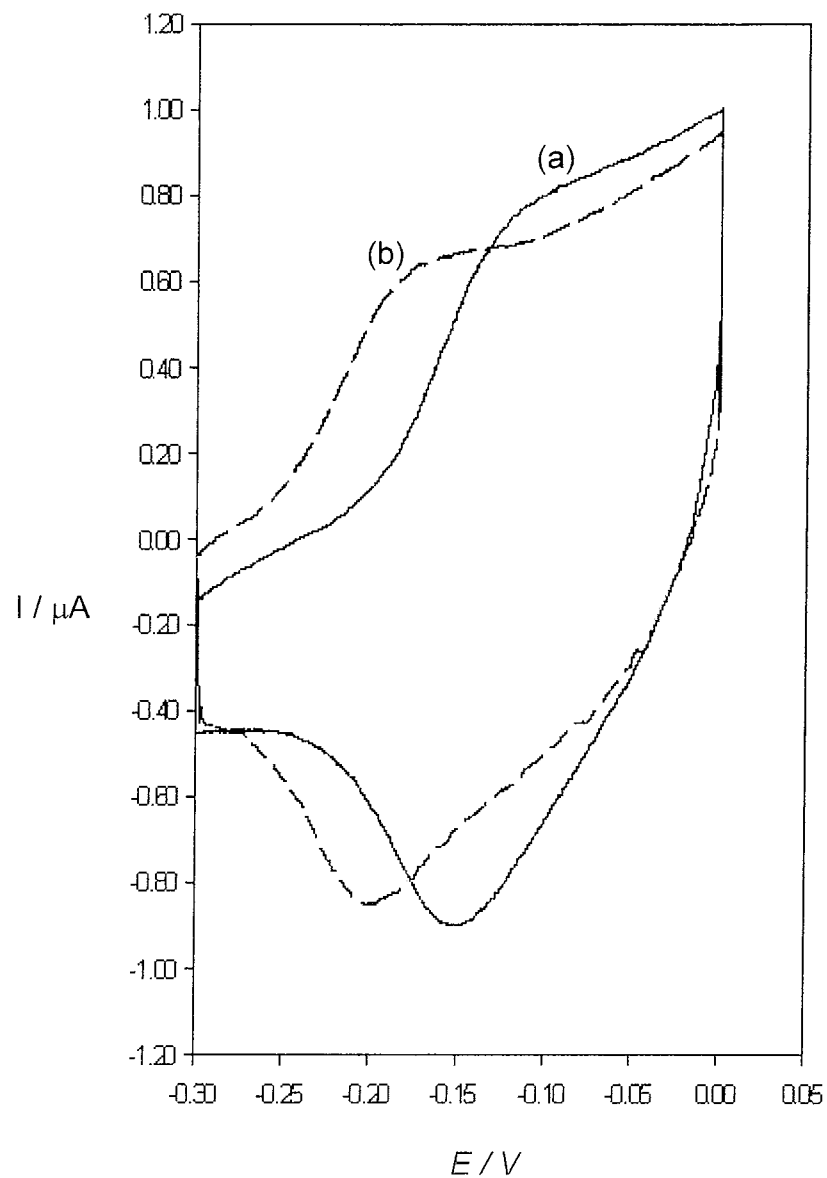


**Figure 5.6:** Cyclic Voltammograms of [Pt] poly-5,6-dimethoxy-N-methylisoindole perchlorate, formed in 0.1M LiClO<sub>4</sub> in CH<sub>3</sub>CN vs SCE sweep (a) in 0.05M LiClO<sub>4</sub> and sweep (b) in 0.75M LiClO<sub>4</sub>, at scan speed 50 mV/sec

Other reported concentration studies on polypyrrole [17], were carried out using a large anion whereby upon reduction of the layer, the anion was immobile and therefore to maintain charge neutrality cation were injected into the layer. Both studies on polypyrrole [17, 18] discussed the movement of cations in and out of the layer and reported cyclic voltammograms showed a positive shift in both the  $E_{pa}$  and  $E_{pc}$ , with increasing the background electrolyte concentration. The opposite trend was observed with the poly-N-methylisindoles, whereby both the  $E_{pa}$  and  $E_{pc}$ , shifted negative with increasing the background electrolyte concentration. This would lead to the conclusion that the movement of the anion i.e.  $ClO_4^-$  was observed. This would seem reasonable, as the perchlorate anion is relatively small and can easily move in and out of the polymer layer.

In the case of polypyrrole [17] the difference in  $E_{pc}$  or  $\Delta E_{pc}$  was far greater than the difference in  $E_{pa}$ ,  $\Delta E_{pa}$ , which was attributed to a barrier to cation ejection at high electrolyte concentrations, i.e. against a concentration gradient. This was not observed for anion movement in polymer film studied here and  $\Delta E_{pa}$  and  $\Delta E_{pc}$  for all three polymers were very similar.

This behaviour of the layer was further analysed to see if Nernst behaviour was followed. A simplified version of equation 5.1 is expressed in equation 5.2, where P is the polymer and X in the counterion, and  $P^+X^-$  is the oxidised polymer.



Assuming that the reaction is at equilibrium, it is governed by the Nernst equation (5.3), where E is the applied potential,  $E_f$  is the formal potential, n = number of electrons transferred, F= Faradays number, R = gas constant and T= temperature.

$$E = E_f + 2.303 \left( \frac{RT}{nF} \right) \text{Log} \left( \frac{[P^+X^-]}{[P][X]} \right) \quad (5.3)$$

From this the formal potential  $E_f$  can be express as in equation 5.4, where  $E^0$  is the standard potential.

$$E_f = E^0 - 2.303 \left( \frac{RT}{nF} \right) \text{Log} [X^-] \quad (5.4)$$

The  $E_{pa}$  and  $E_{pc}$  as a function of  $\log[C_{bulk}]$ , where  $[C_{bulk}]$  is the concentration of the bulk electrolyte solution were plotted for poly-N-methylisindole as in figure 5.7, poly-5-methoxy-N-methylisindole, as seen in figure 5.8 and poly-5,6-dimethoxy-N-methylisindole, see figure 5.9. Linear plots for all three polymers was observed between  $[C_{bulk}] = 0.05$  M and 0.75M, displaying Nernstian behaviour. Figure 5.10 shows a plot of the formal potential  $E_f$ , estimated by  $(E_{pa} + E_{pc}) / 2$ . With polypyrrole there was question mark over whether the  $E_f$  should be determined as halfway between the forward and reverse peaks as the shift in  $E_{pc}$  was greater than the shift in  $E_{pa}$ . However with the poly-N-methylisindoles this question does not arise, as the shift in the forward peak equalled that of the reverse peak.



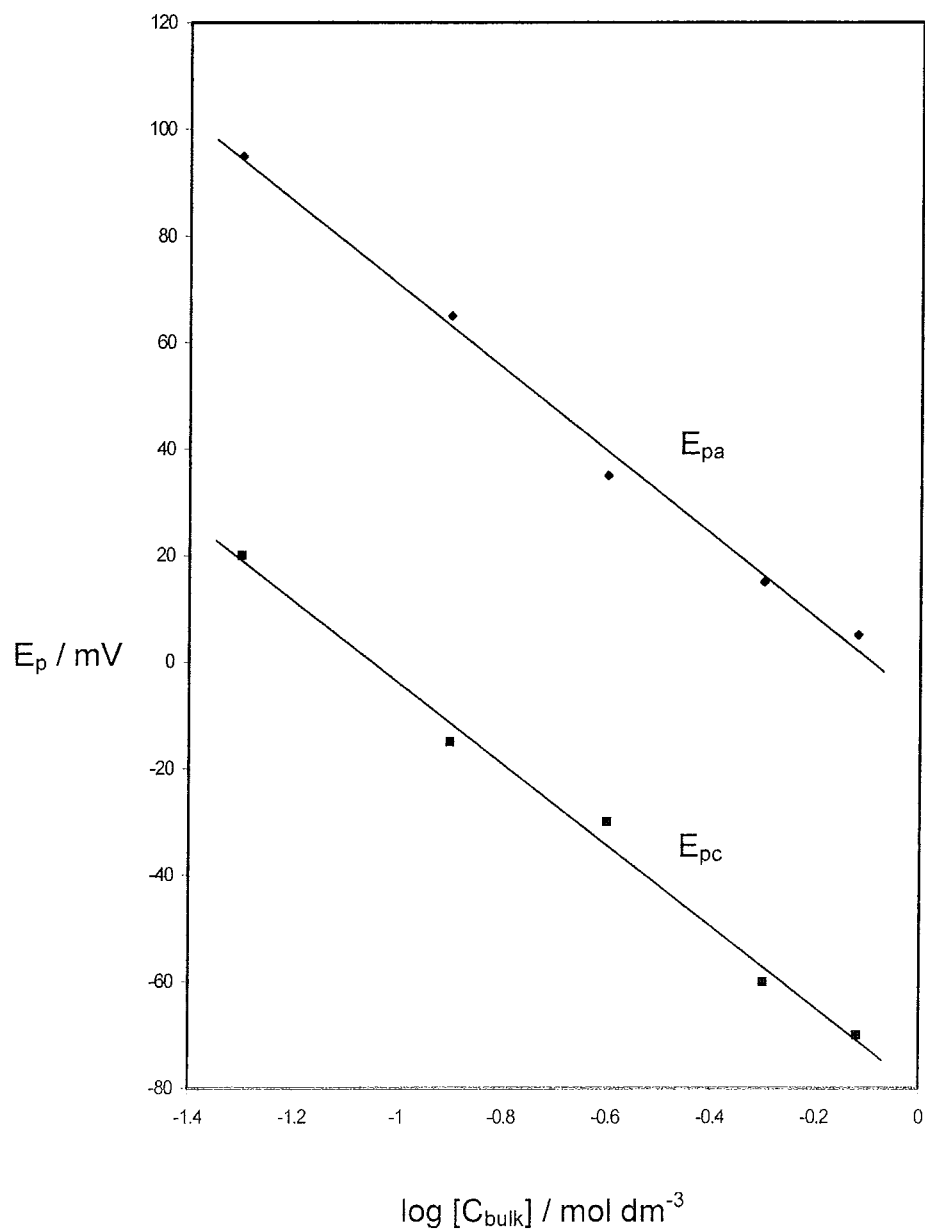


**Figure 5.7:** Plots of  $E_{\text{pa}}$  and  $E_{\text{pc}}$  versus  $\log [C_{\text{bulk}}]$ , for [Pt] poly-N-methylisindole perchlorate in various concentrations of  $\text{LiClO}_4$  in  $\text{CH}_3\text{CN}$  vs SCE.

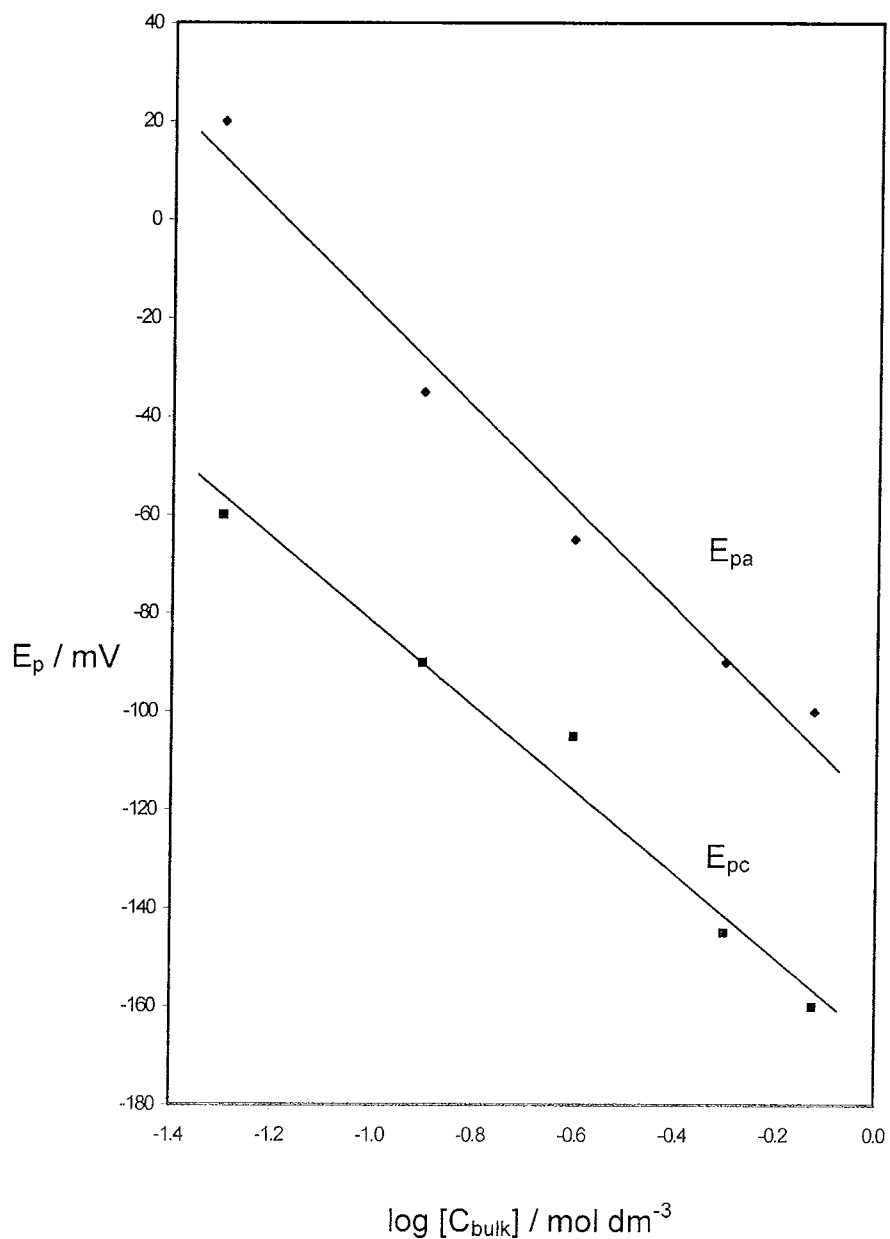


**Figure 5.8:** Plots of  $E_{\text{pa}}$  and  $E_{\text{pc}}$  versus  $\log [C_{\text{bulk}}]$ , for [Pt] poly-5-methoxy-N-methylisindole perchlorate in various concentrations of  $\text{LiClO}_4$  in  $\text{CH}_3\text{CN}$  vs SCE.

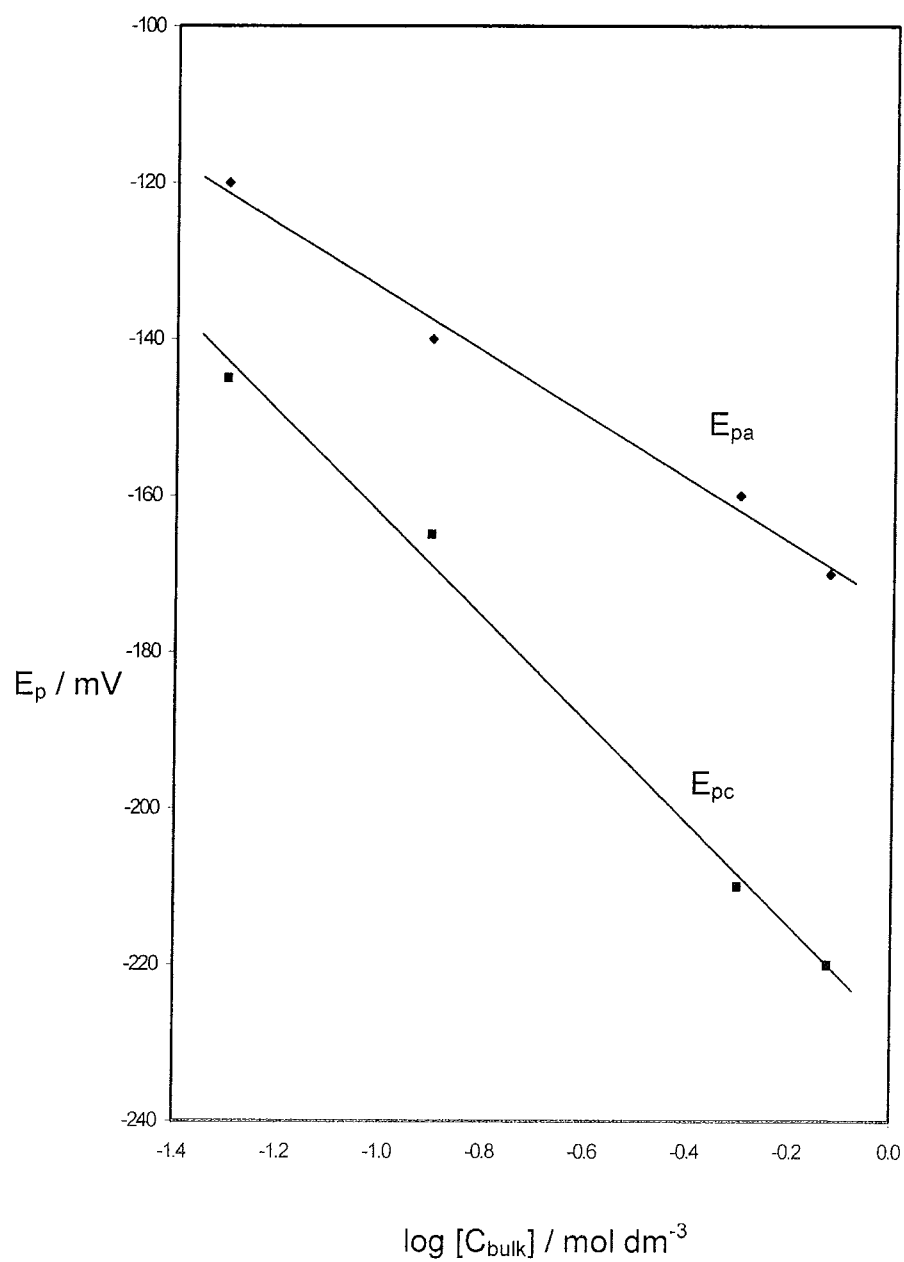


**Figure 5.9:** Plots of  $E_{\text{pa}}$  and  $E_{\text{pc}}$  versus  $\log [C_{\text{bulk}}]$ , for [Pt] poly-5,6-dimethoxy-N-methylisindole perchlorate in various concentrations of  $\text{LiClO}_4$  in  $\text{CH}_3\text{CN}$  vs SCE.

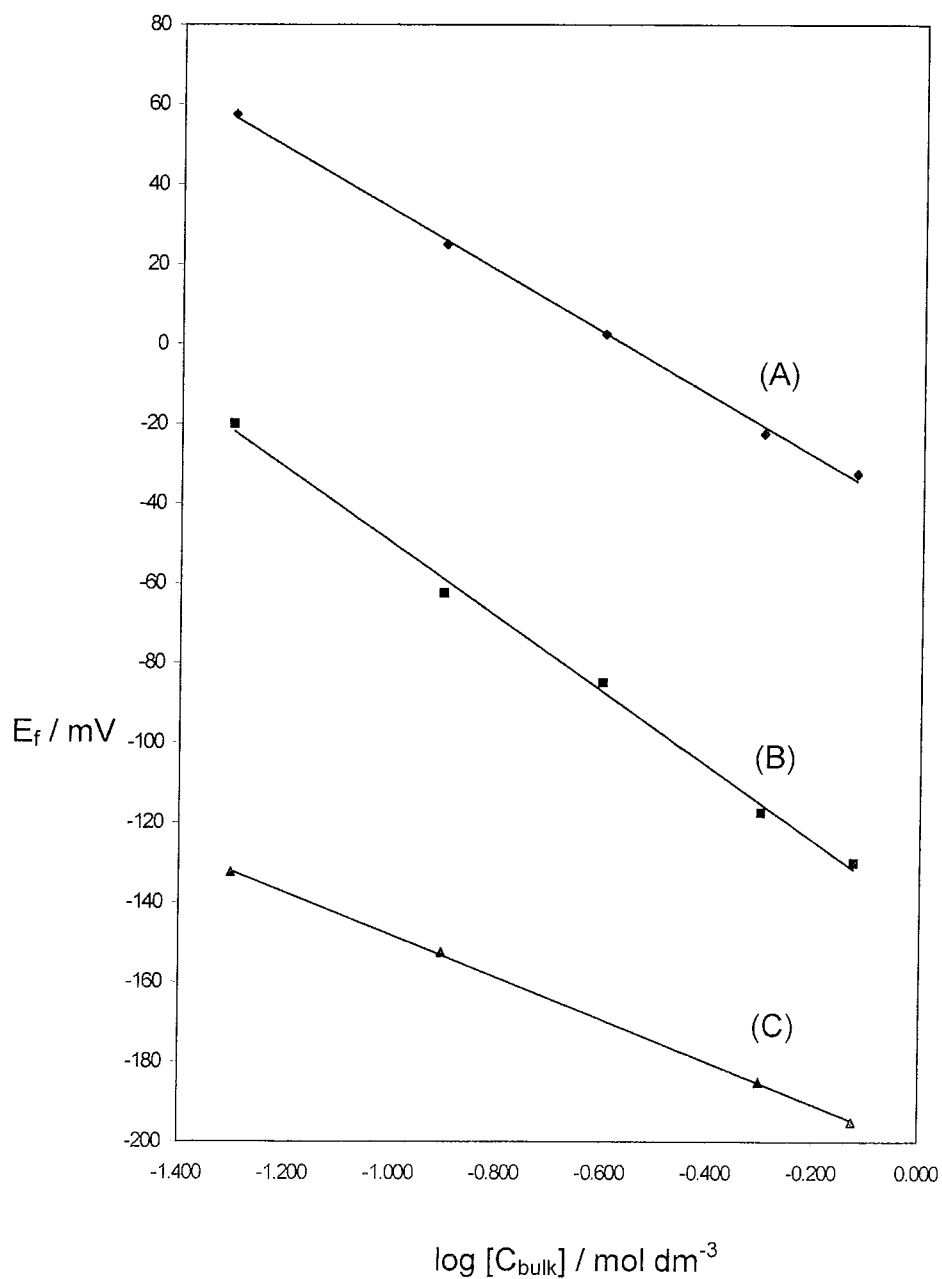


**Figure 5.10:** Plots of  $E_f$  versus  $\log [C_{\text{bulk}}]$ , for (A) poly-N-methylisindole, (B) poly-5-methoxy-N-methylisindole and (C) poly-5,6-dimethoxy-N-methylisindole in various concentrations of  $\text{LiClO}_4$  in  $\text{CH}_3\text{CN}$  vs SCE.

### 5.3 Conclusion

A summary of results of both the ion exchange studies and the ion concentration studies on poly-N-methylisoindole, poly-5-methoxy-N-methylisoindole and poly-5,6-dimethoxy-N-methylisoindole, are tabulated in Table 5.1 and 5.2. With all three polymers studied a similar shift in magnitude and direction of both the  $E_{pa}$  and  $E_{pc}$ , upon ion exchange from perchlorate to p-toluene sulphonate was observed. This shows that with the larger p-toluene sulphonate as anion, the layer was more difficult to oxidise, initially leading to the conclusion that all three polymers had a similar morphology. However the current response of poly-5,6-dimethoxy-N-methylisoindole was slow to attain a steady state compared to poly-N-methylisoindole and poly-5-methoxy-N-methylisoindole which attained a steady state response after three consecutive sweeps in the new electrolyte. This would point to a somewhat different morphology for poly-5,6-dimethoxy-N-methylisoindole to that of the other two polymers.

Both the ion exchange studies and the ion concentration studies show that the electrochemistry of all three polymers is dominated by anion movement. By changing the concentration of the background electrolyte a similar shift in both  $E_{pa}$  and  $E_{pc}$  was observed, as shown by the  $\Delta E_{pa}$  and  $\Delta E_{pc}$  values in table 5.2. Unlike the reported data on polypyrrole [17, 18], the shift in  $E_{pa}$  and  $E_{pc}$  was equal showing the ease of movement of anions. Plot of the  $E_{pa}$  and  $E_{pc}$  versus  $\log[C_{bulk}]$  showed a Nernstian redox nature at the polymer layers. A plot of the formal potential  $E_f$  determined by  $(E_{pa} + E_{pc} / 2)$  would seem to be a reasonable good estimate of the formal potential as the shift in the forward peak potential was equal to that of the reverse peak potential, for all three polymers. Finally, these initial results show that these isoindole polymers have the potential application as ion selective electrodes for anions.

Polymer	LiClO <sub>4</sub>		p-TsO <sup>-</sup>		Shift / mV	
	E <sub>pa</sub> / V	E <sub>pc</sub> / V	E <sub>pa</sub> / V	E <sub>pc</sub> / V	ΔE <sub>pa</sub>	ΔE <sub>pc</sub>
A	+0.06	-0.01	+0.18	+0.08	120	90
B	-0.03	-0.08	+0.08	+0.01	110	90
C	-0.1	-0.13	-0.02	-0.09	98	50

**Table 5.1:** Summary of ion exchange studies of layers in background electrolyte in CH<sub>3</sub>CN (vs SCE), where (A) = poly-N-methylisindole, (B) = poly-5-methoxy-N-methylisindole and (C) = poly-5,6-dimethoxy-N-methylisindole data taken from figures 5.1 – 5.3

Polymer	0.05M		0.75M		Shift / mV		Slope of E <sub>p</sub> vs log [C <sub>bulk</sub> ]/ mV decade <sup>-1</sup>		
	E <sub>pa</sub> / V	E <sub>pc</sub> / V	E <sub>pa</sub> / V	E <sub>pc</sub> / V	ΔE <sub>pa</sub>	ΔE <sub>pc</sub>	at E <sub>pa</sub>	at E <sub>pc</sub>	at E <sub>pf</sub>
A	+0.1	+0.03	+0.02	-0.07	98	100	-78	-76	-77
B	-0.1	-0.07	0.0	-0.16	100	90	-101	-85	-93
C	-0.11	-0.15	-0.17	-0.21	60	60	-40	-65	-53

**Table 5.2:** Summary of background electrolyte studies of layers in CH<sub>3</sub>CN (vs SCE), where (A) = poly-N-methylisindole, (B) = poly-5-methoxy-N-methylisindole and (C) = poly-5,6-dimethoxy-N-methylisindole, data taken from figures 5.4 – 5.10

## 5.4 Experimental

### 5.4.1. General Experimental

All electrochemical experiments were carried out in a 20 cm<sup>3</sup> & 50 cm<sup>3</sup> single compartment cell using a three electrode configuration. A platinum disc, with an exposed surface area of 7.1 mm<sup>2</sup>, sealed in Teflon was employed as a working electrode. In some experiments (where stated) a carbon tip, with an exposed surface area of 7.1 mm<sup>2</sup>, sealed in Teflon was used as a working electrode. A glassy carbon rod was used as auxiliary electrode and all potentials are quoted with respect to a saturated calomel electrode (SCE). The working electrode was pretreated prior to each experiment by polishing with 0.3 μm alumina powder. The auxiliary and reference electrodes were washed thoroughly with deionised water and background electrolyte.

Potential control and current measurement was performed with a H.B. Thompson DGR16 waveform generator and an EG&G model 362 scanning potentiostat and voltammograms were recorded on a Bryans 60100 model X-Y recorder. The cyclic voltammograms were digitised using WinDIG 2.5.

### 5.4.2 Ion Exchange studies

#### *Poly-N-methylisoindole*

A cell containing a freshly made solution of 0.1M LiClO<sub>4</sub> in anhydrous acetonitrile (10 cm<sup>3</sup>) was flushed with nitrogen and N-methylisoindole (17mgs, 1.29 x 10<sup>-4</sup> mole, 12.9 mM) was added as already outlined. A thin film was grown by electrochemically cycling the solution between the limits of -0.5V and +1.0V at a scan speed of 50 mV/sec for 7 cycles. The working electrode containing the layer was then removed and rinsed thoroughly with electrolyte and then placed in fresh electrolyte solution. A cyclic voltammogram was obtained between the limits of -0.3V and +0.3V at 50mV/sec. The working electrode was then immediately removed and

placed in a freshly made solution of 0.1M  $(\text{Et})_4\text{N}(\text{O}_3\text{SC}_6\text{H}_4\text{CH}_3)$  in anhydrous acetonitrile ( $10 \text{ cm}^3$ ) and a cycled between the same limits until a steady state continuous cyclic voltammogram was obtained.

#### *Poly-5-methoxy-N-methylisoindole*

As above with 5-methoxy-N-methylisoindole (15mgs,  $9.31 \times 10^{-5}$  mole, 9.3mM)

#### *Poly-5,6-dimethoxy-N-methylisoindole*

As above with 5,6-dimethoxy-N-methylisoindole (16mgs,  $8.37 \times 10^{-5}$  mole, 8.37mM) and cyclic voltammograms recorded between  $-0.3\text{V}$  and  $0.0\text{V}$

#### 5.4.3 *Electrolyte Concentration studies.*

##### *Poly-N-methylisoindole-perchlorate*

A cell containing a freshly made solution of 0.1M  $\text{LiClO}_4$  in anhydrous acetonitrile ( $10 \text{ cm}^3$ ) and deionised water (1%) was flushed with nitrogen and N-methylisoindole (10mgs,  $7.63 \times 10^{-5}$  mole, 7.63 mM) was added as already outlined. A thin film was grown by electrochemically cycling the solution between the limits of  $-0.5\text{V}$  and  $+1.0\text{V}$  at a scan speed of 50 mV/sec for 5 cycles. The working electrode containing the layer was then removed and rinsed thoroughly with electrolyte. Following this, a "breaking in" process was carried out by placing the electrode in 0.05M  $\text{LiClO}_4$  electrolyte solution and cycling between the limits  $-0.3\text{V}$  to  $+0.25\text{V}$  at 50mV/sec until a steady state continuous cyclic voltammogram was obtained, then one cycle was recorded separately. The electrode was then removed and immediately placed into 0.125M  $\text{LiClO}_4$  whereby the "breaking in" process was repeated and the cyclic voltammograms recorded under identical conditions. The process was further repeated with the same layer in 0.25M, 0.5M and 0.75M  $\text{LiClO}_4$  electrolyte solution.



### *Poly-5-methoxy-N-methylisoindole-perchlorate*

A cell containing a freshly made solution of 0.1M LiClO<sub>4</sub> in anhydrous acetonitrile (10 cm<sup>3</sup>) was flushed with nitrogen and 5-methoxy-N-methylisoindole (15mgs,  $9.31 \times 10^{-5}$  mole, 9.3mM) was added as already outlined. A thin film was grown by electrochemically cycling the solution between the limits of -0.5V and +0.7V at a scan speed of 50 mV/sec for 12 cycles. The working electrode containing the layer was then removed and rinsed thoroughly with electrolyte. Following this, a "breaking in" process was carried out by placing the electrode in 0.05M LiClO<sub>4</sub> electrolyte solution and cycling between the limits -0.3V to +0.3V at 50mV/sec until a steady state continuous cyclic voltammogram was obtained, then one cycle was recorded separately. The electrode was then removed and immediately placed into 0.125M LiClO<sub>4</sub> whereby the "breaking in" process was repeated and the cyclic voltammograms recorded under identical conditions. The process was further repeated with the same layer in 0.25M, 0.5M and 0.75M LiClO<sub>4</sub> electrolyte solution.

### *Poly-5,6-dimethoxy-N-methylisoindole-perchlorate*

A cell containing a freshly made solution of 0.1M LiClO<sub>4</sub> in anhydrous acetonitrile (10 cm<sup>3</sup>) was flushed with nitrogen and 5,6-dimethoxy-N-methylisoindole (16mgs,  $8.37 \times 10^{-5}$  mole, 8.37mM) was added as already outlined. A thin film was grown by electrochemically cycling the solution between the limits of -0.5V and +0.7V at a scan speed of 50 mV/sec for 20 cycles. The working electrode containing the layer was then removed and rinsed thoroughly with electrolyte. Following this, a "breaking in" process was carried out by placing the electrode in 0.05M LiClO<sub>4</sub> electrolyte solution and cycling between the limits -0.3V to +0.0V at 50mV/sec until a steady state continuous cyclic voltammogram was obtained, then one cycle was recorded separately. The electrode was then removed and immediately placed into 0.125M LiClO<sub>4</sub> whereby the "breaking in" process was repeated and the cyclic voltammograms recorded under identical conditions. The process was

further repeated with the same layer in 0.25M, 0.5M and 0.75M LiClO<sub>4</sub> electrolyte solution.

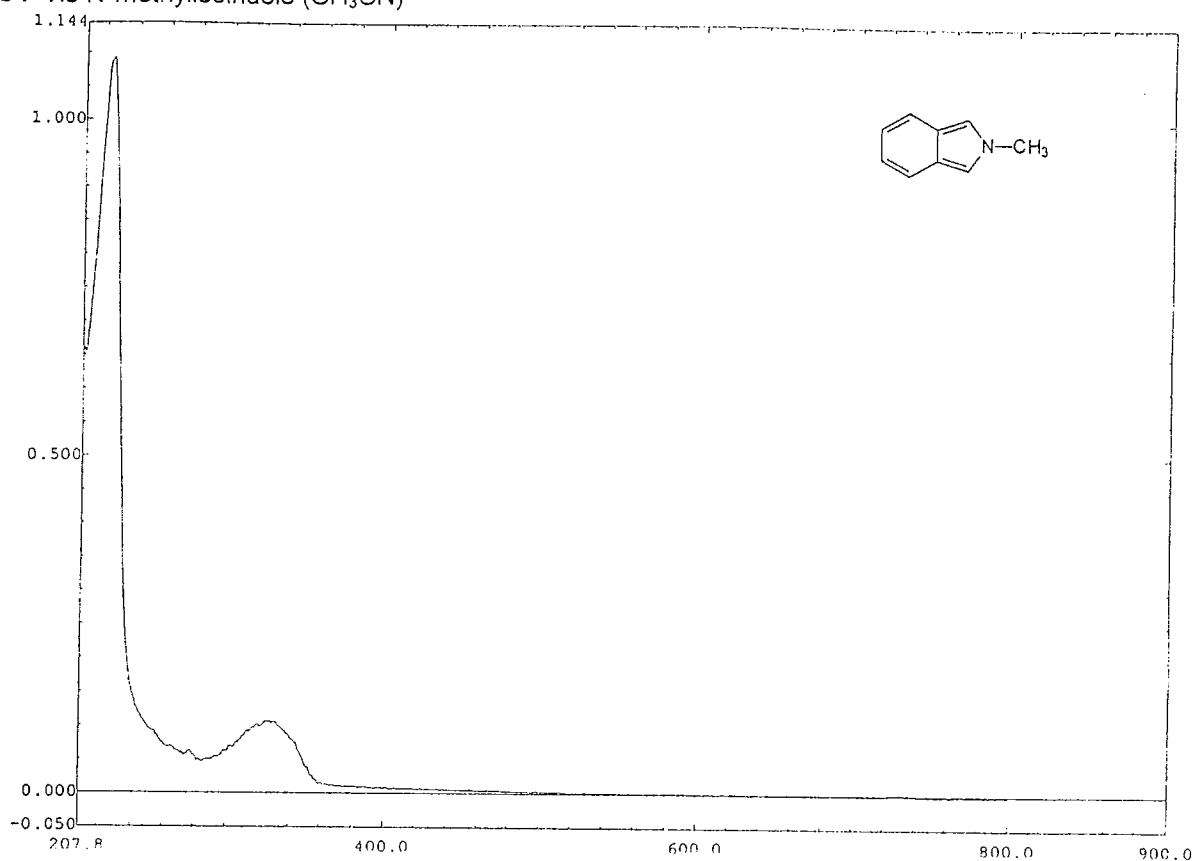
## 5.5 References

- [1] A. Guiseppi-Elie, G.G. Wallace, T. Matsue, Chemical and Biological Sensors based on Electrically Conducting Polymers, *Handbook of Conducting Polymers*. Edited by T.A. Stockheim, R.L. Elesenbaumer and J.R. Reynoldss, (1998), 963.
- [2] H. Shirakawa, E.J. Louis, A.G. MacDiarmid, C.K. Chiang and A.J. Heeger, Synthesis of electrically conducting polymers: Halogen derivatives of polyacetylene,  $(CH)_x$ , *J. Chem. Soc., Chem. Commun.* (1997), 578.
- [3] A.R. Hillman, M.J. Swann and S. Bruckenstein, *J. Electroanal. Chem.* (1990), **291**, 147.
- [4] T.F. Otero and J. Rodriguez, *Intrinsically Conducting Polymers: An Emerging Technology*, edited by M. Aldissi, Kluwer Academic, Dordrecht, (1992) 179.
- [5] P. Marque and J. Roncali, *J. Phys.Chem.*, (1990), **94**, 8614.
- [6] R.M. Penner and C.R. Martin, *J. Phys.Chem.*, (1989), **93**, 984.
- [7] G.M. Genies and J.M. Pernaut, *Synth. Metals*, (1985), **10**, 117
- [8] Z. Cai and C.R. Martin, *J. Electroanal. Chem.* (1990), **35**, 424.
- [9] C. Lee, K. Johyoun and A.J. Bard, *J. Electrochem. Soc.*, (1989), **136**, 3720.
- [10] Y. Tezuka and K. Aoki, *J. Electroanal. Chem.* (1989), **273**, 161.
- [11] T. Iyoda, A. Ohtani, T. Schimidzu, and K. Honda, *Chem. Lett.*, (1986), 687
- [12] T. Schimidzu, A. Ohtani, T. Iyoda, and K. Honda, *J. Electroanal. Chem.* (1987), **224**, 123.
- [13] L.L. Miller and Q. X. Zhou, *Macromolecules*, (1987), **20**, 1594.
- [14] R.C.D. Peres, J-M. Pernaut and M.A. DePaoli, *Synth. Metals*, (1989), **28**, C-59.
- [15] J-M. Pernaut, R.C.D. Peres, V.F. Juliano and M.A. DePaoli, *J. Electroanal. Chem.* (1988), **274**, 225.
- [16] Y-J, Qiu and R.J. Reynolds, *Pol. Eng. Sci.*, (1991), **31**, 417.
- [17] W. Breen, J.F. Cassidy and M.E.G. Lyons, *J. Electroanal. Chem.* (1991), **297**, 445.
- [18] T. McCormac, *Electrochemical Characterisation of Conduction Polymer Layers and their use as gas sensors*, Ph.D. Thesis, Dublin City University, (1994).

# **Appendix A**

## **Spectroscopic data of N-methylisoindole**

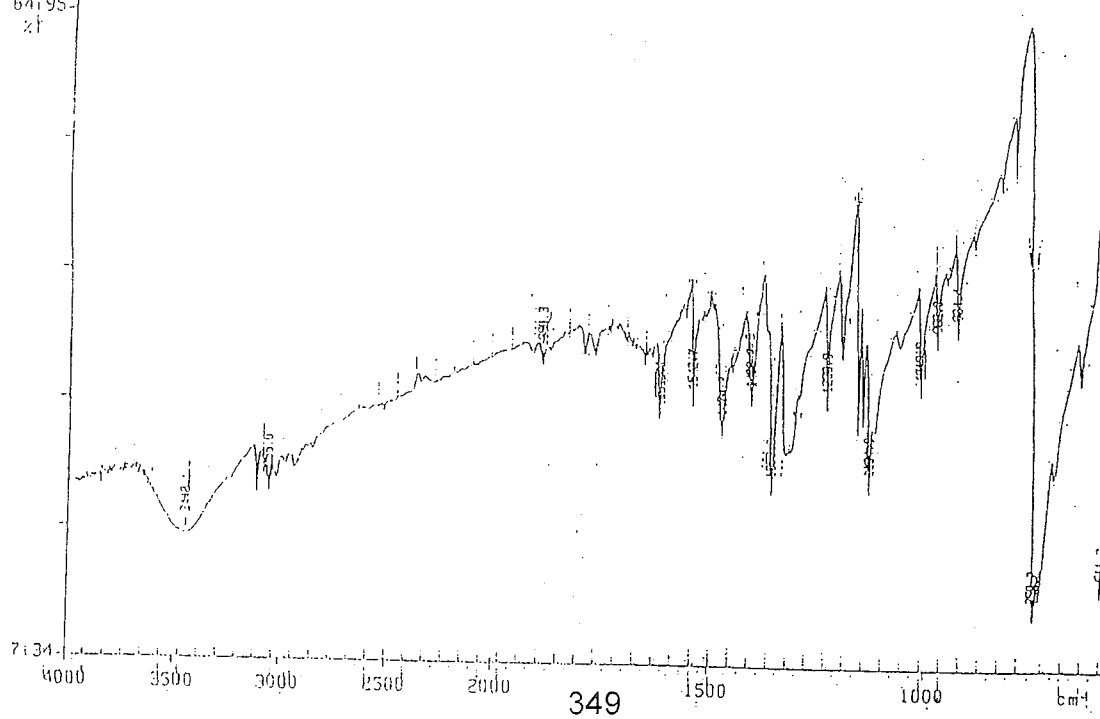
UV-Vis N-methylisoindole (CH<sub>3</sub>CN)



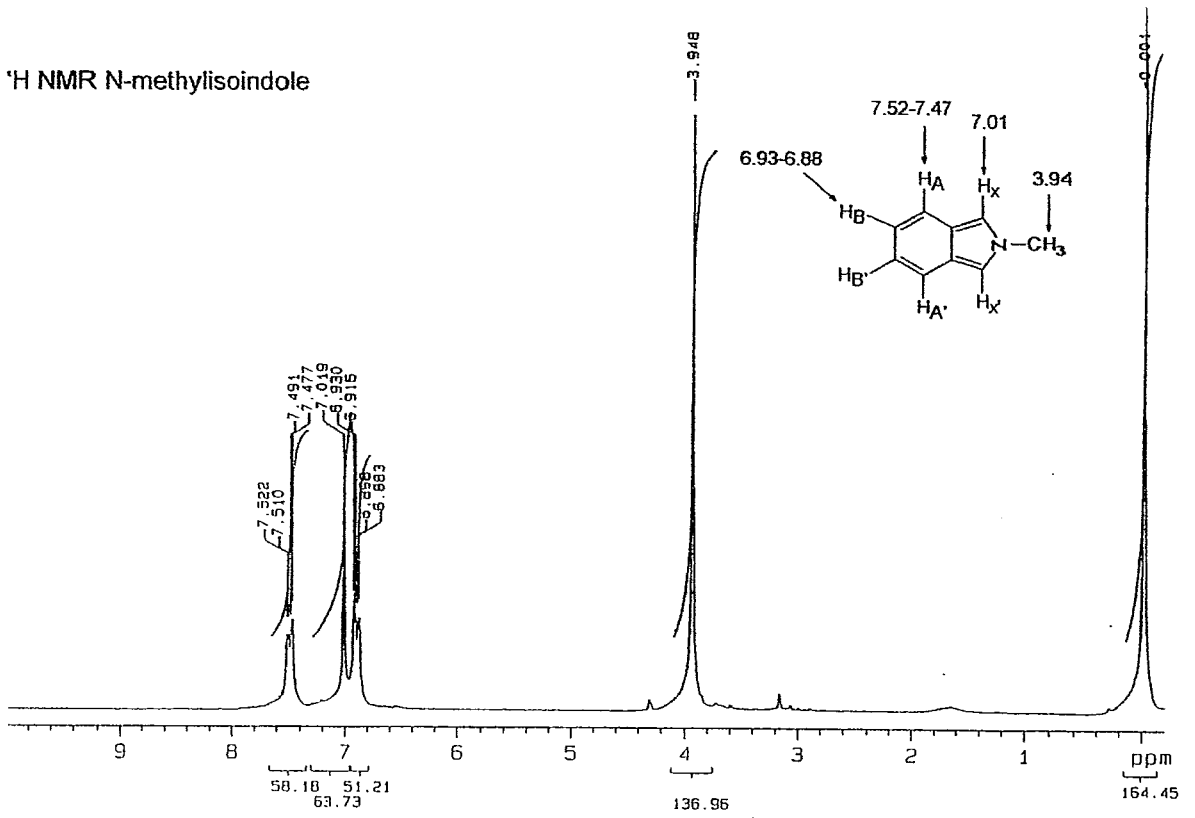
IR N-methylisoindole (KBr)

PARKIN ELMER

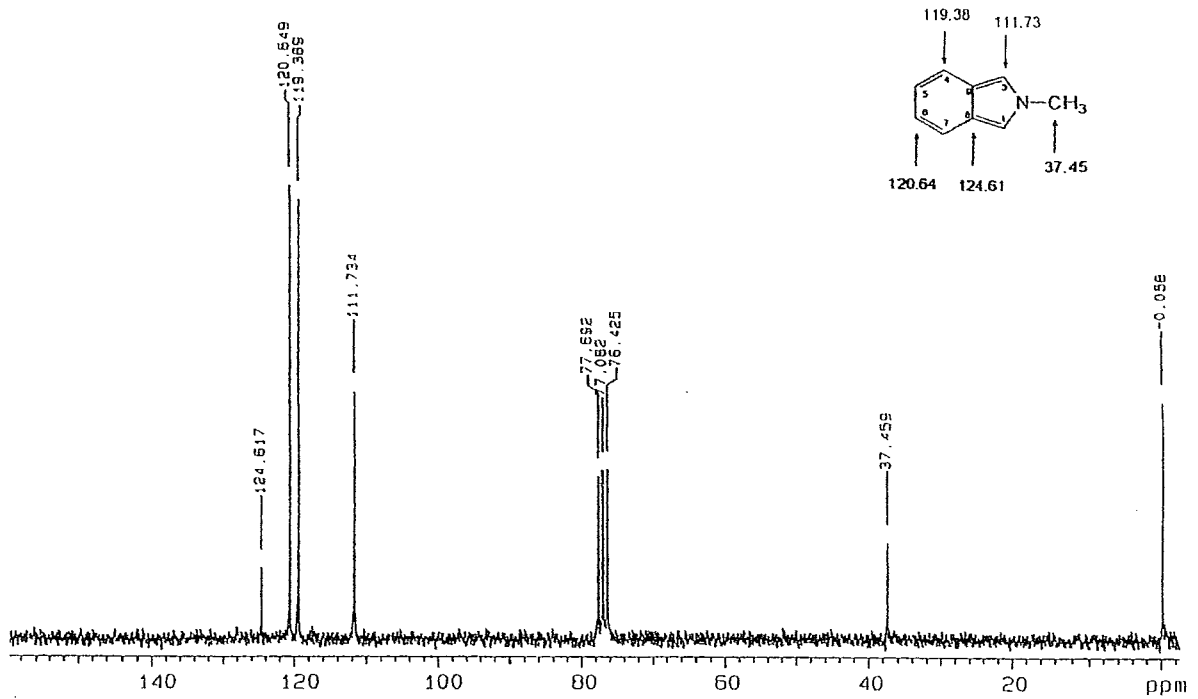
64195-  
zt



<sup>1</sup>H NMR N-methylisindole



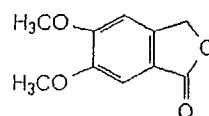
<sup>13</sup>C NMR N-methylisindole



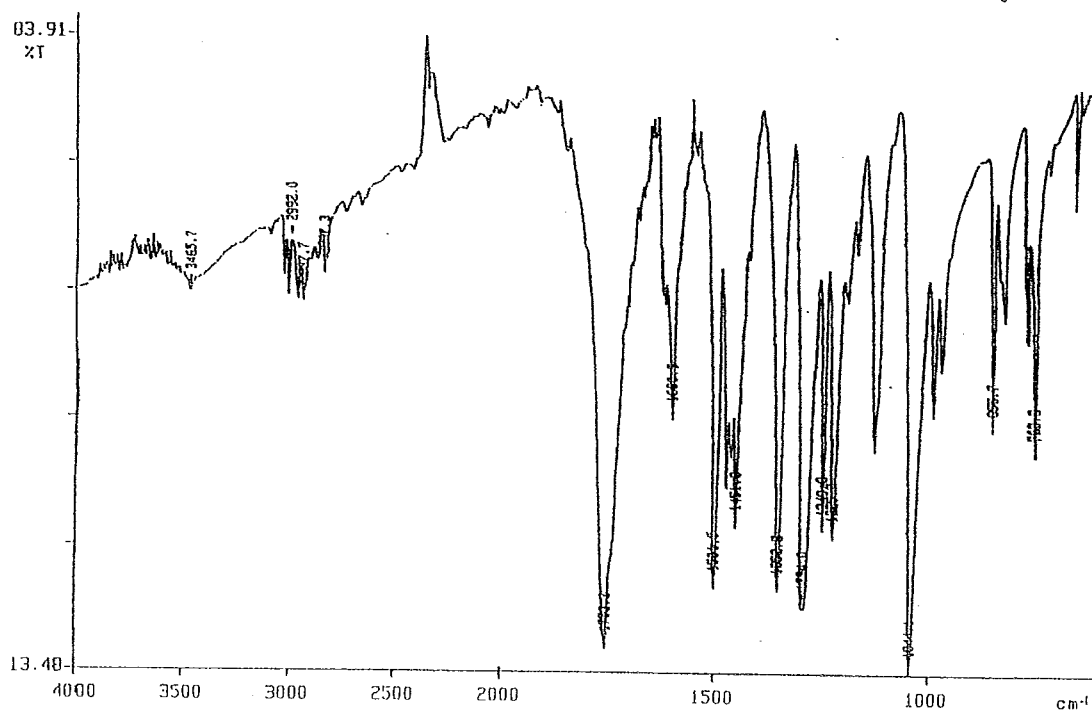
## **Appendix B**

**Spectroscopic data of 5,6-dimethoxyphthalide**

IR 5,6-dimethoxyphthalide (KBr)

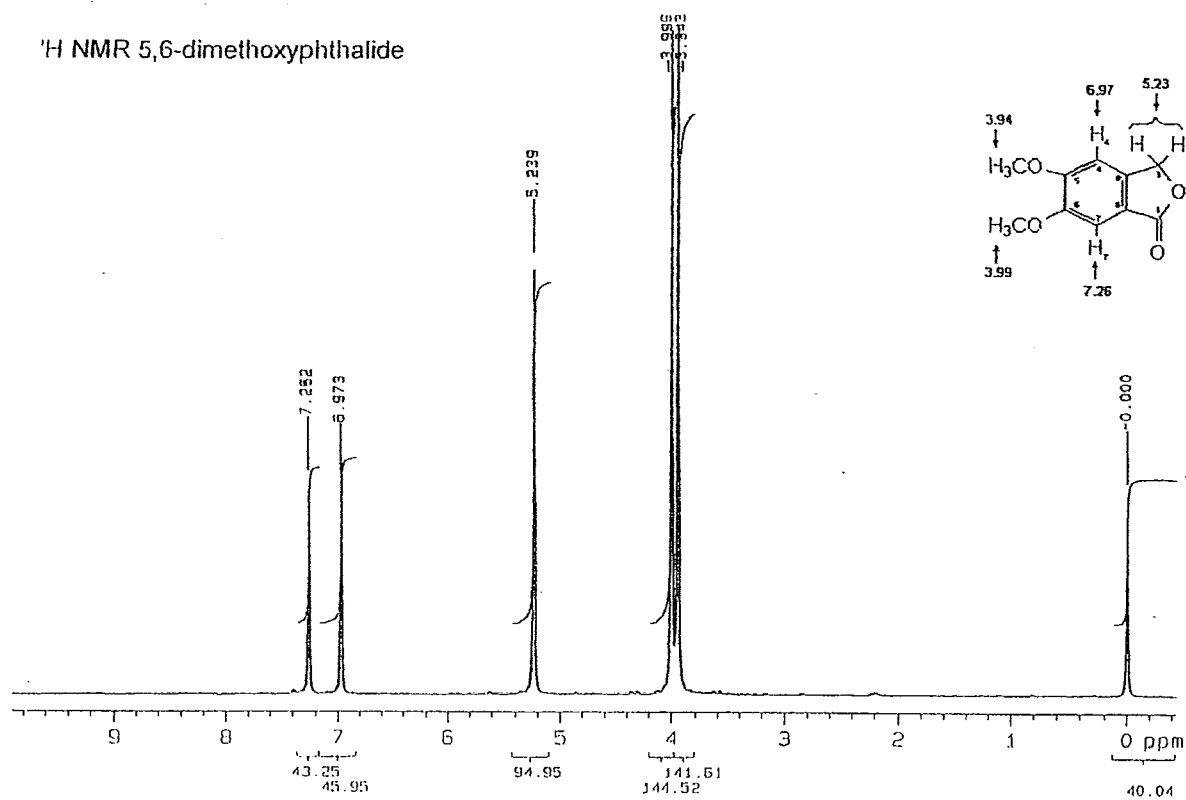


PERKIN ELMER

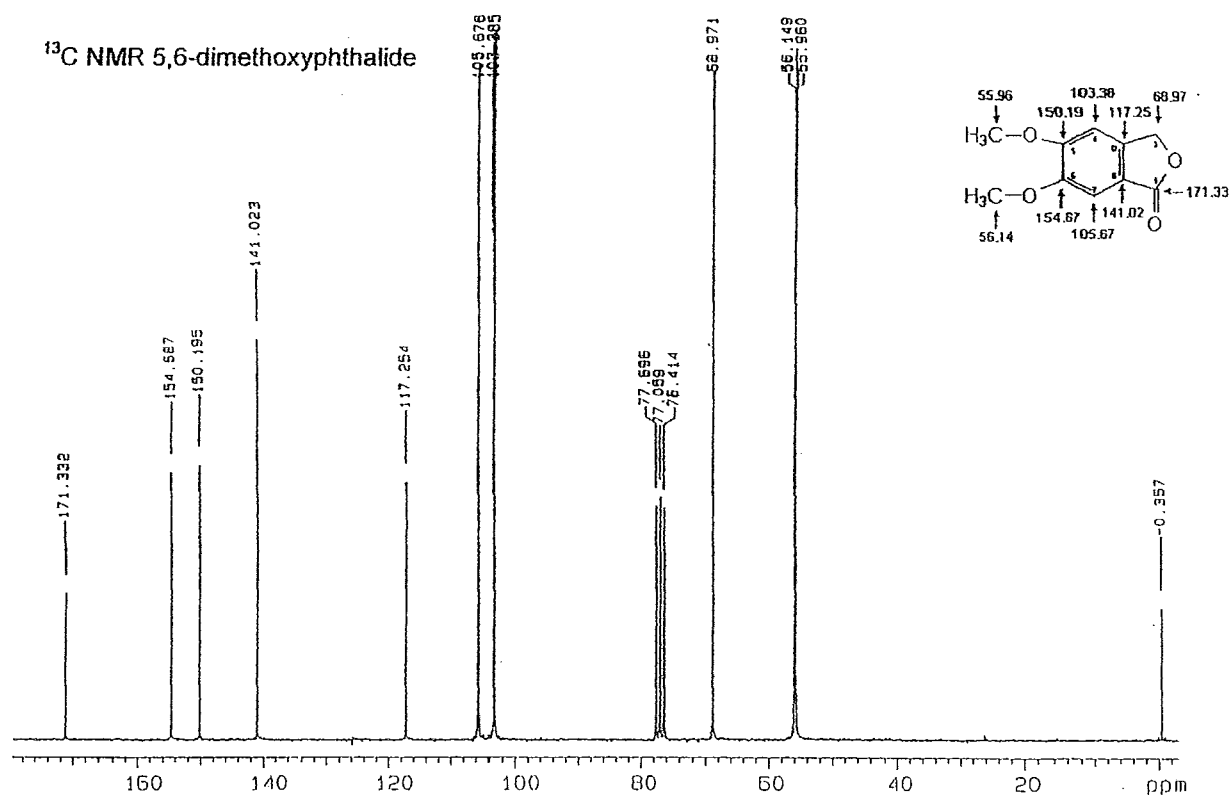




<sup>1</sup>H NMR 5,6-dimethoxyphthalide



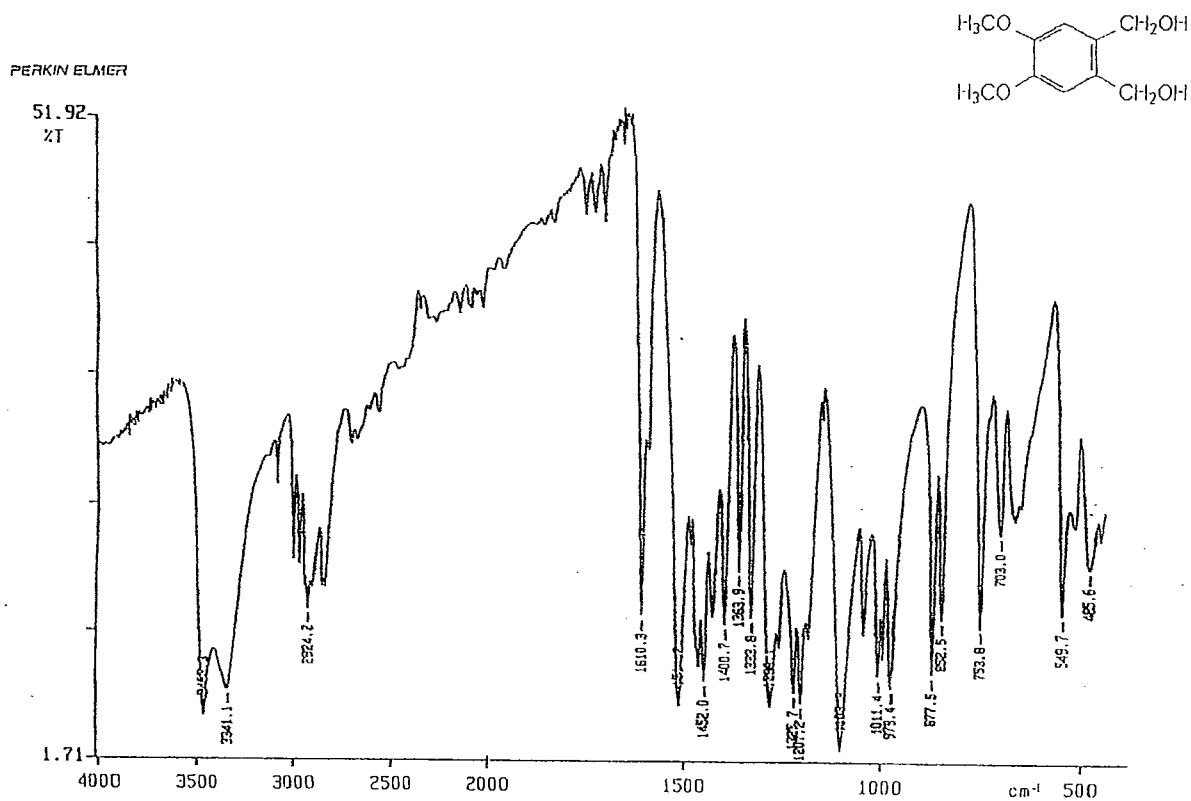
<sup>13</sup>C NMR 5,6-dimethoxyphthalide



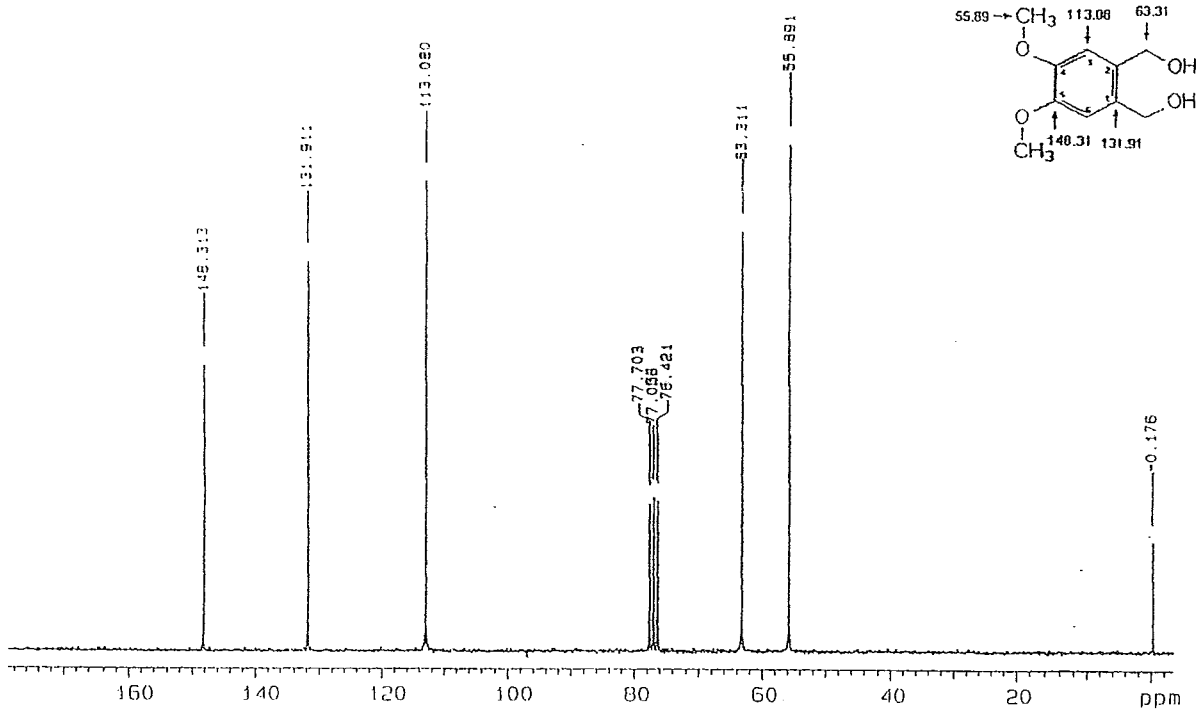
## **Appendix C**

**Spectroscopic data 4,5-dimethoxyphthalyl alcohol**

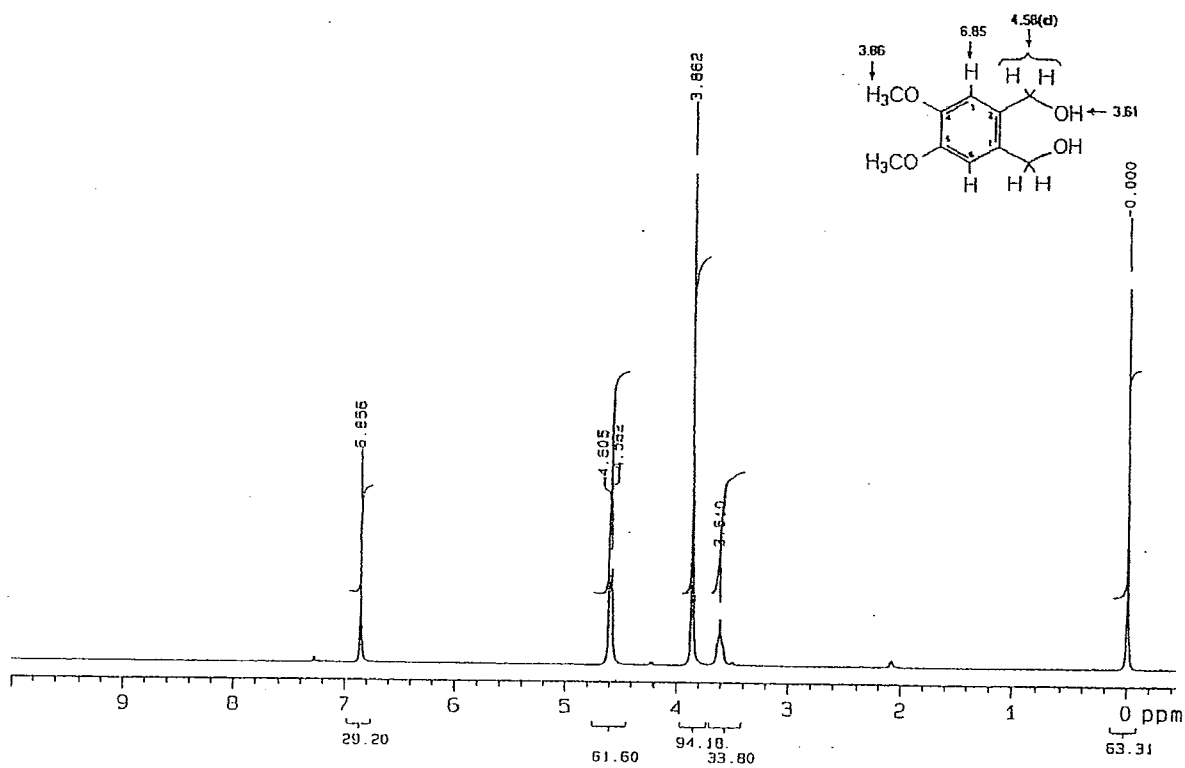
IR 4,5-dimethoxyphthalyl alcohol (KBr)



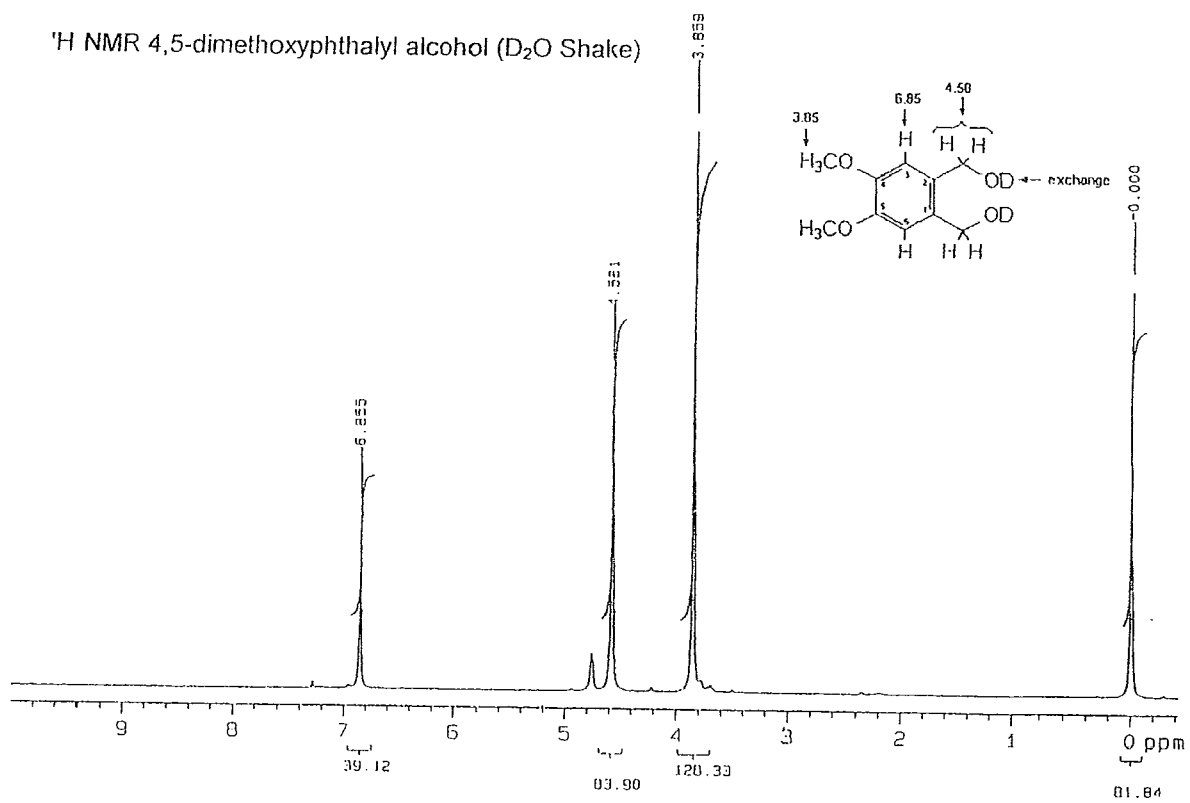
<sup>13</sup>C NMR 4,5-dimethoxyphthalyl alcohol



<sup>1</sup>H NMR 4,5-dimethoxyphthalyl alcohol



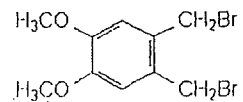
<sup>1</sup>H NMR 4,5-dimethoxyphthalyl alcohol (D<sub>2</sub>O Shake)



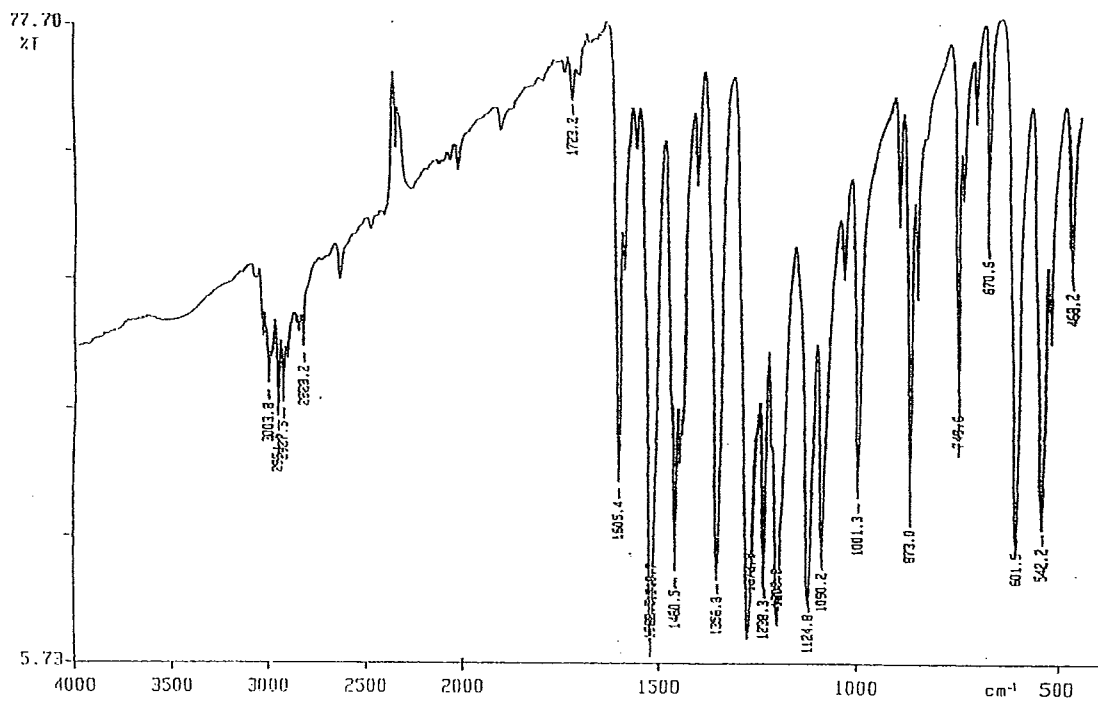
## **Appendix D**

**Spectroscopic data of  
4,5-dimethoxy- $\alpha,\alpha'$ -dibromo-o-xylene**

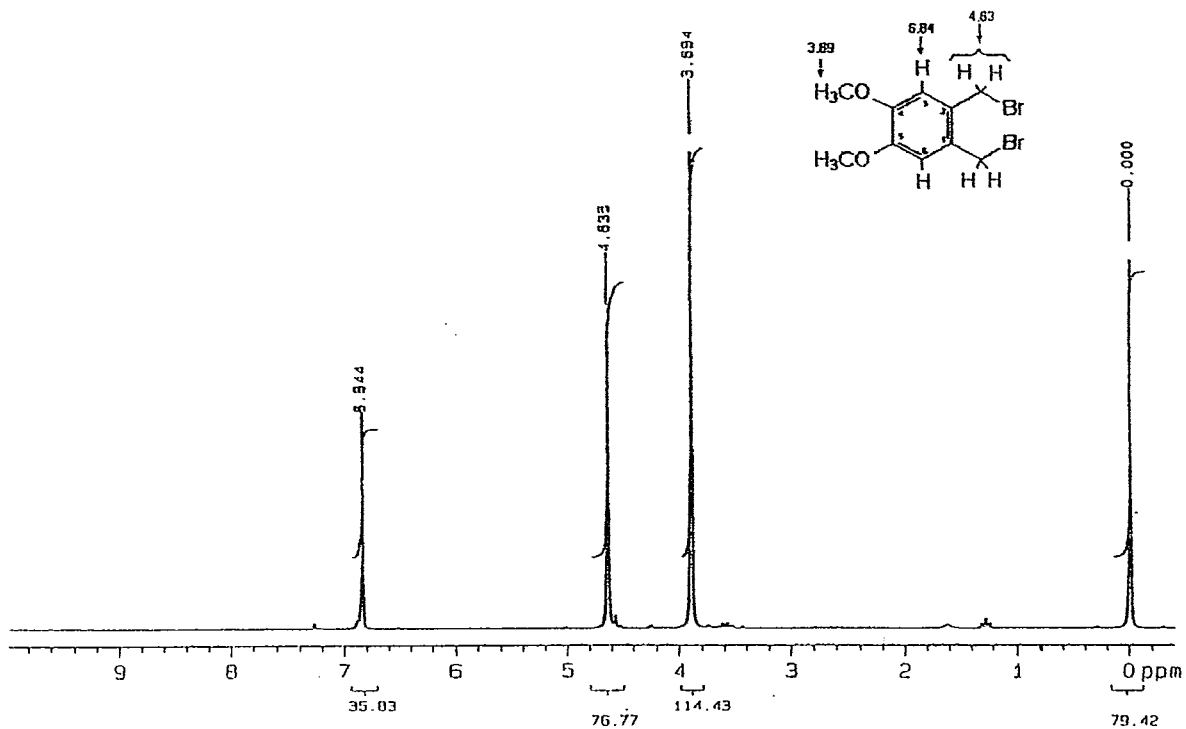
IR 4,5-dimethoxy- $\alpha, \alpha'$ -dibromo-o-xylene (KBr)



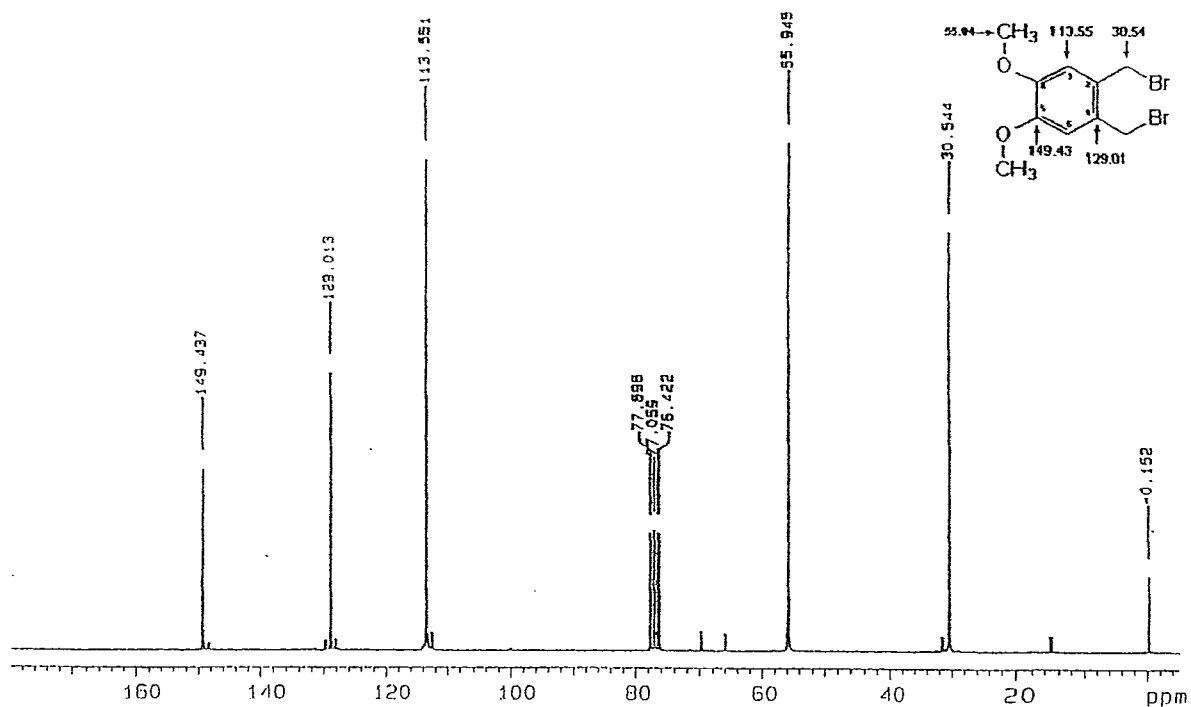
PERKIN ELMER



<sup>1</sup>H NMR 4,5-dimethoxy- $\alpha, \alpha'$ -dibromo-o-xylene



<sup>13</sup>C NMR 4,5-dimethoxy- $\alpha, \alpha'$ -dibromo-o-xylene

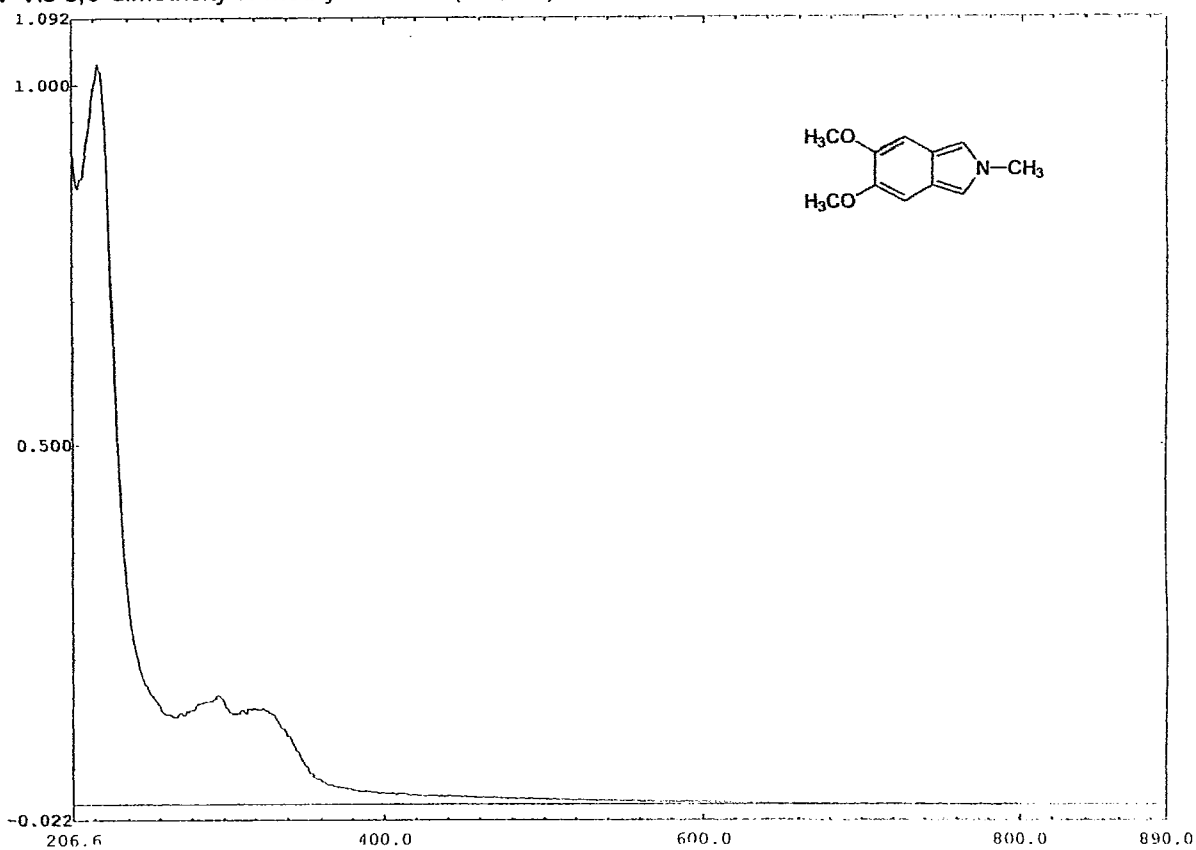


## **Appendix E**

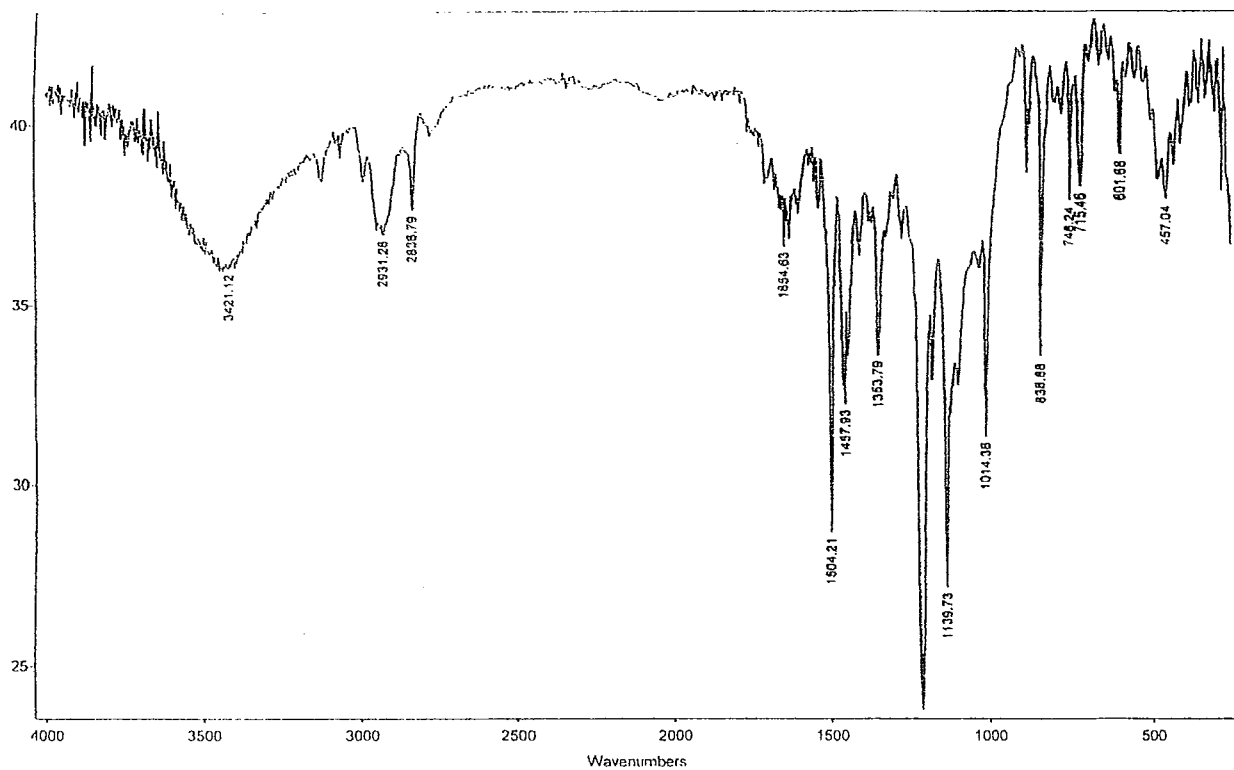
**Spectroscopic data of 5,6-dimethoxy-N-methylisoindole**



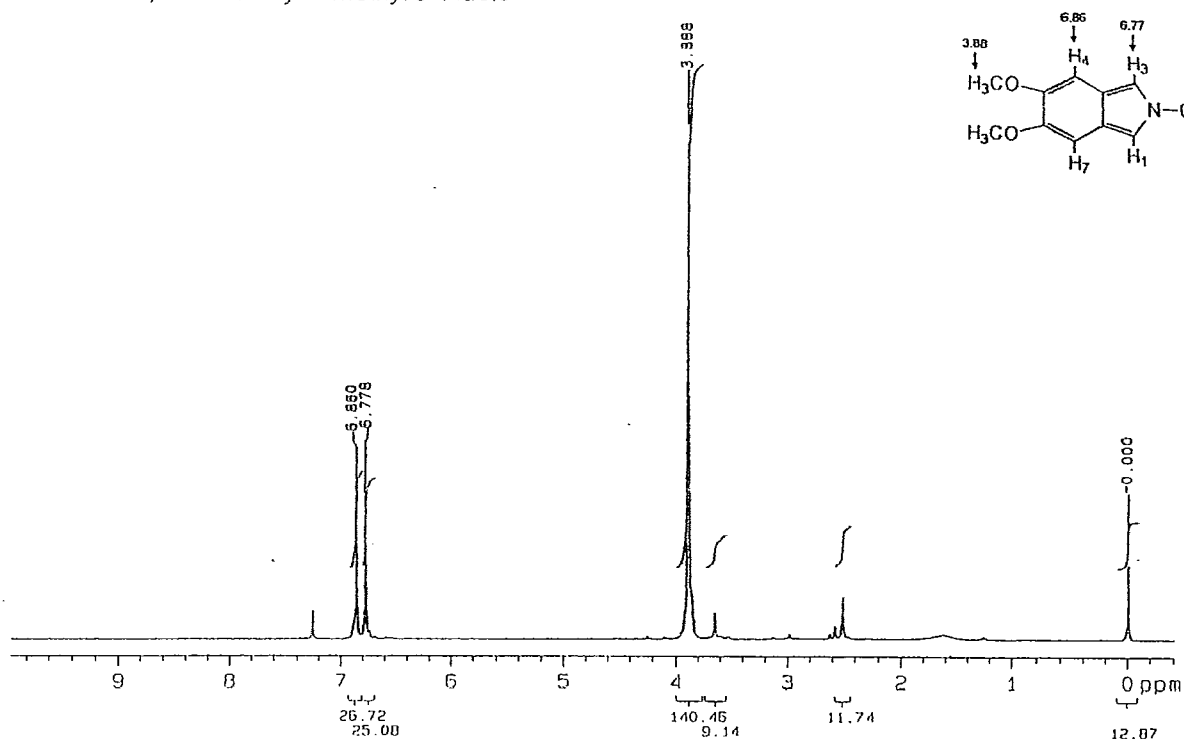
UV-Vis 5,6-dimethoxy-N-methylisindole (CH<sub>3</sub>CN)



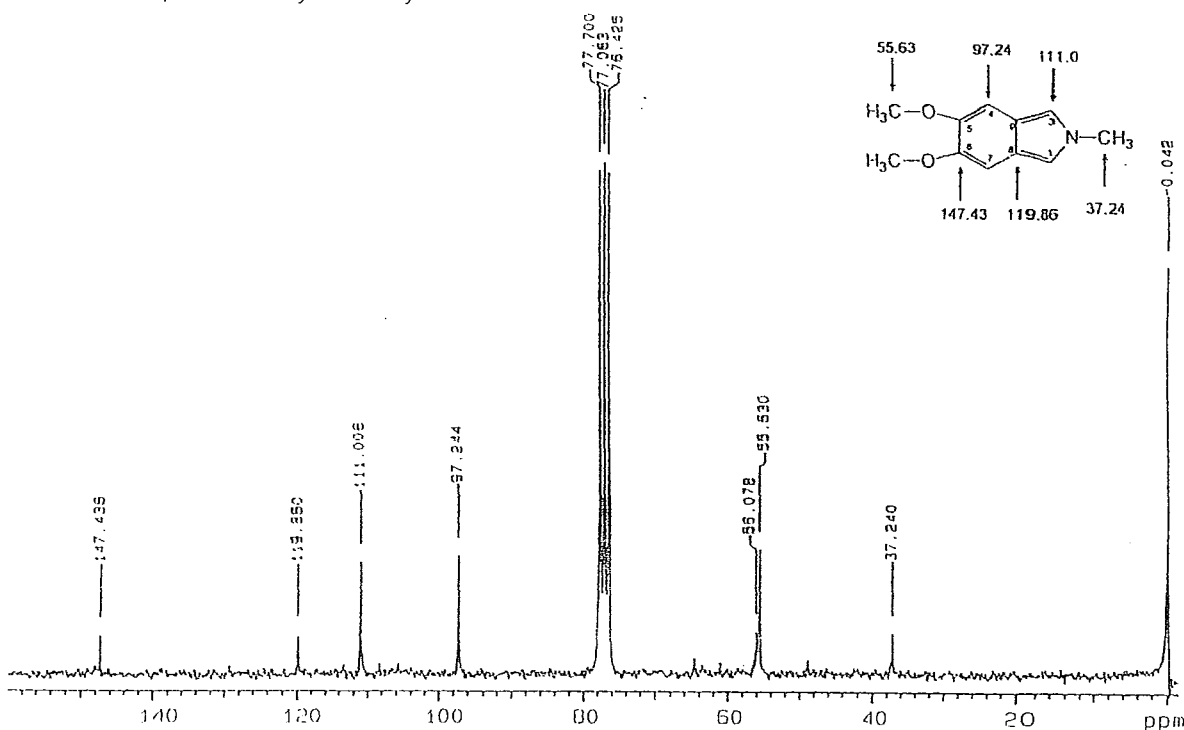
IR 5,6-dimethoxy-N-methylisindole (KBr)



<sup>1</sup>H NMR 5,6-dimethoxy-N-methylisoindole



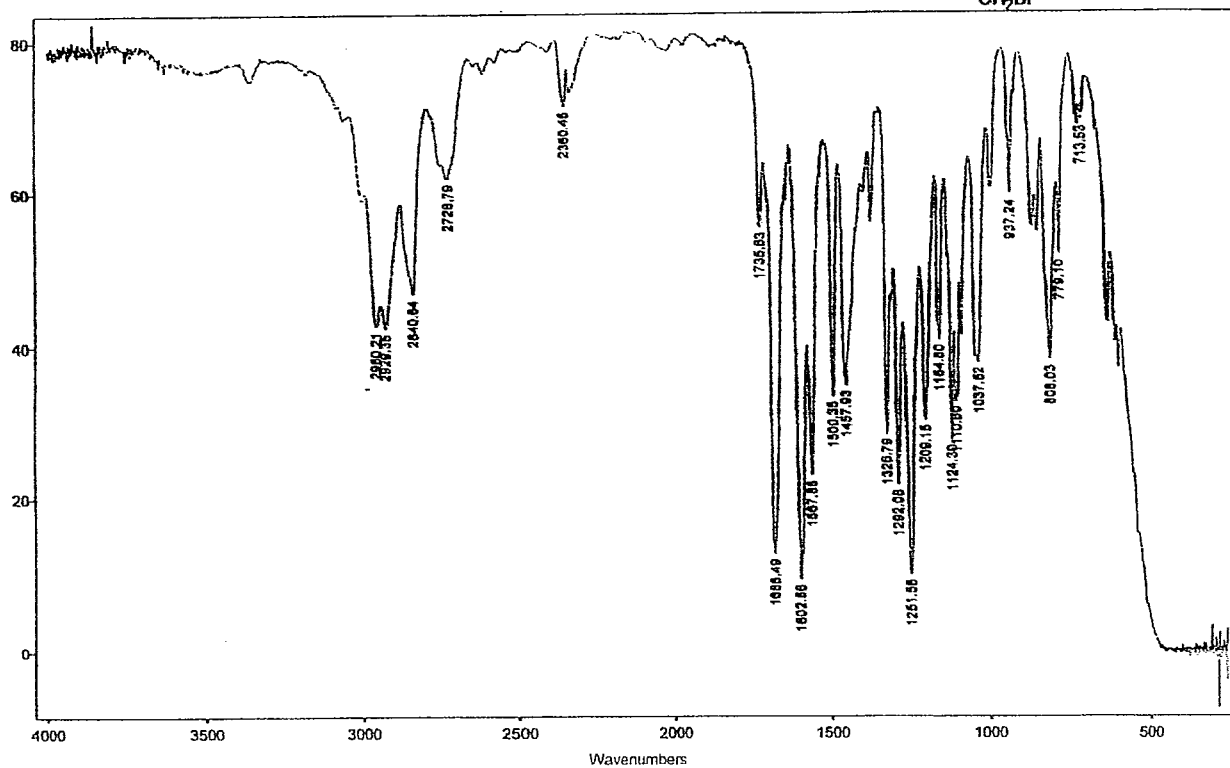
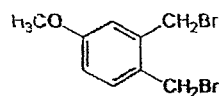
<sup>13</sup>C NMR 5,6-dimethoxy-N-methylisoindole



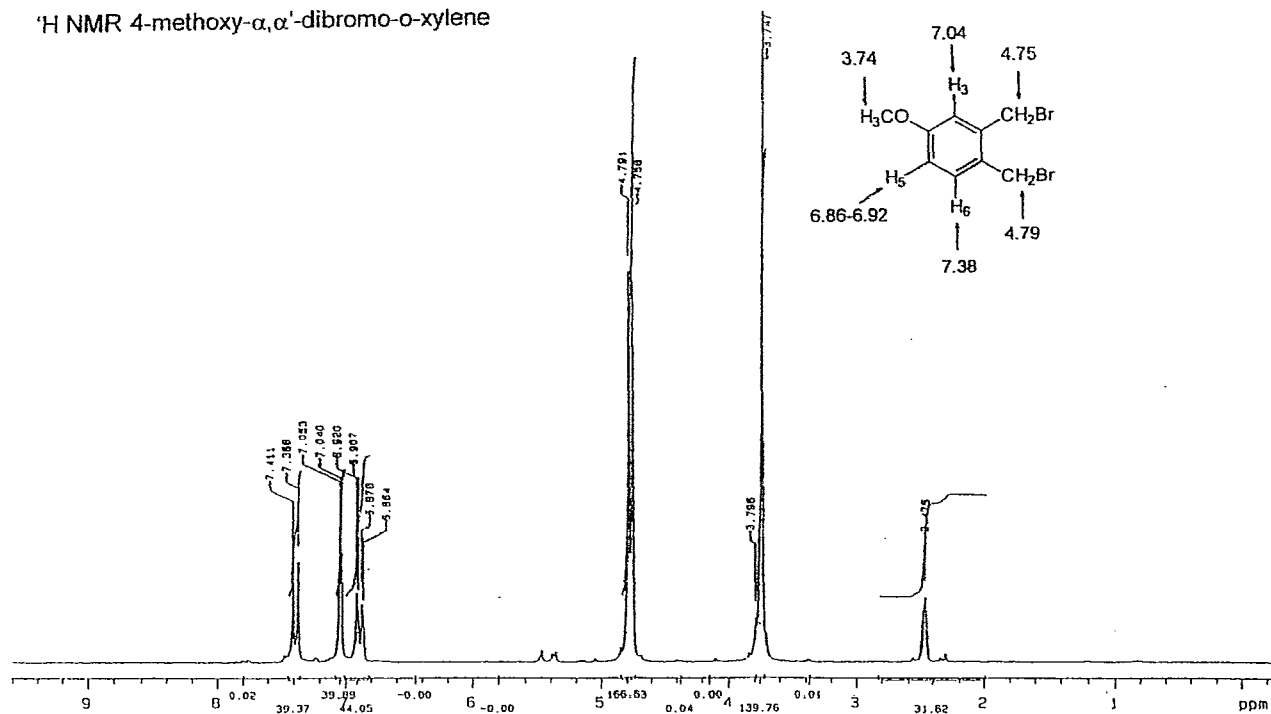
## **Appendix F**

**Spectroscopic data of 4-methoxy- $\alpha,\alpha'$ -dibromo-o-xylene**

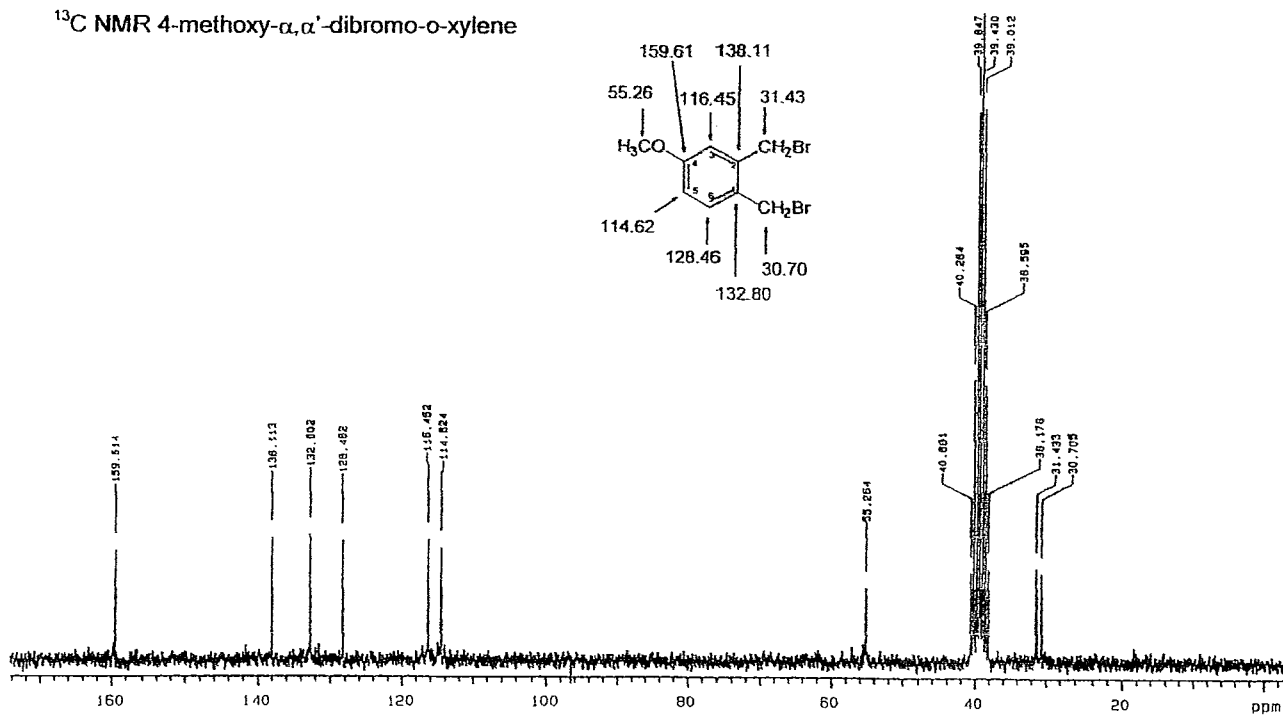
IR 4-methoxy- $\alpha,\alpha'$ -dibromo-*o*-xylene (KBr)



<sup>1</sup>H NMR 4-methoxy- $\alpha,\alpha'$ -dibromo-o-xylene



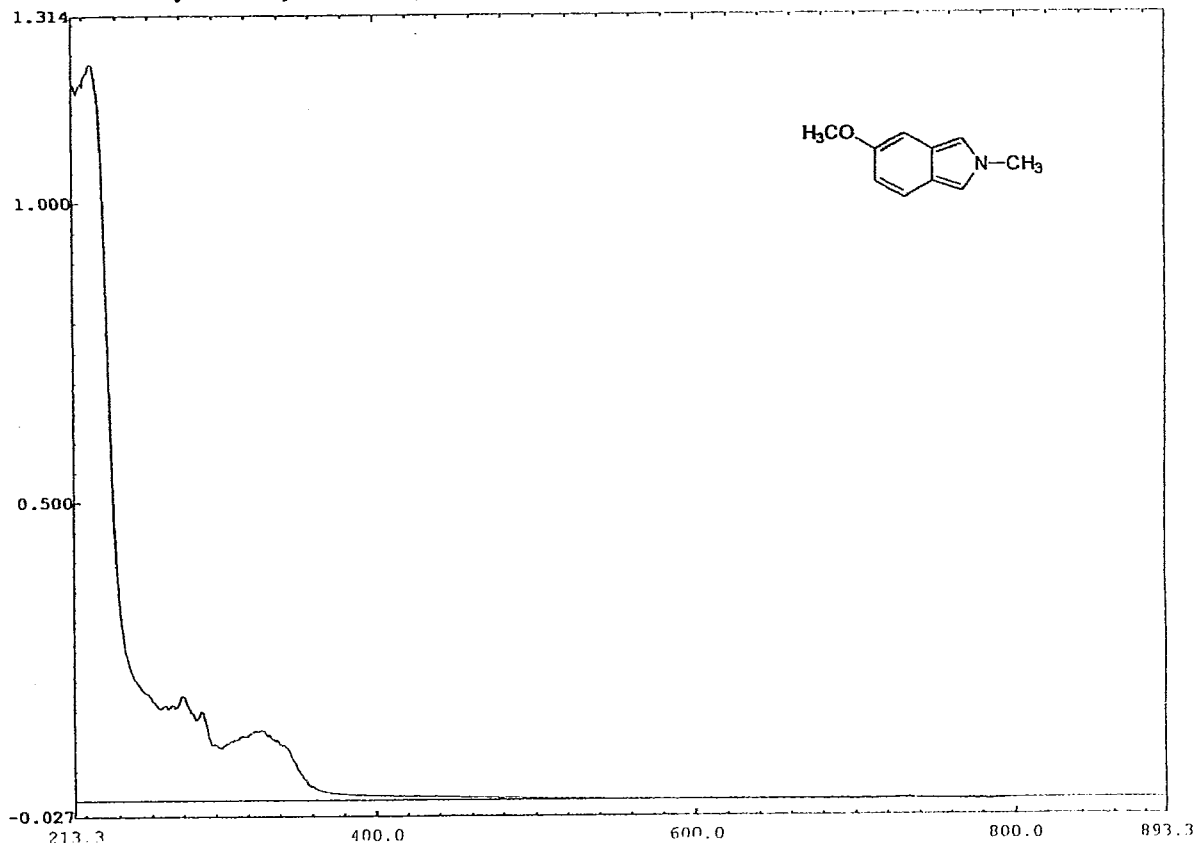
<sup>13</sup>C NMR 4-methoxy- $\alpha,\alpha'$ -dibromo-o-xylene



## **Appendix G**

**Spectroscopic data of 5-methoxy-N-methylisoindole**

UV-Vis 5-methoxy-N-methylisindole (CH<sub>3</sub>CN)



IR 5-methoxy-N-methylisindole (neat)

